

Sonderforschungsbereich 546

**Struktur, Dynamik und Reaktivität von Übergangsmetalloxid-
Aggregaten**

der Humboldt-Universität zu Berlin



Abschlussbericht
1999/2 – 2011/1

Deutsche Forschungsgemeinschaft
- Sonderforschungsbereiche -
53170 Bonn

Abschlussbericht des Sonderforschungsbereichs 546

"Struktur, Dynamik und Reaktivität von Übergangsmetalloxid-Aggregaten"

"Structure, Dynamics and Reactivity of Aggregates of Transition Metal Oxides"

gefördert seit 01.07.1999
bis: 30.06.2011
Sprecherhochschule: Humboldt-Universität zu Berlin

Sprecher des SFB:
Prof. Dr. Joachim Sauer

Dienstanschrift:
Humboldt-Universität zu Berlin
Institut für Chemie
Unter den Linden 6
10099 Berlin

Telefon: 030-2093 7135
Telefax: 030-2093 7136
E-Mail: js@chemie.hu-berlin.de

Stellvertretende Sprecher:
Prof. Dr. Christian Limberg
Prof. Dr. Reinhard Schomäcker

Geschäftsführung oder Sekretariat des SFB:
Dr. Andrea Zehl

Dienstanschrift:
Humboldt-Universität zu Berlin
Institut für Chemie
Unter den Linden 6
10099 Berlin

Telefon: 030-2093 7141
Telefax: 030-2093 7136
E-Mail: sfb546@chemie.hu-berlin.de

Berlin, Dezember 2011

Inhaltsverzeichnis

	Seite	
1	Allgemeine Angaben zum Sonderforschungsbereich	1
1.1	Teilprojektleiterinnen und Teilprojektleiter	1
1.2	Teilprojekte	3
1.3	Beteiligte Einrichtungen	8
1.4	Finanzielle Ausstattung	9
2	Zentrale Ergebnisse des Sonderforschungsbereichs	10
2.1	Results	10
2.1.1	Supported transition metal oxide catalysts	10
2.1.2	Research Program	15
2.1.3	Oxides of reduced dimensionality as model systems	17
2.1.4	Preparation and characterization of single crystals and thin films	21
2.1.5	UHV model catalysts: the VO _x /CeO ₂ (111) example	22
2.1.6	Molecular models	25
2.1.7	Mechanistic studies on molecular models	27
2.1.8	Re-oxidation of the catalyst and the role of peroxy species	30
2.1.9	Deep oxidation of propane	31
2.1.10	Different silica supports	32
2.1.11	Reactivity descriptors for C-H activation catalysts	33
2.1.12	Gas phase models: The perfectly isolated active site	35
2.1.13	Ionization and excitation of transition metal oxo bonds	37
2.1.14	Effect of the particle size	37
2.1.15	Different supporting oxides	39
2.1.16	Summary: Support effects	41
2.2	Interne Kooperation und Organisation	45

II

2.3	Außenwirkung	46	
2.3.1	Wesentliche Publikationen des Sonderforschungsbereiches	46	
2.3.2	Weitere Informationen zur Außenwirkung	50	
3	Strukturwirkung des Sonderforschungsbereichs am Standort	52	
3.1	Personelle Auswirkungen	52	
3.1.1	Personelle Entwicklung, Strukturwirkung und Berufungspolitik	52	
3.1.2	Auswirkungen auf die personelle Grundausstattung	55	
3.1.3	Gleichstellungsmaßnahmen	55	
3.1.4	Förderung der Vereinbarkeit von Familie und Beruf	56	
3.1.5	Förderung des wissenschaftlichen Nachwuchses	56	
3.1.5.1	Verzeichnis der abgeschlossenen Dissertationen und Habilitationen im Sonderforschungsbereich	57	
3.2	Infrastruktur	57	
4	Hinweise an die Deutsche Forschungsgemeinschaft	59	
5	Berichte über die einzelnen Teilprojekte der letzten Förderperiode	61	
A3	Asmis/ Siebert/ Wöste	Struktur, Reaktivität und Dynamik von Übergangsmetalloxid-Aggregaten; Cluster in der Gasphase	61
A4	Sauer	Struktur und Reaktivität unterschiedlicher Übergangsmetalloxid-Aggregate mit quantenchemischen Methoden	83
B1	Freund/ Shaikhutdinov	Untersuchungen zur Struktur-Reaktivitäts-Beziehung von Vanadiumoxid-Aggregaten auf geordneten Übergangsmetalloxidoberflächen	97
B2	Schlögl	Partialoxidation kleiner Kohlenwasserstoffmoleküle mit mikroskopischen Mengen von V_xO_y -Katalysatorsystemen	109
B3	Kondratenko/ Schomäcker	Interaction of oxidants (O_2 , N_2O , CO_2 und H_2O) with well defined VO_x aggregates and its influence on partial oxidation of low alkanes	129

III

B5	Limberg	Synthese und Reaktivität von Molekülmodellen für die aktiven Zentren Vanadiumoxid-basierter Katalysatoren	147
B6	Schomäcker	Untersuchungen zur Selektivität der oxidativen Dehydrierung von Propan an VO _x -Trägerkatalysatoren durch Struktur-Wirkungs-Analysen	171
B7	Schubert	Technische V ₂ O ₅ /TiO ₂ -Modellkatalysatoren: Untersuchung der Aktivkomponente-Träger-Wechselwirkung	195
C1	Kuhlenbeck/ Freund	Adsorptions- und Reaktionsstudien an Vanadium- und Molybdän-gedopten dünnen TiO ₂ -Filmen	211
C4	Hucho	Der Einfluss der elastischen Eigenschaften auf Reaktivität und Selektivität des katalytischen Prozesses	227
C5	Paier/ Sauer	DFT-Rechnungen mit periodischen Randbedingungen zur Struktur, Dynamik und Reaktivität von Übergangsmetalloxiden auf Trägern im Vergleich zu Einkristallen	241
C6	Hermann	Ab-initio-Clustermodelle zur Struktur, Reaktivität und Spektroskopie an komplexen Vanadium- und Molybdänoxidoberflächen	255
C8	Woodruff/ Sauer	Structure determination of VO _x and related surfaces, thin films and interfaces based on scanned-energy mode photo-electron diffraction	275
C11	Winter	Untersuchungen der Eigenschaften von Übergangsmetalloxid-Oberflächen mittels streifender Ionen-Streuung	287

1 Allgemeine Angaben zum Sonderforschungsbereich

1.1 Teilprojektleiterinnen und Teilprojektleiter

Name, Vorname, akad. Titel	w/m	geb.	Institution	TP	Zeitraum der Förderung
Asmis, Knut, Dr.	m	1968	FHI	A3	07/2002 – 06/2011
Baerns, Manfred, Prof. Dr.	m	1934	ACA	B3	07/1999 – 06/2005
Bäumer, Marcus, PD Dr.	m	1966	FHI	B1	07/2001 – 06/2003
Buyevskaya, Olga, Dr.	w	1959	ACA	B3	07/1999 – 06/2002
Dingerdissen, Uwe, Dr.	m	1959	ACA	B3	07/2005 – 04/2007
Döbler, Jens, Dr.	m	1972	HU	A4	07/2008
Freund, Hans-Joachim, Prof. Dr.	m	1951	FHI	B1,C1	07/1999 – 06/2011
Ganduglia-Pirovano, M. Veronica, Dr.	w	1962	HU	C5	07/2002 – 07/2009
Haase, Frank, Dr.	m	1959	HU	C5	07/1999 – 06/2000
Hermann, Klaus, Prof. Dr.	m	1946	FHI	C6	07/1999 – 06/2011
Hess, Christian, Prof. Dr.	m	1972	FHI	B2	07/2005 – 02/2008
Hucho, Carsten, Dr.	m	1964	PDI	C4	07/1999 – 06/2011
Kemnitz, Erhard, Prof. Dr.	m	1951	HU	B4	10/2002 – 06/2005
Kondratenko, Evgueni, Dr.	m	1967	LIKAT	B3	07/2005 – 06/2011
Kuhlenbeck, Helmut, Dr.	m	1957	FHI	C1	07/1999 – 06/2011
Limberg, Christian, Prof. Dr.	m	1965	HU	B5	08/2003 – 06/2011
Manzke, Recardo, Prof. Dr.	m	1949	HU	C10	07/2005 – 06/2008
Moresco, Francesca, Dr.	w	1965	FU	C3	07/1999 – 06/2005
Niehus, Horst, Prof. Dr.	m	1944	HU	C2	07/1999 – 06/2005
Paier, Joachim, Dr.	w	1978	HU	C5	09/2009 – 6/2011
Pelzer, Katrin, Dr.	w	1975	FHI	B2	07/2008 – 02/2010
Ploog, Klaus H., Prof. Dr.	m	1941	PDI	C4	07/1999 – 09/2006

Rademann, Klaus, Prof. Dr.	m	1953	HU	A3	07/1999 – 06/2005
Rieder, Karl Heinz, Prof. Dr.	m	1942	FU	C3	07/1999 – 06/2005
Sauer, Joachim, Prof. Dr.	m	1049	HU	A4,C5,C8	07/1999 – 06/2011
Schilbe, Peter, Prof. Dr.	m	1964	FU	C4	07/2002 – 07/2003
Schlögl, Robert, Prof. Dr.	m	1954	FHI	B2	07/1999 – 06/2011
Schomäcker, Reinhard, Prof. Dr.	m	1959	TU	B3,B6	07/2005 – 06/2011
Schröder, Detlef, Dr.	m	1963	TU	A2	07/1999 – 12/2006
Schubert, Helmut, Prof. Dr.	m	1951	TU	B7	07/2005 – 06/2011
Schwarz, Helmut, Prof. Dr. Drs. h.c.	m	1943	TU	A2	07/1999 – 06/2008
Shaikhutdinov, Shamil, Dr.	m	1960	FHI	B1	03/2004 – 06/2011
Siebert, Torsten, Dr.	m	1969	FU	A3	07/2008 – 06/2011
Sierka, Marek, Dr.	m	1971	HU	A4	06/2010 – 06/2011
Su, Dangsheng, Dr.	m	1961	FHI	B2	07/1999 – 06/2008
Theis, Wolfgang, Dr.	m	1965	FU	C3	07/1999 – 06/2005
Urban, Joachim, Prof. Dr.	m	1940	FHI	B2	07/2002 – 06/2005
Van Wüllen, Christoph, Prof. Dr.	m	1963	TU	A1	07/2001 – 08/2007
Widdra, Wolf, Prof. Dr.	m	1961	TU, MBI	C7	07/2002 – 03/2003
Winter, Helmut, Prof. Dr.	m	1949	HU	C11	07/2008 – 06/2011
Woodruff, David Phillip, Prof. Dr.	m	1944	UW, FHI	C8	07/2002 – 06/2011
Wöste, Ludger, Prof. Dr.	m	1946	FU	A3	07/1999 – 06/2011

Die Abkürzungen bedeuten:

- ACA Institut für Angewandte Chemie Adlershof, 2006 fusioniert zum LIKAT
 FHI Fritz-Haber-Institut der Max-Planck-Gesellschaft
 FU Freie Universität Berlin
 HU Humboldt-Universität zu Berlin
 LIKAT Leibniz-Institut für Katalyse e.V. an der Universität Rostock, ehemals ACA
 MBI Max-Born Institut Berlin
 PDI Paul-Drude-Institut für Festkörperelektronik
 TU Technische Universität Berlin
 UW University of Warwick

1.2 Teilprojekte

TP	Titel	Fachgebiet	Leiter/in	Zeitraum der Förderung des TP
A1	Quantenchemische Rechnungen zur elektronischen Struktur und Reaktivität ein- und mehrkerniger Vanadiumoxid-Cluster	Theoretische Chemie	C. van Wüllen	07/2001 – 06/2008
A2	Übergangsmetalloxide in der Gasphase	Physikalisch-Organische Chemie	D. Schröder H. Schwarz	07/1999 – 06/2008
A3	Spektroskopische Untersuchungen von Clustern in der Gasphase	Physikalische Chemie, Experimentalphysik, Cluster	K. Rademann L. Wöste	07/1999 – 06/2002
A3	Struktur, Stabilität und Reaktivität von Übergangsmetalloxiid-Aggregaten; $V_mO_n^{-/0+}$ Cluster und Clusterionen ($m \leq 10$)	Physikalische Chemie, Experimentalphysik, Cluster	K. Asmis K. Rademann L. Wöste	07/2002 – 06/2005
A3	Struktur, Stabilität und Reaktivität von Übergangsmetalloxiid-Aggregaten; $V_mO_n^{-/0+}$ Cluster und Clusterionen ($m \leq 10$)	Clusterphysik, Massenspektrometrie, Spektroskopie,	K. Asmis L. Wöste	07/2005 – 06/2008
A3	Struktur, Reaktivität und Dynamik von Übergangsmetalloxiid-Aggregaten; Cluster in der Gasphase	Massenspektrometrie, frequenz- und zeitaufgelöste Spektroskopie, Cluster, chemische Reaktivität	K. Asmis T. Siebert L. Wöste	07/2008 – 06/2011
A4	Cluster- und Embedded Cluster-Rechnungen an unterschiedlichen Aggregaten von Vanadiumoxiden	Theoretische Chemie, Quantenchemie	J. Sauer	07/1999 – 06/2002
A4	Vergleich von Struktur, Dynamik und Reaktivität unterschiedlicher Aggregate von Vanadiumoxiden mit Dichtefunktionalmethoden	Theoretische Chemie, Quantenchemie	J. Sauer	07/2002 – 06/2005

A4	Struktur, Schwingungsspektren und Reaktivität unterschiedlicher Vanadiumoxid-Aggregate mit Dichtefunktionalmethoden	Theoretische Chemie, Quantenchemie	J. Sauer	07/2005 – 06/2008
A4	Struktur und Reaktivität unterschiedlicher Übergangsmetalloxid-Aggregate mit quantenchemischen Methoden	Theoretische Chemie, Quantenchemie	J. Sauer M. Sierka J. Döbler	07/2008 – 06/2011
B1	Kleine Oxidaggregate und dünne Oxidfilme auf Oxidoberflächen	Physikalische Chemie, Festkörperoberflächen	M. Bäumer H.-J. Freund	07/1999 – 06/2002
B1	Kleine Oxidaggregate auf Oxidoberflächen	Physikalische Chemie, Festkörperoberflächen	S. Shaikhutdinov H.-J. Freund	07/2002 – 06/2005
B1	Struktur-Reaktivitätsbeziehung von Vanadiumoxid-Aggregaten auf geordneten Übergangsmetalloxidoberflächen	Chemische Physik, Oberflächen, Modellkatalyse	S. Shaikhutdinov H.-J. Freund	07/2005 – 06/2008
B1	Struktur-Reaktivitäts-Beziehung von Vanadiumoxid-Aggregaten auf geordneten Übergangsmetalloxidoberflächen	Chemische Physik, Oberflächen, Modellkatalyse	S. Shaikhutdinov H.-J. Freund	07/2008 – 06/2011
B2	Elektronenmikroskopie und Reaktionsstudien an deponierten Clustern	Physikalische Chemie, Strukturchemie	R. Schlögl	07/1999 – 06/2002
B2	Partialoxidation kleiner Kohlenwasserstoffmoleküle mit mikroskopischen Mengen von V_xO_y -Katalysatorsystemen	Physikalische und Anorganische Chemie	R. Schlögl J. Urban	07/2002 – 06/2005
B2	Partialoxidation kleiner Kohlenwasserstoffmoleküle mit mikroskopischen Mengen von V_xO_y -Katalysatorsystemen	Physikalische und Anorganische Chemie	R. Schlögl C. Hess, D. Su	07/2005 – 06/2008
B2	Partialoxidation kleiner Kohlenwasserstoffmoleküle mit mikroskopischen Mengen von V_xO_y -Katalysatorsystemen	Physikalische und Anorganische Chemie	R. Schlögl K. Pelzer	07/2008 – 06/2011
B3	Wechselwirkung von kurzkettigen Alkanen und Sauerstoff an Oberflächen von Übergangsmetalloxiden insbesondere von V_xO_y	Anorganische Chemie, Heterogene Katalyse	O.V. Buyevskaya M. Baerns	07/1999 – 06/2002

B3	Katalytische Wirkungsweise von VO _x -Aggregaten bei der Oxidation von Ethan und Propan	Anorganische Chemie, Heterogene Katalyse	M. Baerns	07/2002 – 06/2005
B3	Dehydrierung und partielle Oxidation kurzkettiger Alkane	Katalyse	U. Dingerdissen E. Kondratenko	07/2005 – 06/2008
B3	Wechselwirkung von Oxidationsmitteln (O ₂ , N ₂ O, CO ₂ und H ₂ O) mit definierten VO _x -Aggregaten und deren Einfluss auf die partielle Oxidation kleiner Kohlenwasserstoffe	Heterogene Katalyse, Technische Chemie	E. Kondratenko R. Schomäcker	07/2008 – 06/2011
B4	Synthese VO _x -dotierter SiO ₂ - und ZrO ₂ -Aerogele und Cryogele sowie Sauerstoffaustauschuntersuchungen mittels ¹⁸ O-Isotopenaustausch	Anorganische Chemie, Heterogene Katalyse	E. Kemnitz	07/2002– 06/2005
B5	Synthese und Reaktivität von Molekülmodellen für die aktiven Zentren Vanadiumoxid-basierter Katalysatoren	Anorganische Chemie, Molekülsynthese, Übergangsmetall-oxokomplexe, Oxygenierungschemie	C. Limberg	08/2003 – 06/2011
B6	Entwicklung eines kinetischen Modells für die oxidative Dehydrierung von Propan für eine Struktur-Wirkungsanalyse	Heterogene Katalyse	R. Schomäcker	07/2005 – 06/2008
B6	Untersuchungen zur Selektivität der oxidativen Dehydrierung von Propan an VO _x -Trägerkatalysatoren durch Struktur-Wirkungs-Analysen	Technische Chemie	R. Schomäcker	07/2008 – 06/2011
B7	Technische V ₂ O ₅ /TiO ₂ -Modellkatalysatoren: Herstellung und Untersuchung der Aktivkomponente-Träger-Wechselwirkung	Materialwissenschaft, Grenzflächen	H. Schubert	07/2005 – 06/2011
C1	Untersuchungen zu Elektronenstruktur und Adsorptionsverhalten von geordneten und modifizierten Vanadiumoxidoberflächen	Physikalische Chemie, Festkörperoberflächen	H. Kühlenbeck H.-J. Freund	07/1999 – 06/2002

C1	Untersuchungen zu Elektronenstruktur und Adsorptionsverhalten von geordneten und defektbehafteten geordneten Vanadiumoxidoberflächen	Physikalische Chemie, Festkörperoberflächen	H. Kühlenbeck H.-J. Freund	07/2002 – 06/2005
C1	Elektronenstruktur und Adsorptionsverhalten von geordneten Vanadium-, Molybdän- und Nioboxidoberflächen	Physikalische Chemie, Festkörperoberflächen	H. Kühlenbeck H.-J. Freund	07/2005 – 06/2008
C1	Adsorptions- und Reaktionsstudien an Vanadium- und Molybdängedopten dünnen TiO ₂ -Filmen	Physikalische Chemie, Festkörperoberflächen	H. Kühlenbeck H.-J. Freund	07/2008 – 06/2011
C2	Ionen- und Neutralteilchenstreuung an Oxidoberflächen und adsorbierten Clustern	Experimentalphysik, Festkörperoberflächen	H. Niehus	07/1999 – 06/2002
C2	Geometrische und elektronische Struktur von Oxidoberflächen und adsorbierten Clustern	Oberflächenphysik, Ionenstreuung	H. Niehus	07/2002 – 06/2005
C3	Atomstrahlbeugungsuntersuchungen an Oxidoberflächen und dünnen Oxidfilmen	Experimentalphysik, Festkörperoberflächen	K.-H. Rieder D. Farias	07/1999 – 06/2002
C3	Atomstrahlbeugungs- und Tieftemperatur-Rastertunnel-Mikroskopie-Untersuchungen an Oxidoberflächen und dünnen Oxidfilmen	Oberflächenphysik	K.-H. Rieder W. Theis F. Moresco	07/2002 – 06/2005
C4	Herstellung und Charakterisierung einkristalliner Übergangsmetall-oxide	Experimentelle Festkörperphysik, Materialwissenschaft	P. Schilbe K.-H. Rieder K. Ploog	07/1999 – 06/2008
C4	Der Einfluss der elastischen Eigenschaften auf Reaktivität und Selektivität des katalytischen Prozesses	Physik	C. Hucho	07/2008 – 06/2011
C5	Periodische Ab initio-Rechnungen zur Struktur, Dynamik und Reaktivität von Vanadiumoxid-Aggregaten	Theoretische Chemie, Festkörperoberflächen	F. Haase J. Sauer	07/1999 – 06/2002

C5	DFT-Rechnungen mit periodischen Randbedingungen zur Struktur, Dynamik und Reaktivität von Vanadiumoxid-Aggregaten	Theoretische Chemie, Festkörper-Oberflächen	M.V. Ganduglia-Pirovano J. Sauer	07/2002 – 06/2008
C5	DFT-Rechnungen mit periodischen Randbedingungen zur Struktur, Dynamik und Reaktivität von Übergangsmetalloxiden auf Trägern im Vergleich zu Einkristallen	Theoretische Chemie, Quantenchemie	J. Paier J. Sauer M.V. Ganduglia-Pirovano	07/2008 – 06/2011
C6	Lokale und periodische Modelle zur geometrischen und elektronischen Struktur an Vanadiumoxid-Oberflächen	Theoretische Physik, Festkörper-Oberflächen	K. Hermann	07/1999 – 06/2005
C6	Ab-initio-Clustermodelle zur Struktur, Reaktivität und Spektroskopie an komplexen Vanadiumoxid- und Vanadiumphosphat-Oberflächen	Theoretische Oberflächenphysik, Oberflächenchemie	K. Hermann	07/2005 – 06/2008
C6	Ab-initio-Clustermodelle zur Struktur, Reaktivität und Spektroskopie an komplexen Vanadium- und Molybdänoxid-oberflächen	Theoretische Oberflächenphysik, Oberflächenchemie	K. Hermann	07/2008 – 06/2011
C7	Adsorption und Reaktion ungesättigter Kohlenwasserstoff auf Vanadiumoxidoberflächen	Oberflächenphysik	W. Widdra	07/2002 – 12/2003
C8	Structure determination of VO _x and related surfaces, thin films and interfaces based on scanned-energy mode photoelectron diffraction	Experimental surface science	D.P. Woodruff J. Sauer	07/2002 – 06/2011
C10	Unbesetzte elektronische Zustände von Übergangsmetalloxid - Oberflächen und deponierten Clustern	Experimentalphysik, Festkörperoberflächen	R. Manzke	07/2005 – 06/2008
C11	Untersuchungen der Eigenschaften von Übergangsmetalloxid-Oberflächen mittels streifender Ionenstreuung	Physik, Oberflächenphysik	H. Winter	07/2008 – 06/2011

1.3 Beteiligte Einrichtungen

Universitäre Einrichtungen:

- Freie Universität Berlin - Institut für Experimentalphysik (FU-P)
- Humboldt-Universität zu Berlin - Institut für Chemie (HU-C)
- Institut für Physik (HU-P)
- Technische Universität Berlin - Institut für Chemie (TU-C)
- Institut für atomare Physik und Fachdidaktik (TU-P)
- Institut für Werkstoffwissenschaften und
-technologien (TU-W)
- University of Warwick - Physics Department (UW-P)

Außeruniversitäre Einrichtungen:

- Fritz-Haber-Institut der Max-Planck-Gesellschaft, Berlin-Dahlem (FHI)
- Leibniz-Institut für Katalyse e. V. an der Universität Rostock, Außenstelle Berlin (LIKAT)
- Max-Born-Institut für Nichtlineare Optik und Kurzzeitspektroskopie, Berlin-Adlershof (MBI)
- Paul-Drude-Institut für Festkörperelektronik, Berlin-Mitte (PDI)

1.4 Finanzielle Ausstattung

Ergänzungsausstattung				
Haushaltsjahr	Personalmittel	Sachmittel	Investitionsmittel	Summe
1999/2	225,9	61,6	373,8	661,3
2000	474,9	132,9	70,3	678,1
2001	527,9	133,4	20,5	681,8
2002/1	283,8	73,4	-	357,2
Zwischensumme - erste Förderperiode:				2.378,4
Haushaltsjahr	Personalmittel	Sachmittel	Investitionsmittel	Summe
2002/2	442,6	95,6	422,3	960,5
2003	893,9	172,4	74,4	1.140,7
2004	932,0	186,4	-	1.118,4
2005/1	470,7	85,3	-	556,0
Zwischensumme - zweite Förderperiode:				3.775,6
Haushaltsjahr	Personalmittel	Sachmittel	Investitionsmittel	Summe
2005/2	474,0	100,7	412,0	986,7
2006	911,2	179,9	75,0	1.166,1
2007	896,5	189,1	0	1.085,6
2008/1	440,9	84,7	0	525,6
Zwischensumme - dritte Förderperiode:				3.764,0
Haushaltsjahr	Personalmittel	Sachmittel	Investitionsmittel	Summe
2008/2	428,0	112,6	185,3	725,9
2009	856,0	172,1	-	1.028,1
20010	928,6	167,1	-	1.095,7
2011/1	441,8	112,4	-	554,2
Zwischensumme - vierte Förderperiode:				3.403,9
Gesamtsumme:				13.321,9

(Alle Angaben in Tausend Euro)

2 Zentrale Ergebnisse des Sonderforschungsbereichs

2.1 Results

2.1.1 Supported transition metal oxide catalysts

Supported transition metal oxide catalysts in general, and vanadium oxides in particular are suitable materials to study the structure, dynamics and reactivity of different aggregates of transition metal oxides. Vanadium oxides are industrially used catalysts, e.g. for selectively oxidizing SO_2 to SO_3 or benzene to maleic acid anhydride. As vanadium forms sufficiently stable compounds with oxygen in three oxidation states, +3, +4, and +5, there is a large variety of structures. There is an even larger number of structurally distinguishable positions at which oxygen defects can be formed and steer the reactivity. Since under the conditions of catalytic reactions the surface may be partially hydroxylated, the complexity increases even more.

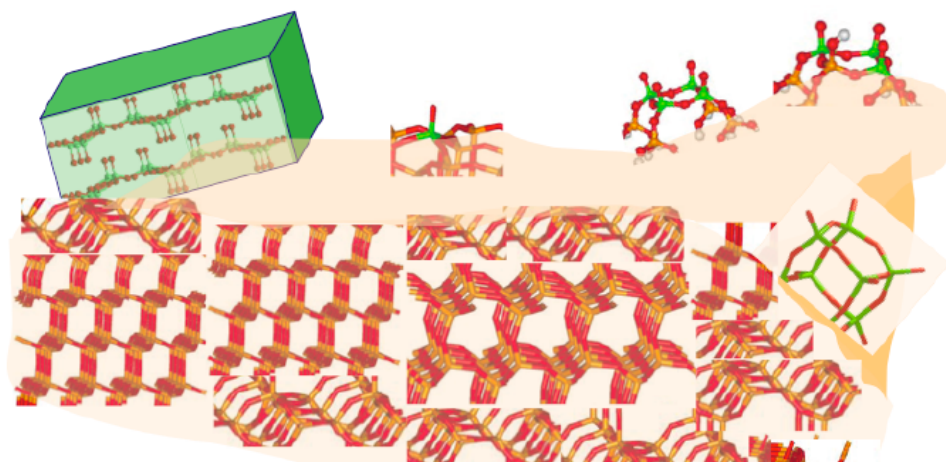


Fig. 1. Vanadium oxide on silica as supporting oxide.

Structures. Fig. 1 shows schematically vanadium oxide particles of different type (monomeric species, clusters and small crystallites of bulk V_2O_5) and different size on a SiO_2 support. The support itself may be differently structured, crystalline or amorphous, dense or nanoporous. The atoms of such catalysts are not ordered into unit cells (no translational symmetry) and therefore, the atomic positions cannot be determined by diffraction techniques. Neither is the assignment of spectroscopic signatures safe, which makes it difficult to identify surface species of given size and structure.^[1] Therefore, the distribution of different species on the catalyst surface is not known in general.

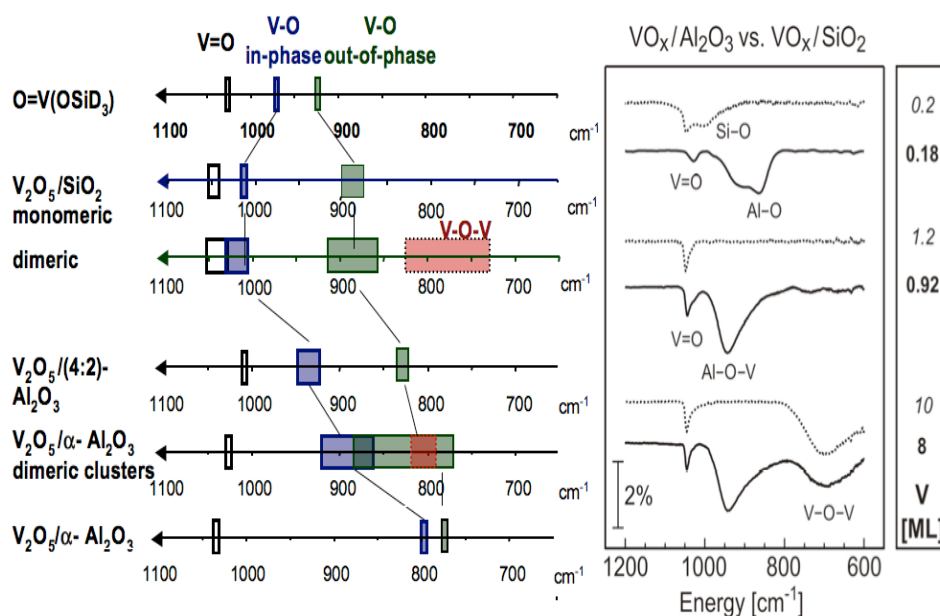
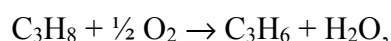


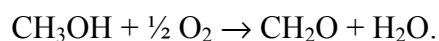
Fig. 2. Observed IR spectra of $\text{VO}_x/\text{Al}_2\text{O}_3$ and VO_x/SiO_2 model catalysts (right) and calculated (DFT) wave number range of different types of vibrations (left).^[1]

A major problem with supported catalysts is the identification of surface species by vibrational spectroscopy. For example, the Raman band observed around 950 cm^{-1} was considered as proof for the presence of V-O-V bonds in supported vanadia species and, hence, believed to be indicative of oligomeric species.^[2-7] In an early joint effort of TP B1 (model catalysts), B3 (powder catalysts), and A4 (DFT calculations), and in cooperation with P. Stair, Northwestern University,^[1] it could be shown that the V-O-V modes do not fall into the 950 cm^{-1} range, but are located around $735\text{--}825\text{ cm}^{-1}$ (Fig. 2, left), where they are covered by support phonons. While the band due to an interfacial V-O-Al-vibration is found around 940 cm^{-1} , the corresponding V-O-Si vibrations overlap strongly with the vanadyl vibration and can lead to a more complex behaviour of the vibrational spectra in the range around $1000\text{--}1050\text{ cm}^{-1}$. This was the explanation for the different IR spectra observed for $\text{VO}_x/\text{silica}$ and $\text{VO}_x/\text{alumina}$ model catalyst which are shown as function of vanadia loading in Fig. 2, right. A band at 940 cm^{-1} shows up for $\text{VO}_x/\text{alumina}$ but not for $\text{VO}_x/\text{silica}$, although the morphology of the two model systems as imaged with STM was almost indistinguishable making it very unlikely that polymeric species are present in the former case, but not in the latter. These findings correlate also very well with the spectra of powder catalysts^[1] and our assignment became widely accepted in the field. Our publication in *Journal of Catalysis*^[1] has been cited 120 times so far (15 citations per year), and was distinguished as top cited article by the journal.

Reactivity. As model reactions for characterizing the reactivity of transition metal catalysts we have selected two C-H activation reactions, the selective oxidation of propane to propene,



and of methanol to formaldehyde,



The catalyst activity is usually characterized by the „turnover frequency (TOF)“ which is a rate divided by the number of active sites, leading to units such as $\text{mol}_{\text{propene}}/\text{mol}_V \cdot \text{s}$, e.g. for the propane oxidation. For a supported catalyst as sketched in Fig. 1, only the total amount of vanadium present in the whole sample is known, but not the share that is active or at least located on the surface of the vanadium oxide particles. This complicates the interpretation of TOF-values.

The support effect on the catalytic activity has been studied by Wachs et al. in detail, and the statement^[8] „The methanol oxidation TOFs vary by approximately four orders of magnitude with the specific oxide support...“ has become a citation classic when motivating studies on support effects.

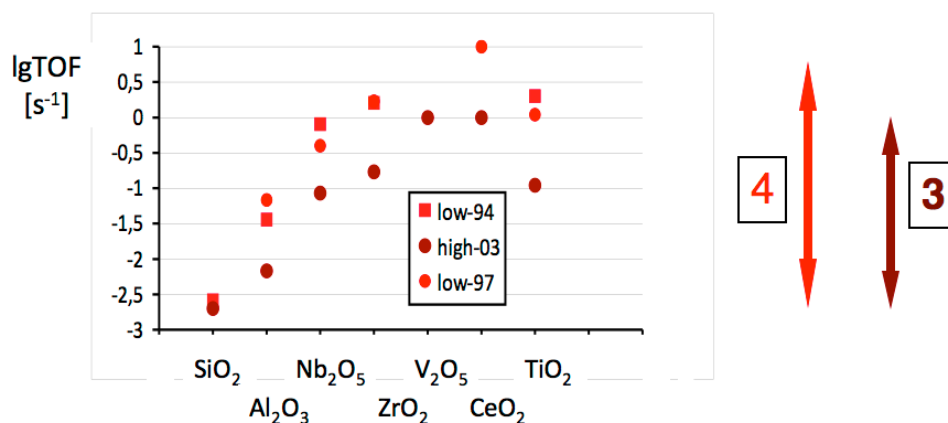


Fig. 3. Turnover frequency (TOF) for the methanol oxidation to formaldehyde by vanadium oxide on different supporting oxides.

Fig. 3 shows a logarithmic plot of TOF values for the oxidation of methanol to formaldehyde for vanadium oxide supported on SiO₂, Al₂O₃, Nb₂O₅, ZrO₂, V₂O₅, CeO₂, and TiO₂ from different publications of Wachs et al.. They all consider catalysts with a vanadium oxide loading up to one monolayer. The “low-94”^[3] and “low-97”^[9] results have both been obtained for a low loading for which the assumption that all vanadium oxide on the surface is active may be justified. With some differences between the results for the same support from different publica-

tions, this data set shows the four orders of magnitude overall variation. The “high-03”^[10] data set refers to vanadium oxide loadings close to monolayer coverage, but without V₂O₅ crystallites as far as X-ray diffraction can prove. For this series an attempt has been made to determine the active part of vanadium. About the same activity distribution is found, but the variation is smaller, within three orders of magnitude.

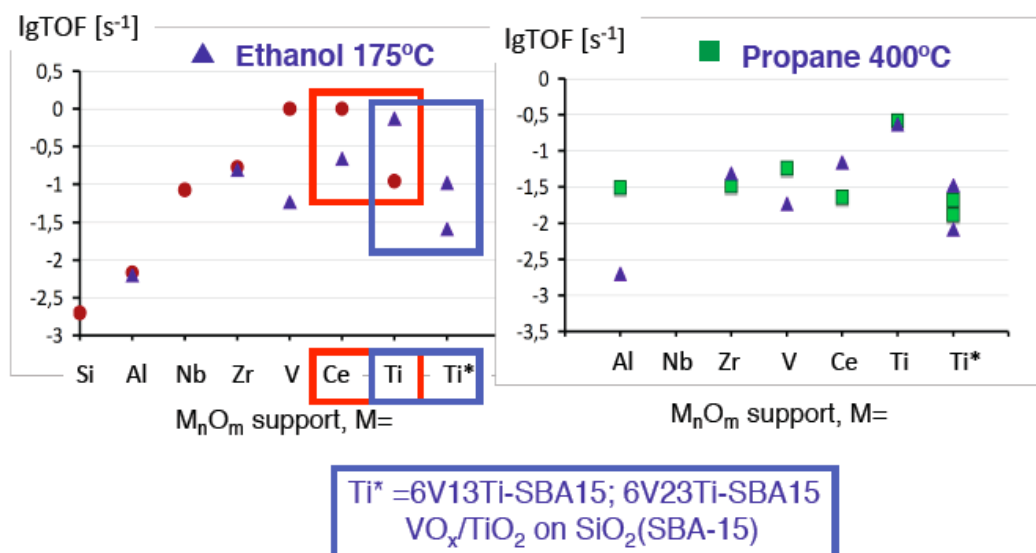


Fig. 4. Turnover frequency for the oxidation of ethanol (blue triangles) and propane (green squares) by vanadium oxide on different supporting oxides (TPs B6 and B2). The red dots are the “high-03” methanol data from Fig. 3.

This Collaborative Research Center (CRC) wanted to make sure that the Wachs data, which apparently originate from very few experiments could be independently confirmed.

Fig. 4 shows results from TP B6 (Schomäcker) and TP B2 (Schlögl), which have been obtained with ethanol instead of methanol to avoid degradation of some of the oxides when exposed to methanol under reaction conditions. There is by and large the same variation, but the activity order of CeO₂- and TiO₂-supported catalysts shows an interesting switch between the methanol and ethanol oxidation data sets. However, the higher activity of V₂O₅ on the TiO₂ support compared to the CeO₂ support disappears, when it is supported on TiO₂ that is dispersed on mesoporous silica (SBA-15) as prepared in TP B2.

Nevertheless, the V-Ti/SBA-15 system (TP B2) is a prominent example for a well-defined model system of practical potential. Under the explored reaction conditions (TP B6) the productivity of this catalyst exceeds the requirements for industrial application of 1 g_{C₃H₆}g_{cat}⁻¹h⁻¹ by far.

The TOF for propane oxidation, obtained at higher temperature, show a smaller variation across different supporting oxides than found for the oxidation of methanol and ethanol, and they also indicate a different activity order of the catalysts with different supports. A variation of only two orders of magnitude (instead of three or four) had already been reported by Wachs et al.^[10] The Wachs data were more or less confirmed by our analysis, and the CRC experiments underline the relevance of the particular reaction considered and the reaction conditions on the TOF.

Results from TP B3 (Fig. 5) illustrate the effect of the operation mode on the oxidative dehydrogenation of propane (and iso-butane), in particular on the alkene selectivity. Operating with a high alkane/O₂ feed ratio (>10) improves significantly the propene selectivity at high propane conversions.^[11]

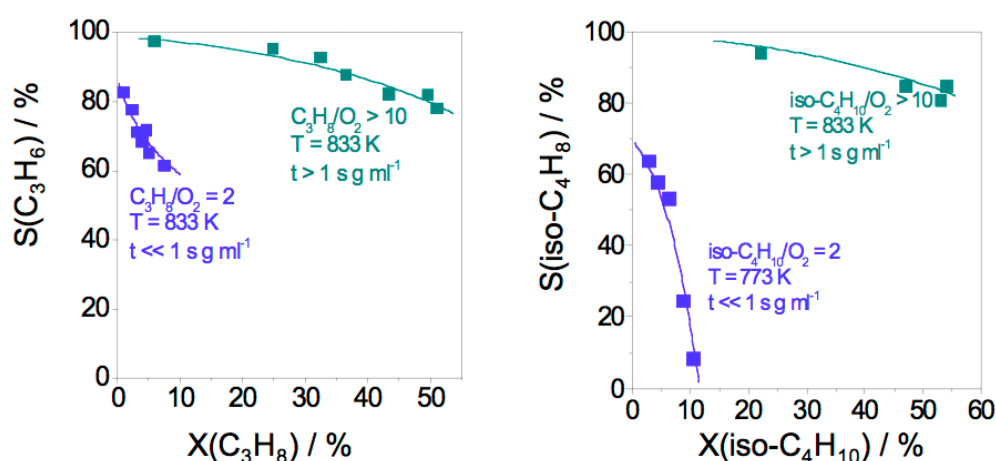


Fig. 5. Alkene selectivity S as function of alkane conversion X for a vanadium oxide (3wt.%) catalyst supported on mesoporous silica (MCM-41).

In summary we have presented evidence that

- the activity depends on the loading, not all vanadium oxide of a sample may be active
- the activity and selectivity depend on reaction conditions.

Attempts to correlate the catalytic activity with a single global parameter of the supporting oxide, the electronegativity,^[8,12,13] are not expected to be successful and do not reflect the multi-dimensional nature of the problem.

To understand the support effect we need to understand

- the reaction mechanism
- the materials properties
- the surface structure: VO_x particles of different size, structure and distribution.

2.1.2 Research Program

Key to our research program (Fig. 6) is the use of different types of model catalysts to gain understanding at the atomic level

- gas phase clusters
- thin films as supports studied in ultra-high vacuum (UHV) using surface science techniques
- molecular model compounds

To reveal the relations between the structures of different aggregates of transition metal oxides and their function, we prepared them in different aggregation forms, characterized their structures and electronic properties and studied their reactivities. The research of this CRC covers the whole range from gas phase reactivity studies in the mass spectrometer to catalytic studies on supported oxides as powder catalysts under realistic conditions.

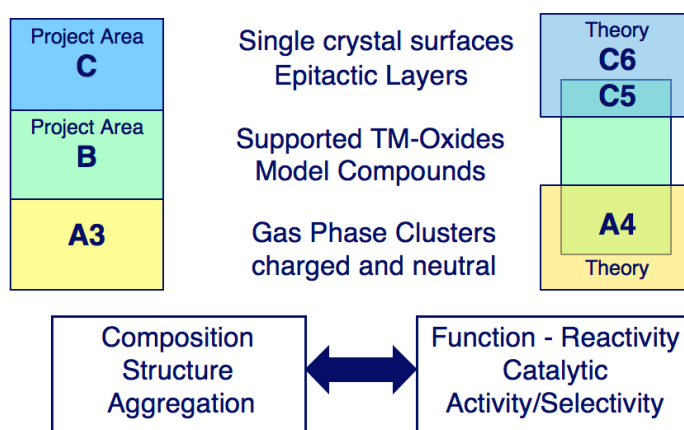


Fig. 6. Research program.

The study of mononuclear transition metal compounds and of small polynuclear clusters in the gas phase provides basic information on “the active sites in isolation”, about their redox properties and their ability to activate C-H bonds. Single crystals and thin films provide the limiting case of ordered aggregates, in which, however, also defects may be created in a defined way. Transition metal oxide clusters can also be prepared on single crystal surfaces or thin films as supports and compared with isolated clusters in the gas phase. Deposited clusters, molecular model compounds and deposited aggregates on powder catalysts form the bridge to industrially used catalyst systems.

Before **structure - reactivity** relations can be discussed, solid structural knowledge is required which must not be flawed by experimental artefacts such as undefined interactions with the support or ill-defined stoichiometric composition, or by deficiencies of badly tested computa-

tional tools. Accordingly, in the early funding periods our focus was on **structure** and methodology, while in later periods, when more reliable structure information became available, the focus was on **reactivity**, specifically the selective oxidation of methanol to formaldehyde and the oxidative dehydrogenation of propane to propene. In the last funding period, **selectivity** was a major subject, with respect to competing reactions and deeper oxidation products down to total oxidation, but also with respect to the oxidizing agent (N_2O compared with O_2) and with respect to comparing different supports.

The strong role of theory groups proved fruitful in two respects. On the one hand, theoretical studies on model systems of different aggregation type (clusters of different size in the gas phase and on surfaces, thin films, inert and strongly interacting supports) yield results that cannot easily be obtained by experimental techniques and provide direct answers to important questions of the CRC. In this respect, theory is complementary to experimental studies. In particular theory helps to bridge the gap between small clusters that can be studied in the gas phase and larger deposited clusters whose structure is not experimentally accessible. Theoretical information on possible elementary steps is also indispensable for establishing reaction mechanisms as foundation of kinetic models.

On the other hand, the complexity of the experiment requires a close coupling with theoretical studies, for example when assigning spectroscopic signatures or STM patterns to atomic structures. The vibrational infrared (IR) spectra resulting from experiments on the free electron laser (FELIX) are our main source of information for the structure of gas phase clusters (TP A3). Structure determination is not possible without comparison of observed with calculated spectra for structural isomers that have been obtained by DFT structure optimization. A major achievement was the implementation of a genetic algorithm for locating unusual and unexpected isomers (TP A4).^[14] The calculation of core excitation spectra using DFT (TP C6) has been essential to explain experimental NEXAFS spectra (TP B2, C1) and to deduce structural details of VO_x and MoO_x compounds.^[15,16]

The achievements in this area profited from the development of modern density functional theory (DFT), which rendered studies of large systems possible. Deposited aggregates and crystalline structures are described by embedded cluster models or by applying periodic boundary conditions (super cell method). The cooperation of theory groups with different, but overlapping competence made validation studies possible, by comparison of both (embedded) cluster models (TP A4, C6) with periodic calculations (TP C5) and density functional theory (all theory projects) with wave-function based methods (TP A1, A4).

2.1.3 Oxides of reduced dimensionality as model systems

Fig. 7 provides an overview of different types of model systems used in this CRC. In ultra-high vacuum (UHV) surface science is used to investigate model catalysts consisting of active oxide particles on a thin film of the supporting oxide (area C). Both the active oxide and the supporting oxide can be studied independently as single crystal surfaces or thin films. The latter are grown on a metal substrate. In the gas phase (area A), clusters of the supporting oxide and the active metal oxide can be studied separately, but also as mixed metal oxide clusters.

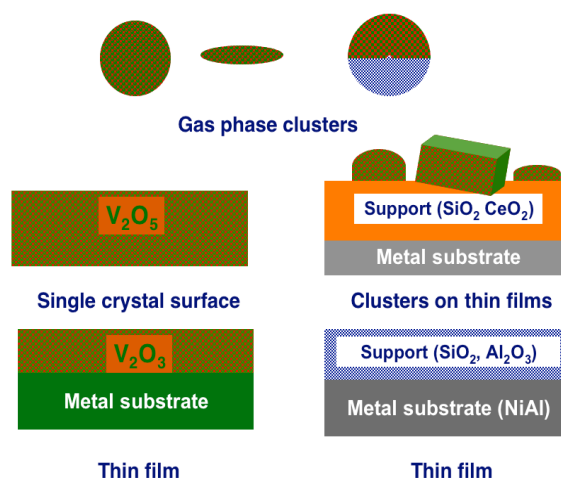


Fig. 7. Types of model systems studied in CRC 546.

Before we turn to complex model catalysts, we will first consider gas phase clusters of vanadium oxide and thin films of SiO_2 as supporting oxide. Both are examples of oxides of reduced dimensionality that are studied under unusual conditions (low pressure, low temperature) compared to ambient conditions. The fundamental question that goes beyond this CRC is: How do their structures differ from the corresponding bulk structure?

Gas phase clusters. Early in the CRC this question could be answered for V_2O_5 (TP A3, A4, C1).^[17,18] Fig. 8 compares the IR spectrum of the $(\text{V}_2\text{O}_5)_4$ gas phase cluster (more precisely, the cluster anion with an additional unpaired electron)^[17] with the HREELS spectrum of the V_2O_5 bulk surface.^[18]

The three bands in the HREELS spectrum^[18] are assigned to O sites with different bonding situations as known from the layered bulk structure - singly coordinated O in the terminal vanadyl groups, two-fold coordinated O in V-O-V bridges, and three-fold coordinated O in the vanadium oxide ribbons. In the gas phase spectrum the band for three-fold coordinated O

atoms is missing. This matches the cage-type structures predicted before as most stable isomers of $(V_2O_5)_n$ clusters by DFT calculations (TP A4).^[19] The smallest cage, V_4O_{10} , was not only studied in the gas phase as $V_4O_{10}^-$ anion,^[17] but also as neutral species in a matrix (TP B5).^[20] Ligand-to-metal charge transfer excitations of the V=O bonds were probed directly by UV-vis spectroscopy of the neutral V_4O_{10} ,^[20] and also by gas phase photoelectron spectroscopy (PES) of the anion (TP A4 with external partner).^[21] These excitations weaken the V=O bond and make it more reactive, see section 2.1.12.

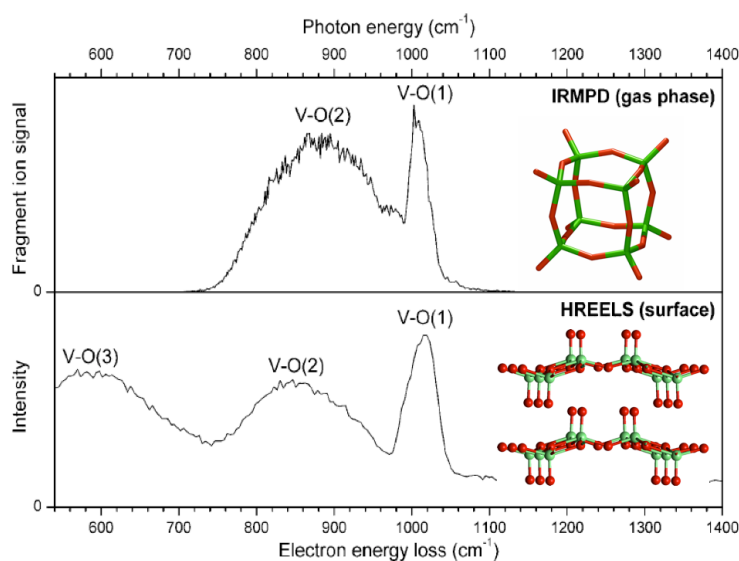


Fig. 8. IR-multi photon dissociation (IRMPD) spectrum of the $[(V_2O_5)_4]^-$ gas phase cluster anion (top) and high resolution electron energy loss spectrum (HREELS) of the V_2O_5 crystal surface.

Thin oxide films. As a UHV model for silica as supporting oxide, an atomically thin SiO_2 film on a Mo(112) substrate was prepared (TP B1). Low energy electron diffraction (LEED) pointed to a $c(2 \times 2)$ surface unit cell, whereas STM showed a hexagonal pattern and the very few and sharp lines in the IR absorption spectrum pointed to a highly-symmetric structure. The question was: Which atomic structure belongs to this signature? The basic building block of silica are corner-sharing SiO_4 tetrahedra which can form a large variety of structures of different dimensionality.^[22]

Among the two-dimensional structures are hexagonal mono- and bilayers, which served as starting point for DFT structure optimizations (A4, C5).^[23] Monolayers of both isolated (composition SiO_4) and corner-sharing (composition $SiO_{3/2} \cdot O$, Fig. 9) tetrahedra proved to be local minimum structures, but only the latter did explain the observed vibrational spectrum (Fig. 9). This also applies to the STM pictures that had been obtained for two different tunnelling condi-

tions. Although atomic resolution was achieved, from the simulation alone it was unclear which atoms or electronic states give rise to the bright features. DFT calculations showed that the six bright spots seen in one experiment belong to Si atoms (which all are in one plane), whereas the four bright spots seen in the other experiment correspond to oxygen positions. Two of the six oxygen atoms in the ring were not visible as bright spots because they are at a more inward position with respect to the surface.

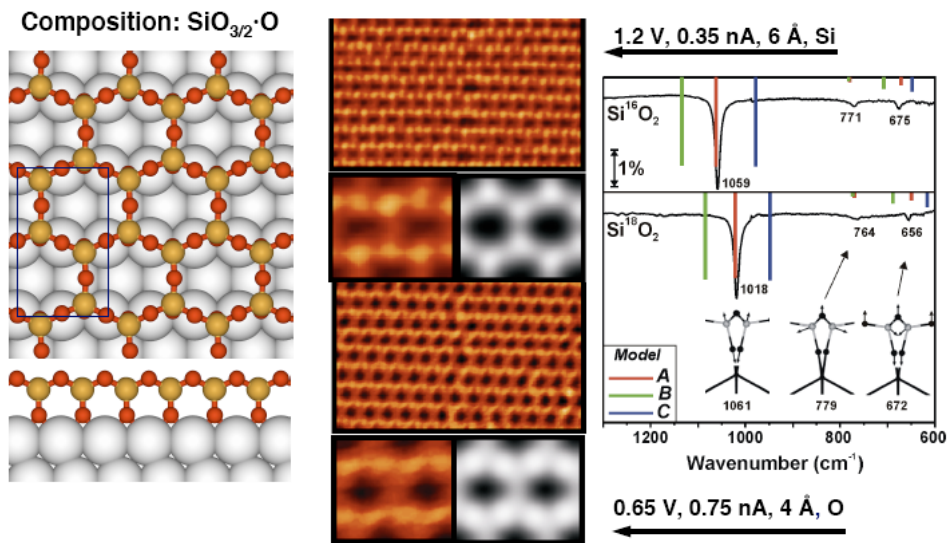


Fig. 9. Hexagonal $\text{SiO}_{3/2}\cdot\text{O}$ monolayer on the Mo(112) metal substrate.^[23]

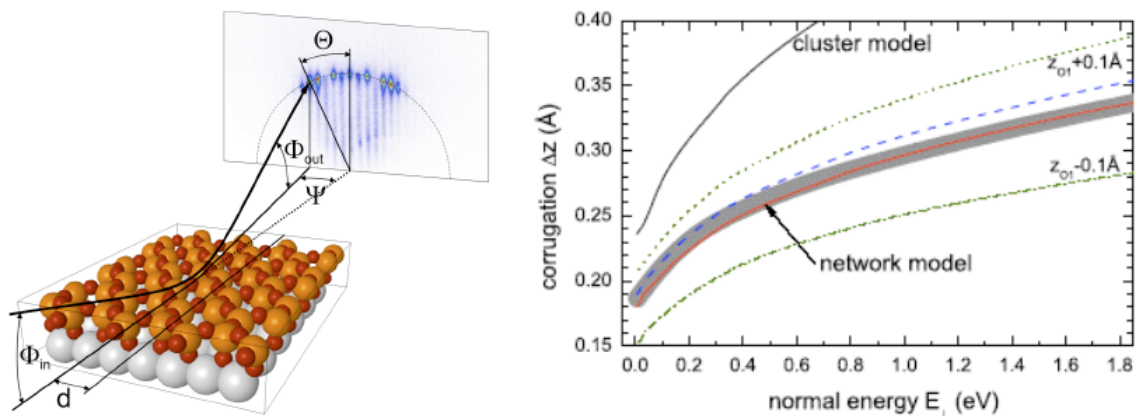


Fig. 10. Coherent quantum scattering of fast atoms from strings of well-ordered surface structures (left) and results for the positions of the top most O atoms of the silica film (right) (TP C11).^[24]

The relative stability of the different surface phases depends on the O_2 partial pressure because of their different composition. The $SiO_{3/2}\cdot O$ -monolayer consisting of corner-sharing tetrahedra is thermodynamically the most stable surface at the experimentally relevant (UHV) conditions, whereas the monolayer of isolated tetrahedra advocated by Goodman et al. has the lowest energy of formation, but would be stable only at very high O_2 partial pressure.^[25] Extension of these DFT calculations resulted in a two-dimensional phase diagram (O_2 partial pressure and loading of the surface with SiO_2)^[26] which lead to the prediction that on increasing the O_2 partial pressure an oxygen rich monolayer with additional oxygen atoms directly attached to the metal substrate should form. Such a phase could indeed be identified when the oxygen pressure was increased in the UHV experiments.^[26]

Additional support for our conclusion that a monolayer of connected tetrahedra (“network model”) is observed and not isolated tetrahedra (“cluster model”) came from fast atom diffraction experiments in TP C11 (Fig. 9).^[24] DFT calculations for the “network model” of the silica film reproduce the experimentally derived positions of the top-most O atoms within a few hundredths of Å.^[24]

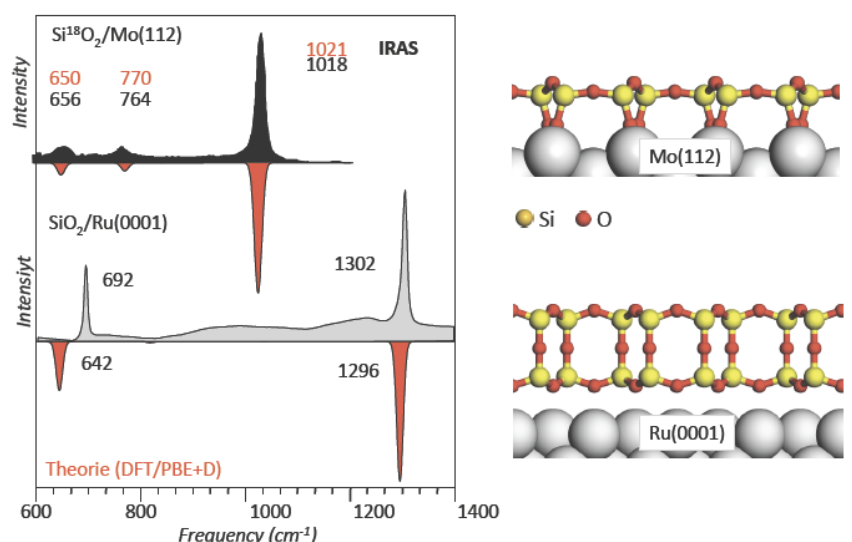


Fig. 11. Si_2O_5 monolayer on $Mo(112)$ and SiO_2 double layer on $Ru(0001)$.^[27]

More recently, using $Ru(0001)$ as a substrate, hexagonal double layers of SiO_2 have been observed (TP B1, C5, A4).^[27] DFT calculations helped to assign the vibrations observed at unusually high wavenumbers in the Si-O stretching region to the nearly linear Si-O-Si interlayer bonds. These calculations also showed that both structures exist as local minima at both metal substrates: On $Mo(112)$ the monolayer is more stable, whereas on $Ru(0001)$ the bi-layer is more stable.

This is an example how two experimental groups (TP B1 and C11) and two theoretical projects (A4 and C5) worked successfully together to prepare these new forms of silica, to characterize their structure and to understand their stability.

2.1.4 Preparation and characterization of single crystals and thin films

One of the major achievements of the CRC 546 is the preparation and characterization of a number of single crystals and thin films

- V_2O_5 and VO_2 single crystals (TP C4)
- V_2O_5 single crystal surfaces by cleaving (TP C4, C2, C1, C5)
- $V_2O_5(001)/Au(111)$ (TP C1)
- $V_2O_3(0001)$ (TP C1, C6, C8)
- $MoO_3(010)/Au(111)$ (TP C1, C6)
- $SiO_2/Mo(112)$ (TP B1, C5, C11), $SiO_2/Ru(0001)$ (TP B1, C5)
- $[V_x]Ti_yO_2/Ta_uTi_vO_2/TiO_2(110)$ (TP C1)

The preparation work started from the beginning of this CRC with the basic materials and continued in later periods with the more difficult and challenging problems. One of the latter was the preparation of films of the supporting oxide that contain the active oxide not as deposited clusters but as dopant in the surface layer. It was not before the last funding period that TP C1 succeeded in preparing a vanadium doped TiO_2 (mixed V/Ti oxide) film. The key step was to insert a mixed tantalum/titanium oxide layer between the $TiO_2(110)$ substrate and the vanadium doped overlayer to prevent vanadium diffusion into the substrate (Fig. 11).

With regard to their function as oxidation catalysts, oxygen defect formation and surface reduction were in the focus of the CRC. Preparation of the V_2O_5 single crystal surface was prerequisite to an *in situ* band gap mapping of this surface which revealed a reversible metal-to-insulator transition at 350–400 K (TP B1, C2, C4, C5).^[28] This transition does not occur homogeneously across the surface but expands preferentially in the direction of the vanadyl (V=O) double rows. DFT calculations rationalized these observations on the basis of the anisotropic growth of vanadyl oxygen vacancies along the V=O double rows.^[29]

There are many possibilities for the termination of the $V_2O_3(0001)$ surface (corundum structure). TP C1 found evidence for vanadyl species (IR band and characteristic XPS core level shifts) on this surface.^[30] They form after O_2 adsorption on the metal terminated surface (TP C1, A4, C5)^[31] and can be removed by electron bombardment.^[32] LEED calculations yielded a

strong inward relaxation of the V surface atoms in the metal terminated surface, which is partially removed when the vanadyl species are formed.

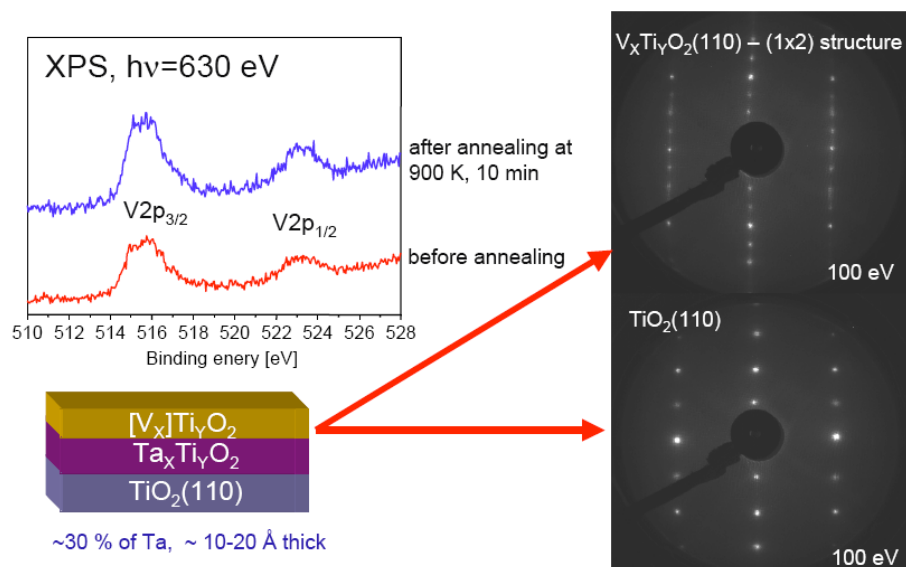


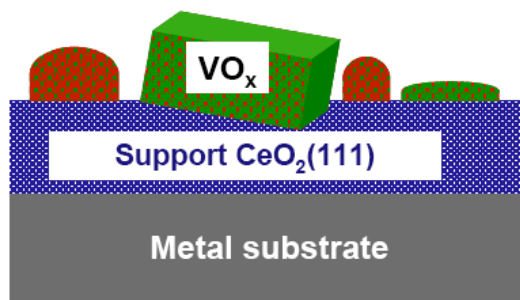
Fig. 12. Mixed V/Ti oxide film on a $\text{TiO}_2(110)$ substrate with a diffusion blocking layer of mixed Ta/Ti oxide.

Photoelectron diffraction studies on a similarly prepared surface (TP C8, C2) showed much better agreement between experiment and simulation for a different termination model (O3 reconstruction,^[33] TP C5, see also Ref. ^[34,35]). Further support for this termination came from medium energy ion scattering (MEIS) (TP C8) and, independently, from a new quantitative analysis of earlier low energy ion scattering results (TP C2).^[36] Further work is necessary to understand in detail under which conditions which surface termination is observed.

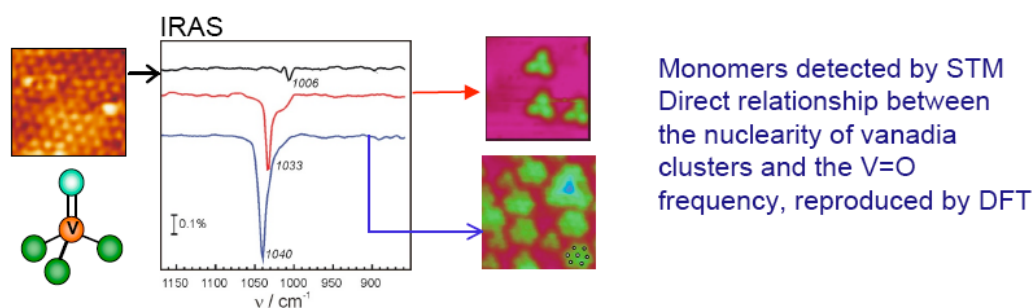
In joined experimental and theoretical work (TP C8 and C6) the local structure of OH species on the $\text{V}_2\text{O}_3(0001)$ surface was determined by photoelectron diffraction.^[37]

2.1.5 UHV model catalysts: the $\text{VO}_x/\text{CeO}_2(111)$ example

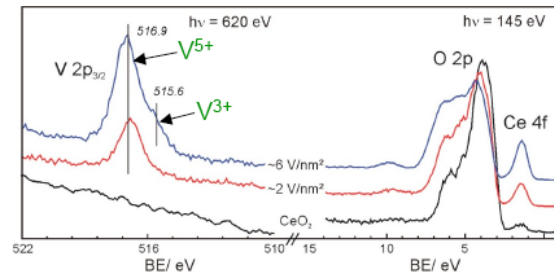
A model catalyst has been prepared by depositing vanadium oxide on the $\text{CeO}_2(111)$ surface (TP B1).^[38]



Vanadium oxide species of different size have been identified by STM and the observed direct relationship between the nuclearity of these clusters and their V=O frequency has been reproduced by DFT calculations (Fig. 13, TP B1, C5).^[38] This is very important because for powder catalysts it is usually not possible to distinguish species of different size.



XPS:
Formation of V=O species is accompanied by chemical reduction of ceria surface



DFT(+U)
Ceria stabilizes
V^{+V} oxidation state

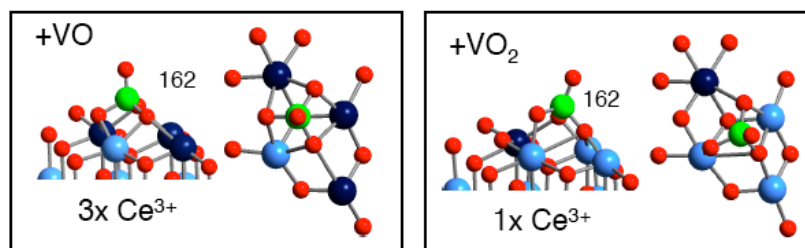
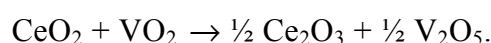


Fig. 13. VO_x/CeO₂(111) model catalysts: STM pictures and IR spectra (top), XPS results (middle) and DFT(+U) calculations (bottom, V green, O red, Ce⁴⁺ light blue, Ce³⁺ dark blue).

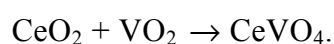
The presence of a Ce-4f XPS peak (Fig. 13) showed that formation of the V=O surface species is accompanied by chemical reduction of the ceria surface. This was in line with DFT(+U) calculations. Regardless whether VO (V oxidation state +2, d³ configuration) or VO₂ (V oxidation

state +4, d^1 configuration) was deposited on the surface, the surface complex formed always had V in its highest (+5) oxidation state, and all electrons are found in Ce 4f states that were populating V d-states in the gas phase VO or VO₂ species. Hence, in VO_x/CeO₂(111) systems, ceria gets partially reduced and stabilizes vanadium in its highest (+5) oxidation state.^[38] This fits with earlier DFT(+U) calculations on crystalline CeVO₄ for which, in agreement with XANES studies,^[39] a Ce⁽⁺³⁾(f¹)V⁽⁺⁵⁾(d⁰) electronic structure was found instead of Ce⁽⁺⁴⁾(f⁰)V⁽⁺⁴⁾(d¹).^[40]

This Ce⁽⁺³⁾(f¹)V⁽⁺⁵⁾(d⁰) preference is by no means trivial. For example, it is in contrast to the Ce⁽⁺⁴⁾(f⁰)V⁽⁺⁴⁾(d¹) preference inferred from both of the reduction potentials in aqueous solution (1.3 - 1.7 eV for Ce⁺⁴ depending on pH and 1.0 eV for V⁺⁵ in VO₂⁺) and the heats of formation for the bulk oxides.^[41] The latter yield endothermicity ($\Delta H_{298}^{\circ} = 1.1 - 1.3$ eV) for the reaction



DFT+U calculations also show that the above reaction is unfavourable ($\Delta H_0^{\circ} = 0.25$ eV), whereas the reaction yielding bulk Ce(f¹)VO₄



is strongly exothermic, $\Delta H_0^{\circ} = -1.53$ eV.^[40]

What is different in CeVO₄ compared to Ce₂O₃ + V₂O₅ is the coordination of the ions and the average distance to the oxygen ligands which determine the splitting, and hence the stability of f respective d states.^[41]

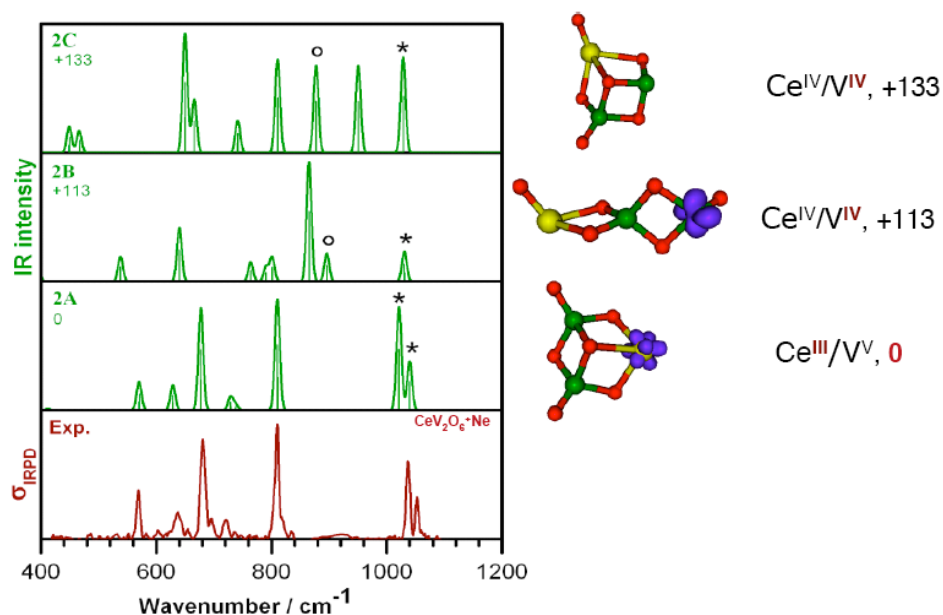
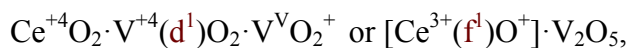


Fig. 14. Different CeV₂O₆⁺ isomers, their relative energies and their IR spectra predicted by DFT in comparison to experiment (TP A3, A4).^[41]

Additional evidence for the interplay of Ce(f)/V(d) preference and geometric structure comes from gas phase IR spectroscopy on mixed metal oxide clusters (Fig. 14).^[41]

For the CeV_2O_6^+ species, which can also be written as $(\text{CeVO}_4)(\text{V}^{(+5)}\text{O}_2^+)$, the same question arises as for crystalline CeVO_4 : Is the Ce-4f or the V-3d state populated with an electron:



and does this lead to geometrically different isomers? Fig. 14 shows that in the cage-type isomer the electron is preferentially located in Ce-f states, whereas in the chain isomer it is located in the V-d states. Comparison with the experimental IR photon dissociation spectrum shows unequivocally that the cage isomer is observed and we may safely conclude that this is the most stable isomer.

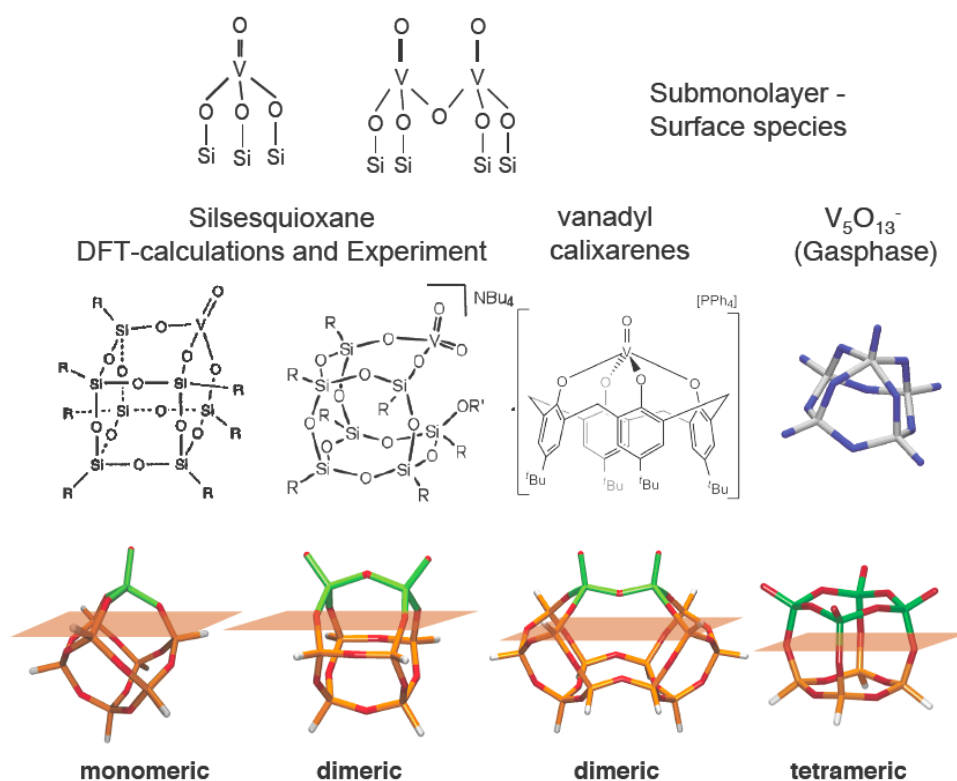


Fig. 15. Submonolayer vanadium oxide species on SiO_2 surfaces (top), different types of model compounds for experimental and computational studies (middle), and models employed in DFT studies of monomeric, dimeric and tetrameric vanadium oxide species on SiO_2 (bottom).

2.1.6 Molecular models

Fig. 15 shows different types of model compounds that are used in TP A4, B5 and A3 for experimental and computational studies on typical submonolayer vanadium oxide surface spe-

cies. Vanadyl containing silsesquioxanes first synthesized by Feher,^[42] were adopted as models for computational studies of monomeric and oligomeric vanadium oxide species on silica surfaces in TP A4^[1,43] and for experimental studies in TP B5.^[44,45] Silsesquioxanes are known to be well-suited models for silica and have been used in computational studies since 1994.^[46]

Vanadyl Calixarenes^[47,48] provide a different coordination platform for vanadyl units, yielding to complexes that share the penta-coordination with some of the gas phase complexes studied in TP A3 and A4.^[49]

Silsesquioxane models as shown in the bottom row of Fig. 15 have been employed in TP A4 to study the relative stability of species with a different number n of $V=O$ sites and with a different distribution for a given number of sites. Energy differences of a few kJ/mol only have been found. The conclusion was reached that there is no preference for smaller or larger species and that the distribution of VO_x species in silica is rather statistical from the thermodynamic point of view.

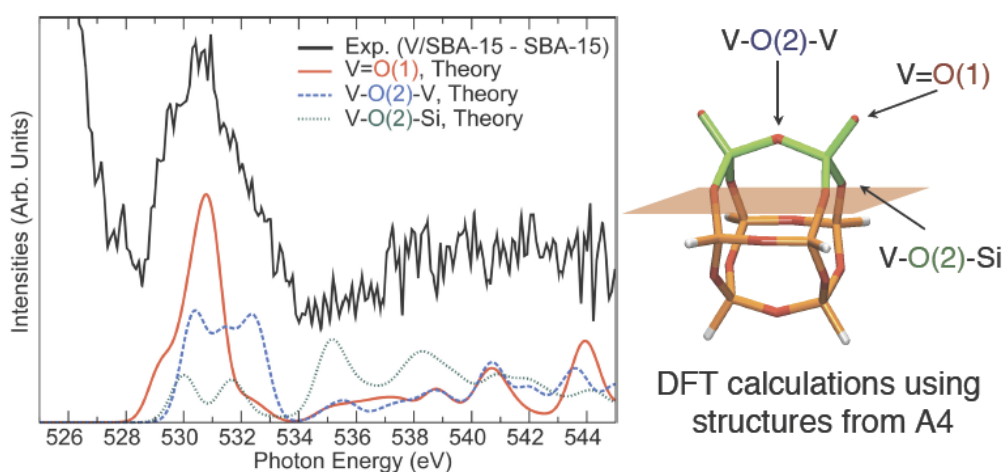
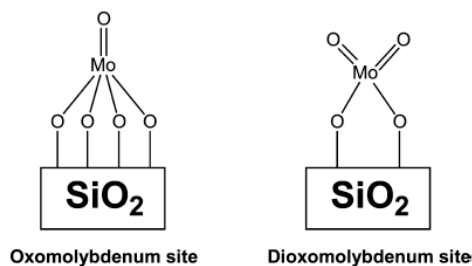


Fig. 16. O(1s) NEXAFS on $VO_x/SiO_2(SBA-15)$ (TP B2, C6, A4).^[15]

Such silsesquioxane models were also employed to predict the wavenumbers for V-O-V vibrations in dimeric vanadia species on silica and alumina (section 2.1.1.).^[1] The conclusion was reached that there is no way to distinguish monomeric from polymeric species by IR or Raman spectroscopy. In search for other options, core level spectroscopy, specifically O(1s) NEXAFS, has been applied in a joined study of TP B2, C6, and A4. The spectra measured in TP B2 have been calculated by DFT in TP C6 using the silsesquioxane type models of TP A4 (optimized structures).^[15] Fig. 16 provides evidence that the presence of species with V-O-V links, i.e. dimeric or oligomeric species, cannot be excluded.^[15]

For isolated MoO_x sites on silica, two types of sites are considered bearing either one

(oxomolybdenum) or two (dioxomolybdenum) terminal oxo ligands.



By the same combined methodology it has been found that the tetrahedral dioxo species fit best with experiments whereas octahedral species can be excluded.^[16]

2.1.7 Mechanistic studies on molecular models

An important contribution of DFT and other quantum chemical methods is information about reaction energies and energy barriers for elementary steps within very complex reaction mechanisms.

Methanol oxidation. Our DFT study for vanadium oxide species supported on silica revealed the key steps of the oxidation of methanol to formaldehyde: First methanol binds on the surface by heterolytically splitting the V–O–Si interface bond (Fig. 17). The second step is the redox step, a hydrogen atom is transferred from the methyl group to the vanadyl oxygen atom which creates a kind of biradical structure with an unpaired electron at the $\cdot\text{CH}_2\text{O}$ – group and one electron in vanadium d-states. The reaction is completed when the V–O(OCH₂ \cdot) bond splits releasing formaldehyde and a second electron goes into the vanadium d-states (Fig. 17).

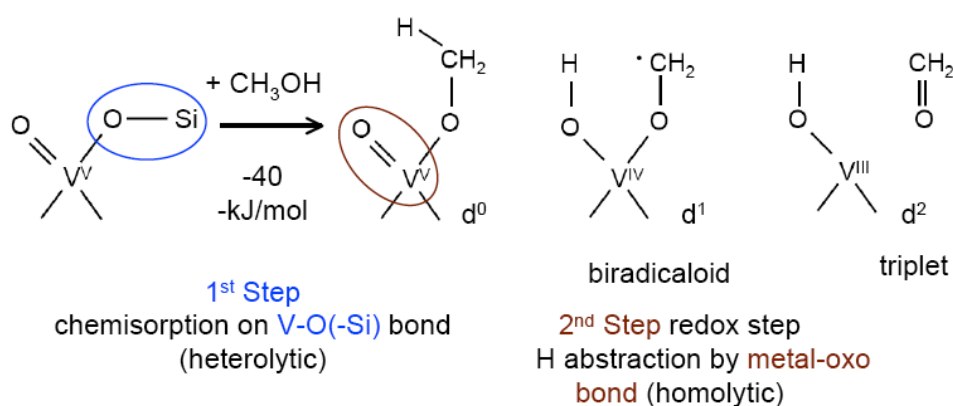


Fig. 17. Structures involved in the first steps of the oxidation of methanol to formaldehyde on VO_x/SiO_2 .^[43]

The B3LYP + $\Delta\text{CCSD(T)}$ prediction $154-17 = 137 \text{ kJ/mol}$ ^[43] falls into the range of reported experimental numbers ($137 \pm 10 \text{ kJ/mol}$).^[3,43] Key to the localization of a biradicaloid transition

structure and the corresponding intermediate on the potential energy surface was looking for a broken symmetry solution in DFT. Previous studies of this reaction, e.g. ref.^[50], were limited to closed shell calculations which cannot describe the decoupling of an electron pair. Our study (76 citations, 11 per year) became a model for many subsequent studies. For example, the Bell group (Berkeley) adopted our silsesquioxane model for isolated vanadia sites on silica and repeated our broken symmetry DFT calculations for methanol oxidation.^[51] In addition, they considered the re-oxidation step involving a peroxide species. Later, they used the same methodology and the same type of model to examine methanol oxidation on VO_x/TiO_2 catalysts.^[52] For isolated molybdenum oxide species on silica we found that the methanol oxidation proceeds with the same fundamental steps (dissociative addition of methanol followed by hydrogen abstraction, Fig. 18).^[53] However, the details differ between monooxo (**1.1**) and dioxo (**4.1**) species. In the former case, the first step leads to cleavage of an Mo-O-Si bond and formation of a surface molybdenum methoxide species. Hydrogen is then abstracted from the methoxide ligand by a terminal oxo ligand in a process entailing a closed-shell transition structure. In contrast, the preferred mechanism on the dioxomolybdenum species involves a addition of the methanol OH group onto one of the M=O double bonds leading to an hydroxomolybdenum methoxide intermediate. The hydrogen abstraction in the second step is effected by the hydroxide ligand formed in the first step and proceeds via an open-shell singlet transition structure.^[53]

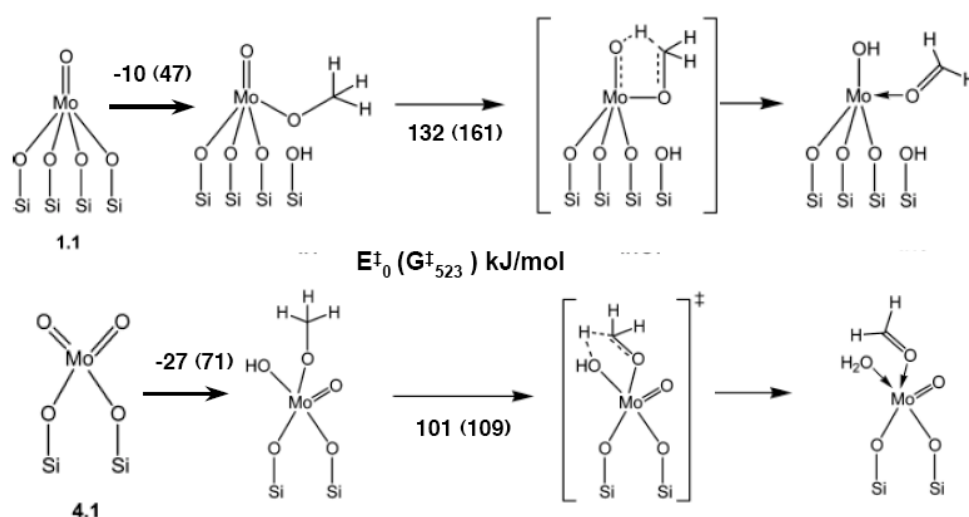
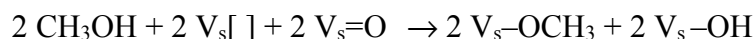


Fig. 18. Oxidation of methanol to formaldehyde on $\text{MoO}_x/\text{SiO}_2$.^[53]

In the focus of a joined experimental-computational study of the formaldehyde formation on $\text{V}_2\text{O}_3(0001)$ and $\text{V}_2\text{O}_5(001)$ surfaces (TP C1, C5, A4)^[54,55] was the question: How does the stable methoxy intermediate form?

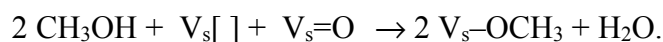
On a partially reduced surface, methanol adsorbs on a oxygen vacancy, $V_s[]$, and undergoes hydrogen transfer to neighbouring $V=O$ group yielding a methoxy and hydroxy group.



Below room temperature, water is found to desorb from the surface, regenerating half of the vacancy sites:



As result, twice as many methoxy species are formed as there were oxygen vacancies on the surface,



Propane oxidation. For the oxidative dehydrogenation of propane, DFT calculations showed that hydrogen abstraction by the vanadyl group is the first step leading to a biradicaloid intermediate which consists of a propyl radical bound to a surface $V^{4+}(d^1)$ species (Fig. 19).^[56] Formation of propene proceeds either by a second hydrogen abstraction by the hydroxyl group attached to the $V^{4+}(d^1)$ species or by a rebound mechanism via propanol bound to a V^{3+} surface site (Fig. 19). The latter is exactly the mechanism by which Cytochrom P450 selectively oxidizes C-H bonds to C-OH bonds.^[57] This points to “unifying concepts” between heterogeneous and enzymatic catalysis. In the enzyme, the porphyrin ligand of the active $[\text{Fe}^{\text{IV}}=\text{O}]^{2+}$ site is “redox-noninnocent”^[58] and this raises the question if among the different supports for vanadium oxide catalysts there are “redox-noninnocent” ones. This is indeed the case as will be shown below although the details of the participation of ligand respective support in the redox process are different.

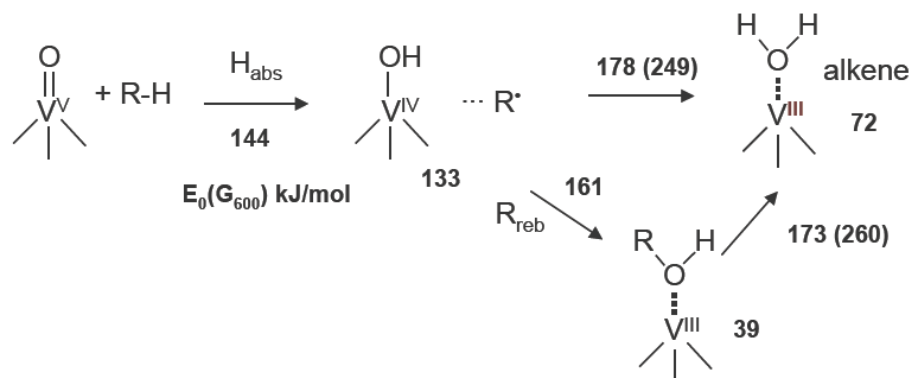


Fig. 19. Elementary steps for oxidative dehydrogenation of propane to propene by vanadyl ($V=O$) species.^[57]

The microkinetic simulation of TP A4 showed that the first H-abstraction step is rate limiting if fast re-oxidation of the catalyst is assumed.^[56] Experiments have also shown that H-abstraction is an irreversible step, and not an equilibrium.^[59] In contrast to reactions with the gas phase vanadium oxide model $V_3O_7^+$,^[60,61] C-H addition on V=O double bonds as proposed in earlier publications^[62-64] does not occur on surfaces.

With these DFT studies the question of the mechanism of the oxidative dehydrogenation of alkenes on transition metal oxide catalysts was settled. Previous DFT studies were not conclusive, either because of non-realistic catalyst models^[65] or because of their self-limitation to electronic closed shell calculations.^[66] Our findings have been confirmed by an independent study on the V_4O_{10} model.^[67] A reactivity study^[68] for crystalline V_2O_5 employed exclusively GGA (generalized gradient approximation) functionals whose suitability for the oxidative dehydrogenation reaction is questionable, however.^[69]

2.1.8 Re-oxidation of the catalyst and the role of peroxo species

The reoxidation part of the catalytic cycle has been studied in less detail, but the role of peroxo species in the re-oxidation process was addressed in several projects. Early, in TP C6 the formation of peroxo species on the $V_2O_5(001)$ surface was examined as intermediates on reoxidation of oxygen defects.^[70] In later funding periods spectroscopic evidence was found for peroxo species being intermediates for the formation of vanadyl species on the $V_2O_3(0001)$ surface from molecularly adsorbed O_2 on an initially metal terminated surface (TP A4, B1, C5).^[31]

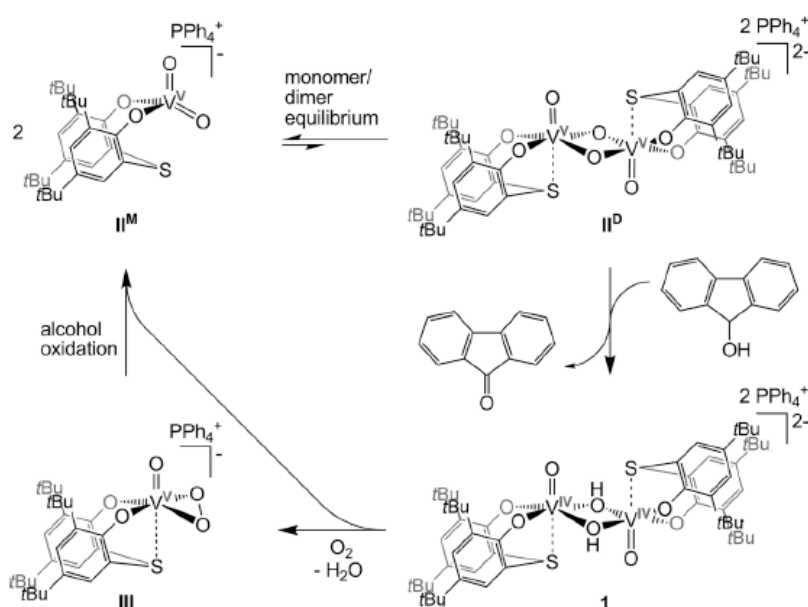


Fig. 20. Functional model involving a peroxo species in the re-oxidation step (TP B5).^[71]

Among the gas phase models, $V_3O_7^+$ is a model of the active catalyst,^[60,61] the oxygen deficient $V_3O_6^+$ a model of the reduced catalyst, and the oxygen rich $V_3O_8^+$ a model for peroxy (or superoxy) species possibly involved in its reoxidation (TP A3, A4). Gas phase IR spectra have been measured for these models (TP A3) and DFT has been used to assign them to predicted structures (TP A4).

TP B5 succeeded in synthesizing a functional calixarene model for the oxidation of alcohols which involves a peroxy intermediate in the re-oxidation step (Fig. 20, TP B5).^[71]

A DFT study on silsesquioxane models confirmed that peroxy vanadate species are intermediates in the reoxidation of partially reduced vanadium oxide catalysts (V^{+4} and V^{+3}) by O_2 , but not by N_2O .^[72] Since peroxy vanadates are highly reactive for propene oxidation, the absence of peroxy vanadates may explain the superior performance of N_2O compared with O_2 as oxidant in the selective oxidative dehydrogenation of propane over catalysts with highly dispersed VO_x species (TP A4, B3).^[72]

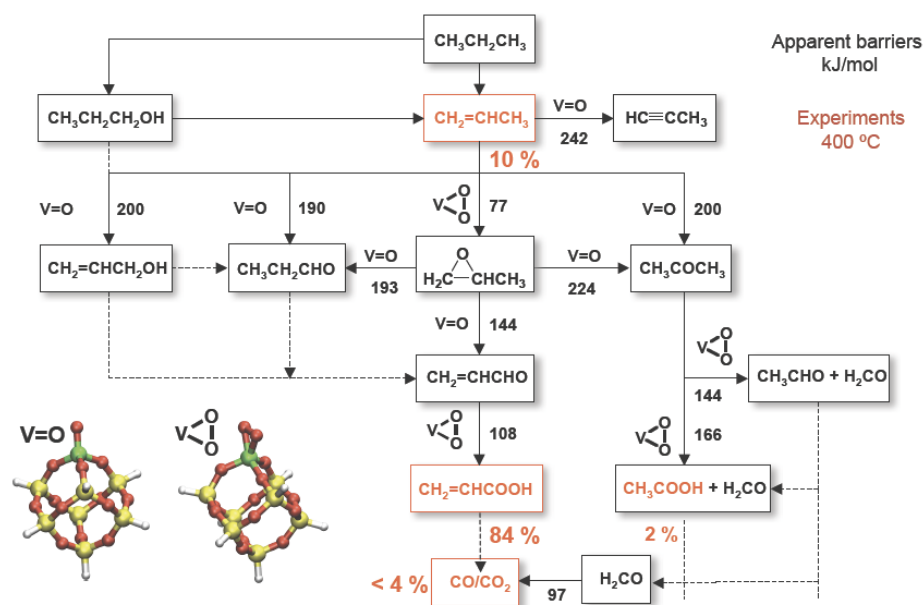


Fig. 21. Free energy barriers (kJ/mol) for elementary steps in the deep oxidation of propane (TP A4). As active sites both vanadyl (V=O) and peroxy vanadate (VO₂) species are considered. The compounds identified as products under specific conditions are indicated in red with the percentage found (TP B2).^[73]

2.1.9 Deep oxidation of propane

Understanding of the selectivity for propene ultimately requires knowledge of all elementary steps down to the total oxidation products CO and CO₂. Fig. 21 shows the results of DFT calculations using the same silsesquioxane model as used for the formation of propane (TP A4).

Peroxo species, formed on re-oxidation are also participating in the reaction network. Quantitative comparison with specific experiments requires a microkinetic simulation, but as a first confirmation for the DFT results we highlight the compounds that have been identified in an experiment conducted in such a way that acrylic acid was the major product (TP B2).^[73]

2.1.10 Different silica supports

Table 1 shows experimental results for the catalytic performance for propane oxidation of differently structured silica supports obtained in TP B2, B3, and B6.^[74-76] Among them are dense, materials (“SiO₂” in the Table), and mesoporous materials of different pore sizes (SBA-15, MCM-41, MCM-48).

Table 1. Turn-over frequency, TOF, and apparent activation energy, $E_{A,app}$, for propane oxidation by vanadia on differently structured silica supports.

Sample	V density $V \cdot nm^{-2}$	TOF (773 K) $mol(C_3H_8)/mol_V \cdot s$	$E_{A,app}$ kJ/mol
VO _x (2.7)MCM-41 ^a	0.4	0.016	112
VO _x (3.4)MCM-48 ^a	0.6	0.011	108
VO _x (2.8)SiO ₂ ^{a,b}	1.4	0.010	97
VO _x (2.7)SBA-15 ^c	0.7	0.013	103
		(±0.002)	(±20)
DFT (750 K; H _{Ts} -H _{S+hc}) ^d		0.26 s ⁻¹	123±5
VO _x /SiO ₂ (Wachs) ^e	< 3	0.003 (623 K)	
VO _x , MoO _x , WoO _x /SiO ₂ ^f			99-126

^a Ref. [74] (TP B3) ^b Ref. [75] (TP B2, B6); ^c Ref.[76] (TP B2, B6)

^d Calculations on monomeric sites on a silsesquioxane model (TP A4).^[56]

^e Ref. [77] ; ^f Ref. [78]

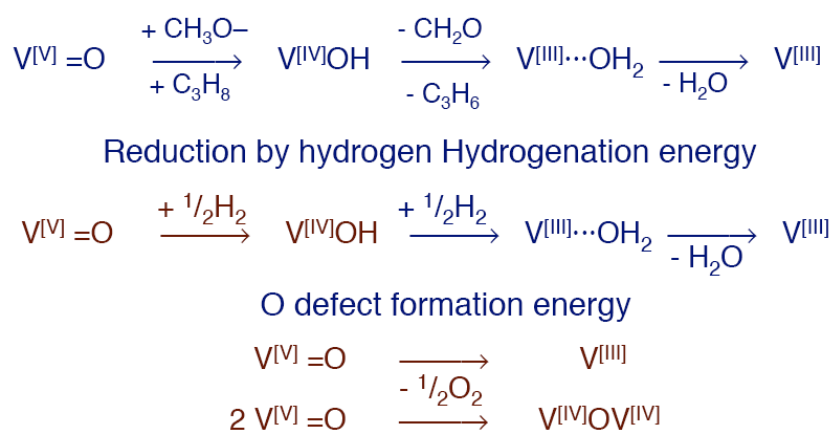
The variation of the TOF across the different supports is only slightly larger than the estimated uncertainty of an individual measurement. The calculated TOF for a similar temperature deviates by a factor of about 20 from these experimental values. This is well within the limits of what is currently achievable with quantum chemical calculations. The smaller TOF value reported by the Wachs group^[77] as compared to the “VO_x(2.8)SiO₂” result is due to the lower temperature (623 instead of 773 K). The observed apparent activation energies vary over 15 kJ/mol and have an estimated uncertainty of about 20 kJ/mol. Their average is 18 ± 25 kJ/mol lower than the DFT result. Given the limited accuracy of DFT in general and the B3LYP functional in particular, the results are still compatible. Barriers reported in the literature^[78] for va-

nadium oxide, molybdenum oxide and tungsten oxide on silica also fit with the experimental and theoretical values of this CRC.

2.1.11 Reactivity descriptors for C-H activation catalysts

The localization of transition structures for C-H activation reactions for catalyst models with different particle sizes and different supports is a formidable task, even if limited to the rate determining step. For screening different catalyst models, reactivity descriptors that are straight forward to compute are therefore extremely useful. We have used two different definitions.

Energy of hydrogenation. For the oxidation of both, methanol and propane, the crucial redox step after the initial binding to the surface is H abstraction by the transition metal oxo (V=O) bond.^[43,56] The simplest molecule for which this step can be studied is H abstraction from the H₂ molecule. If we further apply the Bell-Eyring-Polanyi principle, i.e. if we assume that changes of the energy barrier are parallel to changes of the reaction energy, we arrive at the energy of hydrogenation as a possible descriptor for the activity (Scheme 1, TP A4).^[79]



Scheme 1. Energy of hydrogenation and oxygen defect formation as reactivity parameters.

Before, the energy of hydrogenation had been calculated in TP C6 for different O sites at the V₂O₅ bulk crystal surface to characterize their reactivity.^[70] It has also been used^[80,81] to characterize the activity of MgO-based catalysts for the oxidative coupling of methane.

Oxygen defect formation energy. After the oxidation half-cycle has been completed, a water molecule is formed and an oxygen defect is created on the catalyst (Mars-van Krevelen mechanism). Oxygen defects are therefore very important for understanding the reactivity of oxides, and the oxygen defect formation energy is an obvious descriptor for the activity of oxi-

duction catalysts.^[82-84]

Attempts have also been made to determine oxygen defect formation energies experimentally by Coulometric titration^[85-87] and by conductivity measurements (TP B7). Table 2 shows results for relevant oxide materials and compares them with DFT results for different model systems. Both experimental methods are bulk methods and the role of surface species is not obvious. Moreover, the Coulometric titration follows the change of the oxidation state of the bulk material, whereas conductivity measurements determine a concentration of defects. In the DFT calculations we are looking at isolated defects, a situation that is likely to be close to the catalytic situation with a fast reoxidation of the catalyst. Although we cannot expect a one-to-one correspondence, some similarities between experimental and theoretical data are seen in Table 2. For example, both conductivity measurements and DFT calculations indicate a higher activity of vanadia supported on γ -alumina compared to α -alumina. Further, both experimental methods and the DFT calculations yield a higher activity for vanadia supported on zirconia than for bulk V_2O_5 .

Table 2. Oxygen defect formation energies per $\frac{1}{2} O_2$ (kJ/mol) obtained by different methods.

Red	Conductivity ^a	Coulometric ^b	DFT/GGA ^c	DFT/Hybrid ^d
	ΔH_{def}	ΔH_{def}	ΔE	ΔE
$VO_x/\alpha\text{-Al}_2O_3$	270		386 ^h	
$VO_x/\gamma\text{-Al}_2O_3$	116		270 ^l	
VO_x/MgO	156			
VO_x/SiO_2	(107)		360 ⁱ	256 ⁱ
V_2O_5	125	143 ^e	186 ^{j,p}	113 ^{ij}
VO_x/ZrO_2	82	113 ^e - 129 ^f	150 - 190 ^k	
VO_x/TiO_2	53			
VO_x/CeO_2	58		76 ^m	
CeO_2/Al_2O_3		250 ^g		
CeO_2		375 - 400 ^g	199 ⁿ	256 ^o

^a Conductivity measurement, TP B7, estimated uncertainty ± 10 kJ/mol.

^b Coulometric titration, estimated uncertainty ± 10 kJ/mol.

^c GGA-type functionals, e.g. PBE, PW91; ^d Hybrid functionals, e.g. PBE0, B3LYP

^e Ref.^[85]; ^f Estimated from ΔG (Figure 5, Ref.^[86]) assuming that the entropy is the same as for V_2O_5 reduction (-212 J/K mol); ^g Ref.^[87]; ^h unpublished TP C5; ⁱ Ref.^[84]; ^j Ref.^[29]; ^k Ref.^[88];

^l Ref.^[89]; ^m PBE+U Ref.^[90]; ⁿ PBE+U Ref.^[91]; ^o Ref.^[92]; ^p RPBE result 255 kJ/mol, ref.^[70,82]

2.1.12 Gas phase models: The perfectly isolated active site

Fig. 22 illustrates the fundamental difference between a thermal reaction in condensed phase or on surfaces where systems are crossing barriers of 100 kJ/mol or more and a gas phase reaction under single collision conditions which can only be observed if the energy of the transition structure is below the reactant energy, i.e. if the apparent energy barrier is negative.

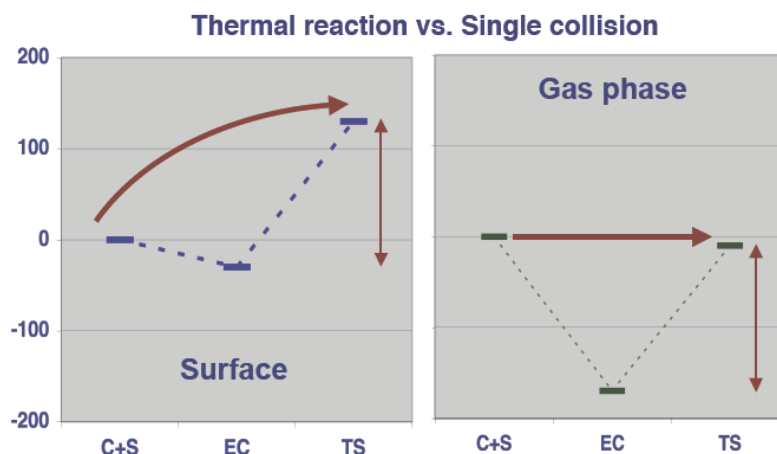


Fig. 22. Energy diagrams for thermal reactions on a surface compared to gas phase reactions under single conditions.

Thus, a reaction with a similar intrinsic barrier as a surface reaction can be observed in the gas phase only if the binding of the reactants compensates for the intrinsic barriers. This is the case for cluster ions, in particular cluster cations, and this means that studying charged systems in the gas phase as models for (non-charged) active sites on surfaces is a meaningful approach. The only condition is that the intrinsic barriers are similar. This is the case, for example, if both the charged gas phase species and the active site on the surface have the same redox properties. Fig. 23 compares the V=O dissociation energy (O defect formation energy in the language of surface science) of different gas phase vanadium oxide clusters with that of a monomeric vanadia surface species supported on silica (silsesquioxane model) (TP A4).^[84] The smaller V=O dissociation energy of the neutral V_4O_{10} cluster suggests a slightly lower intrinsic barrier, but since the binding of the substrate molecule to the neutral cluster will be not stronger than onto the surface, it is unlikely that a reaction of propane or methanol with V_4O_{10} will be observed in the gas phase.

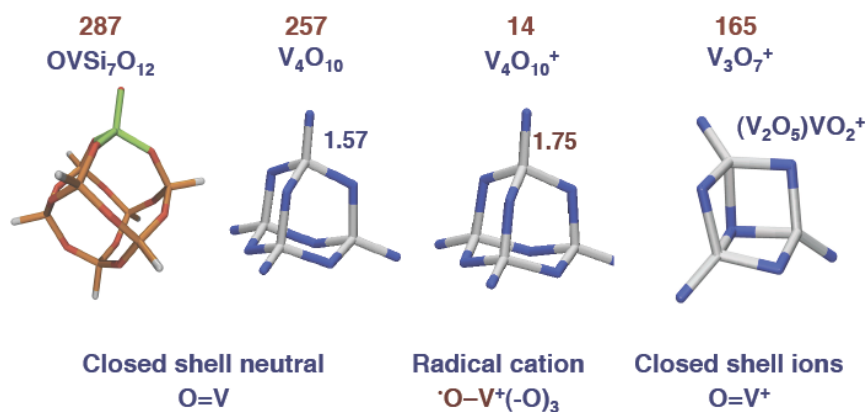


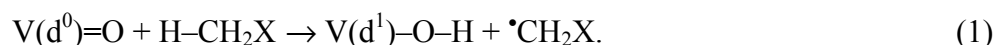
Fig. 23. V=O dissociation energies (kJ/mol per $\frac{1}{2}$ O₂)

The V₃O₇⁺ cluster, which can also be written (V₂O₅)VO₂⁺, is a closed shell cation and has the same V=O bond as active site. Its smaller V=O bond dissociation energy suggests a smaller intrinsic barrier. Indeed, an intrinsic barrier of 108±5 instead of 132±13 kJ/mol has been calculated (TP A4).^[61] In addition, the positive charge increases the binding energy (107 kJ/mol compared to 37±5 kJ/mol)^[56,61] and the resulting apparent barrier is just around zero. That a reaction with propane was not observed in the corresponding mass spectrometric experiment has been explained as follows (TP A2, A4).^[60] After formation of the encounter complex, the system can either cross the barrier or dissociate into the reactants. Since in the latter process two gas phase species are formed instead of one, it is favoured by entropy. To outweigh this entropy effect a substrate that binds more strongly or that has a more active C-H bond (lower intrinsic barrier) is needed. A molecule fulfilling both requirements is butene, and indeed its oxidative dehydrogenation has been observed in the mass spectrometer.^[60]

The V₄O₁₀⁺ cation is a completely different case. Its V=O bond dissociation energy is pathologically low because on ionization of V₄O₁₀ an electron is removed from the V=O bond and a V⁽⁺⁾-O[•] species with an oxyl radical site is created. It is obvious that the redox properties of a radical cation are different from that of a closed shell system, and it does not come as surprise that such species are much more reactive than closed shell species (TP A2, A4).^[82] Mass spectrometry showed that V₄O₁₀⁺ readily abstracts hydrogen even from CH₄ - the least reactive C-H bond,^[93] and reacts also with propane.^[94] The latter study goes beyond mass spectrometric experiments in as far as products have been characterized by IR spectroscopy.

2.1.13 Ionization and excitation of transition metal oxo bonds^[79]

C-H activation by metal oxo bonds involves decoupling of an electron pair in the double bond,



One of the electrons is accommodated in the easily accessible transition metal d-orbitals and the other forms a bond with the H atom of the C-H bond.

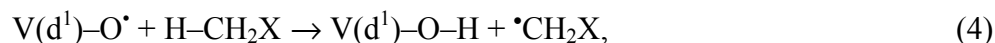
Ionization removes one electron from the electron pair and the unpaired electron left behind reacts readily with the H atom of the C-H bond.



The excited electronic states for V_4O_{10} ^[20,21] and larger aggregates^[21] have been examined in TP A4 and B5. The lowest excited states are ligand to metal charge transfer (LMCT) transitions which also decouple an electron pair in the V=O bond as they populate d states on the V atom and create a radical site



which again reacts readily with C-H bonds,



yielding the same reduced catalyst state as the reaction of the neutral ground state V=O species that is present on the surface.

This explains that photoexcitation may facilitate H abstractions from C-H bonds. Indeed, TP B5 has reported that V_4O_{10} reacts in a matrix with CH_4 after irradiation, but the products could not be identified yet. In TP A3, a complex of $V_4O_{10}^-$ and propane has been generated in an ion trap, but to start the reaction photoexcitation was necessary.^[95] Moreover, supported transition metal oxides are known to be effective photocatalysts.^[96]

2.1.14 Effect of the particle size

For supported powder catalysts, including the catalysts with a loading below a monolayer at which crystallites of bulk vanadia are absent (as far as X ray diffraction can tell) there seems to be always a size distribution of active species. For example, in section 2.1.6. O(1s) NEXAFS evidence has been produced that the presence of vanadium oxide oligomers cannot be excluded (Fig. 16). DFT studies can be made on precisely defined active sites. They can be used to examine how the activity changes with increasing cluster size.

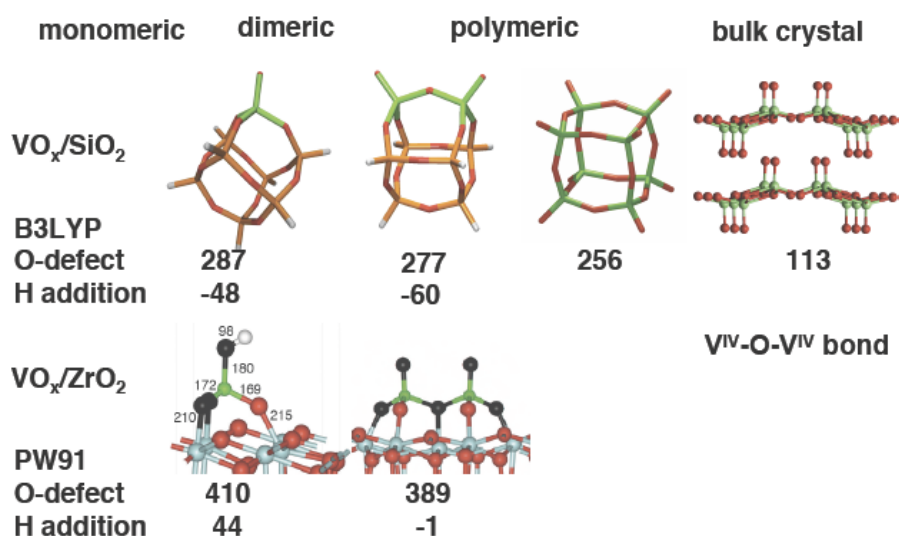


Fig. 24. O defect formation (V=O bond dissociation) and hydrogenation energies

Fig. 24 shows that the O defect formation energies, calculated for silsesquioxane models, decrease with increasing particle size, from monomers to dimers and to polymers (TP A4). The particularly low value of 113 kJ/mol for the V_2O_5 bulk crystal surface is due to formation of an interlayer V-O-V bond on removing a terminal oxygen atom (TP A4, C5, C6).^[29,84,97] This means that an ideal bulk crystal surface will not be present under reaction conditions because it is easily reduced and also partially hydrated.

A higher activity of vanadia dimers compared to monomers is also predicted by a more negative hydrogenation energy, both for silica^[98] and zirconia^[88] supports. For silica, the reaction energies and energy barriers of monomeric and dimeric species have been calculated. The explicit calculations confirm the conclusion from the energy of hydrogenation. The barrier for hydrogen abstraction from propane is 9 kJ/mol lower for the dimer than for the monomer, and the reaction energy is 13 kJ/mol lower in accord with the Bell-Eyring-Polanyi principle. The energy of hydrogenation is also 12 kJ/mol more negative (-60 compared to -48 kJ/mol, cf. Fig. 25).

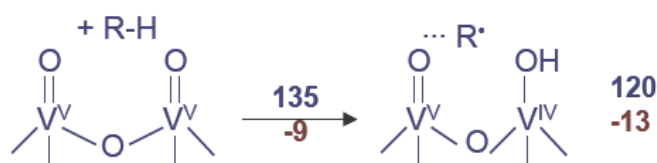


Fig. 25. Energy barrier and reaction energy for hydrogen abstraction from propane by monomeric vanadia sites supported on silica (silsesquioxane model) calculated by DFT (B3LYP) in kJ/mol. In red are given the differences between dimers and monomers.

For the calixarene models of TP B5 it has also been found that the oxidative dehydrogenation proceeds via a dinuclear species whereas the corresponding monomer is inactive. ^[48,71] Moreover, when the redox properties of mixed metal oxides have been measured by Coulometric titration, less favourable reduction energies (per $\frac{1}{2}$ O₂, see Table 1) have been measured for systems which contain only monomeric vanadate species such as Mg₃(VO₄)₂ and CeVO₄ (230 and 270 kJ/mol, respectively)^[86] than for systems with V-O-V bonds such as V₂O₅ and ZrV₂O₇ (143 and 113kJ/mol, respectively).

2.1.15 Different supporting oxides

Fig. 26 compares oxygen defect formation energies of molecular models for active particles of the same size (vanadia dimer) on different supports. The variations across the different supports are of the same order of magnitude as the changes between particles of different size on the same support (Fig. 24).

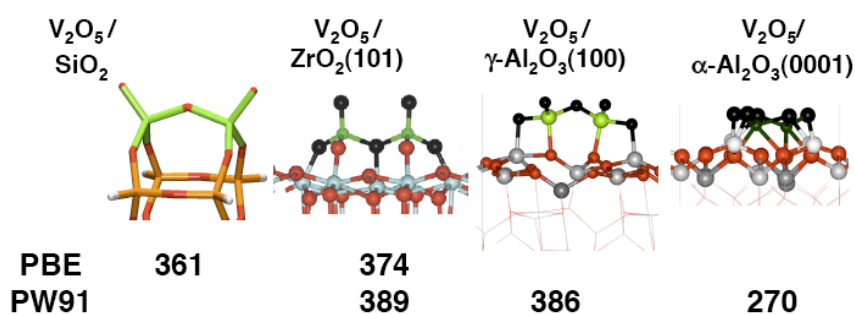


Fig. 26. O defect formation energy (kJ/mol) for dimer sites on different supports.

It has already been shown that ceria stabilizes vanadia particles in their highest oxidation state which results in partial reduction of cerium oxide (Ce³⁺ ions). Further reduction by O defect formation (i.e. in the catalytic reaction) is easy (Fig. 27) and leads to an increase of the number of Ce³⁺ ions. Even for isolated vanadia species on ceria, the O defect formation is much easier than for vanadia species on γ-Al₂O₃(001) or SiO₂ (Fig. 26). On the bare ceria surface, the O defect formation energy is also higher than for the ceria surface bearing vanadia species (Fig. 27). This, however, is entirely a relaxation effect: without relaxation the O defect formation energies are virtually the same (Fig. 27, left).

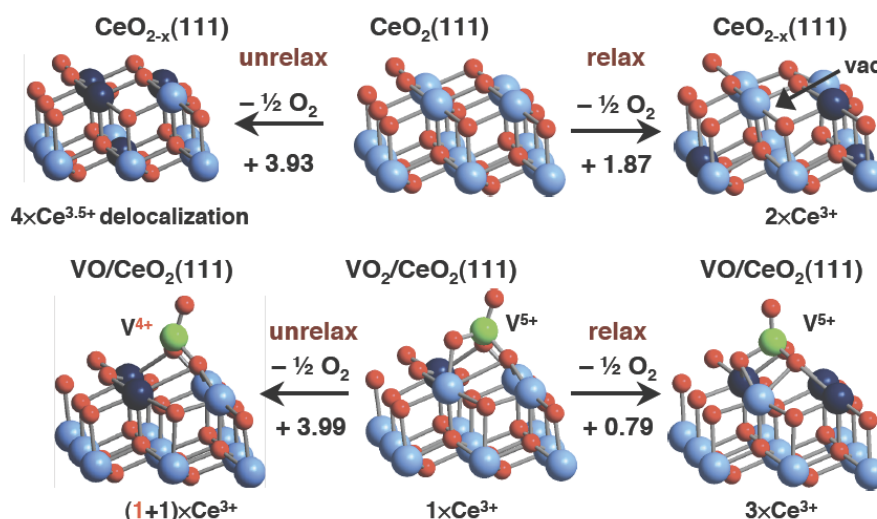


Fig. 27. O defect formation energy (eV) for $\text{CeO}_2(111)$ and $\text{VO}_2/\text{CeO}_2(111)$ (TP B1, C5).^[90,99]

We conclude that the remarkably high activity observed for oxidation catalysts supported on ceria directly relates to this special synergy between the ceria support and the supported oxide (vanadia). Temperature programmed desorption of formaldehyde from the methanol covered model surface of section 2.1.5. shows a low temperature peak (α) for VO_x/CeO_2 that is not present on the clean CeO_2 surface and hence, confirms the higher activity predicted by the lower O defect formation energy.

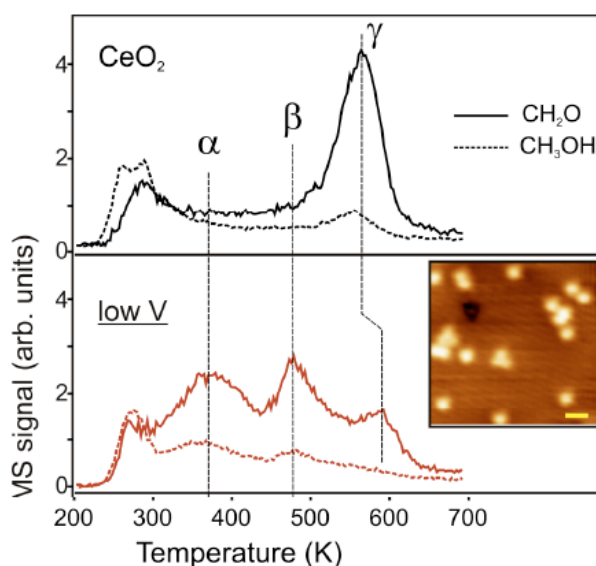


Fig. 28. Temperature programmed desorption of formaldehyde from a surface loaded at low temperature with methanol. In contrast to the clean $\text{CeO}_2(111)$ surface, the vanadia loaded $\text{CeO}_2(111)$ surface produces formaldehyde at lower temperatures (α -peak at 340 K) than the clean CeO_2 surface (γ -peak, 600 K) or vanadia on silica (675 K) (TP B1, C5).^[90]

2.1.16 Summary: Support effects

The results of this CRC with regard to the support effect can be summarized as follows:

The effect of the support on the catalytic reactivity

- depends on the reaction (substrate molecules - methanol, ethanol, propane) and its condition
- can not be described by a single parameter such as electronegativity

The reactivity difference between monomers and dimers of the active species on the same support can be as large as the differences between different supports.

Size (distribution) and atomic structure of active oxide species are different on different supports.

The hydroxylation/hydration state of the surface can affect the particle size, e.g. on zirconia.

The support properties, e.g. its acidity, may play a role in the binding of the substrate and, hence, affect the measured apparent rates.

Electronic effects of the support should only be discussed for the same or similar structure of the active species, comparing, for example, monomers on different supports.

Synthesis of a well-defined model system (vanadia supported on Ti-substituted mesoporous silica) with industrial application potential shows that both structure and composition are important ingredients of the support effect.

Redox active (non-innocent) supporting oxides affect the redox properties of the catalyst system.

The VO_x/CeO_2 system is more reactive than each oxide component alone.

CeO_2 is a very special support. It easily accommodates electrons in f-states. In the VO_x/CeO_2 system this leads to stabilization of vanadium in the +5 oxidation state, even under reducing conditions.

References

- [1] N. Magg, B. Immaraporn, J. B. Giorgi, T. Schroeder, M. Bäumer, J. Döbler, Z. Wu, E. Kondratenko, M. Cherian, M. Baerns, P. C. Stair, J. Sauer, H.-J. Freund, *J. Catal.* **2004**, *226*, 88-100.
- [2] G. C. Bond, S. F. Tahir, *Appl. Catal.* **1991**, *71*, 1-31.
- [3] G. Deo, I. E. Wachs, *J. Catal.* **1994**, *146*, 323-334.
- [4] B. M. Weckhuysen, D. E. Keller, *Catal. Today* **2003**, *78*, 25-46.
- [5] I. E. Wachs, *Catal. Today* **1996**, *27*, 437-455.
- [6] A. Khodakov, B. Olthof, A. T. Bell, E. Iglesia, *J. Catal.* **1999**, *181*, 205-216.
- [7] G. Deo, I. E. Wachs, J. Haber, *Crit. Rev. Surf. Chem.* **1994**, *4*, 141-187.
- [8] I. E. Wachs in *Catalysis, Vol. 13* (Ed. J. J. Spivey), The Royal Society of Chemistry, **1997**, pp. 37-54.

- [9] I. E. Wachs, G. Deo, M. V. Juskelis, B. M. Weckhuysen in *Dynamics of Surfaces and Reaction Kinetics in Heterogeneous Catalysis* (Eds.: G. F. Froment, K. C. Waugh), Elsevier, Amsterdam, **1997**, pp. 305-314.
- [10] I. E. Wachs, Y. Chen, J.-M. Jehng, L. E. Briand, T. Tanaka, *Catal. Today* **2003**, *78*, 13-24.
- [11] O. Ovsitser, E. V. Kondratenko, *Chem. Commun.* **2010**, *46*, 4974-4976.
- [12] L. J. Burcham, L. E. Briand, I. E. Wachs, *Langmuir* **2001**, *17*, 6164-6174.
- [13] I. E. Wachs, *Catal. Today* **2005**, *100*, 79-94.
- [14] M. Sierka, J. Döbler, J. Sauer, G. Santambrogio, M. Brümmer, L. Wöste, E. Janssens, G. Meijer, K. R. Asmis, *Angew. Chem., Int. Ed.* **2007**, *46*, 3372-3375, *Angew. Chem.* **2007**, *119*, 3437-3440.
- [15] M. Cavalleri, K. Hermann, A. Knop-Gericke, M. Hävecker, R. Herbert, C. Hess, A. Oestereich, J. Döbler, R. Schlögl, *J. Catal.* **2009**, *262*, 215-223.
- [16] C. S. Guo, K. Hermann, M. Havecker, J. P. Thielemann, P. Kube, L. J. Gregoriades, A. Trunschke, J. Sauer, R. Schlögl, *J. Phys. Chem. C* **2011**, *115*, 15449-15458.
- [17] K. R. Asmis, G. Santambrogio, M. Brümmer, J. Sauer, *Angew. Chem.* **2005**, *117*, 3182-3185, *Angew. Chem., Int. Ed.*, *44*, 3122-3125.
- [18] B. Tepper, B. Richter, A. C. Dupuis, H. Kuhlenbeck, C. Hucho, P. Schilbe, M. A. bin Yarmo, H. J. Freund, *Surf. Sci.* **2002**, *496*, 64-72.
- [19] S. F. Vyboishchikov, J. Sauer, *J. Phys. Chem. A* **2001**, *105*, 8588-8598.
- [20] C. Herwig, C. Limberg, *Inorg. Chem.* **2008**, *47*, 2937-2939.
- [21] H. J. Zhai, J. Dobler, J. Sauer, L. S. Wang, *J. Am. Chem. Soc.* **2007**, *129*, 13270-13276.
- [22] F. Liebau in *Structural Chemistry of Silicates*, Springer-Verlag, Berlin, **1985**.
- [23] J. Weissenrieder, S. Kaya, J.-L. Lu, H.-J. Gao, S. Shaikhutdinov, H.-J. Freund, M. Sierka, T. K. Todorova, J. Sauer, *Phys. Rev. Lett.* **2005**, *95*, 0761031.
- [24] J. Seifert, A. Schüller, H. Winter, R. Wlodarczyk, J. Sauer, M. Sierka, *Phys. Rev. B* **2010**, *82*, 035436.
- [25] T. K. Todorova, M. Sierka, J. Sauer, S. Kaya, J. Weissenrieder, J.-L. Lu, H.-J. Gao, S. Shaikhutdinov, H.-J. Freund, *Phys. Rev. B* **2006**, *73*, 165414.
- [26] M. Sierka, T. K. Todorova, S. Kaya, D. Stacchiola, J. Weissenrieder, J. Lu, H. Gao, S. Shaikhutdinov, H.-J. Freund, J. Sauer, *Chem. Phys. Lett.* **2006**, *424*, 115-119.
- [27] D. Löffler, J. J. Uhlrich, M. Baron, B. Yang, X. Yu, L. Lichtenstein, L. Heinke, C. Büchner, M. Heyde, S. Shaikhutdinov, H.-J. Freund, R. Wlodarczyk, M. Sierka, J. Sauer, *Phys. Rev. Lett.* **2010**, *105*, 146104.
- [28] R.-P. Blum, H. Niehus, C. Hucho, R. Fortrie, M. V. Ganduglia-Pirovano, J. Sauer, S. Shaikhutdinov, H.-J. Freund, *Phys. Rev. Lett.* **2007**, *99*, 226103.
- [29] M. V. Ganduglia-Pirovano, J. Sauer, *Phys. Rev. B* **2004**, *70*, 045422.
- [30] A. C. Dupuis, M. Abu Haija, B. Richter, H. Kuhlenbeck, H. J. Freund, *Surf. Sci.* **2003**, *539*, 99-112.
- [31] M. Abu Haija, S. Guimond, Y. Romanyshyn, A. Uhl, H. Kuhlenbeck, T. K. Todorova, M. V. Ganduglia-Pirovano, J. Döbler, J. Sauer, H.-J. Freund, *Surf. Sci.* **2006**, *600*, 1497-1503.
- [32] S. Guimond, M. Abu Haija, S. Kaya, J. Lu, W. J. S. Shaikhutdinov, H. Kuhlenbeck, H.-J. Freund, J. Döbler, J. Sauer, *Top. Catal.* **2006**, *38*, 117-125.
- [33] G. Kresse, S. Surnev, J. Schoiswohl, F. P. Netzer, *Surf. Sci.* **2004**, *555*, 118-134.
- [34] T. K. Todorova, M. V. Ganduglia-Pirovano, J. Sauer, *J. Phys. Chem. B* **2005**, *109*, 23523-23531.
- [35] T. K. Todorova, M. V. Ganduglia-Pirovano, J. Sauer, *J. Phys. Chem. C* **2007**, *111*, 5141-5153.

- [36] A. J. Window, A. Hentz, D. C. Sheppard, G. S. Parkinson, H. Niehus, D. Ahlbehrendt, T. C. Q. Noakes, P. Bailey, D. P. Woodruff, *Phys. Rev. Lett.* **2011**, *107*, 016105.
- [37] E. A. Kroger, D. I. Sayago, F. Allegretti, M. J. Knight, M. Polcik, W. Unterberger, T. J. Lerotholi, K. A. Hogan, C. L. A. Lamont, M. Cavalleri, K. Hermann, D. P. Woodruff, *Surf. Sci.* **2008**, *602*, 1267-1279.
- [38] M. Baron, H. L. Abbott, O. Bondarchuk, D. Stacchiola, A. Uhl, S. Shaikhutdinov, H.-J. Freund, C. Popa, M. V. Ganduglia-Pirovano, J. Sauer, *Angew. Chem., Int. Ed.* **2009**, *48*, 8006-8009.
- [39] R. F. Reidy, K. E. Swider, *J. Am. Ceram. Soc.* **1995**, *78*, 1121.
- [40] J. L. F. Da Silva, M. V. Ganduglia-Pirovano, J. Sauer, *Phys. Rev. B* **2007**, *76*, 125117.
- [41] L. Jiang, T. Wende, P. Claes, S. Bhattacharyy, M. Sierka, G. Meijer, P. Lievens, J. Sauer, K. R. Asmis, *J. Phys. Chem. A* **2011**, *115*, 11187-11192.
- [42] F. J. Feher, J. F. Walzer, *Inorg. Chem.* **1991**, *30*, 1689-1694.
- [43] J. Döbler, M. Pritzsche, J. Sauer, *J. Am. Chem. Soc.* **2005**, *127*, 10861-10868.
- [44] C. Ohde, M. Brandt, C. Limberg, J. Döbler, B. Ziemer, J. Sauer, *Dalton Trans.* **2008**, *5*, 326-331.
- [45] C. Ohde, C. Limberg, R. Stöber, S. Demeshko, *Inorg. Chem.* **2010**, *5*, 2479-2485.
- [46] J. Sauer, J.-R. Hill, *Chem. Phys. Lett.* **1994**, *218*, 333-337.
- [47] B. Castellano, E. Solari, C. Floriani, R. Scopelleti, *Inorg. Chem.* **1999**, *38*, 3406.
- [48] E. Hoppe, C. Limberg, *Chem. Eur. J.* **2007**, *13*, 7006-7016.
- [49] G. Santambrogio, M. Brümmer, L. Wöste, J. Döbler, J. Sauer, G. Meijer, K. Asmis, *Phys. Chem. Chem. Phys.* **2007**, *10*, 3992-4005.
- [50] R. Z. Khaliullin, A. T. Bell, *J. Phys. Chem. B* **2002**, *106*, 7832-7838.
- [51] A. Goodrow, A. T. Bell, *J. Phys. Chem. C* **2007**, *111*, 14753-14761.
- [52] A. Goodrow, A. T. Bell, *J. Phys. Chem. C* **2008**, *112*, 13204-13214.
- [53] L. J. Gregoriades, J. Döbler, J. Sauer, *J. Phys. Chem. C* **2010**, *114*, 2967-2979.
- [54] D. Göbke, Y. Romanyshyn, S. Guimond, J. M. Sturm, H. Kühlenbeck, J. Döbler, U. Reinhardt, M. V. Ganduglia-Pirovano, J. Sauer, H.-J. Freund, *Angew. Chem., Int. Ed.* **2009**, *48*, 3695-3698.
- [55] Y. Romanyshyn, S. Guimond, D. Goebke, J. M. Sturm, H. Kühlenbeck, J. Döbler, M. V. Ganduglia-Pirovano, J. Sauer, H. J. Freund, *Top. Catal.* **2011**, *54*, 669-684.
- [56] X. Rozanska, R. Fortrie, J. Sauer, *J. Phys. Chem. C* **2007**, *111*, 6041-6050.
- [57] S. Shaik, S. P. d. Visser, F. Ogliaro, H. Schwarz, D. Schröder, *Curr. Opinion Chem. Bio.* **2002**, *6*, 556-567.
- [58] K. Ray, E. Bill, T. Weyhermüller, K. Wieghardt, *J. Am. Chem. Soc.* **2005**, *127*, 5641-5654.
- [59] K. D. Chen, E. Iglesia, A. T. Bell, *J. Phys. Chem. B* **2001**, *105*, 646-653.
- [60] S. Feyel, D. Schröder, X. Rozanska, J. Sauer, H. Schwarz, *Angew. Chem., Int. Ed.* **2006**, *45*, 4677-4681, *Angew. Chem.*, *118*, 4793-4797.
- [61] X. Rozanska, J. Sauer, *J. Phys. Chem. A* **2009**, *113*, 11586-11594.
- [62] S. T. Oyama, *J. Catal.* **1991**, *128*, 210-217.
- [63] T. Blasco, J. M. Lopez Nieto, *Appl. Catal. A* **1997**, *157*, 117-142.
- [64] T. Blasco, A. Corma, M. Navarro, J. Perez-Pariente, *J. Catal.* **1995**, *156*, 65.
- [65] F. Gilardoni, A. T. Bell, A. Chakraborty, P. Boulet, *J. Phys. Chem. B* **2000**, *104*, 12250-12255.
- [66] P. C. Redfern, P. Zapol, M. Sternberg, S. P. Adiga, S. A. Zygmunt, L. A. Curtiss, *J. Phys. Chem. B* **2006**, *110*, 8363-8371.
- [67] M.-J. Cheng, K. Chenoweth, J. Oxgaard, A. v. Duin, W. A. Goddard III, *J. Phys. Chem. C* **2007**, *111*, 5115-5127.

- [68] H. Fu, Z.-P. Liu, Z.-H. Li, W.-N. Wang, K.-N. Fan, *J. Am. Chem. Soc.* **2006**, *128*, 11114-11123.
- [69] X. Rozanska, J. Sauer, *Int. J. Quantum Chem.* **2008**, *108*, 2223-2229.
- [70] K. Hermann, M. Witko in *The Chemical Physics of Solid Surfaces, Vol. 9* (Ed. D. P. Woodruff), Elsevier, Amsterdam, **2001**, pp. 136-198.
- [71] C. G. Werncke, C. Limberg, C. Knispel, S. Mebs, *Chem. Eur. J.* **2011**, *17*, 12129-12135.
- [72] X. Rozanska, E. V. Kondratenko, J. Sauer, *J. Catal.* **2008**, *256*, 84-94.
- [73] C. Hess, M. H. Looi, S. B. A. Hamid, R. Schloegl, *Chem. Commun.* **2006**, 451-453.
- [74] O. Ovsitser, M. Cherian, E. Kondratenko, *J. Phys. Chem. C* **2007**, *111*, 8594-8602.
- [75] A. Dinse, B. Frank, C. Hess, D. Habel, R. Schomäcker, *J. Mol. Catal. A* **2008**, *289*, 28-37.
- [76] A. Dinse, S. Khennache, B. Frank, C. Hess, R. Herbert, S. Wrabetz, R. Schlögl, R. Schomäcker, *J. Mol. Catal. A* **2009**, *307*, 43-50.
- [77] H. Tian, E. I. Ross, I. E. Wachs, *J. Phys. Chem. B* **2006**, *110*, 9593-9600.
- [78] K. Chen, A. T. Bell, E. Iglesia, *J. Phys. Chem. B* **2000**, *104*, 1292-1299.
- [79] J. Sauer in *Computational Modeling for Homogeneous and Enzymatic Catalysis* (Eds.: K. Morokuma, D. G. Musaev), Wiley-VCH, Weinheim, **2008**, pp. 231-244.
- [80] M. Y. Sinev, Z. T. Fattakhova, V. I. Lomonosov, Y. A. Gordienko, *J. Natural Gas Chem.* **2009**, *18*, 273-287.
- [81] K. Kwapien, M. Sierka, J. Döbler, J. Sauer, *ChemCatChem* **2010**, *2*, 819-826.
- [82] K. Hermann, M. Witko, R. Druzinic, R. Tokarz, *Appl. Phys. A* **2001**, *72*, 429-442.
- [83] H. Y. Kim, H. M. Lee, R. G. S. Pala, V. Shapovalov, H. Metiu, *J. Phys. Chem. C* **2008**, *112*, 12398-12408.
- [84] J. Sauer, J. Döbler, *Dalton Trans.* **2004**, *19*, 3116-3121.
- [85] P. R. Shah, M. M. Khader, J. M. Vohs, R. J. Gorte, *J. Phys. Chem. C* **2008**, *112*, 2613-2617.
- [86] P. R. Shah, J. M. Vohs, R. J. Gorte, *Catal. Lett.* **2008**, *125*, 1-7.
- [87] R. Gorte, *AIChE Journal* **2010**, *56*, 1126-1135.
- [88] A. Hofmann, M. V. Ganduglia-Pirovano, J. Sauer, *J. Phys. Chem. C* **2009**, *113*, 18191-18203.
- [89] V. Brázdová, M. V. Ganduglia-Pirovano, J. Sauer, *J. Phys. Chem. B* **2005**, *109*, 23532-23542.
- [90] M. V. Ganduglia-Pirovano, C. Popa, J. Sauer, H. L. Abbott, A. Uhl, M. Baron, D. Stacchiola, O. Bondarchuk, S. Shaikhutdinov, H.-J. Freund, *J. Am. Chem. Soc.* **2010**, *132*, 2345-2349.
- [91] J. F. Jerratsch, X. Shao, N. Nilius, H.-J. Freund, C. Popa, M. V. Ganduglia-Pirovano, A. M. Burow, J. Sauer, *Phys. Rev. Lett.* **2011**, *106*, 246801.
- [92] M. V. Ganduglia-Pirovano, J. L. F. Da Silva, J. Sauer, *Phys. Rev. Lett.* **2009**, *102*, 02610101 - 02610104.
- [93] S. Feyel, J. Döbler, D. Schröder, J. Sauer, H. Schwarz, *Angew. Chem., Int. Ed.* **2006**, *45*, 4681-4685, *Angew. Chem.*, *118*, 4797-4801.
- [94] T. Wende, J. Döbler, L. Jiang, P. Claes, E. Janssens, P. Lievens, G. Meijer, K. R. Asmis, J. Sauer, *Int. J. Mass Spectrom.* **2010**, *297*, 102-106.
- [95] S. Li, A. Mirabal, J. Demuth, L. Wöste, T. Siebert, *J. Am. Chem. Soc.* **2008**, *130*, 16832-16833.
- [96] F. Amano, T. Tanaka, *Chem. Lett.* **2006**, *35*, 468-473.
- [97] K. Hermann, M. Witko, R. Druzinic, R. Tokarz, *Appl. Phys. A* **2001**, *72*, 429-442.
- [98] X. Rozanska, J. Sauer **2007**; unpublished.
- [99] C. Popa, M. V. Ganduglia-Pirovano, J. Sauer, *J. Phys. Chem. C* **2011**, *115*, 7399-7410.

2.2 Interne Kooperation und Organisation

Die Arbeit erfolgte in drei verschiedenen **Projektbereichen**, die nach der Aggregation der untersuchten Katalysatorsysteme unterschieden sind:

A: Gasphasencluster

B: Deponierte Cluster

C: Epitaktische Schichten und Einkristalle

Innerhalb dieser Bereiche arbeiteten Experimentatoren und Theoretiker eng zusammen, und es erfolgte eine enge Abstimmung der täglichen Arbeit, z. B. welche ganz konkreten Systeme präpariert, spektroskopiert und schließlich mit theoretischen Methoden untersucht werden sollten. Hierzu, aber auch zur Diskussion der Resultate, fanden gemeinsame Seminare von zwei oder mehr Teilprojekten zu speziellen Themen statt.

Die Aufteilung in die einzelnen Projektbereiche war jedoch nicht scharf. Zum Beispiel wurden im Projekt B1 (Shaikhutdinov/Freund) deponierte Cluster sowie dünne Schichten untersucht. Im Projekt A4 (Sauer) wurden theoretische Untersuchungen sowohl an Gasphasenclustern als auch an eingebetteten Clustern durchgeführt, mit denen deponierte Cluster, Einkristalloberflächen und epitaktische Schichten modelliert werden können. Ein weiteres Beispiel ist die Untersuchung katalytisch relevanter Systeme mit ELNES/NEXAFS-Methoden im Projekt B2 (Schlögl), deren Interpretation mit Hilfe theoretischer Ergebnisse aus dem Projekt C6 (Hermann) erfolgte.

Wichtig für die Zielstellung des Gesamtprojektes waren die Vergleiche zwischen den verschiedenen Aggregationsstufen. Dies geschah nicht nur innerhalb einzelner Projekte, die unterschiedliche Aggregate untersuchten, sondern gerade auch durch Vergleich von Ergebnissen aus Teilprojekten verschiedener Projektbereiche. Zum Beispiel veranstalteten die Teilprojekte A2 (Schwarz/Schröder), A3 (Asmis/Wöste), A4 (Sauer), B2 (Schlögl/Hess/Su), B3 (Dingerdisen/Kondratenko) und B6 (Schomäcker) Anfang 2007 einen Miniworkshop zur Thematik der oxidativen Dehydrierung von Propan. Dabei wurde eine zentrale Frage des Sonderforschungsbereichs diskutiert, nämlich ob und wie sich die Reaktivitäten von Gasphasenclustern und festen Katalysatoren unterscheiden.

Einmal im Jahr gab es zweitägige Jahrestreffen außerhalb Berlins, die der intensiven Diskussion der Arbeit in den Teilprojekten dienten. Neben Vorträgen aus allen Teilprojekten gab es einen speziellen Vortrag eines auswärtigen Gastes. In den Jahren 2004, 2007 und 2011 wurden anstelle dieser Jahrestreffen Internationale Symposien durchgeführt, etwa die Hälfte der Red-

ner waren SFB-Mitglieder, die andere Hälfte Gäste aus dem In- und Ausland. Bei der Vorbereitung eines Neuantrages wurden zusätzliche Workshops mit Vorträgen aller Teilprojekte durchgeführt. Bei diesen und bei den Jahrestreffen wurden insbesondere die Fortschritte in Bezug auf die Gesamtzielsetzung des Sonderforschungsbereichs diskutiert.

Das Ergebnis war eine große Zahl gemeinsamer Publikationen verschiedener Teilprojekte. Unter den 40 wesentlichen Originalpublikationen des SFB sind 22 Gemeinschaftspublikationen der Zusammenarbeit von zwei (17), drei (4) oder vier (1) Teilprojekten.

Die Verteilung der bewilligten Personal- und Sachmittel an die verschiedenen am SFB beteiligten Institutionen erfolgte anteilig zu Beginn jedes neuen Quartals. Die zentral bewilligten Gäste- und Reisemittel wurden als Kostenerstattung abgerechnet. Dabei konnte zunächst jeder Teilprojekt-Leiter über einen am Jahresanfang bekanntgegebenen Teilbetrag verfügen. In der zweiten Jahreshälfte wurden auf Antrag weitere Mittel gewährt und Beträge, die absehbar in einem Teilprojekt nicht benötigt wurden, anderen Teilprojekten zur Verfügung gestellt. Die Vergabekriterien waren die Begründung und die Aktivität des Teilprojektes im SFB. Grundsätze hat das Kollegium beschlossen. Die Verteilung selbst wurde vom Sekretariat, Sprecher und den Stellvertretern vorgenommen. Ähnlich wurde mit Restmitteln der Teilprojekte verfahren.

2.3 Außenwirkung

2.3.1 Wesentliche Publikationen des Sonderforschungsbereiches

Im gesamten Förderzeitraum von 1999 bis 2011 entstanden im Sonderforschungsbereich 546 ca. 400 Veröffentlichungen in begutachteten Journalen mit wissenschaftlicher Qualitätssicherung. Im Folgenden sind die wichtigsten 40 Originalarbeiten aufgelistet:

- [1] K. Hermann, M. Witko, R. Druzinic, R. Tokarz; Oxygen vacancies at oxide surfaces: ab Initio Density Functional Theory Studies on Vanadium Pentoxide; *Appl. Phys. A* **2001**, 72, 429-442.
- [2] N. Magg, J. B. Giorgi, T. Schröder, M. Bäumer, H. J. Freund; Model catalyst studies on vanadia particles deposited onto a thin-film alumina support. 1. Structural characterization; *J. Phys. Chem. B* **2002**, 106, 8756-8761.
- [3] B. Tepper, B. Richter, A. C. Dupuis, H. Kuhlenbeck, C. Hucho, P. Schilbe, M. A. bin Yarmo, H. J. Freund; Adsorption of molecular and atomic hydrogen on vacuum-cleaved $V_2O_5(001)$; *Surf. Sci.* **2002**, 496, 64-72.

- [4] A. C. Dupuis, M. Abu Haija, B. Richter, H. Kühlenbeck, H. J. Freund; $V_2O_3(0001)$ on Au(111) and W(110): growth, termination and electronic structure; *Surf. Sci.* **2003**, *539*, 99-112.
- [5] N. Pinna, M. Willinger, K. Weiss, J. Urban, R. Schlögl; Local structure of nanoscopic materials: V_2O_5 nanorods and nanowires; *Nano Letters* **2003**, *3*, 1131-1134.
- [6] N. Magg, B. Immaraporn, J. B. Giorgi, T. Schroeder, M. Bäumer, J. Döbler, Z. Wu, E. Kondratenko, M. Cherian, M. Baerns, P. C. Stair, J. Sauer, H.-J. Freund; Vibrational Spectra of Alumina- and Silica-Supported Vanadia Revisited: An Experimental and Theoretical Model Catalyst Study; *J. Catal.* **2004**, *226*, 88-100.
- [7] J. Sauer, J. Döbler; Structure and Reactivity of V_2O_5 : Bulk Solid, Nanosized Clusters, Species Supported on Silica and Alumina, Cluster Cations and Anions; *Dalton Trans.* **2004**, *19*, 3116-3121.
- [8] K. Asmis, G. Meijer, M. Brümmer, C. Kaposta, G. Santambrogio, L. Wöste, J. Sauer; Gas Phase Infrared Spectroscopy of Mono- and Divanadium Oxide Cluster Cations; *J. Chem. Phys.* **2004**, *120*, 6461-6470.
- [9] E. Kondratenko, M. Cherian, M. Baerns, D. Su, R. Schlögl, X. Wang, I. E. Wachs; Oxidative Dehydrogenation of Propane over V/MCM-41 Catalysts: Comparison of O_2 and N_2O as oxidants; *J. Catal.* **2005**, *234*, 131-142.
- [10] J. Weissenrieder, S. Kaya, J.-L. Lu, H.-J. Gao, S. Shaikhutdinov, H.-J. Freund, M. Sierka, T. K. Todorova, J. Sauer; Atomic Structure of a Thin Silica Film on a Mo(112) Substrate: A Two-Dimensional Network of SiO_4 Tetrahedra; *Phys. Rev. Lett.* **2005**, *95*, 0761031.
- [11] K. R. Asmis, G. Santambrogio, M. Brümmer, J. Sauer; Polyhedral Vanadium Oxide Cages: Infrared Spectra of Cluster Anions and Size-Induced d-Electron Localization; *Angew. Chem. Int. Ed.* **2005**, *44*, 3122-3125.
- [12] J. Döbler, M. Pritzsche, J. Sauer; Oxidation of Methanol to Formaldehyde on Supported Vanadium Oxide Catalysts Compared to Gas Phase Molecules; *J. Am. Chem. Soc.* **2005**, *127*, 10861-10868.
- [13] F. Allegretti, S. O'Brien, M. Polcik, D. I. Sayago, D. P. Woodruff; Adsorption bond length for H_2O on $TiO_2(110)$: A key parameter for theoretical understanding; *Phys. Rev. Lett.* **2005**, *95*, 226104.
- [14] S. Feyel, J. Döbler, D. Schröder, J. Sauer, H. Schwarz; Thermal Activation of Methane by Tetranuclear $[V_4O_{10}]^+$; *Angew. Chem. Int. Ed.* **2006**, *45*, 4681-4685.
- [15] M. Abu Haija, S. Guimond, Y. Romanyshyn, A. Uhl, H. Kühlenbeck, T. K. Todorova, M. V. Ganduglia-Pirovano, J. Döbler, J. Sauer, H.-J. Freund; Low temperature adsorption of oxygen on reduced $V_2O_3(0001)$ surfaces; *Surf. Sci.* **2006**, *600*, 1497-1503.
- [16] S. Feyel, D. Schröder, X. Rozanska, J. Sauer, H. Schwarz; Gas phase oxidation of Propane and 1-Butene with $V_3O_7^+$: Experiment and Theory in Concert; *Angew. Chem. Int. Ed.* **2006**, *45*, 4677-4681.

- [17] B. Frank, A. Dinse, O. Ovsitser, E. V. Kondratenko, R. Schomaecker; Mass and heat transfer effects on the oxidative dehydrogenation of propane (ODP) over a low loaded $\text{VO}_x/\text{Al}_2\text{O}_3$ catalyst;
Appl. Catal., A **2007**, 323, 66-76.
- [18] R.-P. Blum, H. Niehus, C. Hucho, R. Fortrie, M. V. Ganduglia-Pirovano, J. Sauer, S. Shaikhutdinov, H.-J. Freund; Surface Metal-Insulator Transition on a Vanadium Pentoxide (001) Single Crystal;
Phys. Rev. Lett. **2007**, 99, 226103.
- [19] X. Rozanska, R. Fortrie, J. Sauer; Oxidative Dehydrogenation of Propane by Monomeric Vanadium Oxide Sites on Silica;
J. Phys. Chem. C **2007**, 111, 6041-6050.
- [20] E. Hoppe, C. Limberg; Oxovanadium(V) tetrathiacalix[4]arene complexes and their activity as oxidation catalysts;
Chem. Eur. J. **2007**, 13, 7006-7016.
- [21] J. L. F. Da Silva, M. V. Ganduglia-Pirovano, J. Sauer, V. Bayer, G. Kresse; Hybrid functionals applied to rare earth oxides: The example of ceria;
Phys. Rev. B **2007**, 75, 045121.
- [22] E. A. Kroger, D. I. Sayago, F. Allegretti, M. J. Knight, M. Polcik, W. Unterberger, T. J. Leriotholi, K. A. Hogan, C. L. A. Lamont, M. Cavalleri, K. Hermann, D. P. Woodruff; The local structure of OH species on the $\text{V}_2\text{O}_3(0001)$ surface: A scanned-energy mode photoelectron diffraction study;
Surf. Sci. **2008**, 602, 1267-1279.
- [23] M. Sierka, J. Döbler, J. Sauer, G. Santambrogio, M. Brümmer, L. Wöste, E. Janssens, G. Meijer, K. R. Asmis; Unexpected structures of gas phase aluminium oxide clusters;
Angew. Chem. Int. Ed. **2007**, 46, 3372-3375.
- [24] C. Herwig, C. Limberg; V_4O_{10} : Spectroscopic fingerprint of a well-defined, molecular metaloxo aggregate;
Inorg. Chem. **2008**, 47, 2937-2939.
- [25] S. Li, A. Mirabal, J. Demuth, L. Wöste, T. Siebert; A Complete Reactant-Product Analysis of the Oxygen Transfer Reaction in $[\text{V}_4\text{O}_{11} \cdot \text{C}_3\text{H}_6](-)$: A Cluster Complex for Modeling Surface Activation and Reactivity;
J. Am. Chem. Soc. **2008**, 130, 16832-16833.
- [26] M. Baron, H. L. Abbott, O. Bondarchuk, D. Stacchiola, A. Uhl, S. Shaikhutdinov, H.-J. Freund, C. Popa, M. V. Ganduglia-Pirovano, J. Sauer; Resolving the Atomic Structure of Vanadia Monolayer Catalysts: Monomers, Trimers and Oligomers on Ceria;
Angew. Chem. Int. Ed. **2009**, 48, 8006-8009.
- [27] D. Göbke, Y. Romanyshyn, S. Guimond, J. M. Sturm, H. Kühlenbeck, J. Döbler, U. Reinhardt, M. V. Ganduglia-Pirovano, J. Sauer, H.-J. Freund; Formaldehyde Formation on Vanadium Oxide Surfaces $\text{V}_2\text{O}_3(0001)$ and $\text{V}_2\text{O}_5(001)$: How does the Stable Methoxy Intermediate Form?;
Angew. Chem. Int. Ed. **2009**, 48, 3695-3698.
- [28] A. Dinse, S. Khennache, B. Frank, C. Hess, R. Herbert, S. Wrabetz, R. Schlögl, R. Schomaecker; Oxidative dehydrogenation of propane on silica (SBA-15) supported vanadia catalysts: A kinetic investigation;
J. Mol. Catal. A: Chem. **2009**, 307, 43-50.

- [29] M. V. Ganduglia-Pirovano, J. L. F. Da Silva, J. Sauer; Density functional calculations of the structure of near-surface oxygen vacancies and electron localization on CeO₂(111); *Phys. Rev. Lett.* **2009**, *102*, 02610101 - 02610104.
- [30] Y.-S. Hu, X. Liu, J.-O. Mueller, R. Schlögl, J. Maier, D. S. Su; Synthesis and Electrode Performance of Nanostructured V₂O₅ by Using a Carbon Tube-in-Tube as a Nanoreactor and an Efficient Mixed-Conducting Network; *Angew. Chem. Int. Ed.* **2009**, *48*, 210-214.
- [31] J. Seifert, D. Blauth, H. Winter; Evidence for 2D-Network Structure of Monolayer Silica Film on Mo(112); *Phys. Rev. Lett.* **2009**, *103*, 4.
- [32] O. Ovsitser, E. V. Kondratenko; Selective and stable iso-butene; *Chem Commun* **2010**, *46*, 4974-4976.
- [33] D. Löffler, J. J. Uhlrich, M. Baron, B. Yang, X. Yu, L. Lichtenstein, L. Heinke, C. Büchner, M. Heyde, S. Shaikhutdinov, H.-J. Freund, R. Wlodarczyk, M. Sierka, J. Sauer; Growth and structure of crystalline silica sheet on Ru(0001); *Phys. Rev. Lett.* **2010**, *105*, 146104.
- [34] M. V. Ganduglia-Pirovano, C. Popa, J. Sauer, H. L. Abbott, A. Uhl, M. Baron, D. Stacchiola, O. Bondarchuk, S. Shaikhutdinov, H.-J. Freund; Role of Ceria in Oxidative Dehydrogenation on Supported Vanadia Catalysts; *J. Am. Chem. Soc.* **2010**, *132*, 2345-2349.
- [35] P. S. Bagus, C. J. Nelin, E. S. Ilton, M. Baron, H. Abbott, E. Primorac, H. Kühlenbeck, S. Shaikhutdinov, H. J. Freund; The complex core level spectra of CeO₂: An analysis in terms of atomic and charge transfer effects; *Chem. Phys. Lett.* **2010**, *487*, 237-240.
- [36] A. J. Window, A. Hentz, D. C. Sheppard, G. S. Parkinson, H. Niehus, D. Ahlbehrendt, T. C. Q. Noakes, P. Bailey, D. P. Woodruff; V₂O₃(0001) surface termination: phase equilibrium; *Phys. Rev. Lett.* **2011**, *107*, 016105.
- [37] L. Jiang, T. Wende, P. Claes, S. Bhattacharyy, M. Sierka, G. Meijer, P. Lievens, J. Sauer, K. R. Asmis; Electron distribution in partially reduced binary metal oxide systems: Ce_nV_mO_o⁺ gas phase clusters; *J. Phys. Chem. A* **2011**, *115*, 11187-11192.
- [38] C. S. Guo, K. Hermann, M. Havecker, J. P. Thielemann, P. Kube, L. J. Gregoriades, A. Trunschke, J. Sauer, R. Schlögl; Structural Analysis of Silica-Supported Molybdena Based on X-ray Spectroscopy: Quantum Theory and Experiment; *J. Phys. Chem. C* **2011**, *115*, 15449-15458.
- [39] C. G. Werncke, C. Limberg, C. Knispel, S. Mebs; Surface-Inspired Molecular Vanadium Oxide Catalysts for the Oxidative Dehydrogenation of Alcohols: Evidence for Metal Cooperation and Peroxide Intermediates; *Chem. Eur. J.* **2011**, *17*, 12129-12135.
- [40] J. F. Jerratsch, X. Shao, N. Nilius, H.-J. Freund, C. Popa, M. V. Ganduglia-Pirovano, A. M. Burow, J. Sauer; Electron localization in defective ceria films: An STM and DFT study; *Phys. Rev. Lett.* **2011**, *106*, 246801.

2.3.2 Weitere Informationen zur Außenwirkung

Man kann sagen, dass der Berliner „Übergangsmetalloxid“-Sonderforschungsbereich zu einer „Institution“ mit großer internationaler Sichtbarkeit und Wertschätzung geworden ist. Diese positive Außenwirkung des SFB gründet sich zunächst auf die große Zahl qualitativ hochwertiger Originalpublikationen in den wichtigsten referierten internationalen Zeitschriften des Gebietes. Unter den 40 aufgelisteten wesentlichen Originalarbeiten sind die führenden Zeitschriften von Chemie (Angew. Chem. 7x, J. Am. Chem. Soc. 3x) und Physik (Phys. Rev. Lett. 8x) sowie die wesentlichen Zeitschriften der bearbeiteten Forschungsgebiete (Surf. Science 3x; J. Catal. 2x; Nano Letters 1x) vertreten. Die große Resonanz, die viele dieser Publikationen gefunden haben, wird nicht zuletzt durch die Zahl der Zitate belegt. Zum Beispiel wurden von der Liste der 40 wichtigsten Originalarbeiten sechs (Nr. 6, 12, 14, 21 und 23 und 29) mehr als 10-mal pro Jahr zitiert (Web of Science). Ein besonderes Beispiel ist die Nr. 6 (J. Catal.), die bisher 120-mal zitiert wurde (15 Zitate pro Jahr) und von der Redaktion als “top cited” hervorgehoben wurde. Durch die Zusammenarbeit dreier Teilprojekte gelang es zu zeigen, dass die Zuordnung der IR-Bande zu dimeren oder polymeren Vanadiumoxidspecies auf Trägeroxiden revidiert werden muss (s. Abschn. 2.1.1.).

Die Außenwirkung des SFB 546 wurde aber auch durch die Übersichtsartikel und Buchkapitel bestimmt, die von den TP-Leitern und Mitgliedern des SFB 546 verfasst wurden. Beispiele sind das von D. P. Woodruff (TP C8) herausgegebene Buch „The Chemical Physics of Solid Surfaces, Vol 9: Oxide Surfaces“ (Elsevier, Amsterdam, 2001), zu dem K. Hermann (TP C6, zusammen mit M. Witko) sowie H.-J. Freund und H. Kuhlenbeck (TP C1, zusammen mit T. Risse) Kapitel beigetragen haben, sowie das von C. Hess und R. Schlögl herausgegebene Buch „Nanostructured Catalyst: Selective Oxidation Reactions“ (RSC Nanoscience & Nanotechnology, Cambridge, 2011) mit (u.a.) Kapiteln der Autoren E. Kondratenko, M. Baerns, C. Hess, R. Schlögl und R. Schomäcker. In dem Buch von K. Hermann „Crystallography and Surface Structure“ (Wiley-VCH, Weinheim, 2011) werden Kristalloberflächen von Oxiden als Beispiele behandelt. H. Kuhlenbeck und H.-J. Freund (TP C1) haben das Kapitel „Oxide Surfaces“ (III/42 A5, 2006) zum Landoldt-Börnstein (Herausg. P. Bonzel) beigetragen.

Übersichtsartikel wurden z.B. in „Surface Science Reports“ von H.-J. Freund (TP B1 mit J. Libuda,) über Molekularstrahlexperimente an Modellkatalysatoren (57, 2005, 157-298) sowie von V. Ganduglia-Pirovano und J. Sauer (TP C5, zusammen mit A. Hofmann) über theoretische Untersuchungen an Übergangsmetalloxiden (62, 2007, 219-270, bereits 157-mal zitiert, 31 Zitate pro Jahr) publiziert. Weitere Übersichtsartikel sind in Faraday Discussions (TP C1,

H.-J. Freund, 114, 1999, 1-31) sowie in Mass Spectrometric Reviews (TP A3, A4, K. Asmis und J. Sauer, 26, 2007, 542-562) erschienen.

Die Sichtbarkeit des SFB wurde sowohl durch die Internationalen Symposien verstärkt, die der SFB in den Jahren 2004, 2007 und 2011 organisiert hat, als auch durch die Organisation Internationaler Tagungen durch Mitglieder des SFB:

- International Congress on Catalysis (2012 München, Mitglieder des Organisationskomitees: Sauer, Schlögl; *Sprecher*: Freund 2012 München)
- International Symposium on Homogeneous and Heterogeneous Catalysis (2011 Organisation Freund, Limberg u.a.; *Sprecher*: Sauer 2011 Berlin; Freund 2007 Berkeley)
- International Conference on Theoretical Aspects of Catalysis (Organization 2006 Hermann u. Sauer; *Sprecher*: Hermann 2008 Varna, Sauer und Hermann 2010 Matsushima)

Die positive Resonanz auf die Arbeit wird auch durch Preise belegt, die Mitglieder des SFB erhalten haben:

- Freund 2011, Karl-Ziegler-Preis der GdCH
- Woodruff 2011, Max-Born-Preis der DFG
- Schlögl 2010, Dechema-Medaille
- Sauer 2010, Liebig-Denkmünze der GdCH
- Limberg 2009, Horst Dietrich Hardt-Preis der Universität des Saarlandes
- Freund 2007, Gabor S. Somorjai Award of the ACS in Creative Catalysis
- Wöste 2006 Gay-Lussac-Humboldt-Preis des Französischen Wissenschaftsministers
- Schwarz 2003, Otto Hahn-Preis für Chemie und Physik,

sowie durch Einladungen zu Keynote- und Plenarvorträgen bei den einschlägigen internationalen Konferenzen:

- European Congress on Catalysis (EUROPA-CAT) (Schlögl 2005, Sofia; Freund 2001, Limerick)
- North American Catalysis Society Meeting (Schlögl 2007, Houston; Sauer 2009, San Francisco)
- Tokyo Conference on Advance Catalytic Science and Technology (Sauer 2006, Schlögl 2006, Freund 2002)
- Netherlands Catalysis and Chemistry Conference (Limberg 2008, Sauer 2007)

- World Congress on Oxidation Catalysis (Kondratenko 2009, Lille; Freund 2005 Sapporo)
- Gordon Conference on Catalysis (Sauer 2004, Schlögl 2004)
- Gordon Conference on Chemical Reactions at Surfaces (Schlögl 2007; Freund 2005; Sauer 2003)
- Gordon Conference on Clusters, Nanocrystals & Nanostructures (Wöste 2007)
- International Conference on Catalysis in Membrane Reactors (Schomäcker, Lahnstein 2004)
- European Conference on Surface Science (ECOSS) (Freund 2006, Shaikhutdinov 2009, Winter 2011)

Ein wichtiger Aspekt der Außenwirkung war die Vermittlung und Darstellung von Forschungsthemen des Sonderforschungsbereichs bei Vorträgen in Schulen oder für Schüler, sowie bei öffentlichen Veranstaltungen wie der *Langen Nacht der Wissenschaften* oder dem *Girls Day* an der FU Berlin. Als besonderes Beispiel kann hier das TP A3 dienen, in dem viele der Reaktivitätsuntersuchungen in Teilchenfallen durchgeführt werden. Das Instrument ermöglicht es, einzelne Atome, Ionen, Moleküle, Cluster oder Nanopartikel lange Zeit im Visier zu halten. Die Wissenschaftler erläuterten die Funktion ihrer wissenschaftlichen Instrumente anhand eines mechanischen Analogons einer solchen Teilchenfalle - einer rotierenden Sattelfläche. Daneben waren reale Teilchenfallen aufgestellt wie sie im Labor verwendet werden.

3. Strukturwirkung des Sonderforschungsbereichs am Standort

3.1 Personelle Auswirkungen

3.1.1 Personelle Entwicklung, Strukturwirkung und Berufungspolitik

Der Sonderforschungsbereich 546 hat profilbildend in Forschung und Lehre der Humboldt-Universität zu Berlin am Standort Adlershof gewirkt. Es wurden „Mesoskopisch strukturierte Materialien“ und „molekulare Strukturen“ im Hinblick auf die Katalyse und andere Funktionen erforscht. Auch die Kooperation zwischen den Instituten für Chemie und Physik der Humboldt-Universität wurde durch den SFB gefördert.

Das sichtbarste Zeichen der Strukturwirkung des Sonderforschungsbereichs ist, dass sechs seiner Teilprojektleiter aus den drei Universitäten und dem Fritz-Haber-Institut als „Principal In-

investigators“ am Exzellenzcluster „Unifying Concepts in Catalysis“ beteiligt sind. Zu diesen Personen gehört C. Limberg, dessen Berufung auf eine Eckprofessur in Anorganischer Chemie an die Sprecherhochschule (HU) ohne den SFB 546 nicht erfolgt wäre (Der Sprecher war Mitglied der Berufungskommission). C. Limberg war zuletzt Stellvertreter des Sprechers dieses Sonderforschungsbereiches und ist designierter Sprecher des beantragten SFB 1048.

Insgesamt verlief die personelle Entwicklung so dynamisch wie man das für eine erfolgreiche Forschung erwartet und benötigt. Zahlreiche Teilprojektleiter wurden an andere Institutionen berufen

- W. Koch (noch vor 1. Förderperiode) als Geschäftsführer der GDCh
- W. Widdra (C7E; 2003) auf eine C4-Stelle in Halle
- M. Bäumer (B1; 2003) auf eine C4-Stelle in Bremen
- C. van Wüllen (A1E; 3. Förderperiode) auf eine W3-Stelle in Kaiserslautern
- C. Hess (B2; 3. Förderperiode) auf eine W2-Stelle in Darmstadt
- D. Schröder (A2E; 3. Förderperiode) an das Institut für Organische Chemie und Biochemie der Tschechischen Akademie in Prag
- M. V. Ganduglia-Pirovano (C5; 2009) auf eine permanente Stelle als Forscherin in Madrid

M. Baerns (ACA, B3), J. Urban (FHI, B2), H. Niehus (HU, C2), und K.H. Rieder (FU, C3), und K.H. Ploog (C4) schieden altersbedingt aus.

Jüngere Teilprojektleiterinnen und Teilprojektleiter wurden ernannt, die teilweise zuvor in den Projekten beschäftigt waren und teilweise später wieder ausgeschieden sind, um an anderer Stelle ihre Karriere fortzusetzen: K. Asmis, T. Siebert (A3), J. Döbler und M. Sierka (A4), S. Shaikhutdinov (B1), C. Hess, D. Su und K. Pelzer (B2), E. Kondratenko (B3), W. Theis, F. Moresco (C3), C. Hucho (C4), M.V. Ganduglia-Pirovano und J. Paier (C5).

Die besondere Konstellation von Theoriegruppen an der HU, der TU und dem FHI, die auf den Gebieten heterogene Katalyse, Gasphasenchemie und Oberflächenphysik in der Kooperation erfahren sind, war eine wichtige Voraussetzung für die erfolgreiche Arbeit des Sonderforschungsbereichs. Es war deshalb erfreulich, dass unter Mitwirkung des Sprechers in der Berufungskommission noch in der ersten Förderperiode mit C. van Wüllen ein kompetenter Nachfolger für den ausgeschiedenen W. Koch im TP A1 seine Arbeit antreten konnte. Nach dem Wechsel von C. van Wüllen nach Kaiserslautern war zwar eine Nachfolgeberufung an der TU

vorgesehen (auch im Interesse des Exzellenzclusters UNICAT), jedoch konnte der SFB für die 4. Förderperiode damit nicht mehr planen und das TP A1 endete deshalb mit der 3. Förderperiode. Einige Aufgaben wurden im TP A4 bearbeitet, das deshalb gegenüber der Vorperiode um eine Doktorandenstelle erweitert wurde.

Auch das TP A2 endete nach der 3. Periode im Juni 2008, da D. Schröder ein attraktives Angebot des Instituts für Organische Chemie und Biochemie der Tschechischen Akademie der Wissenschaften annahm (inzwischen Inhaber eines ERC Grants), und H. Schwarz wegen seiner Berufung zum Präsidenten der Alexander von Humboldt-Stiftung die Aufgaben eines Teilprojektleiters nicht länger wahrnehmen konnte. Eine Nachfolge auf dem Gebiet der Gasphasenchemie war in der TU nicht vorgesehen. Die Konsequenzen für die Arbeit des Sonderforschungsbereichs in der letzten Antragsperiode waren aber nicht kritisch. Einerseits war das TP A2 im Hinblick auf die Reaktivitätsuntersuchungen allen anderen immer voraus, andererseits wurden im TP A3 in der 4. Förderphase verstärkt Reaktivitätsuntersuchungen durchgeführt.

Das TP B3 (Institut für Angewandte Chemie) war im Sonderforschungsbereich unverzichtbar, da hier anwendungsnahe Pulverkatalysatoren hergestellt und untersucht wurden. Deshalb war es nach dem Ausscheiden von M. Baerns wichtig, dass mit E. Kondratenko ein jüngerer Kollege gefunden wurde, der die Kontinuität sichern konnte. Nach der Eingliederung des Instituts für Angewandte Chemie als Außenstelle Berlin in das Leibniz-Institut für Katalyse an der Universität Rostock (LIKAT) und dem Umzug nach Rostock im Jahre 2009 konnten die Arbeiten in den Räumen der TU Berlin mit der dafür benötigten Ausstattung des LIKAT bis zum Ende des Sonderforschungsbereichs im Juni 2011 fortgesetzt werden. Der TP-Leiter Kondratenko ist Privatdozent an der TU Berlin und R. Schomäcker (TU) trat als zweiter TP-Leiter in das Projekt ein.

Die Projekte C2 und C3 wurden nach dem altersbedingten Ausscheiden der TP-Leiter (Niehus und Rieder) nach der halben Förderzeit nicht weitergeführt. Dafür wurde gerade im Projektbereich C nach neuen Methoden gesucht, welche die im SFB bereits etablierten Methoden vorteilhaft ergänzen konnten. Während sich die Inverse Photoemission (C10) als nicht so aussagekräftig erwies wie zunächst vermutet (das Projekt wurde nach einer Förderperiode wieder beendet), konnten mit der Photoelektronen-Beugung (C8) und der Ionenstreuung (C11) wichtige Beiträge zu den Zielen des Sonderforschungsbereichs geleistet werden.

3.1.2 Auswirkungen auf die personelle Grundausrüstung

Im Jahre 2004 hat es an allen drei Berliner Universitäten massive Kürzungen im Personalbereich und in der Zahl der Professuren gegeben, welche auch die beteiligten Chemie- und Physik-Institute betroffen haben. Diese strukturellen Einschnitte erfolgten jedoch so, dass der Sonderforschungsbereich 546 an der Humboldt-Universität als strukturell vorrangig betrachtet wurde und somit von den Kürzungen nicht unmittelbar betroffen war. Probleme entstanden dadurch, dass es keine Garantie gab, strukturell bestätigte Personalstellen wiederbesetzen zu können. Letztendlich wurden jedoch den Mitarbeiterstellen Priorität eingeräumt, die zur erklärten Grundausrüstung von Sonderforschungsbereichen gehören.

3.1.3 Gleichstellungsmaßnahmen

Im Rahmen des „Berliner Programms zur Förderung der Chancengleichheit für Frauen in Forschung und Lehre“ werden Mittel zur Förderung von Wissenschaftlerinnen vergeben, darunter auch Postdoc-Stipendien, Gastprofessuren, Lehraufträge, Promotions- und Habilitationsstipendien. Davon hat der SFB keinen Gebrauch machen müssen, da qualifizierten Frauen immer reguläre Haushalts- oder SFB-Stellen angeboten werden konnten.

Das Kollegium des Sonderforschungsbereichs hat sich intensiv bemüht, geeignete Frauen für zu besetzende Stellen zu gewinnen. Der Stellvertreter des Sprechers, C. Limberg, hat z.B. im März 2006 an einer Expertenrunde zum Thema „Bewerbung“ teilgenommen, bei der es um die Unterstützung der Karriere von Frauen ging. Dennoch waren in der letzten Förderperiode nur zwei Frauen unter den 20 Teilprojektleitern. Bei den am SFB beteiligten Wissenschaftlerinnen (ohne Teilprojektleiterinnen) war der SFB bemüht, deren weitere Tätigkeit in der Wissenschaft zu fördern. Zum Beispiel strebten von den neun in der 3. Förderperiode beteiligten Wissenschaftlerinnen sieben eine weitere wissenschaftliche Karriere an, eine ist seit Juli 2007 permanente wissenschaftliche Mitarbeiterin des Deutschen Technik-Museums in München und eine andere seit Februar 2007 Referentin im Bundesamt für Strahlenschutz Berlin.

Im Rahmen des finanziellen Anreizsystems können Wissenschaftlerinnen an der Humboldt-Universität in begrenztem Umfang mit zusätzlichen Sachmitteln gefördert werden. Das geschieht auch am Institut für Chemie, in dem ein Teil der jährlichen Verbrauchsmittel für Frauen reserviert ist. Davon hat der SFB 546 regelmäßig Gebrauch gemacht. Anträge auf finanzielle Unterstützung zum Beispiel für Dienstreisen von Nachwuchswissenschaftlerinnen konnten hieraus berücksichtigt werden.

3.1.4 Förderung der Vereinbarkeit von Familie und Beruf

Da in der Nähe der Berliner Wissenschaftseinrichtungen, gerade auch in Adlershof, Kinderbetreuungseinrichtungen in ausreichender Zahl zur Verfügung stehen, musste der SFB keine speziellen Maßnahmen ergreifen. Bei der Festlegung der Zeiten von SFB-Veranstaltungen wurden Kinderbetreuungspflichten berücksichtigt.

3.1.5 Förderung des wissenschaftlichen Nachwuchses

Eine Vielzahl von Diplom-, Doktor- und Habilitationsarbeiten wurden in die Arbeit des Sonderforschungsbereichs 546 integriert, der damit eine bedeutende Stellung bei der Ausbildung des wissenschaftlichen Nachwuchses einnahm. Es haben sich K. Asmis (FU), V. M. Ganduglia-Pirovano (HU), C. Hess (HU), E. Kondratenko (TU), D. Schröder (TU), M. Sierka (HU) habilitiert und es wurden 93 Dissertationen abgeschlossen.

Die Doktorandenförderung verstärkte sich mit der Einrichtung der Internationalen Max Planck Research School (IMPRS) „Complex Surfaces in Materials Science“, an der Mitglieder des Sonderforschungsbereichs aus der Humboldt-Universität (Sauer, Winter), aus der Technischen Universität (Schomäcker) und aus dem Fritz-Haber-Institut der MPG (Freund, Hermann, Schlögl) maßgeblich beteiligt waren und sind. Mehrere Doktoranden des Sonderforschungsbereichs nahmen an den Lehrveranstaltungen und Doktorandenseminaren der IMPRS teil.

Im SFB beteiligten sich alle Diplomanden, Doktoranden und Habilitanden am intensiven wissenschaftlichen Austausch, der die Verbindung von Experiment und Theorie und den Vergleich unterschiedlicher experimenteller Methoden einbezog. Das weitete das Blickfeld und wirkte der verständlichen Tendenz in Qualifizierungsphasen entgegen, sich zu sehr auf das eigene Thema einzuschränken. Der Sonderforschungsbereich veranstaltete regelmäßig Seminare und Kolloquien und jedes Jahr einen mehrtägigen Workshop. Neben Arbeitsberichten aus dem SFB und Vorträgen eingeladener Gäste waren dort auch Vorträge mit Weiterbildungscharakter, u. a. zu den methodischen Grundlagen, im Programm. Natürlich erhielten Doktoranden dort auch Gelegenheit ihre Arbeiten zur Diskussion zu stellen.

3.1.5.1 Zahl der abgeschlossenen Dissertationen, Habilitationen und Berufungen im Sonderforschungsbereich (Grund- und Ergänzungsausstattung)

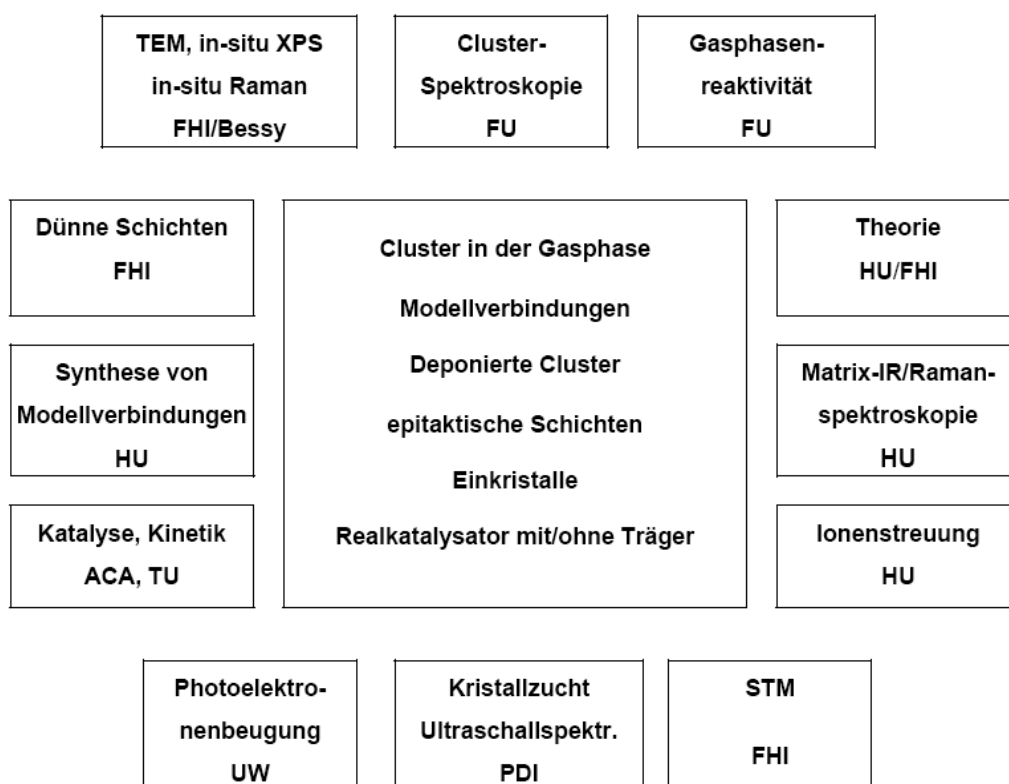
	1. FP 1999-2002		2. FP 2002-2005		3. FP 2005-2008		4. FP 2008-2011		noch lau- fend	
	w	m	w	m	w	m	w	m	w	m
Promotionen	5	29	10	14	8	17	2	8	-	8
Promotionen gesamt	34		24		25		10		8	
Habilitationen	-	-	-	-	-	4	1	1	-	1
Berufungen von Nachwuchswissenschaftlern nach C3, C4, W2, W3	-	-	-	-	-	1	-	-		

3.2 Infrastruktur

Der SFB 546 hat die großen Chancen, die die Berliner Forschungslandschaft mit ihrer hervorragenden Infrastruktur im Allgemeinen und der Standort Adlershof im Besonderen für die Bearbeitung seiner Thematik bietet, konsequent genutzt. Andererseits war die in diesem SFB nachweislich gewonnene Erfahrung in der Zusammenarbeit mehrerer Teilprojektleiter auf dem Gebiet der Katalyse eine wichtige Voraussetzung für den Erfolg des Clusters „Unifying Concepts in Catalysis“ im Exzellenzwettbewerb. Der SFB wird von der Humboldt-Universität getragen und bezieht die beiden anderen Berliner Universitäten sowie außeruniversitäre Forschungsinstitute ein (Fritz-Haber-Institut der MPG, Paul-Drude-Institut für Festkörperelektronik und Leibniz-Institut für Katalyse - Außenstelle Berlin), deren spezielle Expertise und deren Ausstattung unverzichtbar waren. Einige Teilprojektleiter der außeruniversitären Forschungseinrichtung (Freund, Schlögl) sind mit der Humboldt-Universität durch Honorarprofessuren verbunden. Der Sprecher ist auch auswärtiges wissenschaftliches Mitglied des Fritz-Haber-Institutes.

Die besondere Konstellation von Theoriegruppen an der Humboldt-Universität, an der Technischen Universität und am Fritz-Haber-Institut, die auf den Gebieten heterogene Katalyse, Gasphasenchemie und Oberflächenphysik in der Kooperation mit Experimentatoren erfahren sind, ist ein wesentliches Merkmal dieses Sonderforschungsbereiches.

Ein weiterer entscheidender Vorteil war, dass im Sonderforschungsbereich eine außerordentlich breite Palette von oberflächenanalytischen und spektroskopischen Methoden eingesetzt werden kann. In der letzten Antragsperiode wurde die Palette durch die Ionenstreuung (C11) nochmals signifikant erweitert. Da einige Methoden in verschiedenen Arbeitskreisen vertreten sind, war ein Transfer an Know-how sowie die direkte Übertragung methodischer Details möglich. Besondere Erfahrungen bzw. Methoden, welche die beteiligten Gruppen einbrachten, sind im folgenden Schema dargestellt.



Schema: Besondere Erfahrungen/Methoden der beteiligten Gruppen

4. Hinweise an die Deutsche Forschungsgemeinschaft

Das Programm Sonderforschungsbereiche hat sich für uns als ideales Instrument zur Entwicklung der Zusammenarbeit leistungsfähiger Gruppen auf dem wichtigen Gebiet der Katalyse erwiesen. Ohne die Erfahrungen des SFB 546 wäre die erfolgreiche Beantragung des Exzellenzclusters UniCat in Berlin nicht möglich gewesen. Nach den Erfahrungen mit dem SFB und dem Exzellenzcluster gelangt zumindest der Sprecher zu der Auffassung, dass die Größe eines SFB für die Organisation der wissenschaftlichen Zusammenarbeit ideal ist und zu einem guten Verhältnis zwischen Administrationsaufwand, wissenschaftlichen Ergebnissen und strukturbildenden Impulsen führt. Wir sind der DFG für dieses Förderinstrument sehr dankbar - und natürlich auch für die Förderung in unserem konkreten Fall.

Die Begleitung durch die Geschäftsstelle der DFG haben wir stets als unterstützend empfunden und wir sind den verschiedenen Mitarbeiterinnen und Mitarbeitern dafür sehr dankbar. Selbst eine Forderung der Geschäftsstelle, der wir zunächst ohne Verständnis gegenüber standen, erwies sich später als glücklicher Umstand. Das war die Forderung, dass es beim Berichtskolloquium nur einen Gesamtvortrag des Sprechers geben dürfe, wenn wir die Ergebnisse aller Teilprojekte mit Postern darstellen möchten. Letzteres ist in den Naturwissenschaften eine unverzichtbare Diskussionsgrundlage, aber der Verzicht auf jegliche Vorträge aus den Teilprojekten oder Projektbereichen (außer den Neuvorstellungen) schien uns sehr ungünstig. Diese Entscheidung, nur einen Gesamtvortrag des Sprechers zu haben, wurde jedoch von den Gutachtern als äußerst positiv empfunden, da dabei die Synergien und die Beiträge der Teilprojekte zur Gesamtzielsetzung besonders gut sichtbar gemacht werden konnten. Wir haben das dann in späteren Berichtskolloquien, wo es diese Forderung nicht mehr gab, mit großer Zustimmung der Gutachter weiter so gehalten. An dieser Stelle möchten wir den Gutachtern, die teilweise sehr lange den SFB 546 begleitet haben, sehr herzlich für die konstruktiven Diskussionen danken, die ohne Zweifel zu den Erfolgen unseres SFB beigetragen haben.

Mit Beginn der 3. Förderperiode hatte der SFB die Wahl zwischen einer weiteren 4-jährigen oder zwei weiteren 3-jährigen Förderperioden. Wir haben uns - nicht nur im Hinblick auf die Möglichkeit einer längeren Gesamtförderdauer - für letztere Variante entschieden. Das war im Nachhinein betrachtet die beste Entscheidung, nicht nur wegen der zusätzlichen wissenschaftlichen Erkenntnisse, sondern auch wegen des äußeren Zwanges einer vertieften Diskussion der Zusammenarbeit und der weiteren Fokussierung auf die Hauptinteressen des Sonderforschungsbereichs.

5 Berichte über die einzelnen Teilprojekte der letzten Förderperiode

5.1 Allgemeine Angaben zum Teilprojekt A3

5.1.1 Titel: Struktur, Reaktivität und Dynamik von Übergangsmetalloxid-Aggregaten; Cluster in der Gasphase

5.1.2 Projektleitung

Dr. habil. Knut R. Asmis
geb. 25.06.1968

Dr. Torsten Siebert
geb. 17.09.1969

Prof. Dr. Ludger Wöste
geb. 02.05.1946

Fritz-Haber-Institut der
Max-Planck-Gesellschaft
Abteilung Molekülphysik
Faradayweg 4-6
14195 Berlin

Freie Universität Berlin
Institut für
Experimentalphysik
Arnimallee 14
14195 Berlin

Freie Universität Berlin
Institut für
Experimentalphysik
Arnimallee 14
14195 Berlin

030 8413-5735
asmis@fhi-berlin.mpg.de

030 838-56122
siebert@physik.fu-berlin.de

030 838-55566
woeste@physik.fu-berlin.de

5.2 Entwicklung des Teilprojekts

5.2.1 Report

Summary

During the last funding period, the work on gas phase metal oxide clusters and aggregates was continued, focusing on the improvement and extension of the techniques used for the characterization of their structure, reactivity and dynamics. This work can be separated into two categories: Infrared photodissociation (IRPD) spectroscopy of electronic ground state cluster ions (5.2.1.1) and femtosecond spectroscopy of the photoinduced reactivity in electronically excited cluster ions (5.2.1.2).

Within the first category, four distinct goals were put forth in the 2008 proposal: (1) Continuation of the structural characterization of clusters of typical support materials ($M_mO_n^{+/-}$, $M = Ce, Ti, Mo$), (2) extension of these studies to the corresponding binary metal oxide clusters $V_mM_nO_o^{+/-}$, (3) characterization of V_mO_n -adsorbat complexes and (4) construction of a cryogenically-cooled dual laser vaporization for the production of $[(V_mO_n) \cdot (M_oO_p)]^{+/-}$ cluster aggregates. Significant advances were achieved with respect to the first three goals, while the construction of the custom-designed cluster source lagged behind and was only recently completed. These results have led to three publications, summarizing our work on electron localization in binary $Ce_mV_nO_o^+$ clusters [JWC11], the spectroscopic characterization of the

oxidative dehydrogenation of propane by $V_4O_{10}^+$ [WDJ10], as well as the extension of mass-selective IRPD spectroscopy to the far-infrared region [LCH10]. A manuscript on the structure and vibrational spectroscopy of $Ce_mO_n^+$ clusters has been submitted [BSW11] and several other manuscripts are in preparation. Two publications on the structure and IRPD spectroscopy of vanadium oxide anions [SBW08] and aluminum oxide cations [SJS08] had been submitted at the end of the 2005-8 period and these have been accepted for publication in the meantime.

Within the second category (5.2.1.2), exploring photoactivation via electronic excitation within the reactivity of excited state potentials in vanadium oxide cluster ions was proposed [1,2]. This was seen as a complimentary approach to the thermally driven oxidation reactions of small hydrocarbons on vanadium oxide cluster ions investigated in the previous funding period by project A4 (Sauer/Döbler) and the former project A2 (Schwarz/Schröder) [3]. Photoinduced ligand-to-metal charge transfer was proposed for mimicking these reactions in the reduction of vanadium oxide systems and occupation of electronic states with high metal d-state character.[4] This scheme was realized with the photoinduced oxygenation of propene to acrolein on the $V_4O_{11}^-$ system [LMD08]. Within these experiments, the novel technique of identifying neutral reaction participants *in situ* by utilizing the efficiency of intense femtosecond laser pulses in multi-photon ionization was proposed and realized in a fruitful exchange with project A2 (Schwarz/Schröder) [5]. A full description of this technique, which allows for the complete mechanistic analysis of the photoinduced oxygenation of propene, is currently submitted for review [LDM11]. This approach further opens the possibility of temporally resolving the reaction dynamics. This motivated the development of an ultrafast laser source in order to meet the demanding time scales estimated to lie in the lowest end of the femtosecond regime for this reaction. The technique is based on previous work [SUM08] and the manuscript describing the successful compression of standard amplified femtosecond laser pulses down to 5 fs is currently in preparation. The application of this source to cluster reactivity studies remains outstanding due to the significant efforts in its development.

5.2.1.1 Infrared Photodissociation Spectroscopy

Methods and Method Development

The structure of gas phase metal oxide ions is characterized by way of infrared photodissociation (IRPD) spectroscopy as described in the previous reports/proposals (see also Refs. [6,7]). The experimental IRPD spectra are then interpreted on the basis of a comparison to simulated IR absorption spectra, generally derived from harmonic vibrational frequencies and IR intensities. These quantum chemical calculations were either performed within the

project A4 (Sauer/Döbler) or in close collaboration with them.

Several noteworthy methodological improvements were achieved during the past period. First, we extended the accessible wavelength region for our mass-selective IRPD experiments from 500 cm^{-1} down to 100 cm^{-1} range as demonstrated in our study on Au_6Y^+ [LCH10]. While this spectral range is particularly interesting for pure metal clusters, it will also prove useful for characterizing bending and ring breathing vibrations involving heavier transition-metal atoms in metal oxide clusters. Second, we measured the first IRPD spectrum of a metal oxide cluster ion (VPO_4^+) in the $750\text{-}1500\text{ cm}^{-1}$ region using a tunable table-top IR-OPO laser (see Fig.1), as part of a collaboration with the group of H. Schwarz (Technical University Berlin). All our previous IR spectroscopic studies had been limited to the free electron laser facility FELIX, due to the absence of an adequate, commercially available laser system.

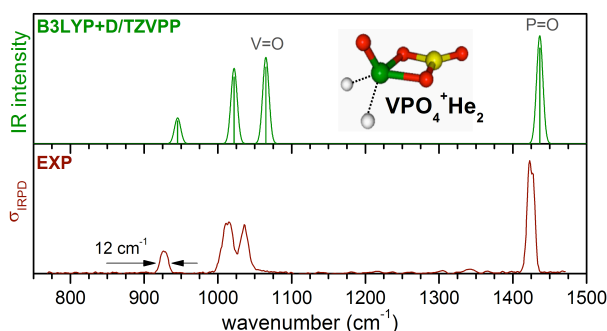


Fig. 1. Simulated linear IR absorption (top) and experimental IRPD spectrum (bottom) from 750 to 1500 cm^{-1} of $\text{VPO}_4^+\cdot\text{He}_2$ measured using a table-top IR-OPO laser system available at the FHI. The observed peak widths are twice as large as the bandwidth of the laser transition and due to rotational excitation.

The development and construction of the cryogenically-cooled dual laser vaporization source, described in the 2008 proposal, turned out to be more challenging than expected. In order to ensure operation of the laser vaporization source over the full temperature range ($10\text{-}300\text{ K}$), the design of the drive system for rotating and translating the metal rods proved to be critical and needed several design iterations. While a single-rod version of the laser vaporization has been fully operational since several months, the dual target version is still under construction. Consequently, the mass spectrometric and IR spectroscopic experiments on mixed-metal oxide clusters aggregates could not be performed during this period.

Clusters of Typical Support Materials

After characterizing aluminum and silicon oxide cluster cations [9,10] during the 2005-8 period, we turned our attention to cerium oxide cluster cations [BSW11] in the recent proposal period. Cerium oxides are widely used in industrial applications, e.g. in fuel cells, ceramics, photosensitive glasses as well as gas sensors. In heterogeneous catalysis cerium oxides serve both as a catalyst as well as a support material (e.g. in self-cleaning ovens and catalytic

converters in automobiles). Interestingly, only little is known about gas phase cerium oxide clusters and, in particular, no spectroscopic information was available. The goal of the present study thus was to characterize the geometric and electronic structure of small, partially-reduced cerium oxide clusters, focusing on testing the predictions of various DFT functionals, in particular how well they would describe the localization of unpaired electrons in Ce 4f states.

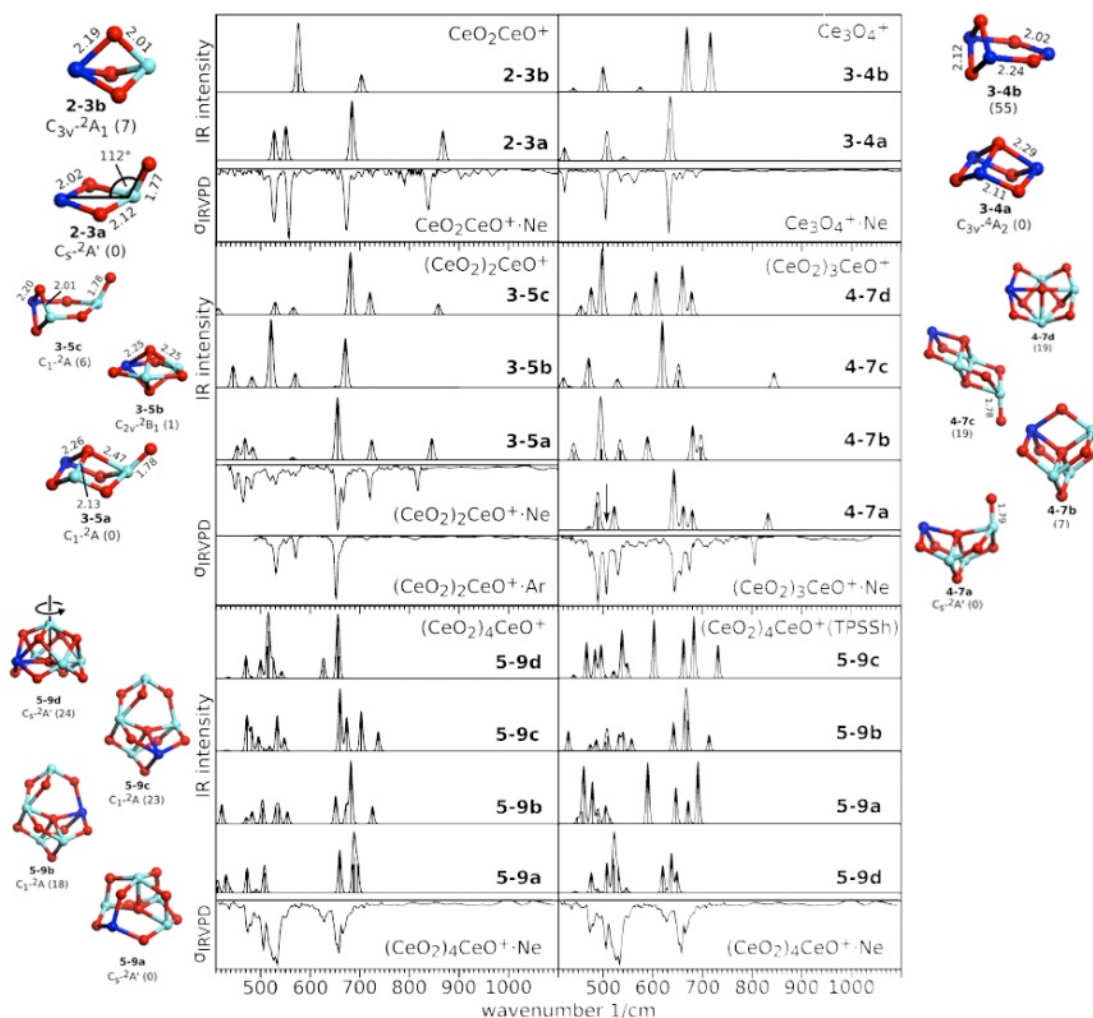


Fig. 2. Optimized B3LYP structures and simulated linear absorption spectra of $Ce_m O_n^+$ clusters with $m = 2-5$. For each cluster size the lowest energy isomers are shown (energies, in kJ/mol, are stated in parenthesis). For $Ce_5 O_9^+$ simulated spectra derived from the TPSSh results (bottom right) are also shown. The experimental IRPD spectra of the corresponding cluster ion - rare gas atom complexes are plotted below the simulated IR spectra for each cluster size.

IR spectra of $Ce_m O_n^+$ clusters with $m=1-5$ were obtained by infrared vibrational predissociation spectroscopy of the corresponding $Ce_m O_n^+$ -rare gas atom complexes clusters. Selected IRPD spectra are compared to simulated linear IR absorption spectra of various low-energy isomers in Fig. 2. The key results are as follows: The CeO^+ -He complex (not shown) is non-linear with

a Ce=O stretching frequency of 891 cm^{-1} and a He binding energy of 5 kJ/mol . Structures containing a terminal Ce=O bond show a characteristic absorption band between 800 and 900 cm^{-1} . Dicerium cluster cations form a four-membered Ce-O-Ce-O ring with a characteristic absorption between 430 and 680 cm^{-1} . In some cases multiple isomers are detected experimentally and their individual spectral signatures are identified by changing the type of messenger atom and thus the relative isomer populations (see for example $\text{Ce}_3\text{O}_5^+\cdot\text{Ne}$ vs. $\text{Ce}_3\text{O}_5^+\cdot\text{Ar}$ in Fig. 2). All larger clusters contain fused Ce-O-Ce-O four-membered rings, characterized by intense IR signals around 500 and 650 cm^{-1} , and show structural properties reminiscent of bulk ceria. However, the spectral signature of the gas phase cerium oxide clusters studied here have not yet fully converged to that of a ceria surface (see Fig. 3). Of the various DFT functionals tested, IR spectra derived from the BP-86 functional do not show as good agreement to experiment compared to B3LYP and TPSSh. For Ce_5O_9^+ B3LYP, in contrast to TPSSh, overestimates the electron localization of the unpaired electron occupying f-orbitals on the Ce-centers and consequently predicts an incorrect ordering of the low-energy isomers.

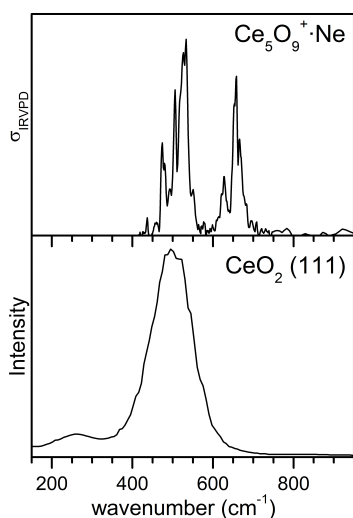


Fig. 3. IR spectrum of $\text{Ce}_5\text{O}_9^+\cdot\text{Ne}$ (top) compared to HREEL spectrum (bottom) of the oxygen-terminated (111) surface ceria.[11]

As part of our IRPD studies on transition metal oxide clusters we also measured spectra of small chromium oxide clusters (Cr_mO_m^+ with $m=2-4$) in collaboration with the group of P. Lievens (KU Leuven, Belgium). These results are currently being written up.

Binary Metal Oxide Clusters

A strong dependence on the type of the supporting oxide has been found for vanadia catalysts, the origin of which is still under debate. Among the factors discussed is the reducibility of the support material, because hydrogen transfer, the rate-determining step in the ODH reaction, leaves an electron on the supported vanadium oxide catalysts. For vanadia supported on ceria,

the catalytic activity is particularly high. Although cerium oxide is known for its ability to store, release, and transport oxygen ions since long, only recently a combined experimental and computational investigation of $\text{VO}_x/\text{CeO}_2(111)$ model catalysts by projects A4 (Sauer/Döbler) and B1 (Freund/Shaikhutdinov) [12] has shown that this remarkable activity is due to the ability of ceria to easily accommodate electrons in localized f-orbitals.

This raises the more general question of the role of the two metals in the partial reduction of a mixed metal oxide system. In order to address this question we studied the binary metal oxide gas phase clusters, CeVO_4^+ (**1**), CeV_2O_6^+ (**2**), and Ce_2VO_5^+ (**3**), by IRPD spectroscopy in combination with DFT [JWC11]. In **1** both metal atoms are fully oxidized. There is no doubt about the $\text{Ce}^{(+4)}\text{O}_2\cdot\text{V}^{(+5)}\text{O}_2^+$ electronic structure with all Ce-4f and V-3d states empty. For **2**, which can also be written as $(\text{CeVO}_4)(\text{V}^{(+5)}\text{O}_2^+)$, and for **3**, which can be written as $(\text{CeVO}_4)(\text{Ce}^{(+3)}\text{O}^+)$, the question arises: Is (are) the extra electron(s) populating the Ce-4f or the V-3d states and does this lead to geometrically different isomers?

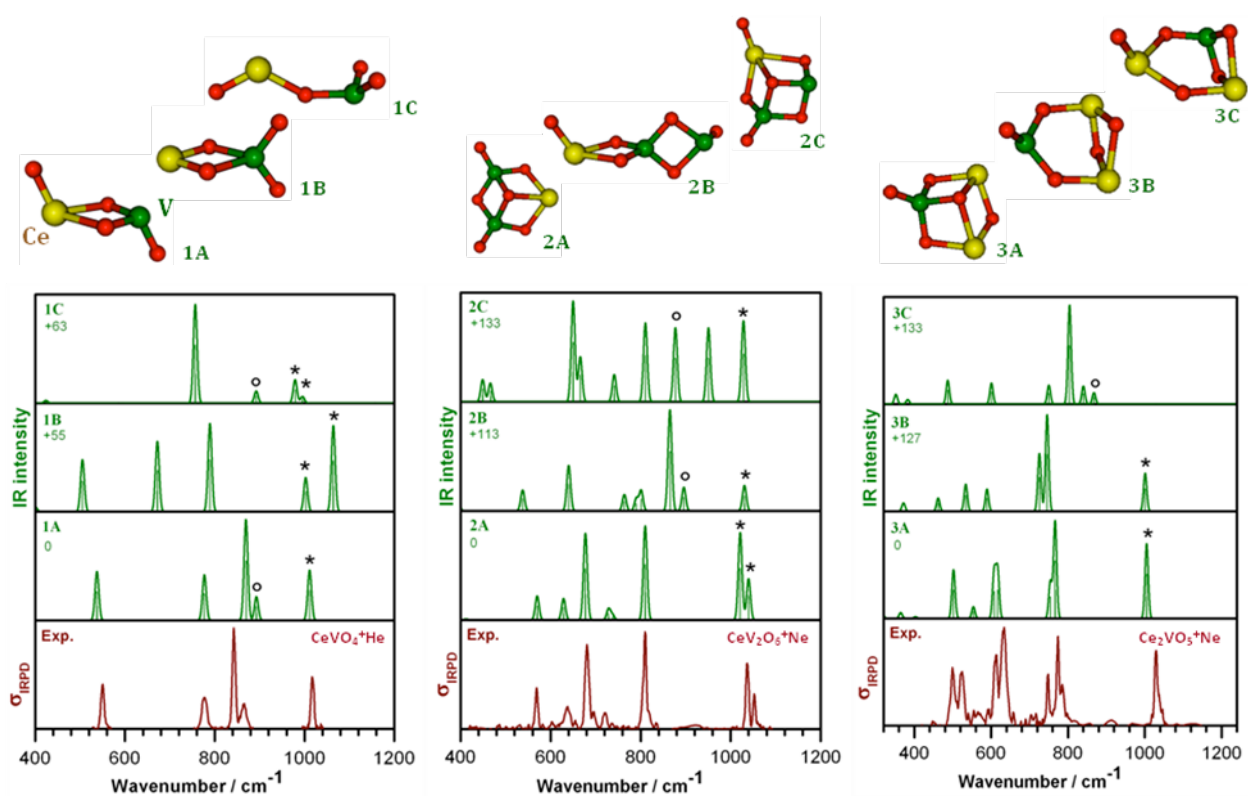


Fig. 4. The structures (top row) of the three lowest energy isomers of CeVO_4^+ (**1A-1C**), CeV_2O_6^+ (**2A-2C**), and $\text{Ce}_2\text{VO}_5^+\cdot\text{Ne}$ (**3A-3C**). The simulated B3LYP/TZVPP IR spectra of these structures are shown in the lower part of the figure and compared to the experimental IRPD spectrum (bottom row) of $\text{CeVO}_4^+\cdot\text{He}$ (left), $\text{CeV}_2\text{O}_6^+\cdot\text{Ne}$ (center), $\text{Ce}_2\text{VO}_5^+\cdot\text{Ne}$ (right). V=O modes are marked with an asterisk and Ce=O modes are marked with an open circle.

The lowest energy B3LYP/TZVPP structures are shown in the top part of Fig. 4. The good

agreement between the experimental IRPD spectra and the simulated IR spectra of the lowest energy structure for the three systems **1-3** considered here shows that the B3LYP/TZVPP calculations yield reliable relative energies and structures and, on this basis, reproduce the vibrational properties of binary Ce/V oxide clusters. The computed spin densities (see Fig. 5) then reveal that in the lowest energy isomer any additional electrons are always localized on the Ce atoms, effectively reducing Ce^{+4} to Ce^{+3} . Summarizing, we find that in our gas phase binary metal oxide clusters the electron distribution leading to $\text{Ce}(\text{f}^1)^{+3}/\text{V}^{+5}$ is more stable than $\text{Ce}^{+4}/\text{V}(\text{d}^1)^{+4}$. These results are in agreement with the work on model catalysts, but in contrast to what one would expect from known reduction potentials in solution. We therefore conclude the $\text{Ce}^{+4}/\text{V}(\text{d}^1)^{+4}$ pair is more stable when the coordination numbers are high as in the bulk solids or in aqueous solution, whereas a low coordination of vanadium, as found for the gas phase clusters or in CeVO_4 or for vanadia species on ceria supports favors the $\text{Ce}^{+3}(\text{f}^1)/\text{V}^{+5}$ pair.

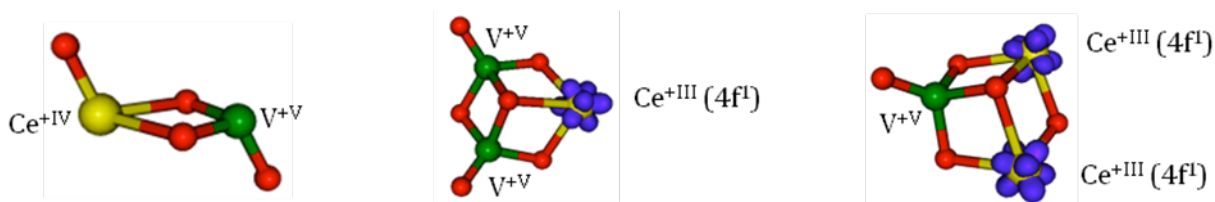


Fig. 5. Oxidation state and spin density isosurface of the lowest energy structures for CeVO_4^+ , CeV_2O_6^+ , and Ce_2VO_5^+ .

Additional calculations show that whereas in the vanadia-ceria clusters Ce^{+4} is easily reduced to Ce^{+3} , stabilizing the V^{+5} center, in vanadia-titania clusters reduction of Ti^{+4} to Ti^{+3} is competitive with that of V^{+5} to V^{+4} , and in vanadia-silica clusters Si^{+4} cannot be reduced. The present results thus confirm that an easily reducible support material, like ceria, may serve as an electron acceptor for the electron transferred to the active site in the rate determining step. In this way IRPD spectroscopy on electronically-tailored binary metal oxide clusters, combined with properly chosen quantum chemical calculations, can contribute to the understanding of complex solid catalysts.

Vanadium Oxide – Adsorbate Complexes

Vanadium oxide cations can react with alkanes and alkenes along several reaction pathways including (i) molecular association, (ii) charge transfer, (iii) dehydrogenation, (iv) oxygen loss, (v) C-C bond cleavage and (vi) oxidative dehydrogenation (ODH). $\text{V}_4\text{O}_{10}^+$ was predicted to be particularly reactive [13] and indeed found to dehydrogenate methane under thermal conditions [3]. Upon reaction with propane ODH is the main channel and involves the transfer of two H

atoms to the cluster, forming $[\text{V}_4\text{O}_{10}\text{H}_2]^+$ concomitant with the elimination of propene [14].

A more detailed insight into the molecular level mechanisms governing these gas phase reactions is clearly of interest, but difficult to extract from mass spectrometric measurements alone. We characterized the reaction of mass-selected gas phase $\text{V}_4\text{O}_{10}^+$ clusters with propane under thermalized, multiple collision conditions in a buffer gas filled ion trap at 100 K [WDJ10]. In contrast to previous mass spectrometric work performed under single collision conditions [14], most clusters in our experiments are fully thermalized prior to a collision with a propane molecule through many collisions with He atoms. The main reaction product, $[\text{V}_4\text{O}_{10}\text{H}_2]^+\cdot\text{C}_3\text{H}_8$, was studied with IRPD spectroscopy, which, in combination with DFT calculations from project A4 (Sauer/Döbler), provided a finger print of its structure.

The IRPD spectrum of $[\text{V}_4\text{O}_{10}\text{H}_2]^+\cdot\text{C}_3\text{H}_8$ is shown in the bottom part of Fig. 6. It is characterized by at least eight discrete absorption peaks, two characteristic vanadyl bands at 1049 and 1037 cm^{-1} , and six bands in-between 600 to 950 cm^{-1} , i.e., in the V-O-V stretching and C-C-H bending region. Simulated linear absorption spectra of three possible structural candidates, labeled A1, A2 and B, are plotted in the upper part of Fig. 6.

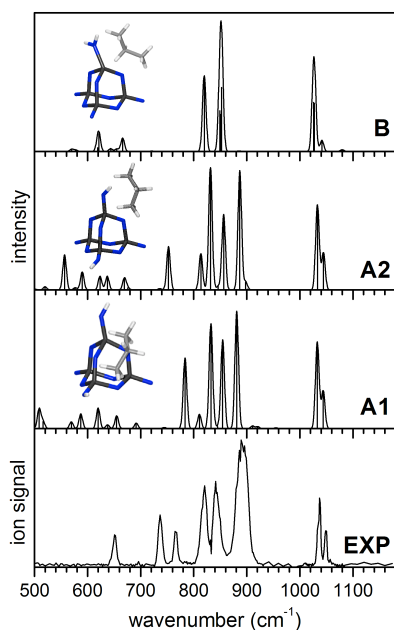


Fig. 6. Experimental IRPD spectrum (bottom) of $[\text{V}_4\text{O}_{10}\text{H}_2\cdot\text{C}_3\text{H}_8]^+$, after trapping mass-selected $\text{V}_4\text{O}_{10}^+$ ions (364 amu) at 100 K for 48 ms in the ion trap filled with a 0.002% propane in Helium gas mixture. Simulated linear IR absorption spectra, derived from B3LYP/TZVP harmonic frequencies and intensities, of three possible structural candidates, labeled B, A1 and A2, are also shown.

Structures A and B differ in the number of vanadyl groups present in the $[\text{V}_4\text{O}_{10}\text{H}_2]^+$ moiety. While structure A contains two vanadyl and two V-OH groups, structure B contains three vanadyl and one V-OH₂ group. Structures A1 and A2, on the other hand, differ in how the propane molecule is bound to the $[\text{V}_4\text{O}_{10}\text{H}_2]^+$ complex, which influences the orientation of the V-OH groups relative to each other. Comparison of the experimental to the simulated spectra clearly favors an assignment to structures A1 and A2 rather than B. The simulated spectrum of

B can neither account for the strongest absorption band at 889 cm^{-1} , nor for the two absorption bands in-between 730 and 780 cm^{-1} . In contrast, the A spectra do account for the absorption in these spectral regions and they also reproduce the relative intensities of the $\text{V}=\text{O}$ bands satisfactorily. The larger width ($\sim 25\text{ cm}^{-1}$) of the 889 cm^{-1} band compared to the other peaks ($<15\text{ cm}^{-1}$) in the experimental spectrum as well as the observation of two peaks of similar intensity in-between 730 and 780 cm^{-1} suggests that both isomers, A1 and A2, are formed and probed in the experiment. This is in agreement with calculated stabilities of A1 and A2, which differ by less than 1 kJ/mol , while B is 33 kJ/mol less stable. Several weaker absorption bands are predicted for all three structures below 700 cm^{-1} .

Based on these results and in combination with the calculations from A4 (Sauer/Döbler) the following reaction mechanism can be postulated (see Fig. 7).

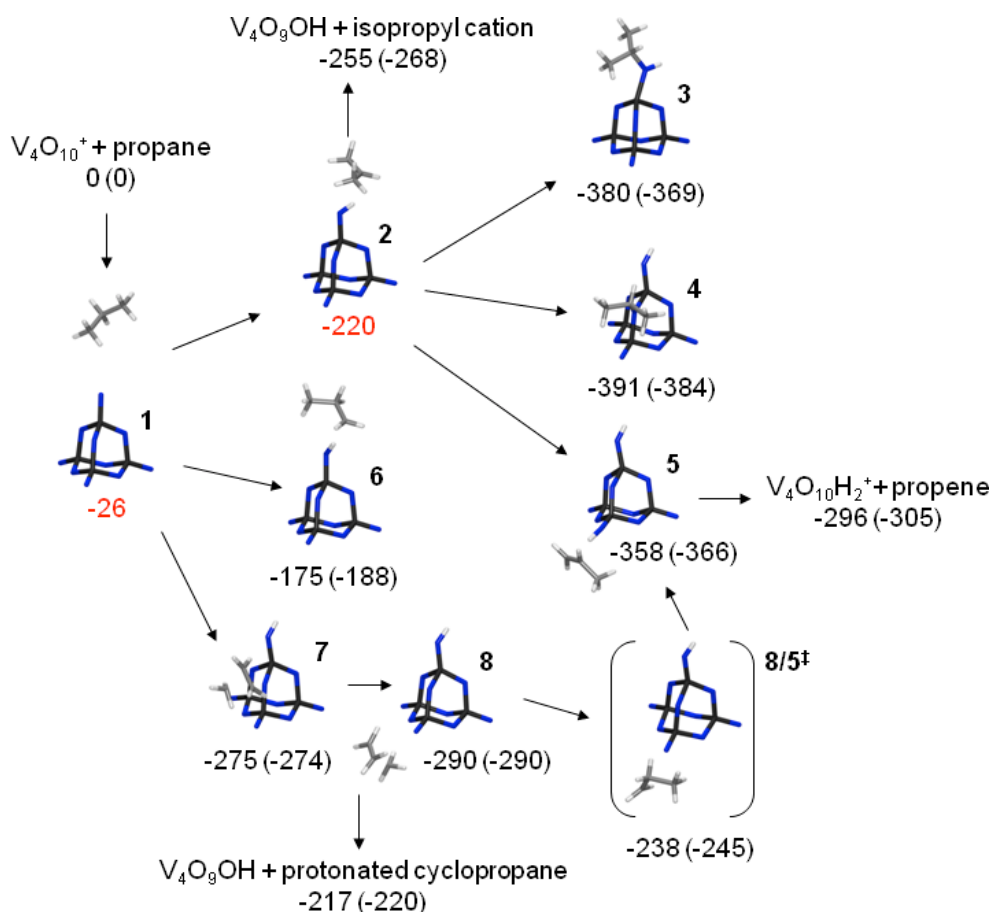


Fig. 7. Calculated B3LYP/TZVP energies (in kJ/mol) and structures and proposed reaction path for the formation of $\text{V}_4\text{O}_9(\text{OH}_2)(\text{C}_3\text{H}_8)^+$.

As $\text{V}_4\text{O}_{10}^+$ and C_3H_8 approach each other, hydrogen abstraction accompanied by electron transfer, i.e. hydride transfer, will occur without a barrier. The reaction system can follow several paths. (a) Direct dissociation leads to formation of C_3H_7^+ (+ $\text{V}_4\text{O}_9\text{OH}$) which is found

experimentally as one of the major products. (b) Abstraction of a second H-atom forms $[\text{V}_4\text{O}_{10}\text{H}_2]^+$ ($+ \text{C}_3\text{H}_6$) which is the dominant reaction observed in the experiment and selectively involves two vanadyl groups rather than a single one, as evidenced by the IRPD spectrum (structures A1 and A2 in Fig. 6). In the latter case a species containing an $-\text{OH}_2$ moiety would be formed (structure B in Fig. 6), which is neither observed in the experiment nor favored by the calculations.

Formation of propene is particularly probable for the case that the initial H-atom was abstracted from a secondary C-atom, in which case the process is effectively barrierless. Even though the binding energy of propene to $\text{V}_4\text{O}_8(\text{OH})_2^+$ is 62 kJ/mol, the reaction proceeds sufficiently fast compared to the cooling rate (10^4 s^{-1}) that the excess energy cannot be dissipated and the complex dissociates. Under the experimental conditions a vanadium oxide ion will, on average experience several collisions with propane molecules and these lead to the formation of the observed, weakly-bound ($\sim 29 \text{ kJ/mol}$ per propane molecule) $\text{V}_4\text{O}_8(\text{OH})_2^+ \cdot (\text{C}_3\text{H}_8)_{1,2}$ complexes, which can be stabilized by three-body collisions.

5.2.1.2 Photochemistry of Vanadium Oxide Cluster Ions

In order to compliment the previous gas phase studies on the thermal reactivity of cluster ions with hydrocarbons in their electronic ground state, a strategy was proposed for the final funding period that pursued the possibilities opened to photoinduced reactions driven by electronic excitation. This approach has generally been discussed in the framework of surface reactivity and catalysis but it is not commonly found in cluster reactivity studies or catalytic strategies [1,2]. In closing this gap in the investigation of vanadium oxide cluster reactivity, a unique possibility was seen to contribute to the general theme of the closing funding period in isolating structural motifs in vanadium oxide species that offer highly selective photoinduced reaction scenarios in their electronic activation. The thermal oxidation reactions with small hydrocarbons on mass-selected vanadium oxide cluster ions investigated by project A4 (Sauer/Döbler) and the former project A2 (Schwarz/Schröder) provided the motivation and background for the photochemical approach [3,4]. Moreover, the general theme innate to photo-catalysis in utilizing electronic excitation for controlling the redox potential of an active site was addressed [1,2].

Insight into the electronic and geometric structure of different vanadium oxide cluster ions necessary for approaching this strategy was provided by the combined efforts of the DFT analysis from project A4 (Sauer/Döbler) together with the IR spectroscopy of mass-selected cluster ions within this project [SBW08]. In this context, the $\text{V}_4\text{O}_{11}^-$ cluster ion was identified

as a highly interesting species for photochemical processes. Not only does this system provide a relationship to bulk material and surface structure with protruding vanadyl units joined by V-O-V bridge structures, the DFT analysis made in cooperation with project A4 (Sauer/Döbler) of the respective IRPD spectrum shows the possibility of different peroxy and dioxy motifs in the structure of this cluster ion. Hereby, the lowest energy dioxy species is derived from a closed superoxy bridge, which mimics oxygen activation on surface structures when opened from the superoxy to the lowest energy dioxy motif. This background provided the starting point for investigating photochemical processes associated with the reaction of the $V_4O_{11}^-$ system with small, unsaturated hydrocarbons such as propene.

A prerequisite for gas-phase studies on photoinduced reactivity is the formation of a structurally defined aggregate complex with the respective reactant for a clearly defined starting point of the photochemistry. The aggregation of propene on the $V_4O_{11}^-$ was accomplished and characterized as shown in the temperature-dependent aggregation kinetics in Fig. 8 [LDM11]. These were analyzed to understand the nature of the complex. Clearly, the temperature dependency of the aggregation process displayed in Fig. 8 violates Langevin theory for gas-phase ion-molecule reactions by showing increasing reaction rates for higher temperatures.

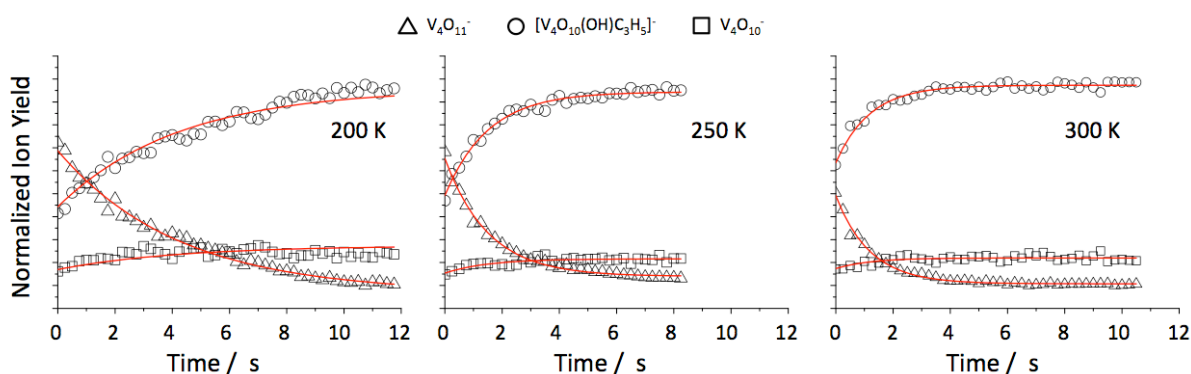
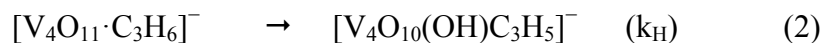


Fig. 8. Aggregation kinetics of propene on $V_4O_{11}^-$ at 200, 250 and 300 K. with $V_4O_{11}^-$ (triangles), $[V_4O_{10}(OH)C_3H_5]^-$ (circles) and $V_4O_{10}^-$ (squares) as well as the fit (red line) with the kinetic model given by reactions (1), (2) and (3).

Circumventing the necessity of stabilizing the collision complex by three-body collisions with the bath could be understood within the first two steps of the DFT model proposed by Tian and coworkers [16], which was motivated by the first report of the photochemistry on the $V_4O_{11}^-$ system from this project [LMD08]. Here, the reaction barrier associated with the irreversible hydrogen transfer reaction from propene to a vanadyl-moiety on the cluster site during the collision compensates coupling to the bath for achieving the aggregation of propene on the

cluster. This interpretation allows for the following model to be formulated for the reaction kinetics:



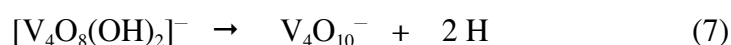
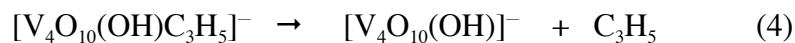
The work on collision-induced dissociation by the Castleman and coworkers on this system further allowed for the temperature-independent behavior of oxygen loss of $\text{V}_4\text{O}_{11}^-$ in the formation of $\text{V}_4\text{O}_{10}^-$ to be understood as an independent reaction channel [17].



From the model according to (1) - (3), an analytical solution for the reaction rates could be found, giving a reaction barrier of $E_a = 70.1 \pm 17.0$ meV for the hydrogen abstraction.. This barrier can be understood when considering the high stability of the transition state in generating the allyl radical species and its further binding to a terminal oxygen of the dioxo moiety in the $\text{V}_4\text{O}_{11}^-$ system. The high radical character on this site as derived by DFT calculations from project A4 (Sauer/Döbler) makes this a logical position for binding the allyl radical. In the formation of the $[\text{V}_4\text{O}_{10}(\text{OH})\text{C}_3\text{H}_5]^-$ aggregate complex, this covalent linkage of the hydrocarbon to the cluster and the general structure of the complex presents the defined starting point for the photoinduced reactivity studies [LDM11].

Approaching the photochemistry of this system, irradiation of the $[\text{V}_4\text{O}_{10}(\text{OH})\text{C}_3\text{H}_5]^-$ aggregate complex with ultraviolet femtosecond pulses centered at 272 nm (4.54 eV) with a pulse duration of 139 fs yields a range of cluster product species. Fig. 9 (left) shows the anionic mass spectrum obtained from the ion trap after irradiation for 500 ms at a pulse rate of 1 kHz. In order to distinguish what motivates the different cluster products seen in the mass range from 360 to 440 amu, the fluence of irradiation is varied over an order of magnitude from 8.07 to 80.7×10^{-2} J/cm² *i.e.* the number of photons supplied for the reaction is correlated to the yield of each reaction channel. Hereby, the photoexcitation at 272 nm (4.56 eV) can be assumed as a one-photon process considering the vertical detachment energy given by Sauer and coworkers at 6.66 eV for the $\text{V}_4\text{O}_{11}^-$ cluster system [SBW08]. From the tendency to higher fluence in the irradiation, two primary reaction channels can be identified. The channel of dissociation involves the cleavage of the C-O linkage of the hydrocarbon at the dioxo unit and the oxygenation channel is associated with the breaking of the V-O bond in linking the hydrocarbon to the cluster at the dioxo site. In the fluence dependency of these two reaction channels, the product yield nearly inverts in favor the oxygenation channel but interestingly,

the yield of the $[\text{V}_4\text{O}_8(\text{OH})_2]^-$ product remains small and is virtually constant in its ratio to the yield in $\text{V}_4\text{O}_{10}^-$. This was taken as a strong indication that the $[\text{V}_4\text{O}_8(\text{OH})_2]^-$ cluster is not the product of a independent reaction channel but rather coupled to the reaction pathway of $\text{V}_4\text{O}_{10}^-$ formation. From this and further analysis that will follow, the two observed photoinduced reaction channels (4) to (5) and (6) to (7) can be formulated as,



in which the loss of hydrogen from the respective cluster in (5) and (7) is motivated by substantial heating from a radiationless non-adiabatic transition into the electronic ground state or from sequential photoexcitation in the train of laser pulses exciting the sample.

At this stage, the experimental approach and analysis of the reactivity is within the standard methodology of tandem mass spectrometry and ion cluster reactivity studies. Within this funding period, the significant enhancement in achieving multi-photon ionization by employing ultraviolet femtosecond pulses allowed for the successful development of a fully novel capability in the analysis of cluster reactivity. When detecting the mass spectrum of the cationic species obtained from the reactor after irradiation, the low mass range clearly shows the capability to efficiently ionize and identify the neutral reaction participants *in situ* [LMD08, LDM11]. While standard techniques applied to analyzing cluster reactivity relate the mass difference observed in the cluster ion products to the formation of possible neutral products, this approach allows for direct verification of the neutral species through *in situ* multi-photon ionization into the cationic charge state with subsequent mass analysis. The results are shown in the intensity dependent mass spectra in Fig. 9 (right), where the product signals in the range between 37 and 42 amu relate to the dissociation channel of reaction (4) and the signals between 52 and 56 amu correlate to the oxygenation channel of reaction (6). Importantly, the diversity of signals in the later mass range indicates that the fragmentation accompanies the ionization of the neutral hydrocarbon product species. This was at first irritating since direct identification of the product stoichiometry is hindered by this effect but a highly fruitful exchange within the colloquia of the collaborative research center, particularly with the former project A2 (Schwarz/Schröder), lead to the realization that these fragmentation channels opens a more precise identification of the neutral reaction products [LMD08,

LDM11]. This was demonstrated in the neutralization-reionization experiments on the allyloxy anion performed by Schröder *et al.* which clearly shows the fragmentation associated with the ionization of the allyloxy radical to match the fragmentation pattern observed in the 52 to 56 mass range of the photoreaction [5].

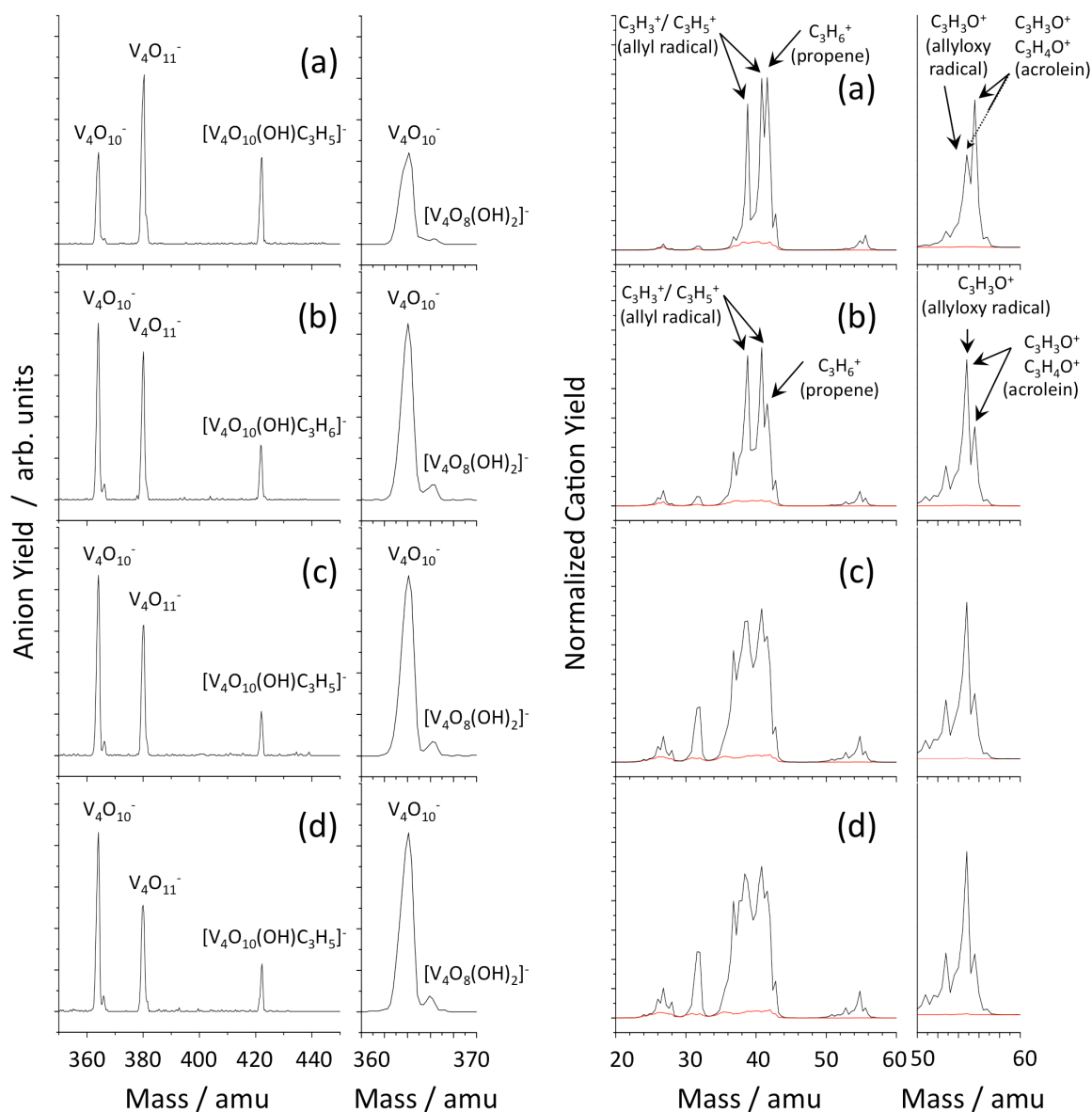


Fig. 9. Complimentary anionic (left) and cationic (right) mass spectrum obtained from the photoreaction of the $[V_4O_{10}(OH)C_3H_5]^-$ complex for 272 nm (4.56 eV) excitation at 139 fs pulse duration. **(left)** Anionic products, $V_4O_{11}^-$ (380 amu) and $V_4O_{10}^-$ (364 amu) as well as the $[V_4O_8(OH)_2]^-$ (366 amu) intermediate and $[V_4O_{10}(OH)C_3H_5]^-$ (422 amu) educt complex for varying fluence at (a) 8.70, (b) 34.8, (c) 60.9 and (d) $80.7 \times 10^{-2} \text{ J/cm}^2$. **(right)** Cationic mass spectrum of the neutral species from *in situ* multi-photon ionization and fragmentation at (a) 1.35, (b) 2.70, (c) 4.73 and (d) $6.75 \times 10^{10} \text{ W/cm}^2$ (black lines) and the background without $V_4O_{11}^-$ in the ion trap (red lines) with characteristic signals for the allyl radical (39, 41 amu) and propene (42 amu) as well as the allyloxy radical (55 amu) and acrolein (56, 55 amu).

the times scales of the characteristic structural dynamics were reviewed. The IR spectra acquired from a wide range of different gas-phase vanadium oxide ion species within the last two funding periods from this project were examined. While there are low frequency modes in these systems not characterized by the frequency range covered in the most of the IRPD spectra, the studies from project A2 (Schwarz/Schröder) and A4 (Sauer/Döbler) for this class of clusters clearly show that the high frequency modes largely dominated by the coordinates of the local stretch and bending vibrations of the vanadyl moieties as well as eventual peroxy and dioxy bonds are the most relevant for the reactivity of these systems [3,4,7]. An evaluation of the time-scale associated with these modes is given in Table 1.

Table 1. Characteristic frequencies in the vibrational modes of the V_4O_{11} cluster anion in the lowest energy dioxo $2A'$ (C_s) structure taken from [SBW08] with the translation to the respective time-scale for a vibrational period.

IRPD Frequency	DFT Assignment	Vibrational Period
999 cm^{-1}	V=O, Vanadyl (989 cm^{-1})	33 fs
990 cm^{-1}	V=O, Vanadyl (973 cm^{-1})	34 fs
976 cm^{-1}	V=O, Vanadyl (960 cm^{-1})	34 fs
899 cm^{-1}	V=O, Vanadyl (891 cm^{-1})	37 fs
874 cm^{-1}	V=O, Vanadyl (868 cm^{-1})	38 fs
824 cm^{-1}	V-O-V, Bridge (848, 834 cm^{-1})	41 fs
785 cm^{-1}	V-O-V, Bridge (732 cm^{-1})	43 fs
684 cm^{-1}	V-O-V, Bridge (672 cm^{-1}) or V-O, Dioxy (642 cm^{-1})	49 fs

The characteristic time scales can be summarized to take place in the sub 50 fs regime. An examination of the vibrational dynamics of hydrocarbons relevant for the reactivity underscores the lower end of this time scale as well as the expected dynamics associated with hydrogen transfer reactions. In order to address this challenging regime, the development of a laser source for meeting the necessary time resolution was approached in the last funding period. This was necessary since commercial amplified femtosecond laser sources based on titanium sapphire technology with the necessary pulse energies in the lower mJ to upper μJ regime are generally limited to pulse durations in the range of 30 fs. Since this time resolution is insufficient, a process for further pulse compression needed to be developed, starting from the parameters of the available laser system with pulse durations of 37 fs at 1.5 mJ per pulse centered at 800 nm. The general approach is based on previous work utilizing filamentation as a pulse compression mechanism together with standard chirped mirror compressors and a refined dispersion control with a spatial light modulator [SUM08]. The initial technique was expanded since it delivers sub 7 fs pulses primarily centered in the near infrared (1.54 eV), making ionization processes of hydrocarbons (at roughly > 9 eV) or photo-electron detachment (at roughly > 4 eV) and ionization processes (at roughly > 15 eV) in small vanadium oxide

cluster ions challenging. The focus of the laser source development was therefore placed on pushing the spectrum of the obtained pulses into the visible spectrum in order to reduce the nonlinearity required for these processes. This is achieved by a two-stage filamentation process with pulse compression after each stage yielding supercontinuum laser pulses with a coherent spectrum that spans over roughly 500 to 900 nm (2.48 – 1.38 eV) and a pulse compression into the 5 fs regime. A characteristic pulse obtained with this technique is shown in Fig. 10.

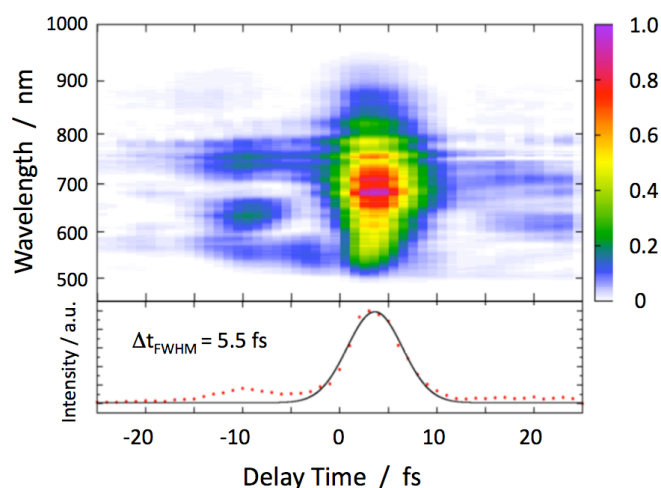


Fig. 10. Supercontinuum laser pulse obtained from multi-stage filamentation with chirped mirror compression after each stage and a final dispersion correction with a spatial light modulator.

The development of this laser source required the full funding period. While an application to cluster reactivity studies is now possible, the challenging development of this source has unfortunately not allowed for its application. Yet it should be noted that the parallel development of a technique offering the isomer identification of neutral reaction intermediates and products via *in situ* multi-photon ionization together with time-resolution and enhanced ionization efficiency offered by pulse durations in the 5 fs regime at ~ 100 μJ pulse energy offers a powerful technique for cluster reactivity studies. The framework of this collaborative research center has allowed for the parallel development of both aspects and this particular combination will allow for detailed mechanistic insight in future studies. The publication describing the development of this ultrafast white-light laser source is currently in preparation and will be submitted in the near future.

References

- [1] Garcia, H., J.M. Lopez-Nieto, E. Palomares, H.D. Roth, B. Solsona, J. Mater. Chem. **16** (2006) 216.
- [2] Linsebigler, A.L., G.Q. Lu, J.T. Yates, Chem. Rev. **95** (1995) 735.
- [3] Feyel, S., J. Döbler, D. Schröder, J. Sauer, H. Schwarz, Angew. Chem. Int. Ed. **45** (2006) 4681.
- [4] Rozanska, X., J. Sauer, Int. J. Quantum Chem. **108** (2008) 2223.
- [5] Schröder, D., H. Schwarz, J. Roithová, Int. J. Mass Spectrom. **301** (2011) 84.

- [6] Asmis, K.R., A. Fielicke, G. von Helden, G. Meijer, "Vibrational Spectroscopy of Gas-Phase Clusters and Complexes", in *The Chemical Physics of Solid Surfaces. Atomic Clusters: From Gas Phase to Deposited*, D.P. Woodruff, Editor. 2007, Elsevier: Amsterdam. p. 327.
- [7] Asmis, K.R., J. Sauer, *Mass Spectrom. Rev.* **26** (2007) 542.
- [8] Asmis, K.R., G. Meijer, M. Brümmer, C. Kaposta, G. Santambrogio, L. Wöste, J. Sauer, *J. Chem. Phys.* **120** (2004) 6461.
- [9] Sierka, M., J. Döbler, J. Sauer, G. Santambrogio, M. Brümmer, L. Wöste, E. Janssens, G. Meijer, K.R. Asmis, *Angew. Chem. Int. Ed.* **46** (2007) 3372.
- [10] Garand, E., D. Goebbert, G. Santambrogio, E. Janssens, P. Lievens, G. Meijer, D.M. Neumark, K.R. Asmis, *Phys. Chem. Chem. Phys.* **10** (2008) 1502.
- [11] Stubenrauch, J., E. Brosha, J.M. Vohs, *Catal. Today* **28** (1996) 431.
- [12] Ganduglia-Pirovano, M.V., C. Popa, J. Sauer, H. Abbott, A. Uhl, M. Baron, D. Stacchiola, O. Bondarchuk, S. Shaikhutdinov, H.J. Freund, *J. Am. Chem. Soc.* **132** (2010) 2345.
- [13] Sauer, J., J. Döbler, *Dalton Trans.* **19** (2004) 3116.
- [14] Feyel, S., D. Schröder, X. Rozanska, J. Sauer, H. Schwarz, *Angew. Chem. Int. Ed.* **45** (2006) 4677.
- [15] Feyel, S., D. Schröder, H. Schwarz, *J. Phys. Chem. A* **110** (2006) 2647.
- [16] Li, H.B., S.X. Tian, J.L. Yang, *J. Phys. Chem. A* **114** 6542.
- [17] Bell, R.C., K.A. Zemski, D.R. Justes, A.W. Castleman Jr., *J. Chem. Phys.* **114** (2001) 798.
- [BSW11] A.M. Burow, T. Wende, M. Sierka, R. Włodarczyk, J. Sauer, P. Claes, L. Jiang, G. Meijer, P. Lievens, K.R. Asmis
Structures and Vibrational Spectroscopy of Partially Reduced Gas-Phase Cerium Oxide Clusters
Phys. Chem. Chem. Phys., **13** (2011) 19393 – 19400.
- [LDM11] S. Li, J. Demuth, A. Mirabal, L. Wöste, T. Siebert
On the Role of Thermal Activation in Selective Photochemistry: Mechanistic Insight to the Oxidation of Propene on the $V_4O_{11}^-$
Phys. Chem. Chem. Phys., DOI: 10.1039/c1cp22550b

5.2.2 Projektrelevante eigene Publikationen

a) erschienene oder angenommene Arbeiten in wissenschaftlichen Zeitschriften oder Buchveröffentlichungen

- [JWC11] L. Jiang, T. Wende, P. Claes, S. Bhattacharyya, M. Sierka, G. Meijer, P. Lievens, J. Sauer, K.R. Asmis,
Electron Distribution in Partially Reduced Mixed Metal Oxide Systems: Infrared Spectroscopy of $Ce_mV_nO_o^+$ Gas-Phase Clusters
J. Phys. Chem. A **115** (2011) 11187 – 11192.
- [LCH10] L. Lin, P. Claes, T. Höltzl, E. Janssens, T. Wende, R. Bergmann, G. Santambrogio, G. Meijer, K.R. Asmis, M.T. Nguyen, P. Lievens
The Structure of Au_6Y^+ in the Gas Phase
Phys. Chem. Chem. Phys. **12** (2010) 13907 – 13913.

- [WDJ10] T. Wende, J. Döbler, L. Jiang, P. Claes, E. Janssens, P. Lievens, G. Meijer, K.R. Asmis, J. Sauer
Infrared Spectroscopic Characterization of the Oxidative Dehydrogenation of Propane by V_4O_{10}
Int. J. Mass Spectrom. **297** (2010) 102 – 106.
- [SJS08] G. Santambrogio, E. Janssens, S. Li, T. Siebert, G. Meijer, K.R. Asmis, J. Döbler, M. Sierka, J. Sauer
Identification of Conical Structures in Small Aluminum Oxide Clusters: Infrared Spectroscopy of $(Al_2O_3)_{1-4}(AlO)^+$
J. Am. Chem. Soc. **130** (2008) 15143 – 15149.
- [SBW08] G. Santambrogio, M. Brümmer, L. Wöste, J. Döbler, M. Sierka, J. Sauer, G. Meijer, K.R. Asmis
Gas Phase Infrared Spectroscopy of Vanadium Oxide Cluster Anions
Phys. Chem. Chem. Phys. **10** (2008) 3992 – 4005.
- [LMD08] S. Li, A. Mirabal, J. Demuth, L. Wöste, T. Siebert
A Complete Reactant-Product Analysis of the Oxygen Transfer Reaction in $[V_4O_{11} \cdot C_3H_6]^-$: A Cluster Complex for Modeling Surface Activation and Reactivity
J. Am. Chem. Soc. **130** 16832 (2008) 16832 – 3
- [SUM08] B. E. Schmidt, W. Unrau, A. Mirabal, S. Li, M. Krenz, L. Wöste, T. Siebert
Poor man's source for sub 7 fs: a simple route to ultrashort laser pulses and their full characterization
Opt. Express **16** (2008) 18910 – 21.

5.3 Rückblick auf die Förderung

Das Teilprojekt wurde seit 07/1999 im Sonderforschungsbereich gefördert. Es wurde mit Ablauf der 4. Förderperiode im Juni 2011 beendet.

5.3.1 Personal im Teilprojekt während der 4. Förderperiode

	lauf. Nr.	Name, akademischer Grad, Dienststellung	engere Fachzugehörigkeit	Institut der Hochschule oder der außeruniv. Einrichtung	Mitarbeit im Projekt Zeitraum, Wochenstunden	Entgeltgruppe
Grundausrüstung						
Wissenschaftlerinnen und Wissenschaftler	1.	Knut R. Asmis, Dr. habil.	Physikal. Chemie	FHI	07/1999 – 06/2011, 8 h	
	2.	Torsten Siebert, Dr.	Physik	FU-P	07/2009 – 07/2011, 10 h	
	3.	Ludger Wöste, Prof. Dr.	Physik	FU-P	07/1999 – 06/2011, 10 h	
	4.	Ling Jiang, Dr.	Physikal. Chemie	FHI	07/2009 – 07/2011, 20 h	
	5.	Shaohui Li, Dr.	Physik	FU-P	07/2008 – 10/2008, 38 h	
	6.	Oliver Gause	Physik	FU-P	07/2008 – 06/2011, 8 h	
nichtwissenschaftl. Mitarbeiterinnen und Mitarbeiter						
Ergänzungsausstattung						
Wissenschaftlerinnen und Wissenschaftler	1.	Torsten Wende, Dr.	Physik	FHI	04/2008 – 06/2010, 20 h	E13, 0,5
					07/2010 – 06/2011, 26,6 h	E13, 2/3
	2.	Franz Hagemann	Physik	FU-P	10/2009 – 06/2011, 20 h	E13, 0,5
	3.	Cristina Stancka-Kaposta, Dr.	Physik	FU-P	07/2008 – 09/2009, 26,6 h	E13, 2/3
4.	Shaohui Li, Dr.	Physik	FU-P	11/2006 – 06/2008, 38 h	E13	
nichtwissenschaftl. Mitarbeiterinnen und Mitarbeiter						

Aufgaben der Mitarbeiterinnen und Mitarbeiter (Grundausrüstung):

1. Dr. habil. Knut Asmis
Teilprojektleiter, wissenschaftliche Gesamtleitung und Koordination. Herr Asmis betreut die IR-Photodissoziationsexperimente, sowie einen der Doktoranden aus der EA.
2. Dr. Torsten Siebert
Teilprojektleiter, wissenschaftliche Leitung und Koordination. Herr Siebert betreut die Femtosekunden-Reaktivitätsexperimente und Entwicklung der Superkontinuuum-Laserquelle sowie Post-Doktoranden und Doktoranden aus der GA und EA.
3. Prof. Dr. Ludger Wöste
Teilprojektleiter, wissenschaftliche Koordination der IR-Photodissoziationsexperimente und Femtosekunden-Reaktivitätsexperimente.
4. Dr. Ling Jiang
Post-Doc aus GA, Koordination und Durchführung der IR-Photodissoziationsexperimente sowie Rechnungen an Metalloxidclustern.
5. Dr. Shaohui Li
Post-Doc aus GA, Koordination und Durchführung von Femtosekunden-Reaktivitätsexperimenten an Metalloxidclustern.
6. Oliver Gause
Doktorand aus GA, Durchführung von Femtosekunden-Reaktivitätsexperimenten an Silsesquioxan-Oxovanadiumkomplexen in Kooperation mit Projekt B5 (Limberg).

Aufgaben der Mitarbeiterinnen und Mitarbeiter (Ergänzungsausstattung):

1. Torsten Wende
Der Doktorand hat im Rahmen seiner Dissertationsarbeit die IR-Photodissoziationsexperimente an Metalloxidclustern durchgeführt.
2. Dr. Cristina Stanca-Kaposta
Die Post-Doktorandin hat eine alternative Methode für die Synthese anionischer Vanadiumoxid-Cluster entwickelt. Im Wechsel von einer Laserablationsquelle zu einer Magnetron-Sputterquelle konnten höhere Ionenströme und Stabilität in der Synthese von Vanadiumoxid-Clustern erzielt werden.

3. Franz Hagemann

Im Rahmen seiner derzeitigen Promotion wurde eine Supercontinuum-Laserquelle für zeitaufgelöste Reaktivitätsexperimente entwickelt. Das optische Verfahren ermöglicht eine Kompression der Pulsdauer in den Bereich von $\Delta\tau_{\text{FWHM}} = 5$ fs und eine Erweiterung der Bandbreite auf $\Delta\lambda = 500\text{-}900$ nm mit 100 $\mu\text{J}/\text{Puls}$ ausgehend von einem Femtosekunden-Verstärkersystem mit Standard-Ausgangsparameter ($\Delta\tau_{\text{FWHM}} = 40$ fs, $\lambda_{\text{center}} = 805$ nm, $\Delta\lambda_{\text{FWHM}} = 40$ nm, 1.5 mJ/Puls).

4. Dr. Shaohui Li

Post-Doc, Koordination und Durchführung von Femtosekunden-Reaktivitätsexperimenten an Metalloxidclustern.

5.1 Allgemeine Angaben zum Teilprojekt A4

5.1.1 Titel: Struktur und Reaktivität unterschiedlicher Übergangsmetalloxiid-Aggregate mit quantenchemischen Methoden

5.1.2 Projektleitung

Prof. Dr. Joachim Sauer
geb. 19.04.1949

Institut für Chemie
Humboldt-Universität zu Berlin
Unter den Linden 6
10099 Berlin
Telefon: 030 / 30 2093-7141
E-Mail: js@chemie.hu-berlin.de

PD Dr. Marek Sierka
geb. 04.07.1971

030 / 30 2093-7477
marek.sierka@chemie.hu-berlin.de

ausgeschieden:
Dr. Jens Döbler, geb. 13.02.1972

5.2 Entwicklung des Teilprojekts

5.2.1 Bericht

The very fruitful cooperation with the project A3 in the structure determination of gas-phase metal oxides clusters has been continued. Structure information has been obtained on mono- and divanadium oxide cluster cations [1], and on vanadium oxide anions [SBW08], [2]. Among the latter were polyhedral vanadium oxide cages, $V_4O_{10}^-$, $V_6O_{15}^-$, $V_8O_{12}^-$, for which size-induced d-electron localization has been observed [2]. It has been demonstrated that successful structure determination of gas-phase clusters can often be achieved only by combining global structure optimization by quantum mechanical methods (this project) with spectroscopic experiments (A3).

5.2.1.1 Structure and spectra of gas phase clusters

Partially reduced cerium oxide clusters. Clusters involving main group and transition metal oxides often display unusual structural features very different from those of their bulk phases [S JL08, SBW08, SDS09]. Our computational investigations combined with experimental studies performed within the project A3 demonstrated that for the rare-earth metal cerium the most stable oxide gas-phase aggregates show structural motifs reminiscent of the bulk ceria [BSW11]. The structures of partially reduced $Ce_2O_2^+$, $Ce_3O_4^+$, and $(CeO_2)_mCeO^+$ clusters

($m = 0-4$) were identified by the combination of global *ab initio* structure optimizations and IR vibrational predissociation (IRVPD) spectroscopy of the cluster-rare gas atom complexes. The most stable structures of Ce_2O_2^+ (**2-2**, Fig. 1) and Ce_2O_3^+ (**2-3**) exhibit a Ce–O–Ce–O four-membered ring with characteristic absorptions between 430 and 680 cm^{-1} . The most stable isomer of Ce_3O_4^+ (**3-4**, Fig. 1) contains three four-membered rings forming three faces of a rhombohedral prism. For Ce_3O_5^+ multiple isomers could be observed (**3-5a** and **3-5b**, Fig. 1). Their individual infrared signatures were identified by tuning their relative population through the choice of Ne and Ar messenger atoms. The structures of the most stable Ce_4O_7^+ and Ce_5O_9^+ clusters (**4-7** and **5-9** in Fig.1, respectively) have common structural features containing fused Ce–O–Ce–O four-membered rings which lead to intense absorption bands around 500 and 650 cm^{-1} . As a common feature all clusters containing a terminal Ce=O bond show a characteristic absorption band between 800 and 840 cm^{-1} . Since these clusters and the bulk cerium oxide exhibit consistent structural features we are convinced that our results provide quite unexpected insight into the intrinsic properties of these systems. This key finding serves also as a strong argument for the comparison of the reactions on gas-phase cerium oxide clusters with catalytic processes on ceria surfaces. In addition, the present results allow to benchmark different DFT functionals which differ in the prediction of the degree of localization of unpaired electrons in Ce 4f states.

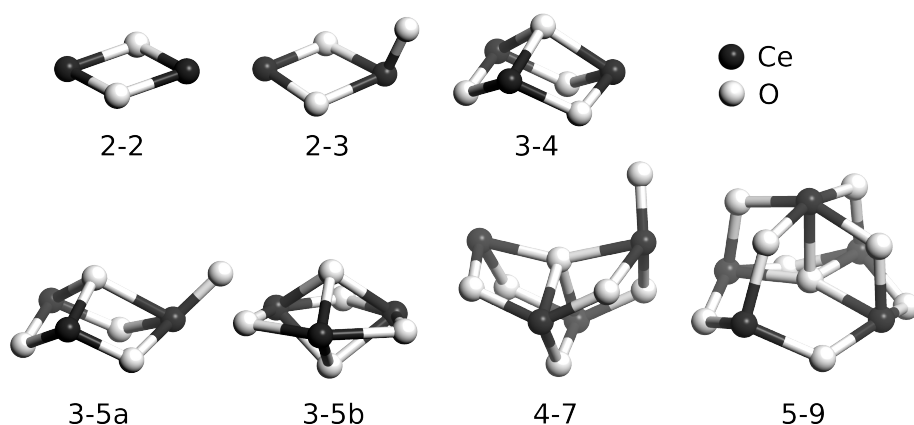


Fig. 1. Structures of the most stable, partially reduced cerium oxide clusters: Ce_2O_2^+ (**2-2**), Ce_2O_3^+ (**2-3**), Ce_3O_4^+ (**3-4**), Ce_3O_5^+ (**3-5a** and **3-5b**), Ce_4O_7^+ (**4-7**) and Ce_5O_9^+ (**5-9**).

Partially reduced mixed cerium and vanadium oxide clusters. For vanadia supported on ceria, the catalytic activity is particularly high. Although cerium oxide has been known for its ability to store, release, and transport oxygen ions for a long time, only recently investigations of model vanadia/ceria catalysts have shown that this remarkable activity is due to the ability of ceria to easily accommodate electrons in localized f orbitals of Ce. In order to shed light on the role of the two metals in the partial reduction of a mixed metal oxide system combined computational and experimental studies of partially reduced $[(\text{CeO}_2)(\text{VO}_2)_{1-2}]^+$ and $[(\text{Ce}_2\text{O}_3)(\text{VO}_2)]^+$ clusters were performed in collaboration with the project A3 [JWC11].

The experimental IRVPD spectra of the cerium vanadium oxide cluster cations were well reproduced by the simulated IR spectra of the lowest energy isomer predicted by DFT calculations using the B3LYP hybrid functional. This confirms that the B3LYP functional properly localizes electrons in the investigated gas-phase Ce-containing binary metal oxide clusters. Experimental evidence was found for the predicted larger stability of $\text{Ce}^{3+}/\text{V}^{5+}$ compared to that of $\text{Ce}^{4+}/\text{V}^{4+}$. Crucial differences were found with respect to the relative reducibility in different binary metal vanadium oxide clusters. Whereas in the vanadia-ceria clusters Ce^{4+} is easily reduced to Ce^{3+} , stabilizing the V^{5+} center, in vanadia-titania clusters, reduction of Ti^{4+} to Ti^{3+} is competitive with that of V^{5+} to V^{4+} , and in vanadia-silica clusters, Si^{4+} cannot be reduced. These results confirm that an easily reducible support material, like ceria, may serve as an electron acceptor for the electron transferred to the active site in the rate-determining step. Hence, IRVPD spectroscopy on electronically tailored binary metal oxide clusters, combined with properly chosen quantum chemical calculations, may contribute to the understanding of complex solid catalysts.

Aluminum oxide clusters. The structure identification of $(\text{Al}_2\text{O}_3)_n\text{AlO}^+$, $n = 1-4$, cluster ions [SJL08] is another example of successful cooperation with the project A3 and application of the genetic algorithm. Here, a combination of HAGA calculations and IRVPD spectroscopy of ion complexes with He has been used. The global minima of all four clusters found in the HAGA calculations differ considerably from bulk alumina structures (Fig. 3). They all contain 3-fold coordinated aluminum, reminiscent of the undercoordinated Al-atoms found at the surfaces of alumina polymorphs, but not in their bulk structures. For $n = 1$ and $n = 4$ only a single, exceptionally stable structure is found (**1** and **4** in Fig. 3). Both clusters show conical structure of C_{3v} symmetry, which is separated from the next lowest isomers by at least 70 kJ/mol. However, for $n = 2$ and $n = 3$ even the combined theory/experiment approach reaches its limits. In case of $n = 2$ a C_s symmetric cage-like structure (**2A** in Fig. 3) is predicted to be

more stable than a sheet-like structure with C2 symmetry (**2B** in Fig. 3), but the best estimate for the energy difference between the two structures is only 2.7 kJ/mol. For $n = 3$, HAGA calculations yield two different structure types. For both, different variants exist, that differ either in the position of the He atom or constitute distorted versions of the same structure type. One type is a cage-like ion (**3A** and **3B** in Fig. 3) and the other sheet-like, with two slightly buckled sheets forming an angle of about 90° (**3C** in Fig. 3). At the DFT level **3C** is the most stable structure, followed by **3B** (+17 kJ/mol) and **3A** (+22 kJ/mol). However, the stability sequence changes when wave function based methods (MP2) are used instead of DFT. At the MP2 level all three structures show similar stability with **3B** predicted as the most stable structure, followed now by **3A** (+1 kJ/mol) and **3C** (+7 kJ/mol). While the characteristic features in IRVPD spectra can be assigned assuming a single **3A** isomer, a slightly better agreement is achieved, when a 3:1 mixture of **3A** and **3B** is assumed. Interestingly, the spectrum of **3C**, the global minimum at the DFT level, does not fit the experimental spectrum.

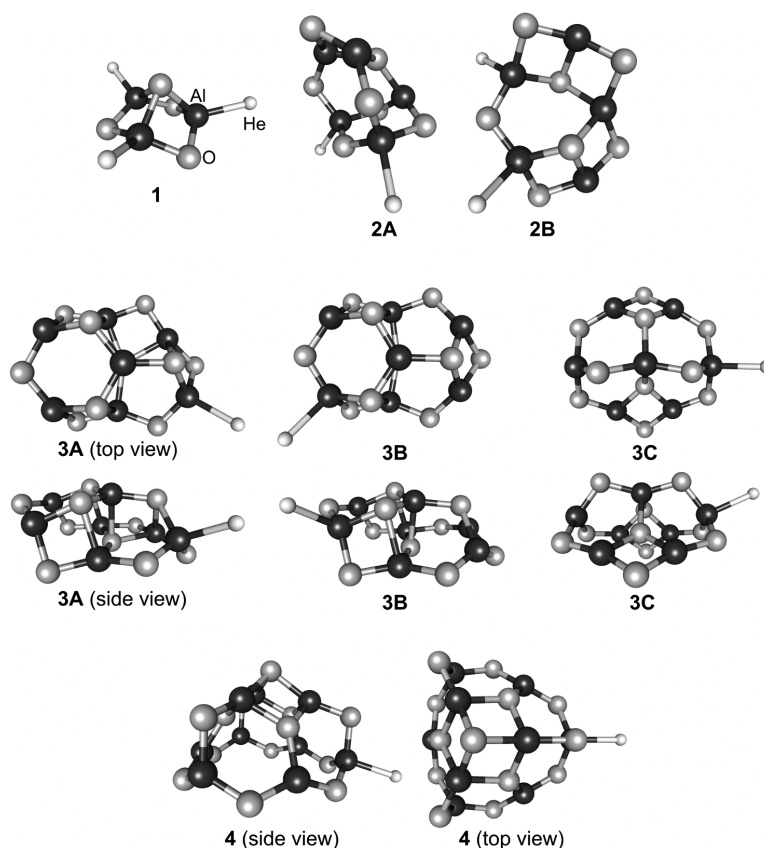


Fig. 2. Calculated structures of low-energy isomers of the complexes of $(\text{Al}_2\text{O}_3)_{1-4}\text{AlO}^+$ clusters with He atoms, $(\text{Al}_2\text{O}_3)_1\text{AlO}\cdot 3\text{He}^+$ (**1**), $(\text{Al}_2\text{O}_3)_2\text{AlO}\cdot 2\text{He}^+$ (**2A** and **2B**), $(\text{Al}_2\text{O}_3)_3\text{AlO}\cdot \text{He}^+$ (**3A**, **3B** and **3C**) and $(\text{Al}_2\text{O}_3)_4\text{AlO}\cdot \text{He}^+$ (**4**).

The studies of aluminum oxide clusters show that the main experimental as well as theoretical limitation is the cluster size. First, the accuracy of theoretical methods, particularly DFT is often not high enough to discriminate between isomers of the same cluster with similar stabilities. For larger clusters, the size and low symmetry make higher level and more accurate calculations prohibitively expensive, so that a definitive answer about the global minimum cannot be based on the calculations. Second, the resolution of the experimental spectra may be insufficient to deduce if a single isomer, several stable isomers or a single one that is quickly interconverting via a low-energy barrier transition state is actually observed.

Electron localization–delocalization isomerism in the $[(\text{Al}_2\text{O}_3)_2]^-$ Anion Cluster. In cooperation with the group of Lai-Sheng Wang from the Washington State University the structures of the $[(\text{Al}_2\text{O}_3)_2]^{0/-}$ clusters were determined by combining photoelectron spectroscopy (PES) and global structure optimization using DFT [SDS09]. The $[(\text{Al}_2\text{O}_3)_2]^-$ cluster anion shows energetically close lying but structurally distinct sheet-like and cage isomers which differ by localization/delocalization of the extra electron (Fig. 3). The experimental results were crucial for benchmarking the different computational methods applied with respect to a proper description of electron localization and the relative energies for the isomers which is of considerable value for future computational studies of aluminum oxide and related systems.

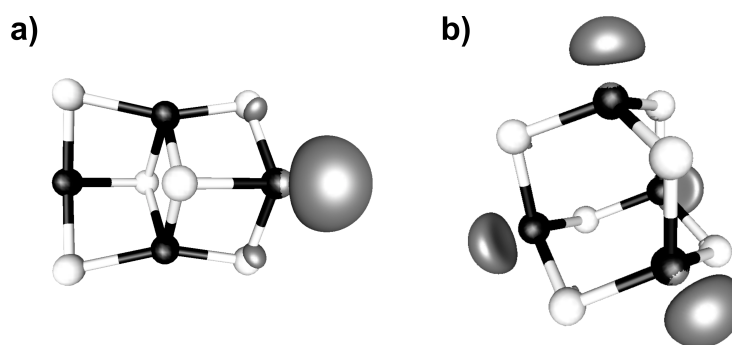


Fig. 3. Optimized structures of $[(\text{Al}_2\text{O}_3)_2]^{0/-}$ clusters along with isosurface plots of spin density for $[(\text{Al}_2\text{O}_3)_2]^-$ cluster anions. a) The C_s symmetric sheet-like structure (unpaired electron of cluster anion localized on one Al atom). b) The T_d symmetric cage structure (unpaired electron of cluster anion delocalized over all four Al atoms). Al black, O gray, spin density dark gray.

5.2.1.2 Gas phase reactivity

The $V_3O_7^+$ cluster, which can also be written $(V_2O_5)VO_2^+$, is a closed shell cation and has the same $V=O$ bond as active site. Therefore, it is a suitable gas phase model for vanadia particles on supporting oxides and we have studied the mechanisms of its reaction with propane in detail [RS09]. The differences and similarities of the reaction mechanism for this system and $O=V(O)_3$ sites supported on silica (Fig. 4) tell us what we can learn about surface reactions from gas phase experiments.

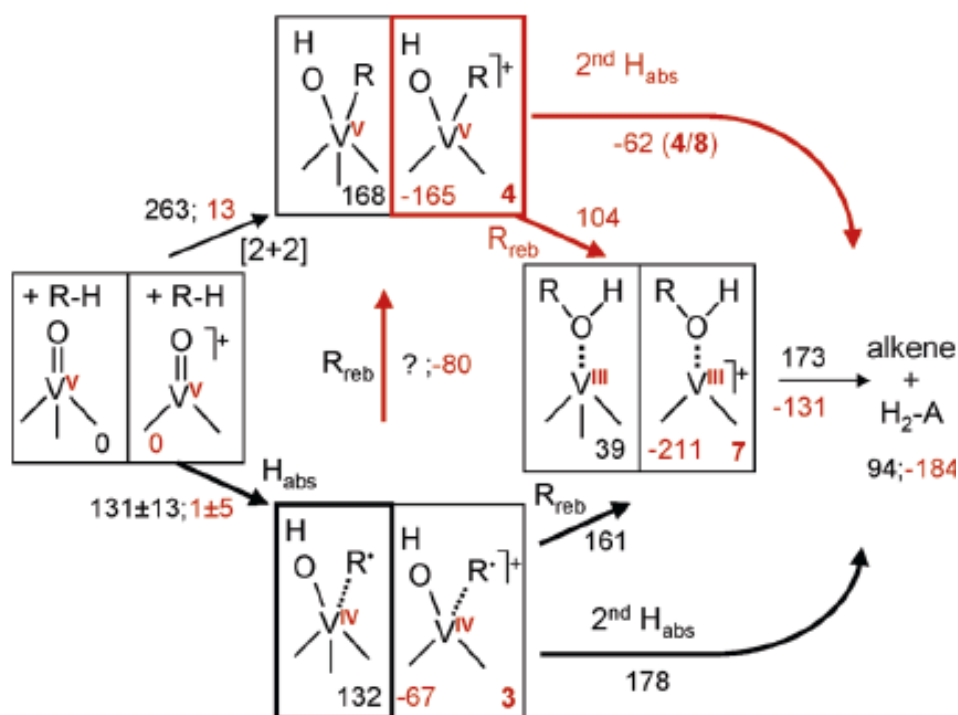
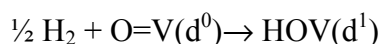


Fig. 4. Comparison of $O=V(O)_3$ surface sites (left boxes) with $V_3O_7^+$ gas phase species (right boxes) in the ODH of propane. H_2-A is the reduced catalyst. Energies of intermediates (within the boxes) and of transition structures near the arrows are E_0 in $\text{kJ}\cdot\text{mol}^{-1}$, first/top figures for $O=V(O)_3$ surface sites, second/bottom figures for $V_3O_7^+$ gas phase ions.

The first difference is in *the binding of the substrate*, which is much stronger with cations. Even for similar *intrinsic* barriers for $V_3O_7^+$ and $O=V(OSi\equiv)_3$ sites for the same initial H abstraction (108 ± 5 vs. 132 ± 13 $\text{kJ}\cdot\text{mol}^{-1}$) the *apparent* barriers become vastly different (1 ± 5 compared to 132 ± 13 $\text{kJ}\cdot\text{mol}^{-1}$, Fig. 4). We should not forget, however, that gas phase reactions can *only* be observed if the (Gibbs free) energies of the transition structures (TS) are below those of the reactants (negative apparent barriers), whereas substantial barriers can be

surmounted (depending on temperature) in condensed phase. The formation of the diradical intermediate $R^{\bullet}\cdots HOV(d^1)$ from the addition complex $RH\cdots O=V(d^0)$, requires more energy for $O=V(OSi\equiv)_3$ sites ($132\text{ kJ}\cdot\text{mol}^{-1}$) than for $V_3O_7^+$ ($40\text{ kJ}\cdot\text{mol}^{-1}$). The difference of $92\text{ kJ}\cdot\text{mol}^{-1}$ is largely due to the $112\text{ kJ}\cdot\text{mol}^{-1}$ difference between the hydrogenation energies,



After the initial H abstraction all subsequent TS have lower energies in the $V_3O_7^+$ case, contrary to what happens for the $O=V(OSi\equiv)_3$ surface site. There are electronic reasons for this, as indicated by the large difference in the reaction energies (-184 vs. $94\text{ kJ}\cdot\text{mol}^{-1}$), but there are also steric reasons. A very stable $[2+2]$ CH addition complex, $R(HO)V$, can be formed at the $O=V^+(O^-)_2$ site of $V_3O_7^+$ ($-165\text{ kJ}\cdot\text{mol}^{-1}$, Fig. 4) extending the coordination on V from 3 to 4, whereas such an addition product on the $O=V(OSi\equiv)_3$ surface site (five-fold coordination on V including one isopropyl ligand) is unstable ($168\text{ kJ}\cdot\text{mol}^{-1}$, Fig. 4). This $[2+2]$ CH addition complex is a central intermediate in the reactions with $V_3O_7^+$ from which the ODH products can be reached on different pathways.

Compared to $V_3O_7^+$, the $V_4O_{10}^+$ cation is a completely different case. Its $V=O$ bond dissociation energy is pathologically low because, on ionization of V_4O_{10} , an electron is removed from the $V=O$ bond and a $V^{(+)}-O^{\bullet}$ species with an oxyl radical site is created. It is obvious that the redox properties of a radical cation are different from that of a closed shell system, and it does not come as surprise that such species are much more reactive than closed shell species and abstract hydrogen even from methane [3]. In collaboration with TP A3, we studied the reaction of $V_4O_{10}^+$ with propane and we found that $V_4O_{10}^+$ readily abstracts hydrogen [WDJ10]. Two main reaction pathways have been identified: (i) oxidative dehydrogenation forming $V_4O_8(OH)_2^+ +$ propene and (ii) direct dissociation leading to formation of $C_3H_7^+ + V_4O_9OH$. Formation of propene is particularly probable for the case that the initial H-atom was abstracted from a secondary C-atom, in which case the process is effectively barrierless. In this experiment additional structural information could be gained from vibrational spectroscopy and quantum chemistry compared to a purely mass spectrometric characterization.

5.2.1.3 Mechanism for the oxidation of hydrocarbons on transition metal oxide surface sites

Methanol oxidation on molybdena sites. For isolated molybdenum oxide species on silica we found that the methanol oxidation proceeds with the same fundamental steps (dissociative

addition of methanol followed by hydrogen abstraction) as for vanadium oxide species on silica [GDS10]. However, the details differ between monooxo and dioxo species. In the former case, the first step leads to cleavage of a Mo-O-Si bond and formation of a surface molybdenum methoxide species. Hydrogen is then abstracted from the methoxide ligand by a terminal oxo ligand in a process entailing a closed-shell transition structure. In contrast, the preferred mechanism on the dioxomolybdenum species involves an addition of the methanol OH group onto one of the M=O double bonds leading to a hydroxomolybdenum methoxide intermediate. The hydrogen abstraction in the second step is effected by the hydroxide ligand formed in the first step and proceeds via an open-shell singlet transition structure [GDS10].

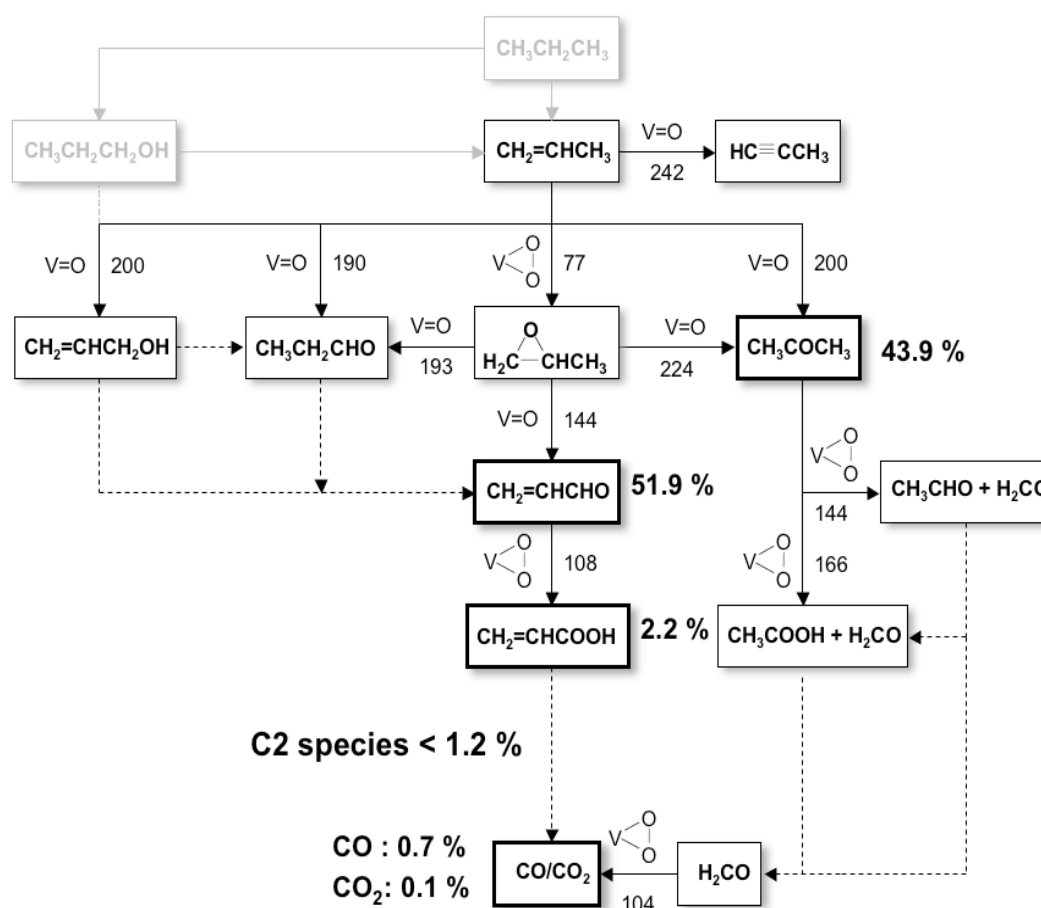


Fig. 5. Free energy barriers (kJ/mol) for elementary steps in the deep oxidation of propane. As active sites both vanadyl ($\text{V}=\text{O}$) and peroxo vanadate (VO_2) species are considered. The compounds identified as products under specific reaction conditions (300 °C) are indicated in bold print with the percentage found (ref. [4]).

Reoxidation step. A DFT study of the reoxidation process [RKS08] showed that peroxovanadates as precursors of vanadyl species are formed on reoxidation of reduced vanadium oxide species with O_2 , but not with N_2O . Peroxovanadates were found highly

reactive for propene oxidation. The absence of peroxovanadates may explain the superior selectivity of N_2O compared with O_2 in the oxidative dehydrogenation reaction over highly dispersed vanadia species.

Deep oxidation of propane. Understanding of the selectivity for propene ultimately requires knowledge of all elementary steps down to the total oxidation products CO and CO_2 . Fig. 5 shows the results of DFT calculations using the same silsesquioxane model as used for the formation of propane. Peroxo species, formed on re-oxidation are also participating in the reaction network. Quantitative comparison with specific experiments requires a microkinetic simulation, but as a first confirmation for the DFT results (Fig. 5) we mention that compounds occurring in Fig. 5 have been identified in two different experiments under different conditions. Whereas in the experiment of Zhao und Wachs [4] at 300 °C acrolein and acetone are the main products, the experiment of Hess et al. was conducted in such a way that acrylic acid was the major product (TP B2) [5]. Beyond such qualitative analysis, these results present a valuable data base for future microkinetic simulations for specific experimental conditions.

References

- [1] K. Asmis, G. Meijer, M. Brümmer, C. Kaposta, G. Santambrogio, L. Wöste, J. Sauer; Gas Phase Infrared Spectroscopy of Mono- and Divanadium Oxide Cluster Cations; *J. Chem. Phys.* **2004**, *120*, 6461-6470.
- [2] K. R. Asmis, G. Santambrogio, M. Brümmer, J. Sauer; Polyhedral Vanadium Oxide Cages: Infrared Spectra of Cluster Anions and Size-Induced d-Electron Localization; *Angew. Chem.* **2005**, *117*, 3182-3185.
- [3] S. Feyel, J. Döbler, D. Schröder, J. Sauer, H. Schwarz; Thermal Activation of Methane by Tetranuclear $[\text{V}_4\text{O}_{10}]^+$; *Angew. Chem., Int. Ed.* **2006**, *45*, 4681-4685.
- [4] C. Zhao, I. E. Wachs; Selective oxidation of propylene over model supported V_2O_5 catalysts: Influence of surface vanadia coverage and oxide support; *J. Catal.* **2008**, *257*, 181-189.
- [5] C. Hess, M. H. Looi, S. B. A. Hamid, R. Schlögl; Importance of nanostructured vanadia for selective oxidation of propane to acrylic acid; *Chem. Commun.* **2006**, 451-453.

5.2.2 Projektrelevante eigene Publikationen

a) erschienene oder angenommene Arbeiten in wissenschaftlichen Zeitschriften oder Buchveröffentlichungen

- [FDH08] S. Feyel, J. Döbler, R. Höckendorf, M. K. Beyer, J. Sauer und H. Schwarz, *Activation of Methane by Oligomeric $(Al_2O_3)_n^+$ ($n = 3, 4, 5$): The Role of Oxygen-Centered Radicals in Thermal Hydrogen-Atom Abstraction*; *Angew. Chem. Int. Ed.* **47** (2008) 1946-1950.
- [SBW08] G. Santambrogio, M. Brümmer, L. Wöste, J. Döbler, M. Sierka, J. Sauer, G. Meijer, K. R. Asmis; *Gas phase vibrational spectroscopy of mass-selected vanadium oxide anions*; *Phys. Chem. Chem. Phys.* **10** (2008) 3992-4005.
- [S JL08] G. Santambrogio, E. Janssens, S. H. Li, T. Siebert, G. Meijer, K. R. Asmis, J. Döbler, M. Sierka, J. Sauer; *Identification of Conical Structures in Small Aluminum Oxide Clusters: Infrared Spectroscopy of $(Al_2O_3)_{1-4}(AlO)^+$* ; *J. Am. Chem. Soc.* **130** (2008) 15143-15149.
- [RKS08] X. Rozanska, E. V. Kondratenko, J. Sauer; *Oxidative dehydrogenation of propane: Differences between N_2O and O_2 in the reoxidation of reduced vanadia sites and consequences for selectivity*; *J. Catal.* **256** (2008) 84-94.
- [ZDS08] H.-J. Zhai, J. Döbler, J. Sauer and L.-S. Wang; *Electronic Structure of Early Transition Metal Oxide Clusters: Polyhedral Cages of $(V_2O_5)_n^-$ ($n = 2-4$) and $(M_2O_5)_2^-$ ($M = Nb, Ta$)*; *J. Am. Chem. Soc.* **130** (2008) 15143 - 15149.
- [RS09] X. Rozanska, J. Sauer; *Oxidative Dehydrogenation of Hydrocarbons by $V_3O_7^+$ Compared to Other Vanadium Oxide Species*; *J. Phys. Chem. A* **113** (2009) 11586-11594.
- [BSD09] A. M. Burow, M. Sierka, J. Döbler, J. Sauer; *Point Defects in CaF_2 and CeO_2 Investigated by the Periodic Electrostatic Embedded Cluster Method*; *J. Chem. Phys.* **130** (2009) 174710-1 - 174710-11.
- [SDS09] M. Sierka, J. Döbler, J. Sauer, H.-J. Zhai, L.-S. Wang; *The $[(Al_2O_3)_2]^-$ Anion Cluster: Electron Localization-Delocalization Isomerism*; *ChemPhysChem* **10** (2009) 2410-2413.
- [WDJ10] T. Wende, J. Döbler, L. Jiang, P. Claes, E. Janssens, P. Lievens, G. Meijer, K.R. Asmis, J. Sauer; *Infrared spectroscopic characterization of the oxidative dehydrogenation of propane by $V_4O_{10}^+$* ; *Int. J. Mass Spectrom.* **297** (2010) 102-106.

- [GDS10] L. J. Gregoriades, J. Döbler, J. Sauer;
Oxidation of Methanol to Formaldehyde on Silica-Supported Molybdena: Density Functional Theory Study on Models of Mononuclear Sites;
J. Phys. Chem. C **114** (2010) 2967-2979.
- [BSW11] A. M. Burow, M. Sierka, R. Wlodarczyk, J. Sauer, T. Wende, P. Claes, L. Jiang, G. Meijer, P. Lievens, K. R. Asmis;
Structures and vibrational spectroscopy of partially reduced gas-phase cerium oxide clusters;
Phys. Chem. Chem. Phys. **13** (2011) 19393-19400.
- [JWC11] L. Jiang, T. Wende, P. Claes, S. Bhattacharyy, M. Sierka, G. Meijer, P. Lievens, J. Sauer, K. R. Asmis;
Electron distribution in partially reduced binary metal oxide systems: $Ce_nV_mO_o^+$ gas phase clusters;
J. Phys. Chem. A **115** (2011) 11187-11192.

5.3 Rückblick auf die Förderung

Das Teilprojekt wurde seit 07/1999 im Sonderforschungsbereich gefördert. Es wurde mit Ablauf der 4. Förderperiode im Juni 2011 beendet.

5.3.1 Personal im Teilprojekt während der 4. Förderperiode

	lauf. Nr.	Name, akademischer Grad, Dienststellung	engere Fachzugehörigkeit	Institut der Hochschule oder der außeruniv. Einrichtung	Mitarbeit im Projekt Wochenstunden, Zeitraum	Entgeltgruppe
Grundausrüstung						
Wissenschaftlerinnen und Wissenschaftler	1.	Joachim Sauer, Dr., Univ.-Prof.	Theoret. Chemie	HU-C	8h, 07/1999 – 06/2011	
	2.	Jens Döbler, Dr.	Theoret. Chemie	HU-C	30h, 03/2002 – 07/2008	
	3.	Marek Sierka, Dr., PD	Theoret. Chemie	HU-C	10h, 04/2004 – 06/2011	
	4.	Laurence Gregoriades, Dr.	Theoret. Chemie	HU-C	30h, 04/2007 – 09/2009	
nichtwissenschaftliche Mitarbeiterinnen und Mitarbeiter	5.	Thomas Dargel, Dipl.-Chem., Systemadministrator	Theoret. Chemie	HU-C	8h, 07/2001 – 06/2011	
	6.	Monika Urban, Dipl.-Ing. FH	Theoret. Chemie	HU-C	5h, 07/1999 – 10/2009	
Ergänzungsausrüstung						
Wissenschaftlerinnen und Wissenschaftler	1.	Witold Piskorz, Dr.	Theoret. Chemie	HU-C	40h, 06/2008 – 02/2009	E13
	2.	Marc Pritzsche	Theoret. Chemie	HU-C	20h, 04/2008 – 10/2008	E13, 50%
	3.	Jianwen Liu, Dr.	Theoret. Chemie	HU-C	40h, 12/2009 – 06/2011	E13
	4.	Andrzej Niedziela	Theoret. Chemie	HU-C	20h, 09/2009 – 06/2011	E13, 50%
	5.	Andreas Mavrantoukakis, Dr.	Theoret. Chemie	HU-C	40h, 07/2009 – 12/2009	E13
	6.	Kaido Sillar, Dr.	Theoret. Chemie	HU-C	40h, 09/2009 – 12/2009	E13
	7.	Torsten Kerber	Theoret. Chemie	HU-C	20h, 11/2010 – 01/2011	E13, 50%
	8.	Matthias Baldofski	Theoret. Chemie	HU-C	20h, 03/2011 – 06/2011	E13, 50%
nichtwissenschaftliche Mitarbeiterinnen und Mitarbeiter						

Aufgaben der Mitarbeiterinnen und Mitarbeiter (Grundausrüstung):

1. Prof. Dr. Joachim Sauer
Projektleitung, Anleitung der Doktoranden und der Mitarbeiter, Rechnungen an Gasphasenclustern
2. Jens Döbler
Projektleitung, Mitwirkung bei der Anleitung der Doktoranden, wellenfunktionsbasierte Elektronenkorrelationsberechnungen zur Einschätzung der Genauigkeit von DFT für die Reaktivitätsprobleme dieses SFB
3. Dr. Marek Sierka
Projektleitung, Entwicklung und Anwendung des genetischen Algorithmus und Entwicklung von quantenchemischen Methoden für große Moleküle und Festkörper
4. Dr. Laurence Gregoriades
Untersuchungen zu selektiven Oxidationsreaktionen an Modellen für Molybdänoxidkatalysatoren
5. Thomas Dargel
Systemadministrator, Betreuung der Rechner und Programme
6. Monika Urban
Technische und organisatorische Mitarbeit

Aufgaben der Mitarbeiterinnen und Mitarbeiter (Ergänzungsausstattung):

1. Dr. Witold Piskorz
DFT-Rechnungen zu den Elementarschritten der oxidativen Dehydrierung von Propan, der Totaloxidation und der Reoxidation an Vanadiumoxidkatalysatoren auf Trägern
2. Dr. Marc Pritzsche
Untersuchung von Modellen fester Katalysatoren mit quantenchemischen Methoden
3. Dr. Jianwen Liu
Untersuchung der Oxidation von Propan an Modellen für Vanadiumoxidkatalysatoren mit quantenchemischen Methoden

4. Andrzej Niedziela
DFT-Rechnungen an Gasphasenclustern und Modellen fester Katalysatoren,
Lokalisierung von Übergangszuständen
5. Dr. Andreas Mavrantonakis
Untersuchung von Modellen fester Katalysatoren mit quantenchemischen Methoden
6. Dr. Kaido Sillar
Untersuchung von Modellen fester Katalysatoren mit quantenchemischen Methoden
7. Torsten Kerber
Untersuchung von Modellen fester Katalysatoren mit quantenchemischen Methoden
8. Matthias Baldofski
Untersuchung von Elementarschritten der katalytischen Oxidation mit quantenchemischen Methoden

5.1 Allgemeine Angaben zum Teilprojekt B1

5.1.1 Titel: Untersuchungen zur Struktur-Reaktivitäts-Beziehung von Vanadiumoxid-Aggregaten auf geordneten Übergangsmetall-oxidoberflächen

5.1.2 Projektleitung

Prof. Dr. Hans-Joachim Freund
geb. 4.3.1951

Dr. Shamil Shaikhutdinov
geb. 29.6.1960

Fritz-Haber-Institut der Max-Planck-Gesellschaft
Abteilung Chemische Physik
Faradayweg 4-6
14195 Berlin

Telefon: 030 / 84134100
E-Mail: freund@fhi-berlin.mpg.de

030 / 84134114
shaikhutdinov@fhi-berlin.mpg.de

5.2 Entwicklung des Teilprojekts

5.2.1 Bericht

The project is aimed at deeper understanding of the structure-reactivity relationships of transition metal oxides by using well-defined model systems where oxide clusters are supported on crystalline thin oxide films grown on metal single crystal surfaces.

The experiments were carried out in ultra-high vacuum (UHV) chambers equipped with all facilities necessary for the controlled preparation of model catalysts. The structural and electronic properties of the systems under study were characterized by scanning tunneling microscopy (STM), infrared reflection-absorption spectroscopy (IRAS), X-ray photoelectron spectroscopy (XPS) and temperature programmed desorption (TPD). STM is used for structural characterization of the oxide film supports and deposited clusters. In particular, particle size distribution as well as nucleation and growth modes (e.g., three-dimensional vs two-dimensional) can be determined. XPS is used for characterization of the electronic structure of the systems and allows determining the oxidation states of the deposits. Vibrational properties of the surfaces (both oxide phonon and stretching regions of adsorbed molecules) are studied with IRAS. TPD studies provide important information on the reactivity of the supported clusters.

Metal oxide clusters were deposited onto oxide films by metal physical vapor deposition in an ambient oxygen. In addition, the metal deposition onto water (ice) precovered films was used to mimic, to some extent, a water-assisted preparation of the real catalysts. In order to combine the results obtained in different chambers, the same preparation conditions were used in each experimental setup.

We first address the vanadia/ceria system which was reported in the literature as one of the most reactive catalysts in the ODH reactions [1]. Vanadia was vapor-deposited onto CeO₂(111) films grown on Ru(0001) ([BAB09], [AUB10]). STM studies revealed the absence of preferential nucleation sites thus indicating a strong interaction between vanadia species and the ceria support. At low V coverage (~ 0.3 at/nm²), highly dispersed and randomly distributed vanadia species are formed (see Fig. 1a). The respective IRA-spectrum features an absorption band at 1006 cm⁻¹ which can be assigned to the vanadyl (V=O) stretching vibration. Finally, XPS studies revealed V in a fully oxidized, i.e., +5 state, as shown by a single peak at ~ 517 eV for the V2p_{3/2} core level (see Fig 1e), which formation is accompanied by reduction of Ce in the fully oxidized CeO₂ film, as indicated by an increase of the Ce 4f peak. When combined, these results provide compelling evidence for the formation of isolated, monomeric V=O species on the ceria surface.

Increasing vanadia coverage first resulted in a higher density of monomeric species and simultaneous formation of dimers, trimers, and ill-defined large aggregates with a relatively broad size distribution. Heating to elevated temperatures (700 K) in UHV caused monomers to sinter, ultimately producing vanadia trimers, as illustrated more clearly by the inset of Fig 1b. The distance of the spots within the trimers is 3.9 ± 0.2 Å matches the lattice constant of CeO₂(111) (3.9 Å). The apparent height of the trimers (1.0 ± 0.3 Å) is about the same as for monomers, thus indicating that the trimers are anchored flat on the surface. The corresponding IR spectrum showed a vanadyl-stretch absorption peak at 1033 cm⁻¹, i.e. blue-shifted by ~ 25 cm⁻¹ as compared to monomeric species. The shift can be attributed to the onset of dipole coupling between neighbouring V=O groups in the trimers. Even larger vanadia species like heptamers are also visible in the middle of Fig 1b, which number increases as the coverage is increased further to 4.3 at/nm² (see Fig. 1c). The heptamers have a hexagonal shape, a lateral distance of 3.7 ± 0.2 Å between the protrusions and an apparent height about the same as for trimers. This means that V=O groups in monomers, trimers and oligomers occupy the same sites with respect to the ceria substrate. At high coverage (4.3 at/nm²), the frequency of the V=O stretch shifts further to 1040 cm⁻¹, ultimately approaching the frequencies (~ 1045 cm⁻¹)

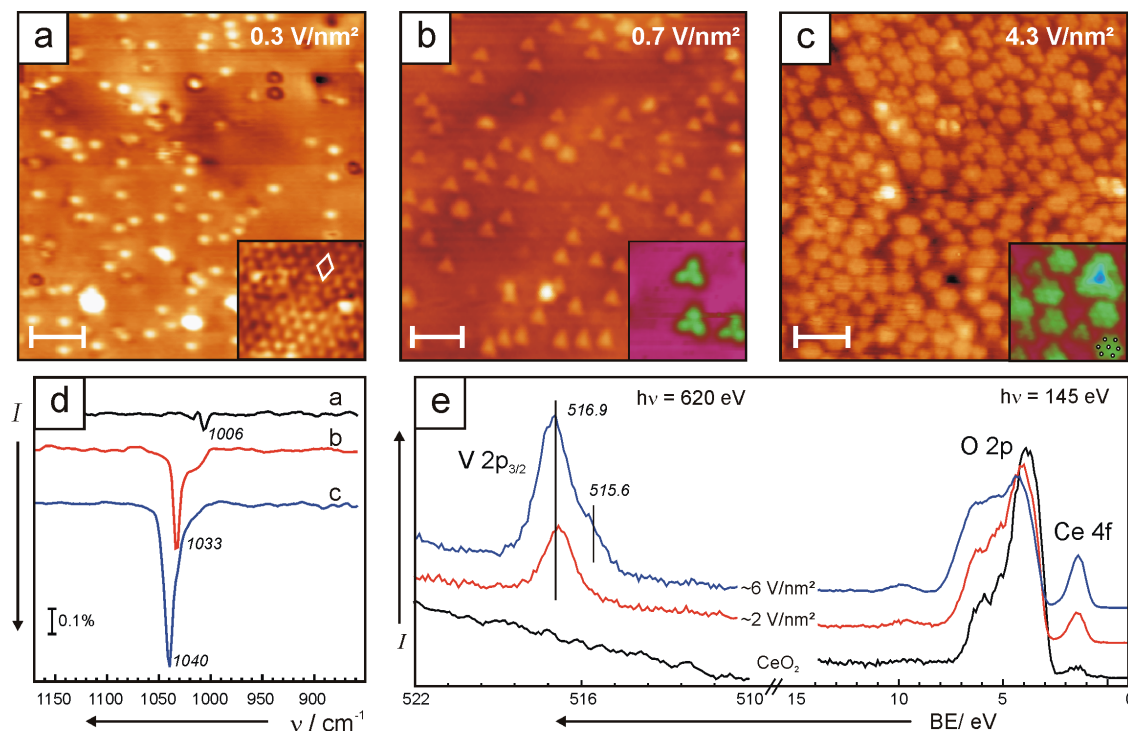


Fig. 1. (a-c) STM images of VO_x/CeO₂(111) for various vanadia coverages as indicated. Sample (a) was annealed to 300 K, while samples (b) and (c) were annealed to 700 K. The insets highlight the atomic structure of the vanadia deposits. (The scale bars are 3 nm). IRA spectra of the vanadyl (V=O) stretching region for the corresponding STM images are shown in (d). XPS spectra of VO_x/CeO₂(111) surfaces are compared to a pristine CeO₂(111) thin film in (e).

observed for V=O terminated V₂O₃ nanoparticles on silica and alumina thin films [2] as well as for V₂O₃(0001) films [3].

Thus, the combined STM, XPS and IRAS results revealed a direct relationship between the nuclearity of vanadia species (monomeric vs polymeric) and the vibrational properties. The experimental results were fully supported by density functional theory (DFT) calculations ([BAB09], see more in TP C5). The results allow one to link the structure of vanadia surface species and the Raman/IR characterization, typically used for real catalysts, in a more definitive manner. The results clearly indicate that ceria surfaces stabilize small vanadia species, such as monomers and trimers that sinter into two-dimensional, monolayer islands wetting the oxide support surface as previously proposed. In addition, it is shown that ceria stabilizes the vanadium +5 oxidation state. It appears that strong vanadia-ceria interaction plays a crucial role in the enhanced reactivity of ceria-supported vanadia in ODH reactions. Indeed, the species of low nuclearity revealed formaldehyde (FA) formation at much lower temperatures as compared to those of higher nuclearity [AUB10]. TPD spectra of the major desorption products after exposure of the VO_x/CeO₂(111) model catalysts to methanol at room

temperature are presented in Fig. 2. The pristine $\text{CeO}_2(111)$ film shows a desorption signal of FA at 565 K (γ peak). Upon vanadia deposition, the γ peak shifts to 590 K. Additionally two new peaks appear at lower temperatures, denoted as α at 370 K and β at 475 K. At high vanadia coverage, the α and γ peaks disappear and the β peak shifts to 505 K. Desorption features similar to the β peak have been observed on silica-supported vanadia and other model systems [2,3] all of which have desorption peak intensities between 450 and 590 K. Thus, the β peak can be assigned straightforwardly to methanol ODH on vanadia nanoparticles and large oligomers imaged by STM at these coverages. In contrast, the α peak is observed at much lower temperature and at coverages where primarily monomeric vanadia species have been identified on these samples by IRAS. In order to rationalize these results DFT studies were performed using O defect formation energy and hydrogenation energy as the reaction descriptors ([GPS10], see more in TP C5). The results indicate an enhanced activity of monomeric vanadia species on ceria surfaces as compared to the bare support, but also to monomeric vanadia species on inert supports such as silica. The effect can also be considered as promoting effect of the vanadia species on the activity of the uncovered ceria support.

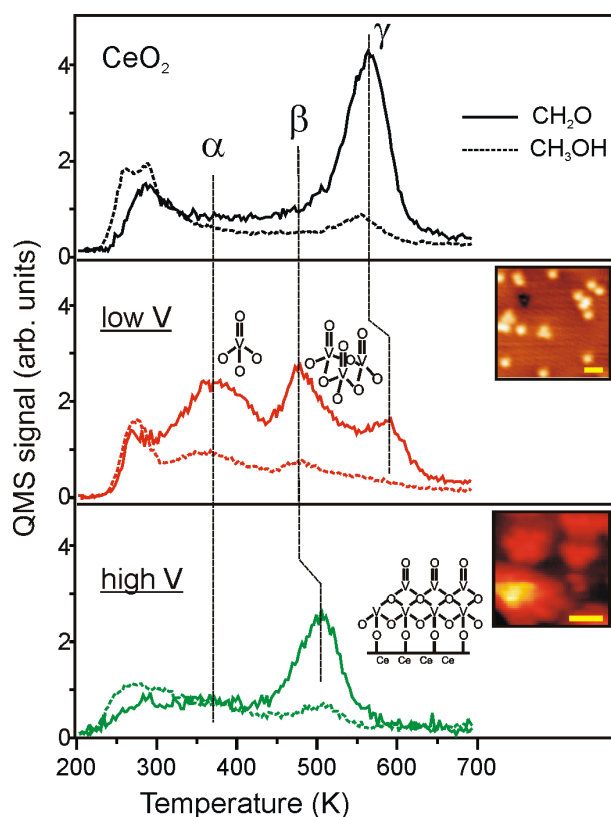


Fig. 2.

TPD spectra for ~ 5 L of methanol adsorbed at 300 K on $\text{CeO}_2(111)$ and $\text{VO}_x/\text{CeO}_2(111)$ surfaces at low (< 2 V at/nm^2) and high (~ 4 V at/nm^2) vanadia loadings. Solid lines indicate the signal for methanol (31 amu), whereas dashed lines indicate formaldehyde (29 amu, corrected for the methanol cracking pattern). Signal intensity below 300 K is assigned to the tail of methanol monolayer desorption. The insets show typical STM images of vanadia species at the respective coverage (see also Fig. 1). The scale bar corresponds to 1 nm.

In order to deduce the role of the support material on the reactivity of vanadia clusters, vanadia was deposited in sub-monolayer quantities on the surfaces of alumina thin films, for

comparison. The alumina films were grown on NiAl(110) using a well-established procedure. The key experimental findings are presented in Fig. 3, from which direct comparison of the reactivity of the vanadia/alumina and vanadia/ceria systems towards ethanol can be made.

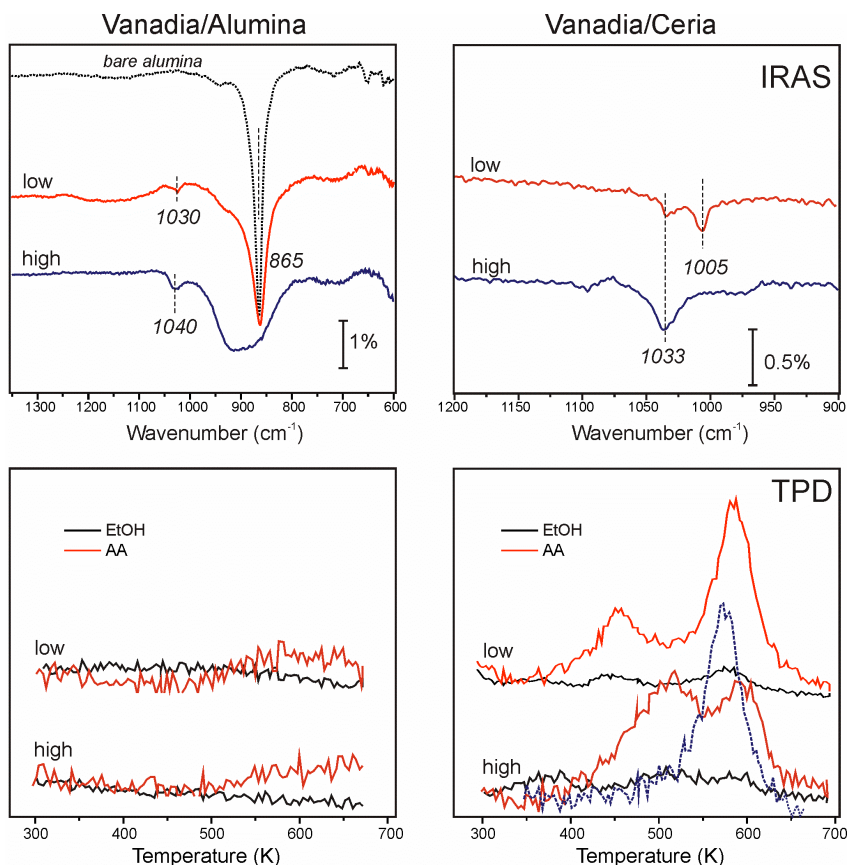


Fig. 3. IRAS (top panel) spectra of vanadia particles deposited onto alumina (on left) and ceria (on right) films at “low” (1 V at/nm^2) and “high” (3 V at/nm^2) coverages. TPD spectra of ethanol adsorbed at 300 K are shown in the bottom panel (see text). The dashed line shows the AA production on the pure ceria film.

Deposition of vanadia onto an alumina film leads to the formation of V=O terminated V_2O_3 nanoparticles as previously studied within this project [4]. The TPD spectra of ethanol adsorbed at 300 K on the respective vanadia/alumina surfaces did not show any detectable reactivity towards acetylaldehyde (AA) regardless of the vanadia coverage (left panel in Fig. 3). In contrast, the vanadia/ceria system containing the same amounts of vanadia showed substantial reactivity in the AA formation (right panel in Fig. 3). The TPD spectra revealed two desorption features, i.e., at 450-500 K and ~ 600 K. The high-temperature reactivity can straightforwardly be assigned to the reactivity of the bare ceria surface showing a similar TPD feature in the experiments performed with pristine ceria films (the dashed line). Obviously, the reactivity at 450 – 500 K must be associated with vanadia species. The structure-frequency

relationship observed for vanadia surface species (see Fig. 1) suggests that, at low coverages, vanadia formed primarily monomeric V=O species exhibiting 1005 cm⁻¹ band. At higher coverage, di- and trimeric as well as larger oligomeric species, showing the 1033 cm⁻¹ band, dominated the surface. Comparison of these two samples clearly show that vanadia species with a lower nuclearity exhibits reactivity at considerably lower temperatures than observed for the large vanadia particles (450 vs 520 K, respectively).

Therefore, the results clearly show the support effect such that vanadia supported on ceria is more active towards ethanol than vanadia/alumina at the same vanadia coverage. In addition, the results again showed that the AA formation on the vanadia/ceria surface proceeds with the lower activation barrier on the smallest vanadia species like monomers and dimers.

However, the smallest vanadia species seems to be the least stable when supported on the extended, well-ordered ceria films. In addition, the results [AUB10] revealed that methanol reacts with the vanadia/ceria surface oxidized at 300 K, but not at 700 K, thus suggesting that the low temperature reactivity relates not only to the high dispersion of vanadia, but also to the degree of reduction of the ceria in close proximity to vanadyls. To validate this hypothesis, we have initiated studies on vanadia/ceria clusters deposited onto inert support such as silica.

Previously, crystalline silica films were grown on Mo(112) resulting in a monolayer honeycomb-like network of corner sharing [SiO₄] tetrahedra (see the most recent review in [5]). However, the principle phonon band of the “monolayer” silica film (at 1060 cm⁻¹) strongly overlaps with V=O stretch band and therefore renders the precise spectral assignment rather vague. All attempts to grow thicker silica films on the Mo substrates resulted in amorphous structures, most likely due to the formation of strong Si-O-Mo bonds at the interface that govern the growth mode. Therefore, considerable effort was put into the preparation of crystalline “multilayer” silica films on other metal substrates.

Now we report the first successful preparation of “multilayer” silica films using Ru(0001) as a substrate. The experimental results, complemented by DFT calculations (in collaboration with TP A4), provided compelling evidence for the formation of a double-layer sheet silicate, with a SiO₂ stoichiometric composition, weakly bound to a metal support [LUB10] (see Fig. 4). These films were further used as a support for ceria and vanadia oxide clusters.

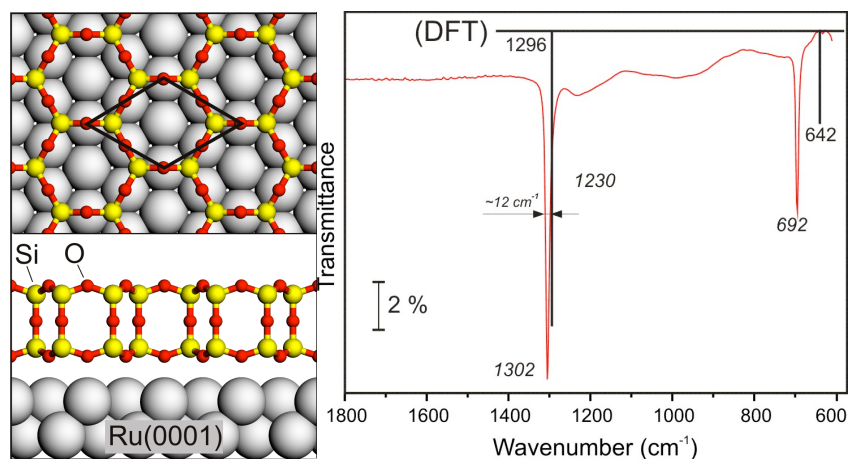


Fig. 4. (Left) Top and side views of a silicate film grown on Ru(0001). (Right) Experimental and calculated IRA-spectra of the film.

Ceria and vanadia were supported by the silicate films using the water (ice)-assisted deposition. First, the ceria/silica surfaces were examined in the dehydrogenation of methanol to formaldehyde. The TPD results, shown in Fig. 5, revealed considerable reactivity at low temperatures (400-450 K) for supported CeO_x nanoparticles, which is not present on well-ordered $\text{CeO}_2(111)$ films (cf. Fig. 2), and which dominates at low ceria coverage. On the other hand, the reactivity of the ceria films is enhanced upon creating surface defects by ion bombardment followed by mild oxidation. These results indicate that the surface defects, naturally present on ceria nanoparticles, and reducibility of the ceria play an important role in

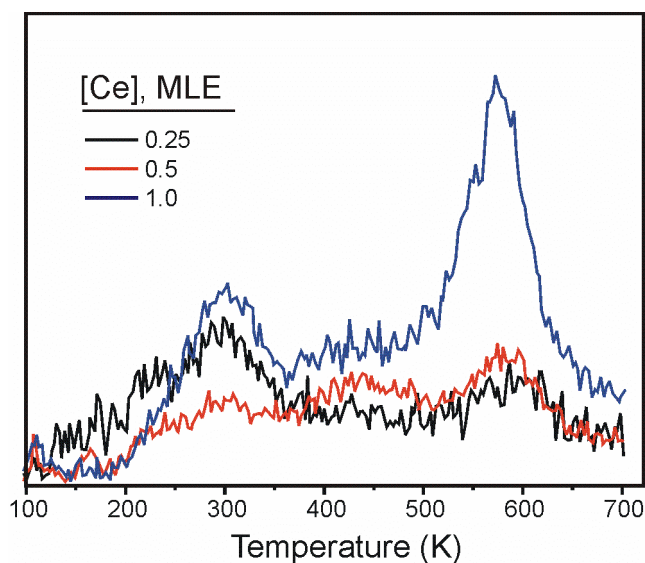


Fig. 5. Formaldehyde signal in TPD spectra of 20 L of methanol exposed at 300 K to ceria nanoparticles supported by silica films as a function of ceria coverage.

the reactivity of ceria surfaces. Indeed, the XPS studies showed that ceria nanoparticles below 5 nm are considerably reduced [BBS09].

In contrast to ceria/silica, the vanadia/silica samples only showed negligible FA production at ~570 K and only at high vanadia loadings. Again, this finding is in a full agreement with the support effects discussed above.

In the next step, vanadia was deposited on the ceria particles or co-deposited with ceria onto the silica films. The preliminary results showed that, in both cases, vanadia is fully oxidized whereas ceria is partially reduced in the presence of vanadia. The vanadia-ceria/silica systems are thermally stable. The reactivity studies of the supported mixed oxide clusters are underway. Finally, we have successfully initiated studies on preparation of well-ordered iron-molybdate thin films as suitable models of methanol oxidation catalysts [USL11]. The studies were motivated by the fact that Fe-Mo oxide catalysts are commercially used for large-scale production of formaldehyde by the partial oxidation of methanol in an excess of oxygen (air). The identity of the active site for the partial oxidation of methanol is still a topic of current research. We have studied Mo deposition onto Fe₃O₄(111) thin films, previously studied in our laboratories, as a function of Mo coverage and annealing temperature. At low temperatures, the iron oxide film is covered by Mo=O terminated molybdena nanoparticles. Upon oxidation at elevated temperatures (T > 900 K), Mo species migrate into the film and form new bonds with oxygen in the film. The resulting films maintain the crystal structure of Fe₃O₄, and the surface undergoes a ($\sqrt{3} \times \sqrt{3}$)R30° reconstruction. STM results showed atomic resolution of the mixed oxide phase, with ordered tripod species on the surface showing a periodicity of ~ 10 Å, consistent with the structure observed by LEED. Five characteristic vibrational transitions were observed using IRAS to serve as a chemical fingerprint of the surface species on the Fe-Mo mixed oxide. A crystalline model is proposed where Mo is substituted for Fe in the surface layers and oxygen vacancies account for the periodicity observed by LEED and STM. Certainly, additional experimental studies using photoelectron and x-ray absorption spectroscopies as well as computational input from theory could provide crucial information in refining the structure of iron molybdate surfaces.

References

- [1] I. E. Wachs, *Catal. Today* 100 (2005), 79.
- [2] N. Magg, B. Immaraporn, J. B. Giorgi et al., *J. Catal.*, 226 (2004), 88.
- [3] S. Guimond, M. Abu Haija, S. Kaya et al., *Top. Catal.* 38 (2006), 117.
- [4] N. Magg, J. Giorgi, T. Schroeder et al., *J. Phys. Chem. B* 106 (2002) 8756.
- [5] S. Kaya, M. Baron, D. Stacchiola et al., *Surf. Sci.*, 601 (2007), 4849.

5.2.2 Projektrelevante eigene Publikationen

a) erschienene oder angenommene Arbeiten in wissenschaftlichen Zeitschriften oder Buchveröffentlichungen

- [KWS08] S. Kaya, J. Weissenrieder, D. Stacchiola, T.K. Todorova, M. Sierka, J. Sauer, S. Shaikhutdinov, H.-J. Freund
Formation of one dimensional molybdenum oxide on Mo (112)
Surf. Sci. **602** (2008) 3338 - 3342.
- [RGK08] Y. Romanyshyn, S. Guimond, H. Kuhlenbeck, S. Kaya, R. P. Blum, H. Niehus, S. Shaikhutdinov, V. Simic-Milosevic, N. Nilius, H.-J. Freund, M. V. Ganduglia-Pirovano, R. Fortrie, J. Döbler and J. Sauer
Selectivity in methanol oxidation as studied on model systems involving vanadium oxides
Top. Catal. **50** (2008) 106 - 115.
- [BAB09] M. Baron, H. Abbott, O. Bondarchuk, D. Stacchiola, A. Uhl, S. Shaikhutdinov, H.-J. Freund, C. Popa, M.V. Ganduglia-Pirovano, J. Sauer
Resolving the atomic structure of vanadia monolayer catalysts: Monomers, trimers and oligomers on ceria.
Angew. Chem. Int. Ed. **48** (2009) 8006 - 8009.
- [BBS09] M. Baron, O. Bondarchuk, D. Stacchiola, S. Shaikhutdinov, H.-J. Freund
Interaction of gold with cerium oxide supports: CeO₂(111) thin films vs CeO_x nanoparticles
J. Phys. Chem. C **113** (2009) 6042 - 6049.
- [AUB10] H. Abbott, A. Uhl, M. Baron, Y. Lei, R. Meyer, D. Stacchiola, O. Bondarchuk, S. Shaikhutdinov, H.-J. Freund
Relating methanol oxidation to the structure of ceria-supported vanadia monolayer catalysts
J. Catal. **272** (2010) 82 - 91.
- [GPS10] M.V. Ganduglia-Pirovano, C. Popa, J. Sauer, H. Abbott, A. Uhl, M. Baron, D. Stacchiola, O. Bondarchuk, S. Shaikhutdinov, H.-J. Freund,
The role of ceria in oxidative dehydrogenation on supported vanadia catalysts
J. Am. Chem Soc. **132** (2010) 2345 - 2349.
- [LUB10] D. Löffler, J.J. Uhlrich, M. Baron, L. Lichtenstein, L. Heinke, C. Büchner, M. Heyde, S. Shaikhutdinov, H.-J. Freund, R. Wlodarczyk, M. Sierka, J. Sauer
Growth and structure of crystalline silica sheet on Ru(0001)
Phys. Rev. Lett. **105** (2010) 146104-1 -146104-4.
- [USL11] J.J. Uhlrich, J. Sainio, Y. Lei, D. Edwards, R. Davies, M. Bowker, S. Shaikhutdinov, H.-J. Freund
Preparation and characterization of iron–molybdate thin films.
Surf. Sci. **605** (2011) 1550 - 1565.

- [NRS11] N. Nilius, T. Risse, S. Schauer mann, S. Shaikhutdinov, M. Sterrer, H.-J. Freund
Model studies in catalysis
Top. Catal. **54** (2011) 4 - 12.

5.3 Rückblick auf die Förderung

Das Teilprojekt wurde seit 07/1999 im Sonderforschungsbereich gefördert. Es wurde mit Ablauf der 4. Förderperiode im Juni 2011 beendet.

5.3.1 Personal im Teilprojekt während der 4. Förderperiode

	lauf. Nr.	Name, akademischer Grad, Dienststellung	engere Fachzugehörigkeit	Institut der Hochschule oder der außeruniv. Einrichtung	Mitarbeit im Projekt Zeitraum Wochenstunden	Entgeltgruppe
Grundausrüstung						
Wissenschaftlerinnen und Wissenschaftler	1.	Hans-Joachim Freund, Prof. Dr., Direktor	Chem. Physik	FHI, Abt. CP	06/2008 – 06/2011, 2h	
	2.	Shamil Shaikhutdinov, Dr., AG Leiter	Chem. Physik	FHI, Abt. CP	06/2008 – 06/2011, 15h	
	3.	Martin Baron, WM	Chem. Physik	FHI, Abt. CP	06/2008 – 04/2010, 20h	
	4.	John Uhlrich, Dr.	Chem. Physik	FHI, Abt. CP	60/2009 – 05/2011, 40h	
nichtwissenschaftl. Mitarbeiterinnen und Mitarbeiter						
Ergänzungsausrüstung						
Wissenschaftlerinnen und Wissenschaftler	1.	Alexander Uhl, WM	Chem. Physik	FHI, Abt. CP	06/2008 – 09/2008, 27h	E13, 2/3
	2.	Daniel Göbke, WM	Chem. Physik	FHI, Abt. CP	11/2008 – 07/2010, 27h	E13, 2/3
	3.	Jan Jerratsch, WM	Chem. Physik	FHI, Abt. CP	08/2010 – 04/2011, 30h	E13, 3/4
nichtwissenschaftl. Mitarbeiterinnen und Mitarbeiter						

Aufgaben der Mitarbeiterinnen und Mitarbeiter (Grundausrüstung):

1. Prof. Dr. Hans-Joachim Freund
Abteilungsleiter übernahm die wissenschaftliche Betreuung.
2. Dr. Shamil Shaikhutdinov
Neben der wissenschaftlichen und organisatorischen Betreuung des Teilprojektes übernahm er die im Rahmen des Projektes anfallenden Verwaltungsaufgaben.
3. Martin Baron
Untersuchungen zur Struktur von Vanadiumoxidclustern auf Ceriumoxid Filmen.
4. John Uhlrich
Untersuchungen zur Präparation und Struktur von Ceriumoxidclustern auf Siliciumoxid Filmen.

Aufgaben der Mitarbeiterinnen und Mitarbeiter (Ergänzungsausstattung):

1. Herr Dipl.-Phys. Daniel Göbke
Untersuchungen zur Struktur, Adsorption und Reaktivität von Vanadiumoxidclustern auf Aluminium- und Silicium-oxid.
2. Herr Dipl.-Phys. Alexander Uhl
Untersuchungen zur Reaktivität von Vanadiumoxidclustern auf Ceriumoxid Filmen.
3. Herr Dipl.-Phys. Jan Jerratsch
Untersuchungen zur Präparation und Struktur von Siliciumoxid Filmen.

5.1 Allgemeine Angaben zum Teilprojekt B2

5.1.1 Titel: Partialoxidation kleiner Kohlenwasserstoffmoleküle mit mikroskopischen Mengen von V_xO_y -Katalysatorsystemen

5.1.2 Projektleitung

Prof. Dr. Robert Schlögl
geb. 23.02.1954

Fritz-Haber-Institut
Max-Planck-Gesellschaft
Faradayweg 4-6
14195 Berlin

Telefon: 030 / 8413 4404
E-Mail: acsek@fhi-berlin.mpg.de

ausgeschieden:

Dr. Katrin Pelzer
geb. 23.02.1975

5.2 Entwicklung des Teilprojekts

5.2.1 Bericht

Project B2 aims at establishing structure-activity relations for partial oxidation reactions of small alkane molecules using the example of supported $(VO_x)_n$ aggregates. An understanding of structure-activity relations requires on one hand the development of well-defined, realistic model systems, on the other hand the thorough characterization of the catalyst before and during reaction.

The last funding period (2005/2 to 2008/1) was focused mainly on the synthesis and structural characterization of vanadia supported on mesoporous silica (SBA-15).[1-6] The individual steps of a novel synthesis approach for highly dispersed vanadium oxide based on controlled ion exchange within the pores of mesoporous SBA-15 were enlightened.[2] On the basis of detailed spectroscopic characterization using XPS and vibrational techniques (DRIFTS, Raman) as well as solid state NMR and thermal analysis, improved understanding of the synthesis steps was achieved.

The role of the support in supported vanadia catalysts is still a matter of discussion. Previous studies have reported a strong influence of the support material on catalytic performance of vanadia catalysts.[7-9] However, the origin of this behaviour is still not well understood as it may either be attributed to differences in the vanadia structure(s) present on the different support materials or different interactions between support and supported phase. Therefore, new synthetic strategies are needed which allow for a more controlled synthesis of supported vanadia catalysts. Ultimately, it would be highly desirable to control the structure of the deposited vanadia aggregates by choice of suitable precursor species and/or ligands. Consequently, our synthetic efforts in the current funding period were directed to modify SBA-15 with a monolayer of a support oxide, such as titania or molybdena, and to synthesize vanadia supported on modified SBA-15. Titania has been chosen, because $(VO_x)_n/TiO_2$ catalysts show exceptional high activity in oxidative dehydrogenation of propane.[10] Molybdenum oxide was selected to link the model studies over silica supported transition metal oxides with molybdenum oxide based high performance bulk catalysts.[11-15]

At the beginning of the current funding period the kinetics of oxidative dehydrogenation of propane over $(VO_x)_n/SBA-15$ catalysts with various V loadings, which have been thoroughly characterized during the last funding period, were investigated for reference. Then, the activities were focussed on synthesis and comprehensive characterization of SBA-15 modified by submono- and monolayers of molybdenum oxide and titanium oxide species. Vanadium oxide species supported on modified SBA-15 materials were studied including the structural dynamics of the catalysts under reaction conditions of oxidative dehydrogenation of propane.

Oxidative dehydrogenation of propane over $(VO_x)_n/SBA-15$ catalysts

SBA-15 is a mesoporous silica material with uniform hexagonal channels, a narrow pore size distribution, surface areas above 800 m²/g, and considerable hydrothermal stability due to a sufficient thickness of the framework walls.[16, 17] All these properties make it a preferable support material for model catalysts. Moreover, vanadia supported on SBA-15 has shown considerable catalytic activity in the ODH of propane.[18, 19] While the possibility to tune the mesoscopic properties of SBA-15 by slight modifications in the synthesis makes it a versatile material, this creates problems in the reproducibility of the support and batch effects are commonly observed. Therefore, a controlled and reproducible synthesis of SBA-15 was developed making use of an automated laboratory reactor (LabMax, Mettler-Toledo).[20] The reactor provides precise control of the operating conditions (temperature, pH, stirring rates)

and process data recording. In particular, practically no temperature gradients occur within the reaction vessel that allows synthesis of homogeneous, well-defined SBA-15 in large batch sizes. The up-scaled SBA-15 batch size should be sufficient for the preparation of a series of catalysts with different loadings from the same support. Since the quality of SBA-15 is critical with respect to stability of the hexagonal pore structure during subsequent calcination of the supported vanadium oxide at 823 K, the SBA-15 synthesis has been optimized resulting in a reproducible and robust procedure achieving batch sizes of approximately 25 g.

A series of vanadia catalysts supported on SBA-15 containing from 0.6 up to 13.6 vanadium atoms per nm² have been synthesized applying the established ion-exchange method.[2] The catalysts are structurally characterized by various techniques (BET, XRD, SEM, TEM, Raman, IR, UV/Vis). Especially the pore diameters of the vanadia containing catalysts are favorably high and decrease only slightly with increasing vanadia content from 7 nm for SBA-15 to 6.5 nm for the catalyst with the highest vanadia loading demonstrating the benefits of the V grafting procedure by ion exchange. Samples containing up to 3.1 V/nm² are structurally rather similar. They all contain a mixture of tetrahedral (VO_x)_n species, both monomeric and oligomeric. The ratio of monomeric and oligomeric species depends on the vanadia loading. Oligomeric species dominate for vanadia concentrations higher than 2.1 V atoms/nm². At the highest loading of 13.6 V/nm², in addition to tetrahedral (VO_x)_n, also substantial amounts of three-dimensional, bulk-like V₂O₅ are present in the catalyst.

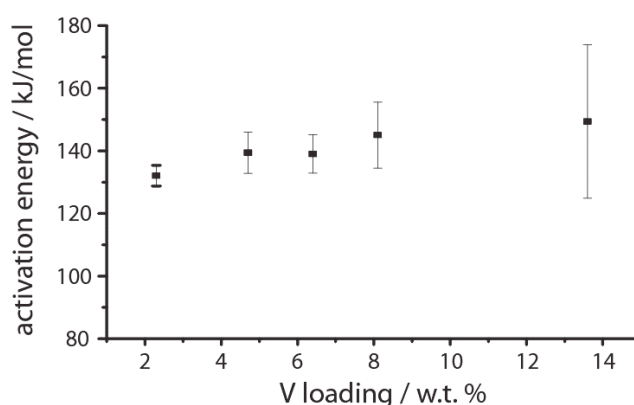


Fig. 1. Apparent activation energy E_a of propane consumption in the oxidative dehydrogenation of propane over V/SBA-15 catalysts with varying vanadia loading.

The structural similarity of the low-loaded catalysts is reflected in their alike catalytic activity during the oxidative dehydrogenation (ODH) of propane between 380 and 480 °C. Propene, CO, and CO₂ are formed as reaction products, while (due to the reaction conditions and the

feed composition) neither the formation of ethene nor acrolein or acrylic acid is observed in other than trace amounts. Iglesia and co-workers found a maximum in propylene selectivity at intermediate vanadia loadings on various supports, which was linked to the prevalence of V–O–V sites.[21, 22] In line with the finding that for vanadia on SBA-15 the molecular structure of the catalyst does not change significantly with loading no obvious trend is visible from the selectivity and all catalysts behave rather similarly.[20] The activation energies are also similar for all catalysts (Fig. 1). For the low loaded species an excellent reproducibility is observed for repeated measurements, also when using a fresh catalyst (squares, circles, and triangles in left panel of Fig. 2). The situation is different in the case of 14V/SBA-15. Using a fresh catalyst, a very high apparent activation barrier of ~ 165 kJ is obtained upon measuring the conversion between 380 and 450 °C (squares in right panel of Fig. 2). In subsequent runs, the activation energy drops to ~ 140 kJ/mol (triangles and circles in right panel of Fig. 2). While the catalysts 2-8V/SBA-15 are very stable and reproducible in their catalytic performance, 14V/SBA-15 behaves highly dynamic. This must be connected to profound changes in the structural properties of this particular catalyst. 14V/SBA-15 is the only sample, for which a substantial amount of bulk-like V_2O_5 was found to be present, as proven by the Raman spectra. The other samples are characterized by a mixture of monomeric and polymeric vanadyl species of different domain size. Thus, it is not the degree of polymerization of the vanadia species that changes the apparent activation barrier for ODH, but it is obviously the ratio of two-dimensional polymeric species and three-dimensional bulk-like V_2O_5 that plays the crucial role.

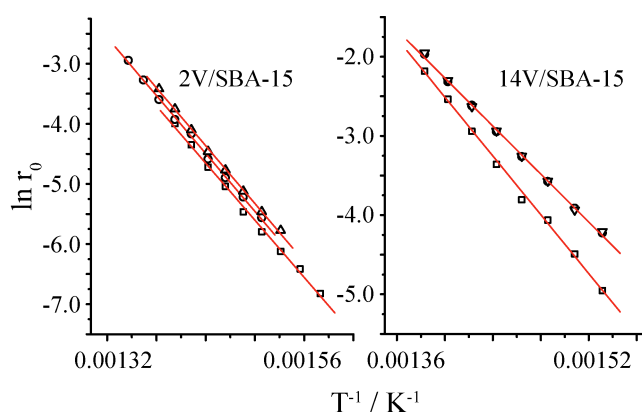


Fig. 2. Arrhenius plots for 2V/SBA-15 and 14V/SBA-15. Three measurements are shown.

Further experimental evidence for the dynamic behaviour of surface vanadia species under reaction conditions of propane oxidation has been obtained by *in-situ* X-ray absorption spectroscopy (NEXAFS).[23] In Fig. 3, left panel, the V $L_{3,2}$ absorption spectra (corresponding

to transition from V 2p to V 3d orbitals) characterized by absorption peaks in the photon energy range between 512-528 eV followed by the oxygen K-edge (transition from O 1s to O 2p) above 528 eV are shown for dehydrated catalysts with various V loadings on SBA-15 support and compared to a reference spectrum of V₂O₅. The spectra have been normalized to the same V edge jump (“A”), *i.e.* to the same V amount. The O K-edge feature in the energy range between 528 eV and 534 eV are determined by peculiarities of the V-O bonding while resonances at photon energy above approximately 534 eV reflect mainly the O 1s excitations of Si-O-Si bonds, *i.e.*, of the support material SBA-15 as explained in great detail previously.[24, 25] The varying intensity ratio of the vanadium NEXAFS relative to the oxygen related NEXAFS reflects directly the different V loading of the catalysts. Restricting a detailed data evaluation on the energy range that serves as a fingerprint for V-O bonds (528 - 534 eV) reveals a similar spectral O K-edge shape on the one hand for a V loading of 12 wt.-% and 14 wt.-% and on the other hand of catalysts with a vanadium loading of 8 wt.-%V and below.

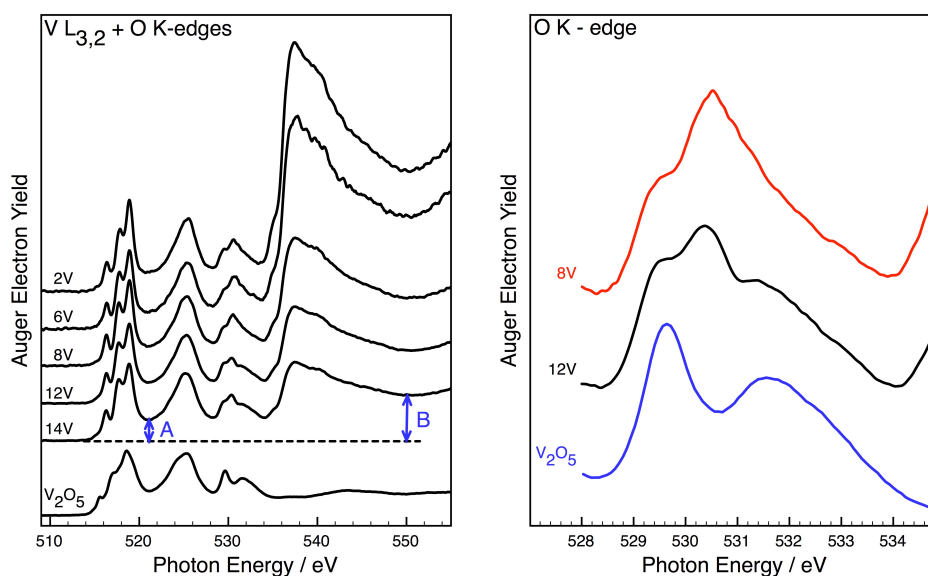


Fig. 3. The left panel presents the V L_{3,2}-and O K-NEXAFS of dehydrated VO_x/SBA-15 catalysts with various V loadings as indicated. Spectra have been recorded in 50Pa O₂ at 673 K. A reference spectrum of V₂O₅ powder is shown as well. The determination of the V edge jump “A” and the total edge jump “B” are marked with arrows (details in the text). In right panel a detail of the O K-NEXAFS is presented for a high loading (12 wt.-% V) and low loading (8 wt.-% V) catalyst and compared to the O K-NEXAFS of V₂O₅. Spectra are offset for clarity.

Details of the O K-NEXAFS in this photon energy range of 8 wt.-% V/SBA-15 and 12 wt.-% V/SBA-15 are compared with the spectrum of V₂O₅ in Fig. 3 in the right panel. As deduced in a recent work by comparison of experimental with theoretical spectra obtained by *ab initio*

DFT calculations,[25] the shape of the O K-NEXAFS of the dehydrated catalysts shown in Fig. 3 with a V loading of 8 wt.-% and below on SBA15 suggests the presence of both monomeric and polymeric species. The O K-edge spectrum of 12 wt.-%V/SBA-15 and 14 wt.-%V/SBA-15 show a more pronounced shoulder at 529.5 eV and about 531.6 eV as the lower loading catalysts. Obviously, these parts of the spectra resemble the characteristic features of V_2O_5 . However, the overall spectral shape is still different from bulk V_2O_5 . Thus, the geometric arrangement of V species in highly loaded catalysts is not the same as in V_2O_5 but possesses only some peculiarities of the V_2O_5 bulk structure, which is in agreement with the results of catalyst characterization by Raman and UV-vis spectroscopy. Based on this observation it seems reasonable to assign some 3-dimensional character to V species with a metal oxide loading equal and above 12 wt.-% while at V loadings of 8 wt.-% and below this character is missing although V-O-V bonds are present (2-dimensional polymers).

X-ray photoelectron spectroscopy is well established among the electron spectroscopy techniques to gather information about atom abundance and dispersion of supported metal particles. Unfortunately, low metal oxide loading on insulating supports like SiO_2 often prevent the recording of high quality XPS spectra due to charging in particular when using high brilliant monochromatic X-ray sources like a synchrotron beam for excitation. To study the evolution of the vanadium oxide species under different reaction conditions also for catalysts with lower transition metal oxide content, we made the attempt to quantitatively analyze the near edge structure of the X-ray absorption spectra. The sudden, step-like increase of the X-ray absorption intensity (“edge jump”) is proportional to the amount of absorbing atoms and therefore a measure of the element abundance. The increase in intensity due to continuous absorption is typically buried by the strong intensity increase due to resonant absorption (bound-bound transition) in the soft energy range. Therefore, it is usually not possible to extract absolute abundance numbers but relative changes can still be evaluated. In our work, the intensity at about 522 eV (indicated as “A” in Fig. 3) after subtraction of the pre-edge intensity was taken as a measure of the vanadium abundance. Silica does not show any absorption feature in this energy range.[25] Intensity “B” in Fig. 3 (at about 548 eV) is the total edge jump that represents vanadium plus all oxygen absorbers. Since the overwhelming part of oxygen is bound to Si this is indeed a good measure for the V+Si abundance. The evolution of the vanadium to total edge jump, *i.e.* the A/B ratio, is shown in Fig. 4 for the catalysts containing 6, 8, and 14 wt.-% V/SBA-15 in O_2 after dehydration and in a mixture of C_3H_8 and O_2 (2:1) below reaction temperature and at temperatures at which the catalyst produces

propylene. Propane conversions of approximately 0.2% were measured in the effluent gas of the *in-situ* XAS cell by gas chromatography. The V / (V+Si) abundance ratio as revealed by XPS is included in Fig. 4 (open blue circles) for 14V/SBA-15. An increase in the edge jump ratio that corresponds to an increase in the V to support ratio suggests an increase in dispersion as in the case of XPS. In this view, the increase of the intensity ratio of catalysts (6V/SBA-15 and 8V/SBA-15) with lower loading during dehydration (298 K to 673 K in O₂) hints that the dispersion of vanadium oxide species is improved during this treatment. The abundance/dispersion of V seems to remain constant under ODH reaction conditions at 773 K for 6V while there is a further slight increase for 8V/SBA-15 that decreases again when heating further to 823 K. The most pronounced effect in the edge jump ratio was observed for the high loading catalyst 14V/SBA-15 with a strong decrease in intensity ratio when applying ODH reaction conditions. Obviously, some of the vanadium species become not further accessible as absorbers to the X-rays. Albeit sublimation of vanadium oxide cannot be excluded under the reduced pressure at the high reaction temperature, spreading of vanadium oxide seems to be more likely as explanation for the observed phenomenon.

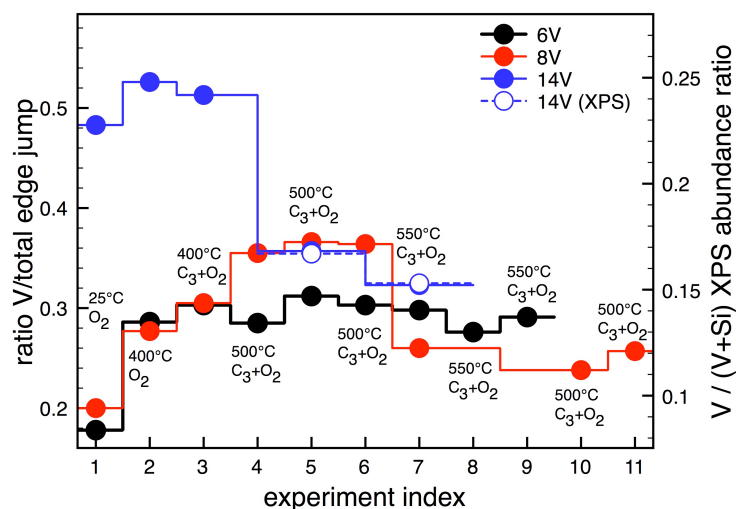


Fig. 4. Evolution of the V-edge/total edge jump ratio (corresponding to the intensity ratio A/B as indicated in Fig. 3 is shown for 3 different V loadings (6, 8, and 14 wt.-% V) at different reaction conditions as designated in the Figure. The V/(V+Si) atom abundance ratio as determined by XPS for the 14V catalysts is included.

Although there was no clear indication of three-dimensional (bulk-like) vanadia by UV-vis spectroscopy in the as synthesized, dehydrated catalyst, vibrational resonances at 144, 284, 303, 404, 482, 525, 702 and 994 cm⁻¹ visible in the Raman spectrum of 14V/SBA-15 suggested the presence of 3D vanadium oxide traces before catalysis.[20] These traces of bulk-like vanadium oxide nano-particles are apparently transformed into 2-D vanadium oxide

species in the feed at reaction temperature, which is also in accord with the catalytic properties of the 14V/SBA-15 catalyst (Fi. 2). Interestingly, the vanadium abundance is similar for all three catalysts under ODH reaction conditions irrespective of the difference in the formal V loading during preparation. The experiment is a good example that attempts to disclose structure-reactivity relationships in heterogeneous catalysis require necessarily surface analysis of the working catalyst.

The details of the O K-NEXAFS measured under reaction conditions reveal that the remarkable evolution in V abundance for 14V/SBA-15 goes along with structural modifications (Fig. 5). The intensity of the resonance at 529.6 eV (marked with an arrow in Fig. 5) is significantly reduced when the catalyst is heated from 673 K (spectrum b) to 773 K (spectrum c) under ODH reaction conditions. As discussed before, this is an indication of a loss of 3-dimensional character of the surface vanadium oxide species, i.e. a spreading of the remaining vanadium species on the catalyst surface. The resulting O K-NEXAFS under ODH reaction conditions (spectrum c and spectrum d in Fig. 5) resembles the spectra found for lower V loading (*i.e.*, ≤ 8 wt-% V) catalyst (compare to Fig. 3). Therefore, it can be concluded that these catalysts are structurally similar under ODH reaction condition. The structural dynamics observed in particular for the 14V/SBA-15 catalyst are in good agreement with the results of kinetic studies in a fixed bed reactor under ambient pressure that indicate a dynamic behavior of the catalyst in repeated runs (Fig. 2). The NEXAFS results provide a rational explanation for the lining-up of activation energies for silica-supported catalysts with different vanadium oxide loading.

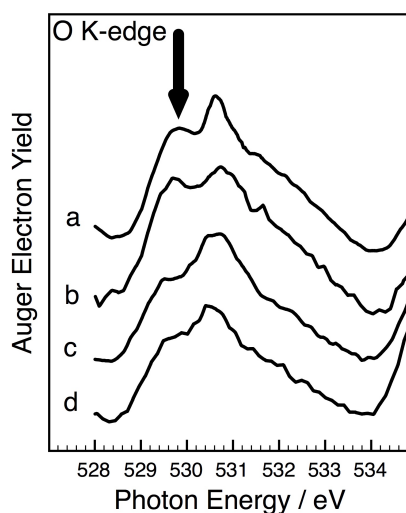


Fig. 5. Evolution of a detail of the O K-edge for the 14V/SBA-15 catalyst at O₂, 673 K (a), C₃H₈+O₂ (2:1), 673 K (b), C₃H₈+O₂ (2:1), 773 K (c), and C₃H₈+O₂ (2:1), 823 K (d).

MoO_x/SBA-15

Molybdenum oxide is catalytically active in a wide range of different organic reactions including oxidation, hydrogenation, metathesis and isomerization that require both redox and acid-base functions. Selective oxidation of propene to acrolein, oxidation of acrolein to acrylic acid, methanol oxidation, olefin metathesis or hydroprocessing applications are prominent examples of commercially implemented molybdenum oxide based catalysts. Aiming at an improved fundamental understanding of oxidation catalysis, supported molybdenum oxide species have been studied as model catalysts in partial oxidation of different substrates, e.g., methanol,[26] propylene,[27] and propane.[28] We have studied the molecular structure of molybdenum oxide species supported on SBA-15 by *in-situ* X-ray absorption fine structure (NEXAFS) measurements near the oxygen K-edge. The results were interpreted by comparing the experimental spectra with theoretical spectra of model clusters obtained by simulations using state of the art density functional theory (DFT), which have been performed in collaboration with Project C6.[29]

The synthesis of MoO_x/SiO₂ was adapted from the functionalization / anion exchange procedure applied in the previous funding period in the preparation of silica supported vanadia catalysts. The mesoporous support, which was synthesized based on the original recipe of Zhao et al.,[17] was functionalized using 3-aminopropyltrimethoxysilane (APTMS) followed by protonation of the resulting amine with HCl. The chloride ions were exchanged by heptamolybdate ions applying ammonium heptamolybdate ((NH₄)₆Mo₇O₂₄·4H₂O) as Mo precursor followed by calcination at 823 K.

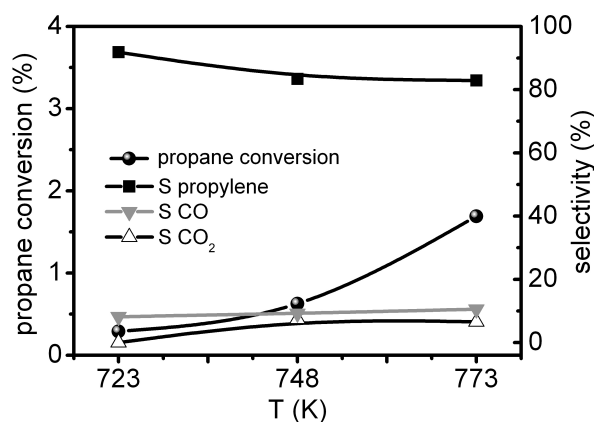


Fig. 6. Propane conversion and product selectivity in oxidative dehydrogenation of propane over 11.1%Mo/SBA-15 for a contact time of 0.6 gs/ml in a feed mixture containing the reactants in a molar ratio of C₃H₈/O₂/N₂=10/5/85.

Due to the well-defined preparation procedure, the present silica supported molybdenum oxide catalyst seems adequately suited as a model to gain new insight into the nature of the active sites as well as into relations between structural properties and activity with emphasis on oxidation reactions. The SBA-15 supported molybdenum oxide catalyst containing 11 wt.-% molybdenum is found to be active in oxidative dehydrogenation of propane. Its activity was studied in a temperature range between 723 and 773 K applying contact times between 0.05 and 0.6 gs/ml and a molar ratio of propane : oxygen = 2 : 1 with nitrogen as balance ($C_3H_8/O_2/N_2=10/5/85$) (Fig. 6). For a contact time of 0.6 gs/ml propane conversion reaches a maximum of approximately 2 %. Under these conditions, only small amounts of total and partial oxidation products CO_2 and CO are formed resulting in a propylene selectivity of more than 80%. The Arrhenius plot using the propane consumption rate yields an apparent activation energy of 162 kJ/mol This is considerably high compared to values reported in the literature for molybdenum oxide species supported on other carrier oxides. The apparent activation energy of propane activation has been determined to be 117 kJ/mol on 11% MoO_x/ZrO_2 ,[30] and 97 kJ/mol on 5% MoO_x/TiO_2 [22] for catalysts with molybdenum oxide loadings corresponding to a theoretical monolayer. This substantiates the strong effect of the support in oxidative dehydrogenation of propane.

The experimental NEXAFS spectra exhibit a pronounced double-peak structure in the O 1s to Mo 4d - O 2p excitation range of 529 - 536 eV (dotted line in Fig. 7). Comparison with the theoretical data (calculations performed in Project C6) gives clear indications that dioxo molybdena species with tetrahedral MoO_4 units can explain the experimental spectrum. This does not fully exclude species with other Mo coordination, like pentahedral surface clusters. But the latter are believed to exist in the present samples in much smaller amounts. The experimental NEXAFS spectrum for the supported molybdena species differs substantially from that for MoO_3 bulk material with octahedral MoO_6 units where the observed asymmetric peak structure is also reproduced by the calculations. It suggests strongly that the dehydrated molybdena prepared in the SBA-15 support of the present study does not contain octahedrally coordinated MoO_6 units.

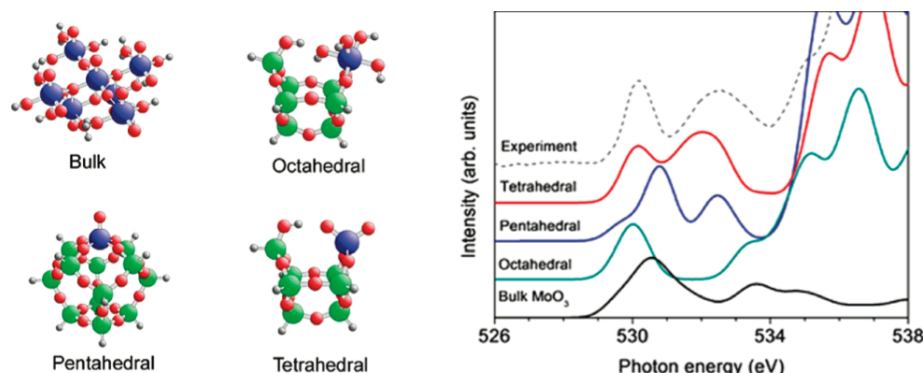


Fig. 7. Geometric structure of the molybdena–silica model clusters (left) and comparison of theoretical O 1s core excitation spectra for $\text{MoO}_x/\text{SiO}_2$ clusters reflecting tetrahedral, pentahedral, and octahedral molybdenum coordination. The figure includes for comparison the corresponding theoretical spectrum for MoO_3 bulk as well as experimental O K-edge NEXAFS data (dashed line) for dehydrated $\text{Mo}_x\text{O}_y/\text{SBA-15}$ with 11.1 wt % Mo.[29]

Synthesis and properties of $(\text{VO}_x)_n$ supported on TiO_x -modified SBA-15

Research from the current funding period has explored the relationship between vanadia and titania guest phases deposited on a high surface area SBA-15 support. The development of an extensive and comprehensive sample matrix has allowed an enhanced understanding of the interaction of both metal oxide guest phases with the support material.

Titania is grafted onto the SBA-15 support via reaction of surface silanol groups with titanium isopropoxide forming Si-O-Ti bonds. A step-wise grafting is used to minimize formation of multilayer titania domains, which occur with single-step grafting, and to approach a titania monolayer surface coverage while maintaining the integrity of the mesopore system. Vanadia is grafted onto such $\text{TiO}_x/\text{SBA-15}$ supports via reaction with Vanadium(V) triisopropoxide ($\text{VO}(\text{OiPr})_3$). This iterative process allows the vanadium and titanium content to be individually incremented, which lead to the generation of a comprehensive sample library (Fig. 8).[31]

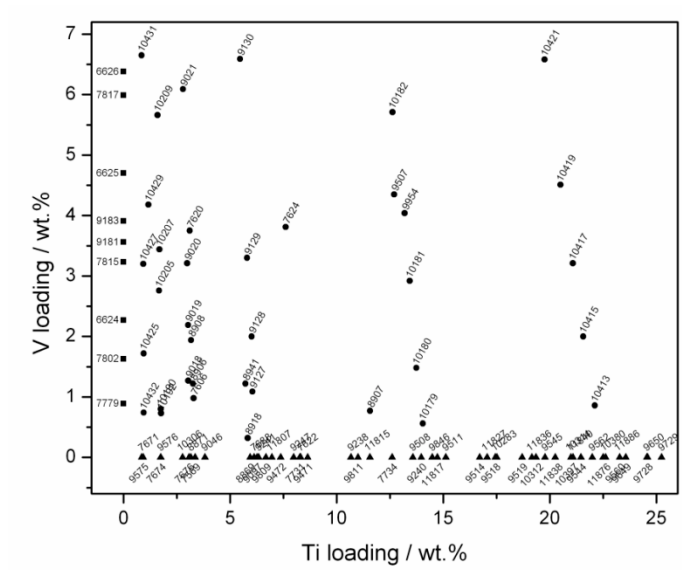


Fig. 8. $(VO_x)_n$ - TiO_x /SBA-15 catalysts library prepared in the current funding period.

Infrared spectroscopy represents a uniquely sensitive method to probe the interaction between support hydroxyl groups (silanols) and deposited surface oxide species. Infrared spectra for both the $(VO_x)_n$ /SBA-15 and TiO_x /SBA-15 sample series reveal the interaction of surface silanol groups with the metal oxide guest phases, showing a consumption of silanol groups with increasing metal loading. Fig. 9 presents the relationship between the ratio of the integrated intensities of the ν_{OH} massif of each V/SBA-15 and Ti/SBA-15 sample and the mother SBA-15, against the ratio of the number of moles of deposited metal and silanol groups present on the mother SBA-15. The trend for vanadia deposition is approximately linear, which, when extrapolated, intersects the x-axis at a value of 0.5 moles of deposited vanadium per mole of silanol groups. This indicates that at theoretical monolayer coverage, where every silanol group is consumed, approximately two OH groups are required to graft each vanadium atom. In contrast, the trend for the Ti/SBA-15 series is represented by a curve, which indicates that less silanol groups are consumed per mole of deposited Ti at high loadings. The curve for the Ti/SBA-15 series does not intersect the x-axis, because the contribution of isolated $\nu(TiO-H)$ modes of a similar energy to $\nu(SiO-H)$ towards the integrated area of the ν_{OH} massif may impose asymptoticity. However the upper limit that can reasonably be proposed for the stoichiometry of a theoretical titania monolayer is 1 mole of deposited Ti per mole of silanol groups, since any ratio less than 1 OH per Ti indicates the formation of Ti-O-Ti bonds perpendicular to the surface; a situation that would demand that a theoretical monolayer coverage had been exceeded. Here, a loading of 17 wt.% titanium corresponds to a surface

density of 2.9 Ti/nm^2 , which, when compared to the surface silanol density (3.1 OH/nm^2), implies a 1:1 ratio between silanol groups and deposited Ti atoms.

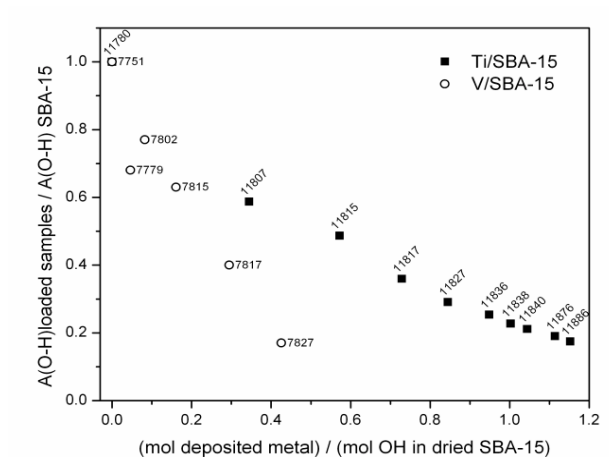


Fig. 9. Relationship between titanium and vanadium loading with OH density as revealed by IR.

Raman spectroscopic measurements show the onset of formation of anatase nano-domains at Ti loadings of 17 wt.% as indicated by a single weak signal located at 154 cm^{-1} (E_g mode of anatase). At higher Ti loadings additional anatase modes indicate the formation of larger anatase domains. However, the absence of anatase reflexes in XRD patterns of catalysts up to 23 wt.-% Ti/SBA-15 indicates the presence of titania nanocrystallites of exceptionally small dimension ($<2 \text{ nm}$).

The relative Lewis and Brønsted acidity was determined by comparing infrared spectroscopic measurements of adsorbed ammonia. For pure V/SBA-15 and Ti/SBA-15 series, increased loading leads to a linear increase in the measured Brønsted acid site density. The trend is more pronounced for the samples containing vanadium than for the Ti/SBA-15 series, indicating that Brønsted acidity is dominated by vanadium species. The Lewis acidity increases also with increasing V or Ti loading. Mixed samples present a greater Lewis acid site density than either of the pure V/SBA-15 or Ti/SBA-15 analogues.

The structure of the binary V-Ti/SBA-15 catalysts was studied by FTIR spectroscopy of adsorbed CO, UV-vis and NEXAFS. Probing the free titania surface in V-Ti/SBA-15 catalysts by CO adsorption at 77 K indicates that vanadia is preferentially, but not exclusively anchored on titania. On sub-monolayer Ti/SBA-15 supports vanadia is also located on residual free silica even in the case when TiO_x sites are still accessible.

For vanadia supported on Ti-SBA-15, the bands in the UV-vis spectra originate from superimposed LMCT transitions of both vanadium and titanium surface oxide species. Apparently, titania in sub-monolayer abundance stabilizes surface vanadium oxide species in tetrahedral coordination, because the peak maxima in the spectra of the catalysts 4V-3Ti/SBA-15 and 4V-8Ti/SBA-15 are shifted to higher energy compared to 4V/SBA-15 (Fig. 10). The interpretation of the 4V-13Ti/SBA-15 spectrum is not that simple. The total metal loading in this catalyst is close to the capacity of a monolayer. This might lead to the formation of a mixed 2D V-Ti surface oxide with unique absorption properties resulting in an absorption maximum close to that of 4V/SBA-15.

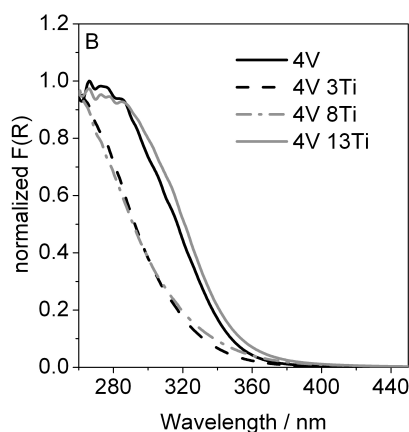


Fig.10. UV-vis spectra of V-Ti/SBA-15 catalysts after dehydration in synthetic air at 723 K.

Similarly, the interpretation of the O K-NEXAFS of vanadia supported on Ti-SBA-15 is complicated by the overlap of absorption features related to oxygen bond only to V, only to Ti or both to V and Ti. The Ti L₃-edge pre-peak intensity is further increased in the mixed system V/Ti/SBA-15. This is the result of a modification of Ti-O bonds by the anchorage of V species at the titania clusters. Interestingly, this spectroscopic fingerprint for an enhanced linkage at the Ti site is the same either when the Ti loading is increased or when the Ti site configuration is modified by adding V. This points to the fact that the newly formed V-O-Ti bonds create a bonding configuration at the Ti site that is similar to the formation of Ti-O-Ti bonds when the Ti loading is increased. This similarity might facilitate the preferential anchorage of V on titania sites instead on the SBA-15 support.

In-situ UV-vis spectroscopic experiments reveal that vanadia species supported on Ti/SBA-15 are structurally more stable under reaction conditions of oxidative dehydrogenation of propane compared to vanadia supported on SBA-15. Furthermore, a clear correlation between the

abundance of vanadium oxide species in tetrahedral coordination and high selectivity of the catalyst in oxidative dehydrogenation of propane towards propylene has been found.[32]

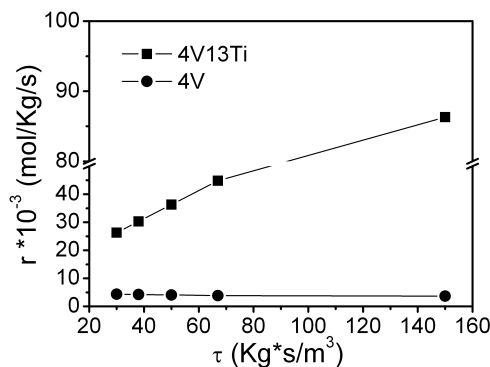


Fig.11. Consumption rate of propane in oxidative dehydrogenation of propane at 500°C as a function of the contact time.

The kinetics of the oxidative dehydrogenation of propane over the catalysts in the V-Ti library have been studied in collaboration with Project B6 and the details regarding the catalytic properties of the catalysts are reported there. Generally, significant improvement in performance is observed when vanadia is deposited on dispersed titanium oxide surface species (Fig. 11) suggesting a threshold for synergy when the titania monolayer is approached. Accordingly, the V-Ti/SBA-15 system has to be considered as a well-defined model system with practical potential. The productivity observed under the explored reaction conditions exceeds the requirement for industrial application of $1 \text{ g}_{\text{C}_3\text{H}_6} \text{g}_{\text{cat}}^{-1} \text{h}^{-1}$ by far. Since the selectivity in propane oxidation to propylene is limited by consecutive reactions and surface titania species contribute also to the ODH activity, there is no simple correlation between V/Ti/Si ratio and reactivity. The optimization parameters are a maximum coverage of silica with non-crystalline titania and a maximum coverage of titania by vanadia in form of $(\text{VO}_x)_n$ oligomers.

References:

- [1] C. Hess, R. Schlögl, Chem. Phys. Lett., 432 (2006) 139.
- [2] C. Hess, U. Wild, R. Schlögl, Microporous and Mesoporous Materials, 95 (2006) 339.
- [3] C. Hess, Journal of Catalysis, 248 (2007) 120.
- [4] C. Hess, G. Tzolova-Muller, R. Herbert, J. Phys. Chem. C, 111 (2007) 9471.
- [5] T.V. Venkov, C. Hess, F.C. Jentoft, Langmuir, 23 (2007) 1768.
- [6] C. Hess, M.H. Looi, S.B.A. Hamid, R. Schloegl, Chemical Communications (Cambridge, United Kingdom), (2006) 451.
- [7] T. Blasco, J.M. Lopez Nieto, Applied Catalysis, A: General, 157 (1997) 117.
- [8] J.M. Lopez Nieto, Topics in Catalysis, 41 (2006) 3.

- [9] E.V. Kondratenko, M. Cherian, M. Baerns, *Catalysis Today*, 112 (2006) 60.
- [10] A. Dinse, B. Frank, C. Hess, D. Habel, R. Schomäcker, *Journal of Molecular Catalysis A: Chemical*, 289 (2008) 28.
- [11] A. Trunschke, Propane selective oxidation to acrylic acid, in: C. Hess, R. Schlögl (Eds.) *Nanostructured Catalysts: Selective Oxidation Reactions*, RSC Nanoscience & Nanotechnology, Cambridge, 2011.
- [12] Y.V. Kolen'ko, W. Zhang, R. Naumann d'Alnoncourt, F. Girgsdies, T.W. Hansen, T. Wolfram, R. Schlögl, A. Trunschke, *ChemCatChem*, accepted (2011).
- [13] M. Hävecker, S. Wrabetz, J. Kröhnert, L.-I. Csepei, R. Naumann d'Alnoncourt, Y.V. Kolen'ko, F. Girgsdies, R. Schlögl, A. Trunschke, *Journal of Catalysis*, submitted (2011).
- [14] W. Zhang, A. Trunschke, R. Schlögl, D. Su, *Angewandte Chemie International Edition*, 49 (2010) 6084.
- [15] A. Celaya Sanfíz, T.W. Hansen, D. Teschner, P. Schnörch, F. Girgsdies, A. Trunschke, R. Schlögl, M.H. Looi, S.B.A. Hamid, *The Journal of Physical Chemistry C*, 114 (2010) 1912.
- [16] D. Zhao, J. Feng, Q. Huo, N. Melosh, G.H. Fredrickson, B.F. Chmelka, G.D. Stucky, *Science*, 279 (1998) 548.
- [17] D. Zhao, Q. Huo, J. Feng, B.F. Chmelka, G.D. Stucky, *Journal of the American Chemical Society*, 120 (1998) 6024.
- [18] Y.-M. Liu, Y. Cao, N. Yi, W.-L. Feng, W.-L. Dai, S.-R. Yan, H.-Y. He, K.-N. Fan, *Journal of Catalysis*, 224 (2004) 417.
- [19] Y.-M. Liu, Y. Cao, K.-K. Zhu, S.-R. Yan, W.-L. Dai, H.-Y. He, K.-N. Fan, *Chemical Communications*, (2002) 2832.
- [20] P. Gruene, T. Wolfram, K. Pelzer, R. Schloegl, A. Trunschke, *Catalysis Today*, 157 (2010) 137.
- [21] M.D. Argyle, K. Chen, A.T. Bell, E. Iglesia, *Journal of Catalysis*, 208 (2002) 139.
- [22] A. Khodakov, B. Olthof, A.T. Bell, E. Iglesia, *Journal of Catalysis*, 181 (1999) 205.
- [23] G. Tzolova-Muller, M. Hävecker, in preparation, (August 2011).
- [24] M. Hävecker, M. Cavalleri, R. Herbert, R. Follath, A. Knop-Gericke, C. Hess, K. Hermann, R. Schlögl, *physica status solidi (b)*, 246 (2009) 1459.
- [25] M. Cavalleri, K. Hermann, A. Knop-Gericke, M. Hävecker, R. Herbert, C. Hess, A. Oestereich, J. Döbler, R. Schlögl, *Journal of Catalysis*, 262 (2009) 215.
- [26] J.-M. Jehng, H. Hu, X. Gao, I.E. Wachs, *Catalysis Today*, 28 (1996) 335.
- [27] A.N. Desikan, W.M. Zhang, S.T. Oyama, *Journal of Catalysis*, 157 (1995) 740.
- [28] K. Chen, A.T. Bell, E. Iglesia, *The Journal of Physical Chemistry B*, 104 (2000) 1292.
- [29] C.S. Guo, K. Hermann, M. Hävecker, J.P. Thielemann, P. Kube, L.J. Gregoriades, A. Trunschke, J. Sauer, R. Schlögl, *The Journal of Physical Chemistry C*, (2011) null.
- [30] E. Heracleous, M. Machli, A.A. Lemonidou, I.A. Vasalos, *Journal of Molecular Catalysis A: Chemical*, 232 (2005) 29.
- [31] N. Hamilton, in preparation, (2011).
- [32] G. Tzolova-Muller, M. Hävecker, in preparation, (2011).

5.2.2 Projektrelevante eigene Publikationen

a) erschienene oder angenommene Arbeiten in wissenschaftlichen Zeitschriften oder Buchveröffentlichungen

- [S11] R. Schlögl,
Active Sites for Propane Oxidation: Some Generic Considerations.
Top. Catal. **54** (2011) 627 - 638.
- [LFZ11] X. Liu, B. Frank, W. Zhang, T.P. Cotter, R. Schlögl, D.S. Su,
Carbon-Catalyzed Oxidative Dehydrogenation of n-Butane: Selective Site Formation during sp^3 -to- sp^2 Lattice Rearrangement / Kohlenstoff-katalysierte oxidative Dehydrierung von n-Butan: Einfluss der sp^3/sp^2 -Phasenumwandlung auf die Produktselektivität.
Angew. Chem. Int. Ed. /Angew. Chem. **50/123** (2011) 3318-3322/3371-3375.
- [GHH11] C. Guo, K. Hermann, M. Hävecker, J. Thielemann, P. Kube, L. Gregoriades, A. Trunschke, J. Sauer, R. Schlögl,
Structural Analysis of Silica-Supported Molybdena Based on X-Ray Spectroscopy: Quantum Theory and Experiment
J. Phys. Chem. **115** (2011) 15449 - 15458.
- [HWK11] M. Hävecker, S. Wrabetz, J. Kröhnert, L.-I. Csepei, R. Naumann d'Alnoncourt, Y.V. Kolen'ko, F. Girgsdies, R. Schlögl, A. Trunschke
Surface chemistry of phase-pure M1 MoVTeNb oxide during operation in selective oxidation of propane to acrylic acid
J. Catal. (2011) DOI: 10.1016/j.jcat.2011.09.012.
- [ZTS10] W. Zhang, A. Trunschke, R. Schlögl, D.S. Su,
Real-Space Observation of Surface Termination of a Complex Metal Oxide Catalyst
Angew. Chem. Int. Ed./Angew. Chem. **49/122** (2010) 6084-6089/6220-6225.
- [GWP10] P. Grüne, T. Wolfram, K. Pelzer, R. Schlögl, A. Trunschke,
Role of dispersion of vanadia on SBA-15 in the oxidative dehydrogenation of propane
Catalysis Today **157** (2010) 137-142.
- [TEW09] J.-P. Tessonnier, O. Ersen, G. Weinberg, C. Pham-Huu, D.S. Su, R. Schlögl,
Selective Deposition of Metal Nanoparticles Inside or Outside Multiwalled Carbon Nanotubes.
ACS Nano **3** (2009) 2081-2089.
- [HWS09] R. Herbert, D. Wang, R. Schomäcker, R. Schlögl and C. Hess,
Stabilization of Mesoporous Silica SBA-15 by Surface Functionalization
ChemPhysChem **10** (2009) 2230-2233.

- [HCH09] M. Hävecker, M. Cavalleri, R. Herbert, R. Follath, A. Knop-Gericke, C. Hess, K. Hermann and R. Schlögl,
Methodology for the structural characterisation of $VxOy$ species supported on silica under reaction conditions by means of in situ O K-edge X-ray absorption spectroscopy.
Phys. Status Solidi B **246** (2009) 1459-1469.
- [FZB09] B. Frank, J. Zhang, R. Blume, R. Schlögl, and D.S. Su,
Heteroatoms Increase the Selectivity in Oxidative Dehydrogenation Reactions on Nanocarbons / Heteroatome steigern die Selektivität der oxidativen Dehydrierung an Nanokohlenstoff.
Angew. Chem. Int. Ed. / Angew. Chem. **48/121** (2009) 6913 - 6917/7046-7051.
- [FFH09] B. Frank, R. Fortrie, C. Hess, R. Schlögl, and R. Schomäcker,
Reoxidation dynamics of highly dispersed VOx species supported on γ -alumina
Appl. Catal. A: General **353** (2009) 288-295.
- [DKF09] A. Dinse, S. Khennache, B. Frank, C. Hess, R. Herbert, S. Wrabetz, R. Schlögl, and R. Schomäcker,
Oxidative dehydrogenation of propane on silica (SBA-15) supported vanadia catalysts: A kinetic investigation.
J. Mol. Catal. A Chemical **307** (2009) 43-50.

b) andere Veröffentlichungen

Nanostructured Catalysts: Selective Oxidations,
RSC Nanoscience & Nanotechnology 19, Cambridge, 2011,
Ed. by C. Hess and R. Schlögl

5.3 Rückblick auf die Förderung

Das Teilprojekt wurde seit 07/1999 im Sonderforschungsbereich gefördert. Es wurde mit Ablauf der 4. Förderperiode im Juni 2011 beendet.

5.3.1 Personal im Teilprojekt während der 4. Förderperiode

	lauf. Nr.	Name, akademischer Grad, Dienststellung	engere Fachzugehörigkeit	Institut der Hochschule oder der außeruniv. Einrichtung	Mitarbeit im Projekt Zeitraum, Wochenstunden	Entgeltgruppe
Grundausstattung						
Wissenschaftlerinnen und Wissenschaftler	1.	Robert Schlögl, Dr., Univ.-Prof..	Phys. Chemie	FHI	07/1999 – 06/2011, 4h	
	2.	Katrin Pelzer, Dr.	Phys. Chemie	FHI	07/2008 – 03/2009, 8h	
nichtwissenschaftl. Mitarbeiterinnen und Mitarbeiter						
Ergänzungsausstattung						
Wissenschaftlerinnen und Wissenschaftler	1.	Di Wang, Dr.	Phys. Chemie	FHI	01/2007 – 05/2009,	E13
	2.	Phillip Grüne	Phys. Chemie	FHI	06/2009 – 11/2009, 20h	E13, 50%
	3.	Till Wolfram	Phys. Chemie	FHI	08/2009 – 06/2011, 20h	E13, 50%
	4.	Genka Tzolova-Müller, Dr.	Phys. Chemie	FHI	05/2009 – 06/2011	E13
nichtwissenschaftl. Mitarbeiterinnen und Mitarbeiter						

Aufgaben der Mitarbeiterinnen und Mitarbeiter (Grundausstattung):

1. Prof. Dr. Robert Schlögl
Leiter des TP, Gesamtkoordination, Fortentwicklung der Konzeption, Anleitung der Doktoranden und der Mitarbeiter
2. Dr. Katrin Pelzer
Synthese von V/SBA-15

Aufgaben der Mitarbeiterinnen und Mitarbeiter (Ergänzungsausstattung):

1. Dr. Di Wang
Durchführung von HRTM- und ELNES-Experimenten sowie Untersuchungen mittels Mikroreaktor, Zusammenarbeit mit TPB6
2. Dr. Philipp Grüne
Synthese, katalytische und spektroskopische Untersuchungen von V/SBA-15 Katalysatoren
3. Till Wolfram
Synthese und spektroskopische Untersuchungen von V-Ti/SBA-15 Katalysatoren
4. Dr. Genka Tzolova-Müller
In-situ spektroskopische Untersuchungen an V-Ti/SBA-15 Katalysatoren

5.1 Allgemeine Angaben zum Teilprojekt B3

5.1.1 Titel: Interaction of oxidants (O₂, N₂O, CO₂ und H₂O) with well defined VO_x aggregates und its influence on partial oxidation of low alkanes

5.1.2 Projektleitung

Priv.-Doz. Dr. Evgenii V. Kondratenko
geb. 02.06.1967

Prof. Dr. Reinhard Schomäcker
geb. 08.01.1959

Leibniz Institut für Katalyse e.V.
an der Universität Rostock

Institut für Chemie,
Fachgruppe Technische Chemie,
Technische Universität Berlin
Strasse des 17. Juni 124-128
10623, Berlin

Albert-Einstein-Strasse 29A
18057, Rostock

Telefon: 0381 / 1281290
E-Mail: evgenii.kondratenko@catalysis.de

030 / 31424973
schomaecker@tu-berlin.de

5.2 Entwicklung des Teilprojekts

5.2.1 Bericht

Functionalization of cheap and in future longer available C₂-C₅ alkanes from natural gas towards corresponding olefins currently produced from oil-derived feeds is a challenging topic in academia and industry. Compared to the commercially applied non-oxidative dehydrogenation, the oxidative dehydrogenation of these alkanes is not thermodynamically constrained and does not suffer from rapid catalyst deactivation requiring often oxidative regeneration. However, the oxidative dehydrogenation is still far from industrial applications. Its main drawback is low olefin selectivity at high alkane conversions due to fast consecutive oxidation of the target olefin to carbon oxides [1-3]. In the previous funding periods of Sfb 546, our research was mainly focused on identifying the nature of VO_x species and their reactivity in the oxidative dehydrogenation of propane. The selectivity-determining factors were not thoroughly dealt with. Therefore, the main focus of the last funding period was to identify origins governing olefin selectivity in oxidative conversion of C₂-C₄ alkanes. The results obtained are summarized below.

Propane dehydrogenation over supported and bulk vanadium oxides

In cooperation with subproject C4, we further investigated catalytic properties of V_2O_5 single crystal in the oxidative dehydrogenation of propane (ODP) and compared them with those of bulk polycrystalline V_2O_5 as well as of highly dispersed surface VO_x species over SiO_2 - TiO_2 ($Ti/Si=0$ - 1.5). Fig. 1 illustrates time-on-stream propane conversion over at V_2O_5 single crystal 773 K. The inserts in this figure are SEM (scanning electron microscopy) images of the single crystal before (at time 0) and after the ODP reaction (after 450 minutes on ODP stream). One can clearly see that the propane conversion was practically zero during first 100 minutes on stream. Hereafter, a strong increase in the conversion was obtained. It should be stressed that neither reaction temperature, nor contact time, nor feed composition were changed. Therefore, such strong conversion increase should be related to catalyst restructuring, which is evident from the SEM images in Fig.1. As a result of the restructuring, the specific surface area of the V_2O_5 crystal after the reaction increased by a factor of 50 as proven by BET measurements with Kr.

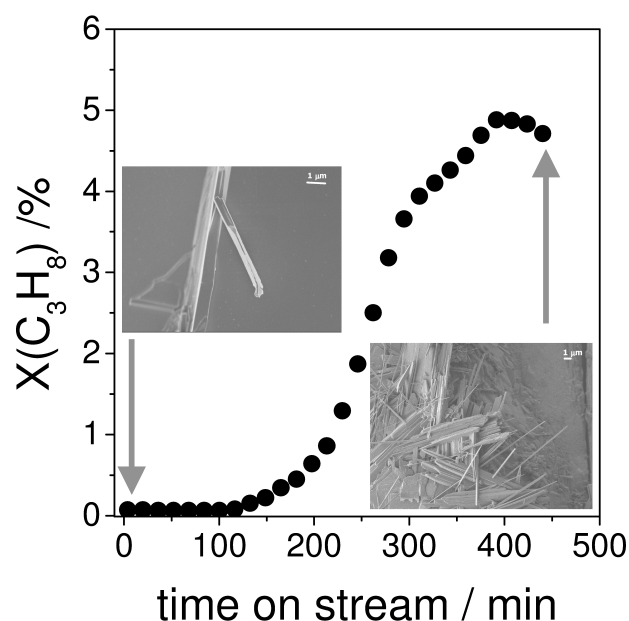


Fig. 1. Propane conversion as function of time on stream upon propane dehydrogenation over V_2O_5 single crystal at 773 K using a $C_3H_8:O_2:Ne=40:20:40$ reaction feed. SEM images of the fresh and used crystals are shown in the inserts.

In order to compare the activity of V_2O_5 single crystal with that of polycrystalline V_2O_5 and highly dispersed VO_x species we calculated the turnover frequencies (TOF) as follows. Since the latter species are either isolated or small 2-dimensional aggregates, it was suggested that all vanadium atoms are available for the ODP reaction and do not differ in their intrinsic activity. According to the crystalline structure of bulk V_2O_5 materials, apparent surface density of active

vanadium species is 5 V/nm^2 . This value was used for calculating the TOF values of propane conversion over V_2O_5 single crystal and polycrystalline V_2O_5 . Fig.2 (a) compares the TOFs obtained over different vanadium-containing materials. It is clearly seen that the highly dispersed VO_x species over $\text{SiO}_2\text{-TiO}_2$ ($\text{Ti/Si}=0\text{-}1.5$) have the lowest activity. The influence of the Ti/Si ratio on the ODP activity is thoroughly discussed in section “*Redox properties of VO_x species and their role in propane dehydrogenation*”. It is important to mention that the single crystal showed the highest activity. The difference in the activity between differently structured VO_x species may be partially related to the strength of vanadium-oxygen bond, which weakens upon increasing the degree of polymerisation of VO_x species. This is indirectly supported by the apparent activation energies of propane conversion in Fig. 2(b). The ODP reaction over bulk VO_x species proceeds with a ca. 20 kJ/mol lower activation energy compared to that over the highly dispersed ones.

From a selectivity point of view, V_2O_5 single crystal showed significantly lower propene selectivity than highly dispersed VO_x species. This is due to an increased activity of the former material for consecutive propene oxidation to carbon oxides.

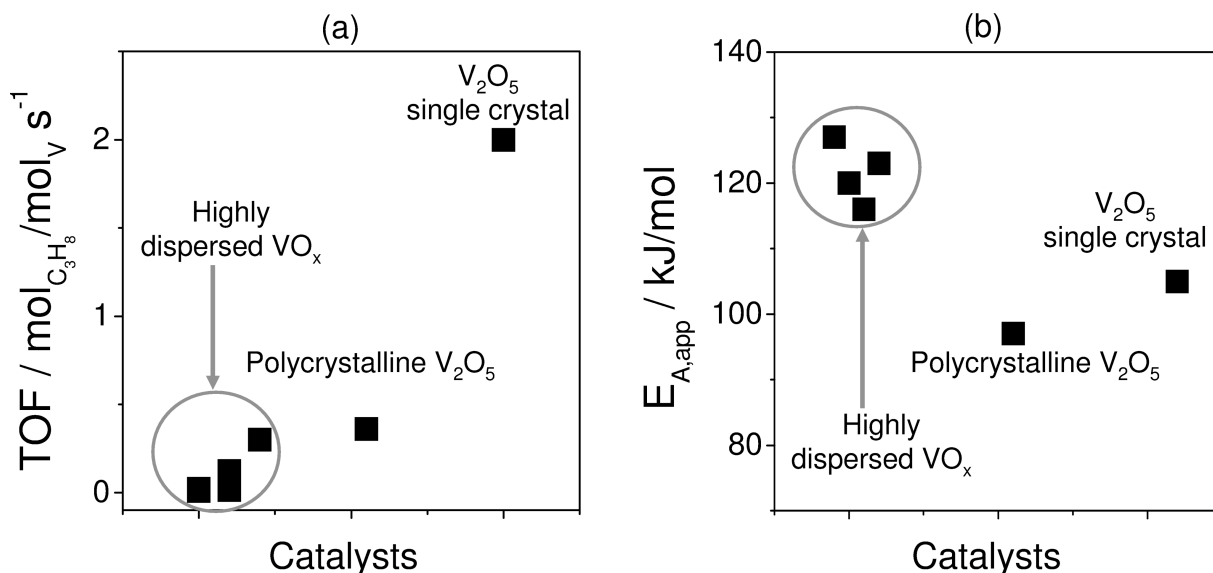


Fig. 2. (a) TOF values and (b) apparent activation energies of propane conversion over different catalytic materials at 773K using a $\text{C}_3\text{H}_8:\text{O}_2:\text{Ne}=40:20:40$ reaction feed.

Effect of oxidising agent of selectivity of $\text{C}_2\text{-C}_4$ alkanes conversion

As demonstrated in our previous studies [4-6] and further supported within this project period, propene selectivity in the ODP reaction is strongly improved when operating with N_2O compared to O_2 irrespective of the nature of VO_x species (from highly dispersed to

polymerized VO_x species and bulk V_2O_3 , VO_2 , and V_2O_5). Since the planned catalytic tests with CO_2 and H_2O showed very low activity in the ODP reaction, we concentrated our studies on the effect of N_2O on alkane dehydrogenation. In [OK09] we demonstrated that this positive effect is of general character and is additionally valid for the oxidative dehydrogenation (ODH) of ethane, n-butane, and iso-butane. As shown in table 1, the overall rate of alkane conversion and the rate of alkene formation decrease by a factor of 3-8 and 1.6-6, while the rates of CO and CO_2 formation (both direct alkane oxidation and consecutive alkene oxidation) become lower in 6-30 and 15-70 times, respectively, upon replacing of O_2 by N_2O . Such a dramatic decrease in the CO_x production clearly distinguishes the ability of N_2O for reducing non-selective reaction pathways in favour of the selective ones (olefin production).

Table 1. Rates of alkane conversion and of alkene, CO and CO_2 formation in ODH reactions of light alkanes at 773 K over VO_x (5 wt.)/MCM-41. Reaction feeds were $\text{C}_n\text{H}_{2n+2}:\text{O}_2:\text{Ne}=40:20:40$ and $\text{C}_n\text{H}_{2n+2}:\text{N}_2\text{O}:\text{Ne}=40:40:20$. $X(\text{C}_n\text{H}_{2n+2}) < 5\%$, $X(\text{O}_2/\text{N}_2\text{O}) < 10\%$.

Alkane	Oxidant	Rate / $\text{mmol g}_{\text{cat}}^{-1} \text{min}^{-1}$			
		$\text{C}_n\text{H}_{2n+2}$	C_nH_{2n}	CO^*	CO_2^*
C_2H_6	O_2	0.85	0.16	0.05	0.57
	N_2O	0.15	0.10	0.04	0.006
C_3H_8	O_2	1.5	0.94	0.15	0.33
	N_2O	0.39	0.34	0.025	0.021
n- C_4H_{10}	O_2	3.1	1.7	0.37	0.39
	N_2O	0.45	0.34	0.02	0.028
i- C_4H_{10}	O_2	4.3	2.6	0.48	0.96
	N_2O	0.56	0.45	0.035	0.041

* the rates of CO and CO_2 formation are a sum of the rates of primary alkane oxidation and consecutive alkene oxidation.

In order to further elucidate the role of oxidizing agent in ODH, catalytic tests were performed at different contact times, i.e. diverse degrees of alkane conversion. The results obtained are presented in Fig. 3. Irrespective of the oxidant applied, olefin selectivity decreases with an increase in the alkane conversion, while CO_x selectivity increases (data are not shown for brevity). For an O_2 -containing feed, primary (extrapolated to zero alkane conversion) alkene selectivity in ODH of propane, n-butane, and iso-butane is close to ca. 70-80%, while significantly lower for the ethane ODH (ca. 40%). This indicates that direct ethane oxidation to CO_x stronger contributes to the overall CO_x production compared to ODH of other alkanes. In case of iso- C_4H_{10} - O_2 mixture, initial iso- C_4H_8 selectivity is ca. 65%, but falls very rapidly to 10% with an increase in iso- C_4H_{10} conversion up to 10%, while CO_x selectivity strongly increases. Upon replacing O_2 with N_2O , olefin selectivity significantly increases, while CO_x

selectivity decreases. The highest effect of N_2O on olefin selectivity at high alkane conversion was found for the iso-butane ODH.

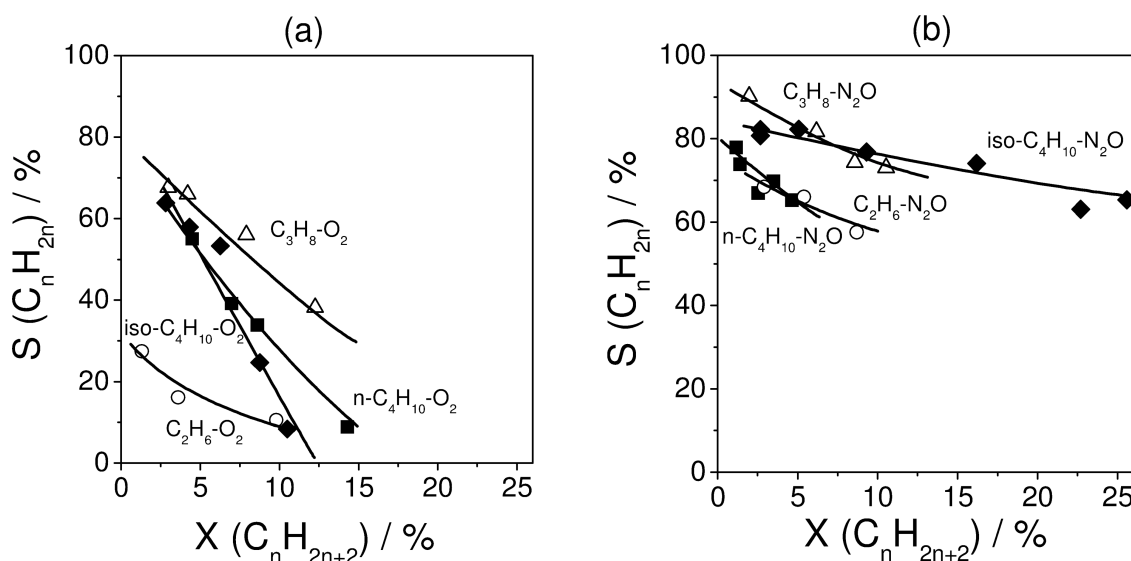


Fig. 3. Selectivity to ethene (○), propene (△), n-butene (■), and iso-butene (◆) over $VO_x(5 \text{ wt.})/MCM-41$ as a function of alkane conversion at 773 K using (a) $C_nH_{2n+2}:O_2:Ne=40:20:40$ and (b) $C_nH_{2n+2}:N_2O:Ne=40:40:20$ reaction feeds.

At this stage it is also important to highlight that the slope of the ODH selectivity-conversion relationships in Fig.3 strongly depends on the alkane and oxidant applied. This slope reflects the catalyst ability for consecutive combustion of primarily formed olefins to CO_x . The following order of consecutive olefin oxidation with O_2 was obtained from Fig.3 (a): $C_2H_4 \leq C_3H_6 < n-C_4H_8 \leq iso-C_4H_8$. It is interesting to note that this order is also valid for the stability of ions or radicals formed from respective alkanes by abstraction of one hydrogen atom. Based on these experimental facts it can be suggested that the long-living ions/radicals are easily oxidized to CO_x . Upon replacing O_2 with N_2O , the slope of ODH selectivity-conversion relationships strongly decreases and does not significantly depend on the alkane applied. The decrease in the slope means that consecutive olefin oxidation is suppressed in the presence of N_2O . In the following, we discuss possible mechanistic reasons of the improving effect of N_2O as derived from experimental EPR (electron paramagnetic resonance) analysis and joint experimental-theoretical studies with the subproject A4.

Structure and reactivity of oxygen species

Taking into account our previous mechanistic analysis using the TAP reactor [7, 8] as well as our current SSITKA studies [OK09] and DFT calculations [RKS08] from A4, a simplified

reaction scheme of product formation from propane/propene over highly dispersed VO_x species in the presence of O₂ and N₂O was developed. Independently of the oxidizing agent (O₂ or N₂O), propene is primarily formed from propane via oxidative dehydrogenation by lattice oxygen of fully oxidized VO_x species. The reduced VO_x species formed can be reoxidized both by O₂ and N₂O. DFT calculations predict that O₂ reoxidizes faster than N₂O as independently proven by kinetic experiments in [OCB09]. This is a possible reason for the lower ODH activity of VO_x (5 wt.)/MCM-41 in table 1 when using N₂O instead of O₂. It is also important to highlight that N₂O and O₂ differ in the nature of oxygen species formed upon reoxidation of reduced VO_x species. While only lattice oxygen is formed upon reaction of N₂O with a reduced VO_x species, O₂ can form peroxovanadates, which then decompose into vanadyl and oxygen [RKS08]. The peroxovanadates are significantly more active for CO_x formation than lattice oxygen. This theoretical conclusion is indirectly supported by the results of SSITKA experiments using ¹⁶O₂-C₃H₈ and ¹⁸O₂-C₃H₈ feeds [OK09]. The distribution of isotopically labeled CO₂ (C¹⁸O₂, C¹⁸O¹⁶O, and C¹⁶O₂) in these experiments did not follow the statistical distribution, assuming CO_x formation with participation of lattice oxygen only. Additionally, our transient experiments in the TAP reactor showed that CO_x formation is increased when O₂ and C₃H₈ were sequentially pulsed when comparing with oxygen-free C₃H₈ pulse experiments.

In order to derive further experimental insights into the mechanism of oxidation of reduced VO_x species with O₂ and N₂O as well as into the nature and reactivity of oxygen species formed from these oxidants we performed EPR studies [KB10]. This technique allows to monitor paramagnetic species. In these experiments, we reduced highly dispersed VO_x species on MCM-41 in vacuum (1.333 mPa) at 773 K for 30 min. During the reduction, the catalyst color changed from white to grey. Since any formation of carbon-containing deposits on the catalyst surface can be excluded during the vacuum treatment, the color change is due to the reduction of V⁵⁺ to V⁴⁺/V³⁺. The reduced catalyst was reoxidized either by O₂ or N₂O at 77 K. No paramagnetic oxygen species were identified in the latter case. However, the hfs (hyperfine structure) signal of V⁴⁺ increased, which clearly indicates that V³⁺ formed during pretreatment in vacuum must have been oxidized by N₂O. This process was even more pronounced when N₂O reoxidized reduced VO_x species at 323 K. In contrast to N₂O, a multiline EPR spectrum occurred upon reoxidation of reduced VO_x species by O₂ at 77 K (Fig. 4).

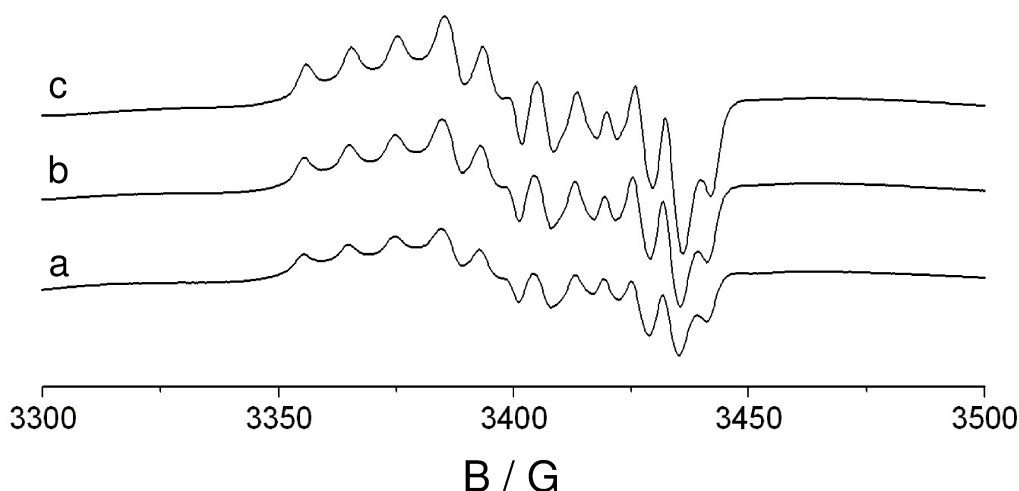


Fig. 4. EPR spectra taken (a) after adsorption of O_2 (5 mbar) over reduced $VO_x/MCM-41$ at 77 K, (b) after warming to 293 K for 1 min and (c) after storage for 1h at 293 K.

This signal became more pronounced after a short warming to 293 K and did not disappear after storage for 1h at 293 K. In other words, this oxygen radical is stable in an oxygen or inert atmosphere. However, its intensity decreased already after 5 min contact with C_3H_8 at 293 K. This signal practically disappeared after further contact with C_3H_8 for 30 min at 293 K and for 5 min at 303 K. When C_3H_6 was used as reactant, the oxygen signal was already gone at 293 K, leaving behind only the hyperfine structure (hfs) signal arising from the coupling of the unpaired electron at the V^{4+} with the nuclear spin of ^{51}V . In agreement with DFT calculations in [RKS08], this proves that C_3H_6 is much more reactive than C_3H_8 .

In order to assign the nature of oxygen species after reoxidation of reduced VO_x species by O_2 at 77 K, the corresponding X-band EPR spectrum has been reproduced by calculation using Eq. 1. Moreover, we also performed EPR measurements of oxidized VO_x species in Q-band at 148 K. Compared to the X-band measurements, higher microwave frequency and magnetic field in the Q-band set-up provide a better resolution of the g tensor components. Based on the results obtained, we concluded that $V^{n+}-O\cdot^-$ species ($n = 4$ or 5) species originates from O_2 . Taking the EPR results and the DFT calculations [RKS08] into account, the following mechanistic scheme of reoxidation of reduced VO_x species by O_2 and N_2O was developed (Fig. 5).

$$H = \mu_B \cdot S \cdot g \cdot B_0 + SAI \quad (1)$$

,in which μ_B is the Bohr magneton, S is the electron spin operator, g is the g tensor, B_0 is the magnetic field vector, A is the hyperfine tensor and I is the nuclear spin operator.

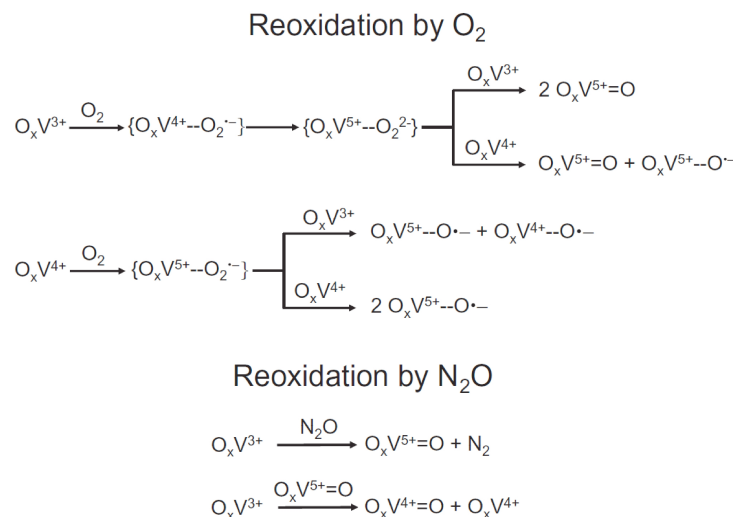


Fig. 5. Suggested pathways of reoxidation of V³⁺O_x and V⁴⁺O_x by O₂ and N₂O.

Redox properties of VO_x species and their role in propane dehydrogenation

In order to investigate the effect of redox properties of VO_x species on the ODP reaction, we applied time-resolved in-situ UV/Vis analysis using a SSITKA-UV/Vis set-up developed in our subproject [OCB09]. Steady-state, time- and spatial-resolved in-situ UV/Vis measurements as well as catalytic tests in combination with isotopic traces can be run simultaneously during heterogeneous catalytic gas-phase reactions from the same solid catalyst under identical reaction conditions. Fig. 6 represents a simplified flowsheet of the set-up and a photo of the reactor together with optical UV/Vis fibres.

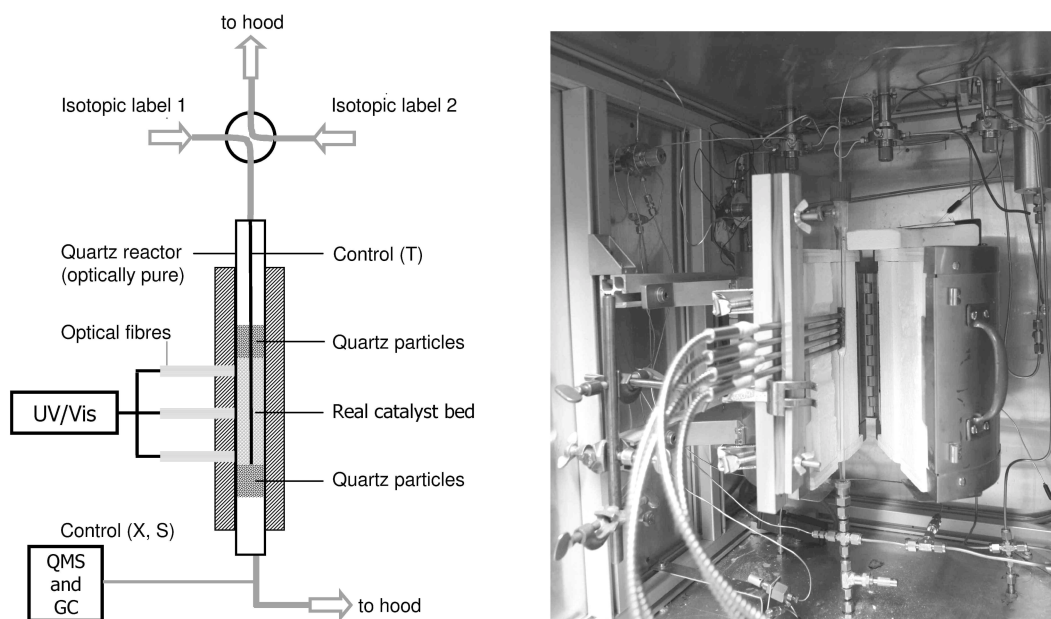


Fig. 6. Schematic representation of set up for simultaneous catalytic testing and catalyst characterization by in-situ UV/Vis spectroscopy.

Catalytic and in-situ UV/Vis characterisation tests were performed with $\text{VO}_x/\text{SiO}_2\text{-TiO}_2$ materials possessing the same amount of vanadium but differing in the ratio of Ti/Si from 0 to 1.5. According to our thorough characterisation studies, all materials had highly dispersed surface VO_x species. Their apparent surface density was $0.4\text{-}1 \text{ V}\cdot\text{nm}^{-2}$, i.e. significantly below one monolayer. Despite the structural similarities of these species, their catalytic activity strongly increased with an increase in Ti loading while propene selectivity did not significantly change. This results in a substantial increase in the propene productivity. Higher propene productivity ($26 \text{ kg}_{\text{C}_3\text{H}_6}\cdot\text{kg}_{\text{cat}}^{-1}\cdot\text{h}^{-1}$) as the state of the art level was achieved over the catalyst with the ratio of Ti/Si of 1.5 (Fig.7). Best literature data in Fig.7 are taken from a recent review of Cavani et al. [1].

In order to elucidate the effect of Ti in SiO_2 support on catalytic performance of VO_x species, we performed a micro-kinetic analysis of reduction and reoxidation of oxidized and reduced VO_x species by C_3H_8 and $\text{O}_2/\text{N}_2\text{O}$, respectively [OCB09]. To this end, we applied time-resolved in-situ UV/Vis analysis for monitoring changes in the oxidation state of vanadium

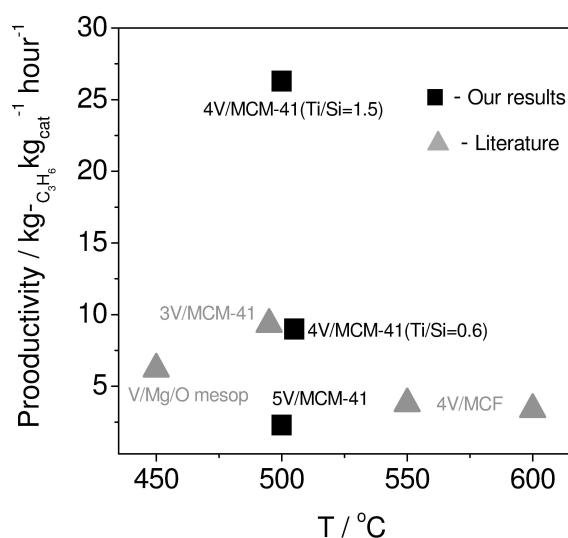


Fig.7. Best obtained propylene productivity over vanadium-based materials. Literature data are from [1].

upon switching from oxidizing ($\text{O}_2/\text{Ne}=20/80$) to reducing ($\text{C}_3\text{H}_8/\text{Ne}=40/60$) and back to oxidizing ($\text{O}_2/\text{Ne}=20/80$ or $\text{N}_2\text{O}/\text{Ne}=40/80$) feeds. This quantitative kinetic study enabled us to determine kinetic parameters of reduction and oxidation steps by oxidized and reduced VO_x species with C_3H_8 and $\text{O}_2(\text{N}_2\text{O})$. The kinetic parameters obtained are summarized in Fig. 8 (a) as a function of the ratio of Ti/Si in $\text{VO}_x/(\text{Ti-Si})\text{O}_2$. Three effects of titanium on redox properties of VO_x species were identified:

i) the reduction constant of oxidized VO_x species by C_3H_8 ($k_{\text{red}}(\text{with } \text{C}_3\text{H}_8)$) increases, ii) the constant of oxidation of reduced VO_x species by O_2 ($k_{\text{ox}}(\text{with } \text{O}_2)$) decreases; and iii) the constant of oxidation of reduced VO_x species by N_2O ($k_{\text{ox}}(\text{with } \text{N}_2\text{O})$) increases. The work in the subproject B6 also highlighted the effect of TiO_2 on redox properties of supported VO_x species.

It is also important to stress that the TOF values of C₃H₈ conversion in the steady-state ODP catalytic tests using O₂ and N₂O increased with the Ti/Si ratio confirming a Mars-van-Krevelen redox cycle involving lattice oxygen and reduced V³⁺ or V⁴⁺ centers. For the ODP with O₂, we found that the k_{red}(with C₃H₈) values determined from our UV/Vis analysis were very close to the TOF value for the corresponding samples. In contrast to the ODP with O₂, k_{red}(with C₃H₈) is significantly higher than the corresponding TOF when operating with N₂O. The ratio of the TOF value to k_{red}(with C₃H₈) was used for determining the fraction of active VO_x sites. We obtained the fraction of 0.9 and 0.15 for the ODP with O₂ and N₂O, respectively.

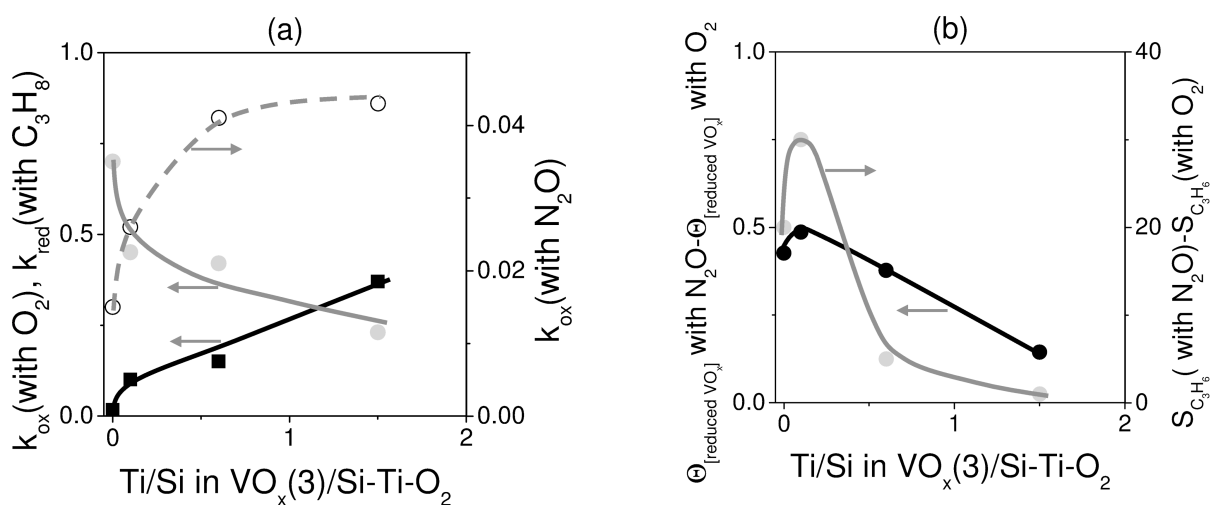


Fig. 8. (a) Kinetic parameters of reduction by (■) C₃H₈ and reoxidation by (●) O₂ and (○) N₂O of VO_x over VO_x(3 wt.%)/(Ti-Si)O₂ materials. (b) Differences in the coverage by reduced VO_x species and in the propene selectivity in the ODP reaction with N₂O and O₂ over these catalysts. Reaction conditions: T=773 K, C₃H₈:O₂:Ne=40:20:40, C₃H₈:N₂O:Ne=40:40:20

The derived kinetic parameters in Fig. 8(a) were used to calculate steady-state reduction degrees of VO_x species under the ODP conditions with O₂ and N₂O assuming the Mars-van-Krevelen mechanism. As shown in Fig. 8 (b), the difference in these degrees between O₂ and N₂O containing feeds passes over a maximum of 0.48 at a Ti/Si ratio of 0.1 and decreases to 0.1 with a further increase in this ratio to 1.5; the smaller this difference, the closer is the reduction degree of VO_x species in the ODP reaction with O₂ and N₂O. It is important to highlight that the difference in steady-state propene selectivity (S(C₃H₆) with N₂O - S(C₃H₆) with O₂) between N₂O- and O₂-mediated ODP (X(C₃H₈) < 2 %, X(N₂O) > 5%, X(O₂) > 5 %) followed the same trend as the difference in the reduction degree of VO_x species (Fig. 8 (b)). Therefore, it was concluded that the reduction degree was an important selectivity-determining factor; the higher the steady-state reduction degree of VO_x species, the higher propene selectivity can be achieved.

Selectivity-determining factors

Based on the results of our catalytic tests, kinetic studies, transient isotopic experiments and DFT calculations from A4, we identified two selectivity-determining factors: i) the nature of surface oxygen and ii) the redox-properties of VO_x species (Fig. 9).

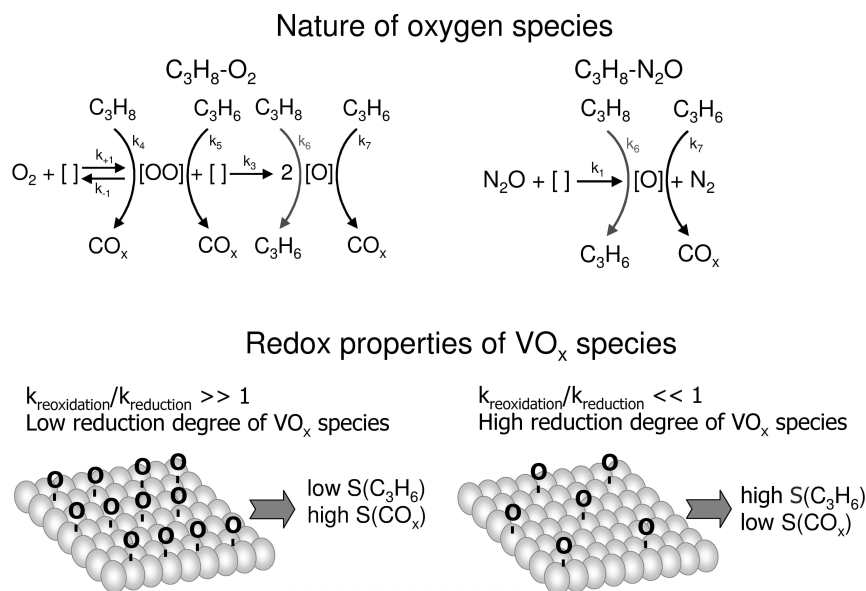


Fig. 9. Selectivity-determining factors in the oxidative dehydrogenation of propane

Lattice oxygen of VO_x species appears to be selective for dehydrogenation of low alkanes to the corresponding olefins. These species are easily formed upon reoxidation of reduced VO_x by O_2 and N_2O and do not significantly contribute to direct C_3H_8 oxidation to CO_x (reaction pathway with k_6 in Fig.9). According to DFT calculations [RKS08], bi-atomic oxygen species are formed from gas-phase O_2 . They are highly reactive for consecutive propene oxidation (reaction pathway with k_5 in Fig.9) but not for direct C_3H_8 oxidation to CO_x (reaction pathway with k_4 in Fig.9). A formal kinetic analysis from the subproject B6 confirms the minor role of CO_x formation from C_3H_8 . Since bi-atomic oxygen species are not formed from N_2O , their participation in CO_x in the ODP reaction with N_2O is excluded. As a result, a higher propene selectivity is achieved with N_2O .

Additionally oxidizing ability of O_2 and N_2O is a crucial parameter governing propene selectivity. O_2 oxidizes reduced VO_x species faster than N_2O therefore higher concentration of active oxygen species is expected in the presence of O_2 . In this case, primarily formed propene is surrounded by active oxygen species and is converted to CO_x before desorption. Since N_2O reoxidizes reduced VO_x species slower than O_2 this results in a lower concentration of active

oxygen species. Therefore, the consecutive propene oxidation is hindered. This ability of oxidants for reoxidation of reduced VO_x species can be tuned by the support and by the nature of VO_x species. Another possibility to tune the kinetics of reduction and reoxidation of VO_x species is variation of partial pressures of reducing and oxidizing agents. This knowledge enabled us to significantly improve the performance of vanadia-catalyzed dehydrogenation of low alkanes. As demonstrated in the following section, when performing the dehydrogenation of propane and iso-butane under oxygen-lean condition (the ratio of $\text{C}_3\text{H}_8/\text{O}_2$ is significantly higher than the stoichiometric one of 2), a strong increase in the olefin selectivity at industrially relevant alkane conversions was obtained.

Improving olefin selectivity via reaction operation

With the aim to improve olefin selectivity in the oxidation dehydrogenation of propane, several approaches dealing with combination of oxidative (ODH) and non-oxidative (DH) processes have already been described in literature [9, 10]. The idea was to use gas-phase O_2 for burning of H_2 in order to shift the thermodynamic equilibrium towards olefins in the non-oxidative dehydrogenation. Additionally, the H_2 combustion provides the heat required for the endothermic DH. For example, Grasselli et al. [9] used two separate reactors loaded with Pt- and Bi-containing materials for the non-oxidative dehydrogenation of propane and selective hydrogen combustion, respectively. Iglesia et al. [10] suggested alkane dehydrogenation over a Pt-containing zeolite in one reactor with staged introduction of O_2 for H_2 removal. Approaches to start from the exothermic ODH process and to use the released heat for DH have been suggested by Schmidt et al. [11] and Forzatti et al. [12] for Pt-catalysts as well as by Buyevskaya et al. [13] for rare-earth oxide catalysts. This auto-thermal reactor operation strongly suffers from the low selectivity towards propene as a result of preferred formation of carbon oxides and C-C scission at high temperature.

Recently we reported on stable and highly selective iso-butane dehydrogenation to iso-butene over VO_x/SiO_2 and $\text{VO}_x/\text{MCM-41}$ under oxygen-lean conditions [OK10]. When combining the oxidative and non-oxidative dehydrogenation, olefin selectivity above 80% at alkane conversions above 40% was achieved (Fig. 10). Compared to $\text{VO}_x/\text{Al}_2\text{O}_3$ catalysts used in [14, 15] for the non-oxidative dehydrogenation of butanes, significantly lower coke formation was observed in our studies. This results in a stable time-on-stream performance over at least 20

hours on stream [OK10]. Since the non-oxidative dehydrogenation of C₃-C₄ alkanes over VO_x/MCM-41 is slower compared to the oxidative dehydrogenation, a sufficient contribution of the non-oxidative dehydrogenation towards alkene production is only possible at higher temperatures (ca. 823-843 K) and longer contact times ($\tau \sim 0.3$ -10 s); the ODP reaction is typically performed in the 673-773 K range and at τ below 0.1 s. A simple increase of the reaction temperature and the contact time results in an increase in the iso-butene selectivity due to the contribution of selective non-oxidative dehydrogenation towards the olefin formation (Fig.10 (b) circle vs. grey squares). However, when using a stoichiometric feed (ratio alkane to O₂ is 2) for the oxidative dehydrogenation, the olefin selectivity was always lower than 70%, and selectivity to CO_x was at least 30 % even at high temperatures and long contact times. Therefore, in order to achieve high olefin selectivity at high alkane conversions, oxygen-lean conditions are necessary (the ratio of oxygen to alkane should be significantly lower than the stoichiometric one for the oxidative dehydrogenation).

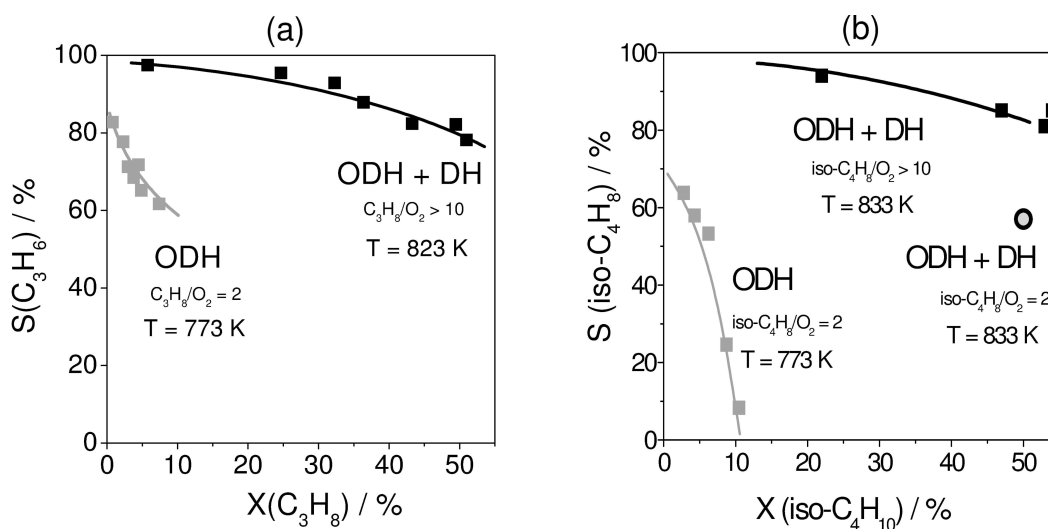


Fig. 10. Selectivity-conversion relationship in (a) propane and (b) iso-butane dehydrogenation over VO_x(5 wt.)/MCM-41. ODH: W/F=0.006 - 0.1 s·g·ml⁻¹; ODH+DH: W/F=0.3 - 18 s·g·ml⁻¹.

References

- [1] F. Cavani, N. Ballarini and A. Cericola, *Catal. Today* 127 (2007) 113.
- [2] M. M. Bhasin, J. H. McCain, B. V. Vora, T. Imai and P. R. Pujado, *Appl. Catal. A* 221 (2001) 397.
- [3] M. Baerns, G. Grubert, E. V. Kondratenko, D. Linke and U. Rodemerck, *Oil Gas-Eur. Mag.* 1 (2003) 36.
- [4] E.V. Kondratenko, M. Baerns, *Appl. Catal. A* 222 (2001) 133.

- [5] E.V. Kondratenko, M. Cherian, M. Baerns, D.S. Su, R. Schlögl, X. Wang, I.E. Wachs, *J. Catal.* 234 (2005) 131.
- [6] E.V. Kondratenko, O. Ovsitser, J. Radnik, M. Schneider, R. Kraehnert, and U. Dingerdissen, *Appl.Catal. A* 319 (2007) 98.
- [7] E.V. Kondratenko, N. Steinfeldt, and M. Baerns, *Phys. Chem. Chem. Phys.* 8 (2006) 1624.
- [8] O. Ovsitser, M. Cherian, and E.V. Kondratenko, *J. Phys. Chem. C* 111 (2007) 8594.
- [9] J. G. Tsikoyiannis, D. L. Stern and R. K. Grasselli, *J. Catal.*, 184 (1999) 77.
- [10] T. Waku, J. A. Biscardi and E. Iglesia, *J. Catal.*, 222 (2004) 481.
- [11] S.S. Bharadwaj, C. Yokoyoma and L.D. Schmidt, *Appl. Catal. A.* 140 (1996) 73.
- [12] A. Beretta, P. Forzatti and E. Ranzi, *J. Catal.* 184 (1999) 469.
- [13] O.V. Buevskaya, M. Baerns, *Catal. Today* 42 (1998) 315.
- [14] M. E. Harlin, V. M. Niemi, A. O. I. Krause and B. M. Weckhuysen, *J. Catal.* 203 (2001) 242.
- [15] S. D. Jackson, S. Rugmini, *J. Catal.* 251 (2007) 59.

5.2.2 Projektrelevante eigene Publikationen

a) erschienene oder angenommene Arbeiten in wissenschaftlichen Zeitschriften oder Buchveröffentlichungen

- [SK11] A. Simon, E. V. Kondratenko
Investigation of the electrical and catalytic properties of materials with $Cs_x(Mo,Nb)_5O_{14}$ composition
Appl. Catal. A 392 (2011) 199 - 207.
- [OK10] O. Ovsitser, E.V. Kondratenko
Selective and stable iso-butene production over highly dispersed VO_x species on SiO_2 supports via combining oxidative and non-oxidative iso-butane dehydrogenation
Chem. Commun. 46 (2010) 4974 - 4976.
- [SK10] A. Simon, E. V. Kondratenko
The flash method: a shortcut for producing the $Cs_x(W,Nb)_5O_{14}$ structure
Chem. Eur. J. 16 (2010) 1765 - 1767.
- [KB10] E.V. Kondratenko, A. Brückner
On the nature and reactivity of active oxygen species formed from O_2 and N_2O on $VO_x/MCM-41$ used for oxidative dehydrogenation of propane
J. Catal. 274 (2010) 111 - 116.
- [OCB09] O. Ovsitser, M. Cherian, A. Brückner, and E.V. Kondratenko
Dynamics of redox behavior of nano-sized VO_x species over Ti-Si-MCM-41 from time-resolved in-situ UV/Vis analysis
J. Catal. 265 (2009) 8 - 18.

- [FAL09] M. Fait, R. Abdallah, D. Linke, E.V. Kondratenko, and U. Rodemerck
A novel multi-channel reactor system combined with operando UV/vis spectroscopy: proof of principles
Catal. Today **142** (2009) 196 - 201.
- [OK09] O. Ovsitser, E.V. Kondratenko
Similarity and differences in the oxidative dehydrogenation of C₂-C₄ alkanes over nano-sized VO_x species using N₂O and O₂
Catal. Today **142** (2009) 138 - 142.
- [KWK09] E.V. Kondratenko, H. Wang, V.A. Kondratenko, and J. Caro
Selective oxidation of CH₄ and C₂H₆ over a mixed oxygen ion and electron conducting perovskite: a TAP and membrane reactors study
J. Molec. Catal. A **297** (2009) 142 - 149.
- [HGT08] D. Habel, O. Goerke, M. Tovar, E.V. Kondratenko, and H. Schubert
Phase relations in the system TiO₂-V₂O_x under oxidizing and reducing conditions
J. Phase Equilib. Dif. **29** (2008) 482 - 487.
- [SHO08] O. Schwarz, D. Habel, O. Ovsitser, E.V. Kondratenko, C. Hess, R. Schomäcker, and H. Schubert
Impact of preparation method on physico-chemical and catalytic properties of VO_x/γ-Al₂O₃ materials
J. Molec. Catal. A **293** (2008) 45 - 52.
- [RKS08] X. Rozanska, E.V. Kondratenko, and J. Sauer
Oxidative dehydrogenation of propane: Differences between N₂O and O₂ in the reoxidation of reduced vanadia sites and consequences for selectivity
J. Catal. **256** (2008) 84 - 94.
- [KO08] E.V. Kondratenko, O. Ovsitser
Catalytic abatement of nitrous oxide coupled with selective production of hydrogen and ethylene
Angew. Chem. Int. Ed. **47** (2008) 3227 - 3229.

b) Patente angemeldet

- [KO10] E.V. Kondratenko, O. Ovsitser,
Verfahren zur Herstellung von Olefinen sowie Katalysator
10 2010 001 910.0 angemeldet am 12.02.2010.

5.3 Rückblick auf die Förderung

Das Teilprojekt wurde seit 07/1999 im Sonderforschungsbereich gefördert. Es wurde mit Ablauf der 4. Förderperiode im Juni 2011 beendet.

5.3.1 Personal im Teilprojekt während der 4. Förderperiode

	lauf. Nr.	Name, akademischer Grad, Dienststellung	engere Fachzugehörigkeit	Institut der Hochschule oder der außeruniv. Einrichtung	Mitarbeit im Projekt Zeitraum Wochenstunden	Entgeltgruppe
Grundausrüstung						
Wissenschaftlerinnen und Wissenschaftler	1.	Evgenii Kondratenko Dr. Priv.Doz.	Techn. Chemie Heterogenkatalyse	LIKAT	07/2008 – 06/2011, 10 h	
	2.	Reinhard Schomäcker, Dr. Prof.	Techn. Chemie	TU-C	07/2008 – 06/2011, 2 h	
	3.	Angelika Brückner, Dr. Prof.	Physikal. Chemie	LIKAT	07/2008 – 06/2011, B	
	4.	Mathias Schneider	Physikal. Chemie	LIKAT	07/2008 – 12/2010, 1 h	
	5.	Sergy Sokolov, Dr.	Physikal. Chemie	LIKAT	07/2008 – 06/2011, 1 h	
	6.	Aniko Simon, Dr.	Heterogenkatalyse	LIKAT	07/2008 – 06/2010, 10 h	
nichtwissenschaftl. Mitarbeiterinnen und Mitarbeiter	7.	Ulrich, Marx		LIKAT	07/2008 – 06/2010, 1 h	
Ergänzungsausrüstung						
Wissenschaftlerinnen und Wissenschaftler	1.	Olga Ovsitser, Dr.	Heterogenkatalyse	LIKAT, TU-C	07/2008 – 06/2011, 40 h	E13
nichtwissenschaftl. Mitarbeiterinnen und Mitarbeiter						

Aufgaben der Mitarbeiterinnen und Mitarbeiter (Grundausrüstung):

1. Priv.-Doz. Dr. Evgenii V. Kondratenko
Als Leiter des TP hat er die wissenschaftliche Betreuung übernommen und koordinierte alle internen und externen Kooperationen. Transientexperimente im TAP Reaktor. Anleitung der Doktorandin (A. Simon) und der TP-Mitarbeiterin (Dr. O. Ovsitser)
2. Prof. Dr. Reinhard Schomäcker
Als Leiter des TP übernahm er die Gesamtkoordination sowie die Anleitung der TP-Mitarbeiterin (Dr. O. Ovsitser)
3. Prof. Dr. Angelika Brückner
Mitwirkung bei der Durchführung der ESR-Experimente sowie bei der Diskussion der UV/Vis- und Raman-Spektroskopie-Ergebnisse.
4. Dr. Mathias Schneider
Verantwortlich für die Interpretation und Auswertung der XRD-Messungen
5. Dr. S. Sokolov
Hilfe bei der Katalysatorherstellung. Durchführung und Interpretation der SEM-Untersuchungen
6. Dr. Aniko Simon (promoviert im April 2011)
Frau Dr. A. Simon hat komplexe Mo-V-Nb-W-Mischoxide hergestellt, charakterisiert und katalytisch für die oxidative Funktionalisierung von C₂-C₄-Alkanen in Ab- und Anwesenheit vom Wasser getestet.
7. Ulrich Marx
Durchführung der ESR- und Raman-Untersuchungen

Aufgaben der Mitarbeiterinnen und Mitarbeiter (Ergänzungsausrüstung):

1. Dr. Olga Ovsitser
Frau Dr. Ovsitser hat katalytische Materialien hergestellt und sie für die Dehydrierung von C₂-C₄-Alkanen mit O₂ und N₂O bei unterschiedlichen Temperaturen, Kontaktzeiten und Partialdrücken der Edukte getestet. Sie hat auch die durchgeführten katalytischen Experimente ausgewertet. Außerdem hat Frau Dr. Ovsitser Untersuchungen zur Ermittlung der Red-Ox-Kinetik der VO_x-Spezies mit Hilfe der zeitaufgelösten in-situ UV/Vis-Spektroskopie und zur Aufklärung der Rolle von Sauerstoffspezies mit Hilfe der SSITKA-Experimente durchgeführt.

5.1 Allgemeine Angaben zum Teilprojekt B5

5.1.1 Titel: Synthese und Reaktivität von Molekülmodellen für die aktiven Zentren Vanadiumoxid-basierter Katalysatoren

5.1.2 Projektleitung

Prof. Dr. Christian Limberg
geb. 12.05.1965

Institut für Chemie
Humboldt-Universität zu Berlin
Brook-Taylor-Str. 2
12527 Berlin

Telefon: 030 / 20937382
E-Mail: christian.limberg@chemie.hu-berlin.de

5.2 Entwicklung des Teilprojekts

5.2.1 Bericht

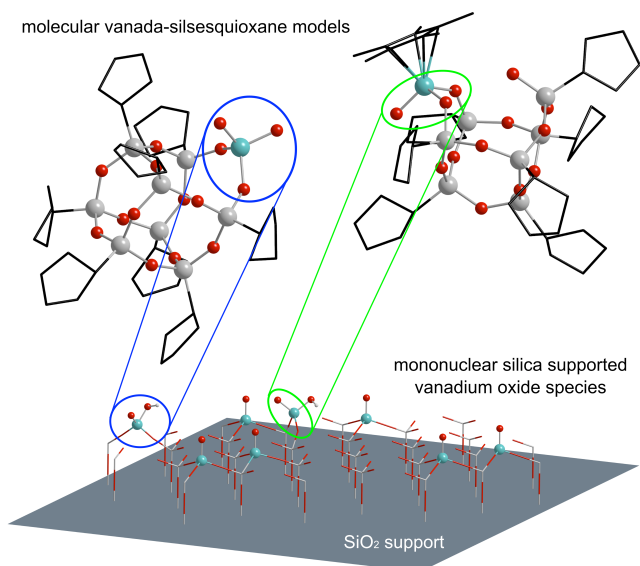
5.2.1.1 Kenntnisstand und Ausgangsfragestellung bei der letzten Antragstellung

Heterogene Katalysatoren spielen eine bedeutende Rolle in der chemischen und pharmazeutischen Industrie. Im Vergleich zu homogenen Katalysatoren bringt ihr Einsatz verschiedene Vorteile mit sich, bspw. hinsichtlich der Produktabtrennung, der Stabilität oder technischer Gesichtspunkte [1]. Allerdings bereitet die eindeutige Identifizierung der Oberflächenkonstitutionen und aktiven Spezies Probleme: Diese werden am besten mit einer Kombination an Methoden wie der IR-, Raman-, und Festkörper-NMR-Spektroskopie sowie mit Hilfe von EXAFS, XANES und XPS untersucht [2], doch diese Techniken mitteln in der Regel über alle vorhandenen aktiven Spezies, und ihre Empfindlichkeit ist oft nicht ausreichend, um auch genaue Daten über die verschiedenen aktiven Zentren zu erhalten, die sich in niedrigen Konzentrationen auf der Oberfläche befinden [3].

Zur Unterstützung entsprechender Arbeiten findet oftmals eine weitere wichtige Methode Anwendung: Die Synthese molekularer Modelle, die in der homogenen Phase untersucht werden und unter Umständen dazu dienen können, Vorschläge zu Mechanismen oder zur Spektrenzuordnung zu stützen bzw. in Frage zu stellen. Darüber hinaus können sich solche

Modelle natürlich auch selbst als neue Homogenkatalysatoren erweisen.

Eine wichtige Klasse von Heterogenkatalysatoren, die demzufolge innerhalb des SFB 546 von zentralem Interesse ist, stellen Vanadiumoxide auf inerten Trägern dar, die Oxidationsreaktionen mit O₂ vermitteln können. Ein Teilbereich des SFBs hat daher zum Ziel, durch Ausnutzung von anspruchsvollen physikalischen Methoden Informationen im Hinblick auf die Natur der aktiven Oxometall-Oberflächenspezies und ihr Verhalten zugänglich zu machen. Der Aufbau molekularer Modelle hierfür – und dies war das Ziel des Teilprojektes B5 – erfordert Liganden, die in der Lage sind, die Umgebung von Oxometall-Einheiten auf den Oberflächen oxidischer Träger nachzuempfinden, und in diesem Zusammenhang haben sich insbesondere zwei Ligand-Systeme in der Vergangenheit hervorgetan: unvollständig kondensierte Silsesquioxane [3,4] und Calixarene [5]. Wie bei der letzten Antragstellung formuliert, zielte Projekt B5 daher auf die Synthese von Oxovanadium-Calixaren und -Silsesquioxan-Komplexen zur Modellierung von Spezies, die bei der oxidativen Dehydrogenierung (ODH) von Alkanen und Methanol [1] auf den Oberflächen der hierzu eingesetzten Vanadiumoxid-Katalysatoren aktiv sind (vgl. Abb. 1). Der Teil 1 des Berichtes beschäftigt sich entsprechend mit den Ergebnissen zur Silsesquioxan-Chemie, während Teil 2

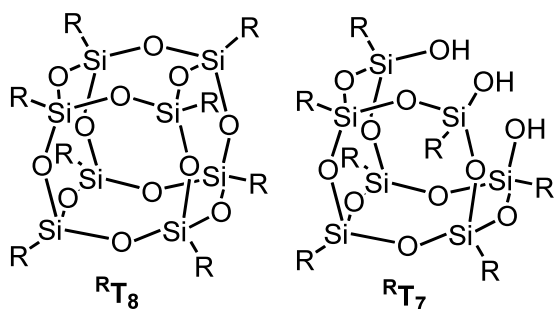


auf Vanada-Calixarene und verwandte Systeme eingeht. Unabhängig von diesen präparativen Projekten war im letzten Antrag ein eher methodisch orientierter Ansatz zur Untersuchung nicht-ligierter Modelle vorgeschlagen worden: Nach dem Durchbruch bei der Isolierung und eingehenden Charakterisierung von V₄O₁₀ sollte dessen Reaktivität intensiv untersucht werden. Mit den Ergebnissen solcher Studien beschäftigt sich Teil 3.

Abb. 1. Modellierung von Oberflächenspezies mit Silsesquioxanen (Titelblatt des Heftes mit OLSE10)

5.2.1.2 Silsesquioxan-Modelle

Oktamere Silsesquioxane, R^T_8 , weisen Gerüststrukturen auf, die denjenigen in kristallinen Formen von SiO₂ gleichen, und sie gelten daher als geeignete molekulare Modelle für die entsprechenden Modifikationen. Um SiO₂-geträgerte Katalysatoren zu modellieren, ist es

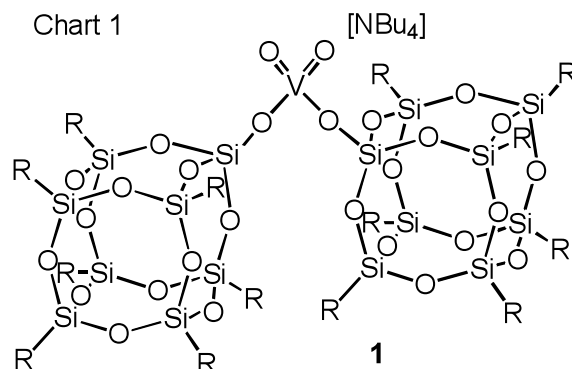


zunächst von Interesse, die Oberfläche des Trägers nachzuempfinden, und in diesem Zusammenhang ist die Substanzklasse der unvollständig kondensierten Silsesquioxane (vgl. R^T_7) von großer Bedeutung. Die Silanolgruppen dieser Verbindungen weisen

strukturelle sowie elektronische Ähnlichkeiten zu OH-Gruppen auf, wie man sie auf SiO_2 -Oberflächen findet [3, 4]. Darüber hinaus lassen sich auch gezielt Silsesquioxane synthetisieren, die geminale und isolierte OH-Gruppen enthalten [3], so dass im Prinzip jede Art der Anbindung eines Metallfragments an einer SiO_2 -Oberfläche simuliert werden kann [3].

Zu Beginn dieses Projektes existierte in der Literatur lediglich ein *Oxovanadium-Silsesquioxan-Komplex* [6]; innerhalb der vorhergehenden Förderperiode war es jedoch gelungen, zielführende Syntheserouten zu weiteren Vertretern dieser Substanzklasse zu entwickeln und auch Bedingungen auszuloten,

Chart 1



die die Kristallisation solcher Verbindungen erlauben [7]. Die Palette an verfügbaren Oxovanadium-Silsesquioxan-Komplexen konnte in der nun ausgelaufenen Förderperiode weiter ausgeweitet werden [OLSE10], so dass für Reaktivitätsuntersuchungen (s.u.) verschiedenste Komplex-Typen zu Verfügung standen. Dabei wurden nicht nur neue, mononukleare Vanadium(V)-Vertreter, wie z.B. **1** (Chart 1), hergestellt: Wie im letzten Antrag in Aussicht gestellt, haben sich diese Arbeiten nun auch auf polynukleare Verbindungen und auf Komplexe mit Vanadium in der Oxidationsstufe +IV erstreckt. Tatsächlich gelang es erstmalig, Oxovanadium(IV)-silsesquioxan-Verbindungen, wie beispielsweise die drei- und vierkernigen Verbindungen **2** und **3**, zu isolieren (Abb. 2), sie vollständig zu charakterisieren und auch ihren Bildungsmechanismus (siehe letzter Antrag) aufzuklären [OLSD10, OLSE10]. Dies erforderte anspruchsvollste und zeitaufwendige Synthesearbeit, denn die Oxovanadium(IV)-Chemie ist aufgrund der Redoxlabilität, der Oxophilie und der Hydrolyseneigung der betreffenden Komplexe nur schwer zu beherrschen. Die am Ende erfolgreich dargestellten Verbindungen können als Modelle für reduzierte Katalysatorspezies auf Silika-Oberflächen betrachtet werden. Demzufolge wurde ihr Verhalten im Kontakt mit O_2 untersucht, um den Reoxidationsschritt der Realkatalysatoren zu untersuchen [OLSD10]. Dabei zeigte sich, dass diese Komplexe sowohl in Lösung als auch im Festkörper sehr schnell

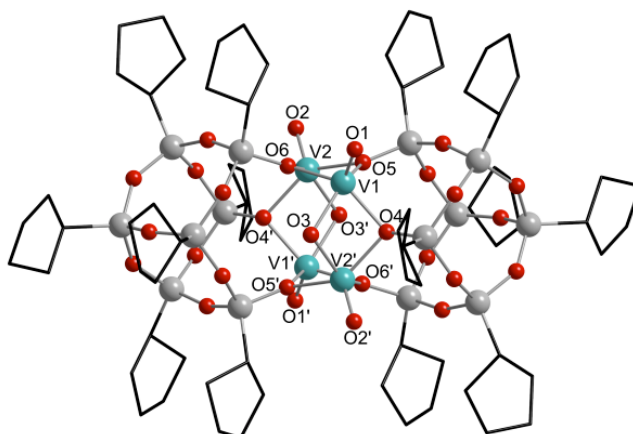
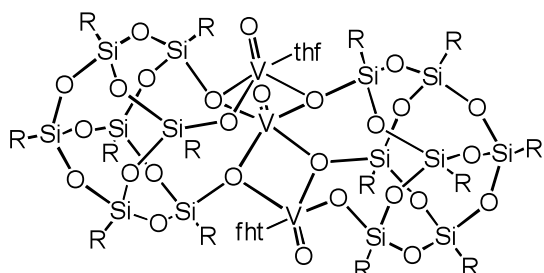
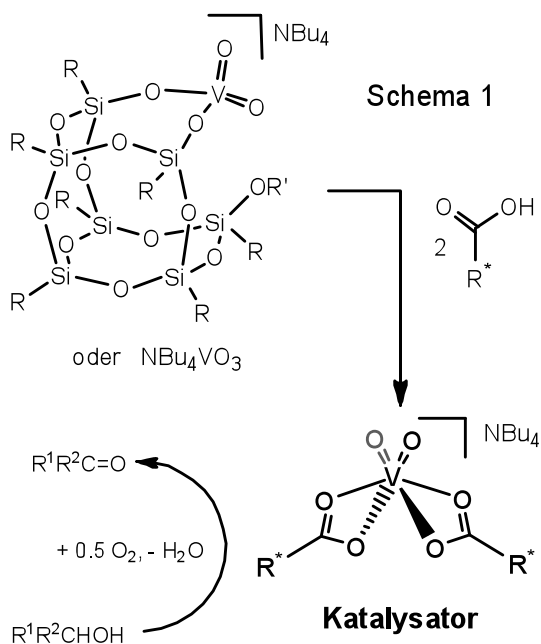


Abb. 2. Das Formelschema von **2** (links) und die Molekülstruktur von **3** (rechts).

zu Oxovanadium(V)-Verbindungen oxidiert werden, was in Übereinstimmung mit den Ergebnissen für Silika-geträgerte Oxovanadium-Katalysatoren steht, die bei der ODH von Propan eingesetzt werden: Die Reoxidation verläuft dort schnell im Vergleich zum Reduktionsschritt, der im Zuge der Propan-Dehydrogenierung erfolgt.



Ein weiteres Ziel war die Untersuchung der Reaktivität der synthetisierten strukturellen Oxovanadium(V)-Modelle im Hinblick auf ihre katalytische Aktivität bei der ODH von Alkoholen. Während sich die ursprünglich eingesetzten Silsesquioxan-Komplexe als nur wenig aktiv erwiesen, zeigten tiefeschürfende Studien, dass „Leaching“, verursacht durch im Zuge von Überoxidation gebildeten Carbonsäuren, die Bildung eines sehr aktiven Katalysators zur Folge hatte, der als Dicarboxylatdioxovanadat(V) (siehe Schema 1) identifiziert werden konnte [OL10]. Mit diesem Wissen gelang es am Ende, ein neuartiges,

einfaches und leicht herstellbares katalytisches System, basierend auf Carbonsäuren und Metavanadat, für die ODH von Alkoholen zu entwickeln, dessen Funktionsweise ebenfalls aufgeklärt wurde: Im geschwindigkeitsbestimmenden Schritt erfolgt eine H-Atom-Übertragung von einer alkoholischen C-H-Einheit auf eine V=O-Funktion des Dicarboxylatdioxovanadats unter Bildung von V(IV)-Spezies. Die Reoxidation letzterer führt zunächst zu Peroxiden, die ihrerseits einen ODH-Schritt bewerkstelligen können [OL10].

Da geträgerte Vanadiumoxide mitunter auch als Heterogenkatalysatoren für die Olefin-

polymerisation eingesetzt werden, wurden ausgewählte Vertreter der von uns dargestellten Oxovanadiumsilsesquioxan-Verbindungen in einer Kooperation als „homogene Varianten“ getestet. Tatsächlich zeigten sie eine moderate Aktivität [OLSE10].

5.2.1.3 Calixaren-Modelle und verwandte Systeme

Calixaren-Liganden bieten Oxo-Koordinationsplattformen, die den allgemeinen Fall eines oxidischen Trägers simulieren, von dem sie sich naturgemäß aufgrund der organischen Reste elektronisch stärker unterscheiden als beispielsweise die Silsesquioxane. Zur Erklärung, warum Calixaren-basierte Modelle dennoch Vorteile haben können, sei an dieser Stelle eine wichtige Konsequenz für elektronisch optimierte Modelle vergegenwärtigt: Silika-getragene Vanadiumoxid-Katalysatoren verhalten sich zwischen 20 und 100°C, also bei Temperaturen, die in der Molekülchemie üblich sind, unreaktiv, und gleiches muss man folglich für sehr realistische molekulare Modelle erwarten; so ist auch die geringe ODH-Aktivität der Silsesquioxan-Komplexe (siehe 5.2.1.2) zu verstehen. Die speziellen elektronischen Eigenschaften der Calixaren-Komplexe machen diese reaktiver, so dass quasi höhere Temperaturen simuliert werden und Reaktivitätsstudien durchgeführt werden können.

In der vorhergehenden Förderperiode hatte sich gezeigt, dass Oxovanadium-Calixaren-Komplexe funktionale Modelle für Oberflächenspezies auf geträgerten Vanadiumoxid-Katalysatoren darstellen [8, 9]. Eine breite Palette verschiedener Komplexe war hergestellt worden, und es hatte sich herausgestellt, dass dinukleare Komplexe in der ODH von Alkoholen aktiver sind als mononukleare [9]. Für die aktivsten Verbindungen (darunter **Ia** in Abb. 3) waren mechanistische Untersuchungen durchgeführt worden, die u.a. auch zur Isolierung eines Katalyseintermediates und zu einem plausiblen mechanistischen Vorschlag für die Alkoholoxidation geführt hatten (Abb. 3) [9].

Es verblieben jedoch noch einige wichtige Fragen, die in der nun ausgelaufenen Förderperiode angegangen wurden. Um zu klären, inwieweit die in **I** zusätzlich vorhandenen OH-Funktionen zur hohen Aktivität der Verbindung beitragen – beispielsweise durch eine Präfixierung der Alkohole – wurde ein Analogon synthetisiert, dessen Ligand, S_L^{2-} , als „halbes Calixaren“ angesehen werden kann und das somit keine freien OH-Funktionen aufweist (**4**, Abb. 3). Beim Einsatz dieser Verbindung **4** als Katalysator für die ODH von Alkoholen wurden jedoch sehr ähnliche TOFs beobachtet, so dass man nun sicher sein kann, dass die OH-Einheiten von **Ia** keine wichtige Rolle spielen [WLK11]. Darüber hinaus brachte die Untersuchung dieses Systems weitere interessante Einblicke: **4** kristallisiert wie **Ia** als Dimer, liegt in Lösung jedoch im Gleichgewicht mit einem Monomer vor, das die Hauptkomponente darstellt.

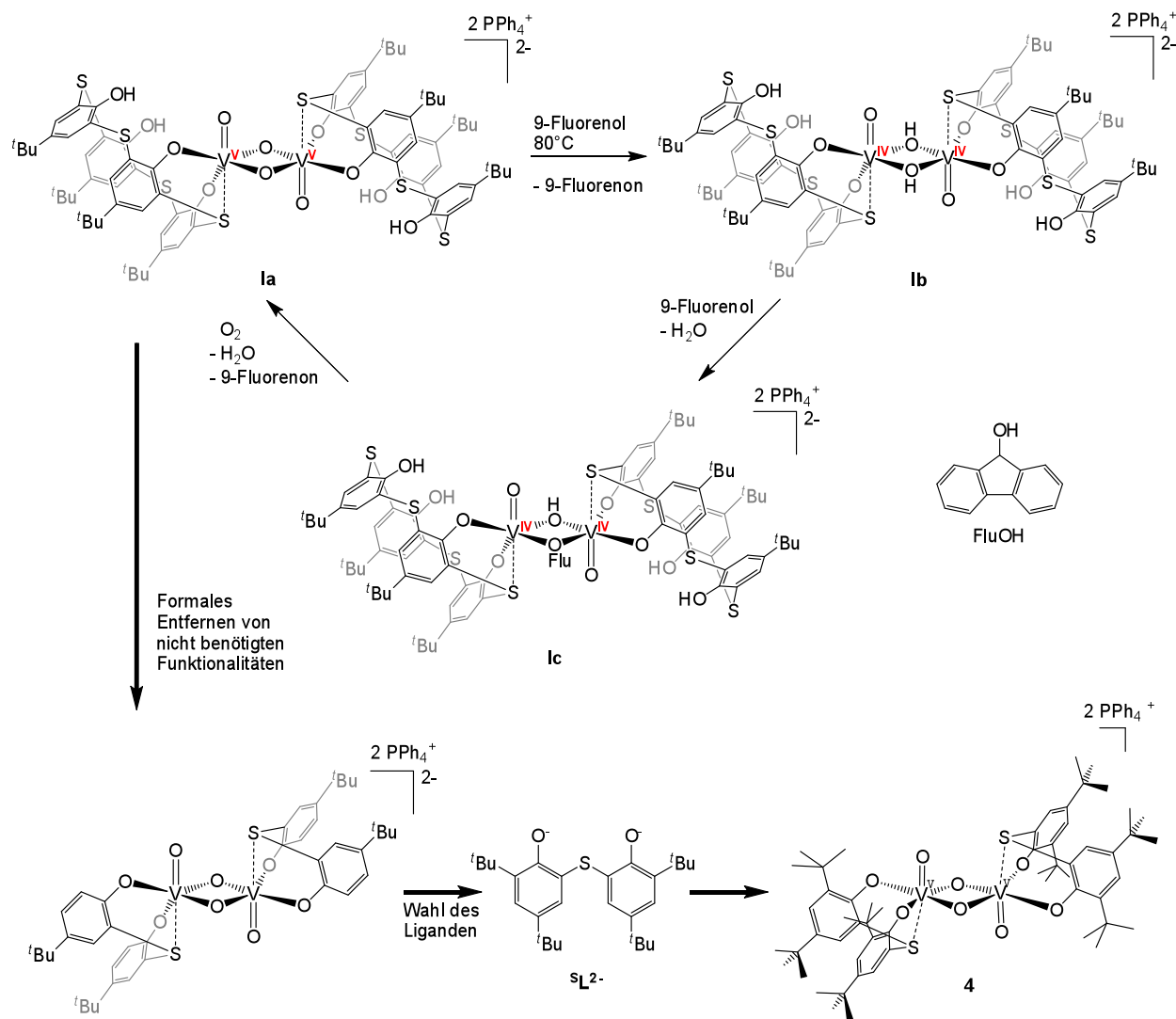


Abb. 3. Vorgeschlagener Katalysezyklus für die Alkoholorxidation mit der Thiacalixaren-basierten Verbindung **Ia** am Beispiel von 9-Fluorenon sowie das vereinfachte Derivat von **Ia**, **4**.

Durch konzentrationsabhängige, mechanistische Untersuchungen konnte gezeigt werden, dass die Alkoholorxidation über das Dimer erfolgt, was die Notwendigkeit der Kooperation zweier V-Zentren für die effiziente ODH unterstreicht [WLK11]. Über Isotopenmarkierungsstudien (Bestimmung KIE für 9-Fluorenon) konnte gezeigt werden, dass im geschwindigkeitsbestimmenden Schritt die C-H-Bindung gespalten wird. Auch im Falle dieses Systems wurden Versuche unternommen, reduzierte Spezies innerhalb des Katalysezyklus zu identifizieren, und interessanterweise führte dies zur Isolierung eines bis- μ -Hydroxo-Komplexes [WLK11], dessen Calixaren-Derivat bereits als Teil des Katalysezyklus des Calixaren-Systems vorgeschlagen (siehe **Ib** in Abb. 3), dort aber nicht isoliert oder nachgewiesen worden war [9]. Schließlich wurde auch die Reoxidation dieses reduzierten Katalysators untersucht, wobei Peroxid-Intermediate nachgewiesen werden konnten, die ihrerseits oxidationsaktiv sind und

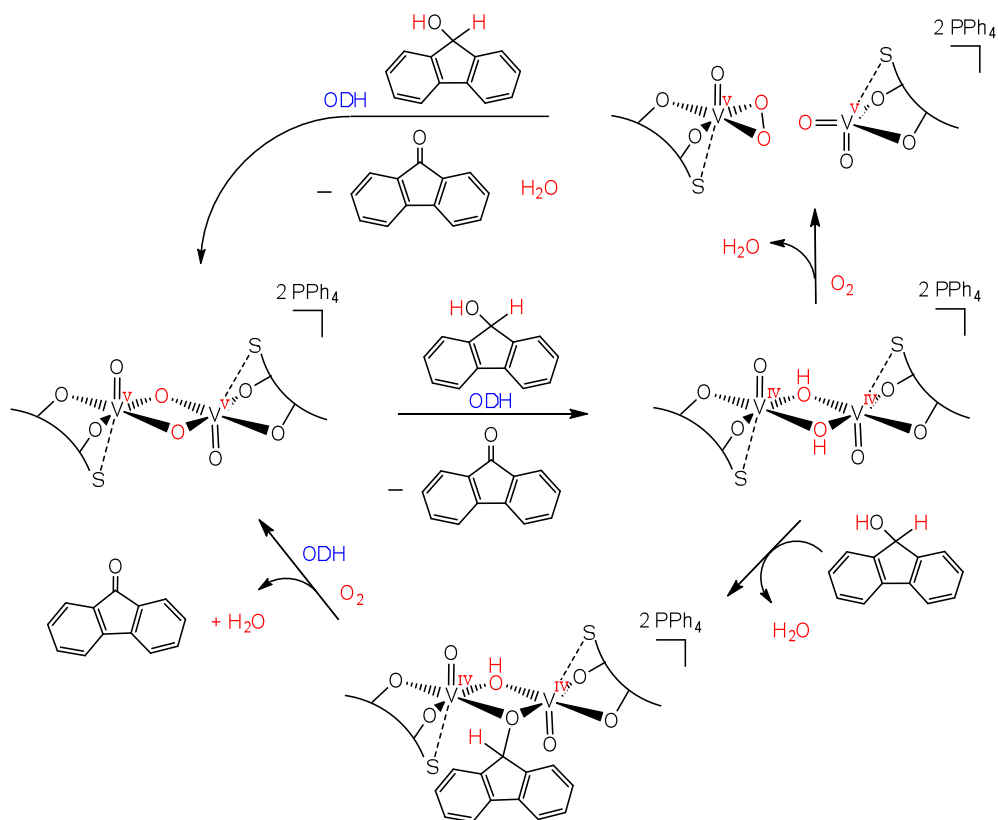


Abb. 4. Allgemeiner Katalysezyklus für die Alkoholorxidation am Beispiel von 9-Fluorenol.

Alkohole in die Carbonyl-Verbindungen überführen [WLK11]. Die Resultate beider Förderperioden zusammen führten nun zu einem allgemeinen Mechanismus, der auf vielen experimentellen Befunden basiert und in der Abb. 4 anhand des Substrates Fluorenol beispielhaft dargestellt ist. Er unterstützt die Annahme, dass Peroxide auch bei den Heterogenkatalysatoren eine intermediäre Rolle spielen [10].

Nachdem sich im Rahmen dieser Arbeiten mit dem Bisphenolat-Ligandsystem Vanadiumperoxide als zugänglich erwiesen hatten, entwickelte sich unabhängig von den ursprünglichen Zielen eine Forschungslinie, die parallel verfolgt wurde und einen bioanorganischen Hintergrund hatte [WLKM11]. Die Peroxide, von denen eines auch isoliert

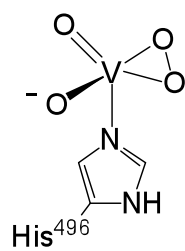
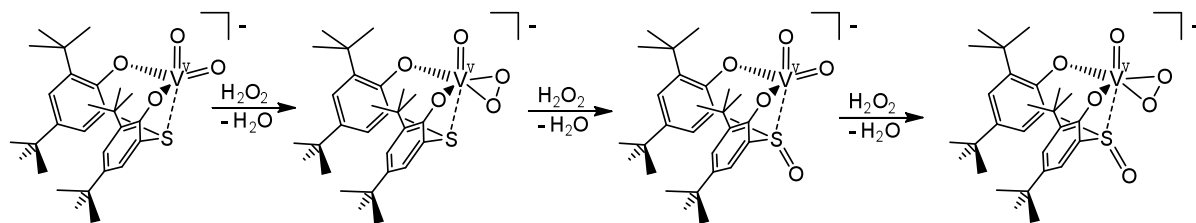


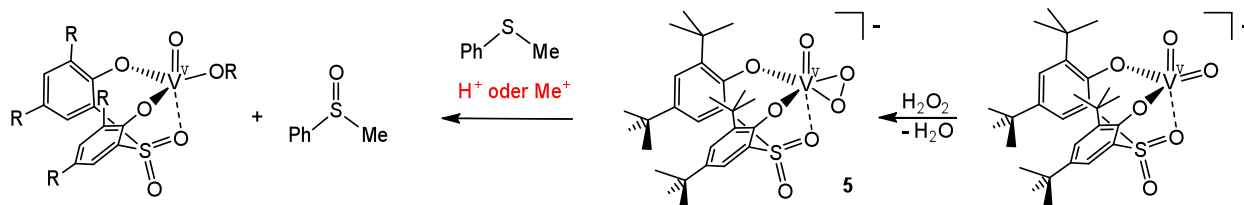
Chart 2

und strukturell charakterisiert werden konnte, erinnern an Intermediate, die innerhalb der Katalysezyklen von Haloperoxidasen – Enzyme, die für die Produktion einer Vielzahl an halogenierten Produkten zuständig sind und gleichzeitig enantioselektive Sulfoxidierungen mit Wasserstoffperoxid vermitteln – auftreten (Chart 2). Da der Ligand $^sL^{2-}$ eine Thioether-Verknüpfung aufweist und somit als eine Art internes Substrat für eine Sulfoxidation angesehen werden konnte, boten sich nun Umsetzungen der entsprechenden V-Komplexe mit Hydroperoxiden an. Dabei zeigte sich, dass im Zuge der Umsetzung mit H_2O_2

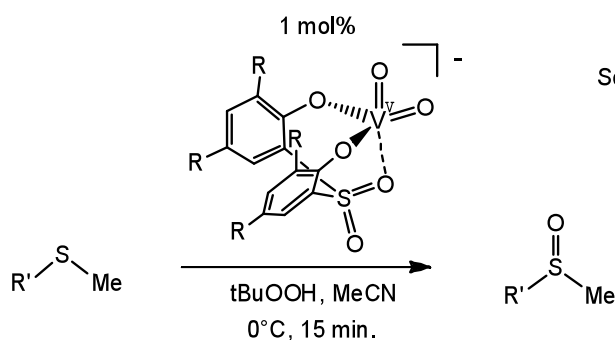
zunächst eine Peroxid Funktion gebildet wird, die dann ein O-Atom auf das koordinierte Schwefel-Atom überträgt, und dieser Reaktionsschritt wiederholt sich, bis der vollständig oxidierte Peroxo-Sulfonyl-Komplex **5** vorliegt (Schema 2). Die Umsetzung von **5** mit externen Thioether-Substraten gelang allerdings erst dann, als Protonen- bzw. Alkylgruppen-



Schema 2



Übertragungsreagentien zur Aktivierung der Peroxid-Einheit zugesetzt wurden (Schema 2),



Schema 3

was wiederum über den für das Enzym postulierten Katalysemechanismus erklärt werden kann. Diese Erkenntnis konnte schließlich zur Entwicklung eines Systems zur selektiven katalytischen Sulfoxidation von Thioethern mit tBuOOH genutzt

werden (Schema 3) [WLKM11].

5.2.1.4 Matrixisolationstudien zu Oxovanadium-Verbindungen

Da im Rahmen der Förderperiode, über die hier berichtet wird, zu diesem Themenkomplex keine Veröffentlichung einreicht wurde (lediglich eine Publikation, die im letzten Bericht als „eingereicht“ angegeben worden war, ist erschienen [HL08]), wird der Bericht an dieser Stelle etwas ausführlicher gehalten. Das Projekt wird auch nach der Förderung weitergeführt und dann zum Abschluss gebracht werden.

In den vergangenen Förderperioden war es gelungen, neutrale V_4O_{10} -Moleküle durch Verdampfung von Vanadium(V)-oxid in einer eigens konstruierten Vakuumapparatur zu erzeugen und nach Abscheidung in eine inerte Argon- oder Stickstoffmatrix bei tiefen

Temperaturen (10 K) mit IR-, Raman- und UV/Vis-Spektroskopie zu charakterisieren [HL08]. Dieses wohldefinierte Modellsystem für deponierte Vanadiumoxidteilchen auf Katalysatorträgern sollte nun auf seine Reaktivität hin untersucht werden. Außerdem sollte ein Massenspektrometer in die Apparatur integriert werden, um den im Vakuum aus dem Ofen austretenden Vanadiumoxiddampf vor der Abscheidung in die Matrix auf seine Zusammensetzung hin untersuchen zu können. Damit sollte zum einen eine Maximierung des V_4O_{10} -Ausstoßes und eine Minimierung von Nebenprodukten (O_2 , CO_2 , H_2O) realisiert werden. Der Anteil dieser Moleküle im Strahl hängt sowohl von der Ofentemperatur als auch von der Experimentdauer ab, so dass eine Echtzeit-Analyse der Verdampfungsprodukte mit einem Massenspektrometer die Voraussetzung für eine Optimierung war. Zum anderen sollte versucht werden, über eine Variation der Ofentemperatur den Anteil an weiteren Vanadiumoxiden zu erhöhen, welche laut massenspektrometrischen Untersuchungen anderer Arbeitsgruppen [11] neben der Hauptspezies V_4O_{10} im Dampf vorliegen sollten. Diese sollten ebenfalls spektroskopisch charakterisiert werden.

Nach der erfolgreichen Entwicklung eines Kopplungsstückes für das Massenspektrometer und dessen Einbau erweckten die ersten Massenspektren den Eindruck, dass eine weitaus größere Anzahl an Vanadiumoxidspezies aus dem Ofen austrat als entsprechend der Literaturberichte [11] zu erwarten gewesen wäre (Abb. 5). Im Zuge einer sorgfältigen Analyse der Ionenintensitäten der verschiedenen Spezies in Abhängigkeit von der Energie der zur

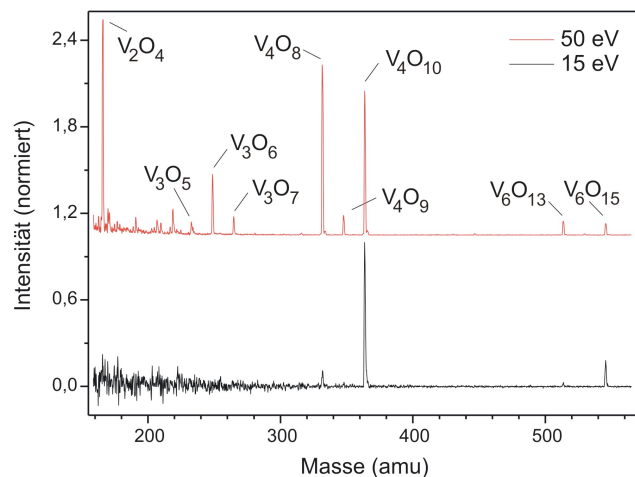


Abb. 5. Massenspektren des erzeugten Vanadiumoxiddampfes, ionisiert mit Elektronen der Energie 50 eV (oben) bzw. 15 eV (unten).

Ionisierung eingesetzten Elektronen zeigte sich jedoch, dass der größte Teil dieser Spezies Fragmentierungsprodukte darstellten, welche sich erst nach der Ionisierung des Vanadiumoxiddampfes durch Zerfall der zunächst erzeugten Ionen gebildet hatten. Wird die Elektronenenergie auf 15 eV gesenkt (was die Aufnahme von Massenspektren experimentell stark erschwert, da die Ionenquelle des Massenspektrometers bei niedrigen Elektronenenergien auch nur niedrige Ionenströme liefert) kann die Fragmentierung weitgehend unterdrückt werden: Neben Signalen für die Spezies $V_4O_{10}^+$ und $V_6O_{15}^+$ waren dann nur noch andeutungsweise Signale für die Fragmentierungsprodukte $V_4O_8^+$ und $V_6O_{13}^+$ im Massen-

spektrum zu sehen (Abb. 5 unten). Es konnte ausgeschlossen werden, dass dieser Befund auf unterschiedliche Ionisierungspotentiale für die verschiedenen Vanadiumoxide zurückzuführen ist: gemäß von eigens dazu durchgeführten Dichtefunktionalrechnungen (B3LYP/TZVP) - und in Übereinstimmung mit experimentellen Daten für ausgewählte V_xO_y -Moleküle [11-13] - haben von allen beobachteten V_xO_y -Spezies gerade die hoch oxidierten Oxide V_4O_{10} und V_6O_{15} die höchsten Ionisierungspotentiale, d.h. Elektronen mit einer Energie, die ausreicht, um diese Moleküle zu ionisieren, ionisieren auch Vanadiumoxidspezies mit geringerem O-Gehalt. Der primäre Fragmentierungskanal nach der Ionisierung der beiden Moleküle V_4O_{10} und V_6O_{15} ist offenbar jeweils die reduktive Eliminierung eines O_2 -Moleküls unter Bildung der Ionen $V_4O_8^+$ und $V_6O_{13}^+$. Diese Art der Reaktivität ist vergleichbar mit derjenigen, die Castlemann et al. [14] in Fotofragmentierungsexperimenten an Vanadiumoxiddkationen in der Gasphase beobachtet haben.

Nach diesen Befunden war offensichtlich, dass mit der in der vorangegangenen Förderperiode aufgebauten Apparatur nur die beiden (nach quantenchemischen Rechnungen hochsymmetrischen) Moleküle V_4O_{10} und V_6O_{15} erzeugt werden (Abb. 6), in denen Vanadium in seiner höchsten Oxidationsstufe +5 vorliegt. Dies war ein überraschendes Ergebnis, da entsprechend der Literaturberichte [11]

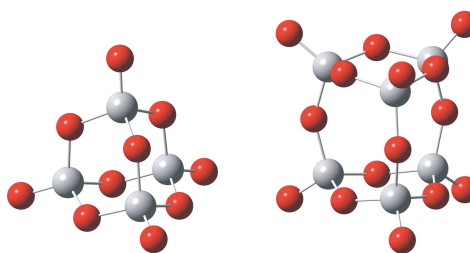


Abb. 6: Strukturen von V_4O_{10} und V_6O_{15} (B3LYP/TZVP).

das Auftreten von weiteren Spezies zu erwarten gewesen wäre. Allerdings wurde in den Literaturexperimenten zum Teil bei Temperaturen gearbeitet, die höher waren als die maximal erreichbare Temperatur des hier verwendeten Ofens, und zum Teil wurde in der Literatur auch die Möglichkeit der Fragmentierung eingeräumt. Nachdem nun klar war, dass die Auswahl an zur Verfügung stehenden V_xO_y -Molekülen wesentlich geringer war als zunächst erwartet, wurde untersucht, ob das Verhältnis von V_4O_{10} zu V_6O_{15} durch die Ofentemperatur zu beeinflussen ist. Es zeigte sich, dass dies innerhalb des zur Verfügung stehenden Temperaturbereiches (Beginn des Ausstoßes von V_xO_y -Molekülen bei 750 °C bis zum Zusammenbruch der V_xO_y -Emission bei etwa 1400 °C) tatsächlich in einem gewissen Rahmen gelingt: das Verhältnis von V_6O_{15} zu V_4O_{10} beträgt bei 800, 900 und 1000 °C etwa 1:5, 1:7 und 1:13; bei höheren Temperaturen sinkt der V_6O_{15} -Anteil noch weiter. Allerdings ist gerade bei vergleichsweise niedrigen Temperaturen (< 850 °C), bei denen der V_6O_{15} -Anteil hoch ist, die Gesamtmenge an Vanadiumoxiddampf, die aus dem Ofen austritt, gering (siehe unten). Eine Abscheidung von V_6O_{15} in größeren Mengen war daher unmöglich, und

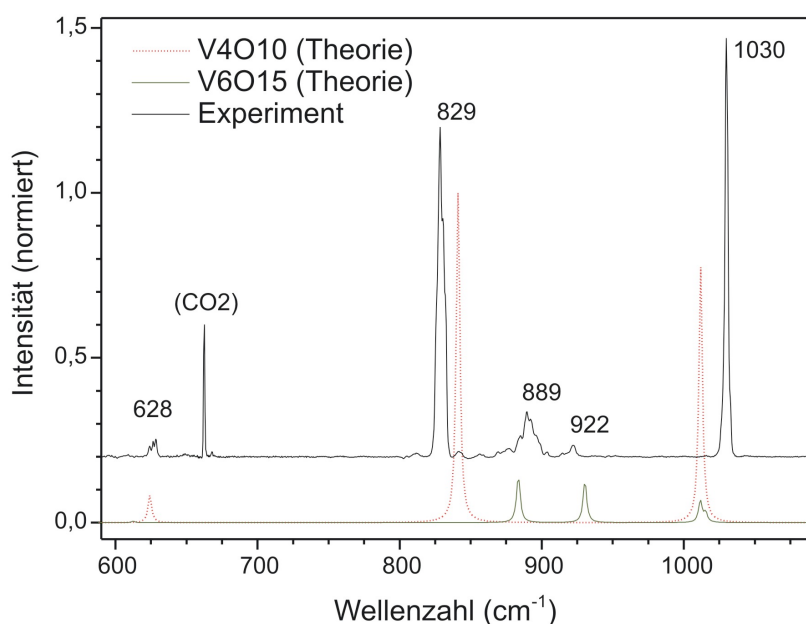


Abb. 7. IR-Spektrum des Vanadiumoxiddampfes isoliert in einer Stickstoffmatrix bei 10 K im Vergleich mit den theoretischen IR-Spektren (B3LYP/TZVP mit Skalierungsfaktoren laut [16]) von V_4O_{10} und V_6O_{15} (IR-Intensitäten gewichtet gemäß der massenspektrometrisch bestimmten Dampfzusammensetzung).

Reaktivitätsstudien waren somit nur mit der Hauptspezies V_4O_{10} zu realisieren. Nichtsdestotrotz gelang die IR-spektroskopische Charakterisierung der Nebenkompente V_6O_{15} : zwei experimentell beobachtete IR-Absorptionen mit geringer Intensität bei 889 und 922 cm^{-1} konnten den beiden laut Dichtefunktionalrechnungen (B3LYP/TZVP, [15]) intensivsten IR-Signalen von V_6O_{15} zugeordnet werden (Abb. 7). Bei Variation der Ofentemperatur zeigte sich außerdem, dass die Gesamtmenge an austretendem Vanadiumoxiddampf stark von der Temperatur abhängt (Faktor 30 zwischen dem Austritt bei 800 °C und bei 1100 °C (= Maximum)). Gegenüber früheren Experimenten konnte der V_4O_{10} -Ausstoß auf Basis dieser Erkenntnis deutlich gesteigert werden, was vor allem im Hinblick auf die Reaktivitätsuntersuchungen und die dabei zu erwartenden vergleichsweise geringen Produktmengen von Bedeutung war. Untersuchungen im Hinblick auf die störenden Nebenprodukte Sauerstoff, Wasser und Kohlendioxid zeigten, dass bei konstanter Temperatur der Anteil an diesen Nebenprodukten mit der Zeit abnimmt. Somit konnte mit Hilfe einer Vorheizperiode vor der Matrixabscheidung die Menge an Nebenprodukten, die in die Matrix gelangt, etwas verringert werden. Nichtsdestotrotz blieben die Anwesenheit insbesondere von Sauerstoff und Wasser unvermeidbar, so dass diese als Matrixbestandteile bei allen Versuchen berücksichtigt werden mussten.

Untersuchungen zur Reaktivität unligierter Vanadiumoxidaggregate wie V_4O_{10} als Modellsysteme für Oberflächenspezies können wichtige Informationen über die prinzipiell zugänglichen Reaktionskanäle liefern. In der Vergangenheit wurden Reaktivitätsstudien vor allem an massenselektierten Vanadiumoxidkationen oder -anionen in der Gasphase durchgeführt [17-21], wobei die Produktanalyse mit Hilfe der Massenspektrometrie (z.B. im Teilprojekt A2) oder mit IR-MPD (infrared multiple photon dissociation) erfolgte (Teilprojekt A3). Beim Vergleich mit Realsystemen ist dabei allerdings die veränderte Elektronenanzahl im Vergleich zu neutralen Vanadiumoxidmolekülen zu berücksichtigen. So ist beispielsweise $V_4O_{10}^+$ im Gegensatz zu neutralem V_4O_{10} ein open-shell-System und reagiert mit Methan und anderen Kohlenwasserstoffen ohne nennenswerte Aktivierungsbarriere [19]. Als Modelle für neutrale Vanadiumoxidkatalysatoren sind solche geladenen Systeme daher nur in Ausnahmefällen geeignet [20]. Die wenigen existierenden Reaktivitätsstudien an *neutralen* V_xO_y [21] beschränkten sich auf eine rein massenspektrometrische Produktanalyse, so dass Strukturinformationen über die Produkte nur über quantenchemische Rechnungen zugänglich waren. Die im Folgenden beschriebenen Reaktivitätsuntersuchungen an matrixisoliertem V_4O_{10} haben daher das Potential, eine wichtige Lücke bei den Modellsystemen für Vanadiumoxidkatalysatoren zu schließen.

Zur Untersuchung der Reaktivität von V_4O_{10} wurde dem Matrixgas (Argon oder Stickstoff) ein Reaktand zugemischt, so dass V_4O_{10} und der Reaktand nach der Abscheidung in der Matrix nebeneinander vorlagen. Im Anschluss erfolgten Experimente zur Initiierung einer Reaktion durch Bestrahlung mit Licht verschiedener Wellenlängen, deren Erfolg durch Vergleich der entsprechenden IR-Spektren überprüft wurde. Dass V_4O_{10} mit Licht im nahen UV-Bereich (410 nm) angeregt werden kann, kann durch sein UV/Vis-Spektrum [HL08] und die Resultate quantenchemischer Rechnungen in Teilprojekt A4 erklärt werden. Danach liegt der energetisch niedrigste $S \rightarrow S$ -Übergang bei 425 nm, auch wenn die Übergangswahrscheinlichkeiten in diesem Energiebereich noch klein sind. Erste Vorexperimente mit einfachen Reaktanden, wie CO , SO_2 und CH_4 , hatten bereits in der vorangegangenen Förderperiode gezeigt, dass die Bestrahlung entsprechender Matrices zu einem Intensitätsverlust für die V_4O_{10} -Banden im IR-Spektrum an Intensität führt und somit offensichtlich eine Reaktion auslöst. Die Reaktion mit Methan schien dabei die bei weitem interessanteste zu sein, da Methan den einfachsten denkbaren Kohlenwasserstoff - mit den stärksten C-H-Bindungen - darstellt; seine Aktivierung und Funktionalisierung wird daher oft als „heiliger Gral“ der Chemie bezeichnet. Eine genauere Untersuchung zeigte, dass bei Bestrahlung von CH_4/V_4O_{10} -Matrices mit Licht der Wellenlänge 410 nm im Bereich der V_4O_{10} -Schwingungen im IR-Spektrum bestimmte Banden

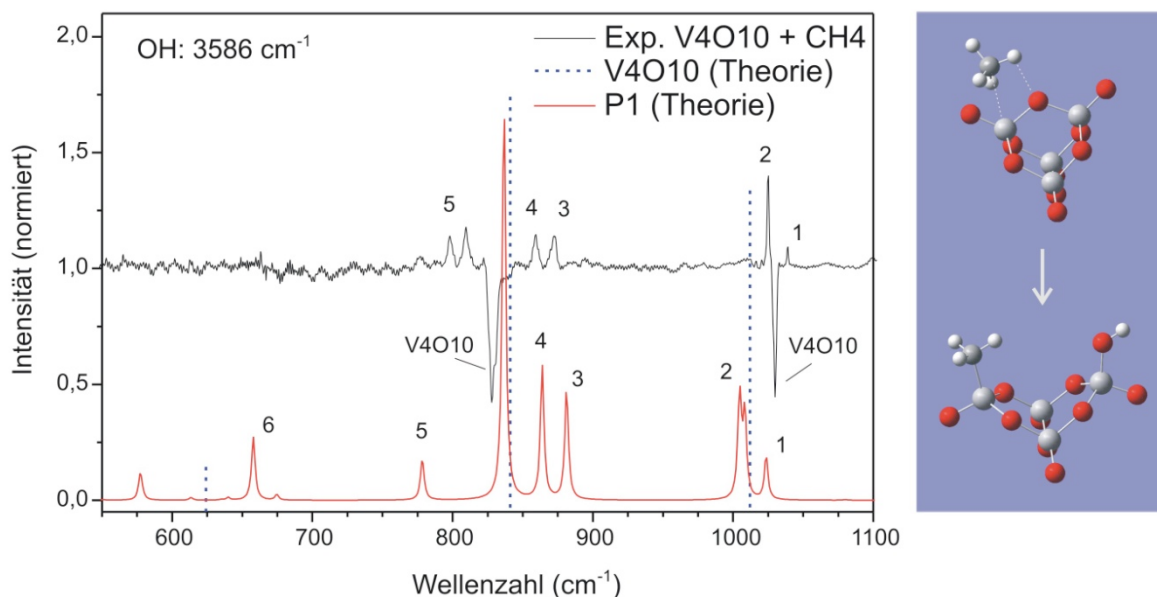


Abb. 8. IR-Spektrum von $V_4O_{10} + CH_4$ in einer Stickstoffmatrix bei 10 K nach Bestrahlung mit 410 nm (Differenzspektrum nach Abzug des Ausgangsspektrums) sowie die theoretischen IR-Spektren (B3LYP/TZVP, skaliert laut [16]) von V_4O_{10} und dem Produkt P1. Der Rückgang von V_4O_{10} überdeckt die intensivste P1-Bande. Das Schema rechts illustriert die Entstehung von P1.

zurückgehen und neue Banden entstehen (Abb. 8 oben). Zeitgleich wird auch eine neue Bande bei 3586 cm^{-1} beobachtet, für die nur eine OH-Schwingung verantwortlich sein kann. Eine Versuchsreihe mit verschiedenen Methankonzentrationen in der Matrix ergab, dass bei höheren Konzentrationen eine zweite, um 40 cm^{-1} zu niedrigeren Wellenzahlen verschobene OH-Bande auftaucht; gleichzeitig werden die Banden im V_4O_{10} -Bereich breiter. Es ist naheliegend, anzunehmen, dass in diesem Fall nicht nur ein, sondern mehrere Methanmoleküle pro V_4O_{10} -Molekül reagieren, was zu verschiedenen Folgeprodukten führen kann. Da für eine erfolgreiche Produktidentifizierung eine wohldefinierte Reaktion (mit nur einem CH_4 - pro V_4O_{10} -Molekül) Voraussetzung ist, musste im Folgenden mit sehr niedrigen Methankonzentrationen gearbeitet werden. Zwangsläufig wurden dadurch auch die Produktkonzentrationen verringert; die entsprechenden IR-Intensitäten waren daher immer am Rande der Beobachtbarkeit und Ramanstudien an den Produkten waren überhaupt nicht möglich. Ein weiteres Problem musste im Zuge der Untersuchungen gelöst werden: Bei der Wiederholung einiger Experimente variierten hin und wieder die Intensitäten oder gar die Lage mancher IR-Banden von Experiment zu Experiment etwas. Eingehendere Untersuchungen zeigten einen Zusammenhang mit der Bestrahlungsintensität: Bei durchgehend niedrigen Lichtintensitäten während der Matrixbestrahlung blieben die Bandenmuster reproduzierbar. Die etwas veränderten Bandenmuster, die zum einen bei hohen Bestrahlungsintensitäten zu beobachten

waren, traten zum anderen auch auf, wenn die Matrix zunächst auf 28 K erwärmt und anschließend mit niedrigen Lichtintensitäten bestrahlt wurde. Dieser Befund lässt sich damit erklären, dass die in der Matrix vorhandenen Wassermoleküle, welche sich aufgrund ihrer geringen Konzentration zunächst nur selten in der Nähe der V_4O_{10} -Moleküle befinden, bei einer Erwärmung (und damit Erweichung) der Matrix mobil werden und in die Nähe der V_4O_{10} - bzw. Produktmoleküle diffundieren können. Hohe Bestrahlungsintensitäten führen ebenfalls zu einer leichten Matrixerwärmung und somit wird der gleiche Effekt beobachtet. Um die Frage zu klären, ob die Wassermoleküle nur Assoziate mit V_4O_{10} ausbilden oder tatsächlich chemische Reaktionen eingehen, wurde V_4O_{10} in Matrices mit verschiedenen H_2O -Konzentrationen (ohne CH_4) abgeschieden. Bei hohen Wasserkonzentrationen zeigten sich bereits direkt nach der Abscheidung im IR-Spektrum Banden an genau den Positionen, zu denen sich in den Experimenten mit CH_4 (in Gegenwart von Wasser als Verunreinigung) manche Banden scheinbar verschoben hatten bzw. an denen Veränderungen beobachtet worden waren. Bei niedrigen Wasserkonzentrationen traten diese Banden erst nach Erwärmen der Matrix auf. Die Banden des Systems V_4O_{10}/H_2O überlagern sich also mit denen des Systems V_4O_{10}/CH_4 derart, dass die scheinbaren Bandenverschiebungen erklärt werden. Ein wichtiger Befund war darüber hinaus, dass die Bestrahlung von V_4O_{10} - H_2O -Ar-Matrices mit Licht der Wellenlänge 410 nm nicht zur Entstehung der OH-Banden führte, die bei der Reaktion mit Methan entstehen. Diese ist demnach tatsächlich auf die Reaktion von V_4O_{10} mit CH_4 zurückzuführen (dass die Bildung der OH-haltigen Produkte auf den in der Matrix vorhandenen Sauerstoff (siehe oben) zurückzuführen ist, konnte durch Referenzexperimente ausgeschlossen werden). Quantenchemische Rechnungen zeigten, dass die beobachteten IR-Banden durch einen V_4O_{10} - H_2O -Komplex (Abb. 9) erklärt werden können. Fazit dieser Untersuchungen war somit, dass bei den Reaktivitätsuntersuchungen an V_4O_{10} unbedingt eine Matrixerwärmung vermieden werden muss, da die ansonsten

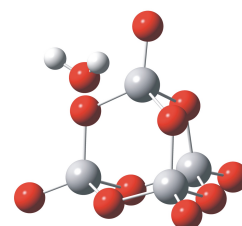


Abb. 9.
 V_4O_{10} - H_2O -Komplex.

mögliche Assoziation von H_2O an Edukte und Produkte die IR-Spektren beeinflusst.

Zur Aufklärung der Reaktion von V_4O_{10} mit Methan wurden die Strukturen möglicher Produkte in Dichtefunktionalrechnungen (B3LYP/TZVP) optimiert und deren IR-Spektren anschließend berechnet, um sie mit den experimentellen IR-Spektren zu vergleichen.

Zunächst wurden nur die aus chemischer Sicht naheliegendsten Produkte berücksichtigt. Abb. 10 zeigt die Produkte der Addition einer C-H-Bindung an eine verbrückende (P1) bzw. eine terminale (P2) V-O-Bindung (Bindungsmetathese) sowie das Produkt einer H-

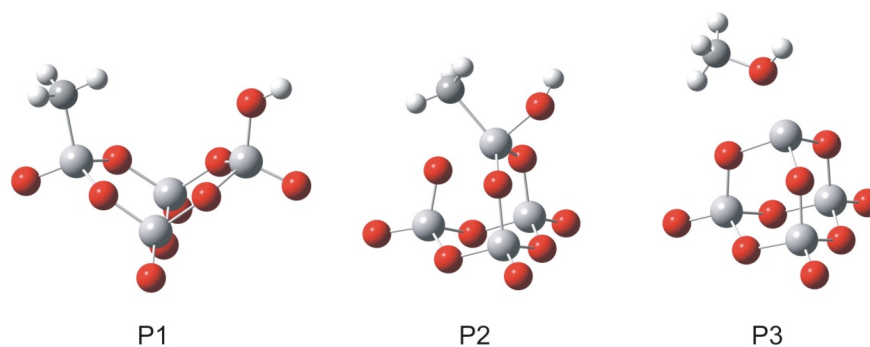


Abb. 10. Auswahl an möglichen Produkten der Reaktion $V_4O_{10} + CH_4$ entsprechend der Ergebnisse von DFT-Rechnungen.

Atomübertragung auf eines der terminalen O-Atome, gefolgt vom Einfang des parallel gebildetem Methyl-Radikals (P3). Die größte Übereinstimmung von Theorie und Experiment wurde für das IR-Spektrum des Produktes P1 (Addition einer C-H-Bindung an eine verbrückende V-O-Bindung) gefunden (Abb. 8). Die theoretisch vorhergesagte Bande bei 658 cm^{-1} (Nr. 6 in Abb. 8) liegt dabei in einen Bereich, in dem die Empfindlichkeit des IR-Spektrometers schon deutlich abfällt, so dass schwache Signale dort schwer detektierbar sind. Die experimentelle Bande bei ca. 808 cm^{-1} (direkt rechts benachbart zu Bande Nr. 5) tritt, mehr oder weniger stark, bei allen Experimenten mit V_4O_{10} auf, unabhängig vom verwendeten Reaktionspartner und kann daher nicht zum Produkt aus $V_4O_{10} + CH_4$ gehören. Um diese Zuordnung zu untermauern, wurden Isotopensubstitutionen vorgenommen. Zum einen wurde CD_4 und zum anderen $V_4(^{18}O)_{10}$ eingesetzt, wobei letzteres ausgehend von $V_2(^{18}O)_5$ generiert wurde, das wiederum zuvor aus den Elementen in einer eigens dafür entwickelten Apparatur hergestellt worden war. Die Experimente bestätigten die Zuordnung der Bande bei 3586 cm^{-1} zu einer OH-Schwingung. Neben den erwarteten Bandenverschiebungen, die in allen Fällen gut mit den theoretisch vorhergesagten Werten übereinstimmten, wurde jedoch bei den Experimenten mit CD_4 eine zusätzliche Bande bei 883 cm^{-1} beobachtet (sowohl bei Reaktionen mit $V_4(^{16}O)_{10}$ als auch mit $V_4(^{18}O)_{10}$), die in den Experimenten mit CH_4 nicht aufgetreten war (Abb. 11, Bande Nr. 3). In den für das deuterierte Produkt P1 berechneten Spektren tritt diese Bande zwar ebenfalls auf, aber mit einer im Vergleich mit den benachbarten Banden (Nr. 4 und 5) um den Faktor 10 geringeren Intensität.

Da diese Diskrepanz nicht akzeptabel schien, wurden die Dichtefunktionalrechnungen auf eine Vielzahl weiterer, chemisch ebenfalls denkbarer Reaktionsprodukte ausgeweitet, wobei zu Grunde gelegt wurde, dass jeweils genau ein CH_4 -Molekül pro V_4O_{10} reagiert und das Produkt genau eine OH-Gruppe aufweist. Dabei wurden unter anderem verschiedene Varianten der Addition je einer CH_3 -Gruppe und eines H-Atoms an zwei verschiedene, mehr oder weniger

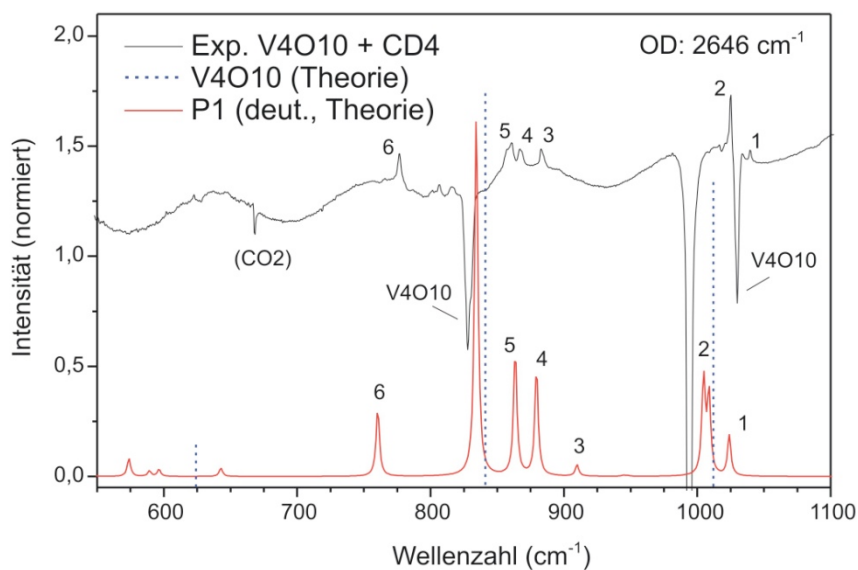


Abb. 11. IR-Spektrum von $V_4O_{10} + CD_4$ in einer Stickstoffmatrix bei 10 K nach Bestrahlung mit 410 nm (Differenzspektrum nach Abzug des Ausgangsspektrums) sowie die theoretischen IR-Spektren (B3LYP/TZVP, skaliert laut [16]) von V_4O_{10} und dem deuterierten Produkt P1. Der Rückgang von V_4O_{10} überdeckt die intensivste P1-Bande. Die Oszillation der Grundlinie rührt von Interferenzen an der Matrixschicht her.

benachbarte O-Atome des V_4O_{10} -Moleküls berücksichtigt, desweiteren eine rebound-Reaktion an einem (sterisch weniger zugänglichen) verbrückenden O-Atom sowie Wanderungen der CH_3 -Gruppe nach einer Öffnung des V_4O_{10} -Käfigs. Es wurden so mehr als zwanzig verschiedene Modelle konzipiert, welche zum Teil in verschiedenen isomeren Formen und in verschiedenen Spinzuständen (inklusive gebrochener Symmetrie) geometrieoptimiert werden mussten, so dass nachfolgend ihre IR-Spektren für die verschiedene Isotopenkombinationen berechnet werden konnten. Keines dieser Spektren gab jedoch das experimentell beobachtete IR-Bandenmuster vergleichbar oder besser wieder als das berechnete IR-Spektrum des Produktes P1.

Um weitere Informationen zu erhalten, wurden auch die Reaktionen von V_4O_{10} mit anderen einfachen Kohlenwasserstoffen untersucht. Als gesättigte Kohlenwasserstoffe kamen Propan und iso-Butan zum Einsatz. Nach der Umsetzung mit Propan wurde die gleiche OH-Bande beobachtet, wie nach der Reaktion mit Methan. Die Intensitäten im IR waren aber sehr gering; überdies lagen zwei IR-Banden des Propan im Bereich der erwarteten Produktsignale. Erst nach Erwärmen der Matrix und nochmaliger Bestrahlung wurden die Produktsignale intensiver. Noch weniger Aufschluss ergab die Umsetzung mit iso-Butan: Danach konnte selbst die OH-Schwingung nicht eindeutig identifiziert werden. Es ist gut möglich, dass eine erfolgreiche Umsetzung von V_4O_{10} mit Molekülen, die drei oder mehr Kohlenstoffatome

besitzen, voraussetzt, dass die Matrix zunächst erwärmt wird, damit die im Vergleich zu Methan sperrigeren Moleküle eine die Reaktion begünstigende Umorientierung vornehmen können. Andererseits muss aber gerade diese Matrixerwärmung experimentell vermieden werden, da ansonsten die oben erwähnten Wechselwirkungen mit Wassermolekülen auftreten. Auf die naheliegende Umsetzung von V_4O_{10} mit dem weniger sperrigen Ethan (zwei C-Atome) musste verzichtet werden, da dessen IR-Banden genau im Bereich der zu erwartenden Produktbanden liegen. Stattdessen wurde Ethen eingesetzt, auch wenn für ungesättigte Kohlenwasserstoffe eine andere Reaktivität zu erwarten war als für gesättigte. Auch Ethen zeigte jedoch bei Bestrahlung nur in geringem Ausmaß eine Reaktion mit V_4O_{10} . Es konnte keine OH-Bande beobachtet werden, dafür eine neue Bande bei ca. 840 cm^{-1} , die eventuell von gebildetem Ethylenoxid herrührt. Alles in allem lieferten die Umsetzungen mit den erwähnten Substraten keine Informationen, die für die Aufklärung der Methanreaktivität hilfreich gewesen wären. Höhere Kohlenwasserstoffe haben noch bandenreichere IR-Spektren, so dass weitere Umsetzungen nicht vielversprechend waren.

Nachdem lediglich die Reaktion von V_4O_{10} mit Methan experimentell klar identifizierbare Produktbanden geliefert hatte und allein die nach der Reaktion mit CD_4 zusätzlich bzw. lt. Rechnung mit zu hoher Intensität auftretende IR-Bande einer eindeutigen Zuordnung des Produktspektrums zu P1 im Wege stand, wurde die zu dieser zusätzlichen Bande gehörende Schwingung des deuterierten P1 noch einmal eingehender betrachtet. Die Rechnungen ergaben, dass hierbei nahezu ausschließlich die CH_3 - bzw. CD_3 -Gruppe schwingt, wobei sie eine symmetrische Deformationsschwingung ausführt (analog der Inversionsschwingung eines NH_3 -Moleküls). Diese Schwingung hat beim deuterierten P1 eine um den Faktor 17 höhere IR-Intensität als beim nicht deuterierten P1. Dies würde erklären, warum die Bande nur beim deuterierten Produkt zu beobachten ist, auch wenn die absolute IR-Intensität in der Theorie zu niedrig wiedergegeben wird. Darüber hinaus sagt die Theorie für diese Bande bei ^{18}O -Substitution keine nennenswerte Verschiebung voraus, da an dieser Schwingung kein O-Atom beteiligt ist. Dies ist im Einklang mit den experimentellen Beobachtungen und unterstützt somit diese Zuordnung. Abschließende Klarheit sollte eine Umsetzung von V_4O_{10} mit $^{13}CD_4$ bringen: im Vergleich mit dem IR-Spektrum des Produktes der $^{12}CD_4$ -Reaktion sollte sich das Spektrum nach der $^{13}CD_4$ -Reaktion ausschließlich in der Lage der in Frage stehenden CD_3 -Inversionsschwingung unterscheiden, die Bandenintensität sollte sich überdies laut Theorie noch einmal erhöhen. Leider konnten nach diesem Experiment anstatt der drei Banden (Nr. 3, 4, 5 in Abb. 11) bei Umsetzung mit $^{12}CD_4$ nur zwei Banden beobachtet werden. Ob eine davon die erwartungsgemäß verschobene Inversionsbande Nr. 3 ist, lässt sich bislang nicht sagen - in

jedem Fall bleibt unklar, wieso eine Bande (im Widerspruch zur Theorie) nicht mehr beobachtbar ist. Eindeutig kann demzufolge bislang nach den innerhalb der Förderperiode realisierbaren Reaktivitätsuntersuchungen an V_4O_{10} lediglich festgehalten werden: V_4O_{10} reagiert mit Methan unter Bildung eines Produktes, das eine OH-Gruppe enthält, und die Reaktion erfordert eine Aktivierung des V_4O_{10} durch Bestrahlung. Unabhängig von der Laufzeit dieses SFB soll in der nächsten Zukunft versucht werden, durch weitere, ergänzende Experimente die noch fehlenden Puzzleteile zu finden, die das Bild der V_4O_{10} -Reaktivität komplettieren.

Literatur

- [1] R. A. van Santen, M. Neurock, *Molecular Heterogeneous Catalysis*, Wiley-VCH, Weinheim, **2006**; J. M. Thomas, W. J. Thomas, *Principles and Practice of Heterogeneous Catalysis*, VCH, Weinheim, **2005**.
- [2] X. S. Zhao, G. Q. Lu, A. K. Whittaker, G. J. Millar, H. Y. Zhu, *J. Phys. Chem. B* **1997**, *101*, 6525-6531; B. A. Morrow, I. D. Gay, In *Adsorption on Silica Surfaces*; E. Papirer, Ed.; Marcel Dekker: New York, **2000**, 9-33.
- [3] T. W. Dijkstra, R. Duchateau, R. A. van Santen, A. Meetsma, G. P. A. Yap, *J. Am. Chem. Soc.* **2002**, *124*, 9856.
- [4] a) R. Duchateau, *Chem. Rev.* **2002**, *102*, 3525 b) V. Lorenz, F. T. Edelmann, *Z. Anorg. Allg. Chem.* **2004**, *630*, 1147; c) C. Copéret, M. Chabanas, R. P. Saint-Arroman, J.-M. Basset, *Angew. Chem.* **2003**, *115*, 164; d) F. J. Feher, T. A. Budzichowski, *Polyhedron* **1995**, *14*, 3239.
- [5] U. Radius, *Z. Anorg. Allg. Chem.* **2004**, *630*, 957; C. Floriani, *Chem. Eur. J.* **1999**, *5*, 19.
- [6] a) F. J. Feher, J. F. Walzer, *Inorg. Chem.*, **1991**, *30*, 1689-1694; b) F. J. Feher, R. L. Blanski, *J. Am. Chem. Soc.*, **1992**, *114*, 5886-5887; c) F. J. Feher, R. J. Blanski, *Makromol. Chem., Macromol. Symp.*, **1993**, *66*, 95.
- [7] C. Ohde, M. Brandt, C. Limberg, J. Döbler, J. Sauer, B. Ziemer, *Dalton Trans.* **2008**, 326-331.
- [8] E. Hoppe, C. Limberg, B. Ziemer, *Inorg. Chem.* **2006**, *45*, 8308-8317; E. Hoppe, C. Limberg, B. Ziemer, C. Mügge, *J. Mol. Cat.* **2006**, *251*, 34-40.
- [9] E. Hoppe, C. Limberg, *Chem. Eur. J.* **2007**, *13*, 7006-7016.
- [10] X. Ding, W. Xue, Y. Ma, Y. Zhao, X. Wu, S. He, *J. Phys. Chem. C* **2010**, *114*, 3161-3169.
- [11] a) J. Berkowitz, W. A. Chupka, M.G. Inghram, *J. Chem. Phys.* **1957**, *27*, 87-90; b) M. Farber, O. M. Uy, R. D. Srivastava, *J. Chem. Phys.* **1972**, *56*, 5312-5315.
- [12] G. Balducci, G. Gigli, M. Guido, *J. Chem. Phys.* **1983**, *79*, 5615-5622.
- [13] E. Jakubikova, A. K. Rappe, E. R. Bernstein, *J. Phys. Chem. A* **2007**, *111*, 12938-12943.
- [14] S. E. Kooi, A. W. Castlemann, Jr., *J. Phys. Chem. A* **1999**, *103*, 5671-5674.
- [15] S. F. Vyboishchikov, J. Sauer, *J. Phys. Chem. A* **2001**, *105*, 8588-8598; E. Janssens, G. Santambrogio, M. Brümmer, L. Wöste, P. Lievens, J. Sauer, G. Meijer, K. R. Asmis, *Phys. Rev. Lett.* **2006**, *96*, 233401.
- [16] S. Feyel, H. Schwarz, D. Schröder, C. Daniel, H. Hartl, J. Döbler, J. Sauer, G. Santambrogio, L. Wöste, K. R. Asmis, *Chem. Phys. Chem.*, **2007**, *8*, 1640-1647.

- [17] a) K. A. Zemski, D. R. Justes, and A. W. Castleman, Jr., *J. Phys. Chem. A* **2001**, *105*, 10237-10245; b) N. A. Moore, R. Mitric, D. R. Justes, V. Bonacic-Koutecky, A. W. Castleman, Jr., *J. Phys. Chem. B* **2006**, *110*, 3015-3022; c) D. R. Justes, R. Mitric, N. A. Moore, V. Bonacic-Koutecky, A. W. Castleman, Jr., *J. Am. Chem. Soc.* **2003**, *125*, 6289-6299.
- [18] a) M. Engeser, D. Schröder, H. Schwarz, *Chem. Eur. J.* **2005**, *11*, 5975-5987; b) S. Feyel, D. Schröder, X. Rozanska, J. Sauer, H. Schwarz, *Angew. Chem.* **2006**, *118*, 4793-4797; *Angew. Chem. Int. Ed.* **2006**, *45*, 4677-4681; c) S. Feyel, L. Scharfenberg, C. Daniel, H. Hartl, D. Schröder, H. Schwarz, *J. Phys. Chem. A* **2007**, *111*, 3278-3286; d) S. Feyel, H. Schwarz, D. Schröder, C. Daniel, H. Hartl, J. Döbler, J. Sauer, G. Santambrogio, L. Wöste, K. Asmis, *Chem. Phys. Chem.* **2007**, *8*, 1640-1647.
- [19] a) S. Feyel, D. Schröder, and H. Schwarz, *J. Phys. Chem. A* **2006**, *110*, 2647-2654; b) S. Feyel, J. Döbler, D. Schröder, J. Sauer, H. Schwarz, *Angew. Chem.* **2006**, *118*, 4797-4801; *Angew. Chem. Int. Ed.* **2006**, *45*, 4681-4685; c) T. Wende, J. Döbler, L. Jiang, P. Claes, E. Janssens, P. Lievens, G. Meijer, K. R. Asmis, J. Sauer, *Int. J. Mass Spectrom.* **2010**, *297*, 102-106.
- [20] a) S. Li, A. Mirabal, J. Demuth, L. Wöste, T. Siebert, *J. Am. Chem. Soc.* **2008**, *130*, 16832-16833; b) X. Rozanska, J. Sauer, *J. Phys. Chem. A* **2009**, *113*, 11586-11594.
- [21] a) F. Dong, S. Heinbuch, Y. Xie, J. J. Rocca, E. R. Bernstein, Z.-C. Wang, K. Deng, S.-G. He, *J. Am. Chem. Soc.* **2008**, *130*, 1932-1943; b) F. Dong, S. Heinbuch, Y. Xie, J. J. Rocca, E. R. Bernstein, *J. Phys. Chem. A* **2009**, *113*, 3029-3040.

5.2.2 Projektrelevante eigene Publikationen

a) erschienene oder angenommene Arbeiten in wissenschaftlichen Zeitschriften oder Buchveröffentlichungen

- [WLK11] C. G. Werncke, C. Limberg, C. Knispel, S. Mebs,
Surface-inspired Molecular Vanadium Oxide Catalysts for the Oxidative Dehydrogenation of Alcohols: Evidence for Metal Cooperation and Peroxide Intermediates
Chem. Eur. J. **17** (2011) 12129 – 12135
- [WLKM11] G. Werncke, C. Limberg, C. Knispel, R. Metzinger, B. Braun,
Haloperoxidase Activity of Oxovanadium(V) Thiobisphenolates
Chem. Eur. J. **17** (2011) 2931 – 2938.
- [OLSE10] C. Ohde, C. Limberg, D. Schmidt, M. Enders, S. Demeshko, C. Knispel,
Progress in the Compilation of an Oxovanada-Silsesquioxane Portfolio and catalytic activity of organometallic Representatives in Ethylene Polymerisation
Z. Anorg. Allg. Chem., **636** (2010) 2315 – 2322.
- [OL10] C. Ohde, C. Limberg,
From Surface-Inspired Oxovanadium Silsesquioxane Models to Active Catalysts for the Oxidation of Alcohols with O₂ - the Cinnamic Acid/Metavanadate System
Chem. Eur. J. **16** (2010) 6892 – 6899.
- [OLSD10] C. Ohde, C. Limberg, R. Stößer, S. Demeshko,
Oxovanadium(IV) Silsesquioxane Complexes
Inorg. Chem. **5** (2010) 2479 – 2485.

- [HL08] C. Herwig, C. Limberg,
V₄O₁₀: Spectroscopic Fingerprint of a Well-Defined, Molecular Metaloxo Aggregate
Inorg. Chem. **47** (2008) 2937 – 2939.

Diese Publikation war bereits im letzten Bericht als “eingereicht” angegeben worden.

5.3 Rückblick auf die Förderung

Das Teilprojekt wurde seit 08/2003 im Sonderforschungsbereich gefördert. Es wurde mit Ablauf der 4. Förderperiode im Juni 2011 beendet.

5.3.1 Personal im Teilprojekt während der 4. Förderperiode

	lauf. Nr.	Name, akademischer Grad, Dienststellung	engere Fachzugehörigkeit	Institut der Hochschule oder der außeruniv. Einrichtung	Mitarbeit im Projekt Wochenstunden, Zeitraum	Entgeltgruppe
Grundausstattung						
Wissenschaftlerinnen und Wissenschaftler	1.	C. Limberg, Dr., Univ.-Prof.	Anorg. Chemie	HU-C	08/2003 – 06/2011, 5h	
	2.	C. Herwig, Dr.	Anorg. Chemie	HU-C	03/2004 – 06/2011, 10h	
	3.	P. Haack, WM	Anorg. Chemie	HU-C	01/2007 – 06/2011, B	
	4.	T. Tietz, Dr., WM	Anorg. Chemie	HU-C	09/2007 – 12/2009, B	
nichtwissenschaftl. Mitarbeiterinnen und Mitarbeiter	5.	S. Oschatz	Anorg. Chemie	HU-C	04/2006 – 06/2011, 2h	
	6.	C. Jankowski	Anorg. Chemie	HU-C	09/2003 – 06/2011, 5h	
Ergänzungsausstattung						
Wissenschaftlerinnen und Wissenschaftler	1.	C. Ohde, Dr., WM	Anorg. Chemie	HU-C	02/2006 – 02/2011, 26,6 h	E13 2/3
	2.	G. Werncke, WM	Anorg. Chemie	HU-C	05/2008 – 06/2011 26,6 h	E13 2/3
	3.	P. Haack, WM	Anorg. Chemie	HU-C	04/2011 – 06/2011 26,6 h	E13 2/3
nichtwissenschaftl. Mitarbeiterinnen und Mitarbeiter						

Aufgaben der Mitarbeiterinnen und Mitarbeiter (Grundausrüstung):

1. Prof. Dr. Christian Limberg
Leiter des Teilprojektes; Anleitung und Beratung der Mitarbeiter, Koordination, Präsentationen
2. Dr. Christian Herwig
Konstruktionsarbeiten, Instandhaltung und Wartungsarbeiten an der Matrix-isolationsanlage, Durchführung von Matrix-Experimenten, DFT-Rechnungen
3. Dipl.-Chem. Peter Haack (B)
Wissenschaftlicher Mitarbeiter, Synthese und Charakterisierung von neuartigen Metalloxo- und peroxo-Spezies
4. Dr. Thomas Tietz (B)
Wissenschaftlicher Mitarbeiter, Synthese und Charakterisierung gemischt valenter Metalloxo-Komplexe
5. Sabine Oschatz
Sekretariat, Verwaltung, Schreibarbeiten
6. Christel Jankowski
Laborantin, Synthese von Ausgangsmaterialien

Aufgaben der Mitarbeiterinnen und Mitarbeiter (Ergänzungsausrüstung):

1. Dipl.-Chem. Gunnar Werncke
Synthese von Oxovanadium-Calixaren- und -bisphenolat-Komplexen (mono- und oligonuklear; unterschiedliche Substituenten und Substitutionsmuster der Liganden; Oxidationsstufen III - V) sowie der dazu benötigten Vorstufen, Identifizierung und Charakterisierung der Modellkomplexe und Prüfung ihrer Reaktivität in Bezug auf organische Substrate, Charakterisierung der Reaktionsprodukte.
2. Dr. Christian Ohde
Synthese von Oxovanadium-Silsesquioxan-Komplexen (mono- und oligonuklear; unterschiedliche Liganden-Substitution; verschiedene Oxidationsstufen) sowie der dazu benötigten Vorstufen und Silsesquioxane, Identifizierung und Charakterisierung der Modellkomplexe und Prüfung Ihrer Reaktivität in Bezug auf organische Substrate.

3. Dipl.-Chem. Peter Haack
Charakterisierung neuartiger Oxo-Funktionen (Raman, UV/Vis, Isotopenmarkierung, Reaktivität)

5.1 Allgemeine Angaben zum Teilprojekt B6

5.1.1 Titel: Untersuchungen zur Selektivität der oxidativen Dehydrierung von Propan an VO_x-Trägerkatalysatoren durch Struktur-Wirkungs-Analysen

5.1.2 Projektleitung

Prof. Dr. Reinhard Schomäcker
geb. 08.01.1959

Institut für Chemie
Technische Universität Berlin
Strasse des 17. Juni 124
10623 Berlin

Telefon: 030 / 314 24973
E-Mail: schomaecker@tu-berlin.de

5.2 Entwicklung des Teilprojekts

5.2.1 Bericht

The initial situation at the beginning of this funding period was characterized by an unclear picture of a variety of influence parameters on the performance of supported vanadia catalysts in the oxidative dehydrogenation (ODH) of propane [1,2]. The general reaction network is shown in Fig. 1, it combines the involved partial and total oxidation reactions. Several research groups showed that the absolute values and the ratios of the rate of these reactions vary substantially with the support material, the loading with vanadia, the preparation method of the catalysts and the oxidizing agent. In general, it was proven that at temperatures below 600°C no homogeneous gas phase reactions are involved [3,4]. Mass transfer limitations are excluded from kinetic studies of catalyst particles smaller than 200 nm in diameter [5,6], In many cases this network can be simplified to the consecutive reactions of the ODH of propane and subsequent total oxidation of propene [7-9].

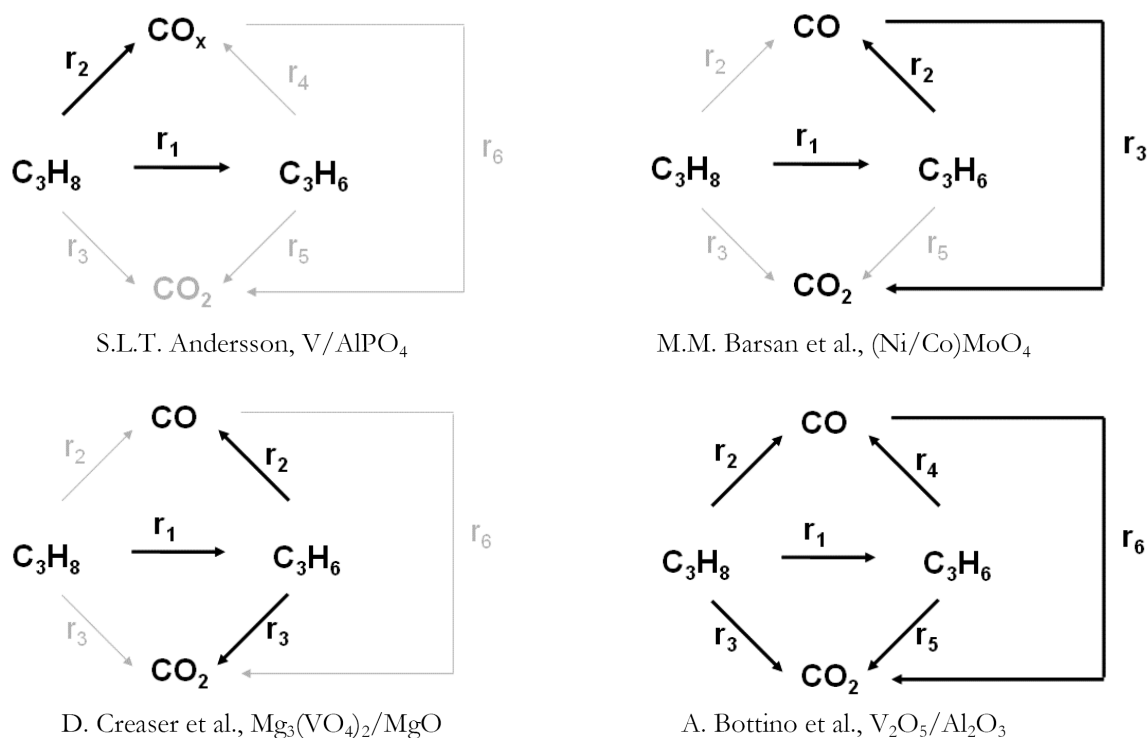


Fig. 1. Reaction network of the ODH of propane considered in different publications [7, 8, 9] for the formal kinetic description (solid lines).

The strong influence of the catalyst loading was known, but not understood in detail due to the difficulties in preparation and characterization of defined vanadia species on different support materials. Only the presence of crystalline vanadia nanoparticles and their disadvantages for the selectivity of the ODH reaction was well understood. In many publications the kinetics was described by simple power law approaches, with reaction orders around 1 for propane and zero for oxygen, indicating a much faster reoxidation of the catalyst in comparison to the reduction by the hydrocarbon. Microkinetic approaches based on Eley-Rideal or Mars-van Krevelen approaches were based on the hydrogen transfer from propane to the vanadyl group as rate determining step and a fast product release and reoxidation of the active sites [2, 10-12]. Theoretical predictions proposed different kinetic behavior of vanadia monomers, oligomers and polymers. In experiments this was difficult to examine, because different equilibria between these species are established at different support materials. A series of low loaded catalysts with different support material showed substantial differences in activity and selectivity, but an assignment of the observations to material properties of the catalysts was not possible, because of very different morphologies, specific surfaces and acidities of the applied support materials [DFH08]. With respect to the selectivity even more open question were

obvious. The oxygen species involved in the total oxidation was identified by isotope labeling and TAP experiments to be the vanadyl oxygen rather than adsorbed molecular oxygen [13-16]. Essential impact factors on the selectivity were not known. On this basis the aims of this project were:

- A detailed kinetic investigation of the ODH of propane with two different well defined and well characterized catalysts, namely V-SBA15 and V-Ti/SBA15.
- Identification of the selectivity determining step within the reaction network.
- Comparison of O₂ and N₂O as oxidizing agent.
- Studied of the impact of water and carbon deposits on the catalyst performance.
- Simulation and testing of different options of reactor concepts.

Because this funding period was focused on the selectivity aspects of the ODH reactions, the work plan was modified already at the beginning, in order to strengthen this aspect. The comparison of O₂ and N₂O was shifted to project B3 and the studies on water and carbon to project B2. Instead of these work packages a detailed investigation of the ODH of ethanol was included, because this reaction is more suitable for comparison with surface science experiments, more simple to study and very sensitive to changes of catalyst properties. With this model reaction an attempt was made to derive a correlation of the catalyst performance with physical properties, especially support effects. The conclusions from this study were used as a guide line to optimize catalysts for the oxidative dehydrogenation of propane and to identify the reaction conditions for the optimal performance of the catalysts.

Support effect on ODH of ethanol and propane

Several authors found a strong impact of the support material to the activity of the surface vanadyl species in various ODH reactions of hydrocarbons and alcohols [17-25]. Some authors assume that the reducibility of the surface vanadia species, which is altered by the support, controls the activity. This is also supported by DFT-calculations for the propane oxidation [26]. It was tried to correlate the activity with the peak maxima of H₂-TPR experiments in dependency of the support material [27] or with the Sanderson electronegativity of the support cation [17]. Besides that, correlations with H₂-TPR and activity data often give insufficient results. The aim of this project was to get a closer insight in the nature of the support effect. The oxidative dehydrogenation of propane, which was investigated before, is not so well suitable to achieve this, because the influence of consecutive reactions is too strong for detailed

kinetic analysis of the primary ODH reaction. Therefore, we choose the partial oxidation of ethanol as probe reaction. This reaction can be performed with very high selectivities to the desired aldehyde and is also very sensitive to the support material [18, 28, 29].

In order to deduce the role of the support material on the reactivity of vanadia, vanadia was deposited by thermal spreading in submonolayer quantities on alumina, zirconia, titania and ceria as support materials using the synthesis facilities of sub-project B2. Additionally, vanadia was deposited in submonolayer quantities on the surfaces of ceria and alumina in thin films as model supports in project B1.

The supported vanadia catalysts were characterized by UV-vis, Raman, TPD, nitrogen adsorption, ICP-OES, impedance spectroscopy and tested for their catalytic capabilities in ethanol dehydrogenation to acetaldehyde. The respective model systems were studied in project B1 by TPD and IRAS in order to elucidate structure-reactivity relationships.

The catalytic tests were done in a fixed-bed reactor system made of stainless steel with an inner diameter of 8 mm. The reactor tubes are coated with a SilcoTek™ silicon coating to prevent catalytic activity and coke formation on the reactor walls. Kinetic measurements were performed under differential conditions with a standard stoichiometric feed composition of 6 kPa oxygen und 12 kPa ethanol at an overall flow rate of 220 Nml/min. The investigated temperature interval was between 140°C and 200°C. The product stream was analyzed by GC. Temperature-programmed reduction was performed in a tubular quartz reactor. Therefore, the catalyst was fully oxidized with synthetic air at 500°C for one hour and cooled down to room temperature. Afterwards the catalyst was quenched in helium, then the gas stream was switched to 3% ethanol in helium at 30 Nml/min and the catalyst was heated to 250 °C at heating rate of 2 K/min. The formed acetaldehyde was measured time resolved by a quadrupole mass spectrometer.

Table 1 shows the surface areas, the loading of vanadia and the resulting surface density of vanadium on the supports. Vanadium surface densities were calculated from the amount of vanadium in the sample by assuming that it is uniformly dispersed over the whole support and surface area. One can see that the surface densities of vanadium on all supports are around 3.5 V at/nm², which is half of a monolayer coverage of polymeric vanadyl species and 1.5 times higher than the theoretical monolayer of monomeric vanadyl species [30]. Only marginal decrease in surface area and a decrease in pore volume over the whole pore size distribution were observed for the thermal spreading and calcination treatment.

Table 1. Physical properties of the catalysts

support	Surface area [m ² /g]	surface density [V/nm ²]	wt% V
TiO ₂	17,1	3,5	0,6 %
Al ₂ O ₃	200,9	3,1	4,9 %
ZrO ₂	52,1	3,1	1,4 %
CeO ₂	19,8	3,9	0,7 %
SiO ₂	820	0,7	2,7 %

The kinetics of the ethanol oxidation to acetaldehyde can be interpreted as a sequence of elementary steps as shown in Fig 2. The kinetic circle is started in the reduced state, where two vanadium atoms in the oxidation state IV are present. DFT-calculations give evidence that this situation is more stable than a V(V) and a V(III) atom [26]. These are getting oxidized via irreversible chemisorption of oxygen to form the active site [18]. Afterwards, ethanol is dissociatively adsorbed resulting in the cleavage of the V-O-V bond. In a consecutive step, the acetaldehyde is formed by H-abstraction from the ethoxide species and by formation of two vanadium (IV) atoms and desorbs.

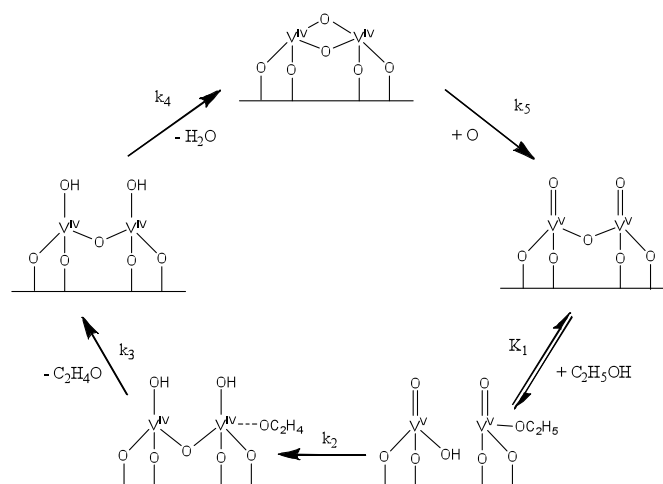


Fig. 2. Mechanistic model of the ethanol oxidation on a dimeric vanadyl species

The catalytic circle is finally closed by the recombination of two OH groups under desorption of water. The irreversibility of this step is proven by the absence of inhibition by water [18]. Based on a pseudo-steady state approach of the shown elementary steps in Fig. 2 the following rate equation is derived:

$$r = \frac{k_2 K_1 p_{C_2H_5OH}^{\frac{1}{n}}}{1 + K_1 p_{C_2H_5OH}^{\frac{1}{n}} + \frac{k_2 K_1 p_{C_2H_5OH}^{\frac{1}{n}}}{k_5 p_{O_2}^{\frac{1}{2}}}} \approx k_2 \quad (1)$$

Here K_1 is the equilibrium constant, k_2 the rate constant of the rate-limiting step, k_5 the rate constant for the reoxidation and n the constant for Freundlich adsorption isotherm.

The initial ODH-rate is calculated at ethanol conversions of less than 10% by division of the acetaldehyde mol stream through the mol amount vanadia in the catalyst. The product distribution for every catalyst was nearly independent of the temperature and exhibited more than 98% acetaldehyde with some diethyl-ether as by-product and carbon oxides as consecutive reaction products. Except for vanadia supported on alumina, a higher selectivity of diethyl ether of 15% is obtained, which is attributed to the Lewis or Brønsted acid sites of alumina [31]. Fig. 3 shows that the initial ODH-rates of the ethanol oxidation differs by almost three orders of magnitude over all support materials with the order $VO_x/Al_2O_3 \ll V_2O_5 < VO_x/CeO_2 < VO_x/ZrO_2 \ll VO_x/TiO_2$. Here titania shows an outstanding performance and one has to mention, that the rate of V_2O_5 is erroneous, because the assumption of a surface density of 5 V/nm² was made. The ethanol conversion over the pure support materials in this temperature range is negligible. Only bare ceria reveals high activity to total oxidation products at temperatures higher than 200°C, which is suppressed by loading with vanadia, which was already observed for different ODH reactions [19, 32].

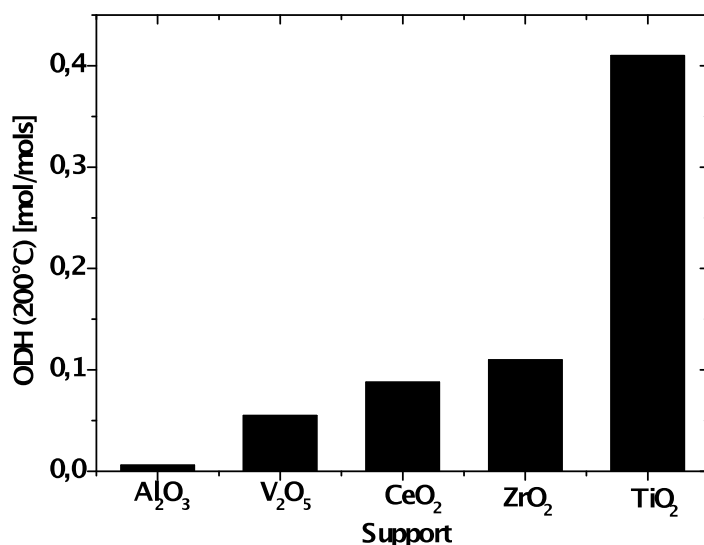


Fig. 3. ODH-rate for vanadia supported on different supports

The apparent activation energies were determined by measuring the initial dehydrogenation rates as a function of temperature and then derived from Arrhenius-plots. The apparent activation energies are shown in Table 2.

Table 2. Apparent activation energy of ODH of ethanol

Catalyst	VO _x /Al ₂ O ₃	VO _x /ZrO ₂	VO _x /CeO ₂	VO _x /TiO ₂	V ₂ O ₅
E _{A,app} [kJ/mol]	92	83	73	67,5	76,5

Fig. 4 shows the produced acetaldehyde in dependency of the temperature for the different supported catalysts for ethanol as reductant. For vanadia supported on titania, zirconia and ceria one product desorption peak can be observed. Vanadia supported on alumina gives two peaks, which are strongly overlapping with the dehydration of ethanol, which starts to take place at temperatures higher than 200 °C. This produces ethylene, which is compromising the MS-measurement, because the main mass peak at 28 m/z is overlapping with the acetaldehyde mass spectra. Exactly the same trend is observed in a comparison of two thin film model catalyst with alumina and ceria as support material investigated in project B1.

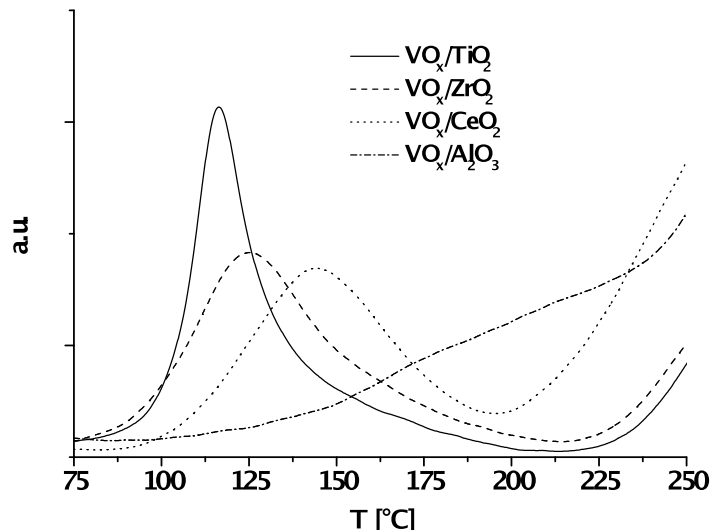


Fig. 4. EtOH-TPR with a heating rate of 2 K/min and 3 mol% EtOH

The integration of the peak areas corresponds roughly to an oxidation state of IV for the different supported vanadia catalysts after reduction, which supports the before mentioned model. The comparison of the peak maxima gives the order for the reactivity of VO_x/TiO₂ > VO_x/ZrO₂ > VO_x/CeO₂ > VO_x/Al₂O₃.

Table 3 summarizes the TPR peak maxima for both reductants ethanol and hydrogen.

Table 3. TPR and TPD peak maxima

Catalyst	VO _x /Al ₂ O ₃	VO _x /ZrO ₂	VO _x /CeO ₂	VO _x /TiO ₂
H ₂ -TPR maximum	425°C	357°C	437°C	399°C
EtOH-TPD maximum	175°C	125°C	145°C	116°C

Previous studies have shown a strong influence of the support material on the ODH rate of various reactants like methanol, ethane and propane. Even though different conditions, respective temperature and feed composition, were used, they found the same order of activity, which is TiO₂ > ZrO₂ > CeO₂ > Al₂O₃ > SiO₂ [19, 22-25]. Except for methanol, the order CeO₂ > ZrO₂ > TiO₂ > Al₂O₃ > SiO₂ was found [17]. Even for the oxidation of propene to acrolein this support effect [33] was found. But one has to be careful with the interpretation, because this reaction needs two active sites and is therefore strongly influenced by the surface density of vanadium.

To be able to find a relation between the ODH of ethanol and propane we investigated the same series of catalysts in the ODH reaction of propane in the temperature range between 400°C and 500°C and found the same order for the activity with exception of V₂O₅ as shown in Fig. 5. The detailed measuring conditions can be found elsewhere [DFH08]. But more important is the observations of the correlation of the apparent activation energies for both reactions as shown in Fig. 6. One can see that there is a close relationship, which can be described by a line through the point of origin. This means that the rate limiting steps in these two reactions are influenced by the same phenomena. This is assumable, because for both reactions the C-H abstraction is proposed as the rate determining step.

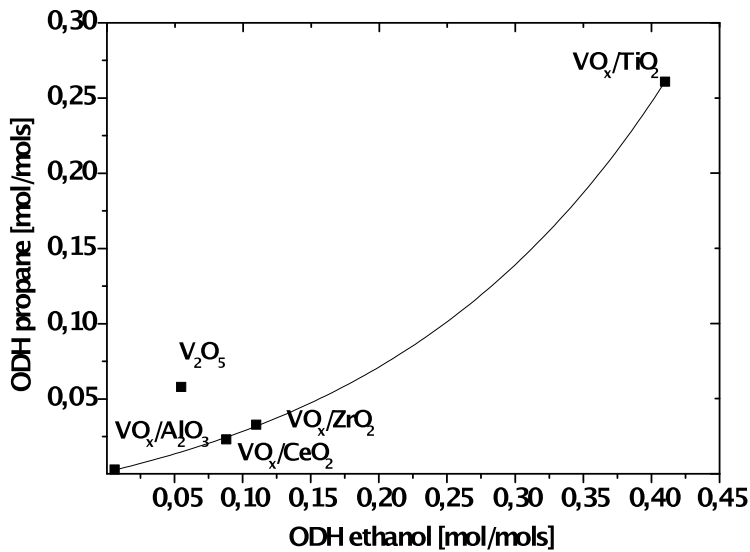


Fig. 5. Correlation of the ODH-rates of ethanol (200°C) and propane (400°C)

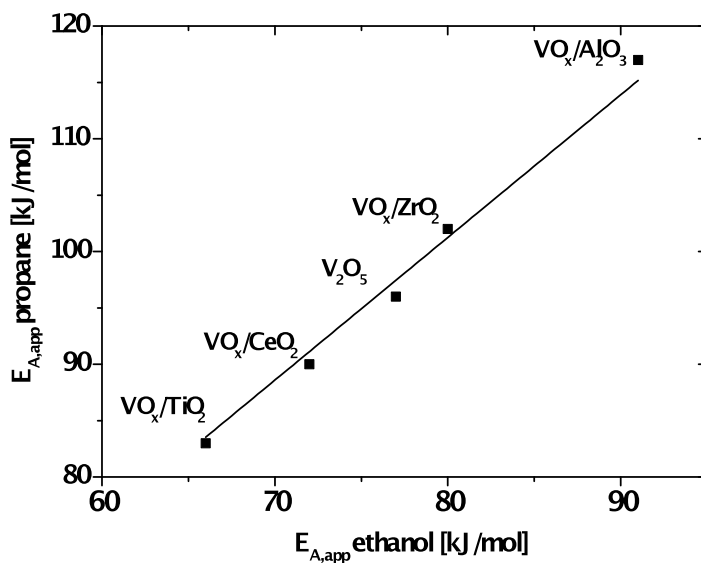


Fig. 6. Correlation of activation energy of ethanol and propane oxidation

Even though every support material exhibits unique singular differences, which can have influences on the catalytic performance, there seems to be a general order parameter for the activity of vanadium catalysts. In particular, EPR measurements show small amounts of vanadium (IV) deposited on alumina, even under oxidizing atmosphere. This could be inactive for the ODH reaction. At elevated temperatures ceria can form a CeVO_4 -phase, which is at least inactive for the ODH of ethanol. This formation gets preferred with increasing surface coverage on vanadium and the reaction conditions [20]. Under reaction conditions ceria and titania are partially reduced to oxidation state three by reoxidizing the vanadium to oxidation

state +V [28]. There is enough evidence to exclude certain phenomena as origin of the different catalytic behaviour:

- Singular differences of each supported catalyst cannot cause changes of orders of magnitude
- no change in surface area during catalyst preparation indicate no pore blocking
- no sign of crystalline V₂O₅ in Raman, XRD, UV-vis
- assumption that all vanadia sites contribute equally to the rate
- different experiments show the same correlation series

It is known that the reducibility of the surface vanadyl species influences the activity of the catalyst [34, 22]. As mentioned a lot of authors tried more or less successful to find a correlation between the ODH-rate and H₂-TPR experiments. We cannot find any good relationship. Nevertheless, the EtOH-TPR experiments suggest that vanadium is only reduced to the oxidation state IV instead of III by the reduction with H₂. Therefore, there is a good correlation between the temperature at maximum acetaldehyde production during TPR of ethanol and the ODH-rate of the catalysts as shown in Fig. 7.

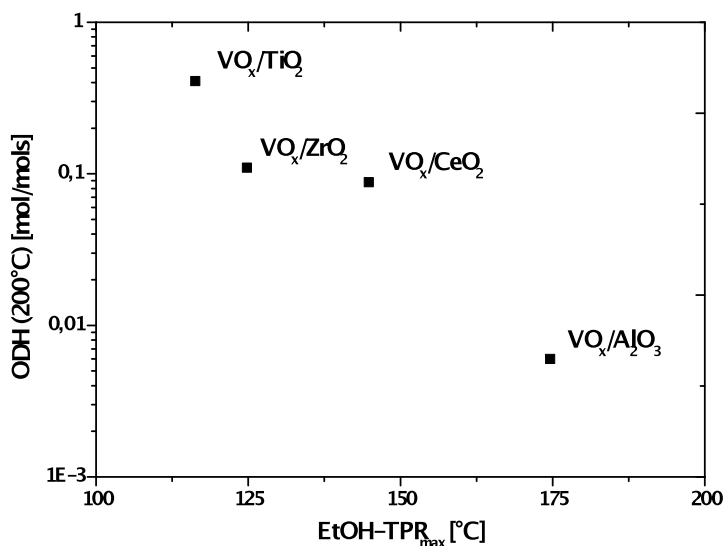


Fig. 7. Correlation of EtOH-TPR maxima with ODH rate of EtOH

The reducibility should be better characterized by the defect formation enthalpy of the catalysts. The reactions



represent the formation of defects as it occurs within a catalytic cycle of an ODH reaction.

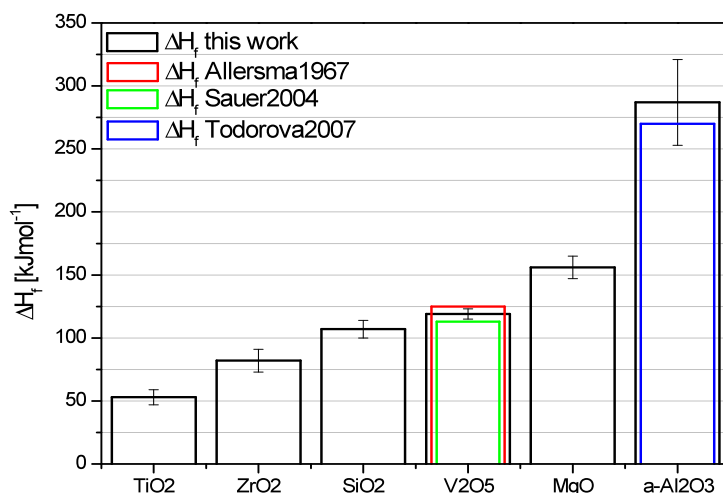


Fig. 8. Measured defect formation enthalpy of high loaded supported vanadia catalysts and comparison with theoretical literature data [35-37].

The thermodynamic parameters of these reactions were proposed as descriptors for the activity of different vanadia catalysts by Sauer *et al.* [36]. Fig. 8 shows defect formation enthalpies of high loaded vanadia catalysts, that were determined in project B7. The data agree well with theoretical predictions and this technique was therefore used to determine the defect formation enthalpies of the sub-monolayer catalysts. The data are given in Table 4 and were used for the construction of energy profiles of the ODH of ethanol at these catalysts.

Table 4. Defect formation enthalpy of low loaded supported vanadia catalysts

Catalyst	VO _x /γ-Al ₂ O ₃	VO _x /ZrO ₂	VO _x /CeO ₂	VO _x /TiO ₂
ΔH _{Def} [kJ/mol]	111	83	58	44

Fig. 9 shows the energy profile of the oxidation of ethanol beginning at the reduced state of the catalyst and the reactants in the gas phase. The first step is the oxidation of the catalyst by oxygen. The transition state TS 0 involves the adsorption and homolytic bond cleavage of the oxygen molecule. The enthalpy of oxidation corresponds to the inverse of the enthalpy of defect formation. Afterwards ethanol is adsorbed. At high ethanol coverage the heat of adsorption is often in the range of the heat of vaporization of 42 kJ/mol [38-40]. The rate limiting step, the H-abstraction, occurs in the transition state TS 1, where the catalyst is being reduced. Experimentally it is only possible to measure the step height between before the adsorption of ethanol and TS 1 in a steady state experiment. This is the apparent activation

energy, which includes the temperature dependency of the adsorption constant and the rate limiting step. The lower the valley after the oxidation, the higher is the apparent activation energy. TS 2 could be a possible transition state, which stands for the comproportionation of one V(III) and one V(V) to two V(IV) atoms and the formation of two hydroxyl groups. The last two steps describe desorption of the products acetaldehyde and water. The overall step size balances to the enthalpy of reaction.

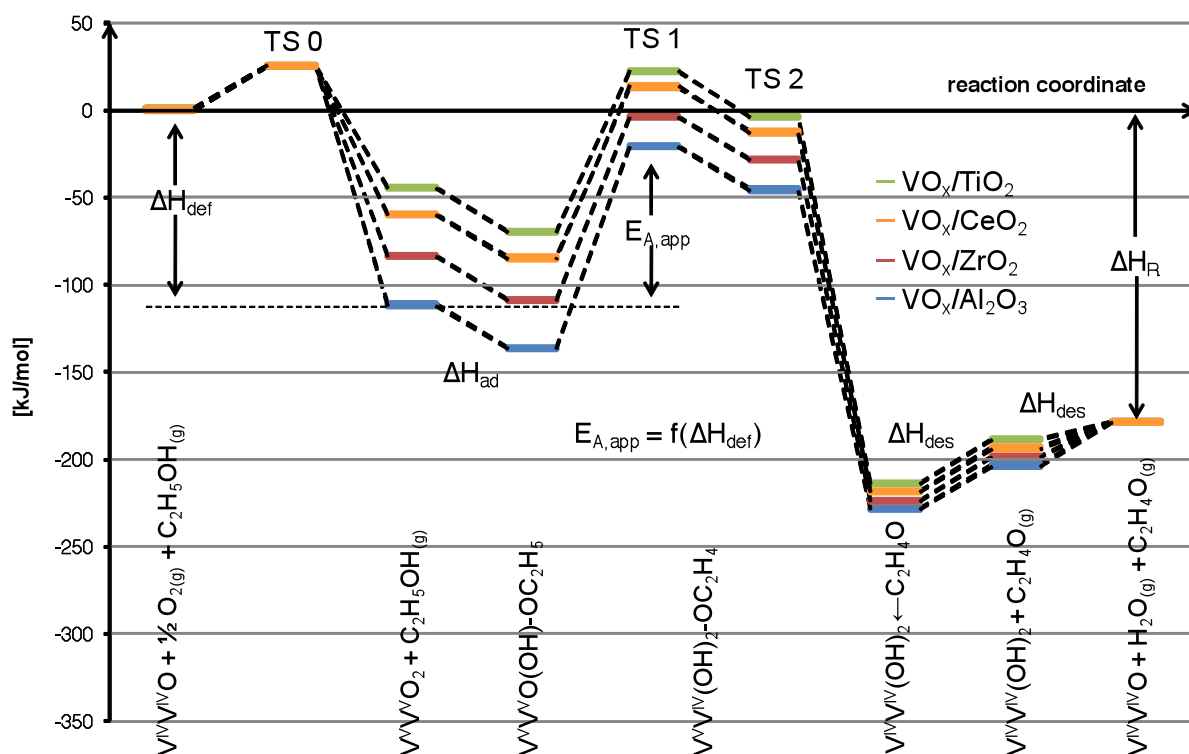


Fig. 9. Energy profile of the oxidation of ethanol

If the energy of adsorption ΔH_{ad} is nearly independent of the support material, there should be a direct correlation between the O defect formation energies and the apparent activation energies as shown in Fig. 10. This gives a very good linear correlation with $r = 0.999$ when omitting the values for the pure vanadia. The straight line has a positive axis intercept at $\Delta H_{Def} = 0$, which is at 60 kJ/mol for propane and at 50 kJ/mol for ethanol. This difference between ethanol and propane could be contributed to the differing strengths of the in the dehydration involved C-H bonds. Between the ODH rate of ethanol and propane and the ΔH_{Def} , can also be found a good correlation, which is shown in Fig. 11 and is in agreement with the C-H bond abstraction being the rate limiting step. The strong connection between the apparent activation energies of the ODH of ethanol and propane with the measured oxygen defect

formation enthalpies prove that the reducibility of the vanadia, which is altered by the support material, is the essential reactivity descriptor.

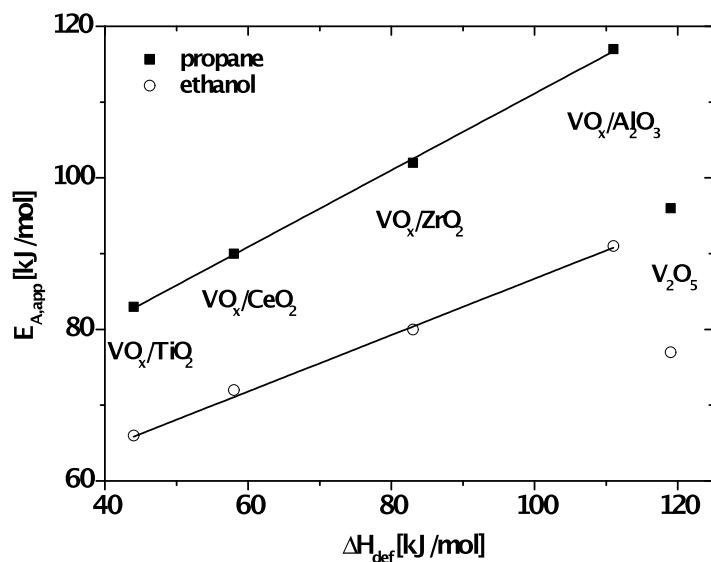


Fig. 10. Correlation of defect formation enthalpy with activation energy of propane and ethanol oxidation

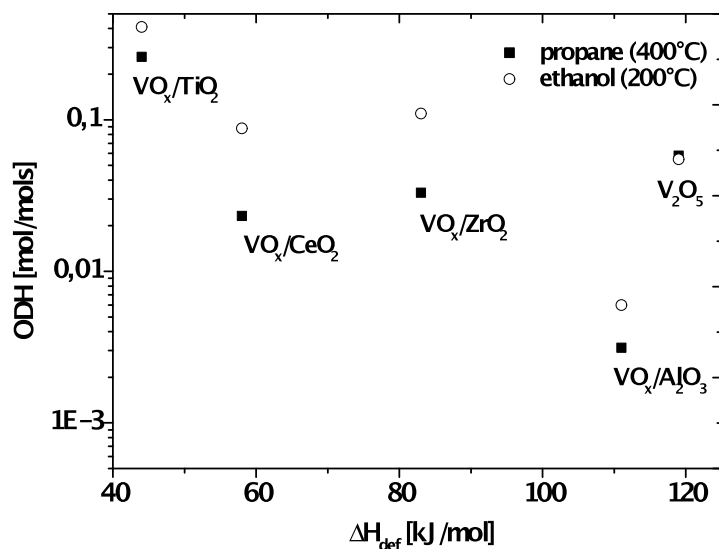


Fig. 11. Correlation of defect formation enthalpy with ODH-rate of propane (400°C) and ethanol (200°C) oxidation

SBA15 supported vanadia catalysts

Silica (SBA-15) supported vanadium oxide was used for a kinetic study of the ODH of propane in a fixed-bed reactor. Prior to this study, spectroscopic characterization using a variety of analytic techniques such as FTIR-, Raman-, DR UV–vis- and XPS revealed the absence of bulk vanadia and a high dispersion of active surface sites for the investigated catalyst. The synthesis and characterizations were performed within project B2 [HWS09].

The kinetic data evaluation was based on a first order rate law, which was derived from a variation of the feed composition. Calorimetric measurements were used to determine the heat of adsorption of propane on the catalyst [DKF09]. The data indicate that the primary combustion of propane is negligible. Reaction orders of 1 for propane dehydrogenation and propene combustion indicate their participation in the respective rate-determining step. The zero reaction order determined for the catalyst reoxidation reveals participation of lattice oxygen in this reaction step. Higher activation energies of propane dehydrogenation as compared to propene combustion indicate the participation of the weaker allylic C–H bond of propene in the rate-determining step of the propene combustion (Table 5). This results in higher propene selectivities at elevated temperatures. Kinetic parameters, including apparent and intrinsic activation energies and the equilibrium constant of propane adsorption allowed a comparison with theoretical predictions and show good agreement.

Table 5. Result of formal kinetic characterization of propane ODH at 2,7V-SBA15

Katalysator	ODP				Totaloxidation			
	E_a [kJ·mol ⁻¹]	$k_{0,eff}$ [m ³ g ⁻¹ s ⁻¹]	m_1	m_2	E_a [kJ·mol ⁻¹]	$k_{0,eff}$ [m ³ g ⁻¹ s ⁻¹]	m_3	m_4
V-SBA-15	103±6	2,3±1,3	1	0	34±18	(7,2±5) · 10 ⁻²	1	0

In comparison to vanadia catalysts supported at other support material this catalyst shows a rather low activity [DFH08]. A comparison of ODH activities of differently supported vanadia catalyst is shown in Fig. 12. This comparison was performed with the catalysts studied above for ethanol ODH. The characterization data are given in Table 1. A substantial increase in activity is observed at 400°C changing the support material to alumina, ceria, zirconia and titania. In this order it increases more than two orders of magnitude. Within the same series of experiments the influence of the support material on the selectivity was studied. At a conversion of 1% the selectivity varies between 50 and 80%, a rather weak variation in comparison to the activity variation. This results means that the rate of the combustion of

propene to CO_x , follows the rate of the ODH of propane almost exactly with the variation of the support material. The observed differences may be caused by additional active sites available at the surface of some of the supports. For a productivity optimization of ODH catalyst for propane this means, that only the activity can be increased by a modification of the catalyst support, not the selectivity. Among this series of catalysts V-TiO₂ shows the highest activity with respect to the vanadia active sites. HF-EPR investigations of differently supported catalyst show a substantial involvement of the titania support in the reduction process of the catalyst. Here VO_x is always in the highest oxidation state, while the support material itself is reduced [DOH08].

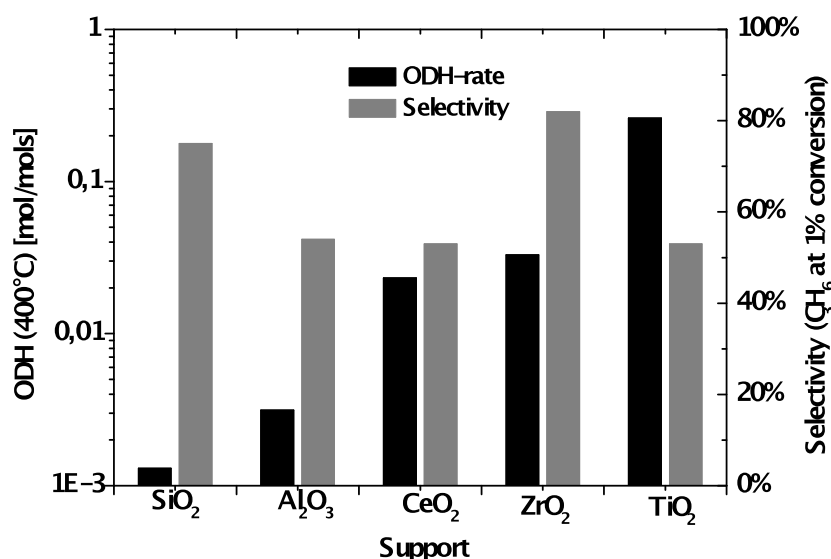


Fig. 12. Comparison of ODH of propane rate and selectivity of differently supported catalyst at 400°C

With its low specific surface of about 20 m²/g its productivity expressed in kg propene per kg of catalyst and hour is still too low for an industrial application. On the other hand, the high surface material SBA-15 results only in a low specific activity of vanadia. This observation motivated the combination of the two materials in a binary support material providing high specific surface for a high loading of vanadia in a highly dispersed state combined with a high reducibility of vanadia cause by the titania. In order to realize this synergetic effect of the binary support material, SBA15 was modified with different loadings of highly dispersed titania. The technique developed in project B2 allows the preparation of sub monolayer coating of the SBA15 material without substantial loss in specific surface of the material [HWS09]. The deposition of vanadia at the surface of these modified support materials resulted in

catalysts with a complex structure depending on the ratio of the titania and vanadia loading. A catalytic screening of a library (Fig. 13) of such catalysts with a systematic variation of titania and vanadia loading showed a strong variation in activity and selectivity of the catalysts.

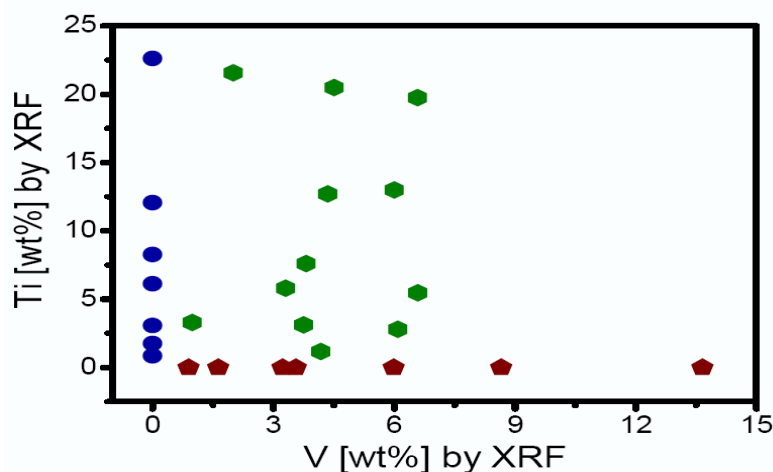


Fig. 13. Catalysts matrix tested to looking for the ideal V/Ti ratio for high propylene productivity.

A variation of vanadia loading on pure SBA-15 results in a linear increase in activity with loading indication the same activity of all deposited species. Titania deposition on SBA15 yields catalysts with increasing total oxidation activity. The performance of catalysts loaded with both depends strongly on the ration of the components. At low titania loading vanadia may be located at silica or titania surfaces, resulting in different activities of individual sites. A low loading with vanadia resulted in catalysts with uncovered titania surfaces that exhibited activity for total oxidation, causing low selectivity. Optimal performance is obtained with a completely vanadia covered titania layer on SBA15 obtained with 13 wt% titania covered by 4 wt% vanadia (Fig. 14).

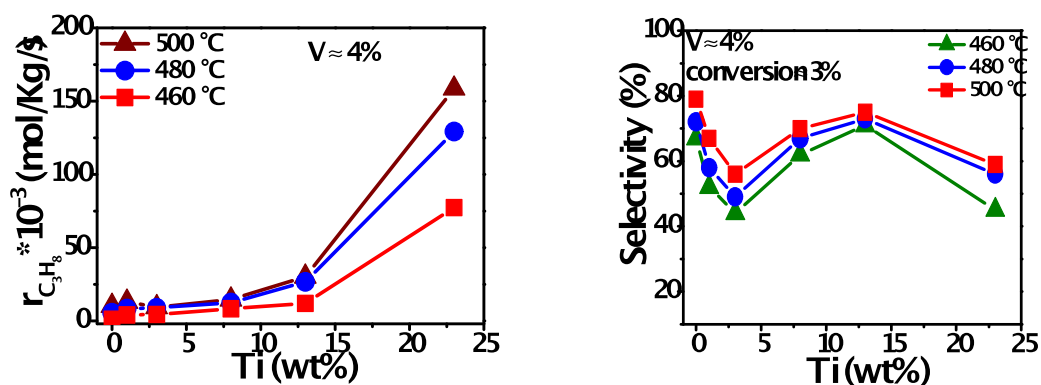


Fig. 14. Catalytic behaviour of V-Ti-SBA15 catalyst with increasing titania content.

The structural characterization of this matrix of catalyst was performed in project B2. More details are described in the report of B2. A kinetic analysis of this catalyst with 4 wt% vanadia and 13 wt% titania and a comparison to the V-SBA15 catalyst shows essentially the same kinetic behaviour (Table 6). The reaction orders are 1 with respect to propane and propene and zero with respect to oxygen. Combustion of propane can be neglected. The activation energy for the ODH of propane is the same as for the unmodified catalyst while the activation energy for the oxidation of propene is slightly higher. The difference in activity per site is about one order of magnitude. This is less pronounced than in the case of pure silica and titania as support, but the combination of the essential features of the two support materials (high surface and facilitated reducibility) results in a catalyst with high productivity per kg of catalyst. The increase in activity may be assigned to the improved reducibility of the vanadia grafted to the titania. This acceleration results still in a rate that is far lower than the rate of catalyst reoxidation by oxygen. Therefore the reaction order for oxygen is still zero.

Table 6. Comparison of kinetic parameter of 2,7V-SBA15 and 4V-13Ti-SBA15

Katalysator	ODP				Totaloxidation			
	E_a [kJ·mol ⁻¹]	$k_{0,eff}$ [m ³ g ⁻¹ s ⁻¹]	m_1	m_2	E_a [kJ·mol ⁻¹]	$k_{0,eff}$ [m ³ g ⁻¹ s ⁻¹]	m_3	m_4
V-SBA-15	103±6	2,3±1,3	1	0	34±18	(7,2±5) · 10 ⁻²	1	0
4V-13Ti-SBA15	101±5	34±18	1	0	57±7	0,2±0,05	1	0

Fig. 15 shows the performance of 5 catalysts from the prepared library with respect to the productivity of propene in kg propene per kg catalyst and hour. For industrial application a minimum of 1 kg_{propene} / kg_{cat}*h should be achieved [41]. The catalyst without TiO₂ modification fails to meet this requirement. Modification with only 3 % TiO₂ decreases the productivity due to a bad selectivity. The modification with 8, 13 and 23 % TiO₂ well exceeds this requirement.

The layer structure of the V-Ti-SBA15 catalyst is beneficial for the performance, but not essential. Similar results were obtained in project B3 with MCM-41 based catalyst with different ratios of Ti to Si within its crystal structure [42].

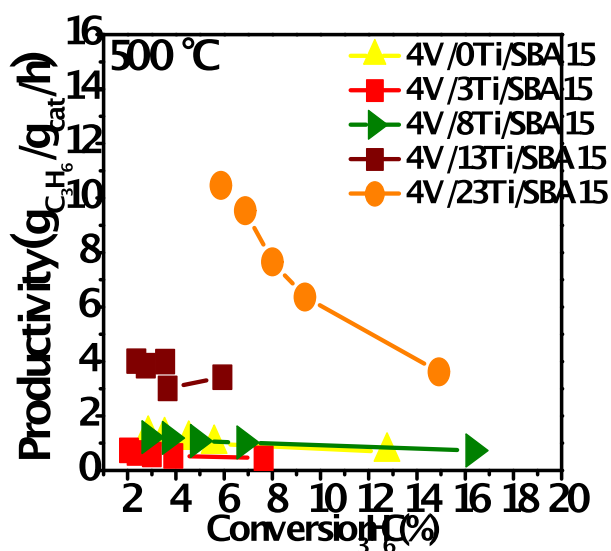


Fig. 15. Productivity of titania modified catalysts at 500°C

Reaction Engineering of ODP

Reactor simulations with the obtained kinetic data show that a plug flow reactor shows always better performance than an ideally mixed reactor like a fluidized bed. The oxidation state of the catalyst decreases with the consumption of oxygen along the reactor length resulting in different selectivity in different zones of the reactor. Experiments with N₂O as less reactive oxidizing agent or with a pre-reduced catalyst [DSB09] demonstrate a higher selectivity of vanadia catalyst in a lower oxidation state than +V. A defined partially reduced catalyst could be obtained in an ideally mixed reactor like a fluidized bed, what is simulated on laboratory scale by a Berty-reactor. Here the catalyst is placed in a rotating basket. All experiments performed in this reactor showed very low selectivity because the back-mixing of the product with oxygen overrules the positive effect of the reduced catalyst.

Another parameter for selectivity control is the temperature. Since the activation energy of the ODH of propane is substantially higher than that of the combustion of propene, the reaction should be performed at a temperature as high as possible, as long unselective gas phase reactions can be excluded. A suitable type of reactor for performing highly exothermic reactions under good temperature control is a micro reactor.

Due to their superior heat transfer properties, microstructured reactors are well suited for performing strongly exothermic heterogeneously catalyzed gas phase reactions. In order to utilize the full potential of this reaction technology, a new low-cost manufacturing concept was developed, using a Ni–Ag–Sn solder system for bonding the individual structured steel

platelets. [SDS09a]. A schematic presentation is shown in Fig. 16. Three different methods for depositing $\text{VO}_x/\alpha\text{-Al}_2\text{O}_3$ material on the micro-channels were investigated with respect to morphology, mechanical stability and catalytic behavior of the obtained coatings [HTG09]. Especially the influence of different binder materials (Al-tri-sec-butylate, tetraethoxysilane, hydroxypropyl cellulose and polyvinyl pyrrolidone) was analyzed. For evaluating the performance of the coatings, the oxidative dehydrogenation of propane (ODP) served as a sensitive test reaction. The modules and the catalytic coatings withstood the applied reaction conditions (400–600°C at ambient pressure), which makes them safe and flexible tools for research activities and small scale production processes.

Catalytic performance in the ODP was predicted on the basis of a kinetic model, showing good agreement for low degrees of propane conversion [SDS09b]. In order to elucidate discrepancies between experimental and forecasted model data at higher degrees of propane conversion (i.e., >12.5%), possible sources of error were systematically investigated. Specifically, heat and mass transport limitations were excluded as well as possible inaccuracies of the applied kinetic model were examined. It could be shown that microstructured reactors are well suited to be applied for strongly exothermic heterogeneously catalyzed gas phase reactions since they allow isothermal reaction conditions over a wide range of concentrations and temperatures.

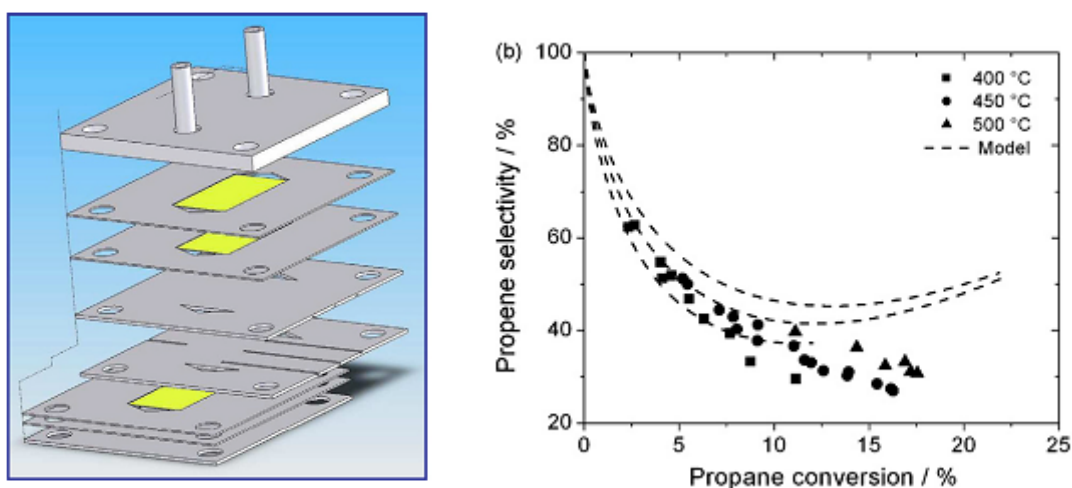


Fig. 16. Schematic presentation of a microreactor with catalyst coating (yellow) before fusion (left) and comparison of predicted and obtained selectivity of this reactor at different propane conversion.

Literature

- [1] R. Grabowski, S. Pietrzyk, J. Slocynski, F. Genser, K. Wcislo, B. Grzybowska-Swierkosz, *Appl. Catal. A* 232 (2002) 277-288
- [2] D. Creaser, B. Andersson, *Appl. Catal. A* 141 (1996) 131-152
- [3] C. Resini, M. Panizza, L. Arrighi, S. Sechi, G. Busca, R. Miglio, S. Rossini, *Chem. Eng. J.* 89 (2002) 75-87
- [4] R. Burch, E.M. Crabb, *Appl. Catal. A* 100 (1993) 111-130
- [5] A. Khodakov, E. Iglesia, A.T. Bell, *J. Catal.* 177 (1998) 343
- [6] M.D. Argyle, K. Chen, A.T. Bell, E. Iglesia, *J. Catal.* 208 (2002) 139
- [7] S.L.T. Andersson, *Appl. Catal. A* 112 (1994) 209
- [8] M. Barsan, F.C. Thyron, *Catal. Today* 81 (2003) 159
- [9] A. Bottino, G. Capannelli, A. Comite, R. Di Felice, *Chem. Eng. J.* 94 (2003) 11
- [10] S. Lars, T. Andersson, *Appl. Catal. A* 112 (1994) 209-218
- [11] R. Grabowski, *Appl. Catal. A* 270 (2004) 37-47
- [12] K. Chen, A. Khodakov, J. Yang, A.T. Bell, E. Iglesia, *J. Catal.* 186 (1999) 325-333
- [13] P. Mars, D.W. van Krevelen, *Chem. Eng. Sci.*, 3 (1954) 41
- [14] A. Pantazidis, S.A. Buchholz, H.W. Zanthoff, Y. Schuurman, C. Mirodatos, *Catal. Today* 40 (1998) 207-214
- [15] S. Albonetti, F. Cavani, F. Trifiro, *Catal. Rev.-Sci. Eng.* 38 (1996) 413
- [16] E.A. Mamedov, V. Cortes Corberan, *Appl. Catal. A* 127 (1995) 1-40
- [17] I.E. Wachs, *Catal. Today*. 100 (2005) 79-94
- [18] B. Kilos, A.T. Bell, E. Iglesia, *J. Phys. Chem. C.*, 133 (2009) 2830-2836
- [19] A. Dinse, B. Frank, C. Hess, D. Habel, R. Schomäcker, *J. Mol. Catal. A*, 289 (2008) 28-37
- [20] T. Blasco, J.M. López Nieto, *App. Catal. A.*, 157 (1997) 117-142
- [21] P. Eisele, R. Killpack, *Ullmann's Enc. of Ind. Chem.* (2000), Propene
- [22] M.A. Bañares, M.V. Martínez-Huerta, X. Gao, J.L.G. Fierro, I.E. Wachs, *Catal. Today*, 61 (2000) 295-301
- [23] A. Khodakov, B. Olthof, A.T. Bell, E. Iglesia, *J. Catal.*, 181 (1999) 205-216
- [24] A.A. Lemonidou, L. Nalbandian, I.A. Vasalos, *Catal. Today*, 61 (2000) 333-341
- [25] H. Tian, E.I. Ross, I.E. Wachs, *J. Phys. Chem. B*, 110 (2006) 9593-9600
- [26] X. Ronzanska, R. Fortrie, J. Sauer, *J. Phys. Chem. C.*, 111 (2007) 6041-6050
- [27] I.E. Wachs, G. Deo, *J. Catal.*, 146 (1994) 323-334
- [28] N.E. Quaranta, J. Soria, V. Cortés Corberán, J.L.G. Fierro, *J. Catal.*, 171 (1997) 1-13
- [29] Y. Lin, C. Chang, C. Chen, J. Jehng, S. Shyu, *Cat. Comm.*, 9 (2008) 675-679
- [30] A. Khodakov, J. Yang, S. Su, E. Iglesia, A.T. Bell, *J. Catal.*, 177 (1998) 343-351
- [31] G. Avgouropoulos, E. Oikonomopoulos, D. Kanistras, T. Ioannides, *App. Catal. B.*, 65 (2006) 62-69
- [32] M.V. Martínez-Huerta, J.M. Coronado, M. Fernández-García, A. Iglesias-Juez, G. Deo, J.L.G. Fierro, M.A. Bañares, *J. Catal.*, 225 (2004) 240-248
- [33] C. Zhao, I.E. Wachs, *J. Catal.*, 257 (2008) 181-189
- [34] H. Feng, J.W. Elam, J.A. Libera, J.M. Pellin, P.C. Stair, *J. Catal.*, 269 (2010) 421-431
- [35] T. Allersma, R. Hakim, T.N. Kennedy, J.D. Mackenzie, *J. Chem. Phys.*, 46 (1967) 154-160
- [36] J. Sauer, J. Döbler, *Dal. Trans.*, 19 (2004) 3116-3121
- [37] T.K. Todorova, M.V. Ganduglia-Pirovan, J. Sauer, *J. Phys. Chem. C.*, 111 (2007) 5141-5153
- [38] V. Majer, V. Svoboda, *Black. Sci. Pub.*, (1985) 300
- [39] M.A. Natal-Santiago, J.A. Dumesic, *J. Catal.*, 175 (1998) 252-268
- [40] J.M. Guil, N. Homs, J. Llorca, P.R. de la Piscina, *J. Phys. Chem. B.*, 109 (2005) 10813-10819
- [41] F. Cavani, N. Ballarini, A. Cericola, *Catal. Today*, 127 (2007) 113-131
- [42] O. Ovsitser, M. Cherian, A. Brückner, E. Kondratenko, *J. Catal.*, 265 (2009) 8-18

5.2.2 Projektrelevante eigene Publikationen

a) erschienene oder angenommene Arbeiten in wissenschaftlichen Zeitschriften oder Buchveröffentlichungen

- [HWS09] R. Herbert, D. Wang, R. Schomäcker, R. Schlögl, C. Hess
Stabilization of Mesoporous Silica SBA-15 by Surface Functionalization
Chem. Eur. J. Chem. Phys. **10** (2009) 2230 – 2233.
- [SDS09a] O. Schwarz, P.-Q. Duong, G. Schäfer, R. Schomäcker,
Development of a microstructured reactor for heterogeneously catalyzed gas phase reactions: Part I. Reactor fabrication and catalytic coatings
Chem. Eng. J. **145** (2009) 420 – 428.
- [SDS09b] O. Schwarz, P.-Q. Duong, G. Schäfer, R. Schomäcker
Development of a microstructured reactor for heterogeneously catalyzed gas phase reactions: Part II. Reactor characterization and kinetic investigations
Chem. Eng. J. **145** (2009) 429 – 435.
- [HGT09] D. Habel, O. Görke, M. Tovar, M. Willinger, M. Ziemann, O. Schwarz,
R. Schomäcker, H. Schubert
Microstraining in titania-, alumina- and silica-supported V₂O₅-catalysts
J. Euro. Cer. Soc. **29** (2009) 1093 – 1099.
- [DKF09] A. Dinse, S. Khennache, B. Frank, C. Hess, R. Herbert, S. Wrabetz, R. Schlögl,
R. Schomäcker
Oxidative dehydrogenation of propane on silica (SBA-15) supported vanadia catalysts: A kinetic investigation
J. Mol. Catal. A **307** (2009) 43 – 50.
- [DSB09] A. Dinse, R. Schomäcker, A. T. Bell
The role of lattice oxygen in the oxidative dehydrogenation of ethane on alumina-supported vanadium oxide
Phys. Chem. Chem. Phys. **11** (2009) 6119 – 6124.
- [DFH08] A. Dinse, B. Frank, C. Hess, D. Habel, R. Schomäcker
Oxidative dehydrogenation of propane over low-loaded vanadia catalysts: Impact of the support material on kinetics and selectivity
J. Mol. Catal. A **289** (2008) 28 – 37.
- [DOH08] A. Dinse, A. Ozarowski, C. Hess, R. Schomäcker, K.-P. Dinse
Potential of High-Frequency EPR for Investigation of Supported Vanadium Oxide Catalysts
J. Phys. Chem. C **112** (2008) 17664 – 17671.

5.3 Rückblick auf die Förderung

Das Teilprojekt wurde seit 07/2005 im Sonderforschungsbereich gefördert. Es wurde mit Ablauf der 4. Förderperiode im Juni 2011 beendet.

5.3.1 Personal im Teilprojekt während der 4. Förderperiode

	lauf. Nr.	Name, akademischer Grad, Dienststellung	engere Fachzugehörigkeit	Institut der Hochschule oder der außeruniv. Einrichtung	Mitarbeit im Projekt Zeitraum Wochenstunden	Entgeltgruppe
Grundausrüstung						
Wissenschaftlerinnen und Wissenschaftler	1.	Reinhard Schomäcker, Dr., Prof.	Techn. Chemie	TU-C	07/2005 – 06/2011, 8h	
	2.	Kirsten Langfeld, Dipl.-Chem.	Techn. Chemie	TU-C	07/2009 – 06/2011, 10h	
	3.	Oliver Schwarz, Dipl.-Ing.	Techn. Chemie	TU-C	07/2005 – 06/2009	
	4.	Carlos Carrero, Dipl.-Chem.	Techn. Chemie	TU-C	07/2009 – 06/2011	
nichtwissenschaftl. Mitarbeiterinnen und Mitarbeiter	5.	Christa Löhr		TU-C	07/2005 – 06/2011, 4h	
	6.	Gabriele Vetter		TU-C	07/2005 – 06/2011, 4h	
Ergänzungsausstattung						
Wissenschaftlerinnen und Wissenschaftler	1.	Arne Dinse, Dipl. Chem.	Techn. Chemie	TU-C	06/2008 – 02/2009, 40h	E13, 66%
	2.	Benjamin Beck, Dipl.-Ing.	Techn. Chemie	TU-C	04/2008 – 10/2008, 40h	E13, 66%
nichtwissenschaftl. Mitarbeiterinnen und Mitarbeiter						

Aufgaben der Mitarbeiterinnen und Mitarbeiter (Grundausrüstung):

1. Prof. Dr. Reinhard Schomäcker
war wissenschaftlicher Leiter des Teilprojektes. Er betreute die wissenschaftlichen Mitarbeiter und koordinierte die Aufgaben innerhalb des Teilprojektes sowie die Zusammenarbeit mit anderen Teilprojekten des SFB.
2. Dipl.-Chem. Kirsten Langfeld
Dipl.-Chem. Kirsten Langfeld ist wissenschaftliche Mitarbeiterin in der Arbeitsgruppe von Prof. Schomäcker. Die Aufgabenstellung ihrer Doktorarbeit bezieht sich auf die Untersuchung der Reoxidation von Oxidationskatalysatoren mit verschiedenen Trägermaterialien und Beladungen durch unterschiedliche Oxidationsmittel. Dieser Beitrag unterstützte die Untersuchung der Einflussparameter auf die Selektivität der oxidativen Dehydrierung von Propan mit kinetischen Informationen zu diesem Teilschritt der Reaktion.
3. Dipl.-Ing. Oliver Schwarz
hatte ein Promotionsstipendium des Landes Berlin erhalten und sich auf das Gebiet der Mikroreaktionstechnik spezialisiert. Er hat den Einfluss der Reaktionsführung auf die Selektivität der oxidativen Dehydrierung von Propan untersucht. Dadurch wird die Anwendungsbezogenheit des Teilprojektes weiter vertieft.
4. Dipl. Chem. Carlos Carrero
hat ein Promotionsstipendium des DAAD und führt kinetische Untersuchungen an TiO₂-modifizierten SBA15-Katalysatoren durch. Die Zielstellung seiner Arbeit ist die Optimierung der Produktivität der ODH von Propan.
5. Christa Löhr
Verwaltungsangestellte, führte die im Rahmen des Teilprojektes anfallenden Verwaltungsaufgaben durch.
6. Gabriele Vetter
Chemotechnikerin, betreute in der Arbeitsgruppe von Prof. Schomäcker das GC- und HPLC-Labor. Im Rahmen des Teilprojektes wurden durch sie die Analysemethoden für die zu untersuchenden Gasgemische ausgearbeitet.

Aufgaben der Mitarbeiterinnen und Mitarbeiter (Ergänzungsausstattung):

1. Dr. Arne Dinse

Diplomchemiker, fertigte von 10/05 bis 12/08 seine Doktorarbeit im Rahmen des SFB-Teilprojektes B6 an und hat den Einfluss von Trägermaterialien auf die Aktivität von Vanadiumoxid-Katalysatoren untersucht. Für einen ausgewählten Katalysator, V-SBA-15, hat er eine detaillierte kinetische Untersuchung und Modellierung durchgeführt, die die Grundlage für die weiteren Arbeiten des Teilprojektes bildet. Im Rahmen eines Auslandsaufenthalts hat er sich mit Isotopenaustauschexperimenten in kinetischen Untersuchungen vertraut gemacht.

2. Dipl- Ing. Benjamin Beck

Herr Beck hat die geplanten kinetischen Untersuchungen an verschiedenen Vanadiumoxid-Katalysatoren fortgeführt und eine detaillierte Struktur-Wirkungs-Analyse anhand von physikalisch-chemischen Daten aus anderen Teilprojekten vorgenommen. Dabei wurde die ODH von Ethanol als zusätzliche Modellreaktion in das Projekt aufgenommen.

5.1 Allgemeine Angaben zum Teilprojekt B7

5.1.1 Titel: Technische V_2O_5/TiO_2 -Modellkatalysatoren: Herstellung und Untersuchung der Aktivkomponente-Träger-Wechselwirkung

5.1.2 Projektleitung

Prof. Dr. Helmut Schubert
geb. 03.10.1951

Institut für Werkstoffwissenschaften und -technologien
Fachgebiet Keramik, Sekr. ES 3
Englische Straße 20
10587 Berlin

Telefon: 030 / 314-23425
E-Mail: Helmut.Schubert@TU-Berlin.de

5.2 Entwicklung des Teilprojekts

5.2.1 Bericht

The research of this project B7 is focussed on the support effect on activity and selectivity, especially the influence of volume properties such as mechanical, thermal and electrical properties.

The previous project aimed on the influence of thermal expansion mismatch on the formation of interfacial stresses, which are a function of both support and active compound. The mismatch was caused by the high anisotropy of thermal expansion of the active compound. Generally the expansion coefficients of those are much higher as compared to the support materials. The mismatch causes the formation of a fine crystallite mosaic structure, which has new interfaces. The material is then characterized by very fine crystallite in the nm-range and a large fraction with low coordinated sites. A mosaic structure correlated with the width (FWHM) of the peaks as well as the catalytic activity.

In this period B7 is embedded in the Poly B group. The focus is on the contribution of transport properties. The central part of the catalytic cycle is the formation of defects. Conductivity measurements are a straight forward possibility of gathering information on the enthalpy of formation for anionic defects.

First, experiments were carried out on pure V_2O_5 for comparison. The conductivity was not

considered as a direct part in catalysis yet, but conductivity measurements a varying partial pressure are one possibility to measure the enthalpy of defect formation, which is one of the key influences in the energy diagram of a reaction.

Defect Equilibrium and Defect Formation Enthalpy

We have studied the defect equilibrium with oxygen partial pressure via conductivity measurements. As it was determined by [1,2], the electrons after formation of an oxygen vacancy $U_{O}^{\bullet\bullet}$ are localized at two adjacent V^{5+} (V_V^x) centers forming two V^{4+} (V_V'):

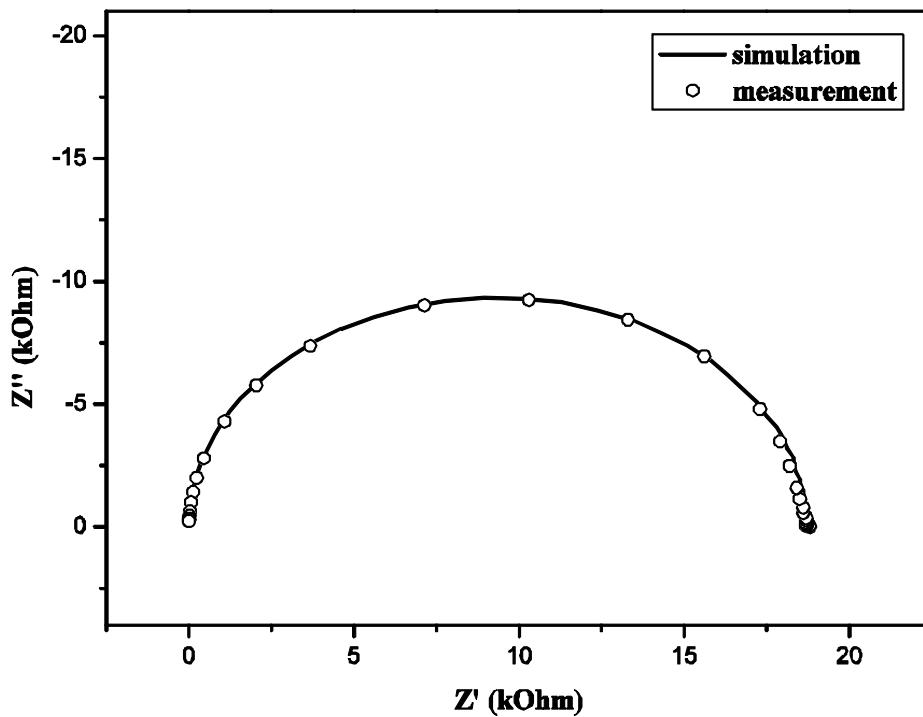


Fig. 1. Nyquist plot of V_2O_5 at room temperature.



This is in agreement with DFT calculations done from [3] where the localization of electrons leads to the formation of a new covalent bond between two a-b layers accompanied by a relaxation of the lattice in c-direction [4]:

A mass action law for this case was given by [5] resulting into an oxygen partial pressure dependence of the conductivity of $-1/6$. The mass balance for the reduction reaction is:

$$K = [V_V']^2 \cdot U_O^{\bullet\bullet} \cdot P_{O_2}^{1/2} \quad (2)$$

As $[V'_V] = 2[U_{O_2}^{\bullet\bullet}]$:

$$K = \frac{1}{2}[V'_V]^3 \cdot P_{O_2}^{-1/3} \quad (3)$$

and

$$[V'_V] = (2K)^{1/3} \cdot P_{O_2}^{-1/6} \quad (4)$$

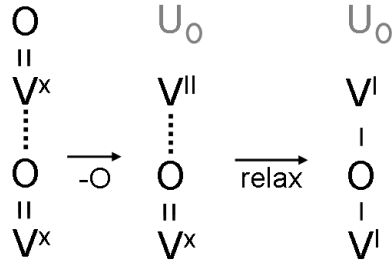


Fig. 2. Relaxation in the V_2O_5 lattice on reduction

From $K = K_0 \cdot \exp(-\Delta H_f^0 / RT)$, where ΔH_f^0 is the enthalpy of formation of the $U_{O_2}^{\bullet\bullet}$ defect follows with equation (5):

$$[V'_V] = K_1 \cdot \exp(-\Delta H_f^0 / 3kT) \cdot P_{O_2}^{-1/6} \quad (5)$$

The conductivity of vanadium pentoxide depends on the concentration of $[V'_V]$:

$$\sigma = [V'_V] \cdot K_2 \cdot \exp(-\Delta E / kT) \quad (6)$$

ΔE is the ionization energy for the localized electron at the $[V'_V]$ site. Substituting $[V'_V]$ in equation (6) with equation (5), the conductivity is described by equation (7-8) with a pressure dependence of $-1/6$:

$$\sigma = K_3 \cdot \exp(-(\Delta H_f^0 / 3kT + \Delta E / kT)) \cdot P_{O_2}^{-1/6} \quad (7)$$

$$\sigma = K_3 \cdot \exp(-\Delta E^* / kT) \cdot P_{O_2}^{-1/6} \quad (8)$$

Therefore at constant P_{O_2} the enthalpy of formation for an oxygen vacancy ΔH_f^0 can be calculated using equation (9):

$$\sigma = K_3 \cdot \exp(-\Delta E^* / kT) \quad (9)$$

where ΔE^* is the measured activation energy derived from the conductivity data. As ΔE^* is

$$\Delta E^* = \Delta H_f^0 / 3 + \Delta E \quad (10)$$

the value of ΔH_f^0 can be derived from the Arrhenius-plot.

The conductivity of a V_2O_5 sample was measured in an oxygen partial pressure range of $p(O_2) = 1.00 - 0.22$ bar at $508\text{ }^\circ\text{C}$ - starting with high oxygen pressure and lowering it subsequently. A re-equilibration after each pressure step was achieved in 1 to 2 days. Fig. 3 displays the data of the conductivity measurements exhibiting a slope of -0.170 ± 0.003 .

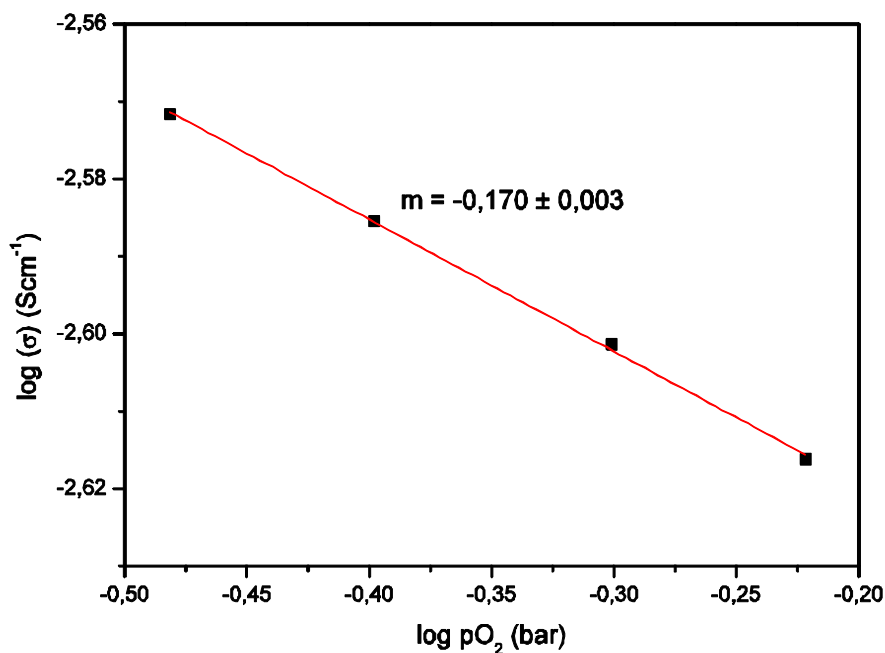


Fig. 3. Oxygen partial pressure dependency of V_2O_5 at $510\text{ }^\circ\text{C}$

The previous considerations showed that conductivity measurements are an appropriate possibility to inspect the formation of defects to judge on their enthalpy of formation. This is one part of the catalytic cycle.

A necessary part of this materials behaviour is a reduction associated by a loss of oxygen. This could be confirmed by measurements of the band gap (cf Fig. 4a). Fig. 4b shows a difference in band gap of heated samples versus room temperature. The specimens are first oxidized and then undergo a reduction. The onset of reduction at $350\text{ }^\circ\text{C}$ coincides with the onset of catalytic activity and the onset of conductivity, cf Fig. 5.

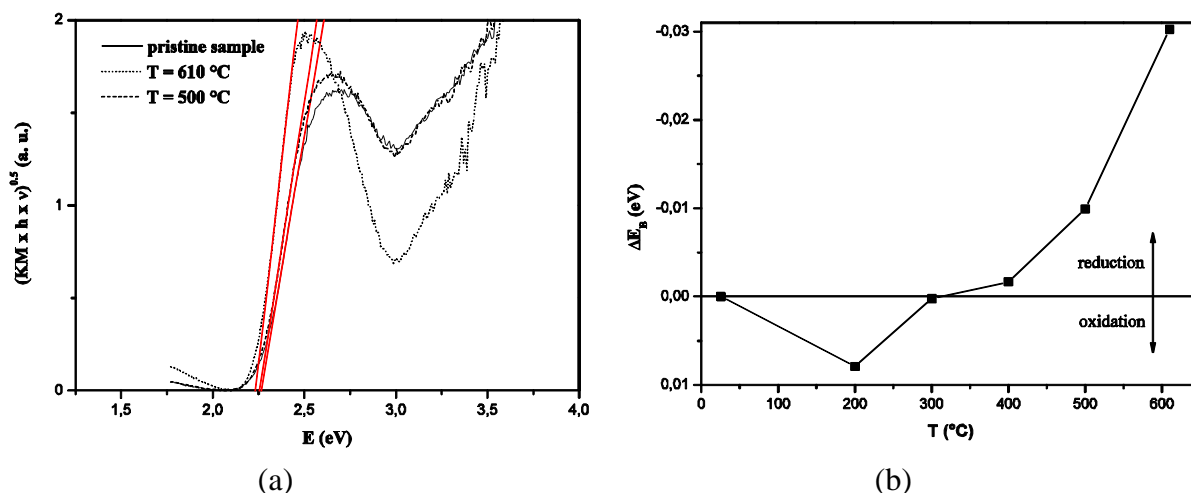


Fig. 4. UV-Vis spectroscopic experiments on thermally treated vanadium pentoxide samples. (a) Analysis of band gap according to [6], (b) difference of band gap in respect to pristine sample.

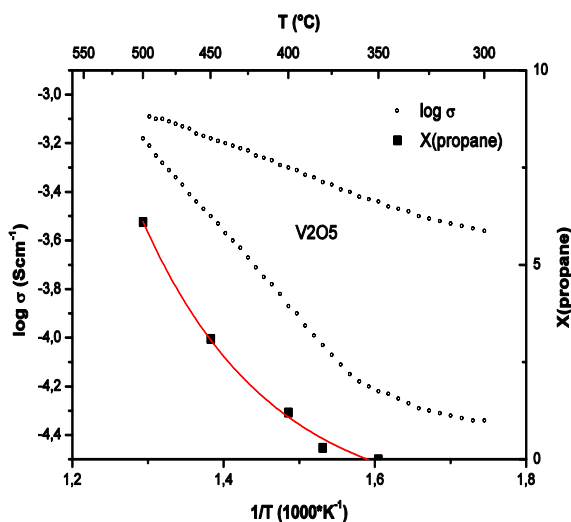


Fig. 5. Arrhenius plot for V_2O_5 in oxygen with the corresponding propane conversion results of the catalytic test.

The Arrhenius plot in Fig. 5 shows a high slope for heating, which consists of migration enthalpy and a contribution of the defect formation. On cooling only the migration enthalpy remains. Thus, the difference between the two slopes is a primary result for the enthalpy of defect formation. The third curve represents the activity as measured in B6. The onset of both conductivity and activity coincide and are basically in agreement with Tamann rule for volume diffusion.

A number of support materials have been tested and give rising enthalpies for defect formation as depicted in Table 1 and 2. The well-known differences in activity are clearly reflected in enthalpy of defect formation. The measurements are entirely independent.

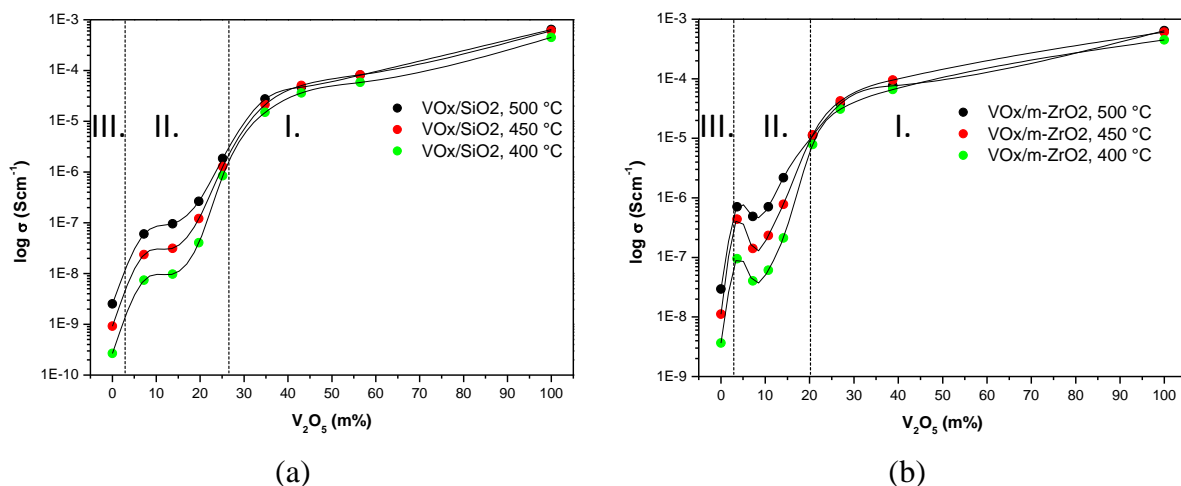


Fig. 6. Conductivity percolation behaviour for (a) VO_x/SiO_2 and (b) $\text{VO}_x/\text{m-ZrO}_2$ catalysts at different temperature in O_2 .

As an example, Fig. 6 shows a series of conductivity test for SiO_2 and ZrO_2 for different loading. Three regimes may be distinguished. At high loading the pathway leads through the V_2O_5 phase (cf. Fig. 7a), i.e. the current is determined by the active compound. The behaviour is mostly electronic, as expected for V_2O_5 . Fig. 8 shows the Nyquist plot for both high a low loading. The low loading shows a contribution for electrode polarization. The general curves are very similar for different support materials.

For decreasing loading the morphology of the active compound changes from crystalline to polymeric species (regime II) and to single sites (regime III). The current path leads through interfaces between the support particles, cf. Fig. 7b.

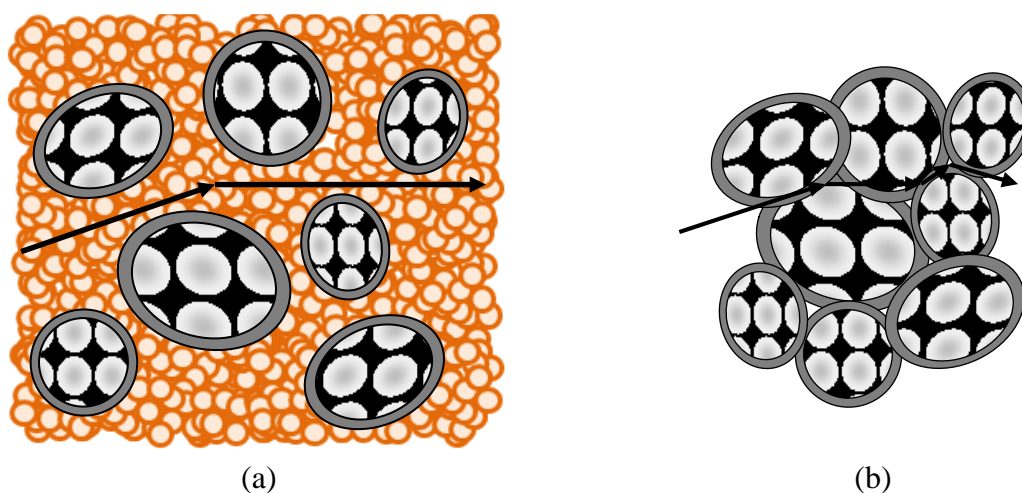


Fig. 7. Conductivity percolation model. The arrows indicate the kinetic path for the charge carriers. At high loading (a) a better conducting V_2O_5 matrix (small circles) is present. At low loading (b) the percolation path through V_2O_5 vanishes and a new kinetic path along the interface $\text{M}_x\text{O}_y/\text{VO}_x$ is formed (shell region).

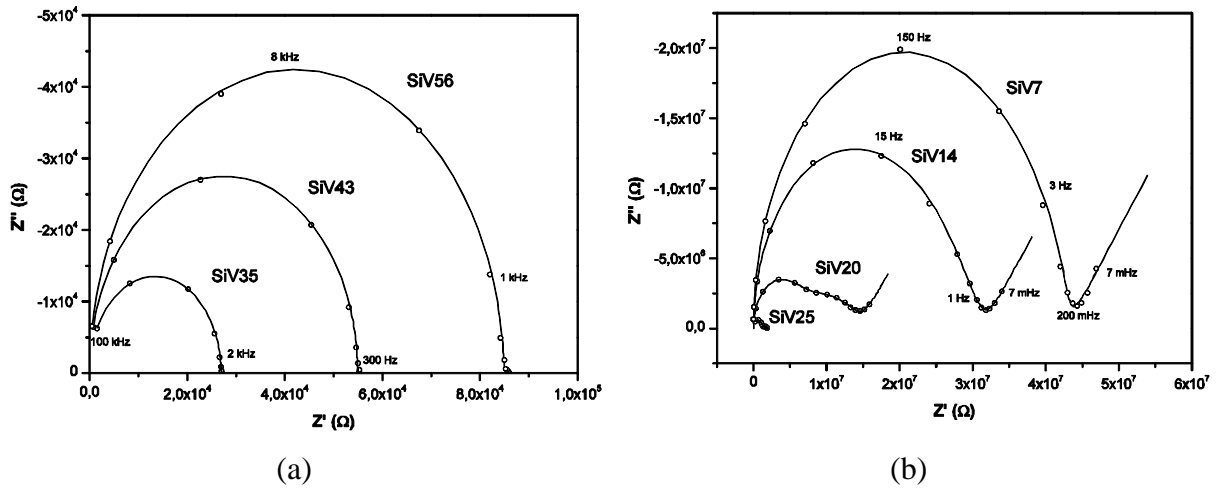


Fig. 8. Nyquist plot of ZrV_x at 500 °C in O_2 . (a) Above threshold in region I and (b) below threshold in region II.

Sample	V_2O_5 (mol%)	V_2O_5 (m%)	BET (m^2/g)	T_{onset} (°C)	ΔE^* (eV)	ΔE_m (eV)	ΔH_f (eV)	E_a (eV)
V_2O_5	100	100,00	2,01	380 -	$0.66 \pm$	$0.23 \pm$	$1.3 \pm$	$0.73 \pm$
				500	0.04	0.01	0.1	0.04
VO_x/TiO_2	30	49,83	4,63	350 -	$0.56 \pm$	0.25	$0.55 \pm$	$0.70 \pm$
				450	0.06	± 0.02	0.06	0.02
$VO_x/m-ZrO_2$	30	38,75	2,38	400 -	$0.63 \pm$	$0.35 \pm$	$0.85 \pm$	$0.67 \pm$
				500	0.02	0.02	0.10	0.05
VO_x/SiO_2	30	56,46	1,73	370 -	$0.57 \pm$	$0.20 \pm$	$1.11 \pm$	$1.06 \pm$
				500	0.01	0.01	0.08	0.06
VO_x/MgO	30	65,92	10,40	375 -	$0.75 \pm$	$0.21 \pm$	1.62	$0.90 \pm$
				430	0.05	0.01	± 0.09	0.01
$VO_x/\alpha-Al_2O_3$	30	43,33	9,04	400 -	$1.4 \pm$	$0.50 \pm$	$2.8 \pm$	$1.13 \pm$
				500	0.1	0.1	0.3	0.09

Table 1. Activation energies (apparent activation energy ΔE^* , migration energy ΔE_m), defect formation enthalpies (ΔH_f) and propane activation energy E_a for support VO_x - catalysts with high loading.

Table 2 shows the activation enthalpies for V_2O_5 on different supports for high loading. In these cases the path of current leads through the vanadia phase. The behaviour is electronic. In contrast specimens with low loading show a more ionic behaviour, cf Table 2. In spite of the difference with respect to mechanism again TiO_2 and ZrO_2 support lead to the lowest energies for defect formation.

	ΔE^*	ΔE_m	ΔH_f
VO_x/TiO_2	1.31 ± 0.02	1.12 ± 0.02	0.6 ± 0.1
$VO_x/m-ZrO_2$	1.35 ± 0.01	1.07 ± 0.01	0.84 ± 0.06
$VO_x/\gamma-Al_2O_3$	1.37 ± 0.02	0.98 ± 0.02	1.2 ± 0.1

Table 2. Defect formation enthalpies and activation energies for the supported monolayer catalysts. All values are given in eV.

Fig. 9. shows an energy diagram, which was derived by the catalytic measurements of B6 and the conductivity measurements in B7. The reaction is briefly described. A comprehensive discussion is given in the report of B6.

The material adsorbs oxygen and then interacts with propane. The following reaction needs the activation enthalpy $E_{A,app}$. In the following step an oxygen is extracted from the surface and reacts with propane to form propene which is then desorbed. The final situation is a reduced catalyst with the products propene and water. The largest contribution in this cycle is the reduction of the material, i.e. the enthalpy of defect formation ΔH_{def} , which has been measured by conductivity investigations at different partial pressure. The second largest contribution is the reaction enthalpy $E_{A,app}$, as determined by B6.

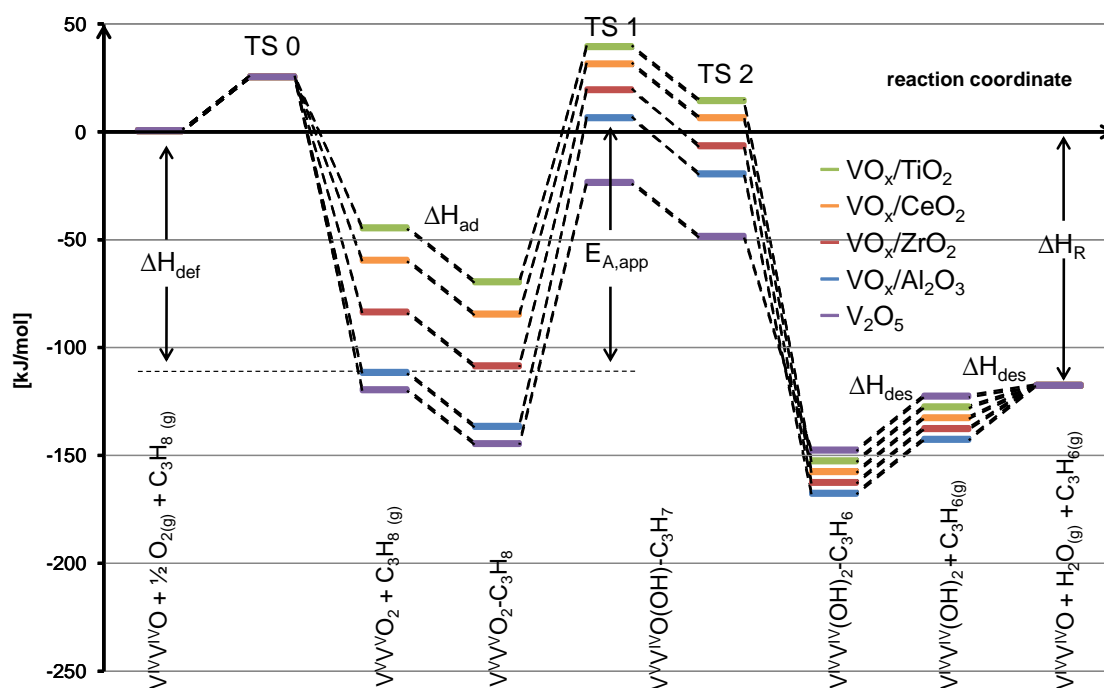


Fig. 9. Energy reaction profile for the ODP with the corresponding defect formation enthalpies.

Both the activation enthalpy $E_{A,app}$ on one side and the enthalpy of defect formation ΔH_{def} on the other hand are structural properties and rely on the same structure. Thus, a linear correlation between the two energies was found as depicted in Fig. 10.

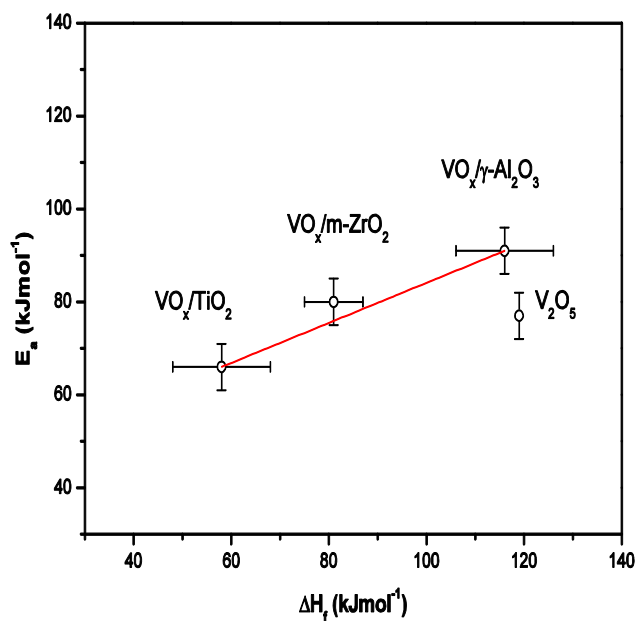


Fig. 10. Correlation plot E_a and ΔH_f

Microstructural Aspects

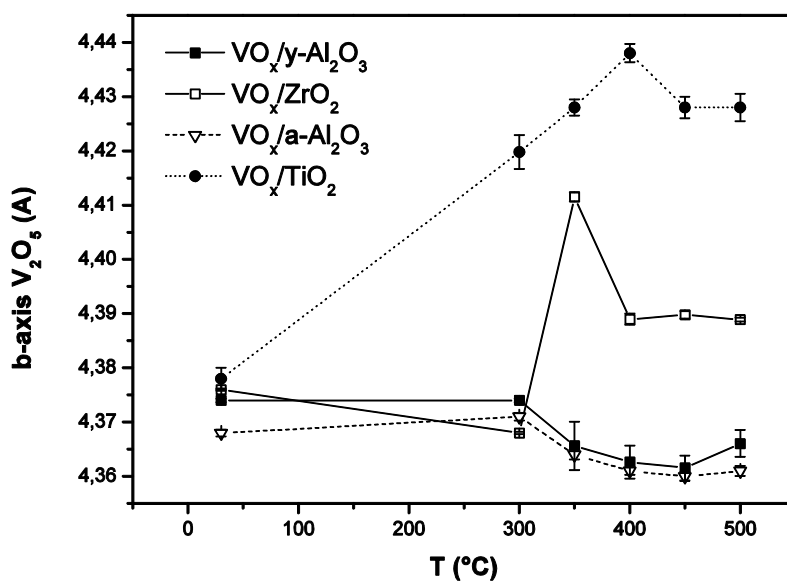


Fig. 11. Temperature dependency of b-axis of V_2O_5 on support.

The lattice parameters of vanadia on different supports has been investigated by high temperature neutron scattering (cf Fig. 11). In spite of using the same vanadia, the supports were able to change the strain behaviour of vanadia. Again, ZrO_2 and TiO_2 showed different behaviour as compared to the alumina supported materials.

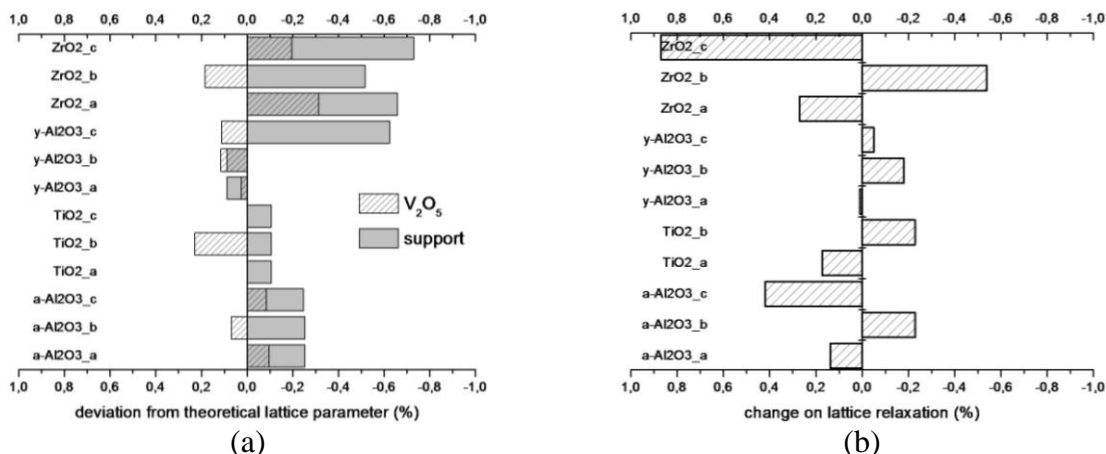


Fig. 12. (a) Deviation of lattice parameters of supported catalysts at 30 °C in oxygen. The V_2O_5 phase is depicted in hatched bars – the support in grey. (b) Relaxation of the V_2O_5 lattice on heating in oxygen.

Fig. 12 shows the deviation of the lattice parameters after processing, heating and cooling. The strain on cooling differs from the heating cycle because of strain hindrance. The b-axis shows the highest deviation in all cases. The high deviation for TiO_2 and ZrO_2 correlated with high activity.

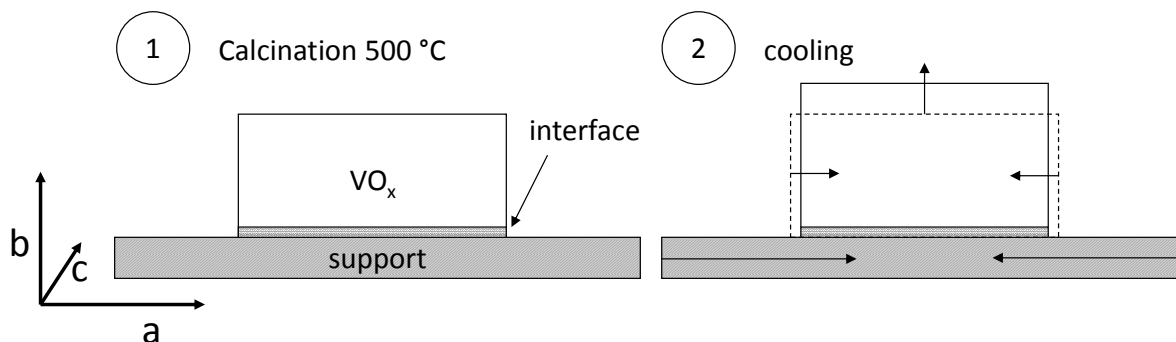


Fig. 13. Evolution of strain fields at the interface.

Since the active compound shows a higher thermal expansion the measured lattice parameter show both tension compress, which shall be illuminated in Fig. 13. The active compound is heated on the support leading to a stable interface. Reaching final temperature the two phases are in equilibrium. On cooling the different thermal contraction lead to stresses in a strain hindered situation (7). Assuming linear elastic behaviour would cause extraordinary high stresses, which are much higher than the materials strength. Thus a non-linear behaviour must occur. If such a material is re-heated, material has passed trough a strain due to the non-linearity but the thermal expansion coefficient is assumed to remain constant. Thus the lattice parameters and therefore the materials dimension -of support and active compound- are smaller after cooling. The following expansion may be high enough.

Summary

The catalytic cycle for vanadia on various supports could be cleared in the cooperative approach of Poly B, especially the two largest contributions were measured in B6 and B7 and found to be in correlation. This implies that they are caused by the same or similar structural origin.

It could be shown, that the support correlated with distinct activation enthalpies. It was also shown, that varying supports causes miscellaneous mosaic structures with substantial differences in domain size and number of interfaces. For the future, microstructural work is needed to clear which structural and microstructural mechanism causes the changes in behaviour.

The method to use conductivity for catalytic purposes had to be established.

The microstructural work needed high-resolution methods. Neutron scattering (HZB) and ASAXS (BessyII) needed long time proposals.

Difficulties

The experimental procedure of combining conductivity data and catalytic performance was not established and needed some interdisciplinary training. The procedure of gaining enthalpy numbers was more or less new.

The project depended on external measuring time proposal, which was managed through external reviewers. The time from the decision to start a measurement to the experiment was certainly over one year.

Cooperation

The cooperation within the Poly B group enabled to address the complex question by different approaches. Specimens have been processed in B2 and B6. Catalytic behaviour has been tested in B6 and B4. The microstructural characterization, especially TEM work, has been carried out in B2 and in an external cooperation with Helmholtz Zentrum Berlin.

Important data have been collected by neutron scattering at elevated temperatures. This work needed extra proposals to Helmholtz Zentrum Berlin BENSCH. The Experiments were run on E6 diffractometer at HZB Wannsee. Further experiment on size and charge of surface structure needed ASAXS spectra. Beamline 7T-MWP-SAXS on Bessy II has been used. The experiments could not be completed and brought to maturity.

A cooperation of rising importance with the group of Prof Wiemhöfer at Münster University was established concerning point defects and conductivity. His expertise on handling different partial pressures, finding the correlation between catalytic, electric behaviour and investigating the structural reasons was needed for this cooperation.

References

- [1] P. Clauws and J. Vennik, *Optical Absorption of Defects in V₂O₅ Single Crystals: As-Grown and Reduced V₂O₅*, Physica Status Solidi, no. 66, pp. 553-560, 1974.
- [2] L. Fiermans, P. Clauws, W. Lambrecht, L. Vandenbroucke, and J. Vennik, *Single Crystal V₂O₅ and Lower Oxides: A Survey of Their Electronic, Optical, Structural, and Surface Properties*, Physica Status Solidi (a), no. 59, pp. 485-504, 1980.
- [3] M. V. Ganduglia-Pirovano, A. Hofmann, and J. Sauer, *Oxygen vacancies in transition metal and rare earth oxides: Current state of understanding and remaining challenges*, Surface Science Reports, no. 62, pp. 219-270, 2007.
- [4] J. Sauer and J. Döbler, *Structure and reactivity of V₂O₅: bulk solid, nanosized clusters, species supported on silica and alumina, cluster cations and anions*, Dalton Transactions, pp. 3116 - 3121, 2004.
- [5] T. Allersma, R. Hakim, T. N. Kennedy, and J. D. Mackenzie, *Structure and Physical Properties of Solid and Liquid Vanadium Pentoxide*, Journal of Chemical Physics, no. 46, pp. 154-160, 1967.
- [6] X. Gao, J.-M. Jehng, and I. E. Wachs, *In Situ UV-vis-NIR Diffuse Reflectance and Raman Spectroscopic Studies of Propane Oxidation over ZrO₂-Supported Vanadium Oxide Catalysts*, Journal of Catalysis, no. 209, pp. 43-50, 2002.
- [7] D. Habel, O. Görke, M. Tovar, M. Willinger, M. Ziemann, O. Schwarz, R. Schomäcker, H. Schubert, *Microstraining in titania-, alumina- and silica-supported V₂O₅-catalysts*, Journal of the European Ceramic Society, no. 26, pp. 1093-1099, 2009.

5.2.2 Projektrelevante eigene Publikationen

a) erschienene oder angenommene Arbeiten in wissenschaftlichen Zeitschriften oder Buchveröffentlichungen

- [MHG11] R. Mitdank, D. Habel, O. Görke, M. Harth, H. Schubert, and H. Winter
Ion beam analysis of a structural phase transition in porous TiO_2/V_2O_5 ceramics with rough surfaces
Nucl. Instrum. Meth. B **269** (2011) 345-352.
- [HGT09] D. Habel, O. Görke, M. Tovar, M. Willinger, M. Ziemann, O. Schwarz, R. Schomäcker, and H. Schubert
Microstraining in titania-, alumina- and silica-supported V_2O_5 -catalysts
J. Eur. Ceram. Soc. **29** (2009) 1093-1099.
- [HGT08] D. Habel, O. Görke, M. Tovar, E. Kondratenko, and H. Schubert
Phase Relations in the System $TiO_2-V_2O_x$ under Oxidizing and Reducing Conditions
J. Phase Equilibria and Diffusion **29** (2008) 482 - 487.
- [SHO08] O. Schwarz, D. Habel, O. Ovsitser, E.V. Kondratenko, C. Hess, R. Schomäcker, and H. Schubert
Impact of preparation method on physico-chemical and catalytic properties of $VO_x/\gamma-Al_2O_3$ materials
J. Mol. Catal. A **293** (2008) 45 - 52.

5.3 Rückblick auf die Förderung

Das Teilprojekt wurde seit 07/2005 im Sonderforschungsbereich gefördert. Es wurde mit Ablauf der 4. Förderperiode im Juni 2011 beendet.

5.3.1 Personal im Teilprojekt während der 4. Förderperiode

	lauf. Nr.	Name, akademischer Grad, Dienststellung	engere Fachzugehörigkeit	Institut der Hochschule oder der außeruniv. Einrichtung	Mitarbeit im Projekt Zeitraum Wochenstunden	Entgeltgruppe
Grundausrüstung						
Wissenschaftlerinnen und Wissenschaftler	1.	Helmut Schubert, Dr., Univ.-Prof.	Werkstoffw.	TU-W	07/2005 – 06/2011, 10 h	
	2.	Oliver Görke, Dr.	Werkstoffw.	TU-W	08/2008 – 06/2011, 2 h	
nichtwissenschaftl. Mitarbeiterinnen und Mitarbeiter	3.	Heinrich Sap, Dipl-Ing	Werkstoffw.	TU-W	08/2008 – 06/2011, 5 h	
	4.	Kai Weisser, Dipl-Ing.	Werkstoffw.	TU-W	08/2008 – 06/2011, 5 h	
	5.	Harald Link	Werkstoffw.	TU-W	08/2008 – 06/2011, 5 h	
	6.	Peter Schnepfmüller	Werkstoffw.	TU-W	08/2008 – 06/2011, 5 h	
Ergänzungsausrüstung						
Wissenschaftlerinnen und Wissenschaftler	1.	Almuth Berthold, Dr.	Werkstoffw.	TU-W	11/2008 – 04/2011, 32 h 05/2011 – 06/2011, 38,5 h	E13
	2.	Manuel Harth, Dipl-Ing.	Werkstoffw.	TU-W	08/2008 – 04/2011, 6,5 h	E13
nichtwissenschaftl. Mitarbeiterinnen und Mitarbeiter						

Aufgaben der Mitarbeiterinnen und Mitarbeiter (Grundausrüstung):

1. Prof. Dr. Helmut Schubert
Projektleitung, Koordination
2. Dr. Ing. Oliver Görke
Herr Dr. Görke ist Werkstoffwissenschaftler. Er ist Ansprechpartner für die
Prozesstechnik und Materialuntersuchung.
3. Dipl.-Ing. Heinrich Sap
Physikingenieur
Hochtemperaturtechnik und thermische Methoden
4. Dipl.-Ing. Kai Weisser
Elektrotechniker, Messtechnik und Datenverarbeitung
5. Harald Link
Chemische Analytik
6. Peter Schnepfmüller
Mechanische Werkstatt

Aufgaben der Mitarbeiterinnen und Mitarbeiter (Ergänzungsausstattung):

1. Dr. Ing. Almut Berthold
Strukturuntersuchungen
2. Dipl.-Ing. Manuel Harth
Leitfähigkeitsmessungen

5.1 Allgemeine Angaben zum Teilprojekt C1

5.1.1 Titel: Adsorptions- und Reaktionsstudien an Vanadium- und Molybdän-gedopten dünnen TiO₂-Filmen

5.1.2 Projektleitung

Prof. Dr. Hans-Joachim Freund
geb. 04.03.1951

Dr. Helmut Kuhlenbeck
geb. 26.08.1957

Fritz Haber Institute of the Max Planck Society
Chemical Physics Department
Faradayweg 4-6
14195 Berlin

Telefon: 030 / 8413 4102/4104

030 / 8413 4222

E-Mail: freund@fhi-berlin.mpg.de

kuhlenbeck@fhi-berlin.mpg.de

5.2 Entwicklung des Teilprojekts

5.2.1 Bericht

The preparation and characterization of V/Ti and Mo/Ti ordered mixed oxides layers as well as adsorption/reaction studies were in the focus of the last project period with the aim of learning about co-operative mechanisms in reactions on the mixed oxide surfaces. According to the project proposal the work should include the preparation and characterization of thin, well ordered TiO₂ layers and mixed oxide layers as well as adsorption and reaction studies. While reports about systems with molybdenum or vanadium deposited onto TiO₂(110) and their interaction with adsorbates are readily available in literature (see e.g. [1]), V/Ti and Mo/Ti ordered mixed oxides were not yet investigated. In mixed oxides surface and bulk can be in equilibrium and they thus can represent more stable and possibly different systems. Both mixed oxide systems could be prepared and were characterized to a large extent. Presently adsorption and reaction studies are performed and preliminary results are available.

Another topic of investigation was the adsorption of methanol on V₂O₅(001) as completion of a project of the preceding period. A summary of the results will be present after the presentation of the results obtained for the V/Ti and Mo/Ti mixed oxide systems.

Studies of V/Ti and Mo/Ti mixed oxide systems

General aspects of the preparation

At the beginning we tried to prepare mixed oxide layers on inert metallic substrates like platinum or gold single crystal surfaces which were chosen in view of possible future reaction studies at higher pressures. However, the preparation attempts were not successful in that ordered layer with regular TiO_2 structure could not be prepared on all the tested substrate surfaces. Faceting, bad order, and de-wetting were the main obstacles which were identified as being due to interface stress induced by the significant lattice mismatch between the substrate and the TiO_2 overlayers in all cases. In order to circumvent this problem, rutile TiO_2 single crystals were used as substrates in future experiments since there is no lattice mismatch in this case. As a consequence $\text{TiO}_2(110)$ films grown on $\text{TiO}_2(110)$ single crystals exhibit good crystalline order as verified with LEED (see Fig. 1) and STM.

V/Ti mixed oxide overlayers on Ti(110)

In a first attempt we tried to prepare such layers by co-deposition of vanadium and titanium at elevated temperature in an oxygen atmosphere which resulted in pure $\text{TiO}_2(110)$ without a detectable vanadium content. This was a clear indication the vanadium ions diffuse into the $\text{TiO}_2(110)$ substrate. Therefore a diffusion blocking layer was introduced between the V/Ti mixed oxide and the $\text{TiO}_2(110)$ substrate. Diffusion blocking was achieved by mixing metal ions with a larger diameter than that of Ti^{4+} into the $\text{TiO}_2(110)$ lattice, which strains the lattice and increases the diffusion barrier. The ions mixed into the TiO_2 lattice were selected among

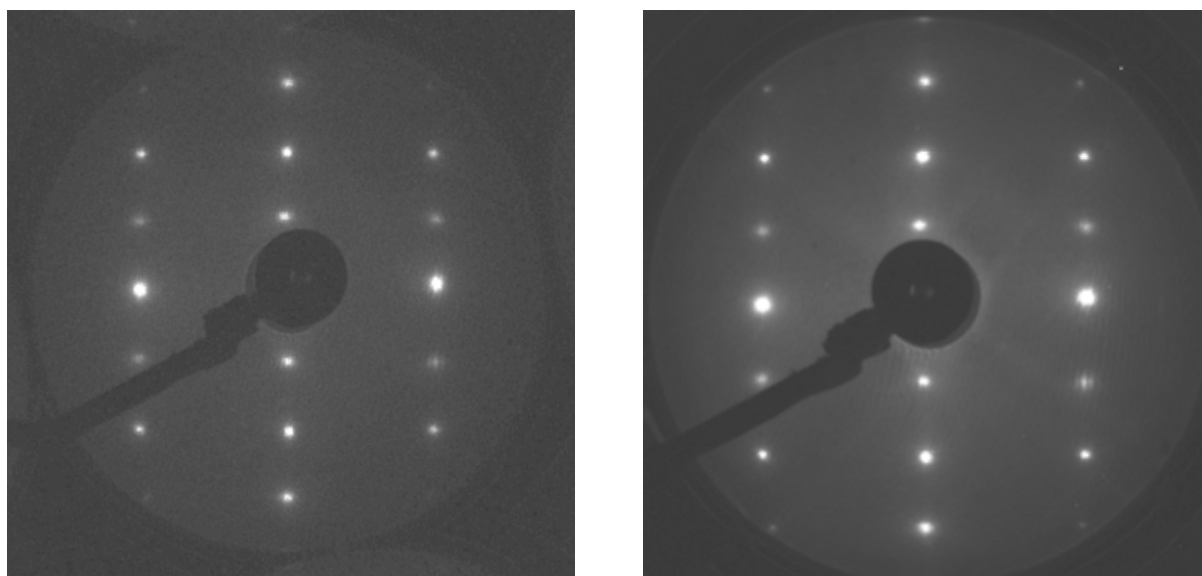


Fig. 1. LEED images of $\text{TiO}_2(110)$ (left) and of a thin $\text{TiO}_2(110)$ layer on $\text{TiO}_2(110)$ (right).

	TiO ₂	VO ₂	PbO ₂	TaO ₂	WO ₂
Ionic radius [Å]	0.745	0.720	0.915	0.82	0.80
Crystal structure	Tetragonal	Tetragonal	Tetragonal	Tetragonal	Monoclinic (distorted rutile)

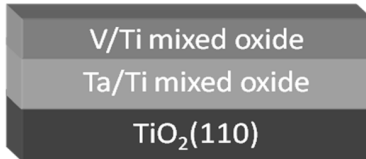


Fig. 2. Left: selected oxides with rutile type structure and the ionic diameter of the metallic ions. Right: schematic drawing of the layer sequence of the V/Ti mixed oxide with the blocking layer between the overlayer and the TiO₂(110) substrate.

elements which form an oxide with rutile structure (for an overview see Fig. 2, left).

In a first try tungsten ions were mixed into the TiO₂ lattice. With this mixed oxide interlayer the diffusion of vanadium could be blocked but the tungsten ions were too mobile at elevated temperature which led to their appearance at the surface after some minutes of annealing at 850 K which is a temperature required for ordering of the surface. In the next try tantalum was used instead of tungsten which turned out to be a feasible approach. The Ta/Ti mixed oxide layer also blocks vanadium diffusion effectively but the tantalum ions diffuse slower than the tungsten ions so that the surface can be kept free of tantalum for more than two hours of annealing at 850 K. Typical film thicknesses are 30 to 40 Å for the Ta/Ti mixed oxide interlayer and 75 Å for the V/Ti mixed overlayer. The diffusion blocking layer and the V/Ti mixed oxide layer are grown by co-deposition of the respective metals at 850 K in an oxygen

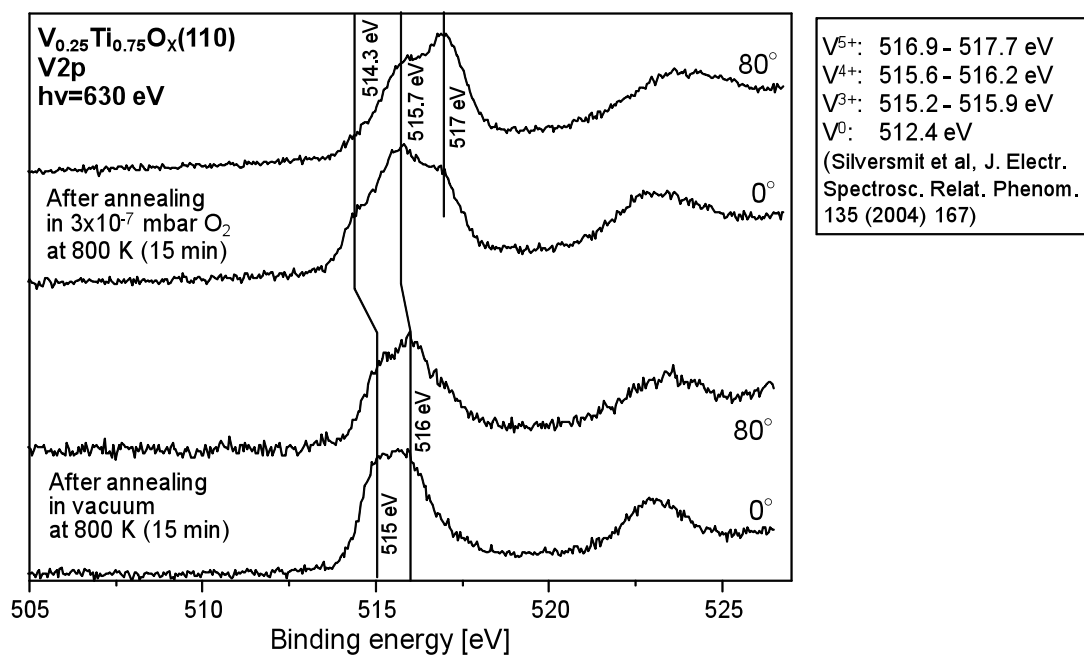


Fig. 3. XPS spectra recorded at 0° and 80° exit angle for a V/Ti mixed oxide layer after reduction by annealing in vacuum and oxidation by annealing in an oxygen ambient.

atmosphere of 10^{-6} mbar. After completion of the deposition the layer is subjected to annealing at 850 K for 5 min in vacuum. The tantalum concentration in the blocking layer is usually about 30 % and the vanadium concentration is varied according to the experimental requirements. A lower limit for the vanadium concentration is imposed by the detection limit of the experimental methods which is a couple of percent for most methods.

The vanadium oxidation state was investigated with XPS (see Fig. 3). Spectra recorded at grazing electron emission (80° relative to the surface normal) and at normal emission (0° , along the surface normal) are compared for two different preparations. The spectra obtained at 80° are more surface sensitive than those recorded at normal emission. If the system is annealed in vacuum then the $V2p_{3/2}$ level consists of two different states which may be assigned to V^{4+} at 516 eV and V^{3+} at 515 eV. Comparison of the spectra recorded at 80° and 0° suggests that the relative concentration of V^{4+} is somewhat higher at the surface than in the bulk. Annealing in 3×10^{-7} mbar of oxygen leads to a different spectrum: a V^{5+} state appears at 517 eV, the V^{4+} state shifts to 515.7 eV, and the V^{3+} state shifts to 514.3 eV or is replaced by a state of vanadium in a different local environment or with a even lower oxidation state (which is not very likely since the sample was annealed in oxygen). From the angular dependence of the spectra it is clear that V^{5+} is located in the surface region whereas the vanadium atoms giving rise to the state at 514.3 eV are located in the bulk. V^{4+} is probably present at the surface as well as in the bulk. Prolonged annealing leads to the accumulation of more and more V^{5+} at the surface where it may form clusters or a layer. It can be removed by annealing at 950 K. An

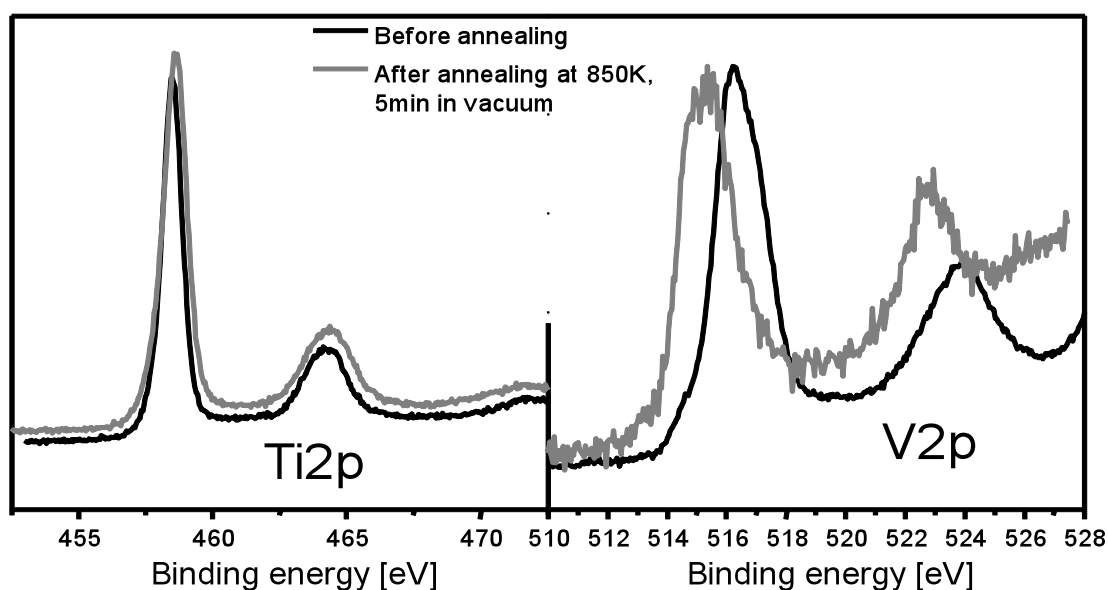


Fig. 4. $V2p$ and $Ti2p$ XPS spectra of a V/Ti mixed oxide layer (33% V) recorded before and after reduction by annealing at 850 K in vacuum.

interesting point is the behavior of the vanadium and titanium oxidation states upon sample reduction. Fig. 3 shows that reduction of the sample by annealing in vacuum induces the formation of a state at 515 eV which may be assigned to V^{3+} . If pure $TiO_2(110)$ is reduced then this leads to the formation of Ti^{3+} ions as is well known. Fig. 4 compares the effect of annealing of a V/Ti mixed oxide layer in vacuum (reduction) onto the V2p and Ti2p levels, demonstrating that reduction affects the V2p level much more than the Ti2p state which means that in the mixed oxide the vanadium ions are preferably reduced instead of the titanium ions as in the case of pure $TiO_2(110)$.

The mixed oxide forms different ordered surface structures (see Fig. 5): up to now two well ordered structures were observed with LEED, namely a (2x1) and a (4x1) structure and some not well ordered structures which are not yet assigned. The existence of LEED patterns different from that of $TiO_2(110)$ may be seen as an indication that the components of the mixed oxide do not segregate at the surface. Studies of the surface structure using STM are planned and photoelectron diffraction studies were performed together with the group of D. P.

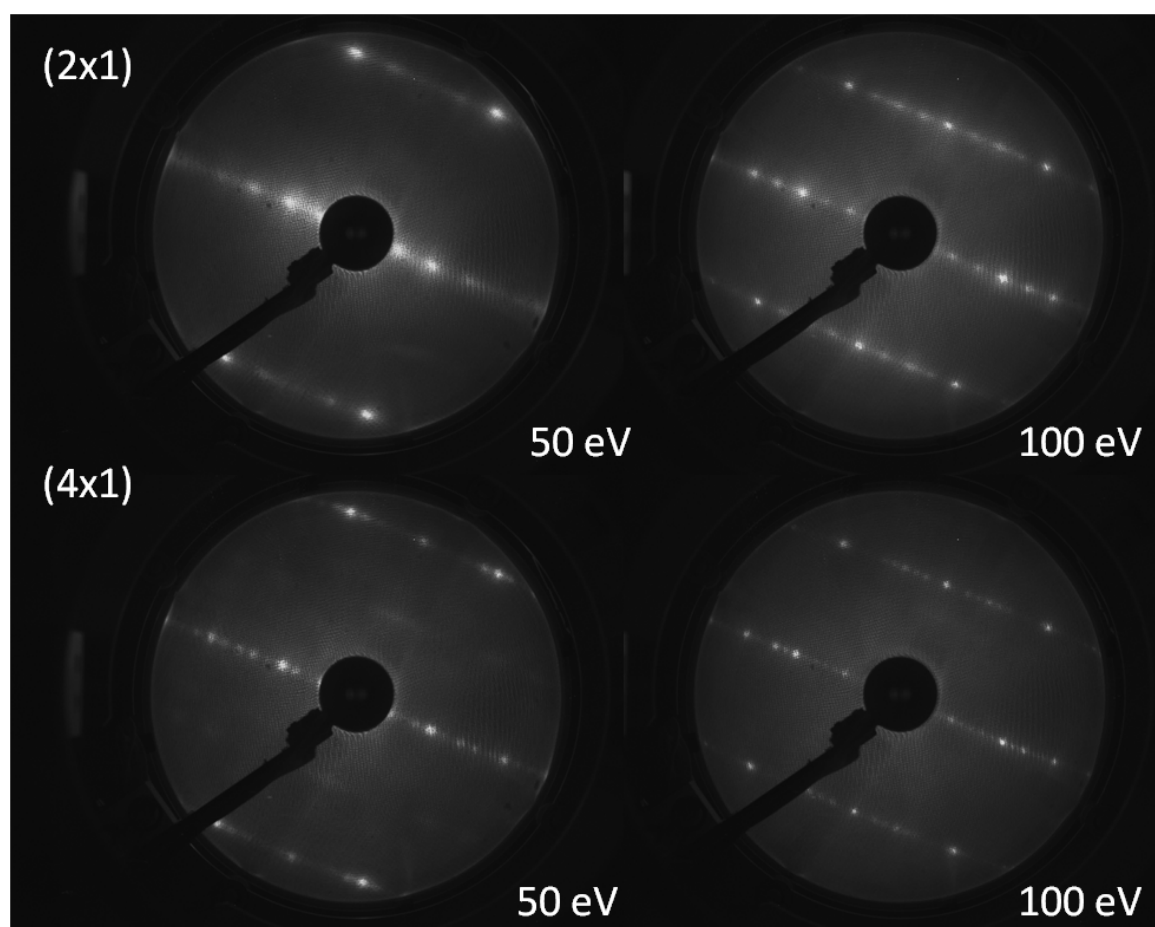


Fig. 5. Photographs of the (2x1) and (4x1) LEED patterns of the mixed oxide at two different electron energies (50 and 100 eV).

Woodruff (project C8). The data are presently evaluated.

In project B6 (Schomäcker) the oxidative dehydrogenation (ODH) of ethanol towards acetaldehyde was studied for vanadium oxide deposited on different substrates. For vanadia on TiO_2 a significantly higher rate of ODH was found than for the other studied substrates (CeO_2 , ZrO_2 , Al_2O_3) which motivated us to study this reaction on the V/Ti mixed oxide with thermal desorption spectroscopy. For the conditions employed until present mostly ethylene with some percent of acetaldehyde is produced by the V/Ti mixed oxide surface. Whether and how the selectivity can be changed towards the production of more acetaldehyde is presently investigated.

Mo/Ti mixed oxide overlayers on $\text{TiO}_2(110)$

Mo/Ti mixed oxide layers were grown by co-deposition of molybdenum and titanium at 850 K in an oxygen atmosphere of 5×10^{-7} mbar followed by an annealing cycle after switching off the evaporators. The desired relative Mo and Ti concentrations were adjusted by choosing the deposition fluxes appropriately. Implementation of a blocking layer was not required since the molybdenum ions diffuse much slower than the vanadium ions.

The oxidation state of the molybdenum ions in the mixed oxide was studied with XPS (see Fig. 6). This figure compares Mo3d spectra recorded at an electron exit angle of 80° with spectra recorded along the surface normal (0°). The former ones are more sensitive than the latter ones. The 4+ and 6+ oxidation states were assigned using binding energy values found in the literature and the remaining state was tentatively assigned to Mo^{5+} since the Mo3d binding

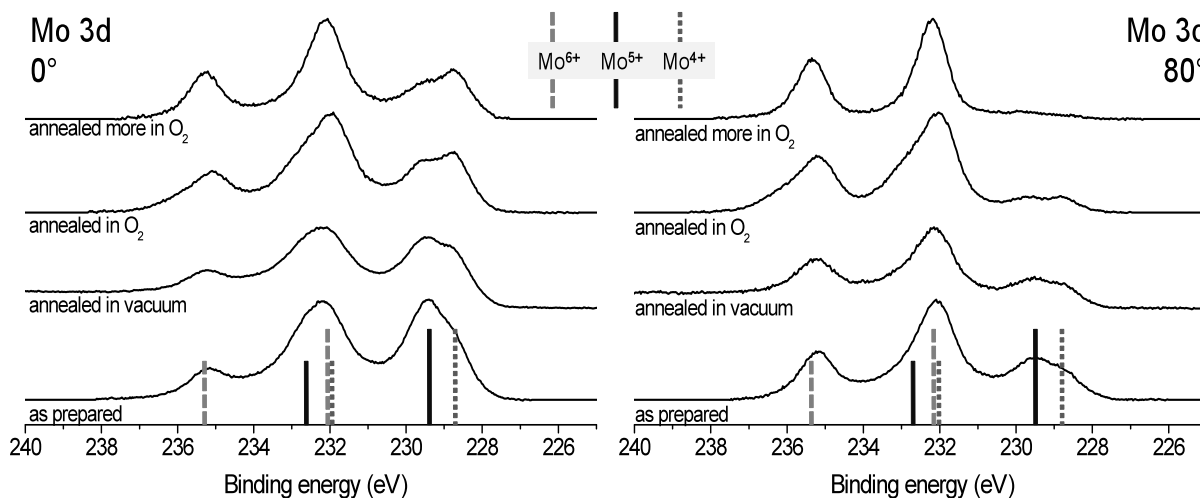


Fig. 6. XPS spectra of a Mo/Ti mixed oxide layer (~50 % Mo) recorded at normal emission and at an electron exit angle of 80° . The data were recorded after subjecting the layer to different treatments.

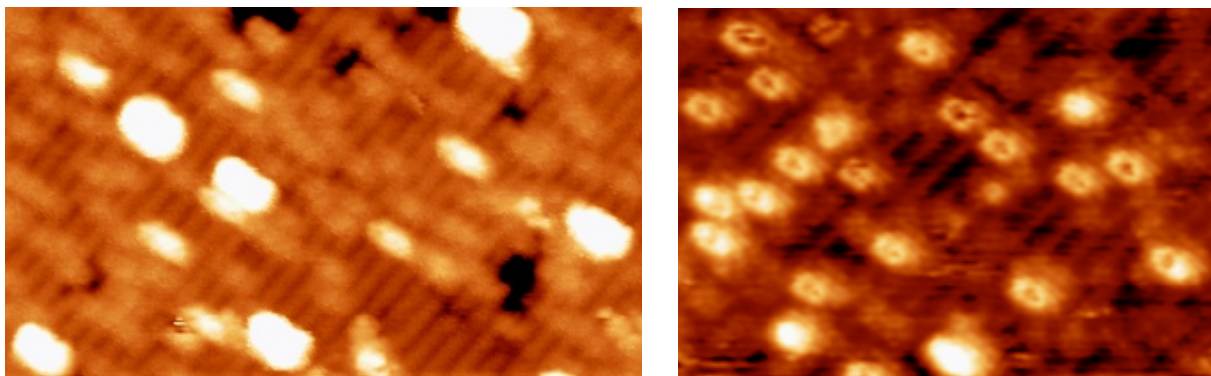


Fig. 7. STM images of the Mo/Ti oxide system. Images of two different surfaces are shown, both with 5% Mo concentration. The different appearances of the clusters are ascribed to different tip terminations. Particle heights are c.a. 3 Å for small particles, getting higher for larger particles.

energies are between those of the 6+ state and the 4+ state. The data reveal that Mo⁴⁺ and Mo⁵⁺ are mainly located within the layer whereas Mo⁶⁺ is more abundant at the surface. Annealing in vacuum reduces the Mo⁶⁺ concentration at the surface and annealing in oxygen leads to Mo⁶⁺ agglomeration at the surface, proving that the Mo ions are also mobile, though less than the vanadium ions. Prolonged annealing in oxygen leads to Mo depletion in the bulk and concomitantly to the pile-up of huge amounts of Mo⁶⁺ at the surface (not shown here). The Mo⁶⁺ aggregates evaporate upon annealing at 850 K and higher according to XPS. Nevertheless, all XPS data show that the molybdenum surface concentration is always higher than the bulk concentration.

The surface structure of the Mo/Ti mixed oxide was studied with LEED, IV-LEED, and STM. STM images (Fig. 7) exhibit small clusters on the surface while the LEED pattern appeared to be not much different from that of TiO₂(110). This led us to speculate that only the bulk of the mixed oxide layer is a mixed oxide while the molybdenum ions at the surface are not embedded within the TiO₂ matrix but form clusters on the surface with the molybdenum ions in a 6+ oxidation state as indicated by XPS. In order to verify this, IV-LEED curves of TiO₂(110) were compared with curves obtained from a Mo/Ti mixed oxide surface (see Fig. 8). The curves of TiO₂(110) and the mixed oxide are very similar which is a strong indication that the LEED pattern is due to TiO₂(110) in both cases. Considering this it is near at hand to assign the cluster seen by STM to molybdenum oxide aggregates with molybdenum in a 6+ oxidation state.

In order to learn about the reactivity of the clusters with respect to partial alcohol oxidation, the surface was exposed to methanol. Exposure at 110 K leads to the formation of methoxy and concomitantly to a reduction of Mo⁶⁺ to Mo⁴⁺. Warming up induces the re-oxidation of the

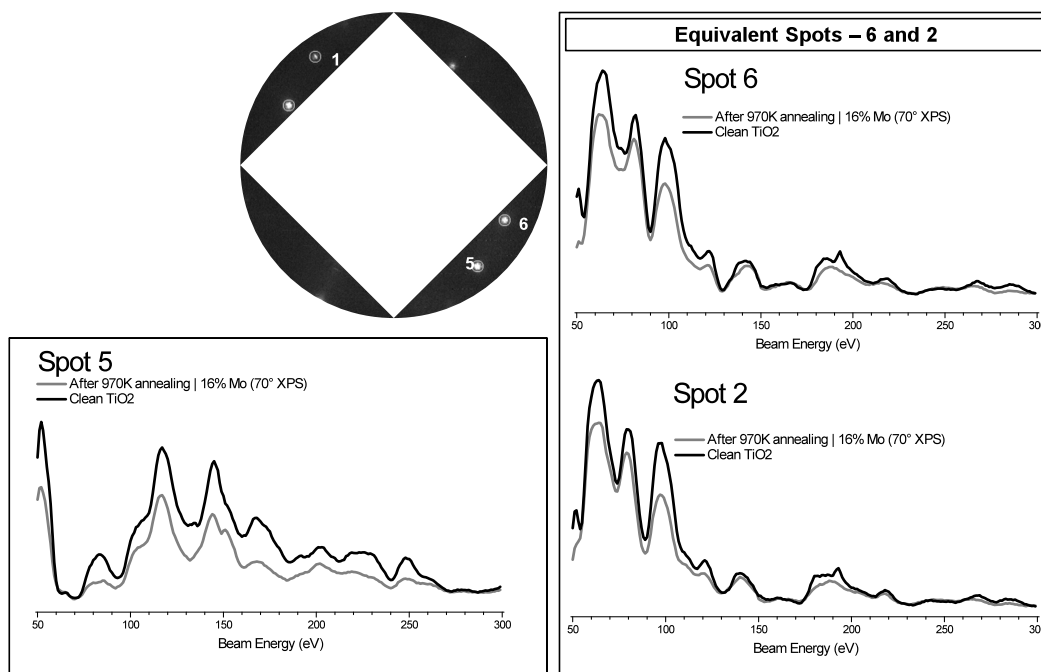


Fig. 8. LEED pattern and IV-LEED curves of some spots recorded for clean $\text{TiO}_2(110)$ and for a Mo/Ti mixed oxide surface.

molybdenum at the surface together with the disappearance of the methoxy groups. Currently thermal desorption measurements and vibrational spectroscopy are performed with the aim of understanding the processes following exposure to methanol.

Adsorption of methanol on $\text{V}_2\text{O}_5(001)$

This work represents a completion of studies which were started in the preceding period and dealt with the role of hydrogen for the partial oxidation of methanol on $\text{V}_2\text{O}_5(001)$. Well-ordered $\text{V}_2\text{O}_5(001)$ layers can be prepared on Au(111) by oxidation of vanadium at 50 mbar oxygen pressure. Similar to the case of $\text{V}_2\text{O}_3(0001)$ [RGG11] defect-free layers do not catalyze the partial oxidation of methanol, but the introduction of surface defects activates the surfaces. Defects are produced by irradiation with low-energy electrons (50 eV) which remove vanadyl oxygen atoms from the surface as studied with STM [SGK09]. These vanadyl oxygen vacancy sites break the methanol molecules up into methoxy which binds to the defect site and hydrogen which forms a surface hydroxyl group [SGK09].

At about 500 K desorption of formaldehyde is detected with thermal desorption spectroscopy (Fig. 9 left). The desorption state is not a single peak which is probably related to the different reactivities of single and multiple defect sites which was investigated with STM [SGK09]. An interesting issue was that methanol adsorption at room temperature appeared to lead to a higher formaldehyde yield than adsorption at 100 K. Initiated by this observation, the formaldehyde

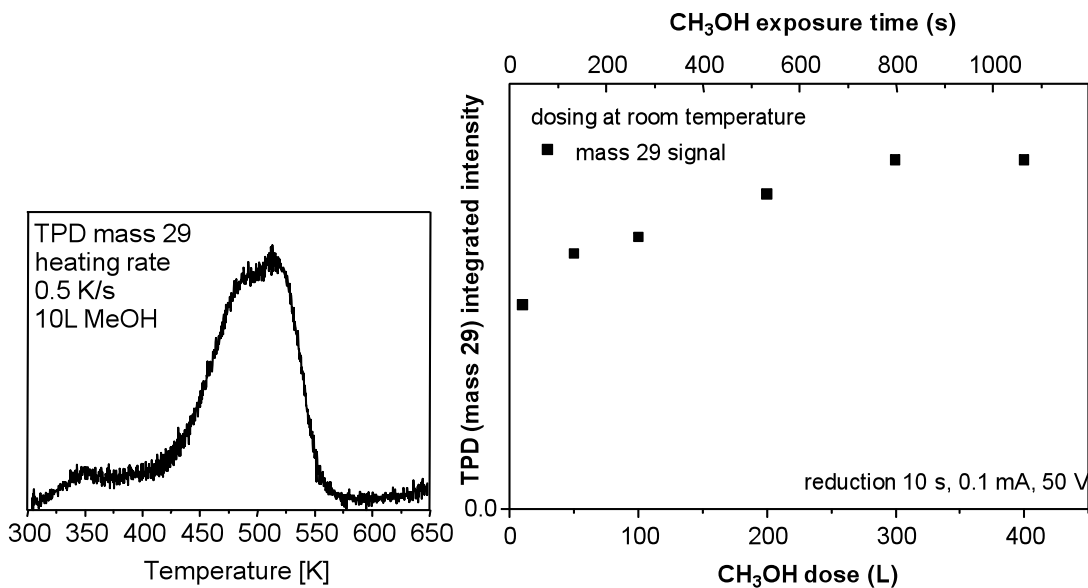


Fig. 9. Left: TPD spectrum (mass 29, formaldehyde) obtained after dosing methanol onto $V_2O_5(001)$ at room temperature. Right: intensity of the formaldehyde desorption peak as a function of the methanol dosing time.

yield was measured as a function of the dosing time for a constant methanol flux of 0.38 L/s (Fig. 9, right). The result cannot be explained by the simple standard model where the sticking probability is proportional to the number of available adsorption sites since the shape of the corresponding curve does not fit very well to the experimental data.

Part of the mechanism leading to the curve can be deduced from C1s XPS data as a function of temperature (Fig. 10, left). The state at 286.5 eV is due to carbon in the V_2O_5 layer, the high-binding energy state at about 288 eV is related to methanol, and the center peak is due to methoxy. If the methoxy covered layer is warmed up to 350 K, then the methoxy peak intensity is reduced to about one third of its intensity at 230 K. At 525 K all methoxy is gone due to the formation of formaldehyde. However, formaldehyde does not form at 350 K and therefore the reduction of the methoxy XPS signal at this temperature must have a different reason. TDS data (Fig. 10, right) show that methanol desorbs at ~ 270 K which means that the methoxy-C1s intensity loss upon warming to 350 K is due to the reaction of methoxy with surface hydrogen to methanol which desorbs at ~ 270 K.

The remaining question in this context is, why did not all of the methoxy groups react with hydrogen? Enough hydrogen should be available since the formation of one methoxy group is accompanied by the formation of a hydroxyl group. However, methanol formation with methoxy is not the only possible reaction of the hydrogen atoms on the surface; they can also react to produce water. If this happens then part of the methoxy groups can not react with hydrogen since there is enough hydrogen available for all methoxy groups. The kinetics of this

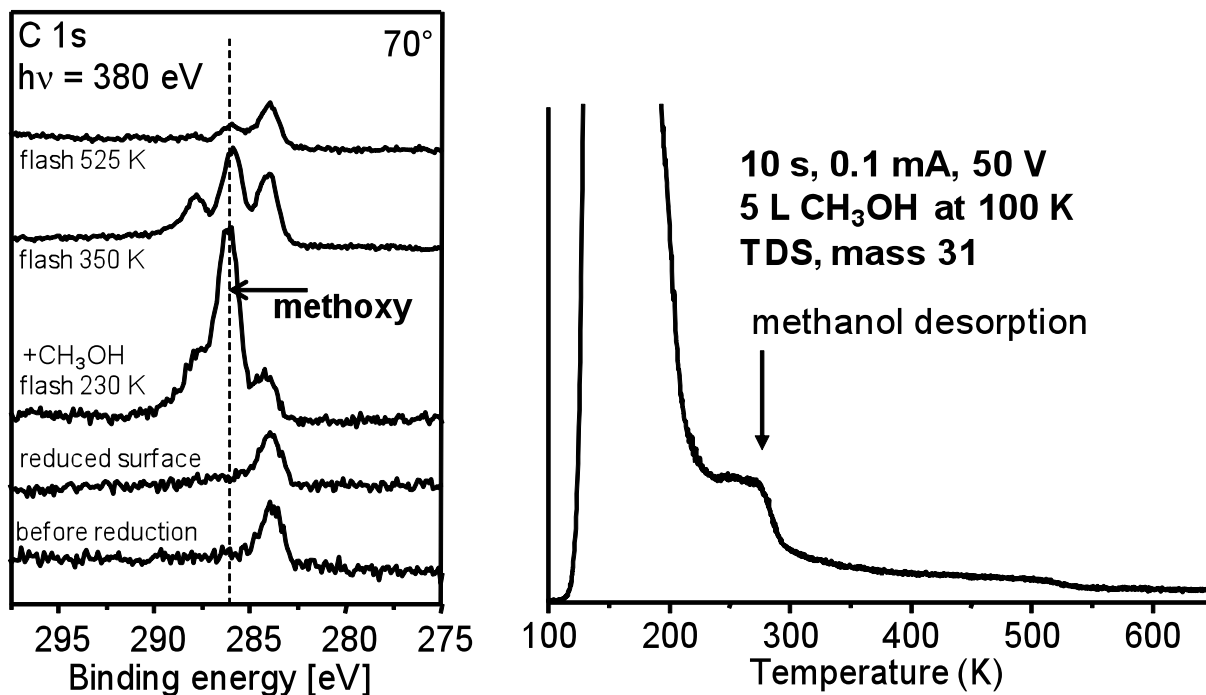


Fig. 10. Left: XPS spectra of methanol on $V_2O_5(001)$ warmed up to different temperatures. Right: TDS spectrum of methanol on $V_2O_5(001)$ (mass 31, methanol).

process was modeled with a set of two coupled differential equations for the concentration of the surface methoxy and hydroxyl groups (Fig. 11).

These equations were used to fit the experimental data in Fig. 9 (right) with E_1 and E_2 as fit parameters. The attempt frequencies were set to standard values (10^{13} s^{-1}). With

$$N_{\text{tot}} \frac{d\theta_M}{dt} = S(\theta) \cdot \Phi_M - N_{\text{tot}} \theta_M \theta_{\text{OH}} \nu_M \exp\left(-\frac{E_1}{kT}\right)$$

$$N_{\text{tot}} \frac{d\theta_{\text{OH}}}{dt} = \underbrace{S(\theta) \cdot \Phi_M}_{\text{adsorption}} - \underbrace{N_{\text{tot}} \theta_M \theta_{\text{OH}} \nu_M \exp\left(-\frac{E_1}{kT}\right)}_{\text{methanol formation}} - \underbrace{2N_{\text{tot}} \theta_{\text{OH}}^2 \nu_{\text{OH}} \exp\left(-\frac{E_2}{kT}\right)}_{\text{water formation}}$$

θ	– coverage
$S(\theta)$	– coverage dependent sticking coefficient (proportional to the density of unoccupied defect sites)
N_{tot}	– number of vanadyl lattice sites ($4.8 \times 10^{18} \text{ m}^{-2}$)
Φ_M	– flux of MeOH molecules per unit area and time (0.38 L/s)
ν_{OH}, ν_M	– attempt frequencies
E_1, E_2	– energy barriers for recombination

Fig. 11. Set of two differential equations for the description of the formaldehyde yield as a function of the dosing time of methanol onto $V_2O_5(001)$.

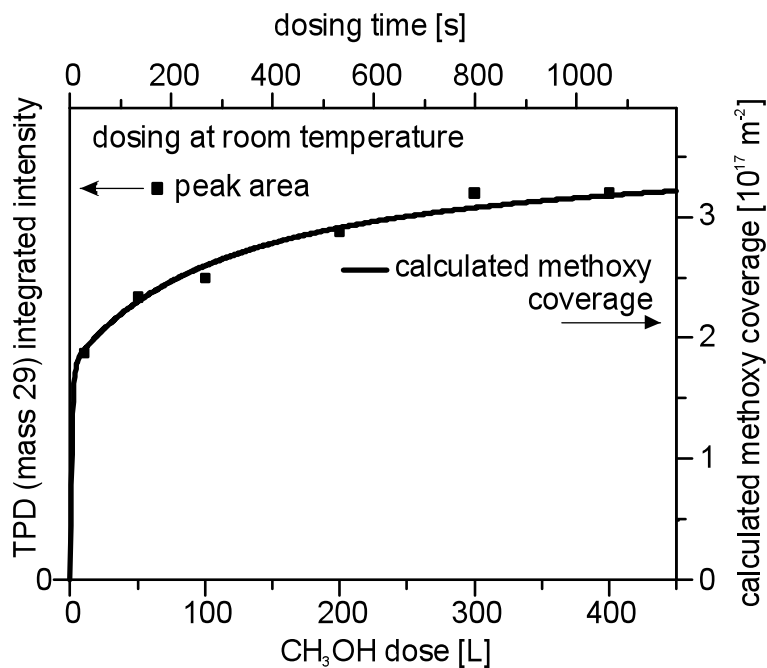


Fig. 12. Methoxy coverage as determined via TDS in comparison with the best fit data.

$E_1=E_2=0.85$ eV an essentially perfect fit to the experimental data could be obtained (see Fig. 12). The result may be explained as follows: the initial steep increase is due to the occupation of the available adsorption sites. At the dosing temperature (300 K) the formation of methanol and water from hydroxyl and methoxy can proceed and therefore water and methanol form and desorb while methanol is dosed. This produces free sites which can again split methanol from the gas stream into methoxy and hydrogen. However, this process leads to a reduction of the hydroxy coverage with increasing dosing time since only methanol is dosed while water and methanol desorb. Due to this effect more and more methoxy groups are blocked on the surface and cannot react to form methanol which is the origin of the slow increase of the formaldehyde desorption signal with increasing dosing time. We note that similar values for E_1 and E_2 (0.75 eV) were obtained from the fit of thermal desorption data using a kinetic model [SGK09].

The slight deviation of the energies from the ones obtained with the above model may be related to weaknesses of the model since the different reactivities of single and multiple defects were not considered in the models. Corresponding calculations were performed in project C5 which gave energies for molecular and dissociative methanol adsorption of 0.64 and 0.67 eV, respectively, and for water energies of 0.64 and 0.43 eV were calculated [SGK09]. The binding energies of 0.67 and 0.64 eV for the most strongly bound methanol and water states are roughly in agreement with the experimental values.

Co-operations within the SFB

- C5 Calculations for methanol adsorption on $V_2O_3(0001)/Au(111)$ and $V_2O_5(001)/Au(111)$ were performed.
- C8 Photoelectron diffraction data of a V/Ti mixed oxide layer were measured at the BESSY II synchrotron. The data are presently being evaluated.
- C11 Ion scattering data of $V_2O_3(0001)/Au(111)$ were recorded in order to determine the surface termination. The experiments are presently running.

References

- [1] Q. Wang, R. J. Madix, *Partial oxidation of methanol to formaldehyde on a model supported monolayer vanadia catalyst: vanadia on $TiO_2(110)$* , Surf. Sci. 496 (2002) 51

5.2.2 Projektrelevante eigene Publikationen

a) erschienene oder angenommene Arbeiten in wissenschaftlichen Zeitschriften oder Buchveröffentlichungen

- [BFK08] P. S. Bagus, H.-J. Freund, H. Kuhlenbeck, and E. S. Ilton
A new analysis of X-ray absorption branching ratios: Use of russell-saunders coupling
Chem. Phys. Lett. **455** (2008) 331 - 334.
- [RGK08] Y. Romanyshyn, S. Guimond, H. Kuhlenbeck, S. Kaya, R. P. Blum, H. Niehus, S. Shaikhutdinov, V. Simic-Milosevic, N. Nilus, H.-J. Freund, M. V. Ganduglia-Pirovano, R. Fortrie, J. Döbler, and J. Sauer
Selectivity in methanol oxidation as studied on model systems involving vanadium oxides
Top. Catal. **50** (2008) 106 – 115.
- [GSG08] S. Guimond, J. M. Sturm, D. Göbke, Y. Romanyshyn, M. Naschitzki, H. Kuhlenbeck, and H.-J. Freund
Well-ordered $V_2O_5(001)$ thin films on $Au(111)$: growth and thermal stability
J. Phys. Chem. C **112** (2008) 11835 - 11846.
- [GGR08] S. Guimond, D. Göbke, Y. Romanyshyn, J. M. Sturm, M. Naschitzki, H. Kuhlenbeck, and H.-J. Freund
Growth and characterization of ultrathin V_2O_y ($y \approx 5$) films on $Au(111)$
J. Phys. Chem. C **112** (2008) 12363 - 12373.

- [SGK09] J. M. Sturm, D. Göbke, H. Kuhlenbeck, J. Döbler, U. Reinhardt, M. V. Ganduglia-Pirovano, J. Sauer, and H.-J. Freund
Partial oxidation of methanol on well-ordered $V_2O_5(001)/Au(111)$ thin films
Phys. Chem. Chem. Phys. **11** (2009) 3290 - 3299.
- [GRG09a] D. Göbke, Y. Romanyshyn, S. Guimond, J. M. Sturm, H. Kuhlenbeck, J. Döbler, U. Reinhardt, M. V. Ganduglia-Pirovano, J. Sauer, and H.-J. Freund
Formaldehyde formation on vanadium oxide surfaces $V_2O_3(0001)$ and $V_2O_5(001)$: how does the stable methoxy intermediate form?
Angew. Chem. Int. Ed. **48** (2009) 3695 - 3698.
- [GRG09b] D. Göbke, Y. Romanyshyn, S. Guimond, J. M. Sturm, H. Kuhlenbeck, J. Döbler, U. Reinhardt, M. V. Ganduglia-Pirovano, J. Sauer, and H.-J. Freund
Formaldehydbildung auf den Vanadiumoxidoberflächen $V_2O_3(0001)$ und $V_2O_5(001)$: wie bildet sich der stabile Methoxy-Zwischenzustand?
Angew. Chem. **121** (2009) 3750 - 3753.
- [BNI10] P. S. Bagus, C. J. Nelin, E. S. Ilton, M. Baron, H. Abbott, E. Primorac, H. Kuhlenbeck, S. Shaikhutdinov, and H.-J. Freund
The complex core level spectra of CeO_2 : An analysis in terms of atomic and charge transfer effects
Chem. Phys. Lett. **487** (2010) 237 - 240.
- [NBI10] C. J. Nelin, P. S. Bagus, E. S. Ilton, S. A. Chambers, H. Kuhlenbeck, and H.-J. Freund
Relationships between complex core level spectra and materials properties
Int. J. Quant. Chem. **110** (2010) 2752 - 2764.
- [RGG11] Y. Romanyshyn, S. Guimond, D. Göbke, J. M. Sturm, H. Kuhlenbeck, J. Döbler, M. V. Ganduglia-Pirovano, J. Sauer, and H.-J. Freund
Methanol adsorption on $V_2O_3(0001)$
Top. Catal. **54** (2011) 669 - 684.

5.3 Rückblick auf die Förderung

Das Teilprojekt wurde seit 07/1999 im Sonderforschungsbereich gefördert. Es wurde mit Ablauf der 4. Förderperiode im Juni 2011 beendet.

5.3.1 Personal im Teilprojekt während der 4. Förderperiode

	lauf. Nr.	Name, akademischer Grad, Dienststellung	engere Fachzugehörigkeit	Institut der Hochschule oder der außeruniv. Einrichtung	Mitarbeit im Projekt Zeitraum Wochenstunden	Entgeltgruppe
Grundausrüstung						
Wissenschaftlerinnen und Wissenschaftler	1.	Hans-Joachim Freund, Prof. Dr.	Physikal. Chemie	FHI	07/1999 – 06/2011, 2h	
	2.	Helmut Kuhlenbeck, Dr.	Physikal. Chemie	FHI	07/1999 – 06/2011, 15h	
	3.	Osman Karlioglu	Chemie	FHI	02/2009 – 06/2011, 38h	
	4.	Elena Primorac	Chemie	FHI	12/2008 – 06/2011, 38h	
nichtwissenschaftl. Mitarbeiterinnen und Mitarbeiter	5.	Mathias Naschitzki			08/2003 – 06/2011, 15h	
Ergänzungsausstattung						
Wissenschaftlerinnen und Wissenschaftler	1.	Jan-Henrik Fischer	Chemie	FHI	10/2008 – 11/2010, 28h	E13, 75 %
	2.	Martin Sterrer, Dr.	Chemie	FHI	01/2010 – 08/2010, 38h 02/2011 – 06/2011	E13
nichtwissenschaftl. Mitarbeiterinnen und Mitarbeiter						

Aufgaben der Mitarbeiterinnen und Mitarbeiter (Grundausrüstung):

1. Prof. Dr. Hans-Joachim Freund
Übernahme von Aufgaben zur Projektverwaltung und zur wissenschaftlichen Leitung.
2. Dr. Helmut Kuhlenbeck
Übernahme von Aufgaben zur Projektverwaltung und zur wissenschaftlichen Leitung.
Unterstützung, Beratung und Anleitung des Technikers (Mathias Naschitzki) und der Doktoranden (Osman Karlioglu, Elena Primorac und Jan-Henrik Fischer) bei den Experimenten.
3. Mathias Naschitzki
Mithilfe bei der Durchführung der Experimente, Konstruktions- und Reparaturarbeiten.
4. Osman Karlioglu
Durchführung von Experimenten (STM, TDS, LEED, XPS) an Mo/Ti-Mischoxiden.
Präparation und Charaktisierung der Mischoxide sowie Optimierung der Präparationsvorschrift.
5. Elena Primorac
Durchführung von Experimenten (ARUPS, TDS, LEED, XPS) an V/Ti-Mischoxiden.
Präparation und Charaktisierung der Mischoxide sowie Optimierung der Präparationsvorschrift.

Aufgaben der Mitarbeiterinnen und Mitarbeiter (Ergänzungsausstattung):

1. Jan-Henrik Fischer
Durchführung von Experimenten (STM, ARUPS, TDS, LEED, XPS) an V/Ti- und Mo/Ti-Mischoxiden zusammen mit Elena Primorac und Osman Karlioglu. Präparation und Charaktisierung der Mischoxide sowie Optimierung der Präparationsvorschriften.
2. Dr. Martin Sterrer
Mitwirkung an den Experimenten der Doktoranden (Fischer, Primorac, Karlioglu), Beratung, Auswertung und Experimentplanung.

5.1 Allgemeine Angaben zum Teilprojekt C4

5.1.1 Titel: Der Einfluss der elastischen Eigenschaften auf Reaktivität und Selektivität des katalytischen Prozesses

5.1.2 Projektleitung

Dr. Carsten Hucho

geb. 28.08.1964

Paul-Drude-Institut für Festkörperelektronik
Abt. Technology and Services
Hausvogteiplatz 5-7
10117 Berlin

Telefon: 030 / 20377-234

E-Mail: hucho@pdi-berlin.de

5.2 Entwicklung des Teilprojekts

5.2.1 Bericht

Nachdem in den ersten Förderphasen des SFB innerhalb des Teilprojektes die Expertise zur Kristallzucht von Vanadiumpentoxid eingebracht und für das Wachstum reduzierter Spezies weiterentwickelt wurde und nachdem ferner Methoden zur elastischen Charakterisierung von kleinen Einkristallen und polykristallinen Materialien entwickelt und studiert wurden, lag der Fokus in der letzten und abschließenden Förderphase auf dem Studium der Wechselwirkung dynamischer Verzerrungsfelder in katalytisch aktiven Proben auf das katalytische Verhalten (wie Reaktivität und Selektivität). Dieses sehr ambitionierte Fernziel erschien erreichbar, da hierzu eine Reihe notwendiger Kompetenzen zusammenkamen: Kristalle des Modellkatalysators V_2O_5 konnten im TP C4 in definierter Qualität und Größe nach Bedarf hergestellt werden. Die elastischen Eigenschaften von polykristallinen Proben und Einkristallen konnten hochgenau bestimmt werden. Es standen Techniken zur Erzeugung und Detektion von Verzerrungsfeldern im Bereich von einigen Hz bis zu einigen 100 MHz (Ultraschall) zur Verfügung. Im Berichtszeitraum waren für die Erreichung des Projektziels mehrere Schritte vorgesehen:

- Untersuchungen des temperaturabhängigen elastischen Verhaltens von Vanadiumoxiden. Es sollten die Ursachen elastischer Anomalien in der Umgebung der Phasenübergänge und der Zusammenhang zwischen Änderungen der strukturellen und elektronischen Eigenschaften untersucht werden.
- elastische Untersuchungen während des Kristallwachstums. Es sollte eine In-situ-Ultraschall-Messtechnik erstellt werden, um die elastischen Veränderungen während des Kristallwachstums studieren zu können.
- Korrelation zwischen Defektdichte und katalytischer Aktivität/Selektivität. Hierbei sollte in Zusammenarbeit mit den Teilprojekten B6 (Prof. Schomäcker) und B3 (Prof. Schomäcker, Dr. Kondratenko) erstmals der Einfluss statischer und dynamischer Verzerrungsfelder auf Reaktivität und Selektivität von Vanadaten untersucht werden.

Kenntnisstand und Ausgangsfragestellung:

Elastische Anregungen und Detektion werden für die Charakterisierung von Materialien in drei Bereichen verwendet: Niederfrequente Verzerrungsfelder (mHz bis kHz) für die Untersuchung von Defekten, Verzerrungsfelder mittlerer Frequenz (kHz bis einige MHz) für das Studium elastischer Konstanten und schließlich Ultraschalluntersuchungen (kHz bis GHz) zur Analyse von Phasenübergängen. Typische Energien an katalytischen Prozessen beteiligter chemischer Bindungen liegen im Bereich von 0.2 eV – dies entspricht ca. 20kJ/mol oder 50THz übersetzt in ‚akustische‘ Anregungsenergien. Die elasto-spektroskopischen Untersuchungen liegen energetisch also weit unterhalb der Bindungsenergie der untersuchten Systeme.

Dies hat zwar einerseits den Vorteil, dass Ultraschalluntersuchungen das beobachtete System nur geringfügig stören, bedeutet aber auch, dass das Aufbrechen von Bindungen, das bei schallinduzierter Katalyse ein wünschenswerter Vorgang sein könnte, durch diese Form elastischer Untersuchungen nicht möglich ist.

Dennoch ist bekannt, dass Verzerrungsfelder hoher Energiedichte massiven Einfluss auf die untersuchten Systeme haben können. So werden Oxid-Schichten auf weichen Metallen durch Ultraschall aufgebrochen, auf harten Metallen können sie auf diese Weise gar entfernt werden. Das schallinduzierte Aufbrechen der Oberflächenstruktur führt zu einer Vergrößerung der aktiven Oberfläche. Kollisionen chemischer Komponenten mit Schallgeschwindigkeit (>1000 m/s) können induziert und elektrische Ladungen transportiert werden. Schließlich wurde in Flüssigkeiten Kavitations-induzierte Sonochemie beobachtet.

In Abbildung 1 zeigen wir beispielhaft für schallinduzierte makroskopische Prozesse den Akustomigration genannten Transport kleiner Partikel durch eine akustische Oberflächenwelle.

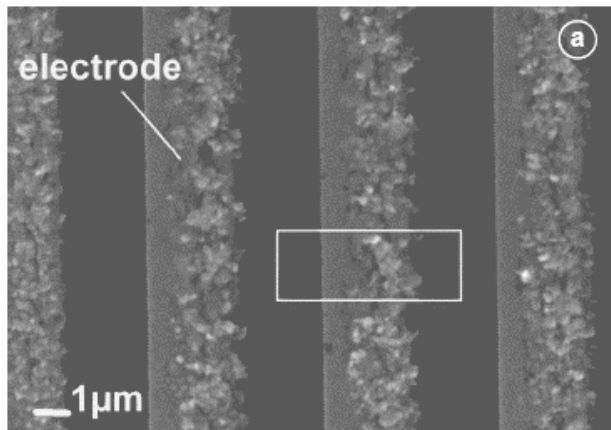


Abb.1.
Aluminiumpartikel werden durch eine akustische Oberflächenwelle transportiert und lagern sich an den Elektroden des Schallwandlers ab (SAW-Transducer, 130MHz, Aluminium).

Untersuchungen des temperaturabhängigen elastischen Verhaltens von Vanadiumoxiden

Bei typischen katalytischen Prozessen wird der Katalysator thermische Zyklen durchlaufen. Zum Studium der Temperaturwechselfestigkeit des Systems wurden Einkristalle von VO_2 mittels Ultraschall untersucht. Der bekannte elektronische und strukturelle Phasenübergang des Materials (ca. 335K) zeichnete sich sowohl in der akustischen Dämpfung als auch in der Schallgeschwindigkeit schon weit jenseits der Umwandlungstemperatur deutlich ab. Die ausgeprägte Hysterese und deren Vergrößerung während thermischen Zykeln gaben klare Hinweise auf elastische Verspannungen und irreversible Prozesse, die schließlich zur Rissbildung und zur Zerstörung des Einkristalls führen.

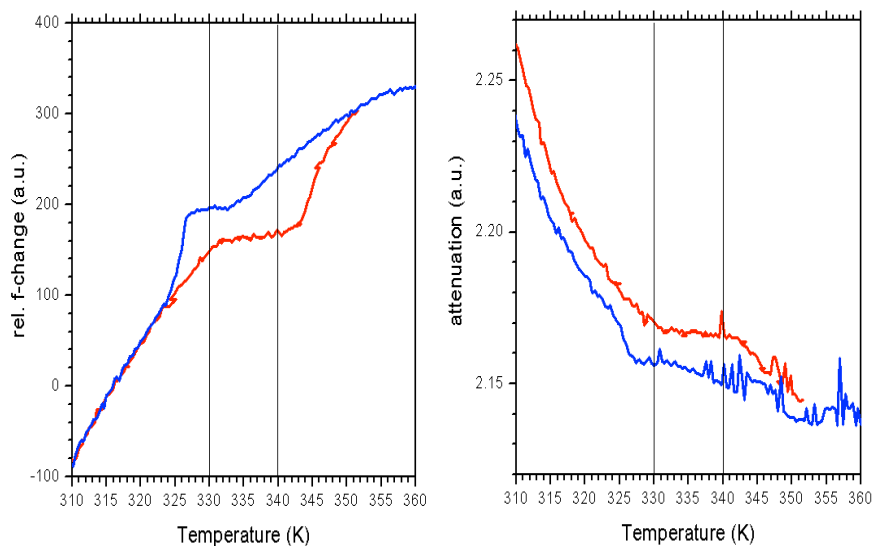


Abb. 2. Untersuchungen der relativen akustischen Resonanzfrequenzänderung (äquivalent zur Änderung der Schallgeschwindigkeit)(links) und akustischen Dämpfung (rechts) zeigen klare Hinweise auf elastische Verspannungen in der Umgebung des Phasenübergangs in VO_2 .

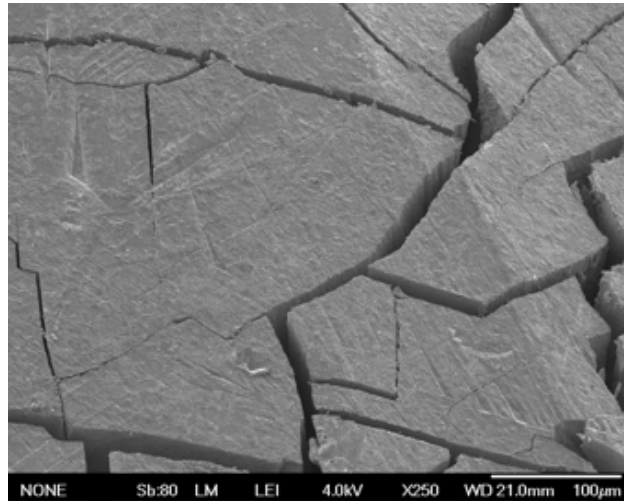


Abb. 3. Elektronenmikroskopische Aufnahme eines VO₂ Kristalls nach thermischem Zyklus durch den Phasenübergang.

Zur Untersuchung des elastischen Verhaltens in Oberflächennähe wurden Schallwandler für die Erzeugung akustischer Oberflächenwellen (surface acoustic waves, SAW) hergestellt. Die Untersuchungen zeigten zum Volumenschall vergleichbare Ergebnisse, brachten an diesem System aber keine zusätzliche Information.

Elastische Untersuchungen während des Kristallwachstums

Es sollte eine In-situ-Ultraschall-Messtechnik erstellt werden, um die elastischen Veränderungen während des Kristallwachstums studieren zu können. Es sollten Aussagen über die Viskosität, die Streumechanismen im Kristall/der Schmelze und über die Ordnungsvorgänge während des Abkühl-Prozesses getroffen werden. Weiterhin sollte die Intensität der Verzerrungsfelder derart gesteigert werden, dass eine gezielte Einbringung von Defekten in die Phasengrenze Schmelze/Kristall ermöglicht wird.

Da einkristalline Proben unterschiedlicher katalytisch aktiver Systeme innerhalb dieses TP hergestellt werden, war es möglich, Proben mit definierten elastischen Eigenschaften herzustellen. Der Einfluss von (insbesondere oberflächennahen) Defekten auf Aktivität und Selektivität der Katalysatoren ist etabliert. Um diesen experimentell genauer zu beschreiben und nach Möglichkeit zu quantifizieren, sollten Proben mit unterschiedlicher, aber definierter Defektdichte hergestellt werden.

Das Einstellen der Defektdichte wurde über unterschiedliche Temperaturprogramme während des Kristallwachstums erreicht – die Charakterisierung sollte über das elastische Verhalten während des Wachstums geschehen. Hierzu wurden Methoden entwickelt, die es erlauben,

gepulste und auch kontinuierliche Schallwellen während des Wachstumsprozesses (bei Temperaturen bis 1500°C) in die Probe einzukoppeln und zu detektieren.

Da die Phasenumwandlungstemperatur des für die Schallanregung verwendeten piezoelektrischen Quarzes bei 850 K liegt, musste die Schallwelle außerhalb des Schmelzofens generiert und in die Schmelzzone geleitet werden. Über einen Sinterkörper wurde das Schallsignal in die Probe eingekoppelt.

Ferner wurde die Messelektronik weiterentwickelt und Software erstellt, die eine Verfolgung der akustischen Antwort des Systems während des Wachstumsprozesses erlaubt (siehe Abbildung 4).

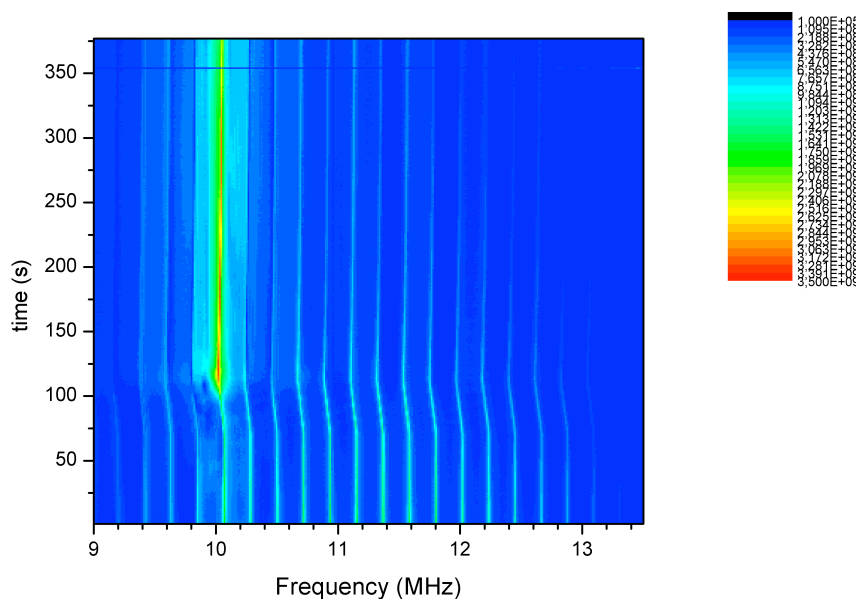


Abb. 4. Der Verlauf der akustischen Resonanzfrequenz während des Kristallwachstums von V_2O_5 in Abhängigkeit von der Zeit. Nach ca. 100 Sekunden verband die Schmelze den Impfkristall und den von oben nachgeführten Sinterkörper. Eine Anhebung der akustischen Antwort ist deutlich erkennbar.

Mit Hilfe der entwickelten Methode konnten unterschiedliche Stadien des Kristallwachstums aufgrund der akustischen Antwort des Gesamtsystems beobachtet werden. Zum einen erlaubte die Lage der Resonanzfrequenzen eine Bestimmung der Schallgeschwindigkeit und insbesondere eine Beobachtung der Änderung während des Schmelzvorganges, zum anderen gaben die Laufzeiten von Ultraschallimpulsen Aussagen über die Lage der Kristallisationsfront der Probe. Dies ist die Basis für eine Automatisierung des Kristallzuchtverfahrens, die nicht – wie sonst üblich – auf reiner optischer Beobachtung der Schmelzzone basiert.

Fundamentale Materialeigenschaften wie thermische Leitfähigkeit oder auch spezifische Wärme lassen sich prinzipiell aus der Zeitabhängigkeit der Resonanzfrequenzen nach einem

thermischen Puls ableiten (siehe Abbildung 5). Wenn die elastischen Eigenschaften im Puls-Echo-Verfahren gemessen werden (was im hier entwickelten Aufbau möglich ist), erlaubt eine Selektion der zurückkommenden Signale nach Laufzeit eine Analyse der Materialeigenschaften an unterschiedlichen Orten (z.B. im Sinterstab, in der Schmelzzone, an der Kristallisationsfront). Eine Verfeinerung dieses Verfahrens war nicht Ziel der Forschung in dieser Förderperiode.

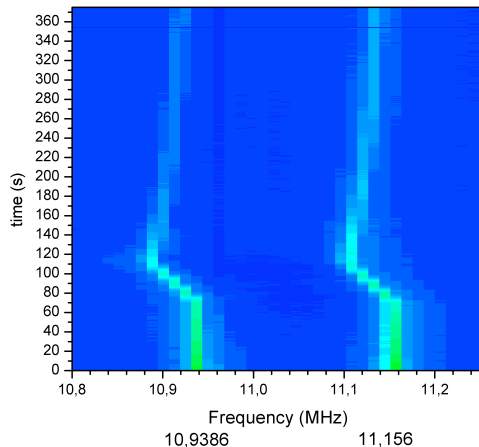


Abb. 5. Nach 60 Sekunden wird der Probe ein Hitzepuls zugeführt. Dies führt zu einer sichtbaren Verschiebung der Resonanzfrequenzen. Nach der Abschaltung des Hitzepulses (100s) klingt die Temperatur exponentiell ab – dies spiegelt sich im exponentiellen Rücklaufen der Resonanzfrequenzen. Aus diesem thermischen Verhalten lassen sich Informationen über die thermische Leitfähigkeit des Systems gewinnen.

Während die elastische Spektroskopie bei nur geringer akustischer Leistung (im Bereich weniger Watt elektrischer Antriebsleistung) durchgeführt wird, wurde für die gezielte Induzierung von Defekten mit großen Schallamplituden experimentiert. Im Puls-Verfahren sind elektrische Anregungen bis zu einigen kW möglich. Es konnte keine Modifikation der unter intensiven Schallfeldern gewachsenen Kristalle beobachtet werden. Für weiter erhöhte Schallamplituden muss auf andere Formen der Schallanregung zurückgegriffen werden. Dies konnte im Berichtszeitraum nicht mehr realisiert werden.

Korrelation zwischen Defektdichte und katalytischer Aktivität/Selektivität

Hierbei sollte in Zusammenarbeit mit den Teilprojekten B6 (Prof. Schomäcker) und B3 (Prof. Schomäcker, Dr. Kondratenko) erstmals der Einfluss statischer und dynamischer Verzerrungsfelder auf Reaktivität und Selektivität von Vanadaten untersucht werden. Es wurde mit hochgradig nichtlinearen Effekten wie plastischer Verformung und Akustomigration

gerechnet, welche einen deutlichen Einfluss auf die Reaktivität und/oder die Selektivität der katalytischen Prozesse erwarten ließen. Es sollte auch versucht werden, eine dynamische, reversible Änderung der Bindungsstärken oder Ladungsdichteverteilung zu erreichen. Hierfür sollte ein in-situ-Aufbau realisiert werden, welcher die Ultraschall- und Kristallzucht-kompetenz von TP C4 und die Analysekompetenz für katalytische Reaktionen von TP B3/B6 kombiniert.

Grundlage für eine sinnvolle Korrelation von Defektdichte mit katalytischer Aktivität oder Selektivität ist ein Verständnis der Wechselwirkung von Verzerrungsfeldern mit relevanten Defekttypen. In der elastischen Spektroskopie werden Defekte aufgrund ihrer Aktivierungsenergie klassifiziert, die sich in einem einfachen Debye-Modell beschreiben lässt. In diesen Experimenten zur ‚internen Reibung‘ (internal friction, IF) ist die akustische Dämpfung (die inverse Güte, Q^{-1}) eine Funktion der eingestrahlten Messfrequenz und der charakteristischen Zeitkonstante τ der Defektanregungen. Die Zeitkonstante ist eine Funktion der Temperatur und mit der Aktivierungsenergie E verknüpft.

$$Q^{-1} = \Delta \frac{\omega\tau}{(1+\omega^2\tau^2)} \quad \text{‚Debye-peak‘, mit } \tau = \tau_0 \exp(E/kT)$$

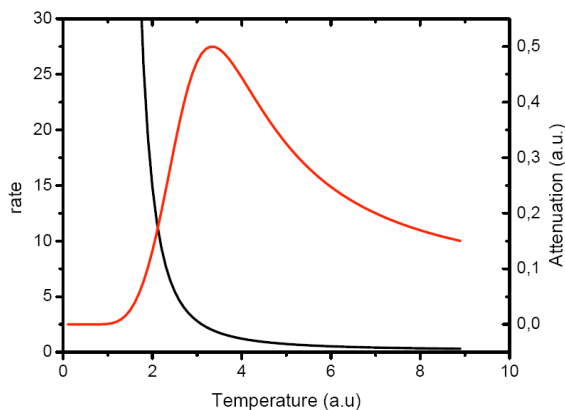


Abb. 6. Bei konstanter Anregungsfrequenz ergibt sich temperaturabhängig ein Maximum in der akustischen Dämpfung. Die frequenzabhängige Lage dieses Maximums erlaubt die Extraktion der Aktivierungsenergie der angeregten Defekte.

Klassische IF-Experimente zur Defektanregung werden mit Torsionspendeln bei Frequenzen von einigen mHz durchgeführt. Der apparative Aufwand ist erheblich, für jede Frequenz muss ein neuer Aufbau realisiert werden, die erforderliche Probengröße liegt im Bereich von mehreren cm.

Der ideale Aufbau zeigt von sehr tiefen Temperaturen bis kurz unter den Schmelzpunkt der zu

untersuchenden Materialien ein stabiles Messverhalten. Weiterhin sollte der Bereich der anregbaren Frequenzen vom Megahertz- bis in den Millihertzbereich verlaufen, um die exponentiellen Effekte der Messungen erfassen zu können. Darüber hinaus müssen auch sehr kleine Proben analysierbar sein. Um all diesen Punkten Rechnung zu tragen, wurden Messköpfe entwickelt, die in einem heizbaren Kryostaten Platz finden, kleine Proben aufnehmen und einen breiten Frequenzbereich abdecken.

Das hier entwickelte Verfahren erlaubt die dynamische elastische Verspannung von kleinen Proben (einige mm) im Bereich von ca. 0.1 Hz bis ca. 15kHz ohne Änderung der Versuchsanordnung. Die elastische Anregung erfolgt mit einem Quarz-Transducer bei Amplituden im Bereich unter 1 Mikrometer und die elastische Antwort sowie Phasenverschiebung wird quasistatisch durch Quarz-Aufnehmer nachgewiesen. Dadurch wird eine geringstmögliche Deformation der Probe gewährleistet – und somit der Arbeitsbereich im wesentlichen auf linear response beschränkt.

Es wurden zunächst gesinterte Proben von V_2O_5 untersucht. Bei unterschiedlichen, konstanten Temperaturen wurden Frequenzläufe durchgeführt und die Phasenverschiebung zwischen Anregung und Antwort detektiert. In Abb. 7 ist deutlich die Temperaturabhängigkeit des Dämpfungspeaks zu erkennen, aus der anschließend die Aktivierungsenergie abgeleitet werden kann.

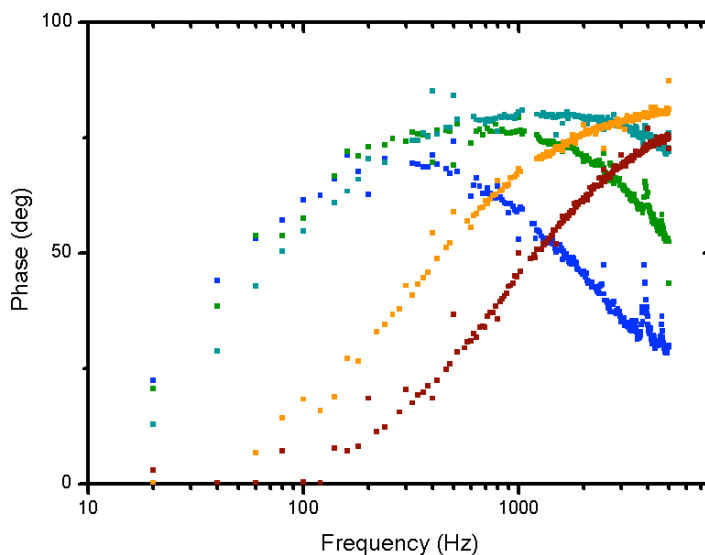


Abb. 7. Die Temperaturabhängigkeit der frequenzabhängigen Phasenverschiebung des elastischen Signals zwischen 200K und 350K in V_2O_5 . Deutlich ist bei zunehmender Temperatur die Verschiebung des Dämpfungsmaximums zu hohen Frequenzen zu erkennen.

Im nächsten Schritt wurde das Messverfahren verbessert, um die Aufnahmezeit für die

Frequenzspektren zu verringern, die Auflösung zu erhöhen und den Parameterraum quasi-kontinuierlich auszumessen. Abb.8 zeigt die Amplitudenantwort in einem Scan derselben Probe.

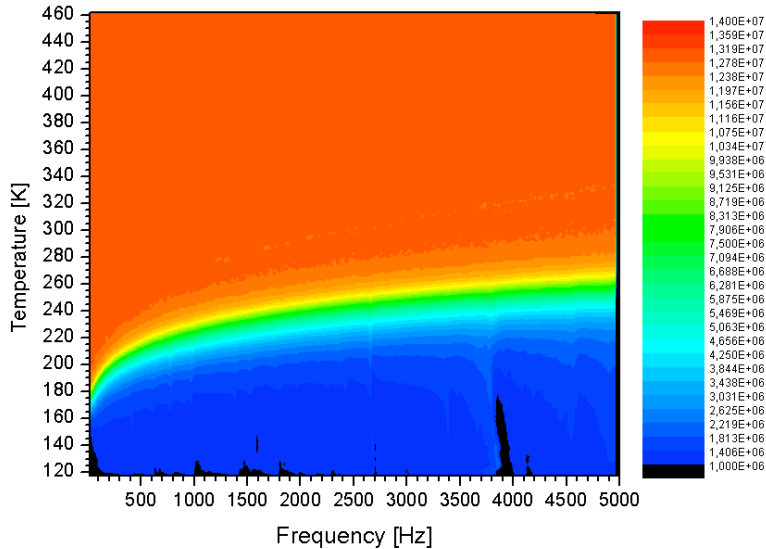


Abb. 8. Temperatur- und Frequenzabhängigkeit der Amplitude des IF-Signals.

Die Analyse erfolgt durch Darstellung der Lage der Dämpfungsmaxima (bzw. der Lage der maximalen Amplitudenänderung) in Form eines Arrhenius-Plots und liefert – bei Dominanz nur einer charakteristischen Anregungsfrequenz – eine Gerade, aus der sich eine Aktivierungsenergie extrahieren lässt. Im Fall der Sinterprobe V_2O_5 konnte eine typische Energie von 0.24 eV für einen dominanten Defekttypen beobachtet werden.

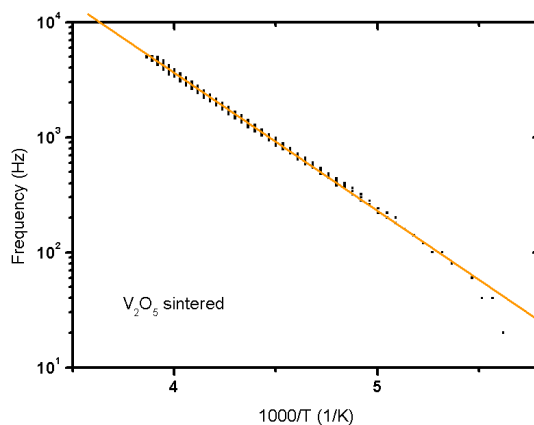


Abb. 9. Arrhenius-Plot der Maxima aus Abb.8.

Diese typische Aktivierungsenergie zeigte sich unabhängig von der Morphologie der Proben – sie war insbesondere vergleichbar für Sinterproben, polykristalline und einkristalline Proben. Die große Reproduzierbarkeit deutet auf einen intrinsischen Prozess hin und erlaubte nun das

Studium der Wechselwirkung zwischen elastischen Feldern und katalytischen Prozessen.

Hier wurden zwei Ansätze verfolgt:

Zum einen wurde der Einfluss einer akustischen Anregung auf Selektivität und Reaktivität einer katalytischen Reaktion im Reaktor studiert, zum anderen wurde der Einfluss der Katalyse auf die charakteristische Anregungsenergie untersucht.

In Zusammenarbeit mit dem Teilprojekt B3 (Schomäcker/Kondratenko) wurden Versuche zur Beeinflussung des katalytischen Verhaltens von V_2O_5 durchgeführt. Es wurde ein Kleinreaktor gebaut, in dem die katalytische Reaktion mittels nachgeschaltetem Gaschromatographen beobachtet werden kann. In dem Quarzreaktor befindet sich ein Stück V_2O_5 -Sinterstab, welcher mittels eines Quarzstabes mit dem außerhalb des Reaktors befindlichen Quarz-Transducer verbunden ist.



Abb. 10. Quarz-Reaktor v.l.n.r.: Quarz-Transducer, Kappe mit Dichtung, Quarzverbindungsstab innen und Reaktorrohr mit Gaseinlass außen, V_2O_5 -Sinterstab, Quarzwolle, Gasauslass

Über den Quarzstab wird der Schall in die Probe eingekoppelt. Während des Versuchs werden die Prozessgase oben in den Reaktor eingeschleust, an der beschallten Probe vorbei geleitet und unten in Richtung Gaschromatograph abgeführt.

Es konnten trotz Variation verschiedener Parameter keine signifikanten und reproduzierbaren Einflüsse von intensivem Ultraschall auf die Reaktivität oder Selektivität von V_2O_5 festgestellt werden. Die Ursache hierfür liegt in den sehr starken Verlusten im akustischen Signal bei der Ankopplung und Weiterleitung der Verzerrungsfelder bis zum katalytisch aktiven Material. Die Schalleistung an der Probe ist offenbar für die Änderung des Verhaltens in der katalytisch aktiven Zone zu gering.

In einem zweiten Ansatz wurden mehrere V_2O_5 Proben aus einem Batch in den Katalysereaktor eingebracht und nach unterschiedlicher Verweildauer unter Katalysebedingungen entnommen. Die Proben wurden anschließend mit IF untersucht und insbesondere die charakteristischen Anregungsenergien verglichen.

Während sich zunächst eine deutliche Abweichung der beobachteten Energien abzeichnete, ließ sich jedoch keine einfache Korrelation mit der Verweildauer unter Prozessgas feststellen.

Bei Betrachtung des hochauflösenden IF-Spektrums zeigt sich aber, dass eine einfache Arrhenius-Analyse des Gesamtspektrums dem Detailreichtum des Datenmaterials nicht gerecht wird. So zeigt Abbildung 11 im Vergleich zu Abbildung 8 wesentlich mehr Struktur in der elastischen Antwort des Gesamtsystems nach der chemischen Reaktion.

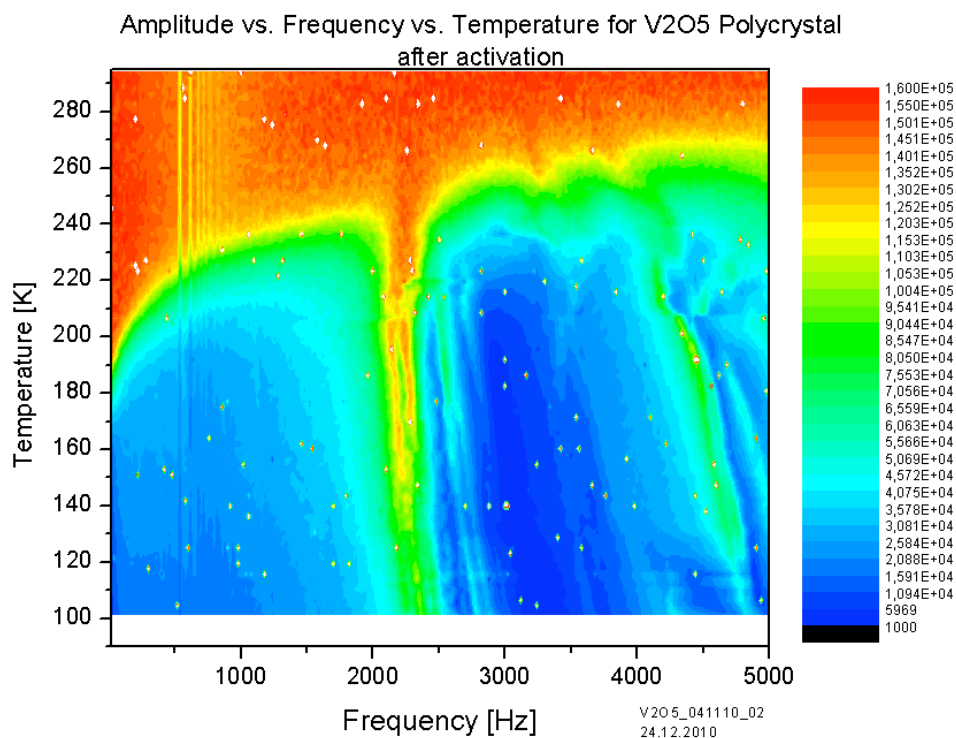


Abb. 11. Die Temperaturabhängigkeit des IF-Spektrums einer V_2O_5 Probe nach mehrstündiger Verweildauer unter Prozessgas im Katalysereaktor. Wichtig ist hier ein Vergleich mit der Probe vor Reaktion (Abbildung 8)

Dies deutet auf eine große Empfindlichkeit der IF-Messtechnik für katalyse-relevante Defektanregungen, belegt aber auch, dass eine komplexere Analyse des Spektrums für ein Verständnis der elastischen Vorgänge unverzichtbar ist. Diese Analyse wird die Kooperation mit theoretisch arbeitenden Gruppen erforderlich machen und war im Rahmen dieser Förderperiode nicht erreichbar.

5.3 Rückblick auf die Förderung

Das Teilprojekt wurde seit 07/1999 im Sonderforschungsbereich gefördert. Es wurde mit Ablauf der 4. Förderperiode im Juni 2011 beendet.

5.3.1 Personal im Teilprojekt während der zu Ende gehenden Förderperiode

	lauf. Nr.	Name, akademischer Grad, Dienststellung	engere Fachzugehörigkeit	Institut der Hochschule oder der außeruniv. Einrichtung	Mitarbeit im Projekt Zeitraum Wochenstunden	Entgeltgruppe
Grundausrüstung						
Wissenschaftlerinnen und Wissenschaftler	1.	Carsten Hucho, Dr.	Physik/Materialwiss.	PDI	07/1999 – 06/2011, 8h	
nichtwissenschaftl. Mitarbeiterinnen und Mitarbeiter						
Ergänzungsausrüstung						
Wissenschaftlerinnen und Wissenschaftler	1.	Arno Wirsig, Dipl.Phys.	Physik/Materialwiss.	PDI	02/2007 – 06/2011, 40h	E13
nichtwissenschaftl. Mitarbeiterinnen und Mitarbeiter						

Aufgaben der Mitarbeiterinnen und Mitarbeiter (Grundausrüstung):

1. Dr. Carsten Hucho
Projektleitung, Anleitung des Doktoranden und der Mitarbeiter, Untersuchung des elastischen Verhaltens katalytisch aktiver Proben.

Aufgaben der Mitarbeiterinnen und Mitarbeiter (Ergänzungsausrüstung):

1. Dipl.-Phys. Arno Wirsig
Untersuchungen zum elastischen Verhalten von katalyserelevanten Proben, Weiterentwicklung der Messverfahren, Probenpräparation.

5.1 Allgemeine Angaben zum Teilprojekt C5

5.1.1 Titel: DFT-Rechnungen mit periodischen Randbedingungen zur Struktur, Dynamik und Reaktivität von Übergangsmetalloxiden auf Trägern im Vergleich zu Einkristallen

5.1.2 Projektleitung

Prof. Dr. Joachim Sauer
geb. 19.04.1949

Dr. Joachim Paier
geb. 19.09.1978

Institut für Chemie
Humboldt-Universität zu Berlin
Unter den Linden 6
10099 Berlin

Telefon: 030 / 20937135
E-Mail: js@chemie.hu-berlin.de

030 / 20937139
paierjoa@chemie.hu-berlin.de

ausgeschieden:

Dr. Maria Veronica Ganduglia-Pirovano
geb. 17.11.1962

5.2 Entwicklung des Teilprojekts

5.2.1 Bericht

5.2.1.1 Related questions and state of knowledge

Vanadium oxide is the major active component of catalysts for selective oxidation reactions. Therefore, a chief part of current research in heterogeneous catalysis has been devoted to the elucidation of the interplay between vanadium oxide and its support. The prevalent mechanistic picture follows the Mars-van-Krevelen mechanism. Theoretical investigations on the mechanism of the oxidative dehydrogenation (ODH) of propane on V_2O_5/SiO_2 model catalysts [“Teilprojekt A4” (TP A4)] have shown that the rate-determining step of the reaction consists of the primary transfer of a hydrogen atom onto a so-called vanadyl oxygen atom [RFS07]. In need of identifying active sites on the surface and the elucidation of the support material’s influence on reactivity and selectivity, there are still open questions yet to be answered.

“Teilprojekt C5” addresses these aforementioned questions using a theoretical approach. Central to its scientific goals are investigations on well defined model systems and the development of models relating structure and reactivity of supported catalysts to each other. Specific aims of the project involved the investigation and comparison of structure, stability, infra-red spectroscopic signature, as well as reducibility of vanadia aggregates on various Al_2O_3 -supports [α - $\text{Al}_2\text{O}_3(0001)$], κ - $\text{Al}_2\text{O}_3(001)$, ordered Al_2O_3 -film on $\text{NiAl}(110)$] [1-3, BGS10]. Furthermore, calculations on stability and reducibility of vanadium oxide species induced by hydroxylation have been done (predominantly surfaces of $t\text{-ZrO}_2$) [HGS09]. The atomic structure of the SiO_2 -model support has been resolved for the VO_x/SiO_2 system. Moreover, questions on the accuracy of the theoretical description of defect formation and reduction of cerium oxide surfaces had to be addressed (see also TP A3/A4). Based on results obtained for the reduced cerium oxide substrate, further calculations on deposited vanadia aggregates on cerium oxide have been envisaged. In this case, the coupling between support and vanadia aggregates via V-O-Ce moieties is of particular interest, because the compound VO_x/CeO_2 system is more reactive than individual components [4,5]. Results on CeVO_4 obtained in the past period of TP C5 have contributed to a more profound understanding on that issue [6]. Additional corroborating calculations on partially reduced $\text{Ce}_m\text{V}_n\text{O}_o^+$ gas-phase clusters have been carried out (TP A3/A4) [7]. Studies on reactivity have been devoted to formation energies of oxygen defects on the above mentioned vanadia aggregates correlating it to corresponding structures. This is well justified supposing that the catalytic reaction follows a Mars-van-Krevelen mechanism. Importantly, the hydrogenation energy relating to the energy barrier of the rate determining step has been previously introduced as a further descriptor on reactivity of ODH reactions [8]. Investigations on the oxidation of methanol on vanadium oxide surfaces have been pursued within TP C5 and results have been published in the literature recently [9,RGG11].

5.2.1.2 Methods

Density functional theory (DFT) within the generalized-gradient approximation (GGA-PW91 and GGA-PBE) to the exchange-correlation energy functional has been applied within periodic boundary conditions and plane-waves as a basis set as implemented in the Vienna Ab-Initio Simulation Package (VASP). VASP is a full-potential all-electron code, restoring the correct shape of the one-electron wave functions by virtue of the projector augmented wave (PAW) method. The PAW pseudo-potentials are particularly efficient for applications involving

transition or rare earth metals. Surfaces of crystalline solids are represented by super-cells of so-called slab models. It is important that the chosen cell dimensions are large enough, in order to prevent unrealistically high defect or adsorbate concentrations. Bulk phases of solids are fully relaxed and vibrational frequencies are obtained by diagonalizing the dynamical matrix, which requires the matrix of the second-derivative of the energy with respect to the atomic positions (Hessian). The latter is obtained using finite differences, i.e. numerical differentiation. Effects induced by finite pressures and finite temperatures of surrounding gaseous phases can be modeled to a good extent by relatively simple statistical thermodynamics. As a consequence questions on the stability of the supported vanadium oxide aggregates under more realistic conditions may be answered. The stability, represented by the surface free energy, can be plotted as a function of the O₂ or H₂O partial pressure, or in case of metallic adsorbates, as a function of activity (concentration). For certain systems, as e.g. cerium oxide, representing a serious challenge for conventional DFT-GGA functionals, the accuracy of various exchange-correlation functionals (e.g. PBE, PBE0, HSE) and methods (DFT+*U*) has been assessed.

5.2.1.3 Results and discussion

Monomeric vanadium oxide species deposited on ceria

In the last funding period, the atomic structure and infra-red absorption spectra of vanadia monolayer catalysts using ceria as a support have been investigated [BAB09] exploiting synergy between high-resolution scanning tunneling microscopy (STM) and theoretical calculations.

Depositing vanadium in an ambient oxygen atmosphere on a well-defined CeO₂(111) thin film at low coverage (0.3 V atoms nm⁻²) yields highly dispersed and randomly distributed species (Fig. 1, upper left-hand picture). The corresponding IR spectrum shows an absorption feature at 1006 cm⁻¹, which has been assigned to the vanadyl (V=O) stretching vibration. Importantly, the IR spectroscopy results suggest that the vanadia monomers observed by STM are positioned with the vanadyl group perpendicular to the surface. Furthermore, XPS data on the VO_x/CeO₂ samples at lower vanadia coverage reveals vanadium only in a fully oxidized, +5 oxidation state, as shown by a single peak at approximately 517 eV for the V 2p_{3/2} core level (lower panel in Fig. 1). Heating the system to 700 K induces sintering to trimers and oligomers as detected by STM (Fig. 1, upper panel). The apparent height of the trimer was found to be 1.0 ± 0.3 Å being about the same as for monomers, which indicates that trimers are anchored

flat on the surface. The associated IR spectrum has a vanadyl stretch absorption peak at 1033 cm^{-1} , which is blue-shifted by about 25 cm^{-1} as compared to the monomeric species.

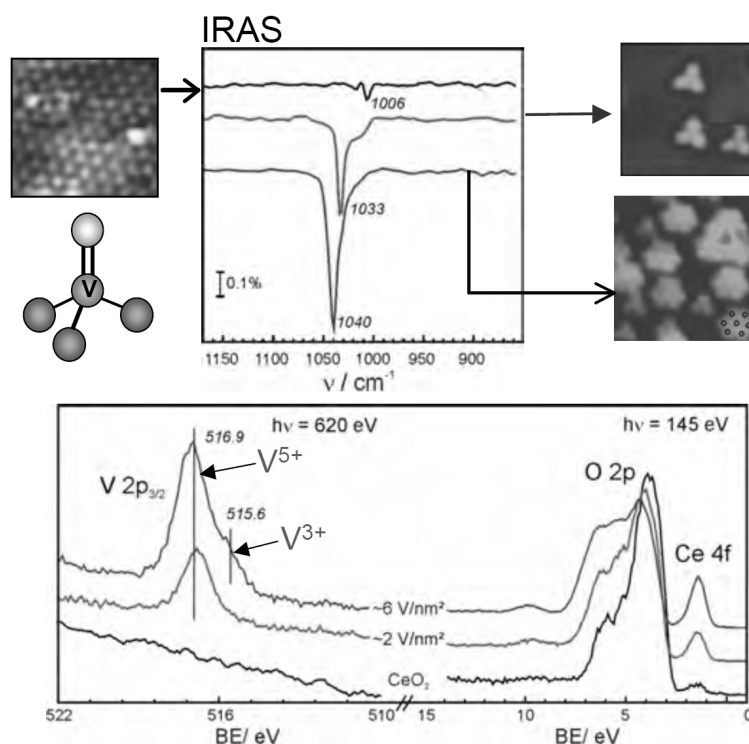


Fig. 1 Vanadia monomers detected by STM. A direct relationship between nuclearity of the vanadia clusters and the V=O, i.e. vanadyl, frequency of the stretching mode could be reproduced by DFT calculations: the higher the nuclearity of aggregates, the more blue shifted the spectra.

DFT+ U results are consistent with the experimental findings for vanadia monomers and trimers. Upon deposition of a V atom on the nondefective CeO₂(111) surface, four electrons are transferred from V 3d states into Ce 4f states, creating four Ce³⁺ ions and leaving V in the +4 oxidation state. However, an isomeric structure to V/CeO₂(111) has been found to be 1.48 eV (= 142.8 kJ/mol) more stable, but oxygen atoms are rearranged. A vanadyl bond is formed and a subsurface oxygen defect is created in the third oxygen layer. This structure is characterized by five Ce³⁺ ions and V in the +5 oxidation state, which is in full agreement with experiment (above mentioned XPS core level shifts). In addition, the trimer structure, 3(VO)/CeO₂(111), where each vanadyl group is oriented perpendicular to the surface, features the characteristic blue-shifted vanadyl stretch frequency by approximately 35 cm^{-1} compared to the monomeric species (see also [PGS11]). This is again in excellent agreement with experimental findings. Note that also here, V is found to be in oxidation state +5 and Ce⁴⁺ ions are reduced to Ce³⁺.

Oxygen defect formation and electron localization in CeO₂(111)

As cerium oxide is known to be an excellent “donor-acceptor system” of oxygen and since it has very favorable properties as a support material in catalytically highly active materials such as VO_x/CeO₂, knowing the structural and electronic properties of oxygen-deficient, i.e. reduced, ceria surfaces is of paramount importance for understanding the reactivity of ceria-based catalysts. In this funding period two major contributions towards such an understanding have been made: (i) structural and energetic trends for various electron localization patterns, i.e. relative positions of Ce³⁺ ions to surface and subsurface oxygen vacancies have been elucidated using DFT [GDS09], (ii) these theoretically calculated localization patterns have been found to be fully in line with actual STM and STS measurements [JSN11]. Concerning (i), strong evidence for the energetic preference of the subsurface position of the oxygen vacancy in ceria compared with the surface oxygen vacancy was provided in agreement with most recent experimental findings [10] and disproving early results obtained using DFT (LDA+U) [11].

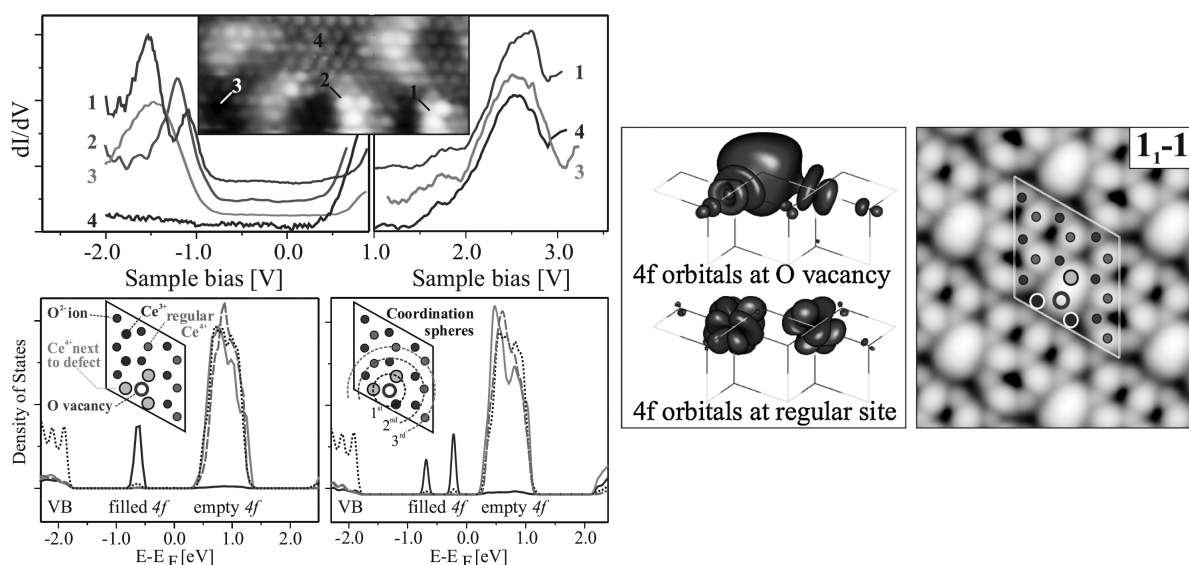


Fig. 2. Observed STS (upper panel, l.h.s.) and STM simulations (lower left and r.h.s. panels) on O-defective CeO₂(111). On the l.h.s., the crystal field splitting of filled f states for different configurations with respect to Ce³⁺ are shown. The panel on the r.h.s. depicts empty 4 f orbitals adjacent to the oxygen defect as well as to a non-reduced regular site calculated using DFT.

Furthermore, it has been shown that nearest-neighbor configurations with respect to the Ce³⁺ ions are not the minimum energy structures, neither for surface nor for subsurface defects. Hence, the oxygen vacancy is prone to be bound to Ce⁴⁺ ions. This is explained by evasion of lattice strain effects. The larger Ce³⁺ ions prefer sites which are located farther apart. Concerning (ii), the impact of so-called crystal field effects on spectroscopic features of the

filled $4f$ states located in the $O_{2p} - Ce_{5d}$ band gap and occupied by the electrons left upon formation of an oxygen vacancy has been demonstrated. A crystal field splitting of the occupied f states induced by different coordination numbers (CN) of the Ce^{3+} ions could be observed experimentally (STS) for different spectral positions on the sample. The electron density of states obtained using DFT+ U and calculated for defects featuring CN differences of one or two were found to perfectly agree with the observed STS. However, the localization of the Ce^{3+} ions with respect to the defect cannot be deduced in this way since it is only sensitive to differences in the local environment. Nevertheless, this information is contained in empty-state STM topographies due to the variance in brightness, which reflects the local electronic structure of a ceria surface. The question where the Ce^{3+} ions are located relative to the defect has been answered by combining the STM measurements with first principles DFT calculations using an electrostatic embedding method [13]. From these calculations the relatively diffuse and extended unoccupied Ce $4f$ states in Ce^{4+} bound to the defect could be visualized providing evidence for the causal connection between brightness of the STM and Ce^{4+} in nearest-neighbor position to the oxygen defect.

Adsorption and oxidation of methanol on $V_2O_3(0001)$ and $V_2O_5(001)$

In [SGK09] the partial oxidation of methanol on $V_2O_5(001)$ films supported on Au(111) was investigated. On non-reduced surfaces methanol adsorbs only in molecular form, consequently no formaldehyde production takes place. On reduced surfaces methanol forms methoxy groups, which react to produce formaldehyde in the temperature range from 400 K to 550 K. Other reaction products were not observed.

Importantly it has been shown that, methoxy groups can be stabilized at room temperature only when the surface is free of hydroxyl groups since otherwise methoxy and hydroxyl groups may react to form methanol, which desorbs between 230 and 300 K. Hydroxyl groups can also react with other hydroxyl groups to form water, which probably desorbs in the same temperature regime. If large amounts of methanol are dosed at room temperature, water formation removes all hydroxyl groups from the surface, which finally stabilizes a layer of methoxy. STM images show that the density of surface defects decreases due to methoxy formation, except for pair defects perpendicular to the vanadyl double rows whose density increases upon methanol dosage. This has been attributed to the promotion of water formation from hydroxyl groups near to a single defect via a reduction of the energy barrier. Water desorption produces another oxygen vacancy so that a vacancy pair results.

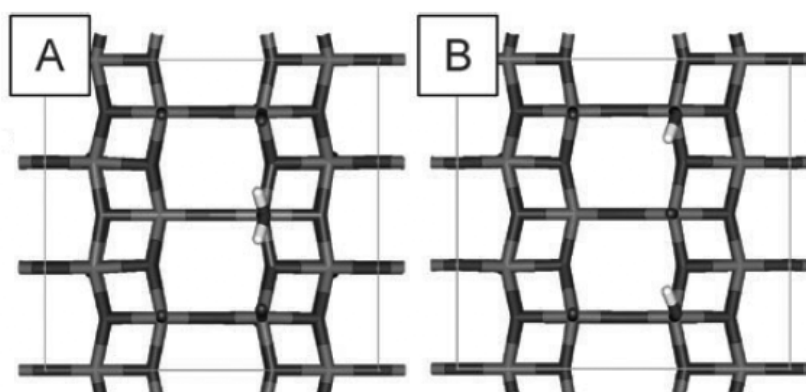


Fig. 3. Calculated structures for water adsorption on a double defect.

DFT calculations pursued within TP C5 essentially support experimental findings. Molecular methanol has been found to be only weakly bound to a non-defective vanadyl-terminated $V_2O_5(001)$ surface (binding energy = 0.16 eV). The bond to a vanadyl oxygen vacancy is stronger (0.64 eV). Dissociation into surface-bound methoxy and hydrogen is only slightly preferred (0.67 eV, with the hydrogen atom bound to a bridging oxygen atom). Molecular water on a defect has the same binding energy as molecular methanol (0.64 eV), but dissociated water is less strongly bound (0.44 eV). Molecular adsorption on a double defect of type B geometry (see Fig. 3), i.e. two oxygen atoms of a vanadyl pair perpendicular to a vanadyl double row are removed, gives a slightly stronger bond for molecular water (0.74 eV) whereas the energy of the dissociated state is reduced (0.38 eV). It is assumed that the presence of the defect not only modifies the binding energies but also the reaction barrier for water formation which might be the reason for the increase of the density of the type B double defects upon methanol adsorption.

In [RGG11] the adsorption of methanol on $V_2O_3(0001)$ has been investigated experimentally as well as by theoretical calculations. Methanol does not react on vanadyl terminated $V_2O_3(0001)$; only molecular adsorption and desorption have been found. If some or all oxygen atoms of the vanadyl groups are removed, methanol may dissociate on the surface already at low temperature (85 K) forming methoxy and hydroxyl groups. In the case of a partial removal of vanadyl oxygen, the hydrogen atoms may bind to vanadyl groups. The resulting hydroxy groups combine to form water at 270 K, producing vanadyl and vanadium sites. These may react with methanol to form more methoxy groups, which finally leads to methoxy density on the surface which is twice as large as the initial defect density. The DFT results also in this particular case basically agree with experimental findings and show that transfer of hydrogen

via co-adsorbed methanol molecules is a critical mechanism for the formation of surface hydroxyl groups and water.

Role of ceria in oxidative dehydrogenation reactions on supported vanadia catalysts

Vanadium oxide is the major active component of catalysts for selective oxidation reactions [4]. The activity of supported vanadia is strongly affected by the specific oxide used as a support [5].

Temperature-programmed desorption (TPD) experiments reveal that methanol oxidation to formaldehyde on the VO_x/CeO_2 model catalyst may occur at much lower temperature than previously reported for vanadia catalysts [14].

The combined experimental and DFT+ U studies [BAB09] and [GPS10], published within this last period of the TP C5 of the SFB 546, have shown that monomeric vanadia species on the ceria support are not reduced, but the support is. These species do not fully cover the support. Further reduction, specifically during the catalytic reaction, is particularly easy and results in an increase of the number of Ce^{3+} ions that have accepted one electron in their f states. Both reactivity parameters, hydrogenation energy and O defect formation energy obtained using DFT+ U , indicate an enhanced activity of monomeric vanadia species on ceria surfaces as compared to the bare support but also compared to monomeric vanadia species on inert supports such as silica. Importantly, as shown in Fig. 4, on the pristine $\text{CeO}_2(111)$ surface, the lowest oxygen defect formation energy has a value of 1.87 eV and is found for a subsurface oxygen site (Fig. 4, top left), which is consistent with recent experimental findings [10]. Creation of an oxygen defect in the $\text{VO}_2/\text{CeO}_2(111)$ structure requires 0.79 eV and yields the supported VO species shown in Fig. 4 (bottom left). Hence, formation of an oxygen defect in the $\text{VO}_2/\text{CeO}_2(111)$ system requires ~ 1.1 eV less than for the uncovered CeO_2 support.

In summary, the stabilization of electrons left upon reduction together with strain release in turn facilitating oxygen defect formation can be considered as a promoting effect of the vanadia species on the activity of the uncovered ceria support. This effect explains the low-temperature formaldehyde peak in the TPD spectra of adsorbed methanol, which was observed at coverages where primarily monomeric vanadia species have been identified. Based on these findings, it was concluded that the remarkably high activity observed for oxidation catalysts supported on ceria as compared to other supports directly relates to this special synergy between the ceria support and the supported oxide.

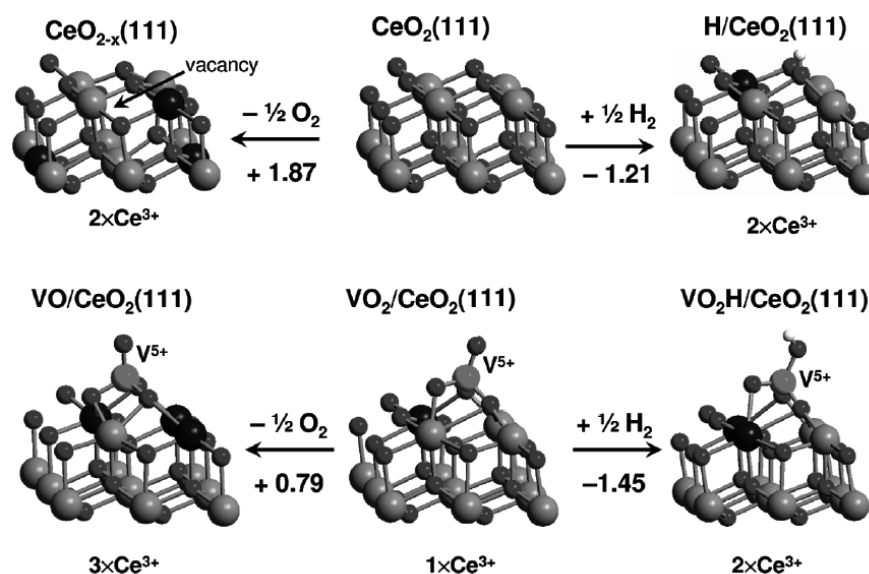


Fig. 4. Top: Side views of the fully oxidized $\text{CeO}_2(111)$ surface (middle), the reduced $\text{CeO}_2(111)$ surface with a subsurface oxygen vacancy (left), and the hydrogenated $\text{CeO}_2(111)$ surface (right). Bottom: Side views of VO and VO_2 species on the defect-free $\text{CeO}_2(111)$ surface (left and middle) as well as of the hydrogenated $\text{VO}_2/\text{CeO}_2(111)$ surface (right). Large light and dark spheres represent Ce^{4+} and Ce^{3+} (f^1) ions, respectively. V ions are represented as smaller light spheres located at the surface. Small dark gray and opaque spheres represent O and H atoms, respectively. Reaction energies are given in electronvolts.

Literature

- [1] T. K. Todorova, M. V. Ganduglia-Pirovano, J. Sauer, *J. Phys. Chem. B* **109**, 23523 (2005).
- [2] V. Brázdova, M. V. Ganduglia-Pirovano, J. Sauer, *J. Phys. Chem. B* **109**, 23532 (2005).
- [3] T. K. Todorova, M. V. Ganduglia-Pirovano, J. Sauer, *J. Phys. Chem. C* **111**, 5141 (2007).
- [4] I. E. Wachs, *Catal. Today* **100**, 79 (2005).
- [5] A. Dinse, B. Frank, C. Hess, D. Habel, R. Schomäcker, *J. Mol. Catal. A* **289**, 28 (2008).
- [6] J. L. F. Da Silva, M. V. Ganduglia-Pirovano, J. Sauer, *Phys. Rev. B* **76**, 125117 (2007).
- [7] L. Jiang, T. Wende, P. Claes, S. Bhattacharyya, M. Sierka, G. Meijer, P. Lievens, J. Sauer, K. R. Asmis, *J. Phys. Chem. A* (2011), doi.: 10.1021/jp203276g.
- [8] X. Rozanska, R. Fortrie, J. Sauer, *J. Phys. Chem. C* **111**, 6041 (2007).
- [9] Y. Romanyshyn, S. Guimond, H. Kühlenbeck, S. Kaya, R. P. Blum, H. Niehus, S. Shaikhutdinov, V. Simic-Milosevic, N. Nilus, H.-J. Freund, M. V. Ganduglia-Pirovano, R. Fortrie, J. Döbler, J. Sauer, *Top. Catal.* **50**, 106 (2008).
- [10] S. Torbrügge, M. Reichling, A. Ishiyama, S. Morita, Ó. Custance, *Phys. Rev. Lett.* **99**, 056101 (2007).
- [11] F. Esch, S. Fabris, L. Zhou, T. Montini, C. Africh, P. Fornarsiero, G. Comelli, R. Rosei, *Science* **309**, 752 (2007).
- [13] A. M. Burow, M. Sierka, J. Döbler, J. Sauer, *J. Chem. Phys.* **130**, 174710 (2009).
- [14] T. Feng, J. M. Vohs, *J. Phys. Chem. B* **109**, 2120 (2005).

5.2.2 Projektrelevante eigene Publikationen

a) erschienene oder angenommene Arbeiten in wissenschaftlichen Zeitschriften oder Buchveröffentlichungen

- [PGS11] C. Popa, M. V. Ganduglia-Pirovano, J. Sauer
Periodic Density Functional Theory Study of Von Species Supported on the CeO₂(111) Surface
J. Phys. Chem. C **115** (2011) 7399 - 7410.
- [JSN11] J.-F. Jerratsch, X. Shao, N. Nilius, H.-J. Freund, C. Popa, M. V. Ganduglia-Pirovano, A. M. Burow, J. Sauer
Electron Localization in Defective Ceria Films: A Study with Scanning-Tunneling Microscopy and Density Functional Theory
Phys. Rev. Lett. **106** (2011) 246801-1 – 246801-4.
- [RGG11] Y. Romanyshyn, S. Guimond, D. Göbke, J. M. Sturm, H. Kuhlenbeck, J. Döbler, M. V. Ganduglia-Pirovano, J. Sauer, H.-J. Freund
Methanol Adsorption on V₂O₃(0001)
Top. Catal. **54** (2011) 669 – 684.
- [BGS10] V. Brázdová, M. V. Ganduglia-Pirovano, J. Sauer
Vanadia Aggregates on an Ultrathin Aluminium Oxide Film on NiAl(110)
J. Phys. Chem. C **114** (2010) 4983 – 4994.
- [GPS10] M. V. Ganduglia-Pirovano, C. Popa, J. Sauer, H. Abbott, A. Uhl, M. Baron, D. Stacchiola, O. Bondarchuk, S. Shaikhutdinov, H.-J. Freund
Role of Ceria in Oxidative Dehydrogenation on Supported Vanadia Catalysts
J. Am. Chem. Soc. **132** (2010) 2345 – 2349.
- [BAB09] M. Baron, H. Abbott, O. Bondarchuk, D. Stacchiola, A. Uhl, S. Shaikhutdinov, H.-J. Freund, C. Popa, M. V. Ganduglia-Pirovano, J. Sauer
Resolving the Atomic Structure of Vanadia Monolayer Catalysts: Monomers, Trimers, and Oligomers on Ceria
Angew. Chem. **121** (2009) 8150 – 8153; Angew. Chem. Int. Ed. **48** (2009) 8006 – 8009.
- [HGS09] A. Hofmann, M. V. Ganduglia-Pirovano, J. Sauer
Vanadia and Water Coadsorption on Tetragonal Zirconia Surfaces
J. Phys. Chem. C **113** (2009) 18191 – 18203.
- [TDS09] T. K. Todorova, J. Döbler, M. Sierka, J. Sauer
Vanadium Oxides Supported on a Thin Silica Film Grown on Mo(112): Insights from Density Functional Theory
J. Phys. Chem. C **113** (2009) 8336 – 8342.

- [GRG09] D. Göbke, Y. Romanyshyn, S. Guimond, J. M. Sturm, H. Kuhlenbeck, J. Döbler, U. Reinhardt, M. V. Ganduglia-Pirovano, J. Sauer, H.-J. Freund, *Formaldehyde Formation on Vanadium Oxide Surfaces $V_2O_3(0001)$ and $V_2O_5(001)$: How does the Stable Methoxy Intermediate Form?* *Angew. Chem.* **121** (2009) 3750 – 3753; *Angew. Chem. Int. Ed.* **48** (2009) 3695 – 3698.
- [SGK09] J. M. Sturm, D. Göbke, H. Kuhlenbeck, J. Döbler, U. Reinhardt, M. V. Ganduglia-Pirovano, J. Sauer, H.-J. Freund *Partial Oxidation of Methanol on Well-Ordered $V_2O_5(001)/Au(111)$ Thin Films* *Phys. Chem. Chem. Phys.* **11** (2009) 3290 – 3299.
- [GDS09] M. V. Ganduglia-Pirovano, J. L. F. Da Silva, J. Sauer *Density Functional Calculations of the Structure of Near-Surface Oxygen Vacancies and Electron Localization on $CeO_2(111)$* *Phys. Rev. Lett.* **102** (2009) 026101-1 – 026101-4.
- [KWS08] S. Kaya, J. Weissenrieder, D. Stacchiola, T. K. Todorova, M. Sierka, J. Sauer, S. Shaikhutdinov, H.-J. Freund, *Formation of One-Dimensional Molybdenum Oxide on $Mo(112)$* *Surf. Sci.* **602** (2008) 3338 – 3342.

5.3 Rückblick auf die Förderung

Das Teilprojekt wurde seit 07/1999 im Sonderforschungsbereich gefördert. Es wurde mit Ablauf der 4. Förderperiode im Juni 2011 beendet.

5.3.1 Personal im Teilprojekt während der 4. Förderperiode

	lauf. Nr.	Name, akademischer Grad, Dienststellung	engere Fachzugehörigkeit	Institut der Hochschule oder der außeruniv. Einrichtung	Mitarbeit im Projekt Zeitraum Wochenstunden	Entgeltgruppe
Grundausrüstung						
Wissenschaftlerinnen und Wissenschaftler	1.	Joachim Sauer Dr., Univ.-Prof.	Theoret. Chemie	HU-C	07/1999 – 06/2011, 5h	
	2.	Joachim Paier, Dr.	Theoret. Chemie	HU-C	09/2009 – 06/2011, 20h	
	3.	Maria Veronica Ganduglia Pirovano, Dr.	Theoret. Chemie	HU-C	07/2001 – 07/2009, 20h	
nichtwissenschaftl. Mitarbeiterinnen und Mitarbeiter	5.	Thomas Dargel, Dipl.-Chem.		HU-C	07/2001 – 06/2011, 5h	
	6.	Monika Urban, Dipl.-Ing. FH		HU-C	07/1999 – 10/2009, 5h	
Ergänzungsausrüstung						
Wissenschaftlerinnen und Wissenschaftler	1.	Cristina Popa, Dr.	Theoret. Chemie	HU-C	03/2008 – 02/2011, 32h	E13, 80%
	2.	Sergio Tosoni, Dr.	Theoret. Chemie	HU-C	10/2010 – 06/2011, 40h	E13
nichtwissenschaftl. Mitarbeiterinnen und Mitarbeiter						

Aufgaben der Mitarbeiterinnen und Mitarbeiter (Grundausrüstung):

1. Prof. Dr. Joachim Sauer
Projektleiter, Wissenschaftliche und organisatorische Leitung des Teilprojekts. Planung der theoretischen Untersuchungen und Auswertung der Ergebnisse.
2. Dr. Joachim Paier
Projektleiter, Wissenschaftliche und organisatorische Leitung des Teilprojekts. Planung der theoretischen Untersuchungen und Auswertung der Ergebnisse. Theoretische Untersuchungen zur Oxidation von Methanol zu Formaldehyd mittels monomeren und oligomeren VO_x auf Ceroxid.
3. Dr. MariaVeronica Ganduglia Pirovano
Projektleiter, Wissenschaftliche und organisatorische Leitung des Teilprojekts. Planung der theoretischen Untersuchungen und Auswertung der Ergebnisse. Theoretische Untersuchungen zur Oxidation von Methanol zu Formaldehyd auf leicht reduziertem $\text{V}_2\text{O}_3(0001)$
3. Thomas Dargel
Betreuung der Rechner und Programme.
4. Monika Urban
Technische Mitarbeit.

Aufgaben der Mitarbeiterinnen und Mitarbeiter (Ergänzungsausstattung):

1. Dr. Cristina Popa
Postdoktorand. Zu den Aufgaben gehören Rechnungen zur Struktur, Schwingungsspektren, Stabilität und Reaktivität von Vanadiumoxidaggregaten auf $\gamma\text{-Al}_2\text{O}_3$ - und CeO_2 -Unterlagen.
2. Dr. Sergio Tosoni
Postdoktorand. Zu den Aufgaben gehören Rechnungen zur Rastertunnelmikroskopie von Thiophenyl-Komplexen adsorbiert auf $\text{Au}(111)$.

5.1 Allgemeine Angaben zum Teilprojekt C6

5.1.1 Titel: Ab-initio-Clustermodelle zur Struktur, Reaktivität und Spektroskopie an komplexen Vanadium- und Molybdänoxidoberflächen

5.1.2 Projektleitung

Prof. Dr. Klaus Hermann
geb. 09.11.1946

Abteilung Theorie
Fritz-Haber-Institut der Max-Planck-Gesellschaft
Faradayweg 4-6
14195 Berlin

Telefon: 030 / 84134812
E-Mail: hermann@fhi-berlin.mpg.de

5.2 Entwicklung des Teilprojekts

5.2.1 Bericht

In the present funding period we built upon the knowledge of the three previous periods focusing on two main subjects as proposed in our application, (a) the evaluation of energetic, structural, and electronic details of reaction steps of small molecule reactions at complex transition metal oxide surfaces, and (b) the elucidation of spectral features of near-edge X-ray absorption structure (NEXAFS, XANES) of transition metal oxide surfaces and small oxide particles on silica support. Due to space limitations only the most important results from these studies will be described in the following.

(a) Reactions at complex transition metal oxide surfaces

Here we discuss as an example details of the selective catalytic reduction (SCR) of NO_x by NH_3 which is one of the most effective NO_x reduction processes. It is widely employed in units of industrial scale where vanadium based metal oxides, VO_x , act as catalysts. The SCR reaction has been studied experimentally in great detail [1]. Here adsorption of NH_x , (de)hydrogenation at the surface, reaction with NO , surface water formation, and diffusion processes at the VO_x catalyst are found to contribute elementary steps [1]. However, details of the reaction mechanism at an atomic scale are still under debate.

In this work elementary steps of the SCR reaction are examined in theoretical cluster studies applying density-functional theory (DFT) together with gradient corrected functionals (cluster code StoBe). In the following we focus only on the main results from this study [GH11] considering adsorption, diffusion, (de)hydrogenation, and further details of different SCR reaction paths.

(a.1) Adsorption of H, NH_x at V₂O₅(010) surfaces

In experiments of the SCR reaction the adsorption of ammonia has been identified as initial reaction step [1] of the SCR. Therefore, we consider first adsorption of hydrogen and different NH_x species, x = 0 – 4. Here we model local sections at the VO_x catalyst substrate by clusters cut out from the ideal V₂O₅(010) surface where peripheral oxygen bonds are saturated by hydrogen [2]. In addition, reduced VO_x surfaces are simulated by introducing oxygen vacancies.

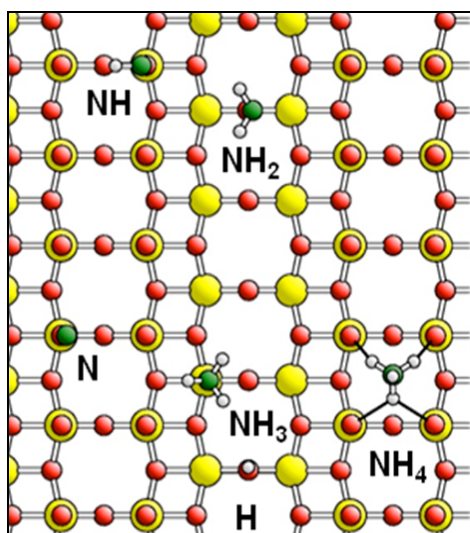


Fig. 1. Balls-and-sticks model of the perfect V₂O₅(010) surface with H, NH_x species, x= 0 – 4, placed at their energetically most preferred adsorption sites. Large light balls denote vanadium atoms while smaller dark balls refer to oxygen and nitrogen and very small light balls to hydrogen. The adsorbates are labeled accordingly.

The calculations show that H and NH_x species can adsorb and bind, except for ammonia itself, rather strongly with the perfect V₂O₅(010) surface at all oxygen sites, singly coordinated vanadyl oxygen O(1), as well as 2-, and 3-fold bridging oxygen O(2, 3). As an illustration Fig. 1 shows the most preferred binding sites for the different adsorbates, O(1) for N, NH, NH₄, and O(2) for H, NH₂. Ammonia, NH₃, is found to prefer the open vanadium site where it binds only relatively weakly ($E_B = 0.3$ eV). While NH₄ itself is bound very strongly to the surface ($E_B = 3.2$ to 3.9 eV) it is very unlikely to occur as an adsorbing molecule. However, during the SCR process it may appear as a consequence of NH₃ adsorbing near pre-adsorbed hydrogen at an oxygen site forming a local OH group (Brønsted acid site). The latter process is found in the calculations to be quite exothermic with binding energies $E_B = 1.4$ eV.

At the reduced $V_2O_5(010)$ surface, simulated by introducing oxygen vacancies, N, NH, and NH_2 are found to adsorb preferentially at vacancy sites where they substitute the missing oxygen and bind quite strongly with the surface. This applies also to NH_3 which stabilizes at the O(1) vacancy site (Lewis acid site) with a sizeable binding energy $E_B = 0.9$ eV, in contrast to only weak binding at the perfect surface. The NH_4 species is too bulky to fit into an oxygen vacancy and, therefore, adsorbs preferentially near the vacancy. There its binding with the V_2O_5 substrate, dominated by electrostatic contributions of the charged NH_4^+ , is affected only little compared with that at the perfect surface.

Altogether, the theoretical adsorption studies yield as the most relevant results for the SCR reaction that ammonia can adsorb at the VO_x catalyst substrate with reasonable binding energies either at Brønsted acid sites, reflecting local OH groups, or near Lewis acid sites represented by bare vanadium of lower coordination after oxygen vacancy formation. This suggests two different scenarios for the initial step of SCR reaction processes originating at the two different sites which will be considered in the following.

(a.2) Diffusion of H, NH_x at the $V_2O_5(010)$ surface

Hydrogenation and dehydrogenation of adsorbed NH_x species must include diffusion at the substrate surface. This has been studied in detail by cluster models where corresponding diffusion paths are evaluated with the nudged elastic band (NEB) method [3]. Here we restrict ourselves to brief comments on the diffusion of hydrogen which is most likely to occur due to its small mass.

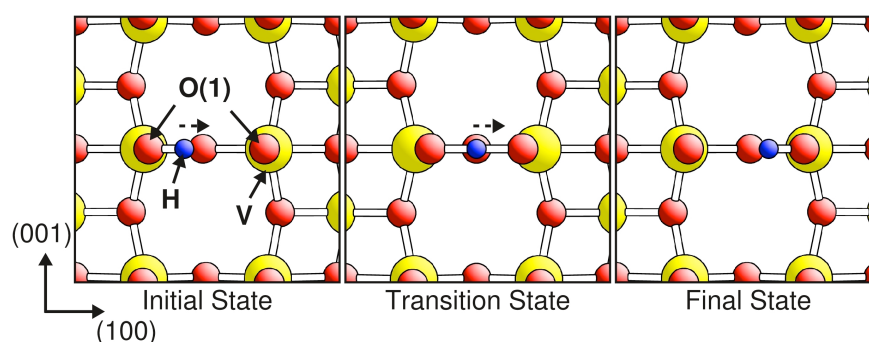


Fig. 2. Diffusion of hydrogen between neighboring vanadyl oxygen sites O(1). The two outer panels illustrate adsorption at the two neighboring sites. The central panel sketches the geometry of the transition state. Large light balls denote vanadium atoms while smaller dark balls refer to oxygen and very small dark balls to diffusing hydrogen. In the left panel atom centers and crystal directions are labeled accordingly.

As discussed earlier, hydrogen stabilizes at the $V_2O_5(010)$ surface preferentially near oxygen sites where binding energies of $E_B = 2.5 - 2.8$ eV have been calculated. This suggests

considering diffusion of hydrogen between adjacent oxygen sites at the surface. As an illustration, Fig. 2 shows the diffusion between two adjacent vanadyl oxygen sites O(1) where the left and right panels refer to adsorption at the two neighboring sites while the central panel sketches the transition state geometry. The geometry of the transition state evidences considerable flexibility of the neighboring vanadyl oxygen atoms at the surface. During H diffusion the two O(1) centers move towards each other which facilitates the O-H bond breaking and making greatly, resulting in a diffusion barrier of only 0.2 eV. This contrasts with hydrogen diffusing between adjacent bridging oxygen O(2) sites where the two surface atoms are further apart and less flexible leading to a computed diffusion barrier of 0.8 eV. These results exemplify the importance of dynamic properties of the substrate surface for its reactivity.

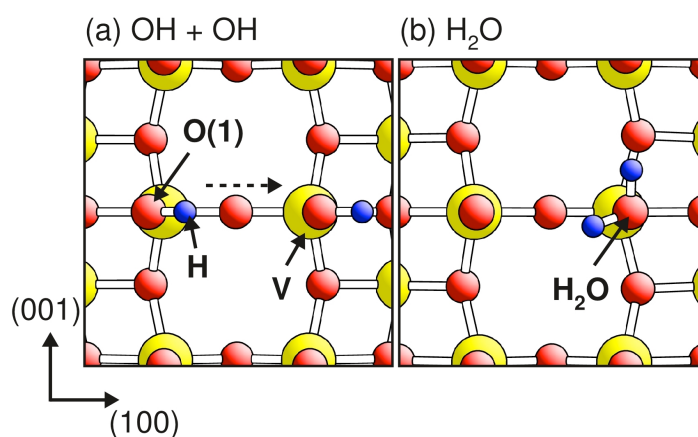


Fig. 3. Interaction of hydrogen from neighboring vanadyl oxygen sites O(1) and surface H₂O formation. (a) Equilibrium geometry of two O(1)H groups at adjacent surface sites. (b) Geometry of surface H₂O(1) formation after diffusion. Large light balls denote vanadium atoms while smaller dark balls refer to oxygen and very small dark balls to diffusing hydrogen. In the left panel atom centers and crystal directions are labeled accordingly.

Another aspect of diffusion comes into play when OH groups as a result of hydrogen adsorption and diffusion approach each other. This is illustrated in Fig. 3 for OH groups at adjacent O(1) sites of the V₂O₅(010) surface. Hydrogen of the left O(1)H group may diffuse towards the right O(1)H which leads to a H₂O(1) group with the diffusion barrier amounting to only 0.3 eV. The resulting surface water is bound rather weakly ($E_B = 0.4$ eV) at the surface and may desorb quite easily leaving an oxygen vacancy behind. This process is expected to occur during the SCR reaction and contributes to water production in gas phase.

(a.3) Hydrogenation and dehydrogenation of NH_x

Hydrogenation and dehydrogenation of adsorbed NH_x species represents important steps of the SCR reaction and corresponding energetics determine reaction probabilities and rates. This is examined in an approximate way by comparing adsorbate binding and dissociation energies of the different species where the catalytic effect of the VO_x substrate becomes obvious. Fig. 4 shows diagrams of corresponding hydrogenation and dehydrogenation energies for different

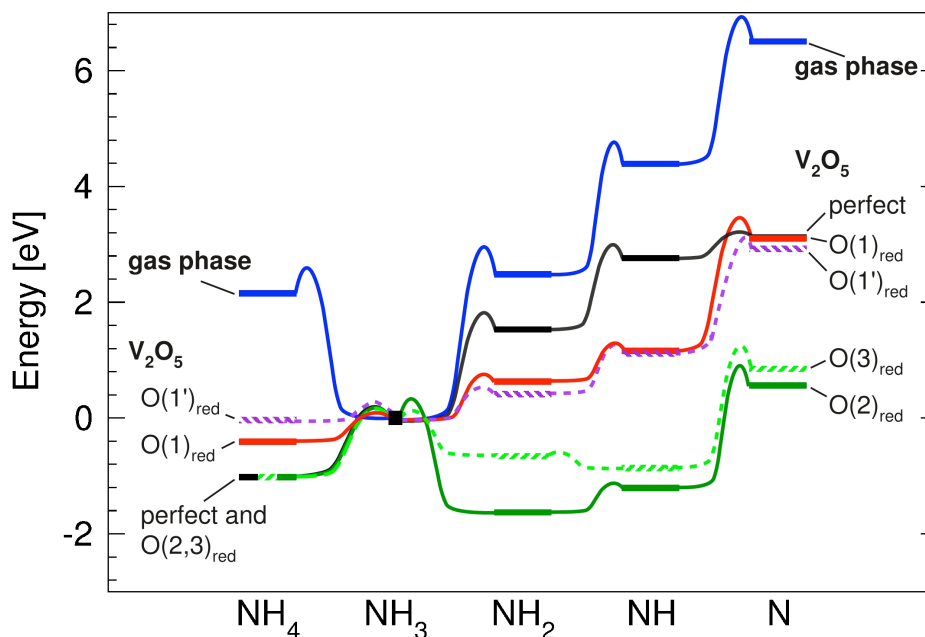
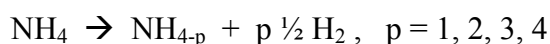


Fig. 4. Energy diagrams for (de)hydrogenation of NH_x , $x = 0 - 4$. Corresponding reaction energies E_R of the gas phase species (“gas phase”) are compared with those of the adsorbed species at the perfect $\text{V}_2\text{O}_5(010)$ surface (“perfect”) as well as at the reduced surface near different oxygen vacancies (“ $\text{O}(i)_{\text{red}}$ ”, $i = 1, 2, 3$), see text

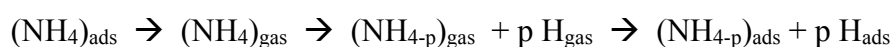
NH_x species. Here the ammonia in its adsorbed state and in gas phase, respectively, is taken as the reference (energy zero). For the gas phase scenario dehydrogenation energies E_R are evaluated successively following the reaction sequence



yielding

$$E_R = | E_{\text{tot}}(\text{NH}_4) - E_{\text{tot}}(\text{NH}_{4-p}) - p \frac{1}{2} E_{\text{tot}}(\text{H}_2) |$$

while for dehydrogenation energies E_R at the substrate surface Born-Haber cycles



with corresponding cluster total energies is considered. The calculated results, shown in Fig. 4, evidence highly endothermic dehydrogenation of ammonia with quite large E_R values in gas phase, about 1.4 eV to 2.5 eV per step. In addition, hydrogenation of gas phase ammonia is

also endothermic with $E_R = 2.2$ eV. The endothermicity of the ammonia dehydrogenation is reduced considerably when the reactions occur at the perfect $V_2O_5(010)$ surface which documents the catalytic effect of the substrate. Further, the hydrogenation of ammonia to yield NH_4 becomes exothermic at the surface due to the strong adsorptive binding of the NH_4 species. Finally, when the reduced surface is considered with different oxygen vacancies, ammonia dehydrogenation becomes even less endothermic and the reaction $NH_3 \rightarrow NH_2 + H$ may even become exothermic. These results are consistent with the experimental findings that during the SCR process NH_3 , NH_2 , and NH_4 species can be identified [4]. However, it should be emphasized that the present arguments are based only on thermodynamic considerations and ignore reaction barriers which are accounted for in evaluations of explicit SCR reaction paths discussed below.

(a.4) SCR reaction paths

As mentioned earlier, there is experimental evidence that the SCR of NO in the presence of NH_3 is initiated by ammonia adsorption. Considering the adsorption studies discussed in Sec. (a.1) there are only two choices for ammonia to stabilize at the VO_x catalyst substrate, either at Brønsted acid sites, reflecting local OH groups, or near Lewis acid sites represented by bare vanadium of lower coordination. This suggests two different SCR scenarios which have been examined in detail by corresponding reaction paths and intermediates: (1) SCR after NH_3 adsorption at a Brønsted acid site, and (2) SCR after NH_3 adsorption at a Lewis acid site of the reduced substrate. While scenario (1) has been discussed earlier in theoretical studies [5], scenario (2) is proposed here for the first time.

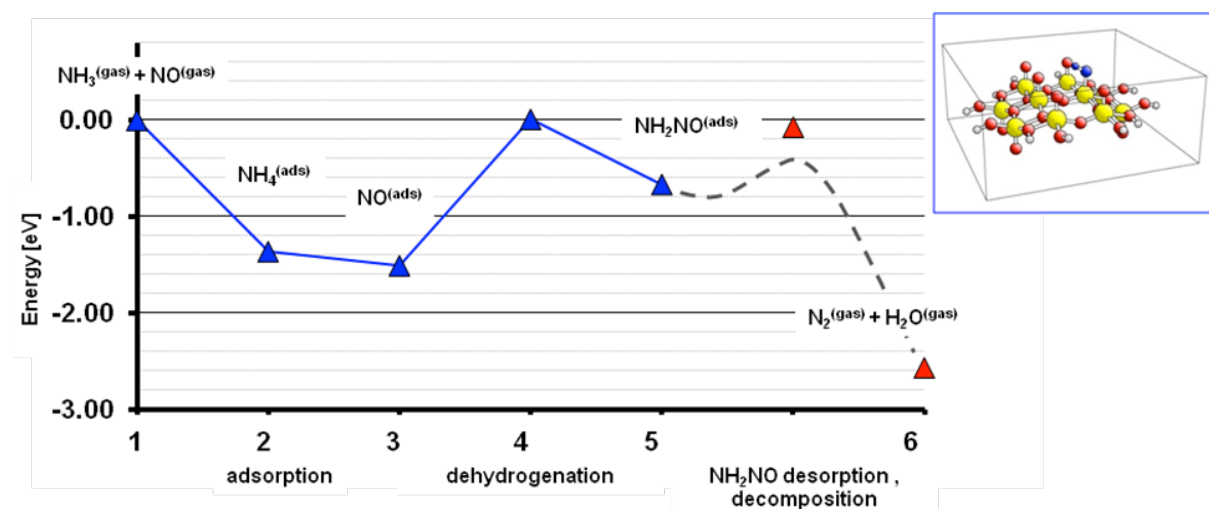


Fig. 5. SCR scenario of NO in the presence of NH_3 starting with NH_3 adsorption at a Brønsted acid site, see text. Reaction energies and barriers from NEB calculations are shown for the optimized reaction path. The inset at the top right sketches the initial surface structure near the Brønsted acid site (indicated by dark balls).

Fig. 5 shows energies and reaction intermediates from NEB calculations for the SCR scenario starting with NH_3 adsorption at a Brønsted acid site. Here the optimized reaction path is described by

- (1) $\text{OH}^{(\text{surf})} + \text{NH}_3^{(\text{gas})} + \text{NO}^{(\text{gas})}$
Initial step of the reaction near a surface OH group.
- (2) $\text{NH}_4^{(\text{ads})} + \text{NO}^{(\text{gas})}$
Ammonia adsorbs at OH forming a surface NH_4 species.
- (3) $\text{NH}_4^{(\text{ads})} + \text{NO}^{(\text{ads})}$
NO from gas phase is attached to NH_4 and fairly weakly binding.
- (4) $2 \times \text{OH}^{(\text{surf})} + \text{NH}_2\text{NO}^{(\text{ads})}$
Transition to the intermediate nitrosamide, NH_2NO , binding to two surface OH groups occurs where (4) characterizes the transition state. This is energetically most costly.
- (5) $2 \times \text{OH}^{(\text{surf})} + \text{NH}_2\text{NO}^{(\text{ads})}$
 NH_2NO equilibrates at the two surface OH groups.
- (6) $2 \times \text{OH}^{(\text{surf})} + \text{N}_2^{(\text{gas})} + \text{H}_2\text{O}^{(\text{gas})}$
 NH_2NO rearranges and dissociates producing the final products in gas phase.

Desorption and decomposition of the reaction intermediate NH_2NO , shown by a dashed line in Fig. 5, has been treated earlier [6, 7] and was not evaluated explicitly in this study.

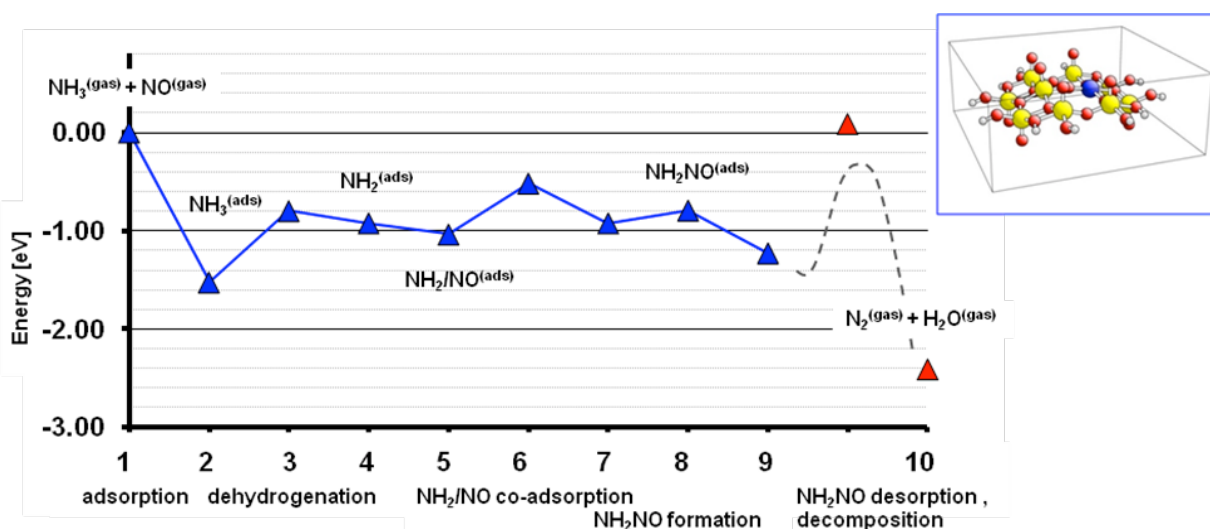


Fig. 6. SCR scenario of NO in the presence of NH_3 starting with NH_3 adsorption at a Lewis acid site, see text. Reaction energies and barriers from NEB calculations are shown for the optimized reaction path. The inset at the top right sketches the initial surface structure near the Lewis acid site (indicated by a dark ball).

Fig. 6 shows energies and reaction intermediates from NEB calculations for the SCR scenario starting with NH_3 adsorption at a Lewis acid site. Here the optimized reaction path is described by

- (1) $\text{O}^{(\text{surf.vac.})} + \text{NH}_3^{(\text{gas})} + \text{NO}^{(\text{gas})}$
Initial step of the reaction near a surface oxygen vacancy.
- (2) $\text{NH}_3^{(\text{ads})} + \text{NO}^{(\text{gas})}$
Ammonia adsorbs at vanadium site near oxygen vacancy.
- (3, 4) $\text{OH}^{(\text{surf})} + \text{NH}_2^{(\text{ads})} + \text{NO}^{(\text{gas})}$
Dehydrogenation of ammonia forming NH_2 and an adjacent surface OH group involving a transition state (3).
- (5) $\text{OH}^{(\text{surf})} + \text{NH}_2^{(\text{ads})} + \text{NO}^{(\text{ads})}$
NO from gas phase is attached to NH_2 and fairly weakly binding.
- (6-9) $\text{OH}^{(\text{surf})} + \text{NH}_2\text{NO}^{(\text{ads})}$
Transition to the intermediate nitrosamide, NH_2NO , binding to oxygen vacancy (Lewis acid site) in various conformations.
- (10) $\text{OH}^{(\text{surf})} + \text{O}^{(\text{surf.vac.})} + \text{N}_2^{(\text{gas})} + \text{H}_2\text{O}^{(\text{gas})}$
 NH_2NO rearranges and dissociates producing the final products in gas phase.

As in the previous reaction scenario, desorption and decomposition of the intermediate NH_2NO , shown by a dashed line in Fig. 6, was not evaluated explicitly in this study.

Altogether, the present theoretical studies suggest two different scenarios of the SCR of NO in the presence of NH_3 which differ by the initial adsorption of NH_3 at the VO_x substrate, either at a Brønsted or at a Lewis acid site. The calculations show that the Brønsted acid site scheme includes a rather large barrier for the formation of the surface intermediate nitrosamide which is lower for the Lewis acid site scheme. For the latter, the main energy barrier appears only during the final dissociation process which may be lowered by additional reaction partners. This would make the Lewis acid site scheme more likely to occur than the Brønsted acid site scheme. However, from the present results no clear preference can be given to either of the two schemes and both may be active in the real catalyst.

(a.5) Other reactions

Theoretical studies on adsorption and reaction steps of different other systems of catalytic interest have been performed within the present project in an attempt to solidify the experience with the theoretical computer codes (StoBe, DMol³) applied to catalytic problems. This includes

- CO Hydrogenation Reactions on Sulfided Molybdenum Catalysts where possible reaction paths have been evaluated [SJH09],
- the catalytic sulfidation of MoO₃ where the sulfur to oxygen exchange process was examined [SWH10a], and
- CO and NO adsorption / dissociation at the β -Mo₂C(0001) surface where surface structure properties [H11] as well as adsorption and dissociation energies were calculated [SWH10b].

Further details can be found in the corresponding publications [SJH09], [SWH10a], [SWH10b].

(b) Structural analysis of small silica-supported transition metal oxide particles

The search for structure-reactivity relationships in catalysts is of paramount interest since it can provide an understanding of elementary steps of catalytic reactions as well as help the design of corresponding catalysts. Here we focus on catalytic transition metal (TM) oxide particles on silica support where both experimental studies on model catalysts, using spectroscopic methods, such as X-ray absorption (NEXAFS), and theoretical work, applying density-functional theory (DFT) methods with small clusters, have been performed. The interplay between theory in this project and experiment in project B2 has proven to yield detailed insight into structural properties of the supported TM oxide particles. Here we restrict ourselves to a short discussion of the most important results of V_xO_y and Mo_xO_y particles on SiO₂ support. Further details can be found in the literature, see [CHK09], [HCH09], [GHH11].

(b.1) Vanadium oxide particles

The choice of the support material is known to modify the activity of vanadia catalysts by several orders of magnitude which can occur by providing specific binding sites for the vanadia surface species. The initial view [8] of monomeric VO_x species dominating the catalytic activity on silica support was based on the assumption that monomeric and polymeric V_xO_y species can be discriminated by vibrational spectroscopy. However, this view has been questioned by studies [9] combining infrared and Raman spectroscopy with DFT calculations. These results show that vibrational modes and frequencies, which are considered to be representative for vanadyl V=O and bridging V-O-V, V-O-Si, and Si-O-Si vibrations, may couple strongly which makes a unique assignment to specific V_xO_y bonds questionable. This suggests that vibrational spectroscopy may not allow definitive conclusions about the presence of different V_xO_y species in a catalyst.

We have performed DFT calculations using the gradient-corrected RPBE functional on oxygen core excitations in vanadia-silica model clusters which can be compared with X-ray absorption fine structure (NEXAFS) measurements near the oxygen K-edge of vanadia model catalysts supported by SBA-15 silica. This allows us to identify structural details of the vanadia species [CHK09, HCH09] beyond vibrational analyses. The calculations, applying the StoBe cluster code, are based on vanadia silica model clusters whose structures are identical with those of Ref. [9]. As an illustration, Fig. 7 shows geometric structures of the eight clusters considered in the calculations, where vanadia units appear in pyramidal conformation. In addition, peroxy (SiO)-V=O(O₂), cluster (g), and hydroxylated (SiO)-V=O(OH)₂ umbrella species, cluster (h) are included.

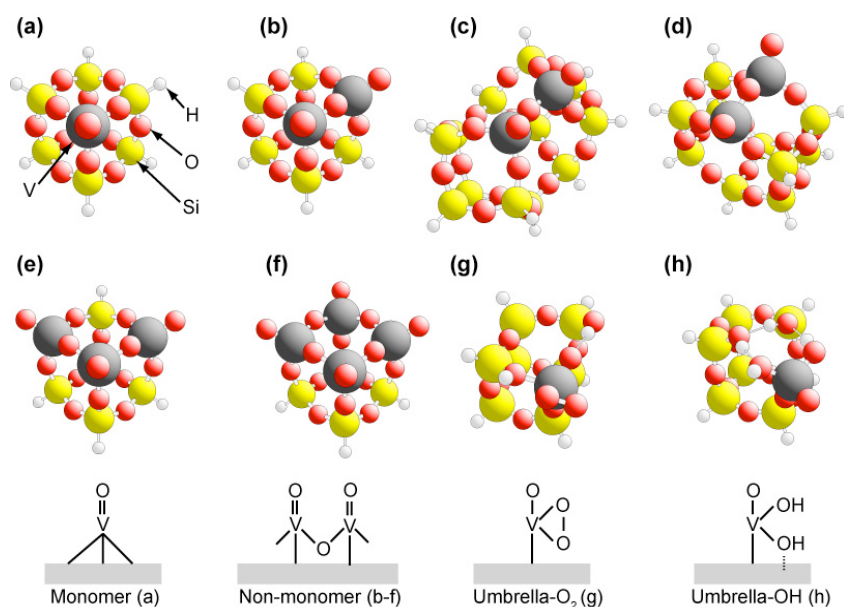


Fig. 7. Clusters used to model silica-supported vanadia units, (a) $\text{VSi}_7\text{O}_{13}\text{H}_7$, (b) $\text{V}_2\text{Si}_6\text{O}_{14}\text{H}_6$, (c) $\text{V}_2\text{Si}_{12}\text{O}_{23}\text{H}_{12}$, and (d) $\text{V}_2\text{Si}_{10}\text{O}_{20}\text{H}_{10}$, see [9], (e) $\text{V}_3\text{Si}_5\text{O}_{15}\text{H}_5$, (f) $\text{V}_4\text{Si}_4\text{O}_{16}\text{H}_4$, see [10], (g) $\text{VSi}_7\text{O}_{15}\text{H}_9$, (h) $\text{VSi}_7\text{O}_{15}\text{H}_{11}$, see [10]. Large dark and light balls refer to vanadium and silicon, respectively, while smaller dark balls denote oxygen and small light gray balls visualize hydrogen. The binding schemes of the clusters are sketched at the bottom.

Calculated O 1s core excitation spectra for differently coordinated oxygen are found to allow a clear discrimination between the different oxygen species and can be used to explain the experimental O K-edge NEXAFS spectrum for vanadia/SBA-15. As an example we consider the $\text{V}_2\text{Si}_6\text{O}_{14}\text{H}_6$ cluster of Fig. 7b which simulates particles containing dimeric vanadia units and offering four different oxygen species indicated in Fig. 8, singly coordinated O(1) of the vanadyl groups $\text{V}=\text{O}(1)$ as well as doubly coordinated O(2) in bridging $\text{V}-\text{O}(2)-\text{V}$, $\text{V}-\text{O}(2)-\text{Si}$, and $\text{Si}-\text{O}(2)-\text{Si}$ groups. Fig. 8 shows theoretical O 1s excitation spectra from the different

oxygen species revealing considerable variations. The spectral contributions due to core excitations at vanadyl oxygen O(1) and oxygen O(2) bridging two vanadium atoms are focused energetically in the region below 534 eV. The excitation spectrum of the vanadyl oxygen is characterized by a large peak centered at 530.7 eV with a much smaller low energy shoulder while the spectrum due to V-O(2)-V bridging oxygen presents a more complex broad peak structure between 530 and 533 eV. The excitation spectrum related to oxygen bridging between vanadium and silicon, denoted by V-O(2)-Si in Fig. 8 and attributed to the vanadia-silica interface, is described by a smaller two-peak structure of 2 eV separation centered near 531 eV and a much larger two-peak structure above 535 eV. Finally, the excitation spectrum of oxygen bridging between silicon, denoted by Si-O(2)-Si in Fig. 8 and connected with the silica support, contributes a broad multi-peak structure above 535 eV near the excitation threshold.

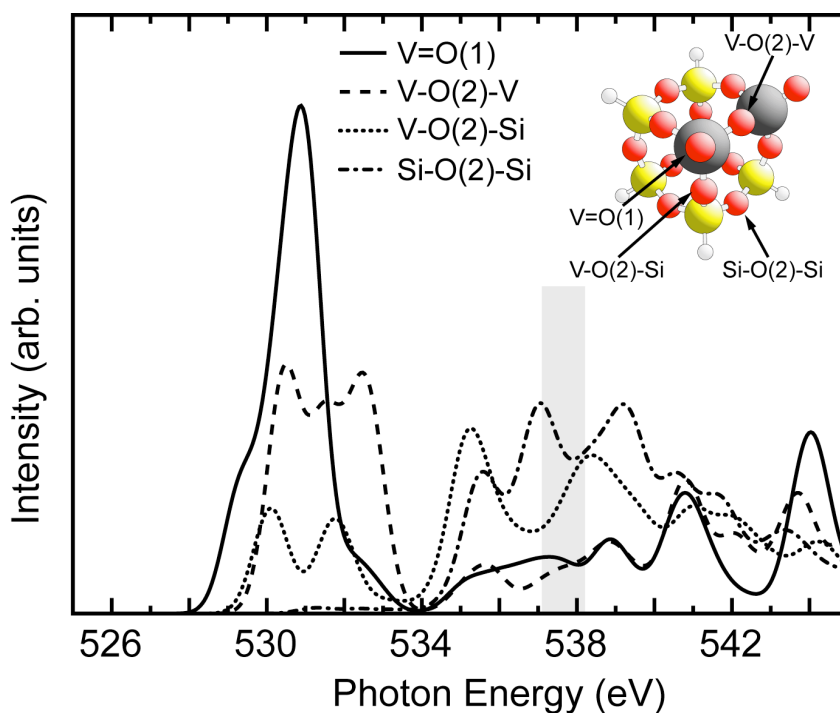


Fig. 8. Theoretical O 1s excitation spectra calculated for four different oxygen species, V=O(1), V-O(2)-V, V-O(2)-Si, and Si-O(2)-Si, of the dimer cluster $V_2Si_6O_{14}H_6$, see Fig. 7b. The light gray vertical block indicates the energy range of the computed ionization potentials of the different oxygen sites.

Altogether, the spectral contributions due to O 1s core excitation provide an obvious distinction between differently coordinated and differently binding oxygen species. This allows a clear spectroscopic discrimination in the O K-edge NEXAFS spectrum. In particular, the theoretical data indicate strongly that spectral intensity near 533 eV could be attributed to bridging V-O(2)-V species characterizing non-monomeric vanadia groups and may, thus, be used to identify different vanadia by O K-edge NEXAFS experiments.

The present theoretical results are used to interpret the NEXAFS spectra obtained in project B2 for corresponding model catalysts. Fig. 9 shows in its upper part (full line) a measured NEXAFS spectrum of SBA-15 supporting surface vanadia species with a weight loading of 2.7 wt% V (0.7 V/nm^2). For comparison, Fig. 9 includes in its lower part theoretical O 1s core excitation spectra from the model clusters (a) to (h) of different stoichiometry and geometry. Based on the theoretical analysis, the broad asymmetric peak observed in the experimental spectrum between 526 eV and 534 eV is clearly due to oxygen 1s core excitations in the vanadia particles. Spectral intensity from oxygen core excitations at singly coordinated V=O, typical for monomeric vanadia species (cluster (a)), are found to focus in a rather small energy region about 530.7 eV which agrees very nicely with the location of the central asymmetric peak in the experimental O K-edge NEXAFS spectrum, see Fig. 9. (Note that the energy scales applied in theory and in experiment have not been calibrated against each other.) However, a

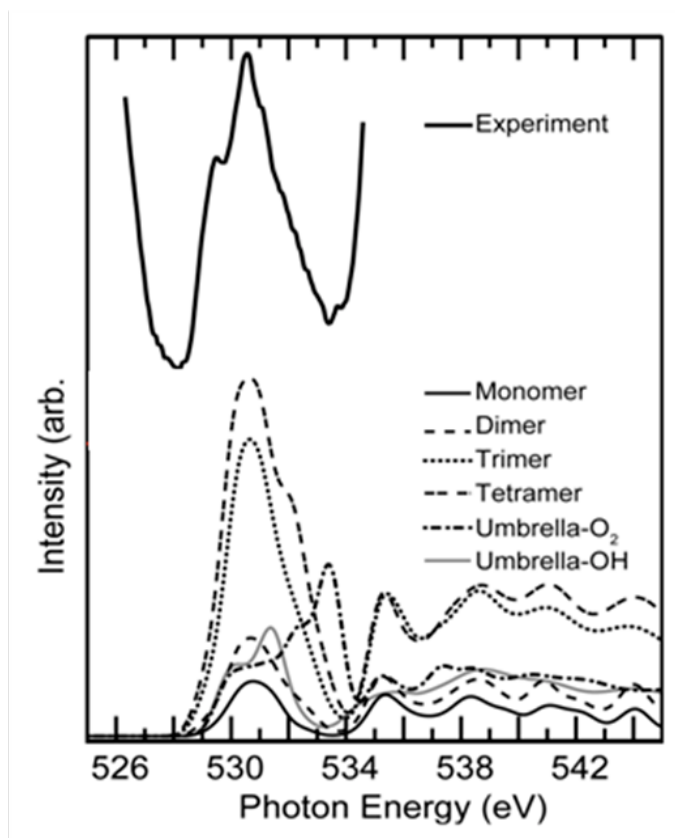


Fig. 9. Comparison of the experimental NEXAFS spectrum of SBA-15 with vanadia particles (2.7% V weight loading) with theoretical O 1s core excitation spectra of the different model clusters shown in Fig. 7, clusters (a) monomer, (b) dimer, (e) trimer, (f) tetramer, (g) umbrella-O₂, (h) umbrella-OH. All theoretical spectra have been normalized according to the total number of oxygen centers in the clusters, see [CHK09].

full explanation of the experimental spectrum must include also contributions from oxygen core excitations at V-O(2)-V bridges, characteristic of non-monomeric vanadia species. These contributions are located at higher energies and extend over a wider range compared with those of vanadyl oxygen excitations which can explain the asymmetric shape of the main peak found in experiment. Thus, the present theoretical results suggest that a successful interpretation of the experimental O K-edge NEXAFS spectrum requires the coexistence of different vanadia species beyond monomeric vanadia considered earlier [8].

(b.2) Molybdenum oxide particles

Molybdenum oxide is catalytically active in a wide range of different organic reactions including oxidation, hydrogenation, metathesis, and isomerization that require both redox and acid-base functions. Aiming at an improved fundamental understanding of oxidation catalysis, supported molybdena species have been widely studied in their structural and electronic behavior, see e.g. [11]. In this work we perform density-functional theory (DFT) calculations using the gradient-corrected RPBE functional on oxygen 1s core excitations in clusters representing bulk MoO₃ substrate as well as in molybdena-silica model clusters simulating local sections of supported molybdena catalysts. The theoretical excitation spectra are then compared with in situ X-ray absorption fine structure (NEXAFS) measurements near the oxygen K-edge of molybdena model catalysts supported by SBA-15 silica in order to identify structural and electronic details of the molybdena species [GHH11].

Fig. 10 shows geometric structures of the nine clusters considered in the calculations on SiO₂ supported vanadia particles, where the Mo centers of the molybdena units are coordinated differently with respect to their oxygen neighbors. Clusters (a) to (c) refer to tetrahedrally coordinated dioxo MoO₄ units, clusters (d) – (f) include octahedrally coordinated MoO₆ units, and clusters (g) – (i) contain pentahedrally coordinated MoO₅ units. These clusters are used to discriminate between differently binding oxygen, in molybdenyl Mo=O as well as in Mo-O-Mo, Mo-O-Si, Mo-OH, and Si-O-Si bridges of the silica-supported molybdena species. They also offer the possibility to identify specifically coordinated molybdena species amongst those prepared in project B2 experimentally at the surface of mesoporous silica, SBA-15. Reference calculations on molybdena environments in bulk MoO₃ substrate are based on a Mo₇O₃₀H₁₈ cluster describing a local section of a (010) oriented bilayer in the orthorhombic crystal. Dangling Mo-O bonds at the cluster periphery are saturated by hydrogen to account for cluster embedding.

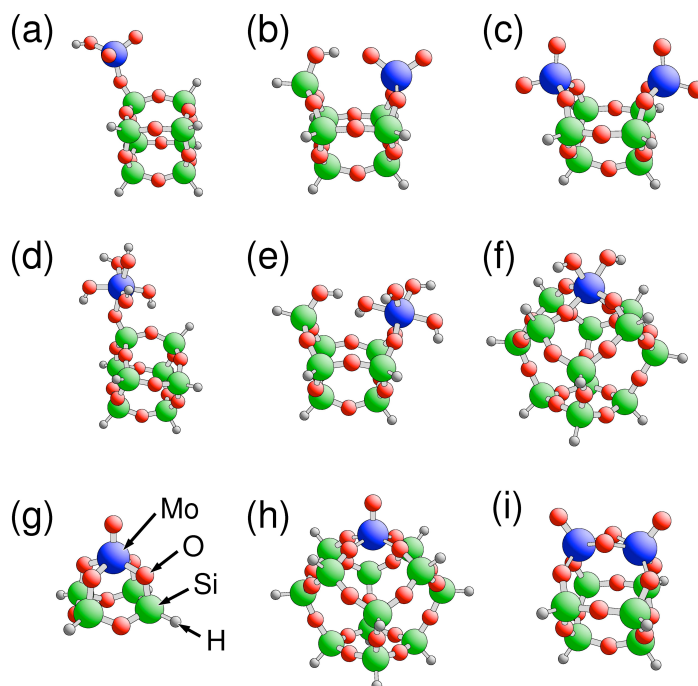


Fig. 10. Clusters used to model silica-supported molybdena units, (a) – (c) tetrahedrally coordinated dioxo molybdena, (d) – (f) octahedrally coordinated molybdena, and (g) – (i) pentahedrally coordinated monooxo molybdena species. Atoms are shown by balls of different radii and labeled accordingly in (g).

The calculated O 1s core excitation spectra for the differently coordinated molybdena units are dominated by excitations O 1s to Mo 4d - O 2p and show characteristic differences which discriminate between the molybdena species. As an illustration, Fig. 11 shows corresponding spectra for model cluster (b) of Fig. 10 (tetrahedral MoO₄ unit), clusters (h) and (e) (pentahedral MoO₅ and octahedral MoO₆ units), as well as for the Mo₇O₃₀H₁₈ cluster representing bulk MoO₃. First, we mention that the theoretical bulk spectrum, with a broad asymmetric main peak at 530.5 eV and less pronounced structures above 533.5 eV, agrees quite nicely with the experimental NEXAFS spectrum measured for bulk MoO₃ (not shown in Fig. 11). The bulk spectrum looks distinctly different from the spectra of all supported molybdena particles. The smallest, yet significant difference appears for particles with octahedral MoO₆ units. This may be explained by the fact that molybdena units in bulk MoO₃ form also distorted octahedra. In contrast, the calculated O 1s core excitation spectrum of pentahedrally coordinated MoO₅ units yields a pronounced double-peak structure with a low-energy shoulder and tetrahedrally coordinated MoO₄ units result in a clear double peak structure.

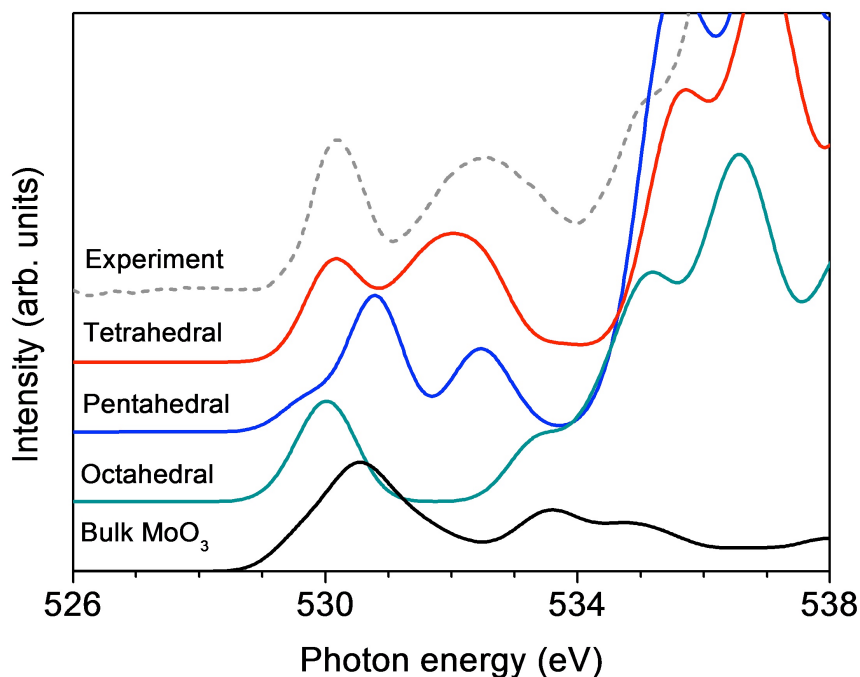


Fig. 11. Comparison of theoretical O 1s core excitation spectra for $\text{MoO}_x/\text{SiO}_2$ clusters reflecting tetrahedral (cluster (b) of Fig. 10), pentahedral (cluster (h)), and octahedral (cluster (e)) molybdenum coordination. The figure includes also the corresponding theoretical spectrum for MoO_3 bulk ($\text{Mo}_7\text{O}_{30}\text{H}_{18}$ cluster). The dashed line shows experimental O K-edge NEXAFS data for dehydrated $\text{Mo}_x\text{O}_y/\text{SBA-15}$ with 11.1 wt% Mo.

The experimental O K-edge NEXAFS spectrum for dehydrated $\text{Mo}_x\text{O}_y/\text{SBA-15}$ with 11.1 wt% Mo [GHH11], obtained in project B2 and included in Fig. 11 (dashed line), exhibits a pronounced double-peak structure in the O 1s to Mo 4d - O 2p excitation range of 529 - 536 eV. Obviously, this agrees most convincingly with the theoretical spectrum of tetrahedrally coordinated dioxo MoO_4 units. Thus, the comparison between theory and experiment can be interpreted by dioxo molybdena species with tetrahedral MoO_4 units characterizing the molybdena particles of the model catalyst under the chosen preparatory conditions. This does not fully exclude species with other Mo coordination, like pentahedral. However, the latter are believed to exist in the present samples in much smaller amounts.

References

- [1] G. Busca, L. Lietti, G. Ramis, and F. Berti, *Appl. Cat. B – Env.* 18 (1998) 1.
- [2] cp. K. Hermann, CH. 18 in “Computational Methods in Catalysis and Materials Science”, IDECAT Course book series, P. Sautet and R. van Santen Hrsg.), Wiley-VCH, Weinheim (2008), ISBN 978-3-527-32032-5, pp. 375.
- [3] H. Jonsson, G. Mille, K.W. Jacobson, in *Classical and Quantum Dynamics in Condensed Phase Simulations*, B.J. Berne, G.Ciccotti, D.F. Coker (Eds.), World Scientific, Singapur 1998.

- [4] G. Ramis, L. Yi, and G. Busca, *Catal. Today* 28 (1996) 373.
- [5] R.-M. Yuan, G. Fu, X. Xu, H.-L. Wan, *PCCP*, 13 (2011) 453.
- [6] M. Anstrom, N.-Y. Topsøe, J.A. Dumesic, *Journal of Catalysis*, 213 (2003) 115.
- [7] S. Soyer, A. Uzun, S. Senkan, I. Onal, *Catalysis Today*, 118 (2006) 268.
- [8] G. Deo, I. E. Wachs, and J. Haber, *Crit. Rev. in Surf. Chem.* 4 (1994) 141.
- [9] N. Magg, B. Immaraporn, J. B. Giorgi, T. Schroeder, M. Bäumer, J. Döbler, Z. L. Wu, E. Kondratenko, M. Cherian, M. Baerns, P. C. Stair, J. Sauer, and H. J. Freund, *J. Catal.* 226 (2004) 88.
- [10] J. Döbler, M. Pritzsche, and J. Sauer, unpublished.
- [11] J.-M. Jehng, H. Hu, X. Gao, and I.E. Wachs, *Catal. Today* 28 (1996) 335.

5.2.2 Projektrelevante eigene Publikationen

a) erschienene oder angenommene Arbeiten in wissenschaftlichen Zeitschriften oder Buchveröffentlichungen

- [CHK09] M. Cavalleri, K. Hermann, A. Knop-Gericke, M. Hävecker, R. Herbert, C. Hess, A. Oesterreich, J. Döbler, R. Schlögl
Analysis of Silica-Supported Vanadia by X-ray Absorption Spectroscopy: combined theoretical and experimental studies
J. Catal. **262** (2009) 215.
- [HCH09] M. Hävecker, M. Cavalleri, R. Herbert, R. Follath, A. Knop-Gericke, C. Hess, K. Hermann, R. Schlögl
Methodology of the Structural Characterization of V_xO_y Species Supported on Silica under Reaction Conditions by Means of in Situ O K-edge X-ray Absorption Spectroscopy
Phys. Stat. Solidi (b) **246** (2009) 1459.
- [SJH09] X. Shi, H. Jiao, K. Hermann, J. Wang
CO Hydrogenation Reaction on Sulfided Molybdenum Catalysts
J. Mol. Catal. A: Chemical 312 (2009) 7.
- [SWH10a] X. Shi, J. Wang, K. Hermann
Theoretical Cluster Studies on the Catalytic Sulfidation of MoO_3
J. Phys. Chem. C **114** (2010) 6791.
- [SWH10b] X. Shi, J. Wang, K. Hermann
CO and NO adsorption and dissociation at the β - $Mo_2C(0001)$ surface: A density-functional theory study
J. Phys. Chem. C **114** (2010) 13630.

- [GHH11] C. Guo, K. Hermann, M. Hävecker, L. J. Gregoriades, J. Sauer, A. Trunschke, R. Schlögl
Structural Analysis of Silica-Supported Molybdena: combined theoretical and experimental studies
J. Phys. Chem. C (2011) : ms jp2034642, in print.
- [GH11] M. Gruber and K. Hermann, in preparation; M. Gruber, PhD thesis, Free University Berlin, 2011, submitted.
- [H11] K. Hermann
Crystallography and Surface Structure, an introduction for surface scientists and nanoscientists
Wiley-VCH, Berlin 2011, ISBN 978-3-527-41012-5, book.

5.3 Rückblick auf die Förderung

Das Teilprojekt wurde seit 07/99 im Sonderforschungsbereich gefördert. Es wurde mit Ablauf der 4. Förderperiode im Juni 2011 beendet.

5.3.1 Personal im Teilprojekt während der zu Ende gehenden Förderperiode

	lauf. Nr.	Name, akademischer Grad, Dienststellung	engere Fachzugehörigkeit	Institut der Hochschule oder der außeruniv. Einrichtung	Mitarbeit im Projekt Zeitraum Wochenstunden	Entgeltgruppe
Grundausstattung						
Wissenschaftlerinnen und Wissenschaftler	1.	Hermann, Klaus, Prof. Dr., MPG-Forschungsgruppenleiter	Theoret. Physik	FHI, FU Berlin	07/1999 – 06/2011, 10h	
	2.	Gruber, Mathis Dipl. Phys., Doktorand	Theoret. Physik	FHI	08/2007 – 06/2011, 20h	
	3.	Shi, Xuerong Dipl. Chem., Doktorandin	Theoret. Chemie	FHI, CAS	11/2007 – 12/2009	
nichtwissenschaftl. Mitarbeiterinnen und Mitarbeiter						
Ergänzungsausstattung						
Wissenschaftlerinnen und Wissenschaftler	1.	Cavalleri, Matteo Dr., wissenschaftlicher Mitarbeiter	Theoret. Physik	FHI	01/2008 – 08/2008, 39h	E13
	2.	Guo, Chunsheng Dr., wissenschaftlicher Mitarbeiter	Theoret. Physik	FHI	08/2010 – 06/2011, 39h	E13
nichtwissenschaftl. Mitarbeiterinnen und Mitarbeiter						

Aufgaben der Mitarbeiterinnen und Mitarbeiter (Grundausrüstung):

1. Prof. Dr. Klaus Hermann
Wissenschaftliche und organisatorische Leitung des Teilprojekts, Anleitung der Doktoranden und der Mitarbeiter. Mitarbeit bei der Planung der theoretischen Untersuchungen, bei methodischen Entwicklungen und bei der Auswertung der Ergebnisse.
2. Dipl. Phys. Mathis Gruber
Der Doktorand hat neben methodischen Erweiterungen Modelluntersuchungen der Adsorption kleiner Moleküle, insbesondere NH_x , C_xH_y an V_2O_5 -Oberflächen, weitergetrieben. Zusätzlich hat er sich ausführlich mit Rechnungen an Clustermodellen zu einfachen Reaktionsschritten dieser Moleküle befasst, insbesondere der selektiven katalytischen Reduktion (SCR) von NO_x mit NH_3 , die wesentlicher Bestandteil seiner Dissertation ist. Herr Gruber hat seine Arbeit an der FU Berlin eingereicht und wird gegen Ende 2011 promovieren.
3. Dipl. Chem. Xuerong Shi
Die Doktorandin hat, teilweise in Zusammenarbeit mit Herrn Gruber, Modellrechnung zur Stabilität und Adsorption, sowie Reaktion kleiner Moleküle an komplexen Oxid-, Sulfid- und Karbidoberflächen des Molybdäns durchgeführt. Sie war als Doktorandin des Instituts für Kohlechemie der Chinesischen Akademie der Wissenschaften in Shanxi Mitarbeiterin im Teilprojekt und hat nach ihrer Rückkehr nach China im März dort 2010 promoviert.

Aufgaben der Mitarbeiterinnen und Mitarbeiter (Ergänzungsausrüstung):

1. Dr. Matteo Cavalleri
Der Postdoktorand hat sich hauptsächlich mit der Entwicklung von Methoden und der Durchführung von Berechnungen röntgenspektroskopischer Parameter aus Clustermodellen beschäftigt. Dies betraf insbesondere die Ermittlung von theoretischen NEXAFS-Spektren an Molybdän- und Vanadiumoxidoberflächen, sowie an kleinen VO_x -Teilchen auf SiO_2 -Substrat, die die Aufklärung experimenteller Spektren aus TP B2 wesentlich unterstützten.

2. Dr. Chunsheng Guo

Der Postdoktorand hat als Nachfolger von Dr. Cavalleri die Berechnung röntgenspektroskopischer Parameter aus Clustermodellen weitergeführt. Dabei hat er insbesondere Untersuchungen zur theoretischen NEXAFS bei kleinen MoO_x - und TiO_x -Teilchen auf SiO_2 -Substrat durchgeführt. Diese konnten wesentliche Details der im TP B2 gemessenen Spektren von Modellkatalysatoren der Familie $\text{MoO}_x/\text{SBA-15}$ bzw. $\text{TiO}_x/\text{SBA-15}$ erklären.

5.1 Allgemeine Angaben zum Teilprojekt C8

5.1.1 Titel: Structure determination of VO_x and related surfaces, thin films and interfaces based on scanned-energy mode photoelectron diffraction

5.1.2 Projektleitung

Prof. David Phillip Woodruff
geb. 12.05.1944

Prof.Dr. Joachim Sauer
geb. 19.04.1949

Physics Department,
University of Warwick,
Coventry CV4 7AL, U.K.

Institut für Chemie
Humboldt Universität zu Berlin,
Unter den Linden 6
10099 Berlin

Telefon: 00 44 24 76523378
Telefax: 00 44 24 76692016
E-Mail: d.p.woodruff@warwick.ac.uk

030 20937135
030 20937136
js@chemie.hu-berlin.de

5.2 Entwicklung des Teilprojekts

5.2.1 Bericht

Gaining a quantitative understanding of the structure of surfaces, including adsorbate species on surfaces, is a key step in understanding many aspects of their electronic and chemical properties, and provides an important test of theoretical modelling. While there are many such studies of metal and semiconductor surfaces, there remains a remarkable dearth of equivalent information on oxide surfaces. The aim of this subproject is to address this problem, particularly with regard to the surfaces and interfaces of VO_x and related surfaces, notably TiO₂. The primary method being used is scanned-energy mode photoelectron diffraction (PhD), a technique developed by a Warwick (Woodruff)/Berlin (Bradshaw) collaboration since the late 1980s, prior to Alex Bradshaw's move to the IPP in Garching in 1999. This technique has been used by this group, through experimental studies using the BESSY synchrotron radiation facility in Berlin, to determine the structure of some 80 surface adsorbate phases. A particular strength of this work is that it is ideally-suited to studies of the local geometry of the light elements C, N and O in the adsorbate layer, and so is especially effective for the investigation of the adsorption structure of chemically-relevant small molecules on surfaces.

The method provides quantitative *local* structural information (adsorption site and bondlengths) which is both *element-specific* and *chemical-state-specific*.

Subproject C8 was initiated in mid-2002 to explore the use of the PhD technique to gain quantitative structural information of appropriate model surface problems of potential relevance to the chemistry of VO_x surfaces. Since that time a Sfb-funded postdoctoral researcher has been based in Berlin with office and laboratory space provided by the Chemical Physics Department of the Fritz Haber Institute (Prof. Freund), working in collaboration with an FHI-funded student and other UK-funded researchers based at the University of Warwick who participate in the experiments at BESSY. Aspects of the oxide-based science programme of the SFB have also been integrated into the Warwick-based studies of other UK-funded graduate students and postdocs.

During the last three years studies have focused on two general areas, namely the determination of the local structure of molecular adsorbates on the rutile $\text{TiO}_2(110)$ surface, and continued efforts to understand the structure of the $\text{V}_2\text{O}_3(0001)$ surface, as detailed below.

The local structure of molecular adsorbates on $\text{TiO}_2(110)$

Perhaps the most ubiquitous and significant adsorbate on oxide surfaces is the hydroxyl species, generally formed as a result of reaction with water in the vapour phase or at a solid/liquid interface. In fact a perfect (defect-free) $\text{TiO}_2(110)$ surface appears to be unreactive to liquid water, but there is considerable evidence from STM and DFT studies that at bridging-oxygen vacancy sites on the surface water dissociated to fill the vacancy with an hydroxyl species, with the H atom that is released hydroxylating an adjacent bridging oxygen atom. Despite this qualitative understanding, there has been no quantitative structural investigation of such a hydroxylated TiO_2 surface. The PhD technique is ideally-suited to such an investigation, because there is a sufficiently large (~ 1.6 eV) chemical shift between the O 1s photoelectron binding energies of oxygen atoms in the surface hydroxyl species and of the oxygen atoms in the underlying oxide. Indeed, our group has identified the local

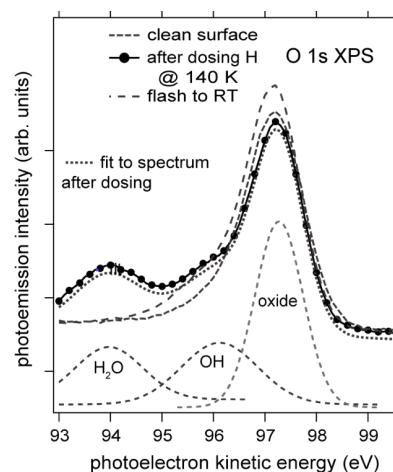


Fig. 1
O 1s photoemission spectrum of the Clean and hydroxylated $\text{TiO}_2(110)$ surface following H exposure

structure of these hydroxyl species on $\text{TiO}_2(110)$ created by atomic hydrogen released through reaction with carboxylic acids (notably formic acid and glycine), but in these cases the local geometry may be influenced by the presence of the coadsorbed carboxylate species. While

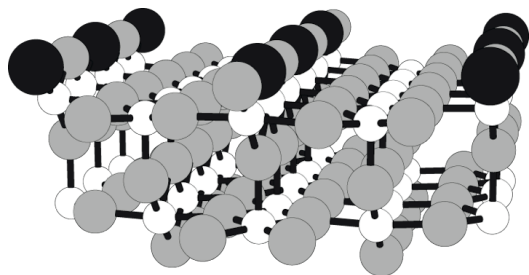


Fig. 2
Schematic diagram of the hydroxylated $\text{TiO}_2(11)$ surface: the hydroxylated O atoms are shown in a darker shading with the H atoms omitted

surface hydroxyl species are formed on a defected $\text{TiO}_2(110)$ surface through reaction with molecular water, the surface concentration achievable is low (a few % of a monolayer), but a higher coverage may be obtained by exposing the surface to atomic hydrogen produced by a thermal gas cracker. As shown above (Fig. 1), the O 1s spectrum from a surface dosed in this way at low temperature contains peaks from coadsorbed OH and molecular water (adsorbed from the gas phase), and the

spectrum recorded after briefly heating to desorb the water. O 1s PhD spectra recorded from the OH species confirm that the associated O atoms are in bridging sites as expected (Fig. 2). Optimisation of the agreement between the experimental PhD spectra and the results of multiple-scattering calculations for different model structures was greatly aided by parallel DFT calculations performed by the A4 group (Sauer/Sierka) which yielded values for the subsurface relaxations; starting from these values an optimised structure was obtained that was closely similar to that obtained from the DFT calculations. In particular, while the hydroxylation of the surface bridging oxygen atoms has very little influence on these near-surface relaxations, the Ti-O_{OH} surface bond is found to be significantly longer (by 0.10-0.15 Å) than that of $\text{Ti-O}_{\text{bridging}}$ bonds on the clean surface. The schematic figure shows these O_{OH} atoms as larger black circles with 0.5 ML coverage. A report of the results of this work has recently been submitted to Physical Review B as a joint C8/A4 publication [1].

The PhD technique has also been used to investigate the local structure of some larger molecules adsorbed on $\text{TiO}_2(110)$. In particular, an investigation of the interaction with the simple amino acid, glycine, reveals that the acid is deprotonated and bonds to the surface in a ‘standing-up’ orientation bridging neighbouring 5-fold-coordinated surface Ti atoms such that the two O atoms are located closed to atop these Ti atoms [TKK09]. Unlike its behaviour on metallic Cu surfaces, the amino N atoms do not form a bond to the surface. This difference can, at least in part, be attributed to steric effects, as adjacent Ti atoms rows on $\text{TiO}_2(110)$ are much more widely-spaced than Cu atom rows on either Cu(100) or Cu(110). Most recently

PhD data have also been collected from the surfaces formed by the reaction of azobenzene, and of aniline, on $\text{TiO}_2(110)$. The motivation is to gain a better understanding of the chemoselective reduction of nitroaromatics over TiO_2/Au which appears, on the basis of the work of Li and Diebold [2] to also occur on the $\text{TiO}_2(110)$ surface. Our results appear to support the contention that both reactants lead to a common phenyl imide adsorbate species, but a full structure determination has not yet been completed.

Most recently we have also been engaged in a collaboration with TP C1 regarding the structure of mixed $\text{Ti}_x\text{V}_{1-x}\text{O}_2$ films grown epitaxially. Detailed analysis of and modelling of PhD data from Ti 2p and V 2p photoemission is ongoing and is expected to lead to a joint publication in due course.

The structure of the $\text{V}_2\text{O}_3(0001)$ surface

A problem that has preoccupied us in this project has been the structure of the (0001) surface of ultra-thin epitaxial films of V_2O_3 grown on Pd(111) and Au(111) substrates by deposition of vanadium in a partial pressure of oxygen. There is clear evidence from vibrational spectroscopy that the surface contains vanadyl, $\text{V}=\text{O}$, species, and combined with STM images showing well-ordered (1x1) surfaces, it has been assumed that the surface of these films has a (1x1)-vanadyl termination. Indeed, our own PhD study of this surface (conducted in an earlier period of the SFB funding) concluded that such a structure was compatible with the experimental data, although a simple half-metal termination (i.e. without the atop O atoms of the vanadyl-terminated structure) was also compatible with the data. We should also note that, as there is no chemical shift between the V 2p and O 1s emission from the bulk and surface atoms, PhD is not ideally-suited to determine the structure of this clean surface. The inferred $\text{V}=\text{O}$ termination is at variance with the results of DFT calculations performed both by the Kresse group in Wien [3], but also within the subproject C5 [4,5], that predict the stable surface phase to be an oxygen-termination, possibly with *partial* coverage of vanadyl species.

As a first step to understand the local structure of adsorbates on this surface we investigated the hydroxylated surface, obtained (as in our more recent study of the hydroxylated TiO_2 surface) mainly by atomic hydrogen adsorption [KSA08]. A surprising result of this study is that the O_{OH} atoms on this hydroxylated surface are clearly *not* in sites atop surface V atoms, as would be expected if the O atoms of surface vanadyl species were hydroxylated. Indeed, this result emerges not only from the O_{OH} 1s PhD data, but also from estimates of the OH coverage achieved that was very significantly greater than one hydroxyl per (1x1) surface unit mesh.

Comparison of the PhD data with the results of multiple-scattering simulations led to the conclusion that, instead, it is O atoms in the outermost oxygen (O_3) atom layer of the underlying solid that are hydroxylated (Fig. 3). DFT calculations performed by the C6 group of Hermann provided some support for this view in indicating no major energetic advantage to hydroxylation of the vanadyl O atoms, and these results were included in the joint publication [KSA08]. Nevertheless, this result was sufficiently surprising that it was decided to undertake further checks on the predictions of the multiple scattering calculations that underpin the PhD data interpretation. In particular, these calculations indicate that if the O atom of a vanadyl species is the photoelectron emitter, and the O 1s PhD is measured along the V-O axis (perpendicular to the surface for a vanadyl species on $V_2O_3(0001)$) then a strong long-period (in electron momentum) modulation should be clearly detectable. It is the absence of any such feature that provides the clearest indication that it is not the vanadyl O atoms that are hydroxylated.

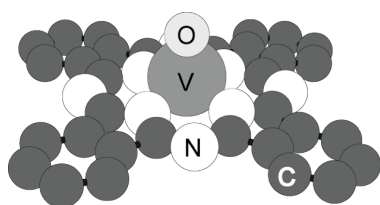


Fig. 4. The VOPc species

adsorbed on Au(111). As shown Fig. 4, the V-O axis in this molecule lies perpendicular to the approximately planar phthalocyanine surroundings, and previous STM studies had confirmed the expected 'lying-flat' orientation of the molecular monolayer on Au(111). The coverage of V=O species is low (~ 0.015 ML) but adequate normal emission PhD data could be obtained from both the O 1s and V 2p emission peaks. Comparison (Fig. 5) of these experimental PhD data with the results of

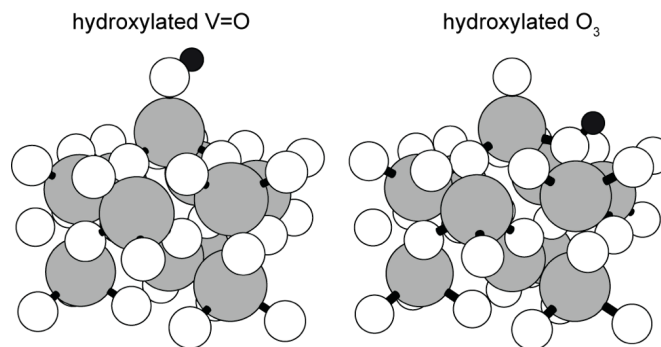


Fig. 3. Schematic diagrams of the $V_2O_3(0001)$ surface showing hydroxylated V=O and surface O_3 species

of theoretical simulations for the optimized surface geometry

To test this in an independent fashion, we measured PhD from the vanadyl phthalocyanine (VOPc) species

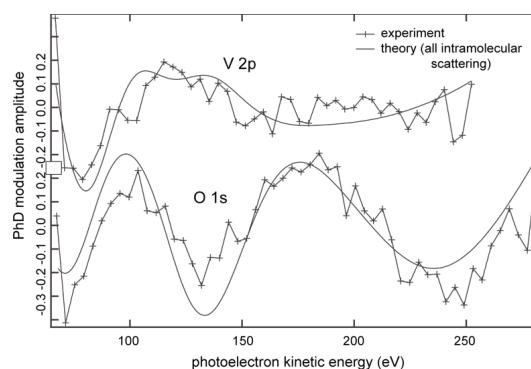


Fig. 5. Comparison of V 2p and O 1s PhD experimental spectra with the results of theoretical simulations for the optimized surface geometry

multiple scattering simulations (assuming the V-O points out from the surface) show excellent agreement [DUH10]. Notice, in particular, that the O 1s PhD shows the expected strong single-period modulations characteristic of the 180° backscattering from the neighbouring V atom. In the light of the absence of any similar effect in the measurements from the hydroxylated V_2O_3 surface, these results thus provide further confirmation of the fact that vanadyl O atoms are not hydroxylated on the oxide surface. Coincidentally, these experiments also provide confirmation of previous suggestions that the V-O direction for adsorbed VOPc on Au(111) is outwards from the surface, and not inwards towards the surface (as does occur in some other adsorbed Pc species). The results also cast some light of minor conformational changes in the VOPc as a result of the adsorption.

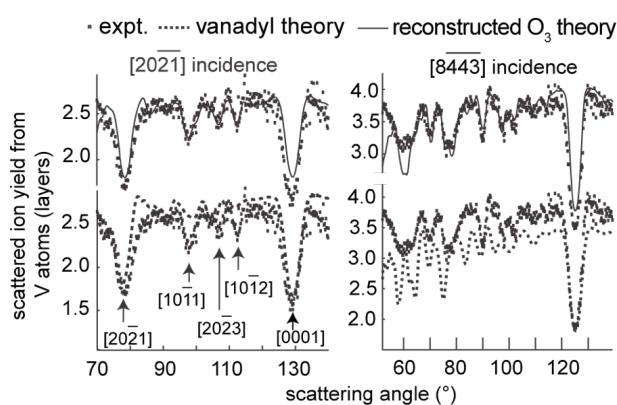


Fig. 6. Comparison of experimental MEIS blocking curves with simulations for the best-fit models based on the vanadyl and reconstructed O_3 termination models

Of course, a key piece of information that is generally a prerequisite for structural studies of adsorbates on surfaces is a knowledge of the clean surface structure. As stated above, our attempts to establish this structure using PhD led to some ambiguity, so we decided to explore a quite different method, namely medium energy ion scattering (MEIS), using the UK national facility in Daresbury. In part, this study was also undertaken in order to check on the quality of the $V_2O_3(0001)$ films grown on Pd(111) and Au(111) that had formed the basis of all of our work; MEIS provides subsurface crystallographic information not available to standard surface methods such as LEED, STM, PhD etc. The technique provides crystallographic information on the bulk through the 'shadowing' of subsurface atoms by near-surface atoms when the incidence is aligned along bulk crystallographic directions. The results of these MEIS studies provided clear confirmation of the good crystalline quality of films grown on these substrates, with thicknesses up to 200 \AA in Au(111). In addition, however, this same elastic-scattering shadowing effect can be exploited in the outgoing ion trajectories, when near-surface

Of course, a key piece of information that is generally a prerequisite for structural studies of adsorbates on surfaces is a knowledge of the clean surface structure. As stated above, our attempts to establish this structure using PhD led to some ambiguity, so we decided to explore a quite different method, namely medium energy ion scattering (MEIS), using the UK national

Of course, a key piece of information that is generally a prerequisite for structural

atoms can ‘block’ ions scattered by subsurface atoms from reaching the detector. Measurement of ‘blocking curves’ – the scattered ion signal as a function of scattering angle – can thus provide information on the surface structure. Experimentally-measured blocking curves are compared with the results of simulations for different model structures using the VEGAS code developed at the AMOLF institute in Amsterdam some years ago. In the case of the $V_2O_3(0001)$ data, the results of these comparisons showed very poor agreement for both the half-metal and (1x1)-vanadyl termination structures (the vanadyl simulations are included in Fig. 6). However, very good agreement was obtained for a previously untested model, namely the reconstructed O_3 termination first identified in the DFT calculations of Kresse *et al.* [3], but also found in the calculations of sub-project C5 [4]. As shown in Fig. 7, in this model the upper half of the second-layer metal atoms are displaced upwards (as shown by the arrow) into the outermost metal layer, creating a termination of the form $O_3V_3O_3$ – resulting in a stoichiometry and local structure closely similar to that of VO_2 . This is actually the structure that is also found, in the DFT calculations, to be in equilibrium with the gas phase under conditions similar to those used in the preparation of the oxide films. Of course, this structure does not have surface vanadyl species and thus is apparently inconsistent with the data from vibrational spectroscopies. However, the DFT calculations do indicate that the preparation conditions correspond to an oxygen chemical potential close to a calculated boundary between this (1x1) O_3 -reconstruction, and a second phase in which the same structure has *partial* (0.33 ML in the calculation) coverage of $V=O$ species. This partial coverage would also be consistent with the results of the vibrational spectroscopy.

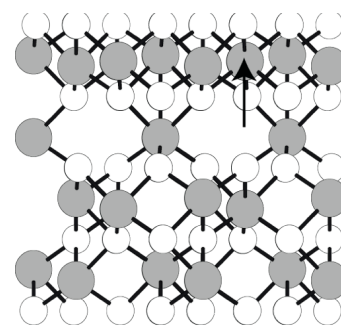


Fig. 7
Schematic diagram of the reconstructed O_3 termination model of the $V_2O_3(0001)$ surface

Interestingly, in earlier work in the Sfb the group of Horst Niehus (subproject C2, which terminated in 2008) had recorded low energy ion scattering data from this surface and argued, on the basis of a qualitative analysis, that these data were also consistent with a (1x1)- $V=O$ terminated surface. While these results were also based on ion scattering, the technique used (low-energy impact collision ion scattering spectroscopy with detection of neutrals – NICISS) is very substantially different in detail and uses 3 keV He^+ incident ions (compared with 100 keV H^+ ions in the MEIS studies). We therefore established a new collaboration with this group who conducted quantitative analysis of their old data, including evaluating the O_3 -

reconstruction model. The results proved to be entirely consistent with those of the MEIS

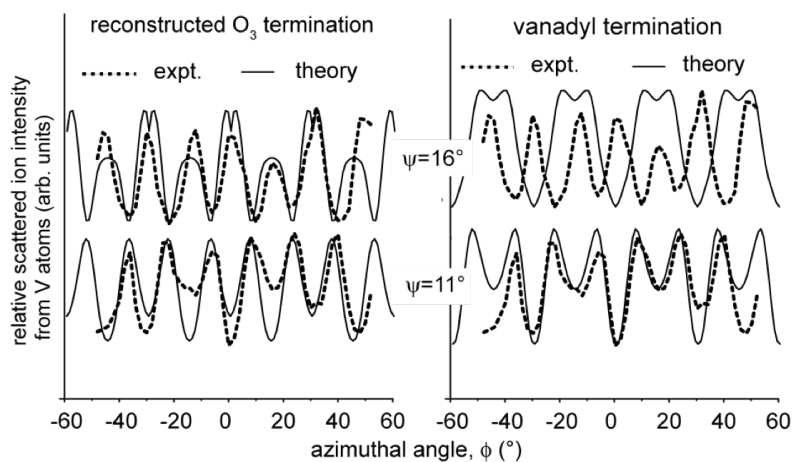


Fig. 8.

Comparison of NICISS experimental data from the $V_2O_3(0001)$ surface with simulations for structural models based on the O_3 -reconstruction and vanadyl termination models

Notice, in particular, that at the angles corresponding to the experimental maxima at a grazing incidence of 11° , the curves show minima for incidence at 16° . This switching of maxima and minima is reproduced by the simulations for the O_3 reconstruction, but not for the vanadyl-termination (nor for a half-metal termination, not shown in the figure). These results have very recently been published in Physical Review Letters [WHS11]. A fuller report of the MEIS results, including a new presentation of the results of the DFT-derived surface phase diagram arising from the work of subproject C5 [4,5] is currently in preparation as a joint publication.

References

- [1] W. Unterberger, T. J. Lerotholi, E. A. Kröger, M. J. Knight, D. A. Duncan, D. Kreikemeyer-Lorenzo, K. A. Hogan, D. C. Jackson, M. Sierka, R. Włodarczyk, J. Sauer, D. P. Woodruff, Phys. Rev. B *submitted for publication*.
- [2] S-C.Li and U. Diebold, JACS 132 (2010) 64.
- [3] G. Kresse, S. Surnev, J. Schoiswohl, F. P. Netzer, Surf. Sci. 555 (2004) 118.
- [4] T.K. Todorova, M. V. Ganduglia-Pirovano, J. Sauer, J. Phys. Chem. **B 109** (2005) 23523.
- [5] T.K. Todorova, M. V. Ganduglia-Pirovano, J. Sauer, J. Phys. Chem. **C 111** (2007) 5141.

study, with simulations clearly being inconsistent with the $(1 \times 1)\text{-V=O}$ model, but showing good agreement with experiment for the O_3 reconstruction.

Fig. 8 shows these comparisons, corresponding to plots of the scattered ion intensity from surface vanadium atoms measured in specular reflection at two different grazing incidence angles as a function of the

5.2.2 Projektrelevante eigene Publikationen

a) erschienene oder angenommene Arbeiten in wissenschaftlichen Zeitschriften oder Buchveröffentlichungen

- [DUH10] D.A. Duncan, W. Unterberger, K.A. Hogan, T.J. Lerotholi, C.L.A. Lamont, D.P. Woodruff,
A photoelectron diffraction investigation of vanadyl phthalocyanine on Au(111)
Surf. Sci. **604** (2010) 47 - 53.
- [KSA08] E.A. Kröger, D. I. Sayago, F. Allegretti, M.J. Knight, M. Polcik, W. Unterberger, T.J. Lerotholi, K. A. Hogan, C.L.A. Lamont, M. Cavalleri, K. Hermann, D.P. Woodruff,
The local structure of OH species on the V₂O₃(0001) surface: a scanned-energy mode photoelectron diffraction study
Surf. Sci. **602** (2008) 1267 - 1279.
- [TKK09] T.J. Lerotholi, E.A. Kröger, M.J. Knight, W. Unterberger, K. Hogan, D.C. Jackson, C.L.A. Lamont, D.P. Woodruff,
Adsorption structure of glycine on TiO₂(110): a photoelectron diffraction determination
Surf. Sci. **603** (2009) 2305 - 2311.
- [WHS11] A.J. Window, A. Hentz, D.C. Sheppard, G.S. Parkinson, H. Niehus, D. Ahlbehrendt, T.C.Q. Noakes, P. Bailey, D.P. Woodruff,
The V₂O₃(0001) surface termination: phase equilibrium
Phys. Rev. Lett. **107** (2011) 016105.

5.3 Rückblick auf die Förderung

Das Teilprojekt wurde seit 07/2002 im Sonderforschungsbereich gefördert. Es wurde mit Ablauf der 4. Förderperiode im Juni 2011 beendet.

5.3.1 Personal im Teilprojekt während der 4. Förderperiode

	lauf. Nr.	Name, akademischer Grad, Dienststellung	engere Fachzugehörigkeit	Institut der Hochschule oder der außeruniv. Einrichtung	Mitarbeit im Projekt Zeitraum Wochenstunden	Entgeltgruppe
Grundausrüstung						
Wissenschaftlerinnen und Wissenschaftler	1.	David Phillip Woodruff, PhD, DSc., FRS, Professor	Physics	Dept. Physics, UW	07/2002 – 06/2011, 10h	
	2.	Sauer, Joachim, Prof. Dr.	Theoret. Chemie	HU-C	07/1999 – 06/2011, 1h	
	3.	Ts'enolo Lerotholi, PhD.	Physics	Dept. Physics, UW	02/2006 – 02/ 2009, 10h	
	4.	Dagmar Kreikemeyer-Lorenzo, PG research student	Physics	FHI, Abt. CP/AC	06/2008 – 06/2011, 40h	
	5.	David Duncan, PG research student	Physics	Dept. Physics, UW	10/2008 – 05/2011, 10h	
	6.	Amanda Window, PG research student	Physics	Dept. Physics, UW	10/2005 – 09/2009, 10h	
nichtwissenschaftl. Mitarbeiterinnen und Mitarbeiter						
Ergänzungsausrüstung						
Wissenschaftlerinnen und Wissenschaftler	1.	Unterberger, Werner, Dr., postdoctoral researcher	Physics	FHI, Abt. CP	11/2006 – 06/2011, 40h	E13
nichtwissenschaftl. Mitarbeiterinnen und Mitarbeiter						

Aufgaben der Mitarbeiterinnen und Mitarbeiter (Grundausrüstung):

1. Prof. Dr. David Phillip Woodruff
Overall scientific direction of sub-project C8
2. Prof. Dr. Joachim Sauer
Administration of finances
3. Ts'eno Lerotholi (Warwick-based)
Responsible for coordinating the Warwick-based component of the photoelectron diffraction structural programme including active participation in all experimental runs at BESSY (on both the SFB project and other systems) and providing some assistance on Sfb project data analysis
4. David Duncan (Warwick-based)
Active collaboration in all BESSY beamtime experiments and responsible for some data analysis, but mainly of adsorption systems falling outside the SFB
5. Dagmar Kreikemeyer-Lorenzo (Berlin-based)
Active collaboration in all BESSY beamtime experiments and responsible for detailed analysis of some of the data on the VO_x and TiO₂ systems within the SFB. Active collaboration in off-line characterisation prior to photoelectron diffraction runs at BESSY
6. Amanda Window (Warwick-based)
Primary responsibility for related ion scattering studies of V₂O₃ in the UK.

Aufgaben der Mitarbeiterinnen und Mitarbeiter (Ergänzungsausrüstung):

1. Dr. Werner Unterberger (Berlin-based)
Responsible for coordinating the Berlin-based (SFB-funded) component of the photoelectron diffraction structural programme including management of the photoelectron spectrometer system used in the experiments. Active participation in all experimental diffraction runs at BESSY and direction of off-line characterization of V₂O₃ and TiO₂ surface systems. Analysis of photoelectron diffraction data on these systems in collaboration with the Berlin-based student.

5.1 Allgemeine Angaben zum Teilprojekt C11

5.1.1 Titel: Untersuchungen der Eigenschaften von Übergangsmetalloxid-Oberflächen mittels streifender Ionen-Streuung

5.1.2 Projektleitung

Prof. Dr. Helmut Winter
geb. 30.09.1949

Institut für Physik
Humboldt-Universität zu Berlin
Newtonstraße 15
D-12489 Berlin

Telefon: 030 / 20937891
E-Mail: winter@physik.hu-berlin.de

5.2 Entwicklung des Teilprojekts

5.2.1 Bericht

Das Teilprojekt C11 wurde in der letzten Förderperiode des SFB546 aufgenommen und begann die Mitarbeit an den Projekten des SFBs im Juli 2008. Durch das Teilprojekt wurde als weitere Untersuchungsmethode der Oberflächen von Oxiden die streifende Streuung schneller Ionen und Atome eingebracht. Dabei haben sich die Arbeiten des Teilprojekts weitgehend auf die Bestimmung von Strukturen der Oberflächen von Oxiden und insb. ultradünnen Oxidfilmen konzentriert, Arbeiten zur reaktiven Streuung von Cs⁺-Ionen zur Bestimmung der Reaktivität von Oberflächenreaktionen wurden auf Empfehlung der Gutachter nicht realisiert.

Im Mittelpunkt der Vorhaben standen methodische Entwicklungen zur Untersuchung der geometrischen Struktur der Oberflächen von Oxidfilmen mittels schneller Atome und Ionen. Dabei spielten die während der Bearbeitung des Projekts entdeckten Beugungseffekte bei der Streuung schneller Atome (typische kinetische Energien von ca. 1 keV) eine wichtige Rolle, die eine sehr empfindliche Untersuchung der Struktur und Atompositionen der obersten Lagen eines Oxidfilms zu bestimmen gestatten. Im Mittelpunkt der untersuchten Systeme stand das System eines ultradünnen Siliziumoxidfilms auf einem Mo(112)-Substrat, dessen Struktur schon in früheren Förderperioden des SFBs546 eine wichtige Rolle gespielt hatte. Durch diverse

neue Untersuchungsmethoden, die im Rahmen der Arbeiten des Teilprojekts entwickelt wurden, konnten maßgebliche Beiträge bezüglich der Klärung der kontrovers diskutierten Strukturmodelle geleistet werden. Es wurde das von Gruppen im Sfb546 vorgeschlagene Strukturmodell eines 2D-Netzwerks für den Silica-Film bestätigt.

Einen weiteren Themenbereich, den wir während der Bearbeitung des Teilprojekts in das Programm aufgenommen haben, ist die Untersuchung von Realkatalysatoren mittels Rutherford-Back-Scattering (RBS). Die Anwendung dieser etablierten Untersuchungsmethode auf raue Proben gestattete, die Struktur und die Elementkonzentrationen von porösen $\text{TiO}_2/\text{V}_2\text{O}_5$ -Keramiken zu untersuchen.

Monolagen-Silica-Film auf Mo(112)

(in Zusammenarbeit mit TP B1 und C5)

Silica-Filme sind vor allem als Substrate für Übergangsmetalloxide von Bedeutung und wurden detailliert im Rahmen des Sfb546 untersucht. Basierend auf Arbeiten im TP B1 und C4 wurde ein 2D-Netzwerk-Modell (Abb.1, linkes Bild) vorgeschlagen, das im Einklang mit den experimentellen Befunden von IRAS und STM steht. Alternativ wurde ein Cluster-Modell (Abb.1, rechtes Bild) vorgeschlagen. In einem Review zur Thematik diskutieren Goodman und Chen diese Problematik und beschreiben die kontroversen Modelle als „an issue yet to be solved“ [1].

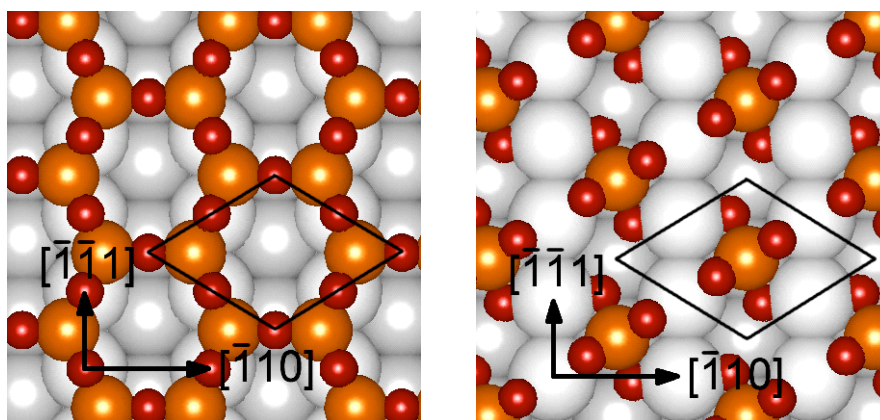


Abb. 1. Strukturmodell für ultradünne Silica-Filme auf Mo(112). Links: 2D-Netzwerk-Modell, rechts: Cluster-Modell.

Zunächst wurde dieses System mit der Ionenstrahl-Triangulation (IST) untersucht, bei der die erhöhte Elektronenemission für das axiale Channeling entlang niedrig indizierter Kristallrichtungen in der Oberfläche ausgenutzt wird. Bei der Detektion der Anzahl emittierter

Elektronen (entspricht der Höhe der Pulse eines Halbleiterdetektors) sinken die Ereignisse für geringe Elektronenzahlen ab, falls der Strahl schneller Atome entlang eines niedrig indizierten Kanals gestreut wird. In Abb. 2 sind diese Ereignisse als Funktion des azimuthalen Drehwinkels für das saubere Mo(112)-Substrat sowie für den SiO₂-Film auf Mo(112) aufgetragen. Die ausgeprägten Minima können niedrig indizierten Kristallrichtungen zugeordnet werden. Dabei erfolgte die Präparation der Filme in enger Kooperation mit den Teilprojekten B1 und C1 im Sfb. Die weiteren Kurven stellen Ergebnisse von Simulationsrechnungen auf der Basis der beiden Strukturmodelle dar, wobei das 2D-Netzwerk-Modell die Daten sehr gut beschreibt, während das Cluster-Modell die Daten nur bedingt reproduziert. Unsere Studien zur Klärung der Struktur von SiO₂/Mo(112) haben wir in Physical Review Letters publiziert [SBW09].

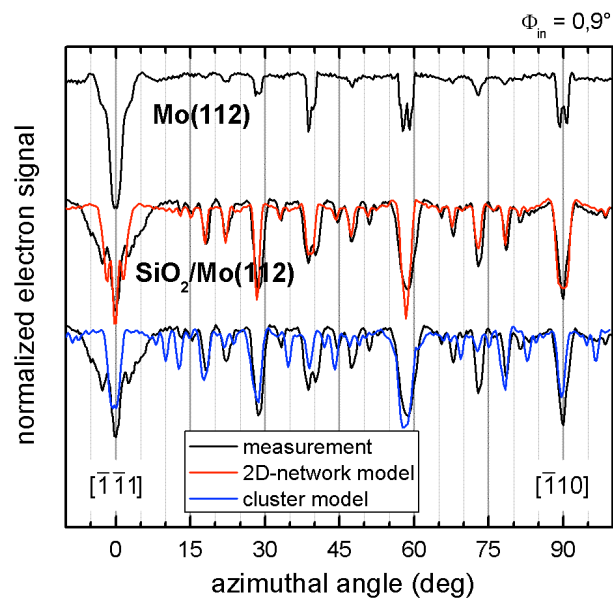


Abb. 2. Triangulationskurve der SiO₂/Mo(112)-Oberfläche mittels 25 keV Protonen. Schwarze Kurven: Experimentelle Daten für Mo(112) und SiO₂/Mo(112). Mittlere Kurven: Vergleich mit Simulationsrechnungen für 2D-Netzwerk-Modell, Untere Kurven: Vergleich mit Cluster-Modell.

Im Fortgang der Studien an diesem System gelang die Regenbogenstreuung im Regime des axialen Oberflächen-Channelings. Dazu wird die Winkelverteilung der gestreuten schnellen Atome mittels eines ortsauflösenden Detektors erfasst, die bei der Streuung an dem korrigierten Oberflächenpotential entlang axialer Atomketten in der Oberfläche ein Maximum der Winkelablenkung mit erhöhtem Wirkungsquerschnitt zeigt, dem sog. „Regenbogen“. Diese Intensitätsverteilung der gestreuten Atome konnten wir nutzen, um die Strukturmodelle in der obersten Atomlage sehr empfindlich zu testen. In Abb.3 ist eine entsprechende Winkelverteilung für die Streuung von 2 keV He Atomen entlang der [-1-11]-Richtung unter einem Einfallswinkel von 1.5° dargestellt.

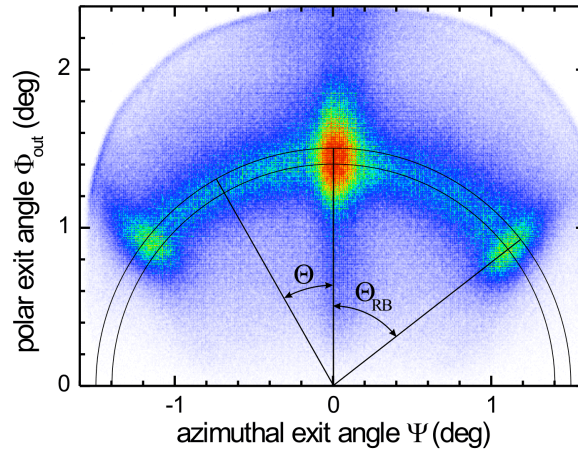


Abb. 3. 2D Intensitätsverteilung des ortsauflösenden Detektors für Streuung von 2 keV He-Atomen von einem ultradünnen Silica-Film auf Mo(112) unter einem Einfallswinkel von 1.5° .

In Abb.4 sind die Projektionen der Intensitäten in einem Kreisring (Energieerhaltung der axialen Bewegung) als Funktion des Ablenkwinkels Θ für die $[-1-11]$ - (linkes Bild) sowie die $[-201]$ -Richtung (rechtes Bild) gezeigt und mit den Ergebnissen von Simulationsrechnungen auf der Basis klassischer Trajektorien für die beiden Strukturmodelle verglichen.

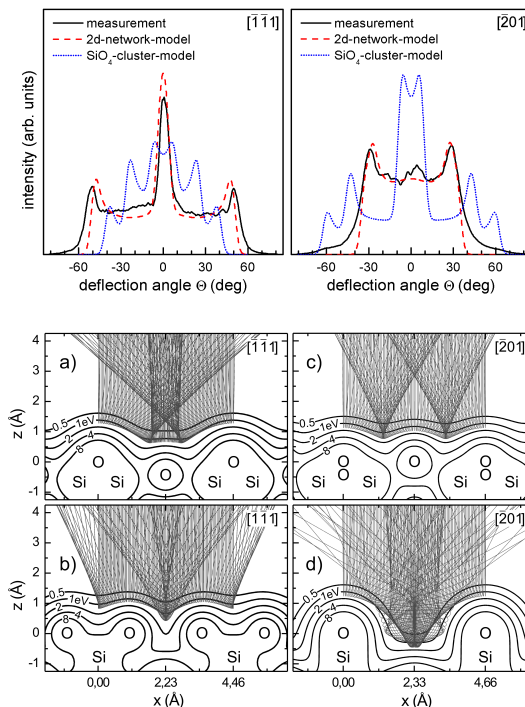


Abb. 4. Projizierte Intensität als Funktion des Ablenkwinkels für die Streuung von 2 keV He-Atomen von der Oberfläche eines ultradünnen Silica-Films auf Mo(112) unter einem Einfallswinkel von 1.5° . Unteren Bilder: Trajektorien-Simulationen für das 2D-Netzwerk- und für das Cluster-Modell (rechts).

Im unteren Teil der Abb.4 sind Projektionen der Trajektorien in eine Ebene senkrecht zu den beiden axialen Kanälen und die Positionen der Atome in den obersten Atomlagen dargestellt. In den Abbildungen sind deutlich sehr unterschiedliche Streubedingungen zu erkennen, insb. ergeben sich für die beiden Modelle sehr unterschiedliche Winkelpositionen für die Regenbögen. Die gestrichelte Linie repräsentiert die Simulationen für das 2D-Netzwerk-Modell, die gut mit den Messdaten übereinstimmen, während mit dem Cluster-Modell das Experiment nicht reproduziert wird. Somit bestätigen auch die Experimente zur Regenbogen-Streuung eindeutig das 2D-Netzwerk-Modell.

Während der Bearbeitung der Thematik wurden von der Arbeitsgruppe (unabhängig von einer französischen Arbeitsgruppe) Beugungseffekte bei der streifenden Streuung schneller Atome an Oberflächen entdeckt, die ein erhebliches Potential für Strukturuntersuchungen von Oberflächen aufweisen. Wir haben deshalb auch die Beugung schneller Atome für die Untersuchungen der ultradünnen Silica-Filme auf Mo(112) eingesetzt. Ein typisches Beugungsbild und die Streugeometrie für diese Methode sind in Abb.5 gezeigt, mit der sich sehr definierte Beugungsmuster für dieses System auflösen lassen.

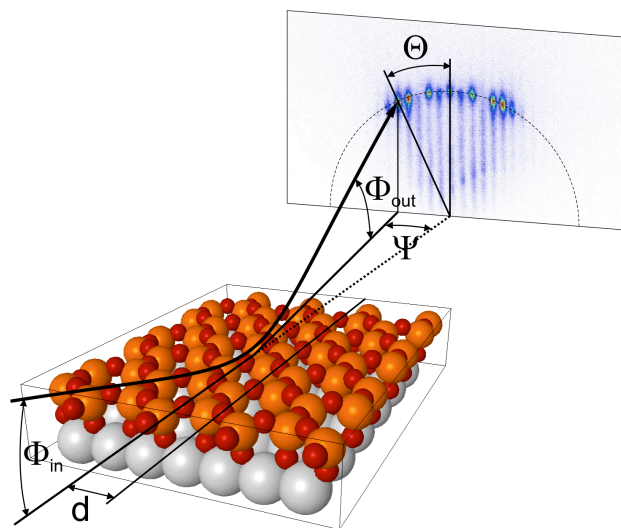


Abb. 5. Streugeometrie für die „Fast Atom Diffraction“ (FAD).

Für die Auswertung der Daten haben wir die experimentellen Beugungsmuster mit semiklassischen Modellrechnungen verglichen, wobei die Atompositionen sowie das atomare Wechselwirkungspotential der He-Atome vor der Oberfläche des Films mittels DFT im TP C5 bestimmt wurden. Der direkte Vergleich der Simulationen mit dem Experiment in Abb. 6 zeigt eine sehr gute Übereinstimmung der Daten für das 2D-Netzwerk-Modell, während zwar die Positionen der Beugungsreflexe auch für das Cluster-Modell reproduziert werden (gleiche

Periodizitätslänge), aber bei den Intensitäten ergibt sich eine gravierende Diskrepanz.

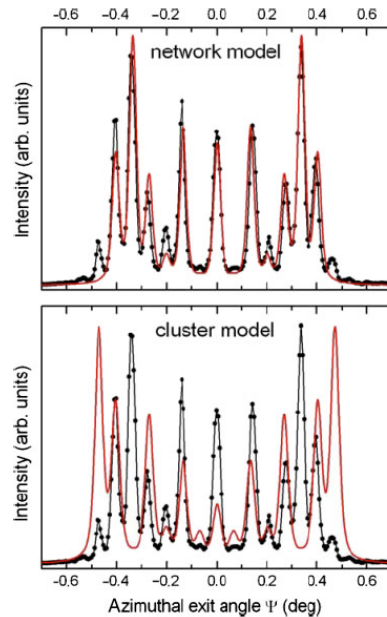


Abb. 6. Projizierte Intensitäten als Funktion des azimuthalen Ablenkwinkels für die Streuung von 2 keV He-Atomen von der Oberfläche eines ultradünnen Silica-Films auf Mo(112) unter 0.9° entlang einer [-110]-Richtung. Kurve mit Punkten: Experiment, Kurven: Semiklassische Modellrechnungen für 2D-Netzwerk- (oberes Bild) und Cluster-Modell (unteres Bild).

Dieses Resultat bestätigt auch eine detaillierte Analyse dieser Beugungsexperimente, bei der die Intensität des Beugungsreflexes 0ter Ordnung als Funktion der Senkrechterenergie der Projektile betrachtet wird (entspricht einer Variation der de Broglie-Wellenlänge der Teilchen). Die resultierende Modulation der Reflex-Intensität steht in enger Beziehung mit der Korrugation des Wechselwirkungspotentials und damit mit den Positionen der Atome in der obersten Lage des Films. In Abb.7 sind die Intensität des Beugungsreflexes 0ter Ordnung (oberes Bild) sowie die Korrugation des Wechselwirkungspotentials als Funktion der Senkrechterenergie der Projektile aufgetragen und mit Modellrechnungen für das 2D-Netzwerk- und das Cluster-Modell verglichen. Durch das interferometrische Verfahren sind die Daten sehr empfindlich auf die Korrugation und somit auf das Potential und die Positionen der Atome. Dies ist durch eine Kurve demonstriert, die auf einer Simulation beruht, bei der die Position der obersten O-Atome um nur 0.1 \AA verschoben wurde. Mit der zusätzlichen Berücksichtigung eines van der Waals-Terms für das Wechselwirkungspotential lassen sich die Daten sehr gut beschreiben, was sich insb. auch für die Korrugation des Potentials (unteres Bild) zeigt. Die gezielte Verschiebung der O-Atome und der resultierende Effekt auf die Korrugation des Potentials belegt, dass die DFT die Atompositionen für dieses System bis auf wenige 0.01 \AA genau zu berechnen gestattet. Entsprechende Berechnungen für das Cluster-

Modell ergeben gravierende Abweichungen und sind nicht im Einklang mit dem Experiment.

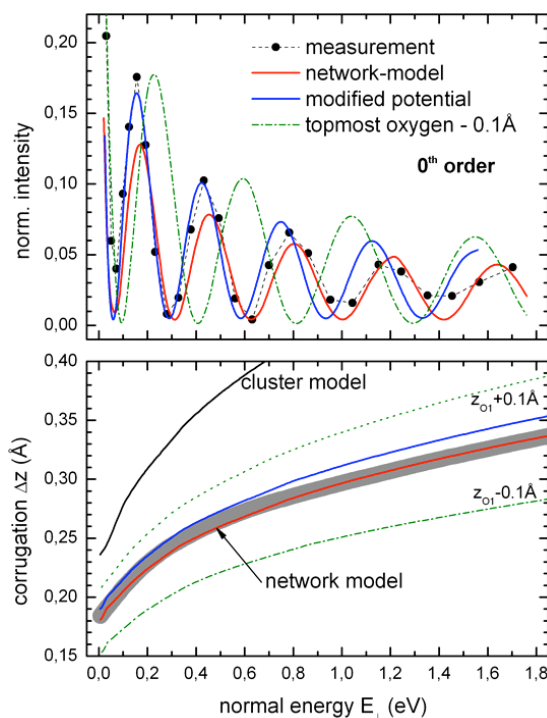


Abb.7. Vergleich der experimentellen (Punkte) und simulierten Intensitätsmodulationen der nullten Beugungsordnung (oben) sowie die Korrgation des Oberflächenpotentials (unten).

Die Experimente zur Beugung schneller Atome bestätigen somit nicht nur in allen Belangen das 2D-Netzwerk-Modell, sondern sie belegen auch sehr eindrucksvoll, dass sich neben der generellen Struktur des ultradünnen Silica-Films auch die Positionen der Atome des Films mit hoher Genauigkeit bestimmen lassen. Auf der Grundlage unserer Untersuchungen erachten wir die Diskussion über die Strukturmodelle für diesen Film als eindeutig geklärt.

O-Adsorption auf Mo(112)

(in Zusammenarbeit mit TP C5)

Bei der Präparation der Silica-Filme auf Mo(112) spielt die anfängliche Oxidation eine wichtige Rolle und wurde bereits in vorangegangenen Arbeiten zu dieser Thematik im Sfb546 in anderen Teilprojekten untersucht. Zunächst auf der Basis von LEED-Studien haben wir erstmals ein vollständiges Phasendiagramm erstellt, das in Abb.8 die verschiedenen Überstrukturen als Funktion der O_2 -Dosis sowie der Ausheiltemperatur zeigt und von einer $p(1 \times 2)$ über eine $c(4 \times 2)$ bis zu einer $p(1 \times 3)$ und $p(2 \times 3)$ Struktur reicht. Ein wichtiger Befund der Studien ist die Tatsache, dass die Strukturen nur von der O_2 -Dosis sowie der Temperatur abhängen.

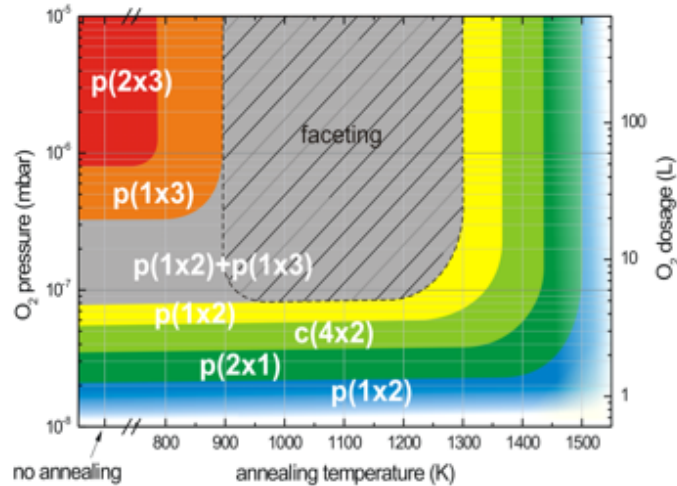


Abb. 8. Phasendiagramm für die Bedeckung von Mo(112) mit O₂.

Die Oxidation der Mo(112)-Oberfläche wurde anschließend mit Methoden der streifenden Ionen-Streuung untersucht. Neben der Ionenstrahl-Triangulation wurden vor allem die gestreuten Projektile untersucht, deren Nachweis mit dem ortsauflösenden Detektor erfolgte. Zunächst konzentrierten sich die Experimente auf die Messung der Intensität der spekulär gestreuten Atome, die empfindlich von der Beschaffenheit der Oberfläche abhängt, d.h. bei einem wohl geordneten Film im Vergleich zu einer ungeordneten Phase erhöht ist. In Abb.9 ist die Intensität der gestreuten Projektile als Funktion der O₂-Dosis für verschiedene Temperaturen aufgetragen. Es werden stets dann maximale Intensitäten beobachtet, wenn geordnete Strukturen vorhanden sind. Somit lässt sich in-situ die Ausbildung der spezifischen Phasen verfolgen.

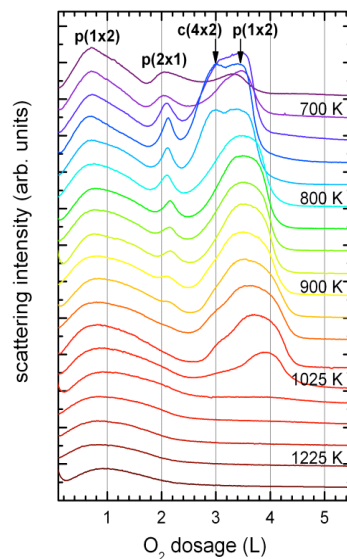


Abb. 9. Intensität der spekulär reflektierten 2 keV He-Atome von einer Mo(112)-Oberfläche als Funktion der O₂-Dosis für Temperaturen des Targets von 700 K bis 1225 K.

Wichtige Informationen kann man aus der zusätzlichen Aufnahme vollständiger Winkelverteilungen gewinnen, die bei Ausbildung einer geordneten Struktur Beugungsmuster zeigen. Durch diese Methode lässt sich die Oxidation in-situ im Detail untersuchen, wie die Winkelverteilungen für 2 keV He-Atome in Abb.10 für ansteigende O₂-Dosierung des Targets demonstrieren. Immer dann wenn eine geordnete Struktur auftritt, die zudem möglichst eine elektronische Bandlücke aufweisen sollte, treten definierte Beugungsmuster auf, die den jeweiligen bereits von den LEED-Studien bekannten Überstrukturen entsprechen. Im Übergangsbereich zwischen zwei Phasen – wie z.B. bei einer Dosis von 2,5 L – fehlt eine periodische Ordnung und es tritt nur die 0. Beugungsordnung auf. Für einen ungeordneten Film – siehe Bild für 4,2 L – führt die raue Oberfläche zu einer breiten, unstrukturierten Winkelverteilung.

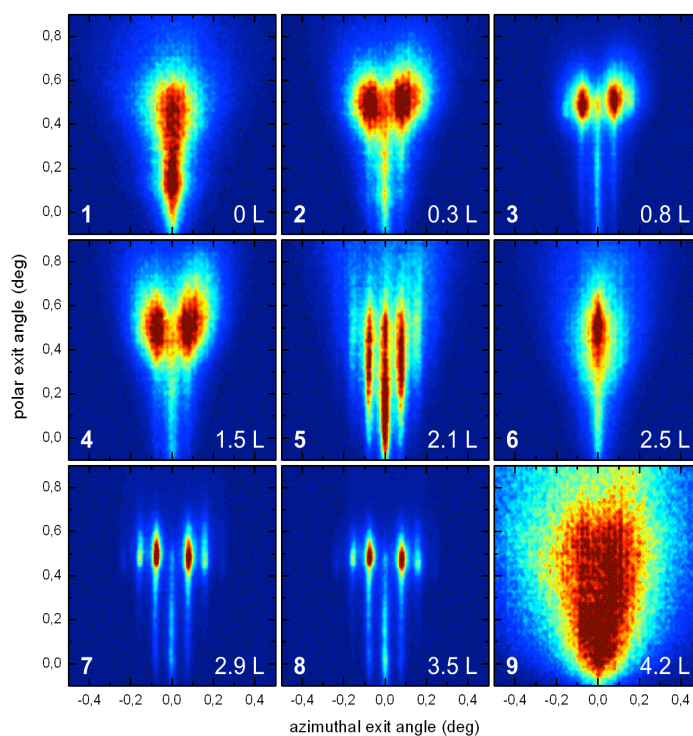


Abb. 10. Winkelverteilung für 2 keV He Atome nach der streifenden Streuung an O/Mo(112) als Funktion der Dosierung mit O₂ von der sauberen Mo(112)-Probe (1) bis zu 4.2 L (9).

Im Rahmen der Analyse der Daten wurden Strukturmodelle aufgestellt, die für die pg(2x1)- und c(2x4)-Überstrukturen in Abb.11 dargestellt sind. Dabei wurden die detaillierten Atompositionen weitgehend durch die Analyse der Daten zur Ionenstrahl-Triangulation bestimmt. Für weitere Überstrukturen wurden ebenfalls Modelle entwickelt. Eine Publikation der Daten ist in Vorbereitung.

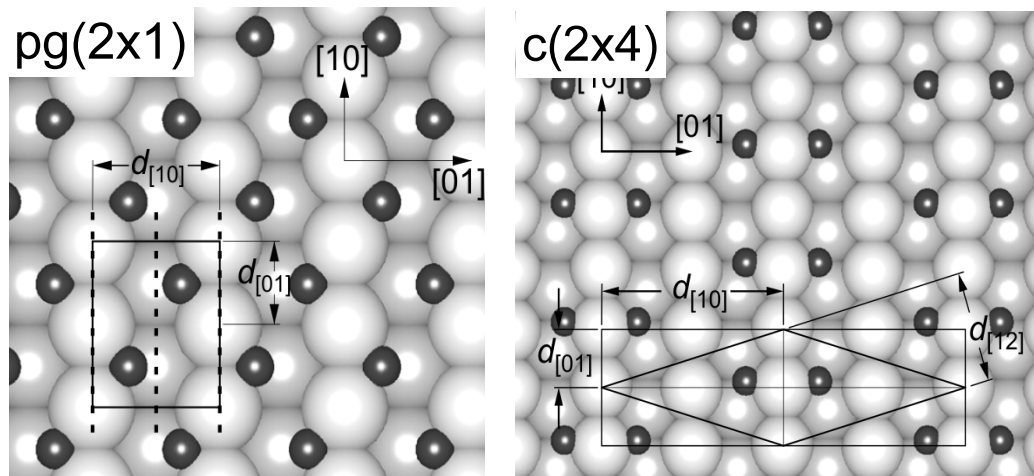


Abb. 11. Strukturmodelle für O/Mo(112). Linkes Bild $pg(2 \times 1)$, rechtes Bild $c(2 \times 4)$.

TiO_x auf Mo(112)

Nach den Vorgaben von Goodman wurde ein Titanoxidfilm mit $p(8 \times 2)$ -Symmetrie auf Mo(112) präpariert, an dem gleichfalls definierte Triangulations-Messungen realisiert werden konnten. Auch die Aufnahme von Beugungsstrukturen war erfolgreich, wie die Winkelverteilungen in Abb.12 zeigen. Aus den Richtungen axialer Ketten in den Triangulationsmessungen sowie den Beugungslinienabständen bei FAD-Messungen kann auf eine Untereinheitszelle von $p(8/7 \times 2)$ mit einem obersten Sauerstoffatom geschlossen werden. Dies ist in Einklang mit dem Strukturvorschlag von Goodman [2] sowie mit einigen mittels DFT von Pacchioni et al. [3] untersuchten Modellen, für die jedoch eine $p(1 \times 2)$ Einheitszelle vorausgesetzt wurde. Den Strukturvorschlag für die Positionen der Sauerstoffatome zeigt Abb.13.

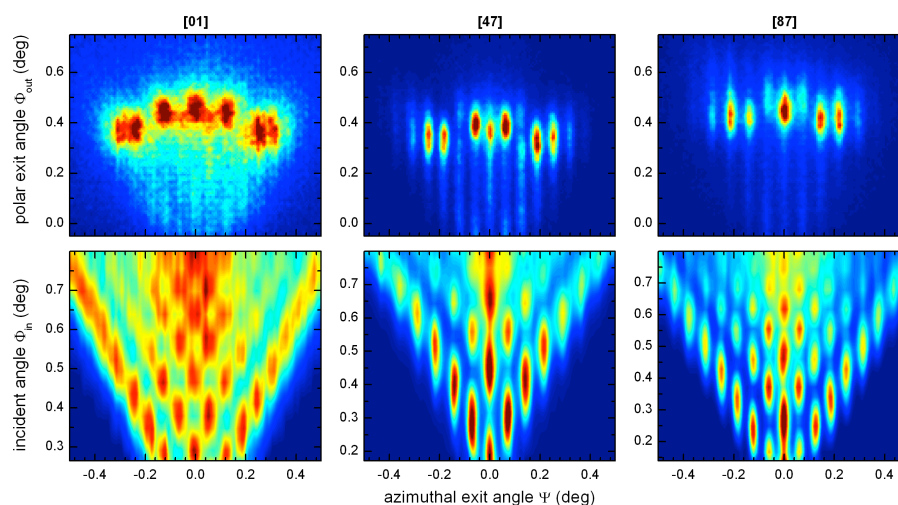


Abb. 12. FAD-Beugungsstrukturen für die Streuung von 2 keV He-Atome von einem TiO_x-Film auf Mo(112).

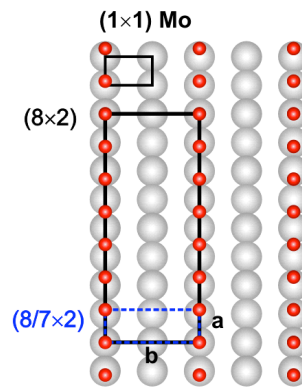


Abb. 13. Strukturmodell für die oberste Lage von Sauerstoffatomen in einer $(8/7 \times 2)$ -Einheitszelle.

V_2O_3 auf Au(111)

(in Zusammenarbeit mit TP C1, C8)

In der Schlussphase der Förderperiode wurden Untersuchungen zur Struktur von dünnen V_2O_3 -Filmen auf Au(111) begonnen, die durch die kontrovers diskutierte Strukturmodelle für die oberste Lage des Films, d.h. insb. die Terminierung, motiviert wurden. Diesbezüglich ist eine aktuelle Publikation des TP C8 zu nennen [4], in der im Gegensatz zu der zuvor diskutierten Vanadyl-Terminierung eine O_3 -Terminierung auf der Basis von Ionen-Steuerexperimenten beschrieben wird.

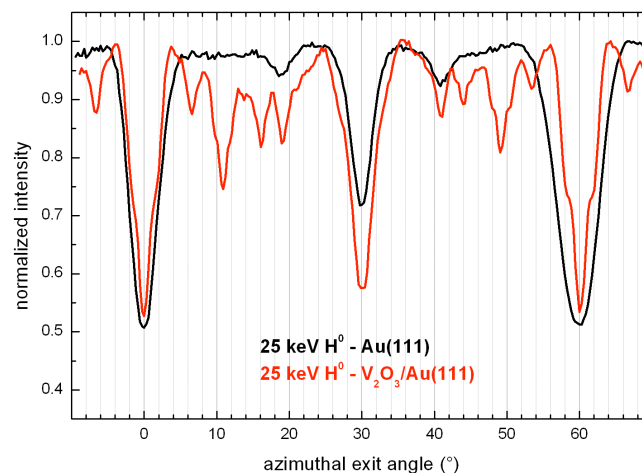


Abb. 14. Triangulationskurve für die Streuung von 25 keV H-Atomen unter 1.5° von einer sauberen Au(111)-Oberfläche und einem Oxidfilm.

Mit einem Au(111)-Kristall aus dem TP C1 wurden V_2O_3 -Filme mit $\sqrt{3} \times \sqrt{3}$ -Struktur gewachsen und Triangulations- sowie FAD-Messungen realisiert. Abb.14 zeigt Triangulationskurven für sauberes Au(111) sowie den Oxidfilm. Auf der Basis einer

vorläufigen Analyse der Daten können wir das O₃-Strukturmodell bestätigen. Eine detaillierte Auswertung sowie die Publikation der Daten steht noch aus.

Untersuchung einer porösen TiO₂/V₂O₅-Keramik mittels Rutherford-Rückstreuung (RBS)

(in Zusammenarbeit mit TP B7, B2)

Mittels Rutherford-Backscattering (RBS) am Beschleuniger des Ionenstrahllabors der Arbeitsgruppe wurden poröse TiO₂/V₂O₅-Keramiken untersucht, wie sie auch in Studien mit Realkatalysatoren zum Einsatz kommen. Durch die Rauigkeit der Oberflächen der gepressten Proben werden die RBS-Energiespektren charakteristisch modifiziert, wie typische Spektren in der Abb.15 zeigen.

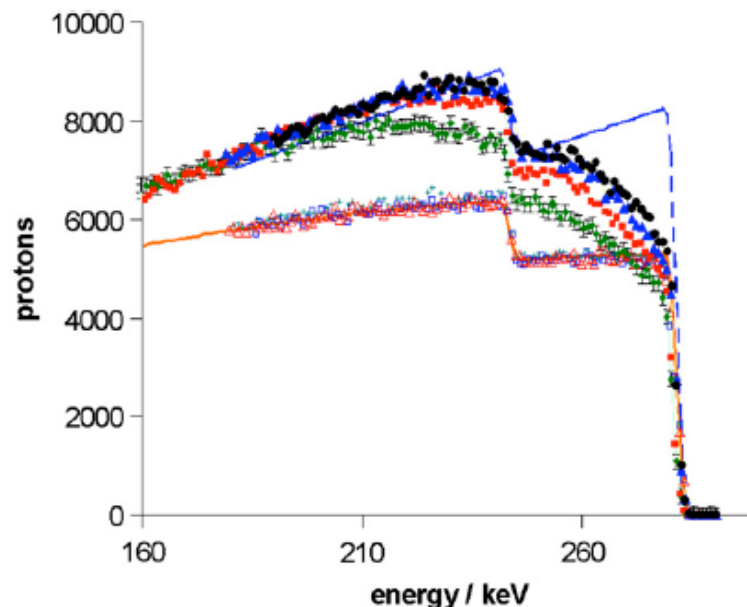


Abb. 15. RBS-Spektren von verschiedenen getemperten Keramikproben. Gestrichelte Kurve: Streuung von V₂O₅-Einkristall.

Während für glatte Proben die typischen scharfen Kanten der Spektren für die Streuung an der Oberfläche beobachtet werden, findet man für die porösen Proben eine ausgeprägte Abrundung der Flanken. In Simulationsrechnungen wurde der Effekt der Rauigkeit der Proben auf die Spektren untersucht und gezeigt, dass das Abflachen der Anstiegskante in unmittelbarem Bezug zu der mittleren Korngröße des Pulvers steht. Somit konnte mittels RBS nicht nur die Stöchiometrie der Probe sondern auch der mittlere Korndurchmesser ermittelt werden.

Als ein Beispiel für die Ergebnisse dieser Studien ist in Abb.16 die so ermittelte Korngröße als Funktion der Prozesstemperatur gezeigt. Die Daten zeigen einen Phasenübergang bei ca.

600°C von „Anatas/Shcherbinaite“ nach „Rutil Solid Solutions“, der mit einer ausgeprägten Änderung der Korngrenzen verbunden ist. Begleitende elektronenmikroskopische Aufnahmen zeigen gleichfalls diese Veränderung. Die Arbeiten sind im Detail in [MHG11] diskutiert.

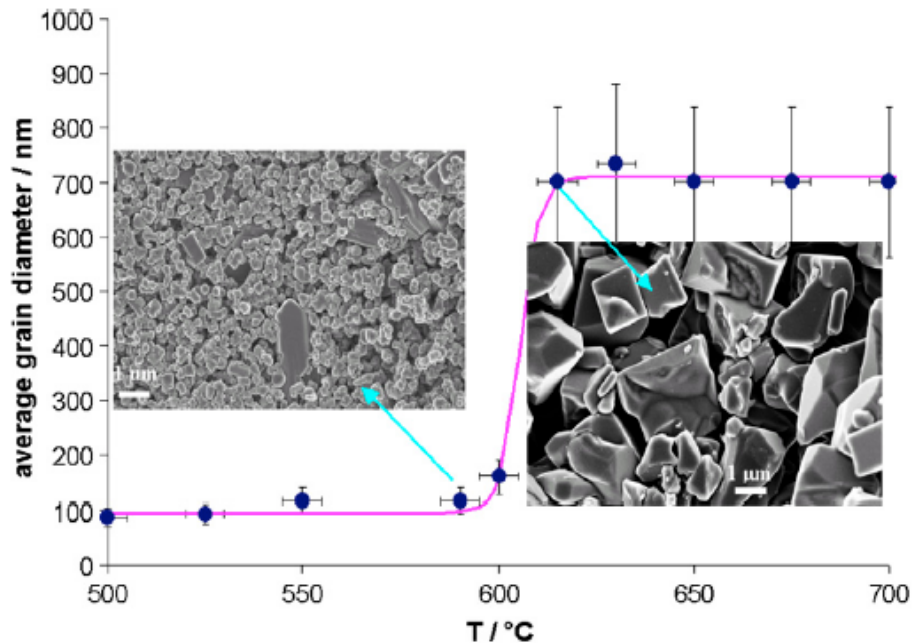


Abb.16. Aus RBS-Messungen abgeleitete mittlere Korngröße als Funktion der Prozesstemperatur sowie elektronenmikroskopische Aufnahmen.

- [1] M.S: Chen and D.W. Goodman, J. Phys.: Condens. Matter **20** (2008) 264013.
- [2] M.S. Chen, K. Luo, D. Kumar, W.T. Wallace, C.-W. Yi, K.K. Gath, D.W. Goodman, Surf. Sci. **601** (2007) 632.
- [3] Y. Zhang, L. Giordano, G. Pacchioni, J. Phys. Chem. C **111** (2007) 7437.
- [4] A.J. Window, A. Hentz, D.C. Sheppard, G.S. Parkinson, H. Niehus, D. Ahlbehrendt, T.C.Q. Noakes, P. Bailey, and D.P. Woodruff, Phys. Rev. Lett. **107** (2011) 016105.

5.2.2 Projektrelevante eigene Publikationen

a) erschienene oder angenommene Arbeiten in wissenschaftlichen Zeitschriften oder Buchveröffentlichungen

- [LSB11] J. Lienemann, A. Schüller, D. Blauth, J. Seifert, S. Wethekam, M: Busch, and H. Winter,
Coherence during scattering of fast atoms from a LiF(001) surface
Phys. Rev. Lett. **106** (2011) 067602(1–4).
- [SSW10] J. Seifert, A. Schüller, H. Winter, R. Wlodarczyk, M. Sierka and J. Sauer,
Diffraction of fast atoms during grazing scattering from the surface of an ultrathin silica film on Mo(112)
Phys. Rev. B. Phys. Rev. B. **82** (2010) 035436(1–10).

- [SBS10] J. Seifert, M. Busch, A. Schüller, D. Blauth, M. Busch, S. Wethekam and H. Winter
Structure of ultrathin silica films on Mo(112) from classical and quantum mechanical rainbow scattering of fast atoms
Surf. Interface Analysis **42** (2010) 1575 – 1580.
- [MHG11] R. Mitdank, D. Habel, O. Görke, M. Harth, H. Schubert and H. Winter,
Ion beam analysis of a structural phase transition in porous TiO₂/V₂O₅ ceramics with rough surfaces
Nucl. Instrum. Meth. B **269** (2011) 345 – 352.
- [SW09] J. Seifert and H. Winter
Structure of monolayer silica layer on Mo(112) from rainbow scattering under axial surface channeling
Surf. Sci. Lett. **603** (2009) L109 – L112.
- [SBW09] J. Seifert, D. Blauth and H. Winter
Evidence for 2D-network structure of monolayer silica film on Mo(112)
Phys. Rev. Lett. **103** (2009) 017601 – 017604.
- [WSB09] H. Winter, J. Seifert, D. Blauth, M. Busch, A. Schüller and S. Wethekam
Structure of ultrathin oxide layers on metal surfaces from grazing scattering of fast atoms
Appl. Surf. Sci. **256** (2009) 365 – 370.
- [WS11] H. Winter and A. Schüller
Fast atom diffraction during grazing scattering from surfaces
Prog. Surf. Sci. **86** (2011) 169 – 221.

5.3 Rückblick auf die Förderung

Das Teilprojekt wurde seit 07/2008 im Sonderforschungsbereich gefördert. Es wurde mit Ablauf der 4. Förderperiode im Juni 2011 beendet.

5.3.1 Personal im Teilprojekt während der 4. Förderperiode

	lauf. Nr.	Name, akademischer Grad, Dienststellung	engere Fachzugehörigkeit	Institut der Hochschule oder der außeruniv. Einrichtung	Mitarbeit im Projekt Zeitraum, Wochenstunden	Entgeltgruppe
Grundausrüstung						
Wissenschaftlerinnen und Wissenschaftler	1.	Helmut Winter Dr., Univ.-Prof..	Experimentalphysik	HU-P	07/2008 – 06/2011, 8h	
	2.	Rüdiger Mitdank, Dr.	Experimentalphysik	HU-P	03/2002 – 07/2008, 30h	
	3.	Marco Busch, Dr.	Experimentalphysik	HU-P	10/2010 – 06/2011, 20h	
	4.	Lienemann Jens, Dipl. Phys.	Experimentalphysik	HU-P	06/2009 – 06/2011, 20h	
	5.	Uwe Specht, SHK	Experimentalphysik	HU-P	07/2008 – 06/2011	
	6.	Eric Meyer, SHK	Experimentalphysik	HU-P	09/2010 – 06/2011	
nichtwissenschaftl. Mitarbeiterinnen und Mitarbeiter	7.	Klaus Maass, Dipl. Ing.		HU-P	07/2008 – 06/2011, 10h	
	8.	Günter Linderberg, TA		HU-P	07/2008 – 06/2011, 10h	
	9.	Birgit Gilsenbach, TA		HU-P	07/2008 – 06/2011, 5h	
	10.	Jürgen Sölle, TA		HU-P	07/2008 – 12/2010, 5h	
	11.	Monika Janetzki, Sekr.		HU-P	07/2008 – 02/2009, 10h	
	12.	Kerstin Hasse, Sekr.		HU-P	05/2010 – 06/2011, 10h	
Ergänzungsausstattung						
Wissenschaftlerinnen und Wissenschaftler	1.	Marco Busch, Dr.	Experimentalphysik	HU-P	07/2008 – 09/2010, 40h	E13
	2.	Andreas Schüller, Dr.	Experimentalphysik	HU-P	10/2010 – 05/2011, 40h	E13
	3.	Jan Seifert	Experimentalphysik	HU-P	06/2011, 40 h	E13
nichtwissenschaftl. Mitarbeiterinnen und Mitarbeiter						

Aufgaben der Mitarbeiterinnen und Mitarbeiter (Grundausrüstung)

1. Prof. Dr. Helmut Winter
Verantwortliche Leitung des Teilprojekts. Mitwirkung bei der Planung und Auswertung der Experimente, Präsentation der Resultate, Erstellen von Publikationen.
2. Dr. Rüdiger Mitdank
Mitarbeit an der Planung, Durchführung und Auswertung der Experimente. Betreuung der beteiligten Doktoranden und Studenten. Betreuung der zum Einsatz kommenden Beschleunigeranlagen.
3. Dr. Marco Busch
Mitarbeit an der Planung, Durchführung und Auswertung der Experimente. Betreuung der beteiligten Doktoranden und Studenten. Betreuung der zum Einsatz kommenden Beschleunigeranlagen. (Stellennachfolger von Mitdank)
4. Jens Lienemann
Mitarbeit an der Planung, Durchführung und Auswertung der Experimente zum Wachstum und zu den Eigenschaften ultradünner Vanadiumoxidfilme auf einer MgO-Oberfläche im Rahmen einer Diplomarbeit.
5. Uwe Specht
Mitarbeit an den Projekten im Rahmen einer SHK.
6. Eric Meyer
Mitarbeit an den Projekten im Rahmen einer SHK.
7. Klaus Maass
Herr Dipl.-Ing. Maass war mit 5 Stunden seiner Wochenarbeitszeit an den apparativen, vor allem elektronischen Aufbauten des Projekts beteiligt.
8. Günter Lindenberg
Herr Lindenberg war an der Planung und Durchführung mechanischer Aufbauten am Projekt beteiligt. Ferner trug er ihm Rahmen logistischer Arbeiten, Mitarbeit bei der Targetpräparation sowie Betreuung der Elektronenstrahlverdampfer zum Projekt bei.
9. Birgit Gilsenbach
Frau Gilsenbach war durch Labortätigkeiten am Projekt beteiligt. Ferner betreute sie das Projekt bei der Auswertung und Präsentation der Daten unterstützen sowie die zum Einsatz kommende Computerausstattung.

10. Jürgen Sölle
Herr Sölle stand als Mitarbeiter des zentralen Präparationslabors des Instituts für die Präparation von Targets sowie Verdampfergut zur Verfügung.
11. Monika Janetzky
Frau Janetzky stand als Sekretärin der Arbeitsgruppe dem Projekt für Schreibarbeiten, Bestellwesen, Mitarbeit bei der Dokumentation, etc. zur Verfügung.
12. Kerstin Hasse
Frau Hasse stand als Sekretärin der Arbeitsgruppe dem Projekt für Schreibarbeiten, Bestellwesen, Mitarbeit bei der Dokumentation, etc. zur Verfügung. (Nachfolgerin von Janetzki)

Aufgaben der Mitarbeiterinnen und Mitarbeiter (Ergänzungsausstattung):

1. Dr. Marco Busch
Verantwortliche Planung, Durchführung, Auswertung sowie Präsentation der Daten, Betreuung der am Projekt beteiligten Studenten. Mitarbeit bei der Erstellung von Publikationen.
2. Dr. Andreas Schüller
Mitarbeit im Teilprojekt. Mitarbeit bei der Erstellung einer Publikation. Durchführung von Simulationsrechnungen. (Stellennachfolger von Busch)
3. Jan Seifert
Vorbereitung und Durchführung der Experimente dünner Titanoxid-Filme auf Mo(112) und dünner Vanadiumoxid-Filme auf Au(111). Durchführung von Simulationsrechnungen. (Stellennachfolger von Schüller)

